# J.C. Bose University of Science and Technology, YMCA, Faridabad

NAAC 'A+' Grade Accredited State Govt. University

GOLDEN JUBILEE YEAR
(1969-2019)

ISBN 978-81-973526-0-7

# Proceedings of International Conference on Trends and Advances in Mechanical Engineering (TAME 2026)

Organized by

**Department of Mechanical Engineering**

Sponsors

IMT Industries Association Faridabad

VICTORA INDUSTRIES PVT. LTD.

NH-2, Sector 6, Faridabad (Haryana) 121006

jcboseust.ac.in /JCBoseUST


Sweden
USA
Germany
Hungary
China
Japan
Mexico
India
Thailand
Indonesia
S. Africa
Supply
Warehouse
Production
EV & H2
Machining
Stamping
Casting
VICTORA INDUSTRIES
Product Design
Fabrication
Forging
Hospitality
Victora Industries Pvt. Ltd.
www.victoraindustries.com info@victoraindustries.com
Head Office: Plot No-1146-47, Sector-58 Faridabad(Haryana)-121004, India


VICTORA
VICTORA LIFTS
ESCALATOR
ELEVATOR
TRAVELATOR
POWER YOUR BUILDING
WITH
PREMIUM ELEVATORS
ELEVAYING INDIA'S
INFRATRAVEL™
FOLLOW US ON :-
victoralifts
Victora-Lifts
victoralifts
victoralifts
SCAN
www.victoralifts.com
Toll Free : 1800 102 8961
info@victoralifts.com



# International Conference

(Hybrid Mode)

## Trends & Advances in Mechanical Engineering

## TAME 2026

16-17 April 2026

### Patron

**Prof. Rajive Kumar**
Vice Chancellor

### Co-Patron

**Prof. (Dr.) Ajay Ranga**
Registrar

**Prof. (Dr.) Rajkumar**
Dean (FET)

### Conference Chair

**Prof. Arvind Kumar**
Chairperson (ME)

### Convener

**Dr. Sandhya Dixit**
Professor (ME)

**Dr. Rajeev Saha**
Associate Prof. (ME)

**Dr. Rajesh Attri**
Asst. Prof. (ME)

### Organizing Secretary

**Sh. Surender Singh**
Asst. Prof. (ME)

**Dr. Nitin Panwar**
Asst. Prof. (ME)

**Dr. Nisha Bhatt**
Asst. Prof. (ME)

### Editors

**Dr. Nitin Panwar**
Asst. Prof. (ME)

**Dr. Rajesh Attri**
Asst. Prof. (ME)

**DEPARTMENT OF MECHANICAL ENGINEERING**

**J.C. BOSE UNIVERSITY OF SCIENCE AND TECHNOLOGY, YMCA, FARIDABAD**

*NAAC 'A+' Grade Accredited State Govt. University*

NH-2, Sector 6, Faridabad (Haryana) 121006

jcboseust.ac.in /JCBoseUST

# INTERNATIONAL CONFERENCE

(Hybrid Mode)

## Trends & Advances in Mechanical Engineering

## TAME 2026

16-17 April 2026

### Internal Research Paper Review Committee

- Prof. Hari Om
- Prof. Vasdev Malhotra
- Prof. Sanjeev Goyal
- Dr. Krishan Verma
- Dr. Mahesh Chand
- Dr. Nitin Panwar
- Dr. Nisha Bhatt

### Organizing Committee

- Dr. Bhaskar Nagar
- Dr. Nikhil Dev
- Dr. Mukesh Gupta
- Dr. Krishan Kumar
- Dr. Mahesh Chand
- Dr. O.P. Mishra
- Dr. Bhupender Singh
- Dr. Sanjay Kumar
- Dr. Nitin Panwar

### Conference Advisors

- Prof. Vikram Singh
- Prof. Vikas Turk
- Prof. Lakhwinder Singh
- Prof. Hari Om
- Prof. Sanjeev Kumar
- Prof. Vasdev Malhotra
- Prof. Sanjeev Goyal
- Prof. Munish Vashishath
- Prof. Atul Mishra
- Prof. Pawan Singh
- Prof. Komal Bhatia
- Prof. Pradeep Dimri
- Prof. Divyajyoti

**DEPARTMENT OF MECHANICAL ENGINEERING**


**J.C. BOSE UNIVERSITY OF SCIENCE AND TECHNOLOGY, YMCA, FARIDABAD**

*NAAC 'A+' Grade Accredited State Govt. University*

NH-2, Sector 6, Faridabad (Haryana) 121006

jcboseust.ac.in /JCBoseUST

# PREFACE

It gives us immense pleasure to present the proceedings of the International Conference on Trends and Advances in Mechanical Engineering (TAME 2026), organized by the Department of Mechanical Engineering, J.C. Bose University of Science and Technology, YMCA, Faridabad. This conference serves as a vibrant platform for academicians, researchers, industry experts, and students from across the globe to come together and exchange knowledge, ideas, and innovations in the rapidly evolving field of mechanical engineering.

In an era marked by unprecedented technological transformation and global challenges, TAME 2026 aims to highlight cutting-edge developments and foster interdisciplinary collaboration. The conference focuses on key thematic areas that are shaping the future of engineering and technology. These include Advanced Manufacturing and Industry 4.0/5.0, emphasizing intelligent production systems and digital transformation; Sustainable & Green Mechanical Systems, addressing energy efficiency, environmental sustainability, and climate-conscious innovations; and Smart Materials, Mechanics & Structural Innovations, exploring next-generation materials and structural solutions.

The conference further delves into Robotics, Mechatronics & Autonomous Systems, showcasing advancements in automation and intelligent machines, as well as Computational Mechanics, AI & Digital Engineering, which integrates simulation, data-driven methods, and artificial intelligence to solve complex engineering problems. Additionally, TAME 2026 recognizes the importance of heritage and sustainability through the theme Indian Knowledge System for Indigenous Technologies, encouraging exploration of traditional wisdom and its relevance in modern technological contexts.

The overwhelming response to this conference reflects the growing interest and significance of these emerging domains. The selected research papers included in these proceedings have undergone a rigorous peer-review process to ensure high academic and technical standards. Collectively, they represent innovative ideas, practical solutions, and forward-thinking approaches that contribute to the advancement of mechanical engineering.

The research papers in the conference are being presented under following tracks:

**Track I: Advanced Manufacturing and Industry 4.0/5.0**

- Additive manufacturing (3D/4D printing)
- Smart factories and digital twins
- Robotics and automation in manufacturing
- Cyber-physical systems
- AI and data analytics in production systems

**Track II: Sustainable & Green Mechanical Systems**

- Renewable energy systems (wind, solar, hydrogen)
- Energy-efficient thermal systems
- Sustainable materials and eco-design
- Life cycle assessment and carbon neutrality
- Waste heat recovery and energy harvesting

**Track III: Smart Materials, Mechanics & Structural Innovations**

- Smart and adaptive materials
- Advanced composites and nano-materials
- Fracture mechanics and durability
- Lightweight structures for aerospace and automotive
- Bio-inspired and multi-functional materials

**Track IV: Robotics, Mechatronics & Autonomous Systems**

- Autonomous robots and mobile platforms
- Human–robot interaction
- Mechatronic system design
- Control systems and sensor integration
- Medical, service, and industrial robotics

**Track V: Computational Mechanics, AI & Digital Engineering**

- Computational fluid dynamics (CFD) and FEA
- AI-driven design optimization
- Machine learning in mechanical systems
- Multiphysics modeling and simulation
- Virtual prototyping and digital engineering workflows

**Track VI: Indian Knowledge System for Indigenous Technologies**

- Philosophical Foundations of Indigenous Innovation
- Traditional Engineering and Architectural Excellence
- Energy Practices in Traditional Systems
- Modern Adaptation of Indigenous Technologies

We extend our sincere gratitude to all authors, reviewers, keynote speakers, and participants for their valuable contributions and enthusiastic participation. We also acknowledge the dedicated efforts of the organizing committee and supporting staff whose commitment has made this conference possible.

We hope that TAME 2026 will inspire meaningful discussions, foster collaborations, and pave the way for future research and technological breakthroughs. May these proceedings serve as a valuable resource for researchers, practitioners, and policymakers striving to shape a sustainable and technologically advanced future.

**Organizing Committee**
**TAME 2026**
**Department of Mechanical Engineering**
**J.C. Bose University of Science and Technology, YMCA, Faridabad**

# NATIONAL ADVISORY COMMITTEE

**Academia**

- Prof. D.S. Chauhan, Pro-Chancellor, GLA University
- Prof. Dinesh Kumar, VC, SVSU, Palwal
- Prof. Narsi Ram Bishnoi, VC, GJUST Hisar
- Prof. Samsher, VC, HBTU, Kanpur
- Prof. Tripta Thakur, VC, UTU
- Dr. Rakesh Mudgal, VC, Atmiya University, Rajkot
- Prof. Vivek Kumar, IIT Delhi
- Prof. D. K. Sharma IIT Delhi
- Prof. D.R. Kaushal, IIT Delhi
- Prof. Harish Kumar, NIT Delhi
- Prof. Anup Shukla IIT Jammu
- Prof. Atul Sharma IIT Bombay
- Prof. Ashish Pandey, IIT Mumbai
- Prof. S.K. Gupta, DCRUST, Murthal
- Prof. Basant Sikarwar, Amity University, Noida
- Prof. Anurag Mishra, Delhi University, Delhi
- Prof. Brijesh Yadav, IIT Roorkee
- Prof. Jaimala Gambhir, PEC University, Chandigarh
- Prof. Manish Jindal, South Asian University, Delhi
- Prof. O. K. Singh, IGDTUW, Delhi
- Prof. Rajesh Singh, Banasthali Vidyapeeth, Rajasthan
- Prof. Ashish Singla, TIET, Patiala
- Prof. Ajay Singholi, GGSIPU, Delhi
- Prof. B.B. Arora, DTU, Delhi
- Prof. Nathi Ram Chauhan, IGDTUW, Delhi
- Dr. Gulshan Sachdeva, NIT Kurukshetra
- Dr. Shivlal, RTU, Kota
- Dr. Siva Reddy, Director (Tech.), National Institute of Solar Energy
- Prof. Sandeep Grover, Retd. Professor (ME), JCBUST
- Prof. Tilak Raj, Retd. Professor (ME), JCBUST
- Prof. M.L. Aggarwal, Retd. Professor (ME), JCBUST

**Industry**

- Sh. S.S. Banga, MD, Victora Industries Pvt. Ltd.
- Sh. Parmod Rana, MD, Spectrum Weighpack & President IIAF
- Sh. Ajay Abrol, MD, UA Consultants
- Sh. Umesh Gupta, Sr. VP, BSES Rajdhani Power Ltd, Delhi
- Sh. S.K. Singhal, Ex DGM, IOCL
- Sh. Naresh Kumar, MD, Dynamic Drilling & Offshore Services Pvt.
- Dr. R.K. Yadav, GM (T), Pragati Power Corporation Ltd.
- Sh. Yogesh Garg, IFS, DFO&DD, Tamil Nadu
- Ms. Chanchal Bhardwaj, Director IRAA, SVSU

# INTERNATIONAL ADVISORY COMMITTEE

- Dr. Biren Prasad, Knowledge Solution, USA
- Dr. Subhas Sharma, Central Queensland University, Australia
- Dr. Ayush Goyal, Texas A&M University, USA
- Dr. Surendra Kumar Singh, President Belmont Scientific, USA
- Prof. Ankur Jain, University of Taxes Arlington USA
- Dr. Ganesh Rathod, University of the Witwatersrand, Johannesburg
- Dr. Gopal Krishan, Wellington Institute of Technology, New Zealand
- Dr. Rahul Sahay, SUTD, Singapore

# ABOUT THE UNIVERISTY

J.C. Bose University of Science and Technology, YMCA, Faridabad (formerly YMCA University of Science and Technology) was established in 2009 by Haryana State Legislative Act No. 21 of 2009 and Haryana Government Gazette Notification No. 29 of 2009, dated 16.9.2009.

Established in 1969 as YMCA Institute of Engineering with an initial intake of 120 students, the institution began as an Indo-German collaboration between the State Government (erstwhile Punjab), the National Council of YMCAs of India, and West German agencies. It aimed to provide practical, industry-oriented technical education on the German model to meet India's growing industrial needs. The State Government allotted 20 acres for campus development, while German expertise supported the establishment of laboratories and workshops. From 1994, the institute received 100% grant-in-aid, and in 1998, its management was fully taken over by the State Government. Elevated to university status under Legislative Act 21 of 2009, it gained UGC 12(B) recognition in 2012. The university is currently accredited with an 'A+' grade by NAAC. In 2018, it was renamed after the eminent scientist Jagadish Chandra Bose.

At present, the University offers a four-year B.Tech. degree in almost all disciplines. Besides, it is offering Science, Management and Arts courses at UG and PG level. At UG level, BSc (Hons) in Physics, Chemistry and Math, BCA, BBA, BA in Journalism & Mass Communication and BA Social Work and BSc (Animation & Multimedia) have been introduced.

Similarly, at PG level, M.Tech. (in all disciplines), MCA, MBA, MSc (Physics, Chemistry, Environment Studies, Math, Bio-Technology, Botany, Zoology and Microbiology, Animation and Multimedia), MA (Journalism & Mass Communication and English) are being offered. The University also offers Ph.D. programs in all disciplines. The University also runs various B.Voc. and skill related diploma and certificate courses under its Community College of Skill Development.

The present campus of the University is situated on National Highway-2, Mathura Road, 30 km from National Capital, Delhi. The University campus is located in the sprawling Faridabad-Ballabgarh Industrial complex. The State Government has also allotted 18 acres of land to the University on Faridabad-Gurugram Road in village Bhakari for its second campus.

# ABOUT THE DEPARTMENT

The Department of Mechanical Engineering offers courses at UG and PG level. At UG level, B.Tech. course in Mech. Engg., started in 1997 has an intake of 120 students. M.Tech. programme in Mech. Engg. with specialization in *Manufacturing Technology and Automation* was started from the academic year 2003-04 and has an intake of 18 students. The University has started PhD Course since 2010 and 53 students have registered themselves for the PhD programme in the department. In 2021-22, the department started 02 more programs i.e. B.Tech. course in Mechanical Engineering (Hindi Medium) and B.Tech. course in Robotics & Artificial Intelligence with intake of 30 each.

The department is actively engaged in research work in the broad area of Design of Mechanical Equipment, Design & Manufacturing, Thermal, Energy conservation, TQM, Product and Service Quality, Computer Integrated Manufacturing, E-Manufacturing, Computer Aided Engineering, Just in Time, etc.

The departmental facilities include 16 labs, 3 workshops (Machine Tools, Refrigeration & Air conditioning, Fabrication & Sheet Metal Technology), 8 lecture halls, and 1 conference room.

The department has highly qualified and experienced faculty including 10 professors, 3 Associate professors and 10 Assistant Professors. 22 of the faculty members are PhD holders with average experience of faculty members being approximately 18 years.

The department also sponsors its faculty for short term courses and conferences on regular basis. During last 5 years, faculty members have published approximately 100 papers in various national and international journals and conferences of repute.

The department is also highly active in co-curricular and technical activities. Two of its club namely *MechNext Club* and *SAE India YMCA Collegiate Club* are actively engaged in practising latest developments in concerned engineering field.

**Prof. (Dr.) Arvind Gupta**
Professor & Chairperson
Department of Mechanical Engg.

# *Faculty Members*

| S. No. | Name | Designation | Qualification |
|---|---|---|---|
| 1 | Dr. Raj Kumar | Professor | PhD |
| 2 | Dr. Arvind Gupta | Professor | PhD |
| 3 | Dr. Vikram Singh | Professor | PhD |
| 4 | Dr. Hari Om | Professor | PhD |
| 5 | Dr. Vikas Turk | Professor | PhD |
| 6 | Dr. Lakhwinder Singh | Professor | PhD |
| 7 | Dr. Sanjeev Kumar | Professor | PhD |
| 8 | Dr. Vasdev Malhotra | Professor | PhD |
| 9 | Dr. Sandhya Dixit | Professor | PhD |
| 10 | Dr. Sanjeev Goyal | Professor | PhD |
| 11 | Dr. Bhaskar Nagar | Associate Prof. | PhD |
| 12 | Dr. Nikhil Dev | Associate Prof. | PhD |
| 13 | Dr. Rajeev Kumar Saha | Associate Prof. | PhD |
| 14 | Dr. Mukesh Gupta | Assistant Prof. | PhD |
| 15 | Dr. Rajesh Kumar Attri | Assistant Prof. | PhD |
| 16 | Dr. Krishan Verma | Assistant Prof. | PhD |
| 17 | Dr. Mahesh Chand | Assistant Prof. | PhD |
| 18 | Dr. Om Prakash Mishra | Assistant Prof. | PhD |
| 19 | Mr. Surender Singh | Assistant Prof. | M. Tech. |
| 20 | Dr. Bhupender Singh | Assistant Prof. | PhD |
| 21 | Dr. Shefali Trivedi | Assistant Prof. | PhD |
| 22 | Dr. Sanjay Kumar | Assistant Prof. | PhD |
| 23 | Dr. Nitin Panwar | Assistant Prof. | PhD |
| 24 | Dr. Nisha Bhatt | Assistant Prof. | PhD |

*ISBN 978-81-973526-0-7*

# AI-DRIVEN SUSTAINABLE SMART MANUFACTURING FRAMEWORK FOR INDUSTRY 5.0: INTEGRATION OF ROBOTICS, ENERGY SYSTEMS, AND DIGITAL ENGINEERING

Bhaskar Nagar*[1], Mayuri[1]
*[1]J.C. Bose University of Science & Technology, YMCA, Faridabad, Haryana, India
*bhasker_nagar@yahoo.com

## Abstract

*A shift to Industry 5.0 focuses on human-centered intelligent manufacturing that is more focused on sustainability. The technologies of artificial intelligence (AI), robotics, and digital engineering are combined with more and more campaigns to positively affect the productivity and reduce the environmental impact. This survey discusses the latest advancement of AI-based smarter manufacturing systems integrating robots and automation, data-driven decision-making systems, and energy-saving operational measures. The importance of machine learning algorithms, industrial robotics and digital engineering platforms in ensuring optimization in the production process, decreasing energy use and enhancing the use of resources are stressed. The paper summarizes the existing research trends and points out technological synergies that can allow manufacturing ecosystems to be environmentally responsible and manufacture energy-efficient, in line with the principles of Industry 5.0.*

## Keywords

Industry 5.0, Smart Manufacturing, Artificial Intelligence, Robotics, Sustainable Engineering.

## Introduction

The recent manufacturing companies are undergoing my paradigm shift as the introduction of the Industry 5.0 paradigm predicts the human-centered production, ecologically friendly environment, and autopilotized machines. In contrast to Industry 4.0 where its main focus was digitalisation and automation, Industry 5.0 incorporates the use of advanced computational tools with sustainable industrial operations to create resilient sustainable industrial manufacturing ecosystems. Recent empirical studies prove that Industry 5.0 models unite artificial intelligence (AI), collaborative robotics, and digital engineering platforms to increase productivity and reduce the environmental blow [20], [14].

The trend of sustainability has become a central force in the modern manufacturing industry due to the increasing energy consumption, the crisis of resources, and strict ecological policies. Data analytics based on AI and smart decision areas are now applied to enhance energy performance, material waste, and industrial processes [8], [17]. At the same time, the sophisticated robotic solutions enable lean and agile production, and contribute to increased safety of the operational process and resource consumption [18].

In addition, digital engineering technologies (i.e., smart sensors, cyber-physical systems and data-driven monitoring structures) enable real-time process optimisation and predictive decisions in the industrial environment [11], [5]. All these technological tools are a foundation of the creation of sustainable smart manufacturing systems which are consistent with the goals outlined by Industry 5.0.

The present manuscript is a review of recent advances in the AI-based sustainable intelligent manufacturing systems with particular focus on the intersection of robotics, digital engineering technologies and the energy-efficient manufacturing solutions.

## Literature Review

The strategic advancement of modern manufacturing systems has triggered the deployment of artificial intelligence and advanced robotic tools to encourage the smart management of production. The generated manufacturing platforms based on artificial intelligence can provide predictive analytics, adaptive control, and in-the-moment process optimisation with the actionable insights generated on the basis of a large volume of industrial data [12].

The use of machine-learning algorithms within industrial control systems has increasingly become a means of adding accuracy and fault-detection to operations in smart factories to achieve better efficiency [19].

### *AI and Robotics in Smart Manufacturing*

Another advancement that has been made in industrial robotics is through the introduction of collaborative or cobots which can work safely in the presence of human operators. These systems increase the flexibility of the manufacturing process along with maintaining high precision and repeatability in complex manufacture and machining operations [1]. The place of AI-powered robotic platforms in adaptive manufacturing settings is further supported by recent empirical studies whereby the intelligent algorithms allow altering the operating parameters of these systems to achieve optimal performance and minimize downtime [10]. Other than the benefit of productivity, the use of AI as a part of robotics will also offer potential resource efficiency through material waste reduction, operational error reduction, and general equipment efficiency. These technologic improvements are a significant platform of sustainable production systems that require more and more-smart energy control and more environmentally conscious production methods. The integration of smart manufacturing solutions with sustainable energy conditions is thus discussed in the subsequent part.

### *Sustainable Energy Integration in Smart Manufacturing*

Introduced as the key consideration of the modern manufacturing systems, sustainable energy integration is regarded as the means to provide industries with the opportunity to reduce carbon emissions, increase resource efficiency, and meet the increasingly strict environmental standards. A large portion of the energy used in the world industry is aimed at manufacturing, and this fact has increased the application of energy-efficient technologies and renewable energy sources in smart factories [21]. Complete monitoring, coupled with artificial intelligence, allows real-time analysis of energy, which ensures manufacturers are able to reduce the manufacturing schedule and reduce unnecessary energy usage [13].

According to recent research, novel sources of renewable energy, such as solar, wind, and hybrid power systems, play an ever-growing role in the support of the creation of infrastructures of sustainable manufacturing [2]. With the help of AI-based energy management systems, production demand and energy resources can actively be adjusted, which can reduce the operational sustainability and the effect on the environment [3]. Additionally, information technologies of digital monitoring and networks of the industrial Internet of Things give rise to incessant data streams that facilitate intelligent energy use and the efficiency of processes. Technological interlocked manufacturing environment is created through the adoption of AI-powered robotics, computer-like engineering environments, and environmentally friendly energy sources. This integration forms the basis in the realization of Industry 5.0 smart manufacturing structures, which are discussed in this following section.

## Conceptual Framework for Industry 5.0 Smart Manufacturing

Artificial intelligence, robotics, and sustainable energy technologies converting are the main pillar of Industry 5.0 smart manufacturing framework. This paper presents a concept map on AI-based sustainable manufacturing ecosystems to exemplify how these technological elements interact with each other.

Figure 1 depicts the conceptual design of an Industry 5.0 smart manufacturing system which comprises AI managed robotics, digital engineering platforms, and sustainable energy management technologies.


Figure 1. Theoretical model associated with AI-based smart manufacturing towards sustainable operations in Industry 5.0 settings.

The model consists of three connected layers. The initial layer is the data gathering and sensing infrastructure, during which the industrial sensors and industrial Internet of Things (IIoT) devices and cyber-physical systems obtain real-time data of operational processes and manufacturing equipment [9]. The second layer includes AI-controlled analytics and online engineering infrastructure; machine learning algorithms are used to process the data obtained to make predictive maintenance, adaptive planning production, and intelligent decision-making [7]. The third is focused on sustainable energy and resource optimization, renewable-energy convergence and energy-monitoring tools aid environmentally friendly production processes [4].
With a combination of these layers, manufacturing systems can reach greater operational efficiency, less use of energy, and greater flexibility in production. As a result, such a harmonized system provides the technological basis of creating sustainable Industry 5.0 manufacturing ecosystems.

## Comparative Analysis of Emerging Technologies in Smart Manufacturing

The successful deployment of the Industry 5.0 smart manufacturing systems depends on the efficient combination of the advanced digital technologies, such as artificial intelligence, industrial machine robots, and sustainable energy management systems. All these technologies bring specific advantages in the efficiency of manufacturing, and its operational flexibility coupled with environmental sustainability. Predictive analytics and data-driven optimisation can be achieved with the help of artificial intelligence, and this allows manufacturers to optimise production scheduling and eliminate operational in-efficiencies [16]. Industrial robotics improves precision in manufacturing, increases the level of automation, and increases production homogeneity, especially in complicated assembly and high-precision tasks [15].
Environmentally responsible manufacturing is also aided by the technologies of sustainable energy management, which allow making the use of energy efficient and employ a renewable energy source in the production locals [6]. These technologies combined will create a technologically connected environment of manufacturing that has the capacity to improve productivity and reduce environmental impact, at the same time.

Table 1. A comparison of the main technological elements in Industry 5.0 smart manufacturing systems.

| Technology | Key Function | Industrial Benefit |
|---|---|---|
| Artificial Intelligence | Data analytics and predictive decision support | Process optimization and fault prediction |
| Industrial Robotics | Data analytics and predictive decision support Automated production and precision manufacturing | Increased productivity and operational accuracy |
| Sustainable Energy Systems | Renewable energy integration and energy monitoring | Reduced energy consumption and environmental impact |

After the comparative evaluation procedure, Figure 2 displays the comparative effects of the technologies on such performance indicators of manufacturing as efficiency, sustainability, and the possibility to automate.

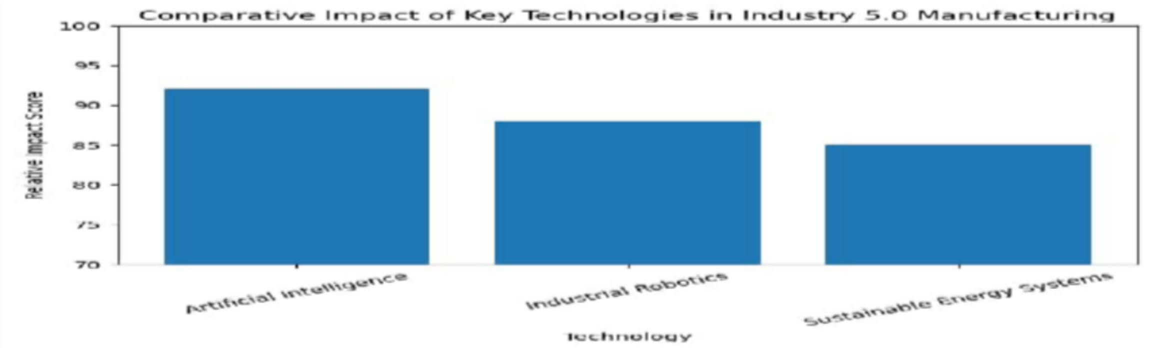


Figure 2. Technological impact comparative on manufacturing performance in Industry 5.0.

## Conclusion

This paper presented a concise review of the emerging technologies that are used to enable smart manufacturing in an Industry 5.0-oriented setting and sustainability. The paper analyses the role played by artificial intelligence, enhanced robotics, and introducing sustainable energy sources in enhancing efficiency in manufacturing workflows, flexibility, and sustainability. The interactions between digital engineering platforms, intelligent automation systems, and energy-efficient manufacturing practices are proposed along with a conceptual framework that provides systematic representation of the interactions between these three entities. The comparative analysis also highlights the supplementary roles of those technologies, highlighting how they all form the basis of establishing intelligent and environmentally friendly productive environments.

## Scope of Future Work

Further research in the field should focus on sophisticated, data-centric optimisation, more extensive integration of renewable energy groups, and also creation of adaptive and AI-oriented manufacturing platforms to further amplify sustainable Industry 5.0 systems.

## References

[1] A. A. Malik and A. Bilberg, “Digital twins of human-robot collaboration in production systems,” Procedia Manufacturing, vol. 38, pp. 108–115, 2019.

[2] C. Bai, P. Dallasega, and G. Orzes, “Renewable energy integration in sustainable manufacturing systems,” Renewable and Sustainable Energy Reviews, vol. 185, p. 113742, 2024.

[3] S. S. Kamble, A. Gunasekaran, and R. Sharma, “Analysis of the driving and dependence power of barriers to adopt Industry 4.0,” Computers in Industry, vol. 101,

pp. 107–119, 2018.
[4] B. Ding, H. Guo, and Y. Li, "Energy-efficient smart manufacturing enabled by digital technologies," Energy, vol. 286, p. 129514, 2024.
[5] M. Ghobakhloo, "Digital transformation and sustainable smart manufacturing: Implications for Industry 5.0," Technological Forecasting and Social Change, vol. 193, p. 122615, 2023.
[6] J. R. Duflou, J. W. Sutherland, D. Dornfeld, et al., "Towards energy and resource efficient manufacturing," CIRP Annals – Manufacturing Technology, vol. 61, no. 2, pp. 587–609, 2012.
[7] M. Javaid, A. Haleem, R. Singh, and R. Suman, "Artificial intelligence applications for sustainable manufacturing systems," Sustainable Operations and Computers, vol. 4, pp. 11–25, 2023.
[8] H. Jiang, Y. Ding, and J. Leng, "Artificial intelligence-driven smart manufacturing: Applications and challenges," Journal of Cleaner Production, vol. 330, p. 129856, 2022.
[9] S. Kamble, A. Gunasekaran, and S. Gawankar, "Sustainable Industry 4.0 framework for smart manufacturing systems," Journal of Cleaner Production, vol. 339, p. 130633, 2022.
[10] L. Wang, M. Törngren, and M. Onori, "Current status and advancement of cyber-physical systems in manufacturing," Journal of Manufacturing Systems, vol. 37, pp. 517–527, 2015.
[11] J. Lee, B. Bagheri, and H. Kao, "Cyber-physical systems architecture for Industry 4.0 manufacturing systems," Manufacturing Letters, vol. 3, pp. 18–23, 2020.
[12] J. Leng, H. Zhang, D. Yan, Q. Liu, and X. Chen, "Digital twin-driven smart manufacturing: A comprehensive review," Journal of Manufacturing Systems, vol. 60, pp. 635–652, 2022.
[13] H. Liu, Y. Chen, and F. Tao, "Intelligent energy management in smart manufacturing using industrial data analytics," Energy Reports, vol. 9, pp. 5568–5580, 2023.
[14] S. Nahavandi, "Industry 5.0—A human-centric solution," Sustainability, vol. 11, no. 16, p. 4371, 2019.
[15] V. Patel, R. Shah, and J. Lee, "Robotics integration in intelligent manufacturing systems," Robotics and Computer-Integrated Manufacturing, vol. 82, p. 102522, 2023.
[16] M. Rahman, S. Ahmed, and D. Kim, "Artificial intelligence in smart manufacturing systems: Applications and challenges," Advanced Engineering Informatics, vol. 51, p. 101511, 2022.
[17] F. Tao, M. Zhang, Y. Liu, and A. Nee, "Digital twins and artificial intelligence in smart manufacturing," CIRP Annals, vol. 72, no. 1, pp. 357–380, 2023.
[18] V. Villani, F. Pini, F. Leali, and C. Secchi, "Survey on human-robot collaboration in industrial settings," Mechatronics, vol. 55, pp. 248–266, 2018.
[19] T. Wuest, D. Weimer, C. Irgens, and K. Thoben, "Machine learning in manufacturing: Advantages, challenges, and applications," Production & Manufacturing Research, vol. 11, pp. 104–123, 2023.
[20] X. Xu, Y. Lu, B. Vogel-Heuser, and L. Wang, "Industry 4.0 and Industry 5.0—Inception, conception and perception," Journal of Manufacturing Systems, vol. 61, pp. 530–535, 2021.
[21] Y. Zhang, S. Wang, and X. Li, "Energy-efficient manufacturing systems for sustainable industrial production," Journal of Cleaner Production, vol. 350, p. 131403, 2022.

# A SYSTEMATIC REVIEW OF CHALLENGES IN ADVANCED DIGITALIZATION OF SMES OF INDIA

Ajay Kumar*[1], Prashant Chauhan[1], Nitin Kumar Chauhan[1]
*[1]JSS Academy of Technical Education, Noida, UP, India
*ajay.jss.me@gmail.com

## Abstract
*The implementation of advanced digitalization has been the basic requirement of SMEs because of the features it provides to the manufacturing system which helps to maintain the trust in the customers and in the different allies of the industry. It has the excellent ability to improve the efficiency by inducing new approaches of production and the productivity by reducing downtime with the help of real time data techniques. But this technology revolution also imposes several challenges along with the features which needs to be mitigated to an extent to achieve the expected result. These challenges can be related to the financial condition of the industry, the skill of the workforce of the industry, the intention of administration of industry towards change and the policies of the government of India.*

## Keywords
Advanced Digitalization, Industry 4.0, SMEs.

## Introduction
The implementation of advanced digitalization in SMEs is changing the methods of production by providing the real-time data which is increasing the customer satisfaction. It is easy to implement the advanced digitalization in large manufacturing units as compared to SMEs because they meet the requirements of resources such as physical and digital infrastructure, skilled manpower and the financial access. The technologies to be adopted by the SMEs in the course of advanced digitalization are Internet of things, cloud computing, additive manufacturing, robotics, cyber security tools, customer relationship management and machine to machine communication. These technologies help the SMEs to improve their quality of production and allows for customized production which add the qualitative value to the product and increases the variety in the product design [1] and empowers the manufacturer to stand steadily even in the completely dynamic market.
The revised definition of MSME by the government of India is in effect from April 1, 2025 [2]. This definition uses investment in plant and equipment and annual turnover as the parameter to differentiate between micro, small and medium enterprises. The lower limit is 2.5, 10 and 125 crore for micro, small and medium enterprises for investment in plant and equipment. The lower limit for annual turnover is 10, 100 and 500 crore for micro, small and medium enterprises. The impact of SMEs on GDP of India is quite considerable because from the annual report of ministry of MSME 2024 – 25 the contribution of MSME in GDP of India is 30% and contribution in exports is 45% [3]. Even with this large contribution of SMEs in GDP of India, there is lack of digitalization and a large segment of workforce is unskilled, this contribution will still take a jump if this unskilled workforce is skilled. The fourth largest economy of world is India as per the normal gross domestic product (GDP).
If the impact of advanced digitalization is considered in a global scenario, it signifies that the disparity between the digitalized nations with large economy and the nations without digitalization with small economy is increasing significantly. The large economies are far ahead in innovations as compared to the small economies because they can fulfill the requirements of the new technologies. The gap of technology and even the infrastructure

ISBN 978-81-973526-0-7

among different nations or among different segments of industries needs to be considered in order to reduce the disparity among the industries and to develop a collaborative network of industries so that they can utilize and share their resources.

## Literature Review

### *Emergence of Advanced Digitalization*

The development of "cyber-physical production system" [4] is the introduction of advanced digitalization also pronounced as 4th Industrial revolution or Industry 4.0. This phase of digitalization which initiated around 2010 and is continue till present followed the era of electronics and IT which is called Automation revolution [5]. The digitalization of production system achieved a significant societal impact [6] and a considerable change in work culture of the industries. Along with the era of advanced digitalization a new concept of industrial revolution is also emerging in a parallel way which is intending to develop a production system that works with Human-AI collaboration, termed as Industry 5.0 [7].

### *Concepts of Advanced Digitalization*

The advanced digitalization of manufacturing systems and even the service industries utilizes the techniques which work on real-time data and also a big data comparatively. The techniques [8] of advanced digitalisation and their benefits are Internet of Things (IoT) (Reduced downtime), Artificial Intelligence (AI) (Improved decision accuracy), Big data (Process optimization), Robotics (Increased throughput), Digital twins (Reduced development time), Cloud computing (Cost-effective data management), Machine to Machine Communication (M2M) (Data Collection and Assessment of Data), End-to-End Software Integration (Production lines and Logistics) and Additive Manufacturing (Mass production of standard products and Customized products) which are helpful in developing Cyber-Physical System (CPS) [9]. These tools of digitalization helps the production system to improve their efficiency and productivity and also to reduce the maintenance time [10].

### *Challenges in Advanced Digitalization of SMEs of India*

When an automated manufacturing system or a service industry intends to adopt advanced digitalization then it confronts the requirements related to the new technologies to be adopted. These requirements are relative and depend on the location, manpower, skill of the workers, physical and digital infrastructure, and intention of the administration and size of the economy of the corresponding industry. These requirements or challenges faced are classified in four categories as shown in figure 1 such as financial challenges, operational challenges, organizational challenges and external challenges and are discussed in further sections.

### *Financial challenges in Advanced Digitalization of SMEs of India*

These challenges are listed there in table 1 and they arise due to economic inability of the industries. This financial inability [11] may exist due to the inertia of administration, lack of trust in adopting the new technologies and the lack of expenditure for the required expenses. It may exist due to location of the industries as the policies of government vary from place to place in terms of disbursement of incentives and subsidies announced by the government. The mitigation for these challenges are awareness programs for the administration of industries, proper disbursement of the incentives and subsidies and phase-wise adoption of the digitalization techniques.

### *Operational challenges in Advanced Digitalization of SMEs of India*

The center of these challenges is skill of workers in operating [13], handling and analyzing the data of the system in operation. The inability of operating and storing the big data produces threat to data which is registered as cyber security concern [17] and hence the lack of trust is promoted in customer as well as in management of the industry. The wrong projections about the required parameters are generated due to inability to analyze the big data and affects the efficiency and productivity of the industry. This lack of digital skills and insufficient infrastructure increases the complexity in integration of the new to technologies with the existing one. The operational challenges faced by the manufacturing systems are listed in table 2.The mitigation of these challenges includes arranging continued skill training programs, involving the academic institutions by government policies to skill the unskilled workers and conducting the awareness programs towards the benefits of the skilled workers.

Table 1. Financial challenges in Advanced Digitalization of SMEs of India

| S. No. | Challenges | Explanation | References |
|---|---|---|---|
| 1 | Investment cost | The substantial investments in hardware, software, and IT infrastructure, tools of advanced technology, coupled with limited working capital. | [12], [13], [14], [15], [16], [17], [18], [11], [19] |
| 2 | Investment in advanced technologies | The cost related to advanced technologies such as IoT, robotics, AI, and automation. | [15], [14], [17] |
| 3 | Cost of scaling | The additional investment in infrastructure, software, and skilled manpower to increase output. | [17], [20], [21] |
| 4 | Maintenance and operation cost | Expenditure on maintenance, software updates, and skilled manpower. | [17], [18], [22] |

Table 2. Operational challenges in Advanced Digitalization of SMEs of India

| S. No. | Challenges | Explanation | References |
|---|---|---|---|
| 1 | Complexity in technology integration | The difficulty in integrating technologies, compatibility issues, managing data, and coordinating digitally connected operations. | [12], [13], [15], [19] |
| 2 | Lack of digital skills | Advanced technologies such as IoT, automation, and data analytics require skilled manpower. | [12], [13], [14], [15], [16], [17], [22], [11], [19] |
| 3 | Cyber security concern | The lack of trust in privacy and data security, unanswered concerns around data privacy and security concerns using external data. | [1], [12], [13], [17], [20], [22], [11], [19] |
| 4 | Data analytics skills | Skilled analytics are required to analyse large volumes of data collected through IoT devices, sensors, and automated systems. | [20] |

## *Organizational challenges in Advanced Digitalization of SMEs of India*

The organizational challenges circumscribe the issues being produced due to lack of awareness of the administration [19] and employees about the new technologies and considering them as threat to the existing jobs and simultaneously the lack of trust [23] in return from the new technologies. This environment of industry produces many of the challenges as listed there in table 3 and makes the digitalization challenging. The government must conduct awareness programs for administration of industries and employees so that they can contribute efficiently in enhancement of the culture of industry contribute to the nation's economy.

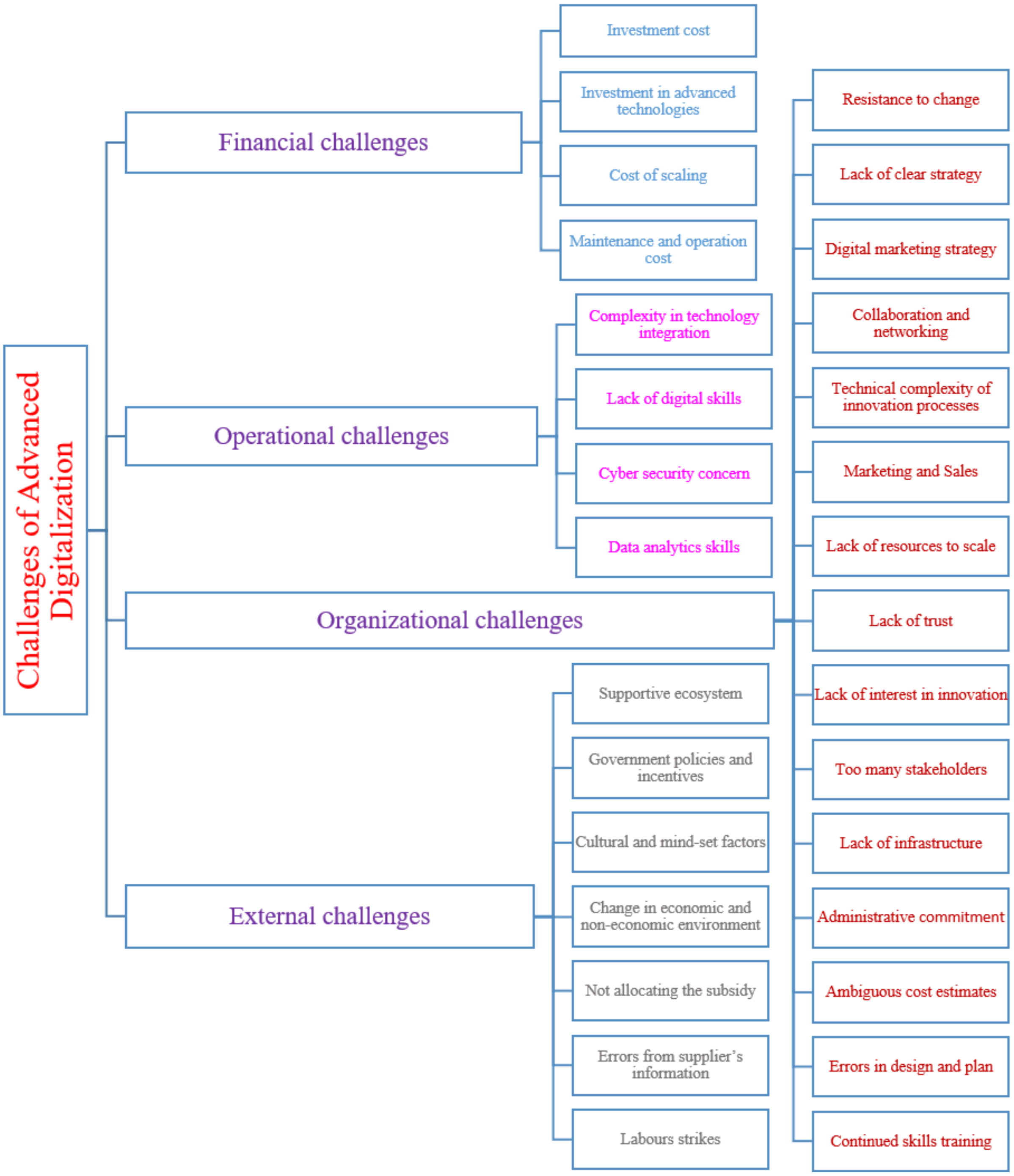


Figure 1. Classification of challenges in Advanced Digitalization of SMEs of India.

Table 3. Organizational challenges in Advanced Digitalization of SMEs of India

| S. No. | Challenges | Explanation | References |
|---|---|---|---|
| 1 | Resistance to change | Employees and managers perceive automation, digitalization, and advanced technologies as threats to existing jobs. | [12], [13], [14], [17], [11], [19] |
| 2 | Lack of clear strategy | Lack of well-defined objectives, roadmaps, or alignment with business goals. | [13] |

| | | | |
|---|---|---|---|
| 3 | Digital marketing strategy | Lack of strategic planning, skilled personnel, and integration with operations. | [24] |
| 4 | Collaboration and networking | Lack of technology providers, research institutions, and industry associations for implementation guidance. | [15], [14] |
| 5 | Technical complexity of innovation processes | Lack of implementing advanced technologies such as IoT, AI, robotics, and analytics requires integration with legacy systems, redesign of workflows, and specialized technical expertise. | [15] |
| 6 | Marketing and Sales | It includes limited digital capabilities, poor integration of operational data, and resource. | [16], [25] |
| 7 | Lack of resources to scale | It includes infrastructure constraints, workforce skill gaps, and management bandwidth. | [16], [20] |
| 8 | Lack of trust | It is the lack of trust of managers that perceive advanced digital technologies as risky due to uncertainty regarding performance, cyber security, and return on investment. | [20], [23], [26], [27] |
| 9 | Lack of interest in innovation | SMEs prioritize short-term operational stability over long-term innovation, leading to reliance on traditional practices and limited experimentation with advanced digital technologies. | [20] |
| 10 | Too many stakeholders | Managing too many stakeholders **(**owners, managers, employees, technology vendors, consultants, financial institutions, government agencies, and customers**)** with diverse interests, expectations, and levels of influence. | [20] |
| 11 | Lack of infrastructure | Lack of robust physical, digital, and organizational infrastructure, including reliable connectivity, modern machinery, data storage systems, and IT support. | [16], [1] |
| 12 | Administrative commitment | It includes the bureaucratic complexity, regulatory burdens, and inefficient internal administrative systems. | [16], [28], [29], [19] |
| 13 | Ambiguous cost estimates | The wrong estimation of hidden implementation costs, and uncertainty regarding long-term financial implications. | [22] |
| 14 | Errors in design and plan | The inadequate system architecture and roadmap, poor alignment between digital technologies and operational processes, and lack of user-centric design. | [12], [22], [30], |

| | | | |
|---|---|---|---|
| 15 | Continued skills training | The rapid evolution of digital technologies demands, ongoing up skilling in areas such as automation, data analytics, and IoT. | [1], [17], [19] |

### *External challenges in Advanced Digitalization in SMEs of India*

The challenges which influence the digitalization of SMEs but cannot be controlled by the internal management of the SMEs are considered as external challenges such as policies of the government [20], subsidy and incentive disbursement by the government lack of availability of research institutions, information from the supplier [22], labor strikes etc. as listed in table 4. The government should take care of these challenges by changing the policies in favor of SMEs and releasing the funds as required and also by providing a supportive ecosystem to the SMEs.

Table 4. External challenges in Advanced Digitalization of SMEs of India

| S. No. | Challenges | Explanation | References |
|---|---|---|---|
| 1 | Supportive ecosystem | It includes policy frameworks, financial institutions, technology providers, research institutions, skill development agencies, and industry networks. | [15] |
| 2 | Government policies and incentives (GPI) | It includes limited awareness, complex application procedures, policy uncertainty, frequent regulatory changes, delayed fund disbursement, and misalignment with SME-specific needs. | [15], [20], [19] |
| 3 | Cultural and mind-set factors | A preference for traditional practices, risk-averse attitudes, limited digital orientation, and hierarchical management structures. | [15] |
| 4 | Change in economic and non-economic environment | It includes economic volatility, supply-chain disruptions, regulatory shifts, social dynamics, and technological uncertainty. | [16] |
| 5 | Not allocating the subsidy | It includes limited budgetary support, administrative delays, uneven distribution, and lack of transparency. | [22] |
| 6 | Errors from supplier's information | It includes errors, inconsistencies, or incomplete information provided by suppliers. | [22] |
| 7 | Labours strikes | The disputes arising from fear of job loss, wage concerns, or poor working conditions. | [22] |

### *Impact of Advanced Digitalization on SMEs of India*

The advanced digitalization is capable to enhance the efficiency and productivity of the industry in excellent manner by ensuring the real time production which will reduce the storage cost and by ensuring the production of customized products as per the customer requirements which will improve the customer satisfaction. The techniques of advanced digitalization can reduce the downtime as it can help to schedule the maintenance of the manufacturing system by the use of condition monitoring. It will also generate a flexible work culture in industries because of skilled manpower.

## Conclusion

To address the expectations of the customers and to stand tall in the competitive market the SMEs must renovate themselves with the techniques of advanced digitalization but while doing so they face different types of challenges as discussed in earlier sections. The different type of manufacturing systems require different techniques of digitalization and hence the priority of techniques changes from industry to industry and hence the priority of challenges also changes. The challenges are categorized as financial, operational, organizational and external but it does not mean that these are independent of each other. Producing skilled workforce and scheduling continued skill training require a continuous flow of financial resources, digital and physical infrastructure, administrative commitment, arranging awareness programs and involvement of institutions in skilling the workforce. All of these requirements belong to different categories of challenges but are so dependent on each other that all of them should be focused simultaneously. The cyber security threat is a great concern because it produces lack of trust in the minds of industry of administration and the consumer both. The government needs to conduct awareness programs at different levels to target the trust deficit towards technologies of advanced digitalization. It will need to develop some model to fix the priority of challenges to address them for a certain manufacturing system.

## References

[1] V. Jain and P. Ajmera, "Modelling the enablers of industry 4.0 in the Indian manufacturing industry," Int. J. Product. Perform. Manag., vol. 70, no. 6, pp. 1233–1262, 2020, doi: 10.1108/IJPPM-07-2019-0317.

[2] M. Srikanth, G. K. Chetan, and S. Paul, "Market Reactions to the Revised MSME Classification in India : An Event Study," pp. 1–16.

[3] Ministry of MSME, "Annual Report 2024-25," 2025.

[4] A. Sharma and B. J. Singh, "Evolution of Industrial Revolutions : A Review," no. 11, pp. 66–73, 2020, doi: 10.35940/ijitee.I7144.0991120.

[5] P. P. Overview, P. P. Groumpos, and P. Peter, "A Critical Historical and Scientific Overview of all Industrial Revolutions," IFAC Pap., vol. 54, no. 13, pp. 464–471, 2021, doi: 10.1016/j.ifacol.2021.10.492.

[6] Prof. (Dr.) Anumita Agarwal, DIGITIZATION AND HUMAN DEVELOPMENT.

[7] M. C. Zizic, M. Mladineo, N. Gjeldum, and L. Celent, "From Industry 4.0 towards Industry 5.0: A Review and Analysisnof Paradigm Shift for the People, Organization and Technology," 2022.

[8] B. Parashar, R. Sharma, G. Rana, and R. D. Balaji, "Foundation Concepts for Industry 4.0 BT - New Horizons for Industry 4.0 in Modern Business," A. Nayyar, M. Naved, and R. Rameshwar, Eds., Cham: Springer International Publishing, 2023, pp. 51–68. doi: 10.1007/978-3-031-20443-2_3.

[9] P. P. Senna, L. Miguel, D. F. Ferreira, A. C. Barros, J. Bonnín, and V. Magalh, "Computers & Industrial Engineering Prioritizing barriers for the adoption of Industry 4 . 0 technologies," vol. 171, no. June, 2022.

[10] O. Fuglsang, "Advancing maintenance strategies through digitalization : A case study," Procedia Comput. Sci., vol. 217, no. 2022, pp. 1522–1531, 2023, doi: 10.1016/j.procs.2022.12.352.

[11] P. Kumara, J. Bhamub, and K. Singh, "Analysis of Barriers to Industry 4 . 0 adoption in Manufacturing Organizations : an ISM Approach," vol. 98, no. March, pp. 85–90,

2023, doi: 10.1016/j.procir.2021.01.010.
[12] D. Horváth and R. Z. Szabó, "Driving forces and barriers of Industry 4.0: Do multinational and small and medium-sized companies have equal opportunities?," Technol. Forecast. Soc. Change, vol. 146, no. May, pp. 119–132, 2019, doi: 10.1016/j.techfore.2019.05.021.
[13] V. Pandey, A. Kumar, and S. Gupta, "Assessing the need for the adoption of digitalization in Indian small and medium enterprises," Open Eng., vol. 14, no. 1, pp. 1–18, 2024, doi: 10.1515/eng-2024-0072.
[14] H. Indrawati, "Barriers to technological innovations of SMEs : how to solve them ?," 2020, doi: 10.1108/IJIS-04-2020-0049.
[15] Toluwalase Vanessa Iyelolu, Edith Ebele Agu, Courage Idemudia, and Tochukwu Ignatius Ijomah, "Driving SME innovation with AI solutions: overcoming adoption barriers and future growth opportunities," Int. J. Sci. Technol. Res. Arch., vol. 7, no. 1, pp. 036–054, 2024, doi: 10.53771/ijstra.2024.7.1.0055.
[16] R. Viswanathan and A. Telukdarie, "A systems dynamics approach to SME digitalization," Procedia Comput. Sci., vol. 180, no. 2019, pp. 816–824, 2021, doi: 10.1016/j.procs.2021.01.331.
[17] A. Telukdarie, T. Dube, P. Matjuta, and S. Philbin, "The opportunities and challenges of digitalization for SME ' s," Procedia Comput. Sci., vol. 217, no. 2022, pp. 689–698, 2023, doi: 10.1016/j.procs.2022.12.265.
[18] N. K. Chauhan, V. Kumar, and S. Dixit, "A Study of Key Challenges in Implementation of Digital Supply Chain in the Context of Indian SMEs", doi: 10.1007/978-981-99-1328-2.
[19] [19] D. Nimawat and B. D. Gidwani, "Identification of cause and effect relationships among barriers of Industry 4.0 using decision-making trial and evaluation laboratory method," Benchmarking An Int. J., vol. 28, no. 8, pp. 2407–2431, Feb. 2021, doi: 10.1108/BIJ-08-2020-0429.
[20] K. P. Bholane, "Adoption, Status and Environmental Sustainability of Industry 4.0 in India," vol. 8, no. 1, pp. 865–870, 2023.
[21] R. Accorsi, M. Bortolini, F. G. Galizia, F. Gualano, and M. Oliani, "Scalability Analysis in Industry 4.0 Manufacturing BT - Sustainable Design and Manufacturing 2020," in Proceedings of the 7th International Conference on Sustainable Design and Manufacturing (KES-SDM 2020), S. G. Scholz, R. J. Howlett, and R. Setchi, Eds., Singapore: Springer Singapore, 2020, pp. 161–171.
[22] M. Hirman and A. Benesova, "Project Management during the Industry 4.0 Implementation with Risk Factor Analysis," Procedia Manuf., vol. 38, no. Faim 2019, pp. 1181–1188, 2020, doi: 10.1016/j.promfg.2020.01.208.
[23] M. F. Mubarak and M. Petraite, "Industry 4.0 technologies, digital trust and technological orientation: What matters in open innovation?," Technol. Forecast. Soc. Change, vol. 161, p. 120332, 2020, doi: https://doi.org/10.1016/j.techfore.2020.120332.
[24] T. Gogia and D. Sitchinava, "The Role of Digital Marketing in Small Business," Shota Meskhia State Teach. Univ. Zugdidi, vol. 45, no. 3, pp. 443–449, 2023, doi: 10.52340/zssu.2022.14.09.
[25] G. T. Ahamed and S. A. A. Raju, "A REVIEW OF CHALLENGES AND OPPORTUNITIES FOR MSMEs IN INDIA: A ROADMAP FOR SUCCESS," Int. J. Adv. Res. Commer., vol. 06, no. 01, pp. 89–98, 2023.
[26] A. Brattström, H. Löfsten, and A. Richtnér, "Creativity, trust and systematic processes in product development," Res. Policy, vol. 41, no. 4, pp. 743–755, 2012,

*ISBN 978-81-973526-0-7*

doi: https://doi.org/10.1016/j.respol.2011.12.003.

[27] J. Lee, M. Azamfar, and J. Singh, “A blockchain enabled Cyber-Physical System architecture for Industry 4.0 manufacturing systems,” Manuf. Lett., vol. 20, pp. 34–39, 2019, doi: https://doi.org/10.1016/j.mfglet.2019.05.003.

[28] D. D. Nirmal, M. Kumari, and K. Gumte, “Analyzing top management commitment, Industry 4.0 technologies and sustainable manufacturing practices through institutional theory and practice-based view,” Benchmarking An Int. J., vol. 32, no. 9, pp. 3492–3523, Sep. 2025, doi: 10.1108/BIJ-12-2024-1120.

[29] M. Curtis, “Supporting small businesses in developing countries: Which programmes work and why?,” Brief. Pap. Funded by Christ. Aid., 2016.

[30] J. M. Müller, M. Julian, M. Julian, and M. Julian, “Assessing the barriers to Industry 4.0 implementation from a workers’ perspective,” IFAC Pap., vol. 52, no. 13, pp. 2189–2194, 2019, doi: 10.1016/j.ifacol.2019.11.530.

# NLP FOR LOW-RESOURCE LANGUAGES IN INDUSTRY 4.0: KNOWLEDGE EXTRACTION FROM MULTILINGUAL MANUFACTURING TEXTS

Chandra KantaYadav*[1], Bharti Nathani[1]
Banasthali Vidyapith, Rajasthan, India
*chanduyadav443@gmail.com

## Abstract

*Industry 4.0 is a field where machine maintenance, operator reports, and document troubleshooting are all done. Most NLP systems are developed for resource-rich languages like English. This hinders the multilingual industry sector, where resource-poor languages like Sindhi and Hindi are widely used. In order to extract knowledge from multilingual manufacturing text produced in low-resource languages, this study suggests an NLP-based approach. To extract functional information from engineering documents, the suggested system combines preprocessing, multilingual word embedding, and word-sense disambiguation techniques using the Lesk algorithm and Naive Bayes classification. The MongoDB database is used to produce a multilingual corpus of maintenance records and manufacturing instructions. Precision, recall, and F1-score metrics are used in an experimental evaluation of a production query interpretation task. The findings demonstrate that the accuracy of information extraction is much increased when multilingual embeddings and disambiguation approaches are used together. The suggested paradigm highlights the significance of creating NLP resources for resource-constrained languages in Industry 4.0 and Industry 5.0 systems and helps with intelligent decision support in smart factories.*

## Keywords

Industry 4.0/5.0, Artificial Intelligence, Natural Language Processing, Low resource language

## Introduction

Intelligent manufacturing environments are made possible by Industry 4.0, which includes cyber systems, the Internet of Things (IoT), big data analytics, and artificial intelligence. In this era, a vast amount of text is generated through the use of digital technology [1]. This data may include equipment manuals, maintenance records, production logs, operator notes, troubleshooting documents, and other items. In this work, the provided useful operational information can assist manufacturing systems in making better decisions. Manufacturing manuals contain important information regarding machine performance, operating procedures, and fault diagnosis. The information derived from research papers can be helpful in detecting faults, improving production, and facilitating predictive maintenance. In a smart manufacturing environment, the automated analysis of text data helps engineers and operators make better decisions and perform real-time monitoring [2]. With the aid of Natural Language Processing techniques, unstructured industrial text can be transformed into structured knowledge representations. Integrating textual insights into digital production systems can help businesses increase productivity and reduce operational downtime.

However, high-resource languages like English are the primary focus of the majority of NLP tools. Workers frequently record procedures in mixed multilingual text or in regional languages like Hindi and Sindhi in many emerging industrial settings [3]. Automated knowledge extraction is limited by these languages' lack of computational resources. For Industry 4.0 systems to be inclusive and multilingual, low-resource language processing is crucial.

This paper suggests an NLP framework that uses word embedding and word sense disambiguation to process multilingual manufacturing language and extract operational knowledge. Low-resource language integration in smart manufacturing settings is supported by this system.
The structure of this article is as follows: the next section introduces resource-poor languages, the development of multilingual methods, and the process of extracting knowledge from literature. The Methodology section focuses on corpus construction, Natural Language Processing (NLP) pipelines, word embedding models, and WSD approaches. The experimental section presents the results and evaluation metrics; the findings are discussed in the Discussion section, followed by a section on the summary and future outlook.

## Related Work

In the field of Natural Language Processing, A brief overview is presented regarding the limitation of low-resource languages; multilingual construction processes andthe process of extracting knowledge from engineering literature. Table 1 illustrates the limitations inherent in NLP manufacturing tasks.

Table 1: Existing NLP work in manufacturing

| Method | Application | Limitations | References |
|---|---|---|---|
| Lightweight BERT | Defect severity detection | Domain specific dataset | [4] |
| Word2Vec/ FastText | Knowledge extraction from technical documents | Small industrial datasets | [5] |
| Data-driven methods, deep learning, | Predictive maintenance | large labeled datasets required | [6] |
| TF-IDF +SVM | Fault classification from machine reports | No multilingual support | [7] |
| FastText | Handles morphology in low resource languages | Limited domain adaption | [8] |

### *Low-resource language limitation*

The majority of current research in industrial Natural Language Processing focuses on ‘high-resource’ languages such as English, German, or Chinese primarily due to the availability of extensive annotated datasets and pre-trained language models for these languages. Nevertheless, various industrial settings operate in multilingual settings, where employees record maintenance-related activities and procedures in local languages such as Hindi, Sindhi, or other regional languages. However, these languages are considered ‘low-resource’ languages, as they lack sufficient corpora, lexical databases, and pre-trained NLP models. Consequently, existing industrial NLP systems are not easily transferable to these languages. Tackling this issue necessitates the creation of multilingual corpora, lexical resources, and language models explicitly tailored for low-resource industrial texts.

### *The challenge of multilingual manufacturing*

Global supply networks, multinational labor cooperation, and dispersed production facilities are common components of contemporary industrial ecosystems. As a result, different languages or mixed-language content may be found in technical manuals, maintenance logs, and operational reports. Many NLP-based industrial research, however, make the assumption that the textual data is monolingual. Multilingual knowledge representation, translation models, and cross-lingual embeddings are some of the methods needed to handle multilingual data [9]. NLP frameworks that can process several languages at once in industrial systems have not received much attention. Models that can extract knowledge from multilingual industrial datasets are therefore required.

### *The hurdle of knowledge acquisition*

Highly technical language pertaining to machinery, production processes, problem diagnostics, and operational procedures can be found in engineering and manufacturing papers. It is difficult to extract organized knowledge from such technical papers because of contextual ambiguity and domain-specific language. The majority of current research concentrates on problems like maintenance prediction or document categorization, whereas fine-grained information extraction from engineering texts is still mostly unexplored. In order to enable intelligent decision-making in smart manufacturing systems, unstructured engineering papers can be transformed into structured knowledge using techniques like word sense disambiguation, semantic embeddings, and information extraction.

## Methodology

The relevant section describes algorithm for the construction of a multilingual corpus, the natural language processing pipelines, and word sense disambiguation and semantic representation in text generation.

### *Corpus Construction*

The corpus is domain-specific, created from industry sources and engineering text, and is used to analyze multilingual manufacturing documents. The dataset contains essential operational information such as machine performance and maintenance tasks, such as equipment manuals, maintenance reports, operator notes, and troubleshooting logs. Within the context of Industry 4.0, these documents represent general text data generated in industrial environments. English, Hindi, and Sindhi are some of the languages frequently used in industrial documents, and which have been included in this corpus. This approach could be helpful in addressing the challenges associated with resource-poor language processing. MongoDB a NoSQL database that facilitates the flexible storage and efficient retrieval of multilingual text documents-is used to store and manage all text data. Since MongoDB facilitates scalable data management and schema-less storage, it is particularly well-suited for large-scale text datasets [10].

### *NLP Processing Pipeline*

A natural language processing pipeline has been developed to extract valuable details from manufacturing records. To assist in making intelligent decisions within a smart manufacturing system, this pipeline is used to convert unstructured technical language into structured information.

### *Word Embedding Model*

We have attempted to train bilingual word embedding using FastText to understand semantic relationships between words in industrial articles. Word embeddings leverage the context-based usage of words to represent them as numerical vectors, thereby making it easier to encode semantic similarity. The reason of choosing FastText is that it utilizes sub-word information, enabling it to handle rare words and morphological variations—characteristics often found in low-resource languages. Therefore, it is particularly suitable for languages such as Hindi and Sindhi, where the complexity of morphology can affect the efficiency of text processing.

### *Word Sense Disambiguation*

Word Sense Disambiguation (WSD) - the objective of which is to determine the correct meaning of a word based on its surrounding context – is an extremely important task in Natural Language Processing [11]. Many technical terms used in articles related to manufacturing may have more than one meaning. The Lesk algorithm is primarily used for Word Sense Disambiguation as an unsupervised approach, whereas the Naive Bayes classifier is a method employed within a supervised approach.

*ISBN 978-81-973526-0-7*

In order to ascertain a word's meaning, the Lesk algorithm compares the dictionary definition of each potential meaning with the word's context [12]. The interpretation that best matches the meaning is selected as the right one. Based on Bayes' theorem, Naive Bayes is a probabilistic classification technique. Based on the contextual elements around the word, it calculates the likelihood that a word belongs to a specific sense [13].

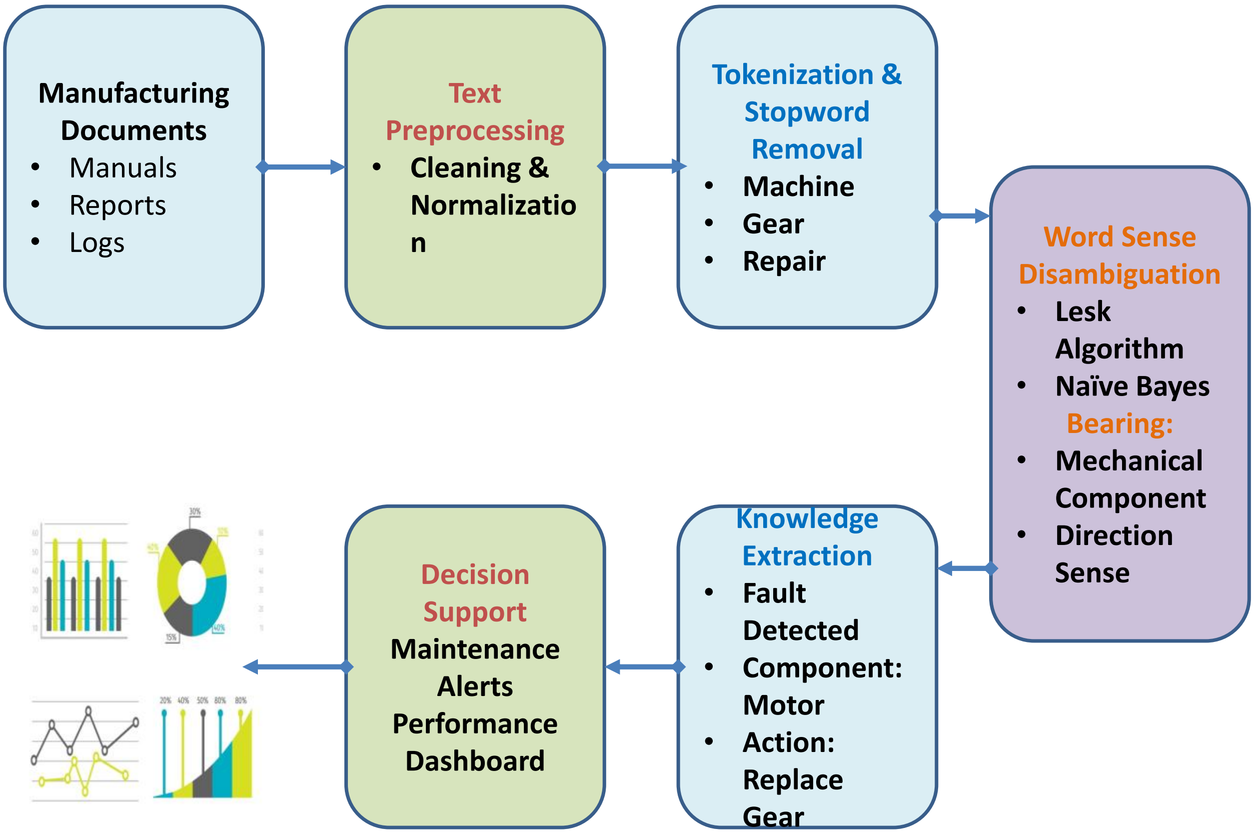


Figure1. Architecture for Knowledge Extraction

## Experiments and Results

This section presents the experimental setup, evaluation metrics, and performance results of the proposed multilingual NLP framework for extracting information from manufacturing text.

### *Experimental Setup*

To assess the effectiveness of the proposed approach, experiments were conducted on the multilingual manufacturing corpus described in methodology section. The main focus of the evaluation was on manufacturing query interpretation tasks, in which the system must accurately determine the intended meaning of ambiguous technical terms within industrial contexts [14].

Manufacturing queries frequently include domain-specific phrases that have context-dependent meanings. For instance, the term "bearing" might refer to a direction or orientation in everyday speech or a mechanical part used in rotating machinery. When examining machine data or maintenance logs in a production setting, the system must accurately interpret "bearing" as a mechanical component. In this case, "The temperature of the machine's bearing is rising rapidly." In this instance, the system must read "bearing" as a mechanical element connected to the machine's functioning and the context as a possible malfunction condition coupled with the unusual temperature increase. A number of approaches to text representation and semantic annotation were assessed, including embedding-based models in conjunction with conventional feature-based methods and semantic annotation strategies.

### *Evaluation Matrix*

Precision, Recall, and F1-score—standard information retrieval measures often used to assess NLP classification and knowledge extraction systems—have been utilized to evaluate the performance of the proposed models. The percentage of correctly identified relevant instances out of all those instances predicted to be relevant is termed Precision.

$$Precision = \frac{TP}{TP + FP} \quad (1)$$

Recall measures the proportion of relevant examples that were correctly identified by the system.

$$Recall = \frac{TP}{TP + FN} \quad (2)$$

The F1-score is used to provide a balanced evaluation of a system's performance, and it represents the harmonic mean of precision and recall.

$$F1 - Score = \frac{2 \times Precision \times Recall}{Precision + Recall} \quad (3)$$

In this context, TP, FP, and FN stand for True Positive, False Positive, and False Negative, respectively. The system's ability to extract useful information from multilingual manufacturing texts may be thoroughly assessed with the use of these criteria.

### *Experimental Results*

The experimental results comparing different text representation and disambiguation approaches are presented in Table 1.

Table 2: Performance comparison of different NLP methods

| **Method** | **Precision** | **Recall** | **F1-Score** |
|---|---|---|---|
| TF-IDF | 0.70 | 0.68 | 0.69 |
| Word2Vec | 0.77 | 0.73 | 0.75 |
| FastText | 0.81 | 0.78 | 0.79 |
| FastText + Lesk | 0.85 | 0.82 | 0.83 |
| FastText + Naïve Bayes | 0.88 | 0.85 | 0.86 |

The evaluation results are presented in Table 2. When utilizing the TF-IDF method, the F1-score was 0.69, while the Word2Vec method yielded a score of 0.75. An F1-score of 0.79 was achieved using the FastText method; theFastText + Lesk method attained a score of 0.83; and the FastText + Naïve Bayes method reached 0.86.

Based on the F1-score results, it is concluded that FastText + Naïve Bayes performs overall better compared to other methods, such as FastText + Lesk, FastText, Word2Vec and TF-IDF. This leads to the conclusion that combining semantic embeddings with probabilistic ambiguity-resolution methods significantly improves the system's ability to correctly interpret ambiguous technical terms present in manufacturing-related articles.

## Discussion

Our study utilized embedding-based models, which perform better than traditional text representation techniques in multilingual industrial NLP tasks. FastText is particularly successful at handling diverse vocabulary forms and modeling sub-word information in low-resource languages. Similarly, incorporating embeddings with 'Word Sense Disambiguation' techniques enhances the contextual understanding of concepts related to a specific domain. The

ambiguity-resolution model based on Naïve Bayes performed better than other models, proving that the ambiguity inherent in industrial language can be successfully quantified through probabilistic contextual modeling.
Thus, this proposed framework appears highly promising for extracting information from multilingual production documents and facilitates intelligent decision-making processes within the Industry 4.0 environment.

## Conclusion

In this research paper, we present multilingual manufacturing texts and an NLP framework for extracting knowledge for resource-poor languages. The proposed work combines bilingual embedding and Word Sense Disambiguation techniques to process engineering documents written in Hindi, Sindhi, and English. Experimental evaluation exhibit that combining embedding-based models with a Naive Bayes classifier achieves significantly improvements compared to baseline approaches. The framework assists in making intelligent decision within smart factories and highlights the importance of developing computational resources for low-resource languages in the Industry 4.0 environment. Future research will focus on real-time knowledge extraction in Industry 5.0 systems, large-scale multilingual industrial corpora, and deep learning approaches.

## References

[1] M. C. May, J. Neidhöfer, T. Körner, L. Schäfer, and G. Lanza, “Applying Natural Language Processing in Manufacturing,” *Procedia CIRP*, vol. 115, pp. 184–189, Jan. 2022, doi: 10.1016/j.procir.2022.10.071.

[2] K. Zhong, T. Jackson, A. West, and G. Cosma, “Natural Language Processing Approaches in Industrial Maintenance: A Systematic Literature Review,” *Procedia Computer Science*, vol. 232, pp. 2082–2097, 2024, doi: 10.1016/j.procs.2024.02.029.

[3] S. Sarwat, H. Kabir, N. Qayyum, and M. Akram, “Language Shift and Maintenance: A Case Study of Pakistani-American Family,” *IJEL*, vol. 11, no. 1, p. 86, Nov. 2020, doi: 10.5539/ijel.v11n1p86.

[4] J. Chen, S. Sheng, J. Lin, C. Xu, and Y. Peng, “A Lightweight BERT-Based Framework for Automated Severity Classification of Power Equipment Defects,” in *2025 3rd International Conference on Data Science and Network Security (ICDSNS)*, Jul. 2025, pp. 1–6. doi: 10.1109/ICDSNS65743.2025.11168711.

[5] T. Mikolov, K. Chen, G. Corrado, and J. Dean, “Efficient Estimation of Word Representations in Vector Space,” Sep. 07, 2013, *arXiv*: arXiv:1301.3781. doi: 10.48550/arXiv.1301.3781.

[6] P. Jieyang *et al.*, “A systematic review of data-driven approaches to fault diagnosis and early warning,” *J Intell Manuf*, vol. 34, no. 8, pp. 3277–3304, Dec. 2023, doi: 10.1007/s10845-022-02020-0.

[7] X. Wang and S. Yang, “A Tutorial and Survey on Fault Knowledge Graph,” in *Cyberspace Data and Intelligence, and Cyber-Living, Syndrome, and Health*, H. Ning, Ed., Singapore: Springer, 2019, pp. 256–271. doi: 10.1007/978-981-15-1925-3_19.

[8] P. Bojanowski, E. Grave, A. Joulin, and T. Mikolov, “Enriching Word Vectors with Subword Information,” *TACL*, vol. 5, pp. 135–146, Dec. 2017, doi: 10.1162/tacl_a_00051.

[9] G. Buchgeher, D. Gabauer, J. Martinez-Gil, and L. Ehrlinger, “Knowledge Graphs in Manufacturing and Production: A Systematic Literature Review,” *IEEE Access*, vol. 9, pp. 55537–55554, 2021, doi: 10.1109/ACCESS.2021.3070395.

[10] C. A. Győrödi, D. V. Dumşe-Burescu, D. R. Zmaranda, and R. Ş. Győrödi, “A Comparative Study of MongoDB and Document-Based MySQL for Big Data

*ISBN 978-81-973526-0-7*

Application Data Management," *Big Data and Cognitive Computing*, vol. 6, no. 2, May 2022, doi: 10.3390/bdcc6020049.

[11] R. Navigli, "Word sense disambiguation: A survey," *ACM Comput. Surv.*, vol. 41, no. 2, p. 10:1-10:69, Feb. 2009, doi: 10.1145/1459352.1459355.

[12] M. Lesk, "Automatic sense disambiguation using machine readable dictionaries: how to tell a pine cone from an ice cream cone," in *Proceedings of the 5th annual international conference on Systems documentation*, in SIGDOC '86. New York, NY, USA: Association for Computing Machinery, Jun. 1986, pp. 24–26. doi: 10.1145/318723.318728.

[13] K. Gull, S. Padhye, and D. S. Jain, "A Comparative Analysis of Lexical/NLP Method with WEKA's Bayes Classifier," vol. 5, no. 2.

[14] D. Chen, X. Jiang, Y. Guo, and B. Xu, "A Transfer Learning Method for Remaining Useful Life Prediction Based on LSTM-KAN-DANN," in *Proceedings of the UNIfied Conference of DAMAS, IncoME and TEPEN Conferences (UNIfied 2025)*, K. Wei, W. Yang, J. Dai, and B. Chen, Eds., Cham: Springer Nature Switzerland, 2026, pp. 1123–1135. doi: 10.1007/978-3-032-00968-5_91.

# EN-41B STEEL NANO POWDER MIXED EDM (NPMEDM) USING GENETIC ALGORITHM

Divya Chandra*[1], Priyanka Singh[1], Nitin Kumar Chauhan[1], Yash Pandey[1], N.R. Chauhan[2]
*[1]JSS University, Noida, India
[2]Indira Gandhi Delhi Technical University for Women, New Delhi
divya.chand@gmail.com

## Abstract
*EN-41B nitriding steel is widely used in components such as gears, connecting rods, extruders, and plastic mould tools due to its high wear resistance, strength, and ductility. However, its high hardness and work-hardening tendency makes it difficult to machine using conventional processes. This study investigates the enhancement of material removal rate (MRR) and reduction of surface roughness (SR) during nano-powder mixed electrical discharge machining (NPMEDM) of EN-41B steel by incorporating silver nanoparticles into the dielectric fluid. Experiments were designed using Dr. Genichi Taguchi's L16 orthogonal array considering four process parameters: nano powder concentration, pulse-on time, pulse-off time, and peak current. Results showed a 21.69% increase in MRR and a 13.35% reduction in SR with the addition of silver nanoparticles. A second-order polynomial regression model was developed to relate input parameters with responses and was used as a fitness function in a genetic algorithm for single and multi-objective optimization. The optimized values obtained were 3.8033 mm³/min for MRR and 2.2141 µm for SR with prediction errors below 4%. Multi-objective optimization produced 35 Pareto-optimal solutions. Validation tests confirmed the effectiveness of the optimization approach, suggesting further studies such as the effect of tool rotation in nano powder-mixed EDM.*

## Keywords
Powder mixed EDM, Nano powder, Material removal rate, Tool wear rate, Surface Roughness.

## Introduction
Modern manufacturing industries increasingly demand machining of advanced and difficult-to-machine materials such as composites, ceramics, and high-strength alloys that possess superior mechanical and thermal properties. Conventional machining methods often face limitations in meeting requirements such as high precision, complex geometries, improved surface quality, and reduced machining costs. Electrical Discharge Machining (EDM), a non-conventional machining process, addresses these challenges by removing material through controlled electrical sparks between a tool and an electrically conductive workpiece in the presence of a dielectric medium [1]. The process enables machining of extremely hard materials without direct contact, thereby eliminating issues such as cutting forces, vibration, and chatter. The phenomenon of metal erosion by electrical sparks was first observed by Joseph Priestley in 1770, while controlled EDM machining was later developed by Boris R. Lazarenko and Natalya I. Lazarenko in 1943. With the introduction of CNC systems in the 1980s, EDM achieved significant improvements in accuracy, automation, and efficiency, leading to widespread industrial adoption and increased research interest in the field.
Electrical Discharge Machining (EDM) is a non-conventional machining process in which electrical energy is converted into thermal energy through a series of controlled sparks generated between a tool electrode and an electrically conductive workpiece separated by a small gap filled with a dielectric medium [2,3]. The working principle is shown in Fig.1.

Common dielectric fluids include kerosene, EDM oil, and deionized water, which help maintain insulation and flush away debris from the machining zone[4]. During machining, the tool advances toward the workpiece until the dielectric becomes ionized, allowing spark discharges to occur. The intense localized heat generated by these sparks melts and vaporizes small portions of the workpiece material, resulting in gradual material removal. This mechanism enables precise machining of hard conductive materials without direct physical contact between the tool and the workpiece [5].
The erosive procedure because of solo electric-spark in E.D.M ordinarily crosses from the ensuing stages is exhibited in Fig.2.

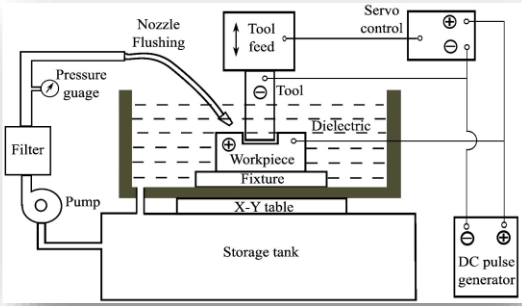


Figure 1. Working Principle of EDM.

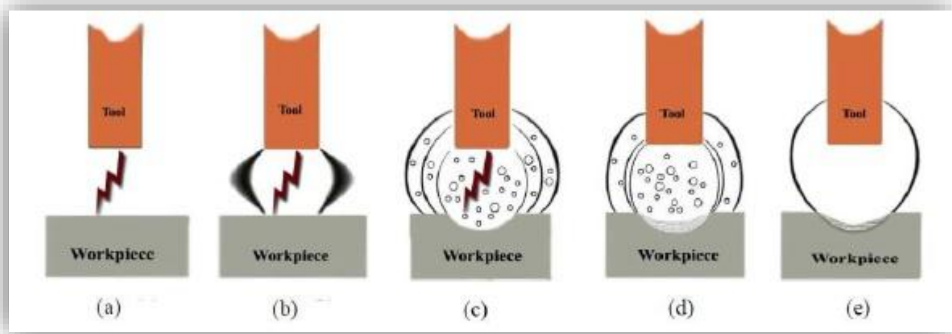


Figure 2. Phases in erosion process.

Electrical Discharge Machining (EDM) operates through a sequence of stages that enable controlled material removal by electrical sparks[6]. Initially, the tool and workpiece are placed very close to each other and a high voltage is applied across the small gap. When the applied voltage exceeds the dielectric strength of the insulating medium, dielectric breakdown occurs, forming an ionized plasma channel between the electrodes[7,8]. During the discharge stage, a high current flows through this plasma channel, generating extremely high temperatures (about 8000–12,000 °C) that melt and partially vaporize the workpiece material. When the current supply stops, the plasma channel collapses and the molten material rapidly cools in the dielectric fluid, forming small craters on the workpiece surface[9]. The dielectric fluid also flushes away debris from the inter-electrode gap, allowing subsequent sparks to occur at new locations. Repeated spark discharges gradually remove material and reproduce the shape of the tool on the workpiece surface[10,11]. Layers of an EDMed surface is shown in Fig 3.

### *Important Parameters of EDM*

Input Parameters:

- Voltage
- Pulse on time
- Pulse off time
- Discharge current
- Polarity

Output Parameters:

- Material Removal Rate (MRR)
- Tool Wear Rate (TWR)
- Surface Roughness (SR)
- Surface Integrity

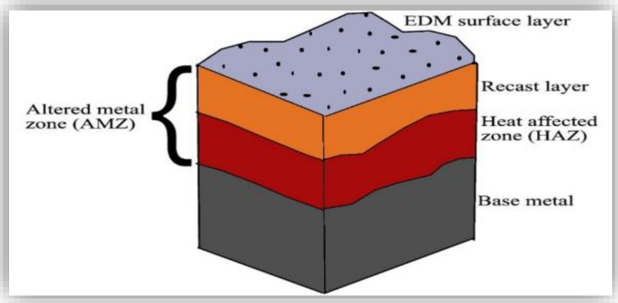


Figure 3. Layers of an EDMed surface.

## Materials and Methods

EN-41B steel is a chromium–aluminum–molybdenum nitriding steel known for its high wear resistance, toughness, and excellent abrasion resistance after nitriding. It is commonly supplied in hardened and tempered conditions and is widely used in components such as connecting rods, small extruders, and valve stems in automotive and textile industries. Due to its superior wear-resistant properties, EN-41B steel plates of size 25 mm × 25 mm × 5 mm were selected as the workpiece material for the study. Chemical constituents and mechanical properties of EN-41B steel is shown in table 1 and 2.

Table 1. Chemical Constituents of EN-41B steel

| Element | C | Si | Cr | Mo | Al | Mn | Ni | P | S |
|---|---|---|---|---|---|---|---|---|---|
| Weight % | 0.35-0.45 | 0.1-0.45 | 1.4-1.8 | 0.10-0.25 | 0.90-1.30 | 0.65 | 0.40 | 0.05 | 0.05 |

Table 2. Mechanical properties of EN41B Steel

| Condition | Tensile strength ($N/mm^2$) | Yield strength ($N/mm^2$) | Elongation (%) | Izod | Hardness Brinell | Density ($kg/m^3$) | Melting point (K) |
|---|---|---|---|---|---|---|---|
| R | 700-850 | 480 | 16 | 28 | 201-255 | 7850 | 1795 |
| S | 775-925 | 525 | 14 | 16 | 223-277 | 7850 | 1795 |

Based, upon the properties and applications, Tungsten Carbide (W-C) has been preferred as tool material. Physical properties of Tungsten Carbide is shown in table 3.

Table 3. Properties of Tungsten Carbide

| Property | Minimum value (S.I) | Maximum value (S.I) |
|---|---|---|
| Density (g/cm3) | 15.25 | 15.88 |
| Bulk Modulus (Gpa) | 350 | 400 |
| Compressive strength (Gpa) | 3347 | 6833 |
| Hardness (Mpa) | 17000 | 36000 |
| Endurance Limit(Mpa) | 285 | 420 |
| Poisson's Ratio | 0.2 | 0.22 |
| Tensile Strength (Mpa) | 370 | 530 |
| Melting point (K) | 3000 | 3193 |
| Thermal Conductivity (W/m.K) | 28 | 88 |

Powder material Silver Nano particles have been employed as additives in dielectric to optimise the performance parameters. Average, size of powder particles in the employed powder is 50nm (Nano meter).
Four process parameters i.e., powder concentration (Pc), peak-current(Ip), pulse-time(on) and pulse-time(off) were selected for the present research work. Choice of parameters has been made bearing in mind the eloquent effect of these parameters on different PMEDM. Besides these some parameters were fixed such as Tool rotation= 1000 rpm, Voltage = 230 V, Flushing pressure= 0.25 kgf/cm$^2$.
This study employs the Taguchi method as an effective experimental design technique to analyze the influence of machining parameters on performance characteristics in Electrical Discharge Machining[12]. Developed by Genichi Taguchi, the method uses orthogonal arrays to systematically study the effects of multiple control factors while minimizing experimental trials and process variability. In this research, the Taguchi L16 orthogonal array with a mixed-level four-factor design was adopted to conduct sixteen experiments for determining optimal machining parameters aimed at maximizing material removal rate (MRR) and minimizing surface roughness (SR)[13].

## *Experimental Setup*

Input parameters, their levels and Design matrix and observation are shown in Table 4 and 5.

Table 4. Input parameters and their levels

| **Machining parameter** | **Symbol** | **Unit** | **Level** | | | |
|---|---|---|---|---|---|---|
| | | | 1 | 2 | 3 | 4 |
| Current | $I_p$ | A | 2 | 3 | 4 | 5 |
| Pulse-on time | $T_{on}$ | Ms | 50 | 100 | 150 | 200 |
| Pulse-off time | $T_{off}$ | Ms | 30 | 70 | 110 | 150 |
| Powder concentration | $P_c$ | g/*l* | 0 | 1 | - | - |

Table 5. Design matrix and observation table

| Run No. | $I_p$ | $T_{on}$ | $T_{off}$ | $P_c$ | Weight of workpiece (grams) in | |
|---|---|---|---|---|---|---|
| | A | Ms | Ms | g/*l* | $W_i$ | $W_f$ |
| 1 | 2 | 50 | 30 | 0 | 26.93098 | 26.80042 |
| 2 | 2 | 100 | 70 | 0 | 26.80042 | 26.76990 |
| 3 | 2 | 150 | 110 | 1 | 26.77237 | 26.71267 |
| 4 | 2 | 200 | 150 | 1 | 26.87035 | 26.77237 |
| 5 | 3 | 50 | 70 | 1 | 26.89935 | 26.87035 |
| 6 | 3 | 100 | 30 | 1 | 26.94502 | 26.89935 |
| 7 | 3 | 150 | 150 | 0 | 26.76990 | 26.69373 |
| 8 | 3 | 200 | 110 | 0 | 26.69373 | 26.59697 |
| 9 | 4 | 50 | 110 | 0 | 26.59697 | 26.53427 |
| 10 | 4 | 100 | 150 | 0 | 26.53427 | 26.50652 |
| 11 | 4 | 150 | 30 | 1 | 26.58315 | 26.45939 |
| 12 | 4 | 200 | 70 | 1 | 26.70420 | 26.58315 |
| 13 | 5 | 50 | 150 | 1 | 26.84580 | 26.70420 |
| 14 | 5 | 100 | 110 | 1 | 26.94634 | 26.84580 |
| 15 | 5 | 150 | 70 | 0 | 26.96815 | 26.91640 |
| 16 | 5 | 200 | 30 | 0 | 26.91640 | 26.82524 |

***Predictive model employing regression method***

After conducting the experiments, regression analysis using MINITAB 17 was applied to develop prediction models relating input parameters—peak current, pulse-on time, pulse-off time, and powder concentration—with the output responses, material removal rate (MRR) and surface roughness (SR)[14]. Quadratic regression equations were established, and statistical tests such as F-test and t-test were performed to evaluate the significance of the models.

$$Y = a_0 + \sum_{i=1}^{n} a_i X_i + \sum_{i=1}^{n} a_{ii} X_i^2 + \sum_{i=1}^{n-1} \sum_{j=1}^{n} a_{ij} X_i X_j,$$

Where Y corresponds to objective i.e., M.R.R and S.R, ao is constant term; ai, aii, and aij are coefficients of linear, quadratic and interaction terms.

Employing MINITAB 17 software ANOVA test is performed to check the significance of design or input parameters vis-s-vis response parameters in other words to check which design parameter has eloquent contribution towards the particular response it is also employed to calculate the percentage variation in response variable explained by a linear model[15].

The predictive response models were optimized using the Genetic Algorithm (GA), an evolutionary search technique based on the principle of survival of the fittest, which explores the solution space through populations of chromosomes to obtain optimal results[16].

## Results and Discussion

In the experiments, a 10 mm diameter tungsten carbide (WC) cylindrical tool was used to machine EN-41B steel with commercial-grade dielectric fluid; MRR was calculated using the weight loss method and surface roughness (SR) was measured with a stylus profilometer, with all results listed in Table 6.

*ISBN 978-81-973526-0-7*

Table 6. Response table

| Order | Run No. | $I_p$ | $T_{on}$ | $T_{off}$ | $P_c$ | MRR | SR |
|---|---|---|---|---|---|---|---|
| | | A | Ms | µs | g/*l* | mm$^3$/min | um |
| 1 | 1 | 2 | 50 | 30 | 0 | 1.29096 | 2.64212 |
| 2 | 2 | 2 | 100 | 70 | 0 | 1.01176 | 2.66309 |
| 16 | 3 | 2 | 150 | 110 | 1 | 1.12834 | 2.32237 |
| 15 | 4 | 2 | 200 | 150 | 1 | 1.00774 | 2.21573 |
| 14 | 5 | 3 | 50 | 70 | 1 | 1.38570 | 2.67940 |
| 13 | 6 | 3 | 100 | 30 | 1 | 2.09026 | 2.94253 |
| 3 | 7 | 3 | 150 | 150 | 0 | 1.33837 | 2.94238 |
| 4 | 8 | 3 | 200 | 110 | 0 | 1.41428 | 2.92880 |
| 5 | 9 | 4 | 50 | 110 | 0 | 1.54594 | 3.05514 |
| 6 | 10 | 4 | 100 | 150 | 0 | 1.63206 | 3.45439 |
| 12 | 11 | 4 | 150 | 30 | 1 | 2.98405 | 2.92283 |
| 11 | 12 | 4 | 200 | 70 | 1 | 2.92938 | 2.57922 |
| 10 | 13 | 5 | 50 | 150 | 1 | 2.58927 | 2.98710 |
| 9 | 14 | 5 | 100 | 110 | 1 | 3.02545 | 2.89205 |
| 7 | 15 | 5 | 150 | 70 | 0 | 2.91633 | 3.56710 |
| 8 | 16 | 5 | 200 | 30 | 0 | 2.93750 | 3.61230 |

MRR increases mainly with peak current (Ip) due to stronger sparks and higher temperature, leading to greater material melting and removal. It also increases with pulse-on time (Ton) up to a certain limit and then decreases, while pulse-off time (Toff) generally reduces MRR. The addition of silver nano powder significantly improves MRR (about 21.69%) by lowering dielectric breakdown strength and increasing spark frequency in NPMEDM compared to conventional EDM. Mean effect and normal probability plots for MRR is shown in Fig 4.

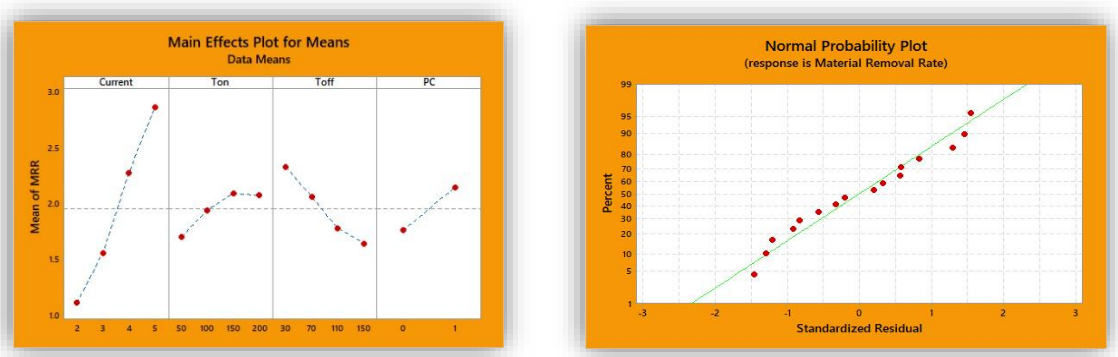


Figure 4. Mean effect and normal probability plots for MRR.

The mean effect plot shows that peak current has the most significant influence on surface roughness (SR), where higher current increases energy and leads to poorer surface finish. Pulse-on time initially increases SR due to higher energy input, but at higher values SR slightly decreases because of reduced energy transfer. Pulse-off time first increases SR but later improves surface finish due to better flushing of debris. Mean effect and normal probability plots for SR is shown in Fig 5.

*ISBN 978-81-973526-0-7*

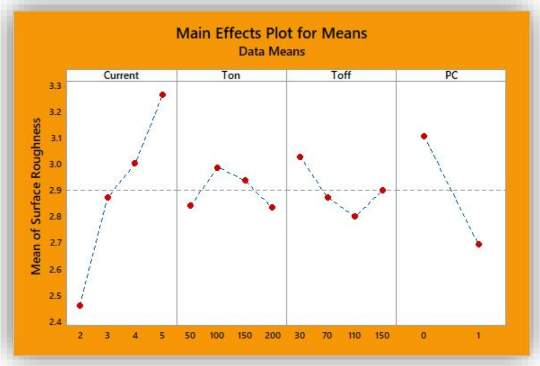


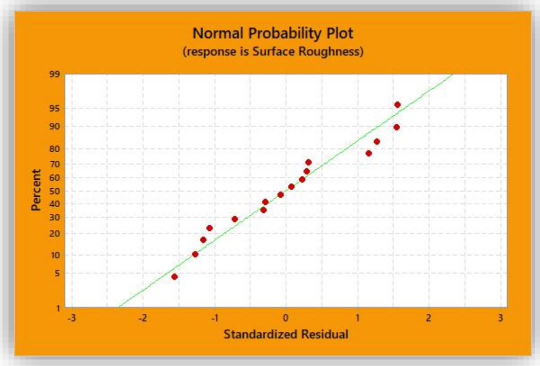


Figure 5. Mean effect and normal probability plots for SR

Through the optimization the initial population of strings is selected randomly and the population ranges covering the entire range of values for Ip, Ton, Toff and Pc were employed to avoid getting the solution into a local optimum and to obtain global optimum solution. The GA was implemented employing optimization toolbox available in MATLAB. Results of confirmation test for GA is given in Table 7.

Table.7 Confirmation test for GA

| Parameters | Responses | Predicted values | Experimental values | Error % |
|---|---|---|---|---|
| $I_p$ = 5 Amp<br>$T_{on}$ = 200 us<br>$T_{off}$ = 30 us<br>$P_c$ = 1 g/l | MRR ($mm^3$/min) | 3.8033 | 3.6933 | 2.8922 |
| $I_p$ = 2 Amp<br>$T_{on}$ = 200 us<br>$T_{off}$ = 110 us<br>$P_c$ = 1 g/l | SR (um) | 2.2141 | 2.1382 | 3.4280 |
| **Multi-objective optimization** | | | | |
| $I_p$ = 2.07149 Amp<br>$T_{on}$ = 194.8065 us<br>$T_{off}$ = 89.46077 us<br>$P_c$ = 0.999442 g/l | MRR<br>SR | 1.39942<br>2.32084 | 1.36021<br>2.24065 | 2.8018<br>3.4552 |

## Conclusion

Following conclusions can be drawn from above research work. Powder concentration was found to have eloquent positive influence on SR. This, is because Plasma channel gets broadened and distended as soon as Nano powder powder particles are incorporated into the di-electric. Following conclusions can be drawn from above research.

- Genetic Algorithm optimization showed that the optimal parameters for MRR are Ip = 5, Ton = 200, Toff = 30, Pc = 1 with a predicted MRR of 3.8033 $mm^3$/min, while the optimal parameters for SR are Ip = 2, Ton = 200, Toff = 110, Pc = 1 with a predicted SR of 2.2141 µm.

- Genetic algorithm optimization produced 35 Pareto-optimal solutions, helping engineers select machining conditions that achieve maximum MRR with surface roughness ranging from 2.304561 µm to 2.607057 µm.

## References

[1] R. Chaudhari, Y. Shah, S. Khanna, V. K. Patel, J. Vora, D. Y. Pimenov, and K. Giasin, "Experimental investigations and effect of nano-powder-mixed EDM variables on performance measures of nitinol SMA," Materials, vol. 15, no. 20, p. 7392, 2022.

[2] R. Chaudhari, I. Ayesta, S. Khanna, V. K. Patel, J. Vora, and L. N. L. De Lacalle, "Experimental investigations of using MWCNTs and nano-graphene particles for the enhancement of machining performance using powder-mixed EDM of Udimet-720," The International Journal of Advanced Manufacturing Technology, vol. 136, no. 1, pp. 145–157, 2025.

[3] K. A. Pillai and P. Hariharan, "Experimental investigation on surface and machining characteristics of micro ED milling of Ti-6Al-4V with different nano powder mixed dielectrics," Silicon, vol. 14, no. 6, pp. 2871–2894, 2022.

[4] P. Sivaprakasam, P. Hariharan, and S. Gowri, "Experimental investigations on nano powder mixed Micro-Wire EDM process of Inconel-718 alloy," Measurement, vol. 147, p. 106844, 2019.

[5] M. Al-Amin, A. M. Abdul Rani, A. A. Abdu Aliyu, M. A. H. Abdul Razak, S. Hastuty, and M. G. Bryant, "Powder mixed-EDM for potential biomedical applications: A critical review," Materials and Manufacturing Processes, vol. 35, no. 16, pp. 1789–1811, 2020.

[6] K. MangapathiRao, D. Vinaykumar, K. Chandra Shekar, and R. R. Kumar, "Investigation and analysis of EDM process—A new approach with $Al_2O_3$ nano powder mixed in sunflower oil," in IOP Conference Series: Materials Science and Engineering, vol. 1057, no. 1, p. 012059, Feb. 2021.

[7] V. Kumar, A. Kumar, S. Kumar, and N. K. Singh, "Comparative study of powder mixed EDM and conventional EDM using response surface methodology," Materials Today: Proceedings, vol. 5, no. 9, pp. 18089–18094, 2018.

[8] S. Yadav, D. Agarwal, A. K. Sharma, R. K. Singh, S. Chauhan, and S. Mohanty, "Experimental investigation of $Al_2O_3$ nano-powder-mixed dielectric in EDM-assisted micro-milling," Micromachines, vol. 16, no. 7, p. 725, 2025.

[9] B. K. Lodhi, S. Agarwal, and S. Ahamad, "Optimization of WEDM parameters on surface roughness of EN41B steel," Materials Today: Proceedings, vol. 25, pp. 816–820, 2020.

[10] M. N. Alam, M. A. Wahid, R. Ahsan, N. Kumar, and S. Sabri, "A comparative investigation on powder mixed EDM machining of steel alloys with multi-objective optimization using fuzzy-TOPSIS method," Diyala Journal of Engineering Sciences, pp. 18–37, 2024.

[11] P. K. Rout and P. C. Jena, "A review of current researches on powder mixed electrical discharge machining (PMEDM) technology," in Advances in Mechanical Processing and Design: Select Proceedings of ICAMPD 2019, pp. 489–497, 2020.

[12] D. Saminatharaja, S. Periyakgounder, M. Selvaraj, and J. Elangandhi, "Performance study of EDM process parameters using TiC/$ZrSiO_4$ particulate-reinforced copper composite electrode," Journal of Mechanical Engineering/Strojniški Vestnik, vol. 67, no. 11, 2021.

[13] T. Saba, A. N. Amin, S. Islam, M. R. Chaity, N. T. Tuli, and A. B. Rashid, "Optimization of process parameters in nano-particle mixed EDM of hardened die

steel AISI H13 using RSM and GA," Results in Surfaces and Interfaces, vol. 19, p. 100458, 2025.

[14] G. Rajkumar, M. Saravanan, A. B. H. Bejaxhin, S. Sharma, S. P. Dwivedi, R. Kumar, and S. Singh, "Parametric optimization of powder-mixed EDM of AA2014/$Si_3N_4$/Mg/cenosphere hybrid composites using fuzzy logic," Journal of Composites Science, vol. 7, no. 9, p. 380, 2023.

[15] S. Ali, A. Kossymbayev, D. Kenesbek, D. Yeregenov, D. Talamona, and A. Perveen, "Experimental surface modification, prediction modeling, and multi-objective optimization of μ-EDM process using GBR-NSGA-II for machining of Ti-6Al-4V + 8% Ta," International Journal of Lightweight Materials and Manufacture, 2025.

[16] D. Chandra, N. R. Chauhan, and S. Rajesha, "Process optimization of EDM parameters using Taguchi while machining aluminium metal matrix composite," in Optimization of Industrial Systems, D. Panchal, M. Tyagi, A. Sachdeva, and D. Pamucar, Eds. Hoboken, NJ, USA: Wiley, 2022. doi:10.1002/9781119755074.ch41.

*ISBN 978-81-973526-0-7*

# DESIGN AND STRUCTURAL ANALYSIS OF MULTIPURPOSE MACHINE FOR SMALL SCALE MANUFACTURING

Faizan Fayaz*[1], Uddeshya Verma[1], Shakil Ahmad[1], Vivek Sheel Yadav[1]
*[1]Department of Mechanical Engineering, Galgotias University, India
faizanfayazganaie6@gmail.com

## Abstract
*This study introduces a compact multipurpose machine that handles drilling, cutting, and grinding all powered by one motor. The system uses an electromagnetic clutch, so you can switch between operations without shutting the motor off, which gives you more control than the typical mechanical setups. The team designed and modelled each part in CAD, then ran finite element simulations to see how the shaft holds up under stress. They used alloy steel and checked the results with von Mises stress criteria. Turns out, the maximum stress on the shaft stays safely below the limit, which means the design is solid and reliable.*

## Keywords
Multipurpose machine, electromagnetic engagement mechanism, shaft analysis, finite element analysis (FEA), power transmission.

## Introduction
In today's manufacturing world, machines need to be small, efficient, and able to do many things. In small workshops and labs, tasks like drilling, cutting, and grinding are often done on separate machines. This way of working is reliable, but it takes more time to set up, needs more handling of materials, and requires more equipment and space. That's why there's a growing interest in machines that can do many tasks at once. These multipurpose machines aim to cut equipment costs, make the workspace more efficient, and make operation simpler, all while keeping safety and mechanical reliability in check. By combining several machining processes into one system, they can help reduce costs and improve overall performance. This approach can be especially useful in small workshops and teaching laboratories, where space and resources are limited. With a multipurpose machine, users can perform multiple tasks without having to switch between different machines, saving time and increasing productivity. Additionally, these machines can help simplify operation and reduce the need for additional handling of materials, making the manufacturing process more efficient and streamlined. Overall, the development of multipurpose machines is an important step forward in modern manufacturing, enabling companies to produce high-quality products while reducing costs and improving efficiency. Researchers have explored different approaches to integrating multiple machining operations in a single machine. Earlier work by Srivastava and colleagues presented a multifunction machine powered by a single motor and driven through mechanical linkages and gear systems, demonstrating that multiple operations could be performed within one structure. Later studies by Urunkar et al. and Perumal et al. examined designs capable of carrying out drilling, sawing, and grinding using shared power transmission systems. These studies showed that multipurpose machines can reduce both space requirements and overall cost, particularly for small-scale production environments. However, many of the existing designs rely on fixed mechanical couplings or manually operated engagement mechanisms. When operations are switched frequently, these mechanisms can introduce vibration, wear, and operational limitations. Machining systems have a major flaw - they don't have a good way to switch between different machining units.

ISBN 978-81-973526-0-7

Older designs use clutches, belt-shifting, or drives that are always connected, which need someone to control the power manually. This can cause problems like sudden changes in load, alignment issues, and wear on mechanical parts. Many studies have focused on building or designing machines, but haven't looked closely at how the important parts work when they're under stress. We need a new approach that combines machining with a reliable way to engage the machines and checks the mechanics thoroughly. This new approach should make sure the machining units work well together and can be controlled properly. It's not just about building a machine, but also about making sure it can handle the stresses of working. By looking at the mechanics of the machine and how it works under stress, we can design a better system. The old way of doing things can cause a lot of problems, like machines wearing out quickly or not working properly. We should focus on creating a system that is integrated and reliable, with a good way to engage the machining units. This will help us build better machines that can handle the demands of machining. It's time to move away from the old designs and create something new and improved. With a good design approach, we can build machines that are efficient, reliable, and can handle the stresses of working. To address these challenges, the present work investigates the modelling and analysis of a multipurpose machine that uses an electromagnet-based engagement and disengagement system. This mechanism allows drilling, cutting, and grinding operations to be activated selectively without stopping the motor, which helps improve operational control and reduces manual intervention. The complete machine assembly was developed using computer-aided design tools, and the main load-carrying shaft was analyzed using both classical strength-of-materials methods and finite element simulation. Shear force and bending moment diagrams were used to determine the loading conditions on the shaft, and the analytical results were verified through SolidWorks simulation. By combining design calculations with numerical analysis, the study evaluates the practicality and structural reliability of using electromagnetic engagement mechanisms in multipurpose machining systems.

## Experimental Setup

In figure 1 the finished hardware of the multipurpose machine. The setup has a steel frame holding everything together: the main shaft, pulleys, gears, and bearings. One electric motor runs the show, sending power to the shaft through a belt and pulley setup. That’s how it drives the drilling If you want to switch between operations, there's an electromagnetic mechanism for that. It lets you choose what you want to do without ever having to shut off the motor.


Figure 1. Experimental setup of the developed Multipurpose machine.

## Modelling

### *Modelling of the Multi-Purpose Machine*

The multi-purpose machine was modelled using CAD software to represent the arrangement of its main components. The system includes a frame, drilling shaft, grinding shaft, cutter shaft, belt drive, and an electric motor.

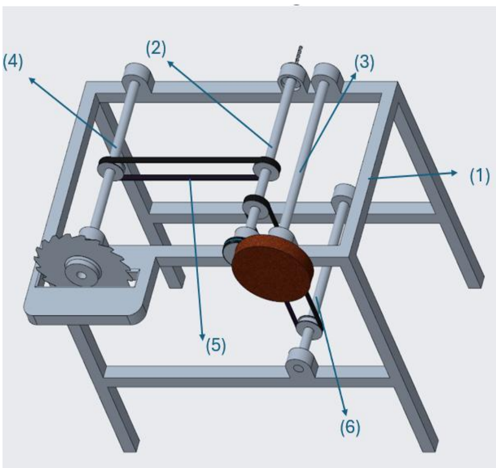


Figure 2. Represents the location of each part in the whole body.

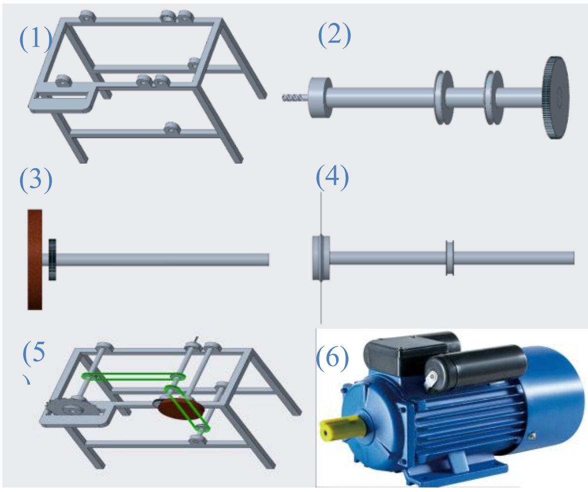


Figure 3. Represents each part separately in the whole body.

Model has 6 parts:

- Frame
- Main shaft with drill
- Bench grinder shaft
- Cutter shaft
- Belts
- Motor

(1) Frame: The frame is the main support structure for the multipurpose machine. It provides a solid base for mounting the motor, shafts, gears, and other parts. The frame keeps the machine elements aligned during drilling, cutting, and grinding. This ensures stability and reduces vibration. It measures about 550 mm × 420 mm × 300 mm and is made of alloy steel, which is strong, durable, and resistant to deformation under load.

(2) Main shaft with drill: The main shaft is the main load-carrying part of the machine. It

transmits power to the drilling unit. The shaft is about 320 mm long and is made of alloy steel. This material can handle bending and twisting forces during operation. The shaft is built to support drilling loads while keeping proper alignment with the gear and pulley system. This design ensures stable and reliable machining performance. Material used to built this is alloy steel.

(3) Bench grinder shaft: The bench grinder shaft is what holds the grinding wheel. The dimensions of the shaft are 250mm in length with the alloy steel material to provide sufficient strength and durability.The grinding wheel mounted on the shaft is composed of aluminium oxide and silicon carbide which enables efficient grinding and finishing for workpieces.

(4) Cutter shaft: And it is the cutter bar that holds cutting tools as well triggers rotational movement from motors to cutter.In the radial type, the cutter holder is hollow, fitted to the spindle of the stand, and fixed by a drawbar.Then the cutter shaft has an approximate length of 250mm and a diameter: 20mm, providing enough strength and stability for use very well.It is made of alloy steel, which is often used in machineries here (including all shafts).

(5) Belt: Used to transfer rotational motion. The motor can be made to drive all sorts of shafts on machine: The power of Link This is where the belt comes in. Wound on the outer wheels of any two adjacent pulleys, it will absorb any irregularities in case speeds are transmitted between two belts. With a length of about 800mm and width of 20 mm, the belt is made of synthetic rubber. This type flexible material not only lasts longer than metal but also gives good grip during power transfer.

(5) Motor: The machine gets its power from a single-phase AC induction motor which provides rotation for drilling, cutting, and grinding. The motor is operated with a line voltage of 230 V ac and at a 2 A rms current. It uses 6-12 µF capacitors for starting and running. It produces an output power of approximately 0.3HP (amounting to about 200–250W) and operates at about 1400 r/min of speed. This design is suitable to ensure smooth processing. The motor couples the whole system together using a belt system of pulleys. This way the multifunction machine, is supplied with a stroke from 0 to 100 mm, there will always be drive power to individual shafts.

## Calculations and Analysis

### Gear mesh calculations

- Type: Spur gears
- Pressure angle, $\alpha = 20°$
- Module, $m = 0.6$ mm
- Teeth on pinion, $Z_1 = 80$
- Teeth on gear, $Z_2 = 100$

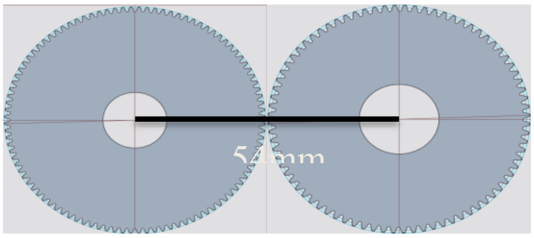

Figure 4. Represents the involute gears

Centre distance: $a = \frac{d_1+d_2}{2}$ =54mm where d1 is the diameter of the pinion and d2 is the diameter of the gear ….....[7]

### Motor calculations

Motor specifications:

- Voltage: 230 V AC
- Current: 2 A
- Capacitor: 6–12 µF
- Output: ~0.3 HP
- Speed: 1400 RPM
- Coefficient of friction of belt material =0.3
- Efficiency =70%
- Power = Voltage × power =230×2=460W
- Efficiency=70%
- Effective power=0.7×460=322W

## Shaft calculations

(A) The power will be transmitted to both the pulleys given by:

Power = (Difference between tension in pulleys) × (Belt velocity) = $(T1 - T2) \times V$……. [7]

Which $T1 - T2 = 51.3N$

(B) The ratio of tensions in a pulley belt is given by $(T2/T1 = e^\wedge\mu\theta)$ ……… [7]

where μ (0.3 for belt) is the coefficient of friction, and θ (180 degrees) is the wrap angle, $T1/T2 = 2.75$

Solving both equations, we get: $T1 = 32.67\ N, T2 = 83.97\ N$

Therefore, the net force on each pulley is $T1 + T2 = 116.64\ N$

## Shear force calculations

(1) Resultant forces

$R^\wedge 2 = (Pv)^\wedge 2 + (Ph)^\wedge 2$…….[7]

where R is the resultant force and Pv,Ph are the forces acting on the pulleys.

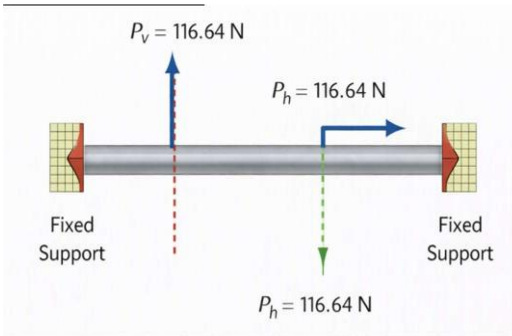


Figure 5. Represents the FBD of the shaft.

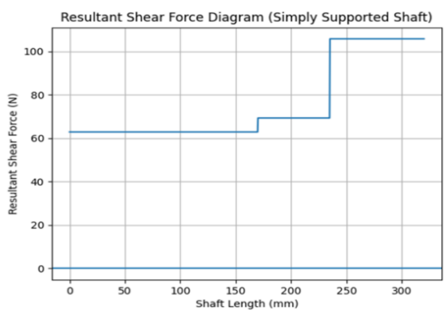


Figure 6. Represents the resultant SFD.

## Bending Movement calculations

The shaft is treated like a simply supported beam ,BM will calculated for pulleys individually.

(1) <u>Considering only 1st load</u>:

Applying, Sum of movements = 0 ($\sum Mc$ =0)….[7]

We get the value of reaction forces as follows:

| |
|---|
| Rc=61.965N |
| Rd=54.675N |

—

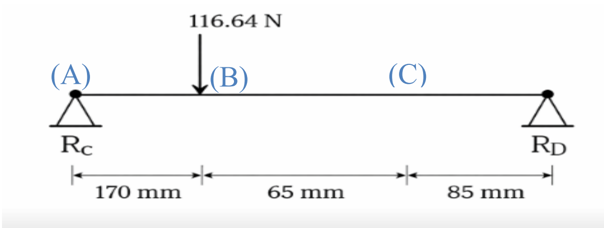


Figure 7. Shows FBD of shaft with 1st load

Bending movements about point B and C:

| |
|---|
| Mb=9294.75 |
| Mc=5267.025 |

(2) <u>Considering the 2nd load</u>:

Applying, Sum of movements = 0 ($\sum Mc$ =0) ….[7]

We get values of reaction forces as follows

| |
|---|
| Rc=85.48N |
| Rd=30.91N |

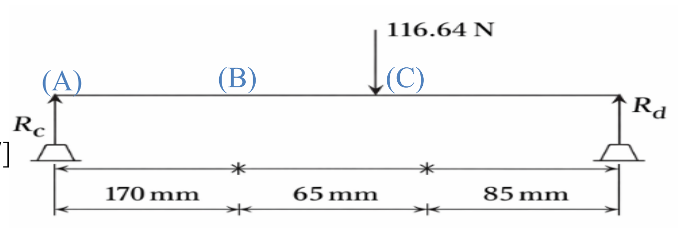


Figure 8. Shows FBD of shaft with 2nd load

Bending movement about point B and C are:

| |
|---|
| Mb=5254.7N |
| Mc=7265.8N |

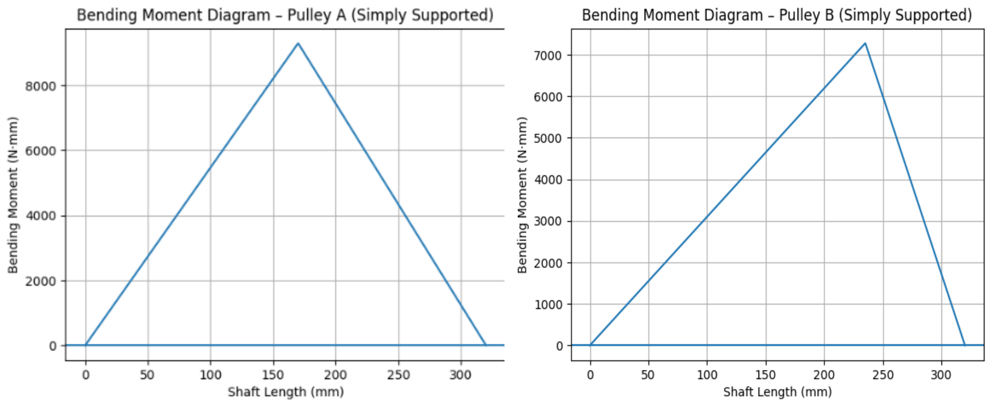


Figure 9. Shows two diagrams of the BMD graph of the shaft considering 1st load and 2nd load.

By applying the formula of resultant bending movement, we can combine both loads and calculate the resultant bending movement.

Resultant bending movement: $M_R = \sqrt{(M_v^2 + M_h^2)}$…….[7]

Where Mv is the vertical BM of the shaft and Mh is the horizontal BM of the shaft.

Table.1 shows the vertical, horizontal bending moments on pully A and B.

| Section | $M_v$(N·mm) | $M_h$(N·mm) | $M_R$(N·mm) |
|---|---|---|---|
| Pully A | 9294.75 | 5254.7 | 10677.3 |
| Pully B | 5267.025 | 7265.8 | 8974 |

Maximum bending movement =10677.3

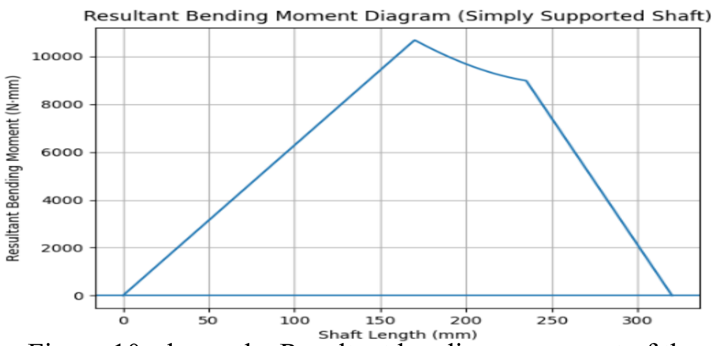


Figure 10. shows the Resultant bending movement of the shaft.

## *Simulation and Analysis*

**Simulation conditions:**

- Material: Alloy Steel
- Constraints: Fixed at both ends
- Loads: Vertical and horizontal forces applied at gear locations
- Mesh: Fine solid mesh

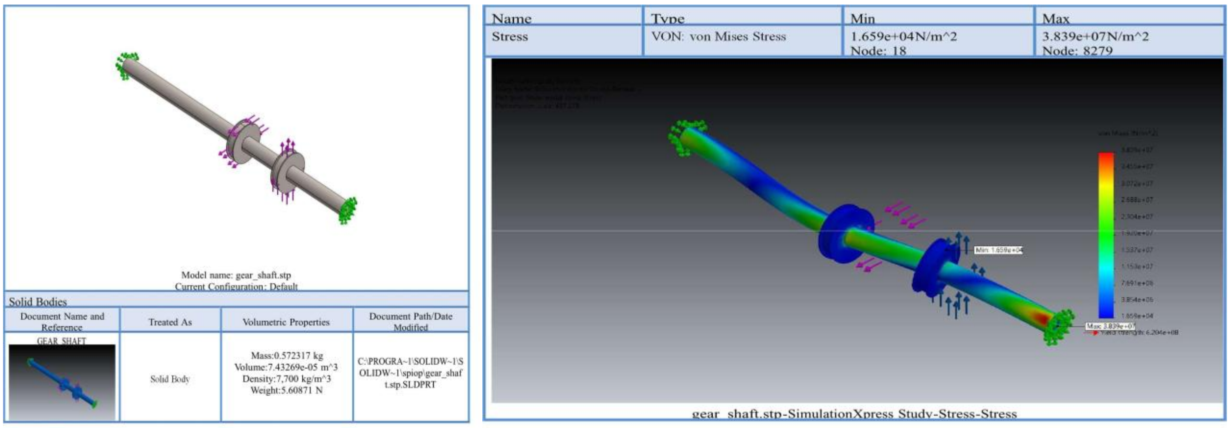


Figure 11. represents the Finite Element Analysis (FEA) stress simulation of your gear shaft model in SolidWorks Simulation.

SolidWorks static structural analysis indicates how the shaft's Von Mises stress is distributed under the condition of fixed supports and loads by pulley. In the shaft, the simulation shows that the maximum stress developed (≈88 MPa), and this is found near the support region because of bending forces. As the contour indicates, most of the shaft is subject to a low level of stress. Most regions on the map are blue or green. The shaft is safely operating within elastic limits, because its maximum stress is significantly lower than that of yield point for alloy steel.

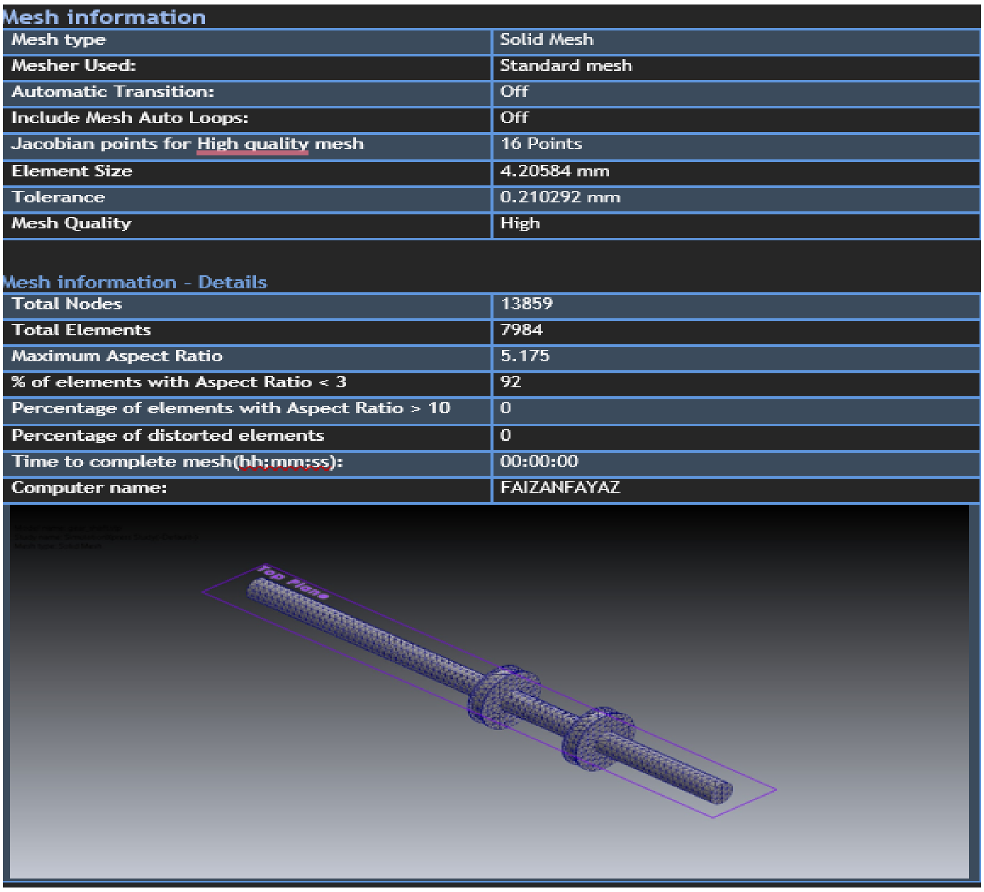

**Mesh information**

| | |
|---|---|
| Mesh type | Solid Mesh |
| Mesher Used: | Standard mesh |
| Automatic Transition: | Off |
| Include Mesh Auto Loops: | Off |
| Jacobian points for High quality mesh | 16 Points |
| Element Size | 4.20584 mm |
| Tolerance | 0.210292 mm |
| Mesh Quality | High |

**Mesh information - Details**

| | |
|---|---|
| Total Nodes | 13859 |
| Total Elements | 7984 |
| Maximum Aspect Ratio | 5.175 |
| % of elements with Aspect Ratio < 3 | 92 |
| Percentage of elements with Aspect Ratio > 10 | 0 |
| Percentage of distorted elements | 0 |
| Time to complete mesh(hh;mm;ss): | 00:00:00 |
| Computer name: | FAIZANFAYAZ |



Figure 12. Represents Mesh generation details of the shaft model used for Finite Element Analysis (FEA) in solidworks Simulation**.**

*ISBN 978-81-973526-0-7*

Table.2 shows the final concluded results from the analysis.

| Parameter | Value |
|---|---|
| Max von Mises stress | $3.84 \times 10^7$ N/m² (≈ 38.4 MPa) |
| Maximum displacement | 0.084 |
| Factor of safety | ≈3 |

## Conclusion

According to theoretical calculations and analysis by computer, the shaft design was then authenticated. Such verified, the fact that the maximum value for von Mises stress is well below alloy steel 's yield point and hardly any displacement were evidenced, would suggest its operating safety. The simulation results also match up with the analytical bending moment proof above, proving that the design is reliable. The new "electromagnetic" engagement mechanism in our compound production room station, though a great many processes are performed carefully thereby eliminating randomness.

## References

[1] S. Shahnawaz and N. Nirwan, “Conceptual Design and Fabrication of Multipurpose Machine,” International Journal for Research & Development in Technology, vol. 8, no. 4, Oct. 2017.

[2] A. Bonde, N. K. Mandavgade, and S. R. Jachak, “Design of Multipurpose Mechanical Machine,” Materials Today: Proceedings, vol. 49, pp. 1180–1184, 2022.

[3] R. Kajabe, O. Gunjal, V. Gupta, S. Godase, and M. Gorde, “Design and Development of Multipurpose Machine,” Journal of Emerging Technologies and Innovative Research (JETIR), vol. 6, no. 2, 2019.

[4] S. Perumal, T. Manikandan, K. Mounaraj, S. Mubarak, and M. Praveen Kumar, “Design and Synthesis of Multipurpose Hand Driller Machine for Various Processes,” International Journal of Science Technology & Engineering, vol. 4, no. 3, 2017.

[5] R. U. Urunkar et al., “Design and Development of Multipurpose Machine for Sawing, Drilling and Grinding,” International Journal of Creative Research Thoughts, vol. 6, no. 1, 2018.

[6] M. A. F. Nagori et al., “Implementation and Development of Multi-Purpose Mechanical Machine,” International Journal for Research in Applied Science & Engineering Technology (IJRASET), vol. 10, no. 4, 2022.

[7] V. B. Bhandari, Design of Machine Elements, 3rd ed., New Delhi, India: Tata McGraw-Hill Education, 2010.

# MULTI-OBJECTIVE OPTIMIZATION IN NPMEDM BY UNITED APPROACH OF TAGUCHI METHOD AND GREY RELATIONAL ANALYSIS

Priyanka Singh[1]*, Divya Chandra[1], Nitin Kumar Chauhan[1], Nathi Ram Chauhan[2], Preetesh Dubey[1]
*[1]JSS University, Noida, India
[2]Indira Gandhi Delhi Technical University for Women (IGDTUW), New Delhi, India
*priyankasingh@jssaten.ac.in

## Abstract

*Electrical Discharge Machining (EDM) is a non-traditional machining process widely employed for machining hard-to-cut materials and producing intricate geometries. With the growing demand for high-precision components possessing superior surface hardness, chemical stability, and wear resistance—Nano Powder Mixed Electrical Discharge Machining (NPMEDM) has emerged as an effective technique to enhance the performance and efficiency of conventional EDM processes. The present study aims to investigate the influence of key process parameters on machining performance during NPMEDM using silver nanoparticles with AISI D3 steel as the work material. The primary machining parameters considered are discharge current (Ip), pulse-on time (Ton), pulse-off time (Toff), and powder concentration (Pc), each varied at four distinct levels. The performance characteristics evaluated in this study include material removal rate (MRR) and surface roughness (SR). Sixteen experiments were conducted using an L16 orthogonal array based on the Taguchi design of experiments. Quadratic regression models were developed to establish relationships between the input parameters and performance responses. Single-objective optimization was carried out using the Taguchi method, whereas multi-objective optimization of MRR and SR was achieved through Grey Relational Analysis (GRA). The experimental results indicate that discharge current is the most influential parameter affecting MRR, followed by pulse-on time. In contrast, discharge current and powder concentration significantly influence surface roughness. Analysis of Variance (ANOVA) reveals that powder concentration contributes 28.907% to the grey relational grade, followed by discharge current (19.667%), pulse-on time (16.908%), and pulse-off time (10.001%). The optimal parameter combination was identified as Ip 5 A, Ton 200 μs, Toff 50 μs, and Pc 1 g/L, resulting in improved machining performance and process efficiency.*

## Keywords

EDM, MRR, SR, discharge current (Ip), pulse-on time (Ton), pulse-off time (Toff).

## Introduction

Electrical Discharge Machining (EDM) is widely used for precision machining of hard and difficult-to-machine materials. Despite its advantages, EDM is often limited by low surface quality (SQ) and low material removal rate (MRR). To overcome these limitations and meet the growing demand for high-precision components with improved chemical resistance and wear properties, Powder Mixed Electrical Discharge Machining (PMEDM) has been developed as an effective modification of the EDM process. In PMEDM, conductive or semi-conductive powders are mixed with the dielectric fluid to enhance machining performance and improve surface characteristics.

Several studies have investigated the influence of different powder materials in PMEDM. Powders such as Ni, Co, Fe, Al, Cr, Cu, Ti, graphite, Mo, Si, SiC, and $MoS_2$ have been used with varying concentrations and particle sizes to improve machining responses.[1-2]

Research indicates that powder additives significantly affect machining characteristics, including material removal rate (MRR), surface roughness (SR), and tool wear rate (TWR). Graphite powder improves MRR, while alumina powder reduces electrode wear [3]. Aluminium powder has been reported to enhance surface integrity with fewer cracks and voids. Similarly, titanium powder increases MRR and SR, whereas carbon nanotubes (CNTs) improve surface quality [4]. Silicon powder has also been shown to significantly improve surface finish and enhance recast layer hardness [5].

In addition to powder material, machining parameters such as discharge current (Ip), pulse-on time (Ton), pulse-off time (Toff), powder concentration (Pc), tool rotation, and dielectric flow rate play a significant role in determining machining performance [6-8.] Studies have shown that peak current and pulse duration strongly influence MRR and SR. Higher powder concentrations can enlarge the spark gap and improve machining efficiency, although excessive concentration may cause powder settling problems [9-15].

Although considerable research has been conducted on PMEDM, limited work has focused on Nano Powder Mixed EDM (NPMEDM). In particular, the influence of silver nanoparticles on machining characteristics has not been widely explored. Furthermore, multi-objective optimization of NPMEDM and the effect of tool rotation have received limited attention. Therefore, further investigation is required to evaluate the effect of silver nanoparticles and machining parameters on EDM performance.

## Material & Methods

### *Material Selection*

The workpiece material selected for machining was AISI D3 tool steel of dimension 25mm x 25mm x 5mm. Dimension of D3 steel workpiece used in machining and copper tool is shown in Fig. 1 (a) and (b). In this investigation 12mm diameter copper electrode of with 99.98% purity have been taken for NPMEDM process. Silver (Ag) Nano powder with grain size of 50nm (Nano meter) is added to working fluid in EDM and its effect was observed on finished texture and material erosion rate of an AISI D3 steel. Ultra-sonication of the silver nano particle is done for about 18 hours to ensure proper blending of nano particles into dielectric oil.

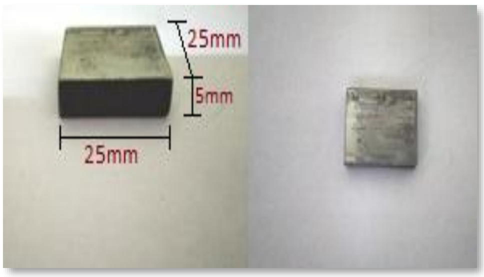


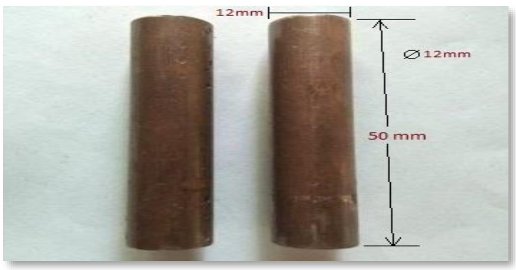


(a) (b)

Figure 1. (a)Dimension of D3 steel workpiece (b) Copper Tool.

### *Process Parameters*

### *Material removal rate*

The MRR of the work material is the quantity of the material eroded per minute. MRR measured on weight base.

### *Surface roughness (SR)*

Surface roughness is the factor of the quality of operated surface. It is expressed in µm and denoted by Ra. If the value comes higher that means the texture is uneven and with low value, Surface roughness of machined work pieces was measured by surface roughness testing machine "Mitutoyo Surface Roughness Tester SJ – 301.

### *Machining parameters*

Table 1. Machining parameters and their level.

| **Machining parameter** | **Symbol** | **Unit** | **Level** | | | |
|---|---|---|---|---|---|---|
| | | | **Level 1** | **Level 2** | **Level 3** | **Level 4** |
| Discharge current | (Ip) | A | 5 | 6 | 7 | 8 |
| Pulse on time | (Ton) | µs | 100 | 150 | 200 | 250 |
| Pulse off time | (Toff) | µs | 20 | 50 | 80 | 110 |
| Powder conc. | (Pc) | g/l | 0 | 1 | - | - |

### *Methodology*

### *Design of experiment*

In this investigation, Taguchi method is employed with parametric optimization based on "Orthogonal Arrays" (OA) experiments. L16 orthogonal arrays design is established to evaluate the influence of the factors.

### *Taguchi design experiments in MINITAB*

This experimental run was conducted on MINITAB 17 software. For this experimental work, a four-factor mixed level design is preferred in which 16 experiments were carried out and thus the L16 OA was chosen.

### *Grey relational analysis (GRA) for Multi-objective optimization*

GRA is the system with partial information and is implemented to specify the grade of similarity among simultaneous series to evaluate the distance of parameters separately.

### *Experimental Setup*

Cylindrical copper tool material having 12 mm diameter is taken for investigation on the die-sinking type ZNC25 EDM machine setup as shown in Fig.2. Ip, Ton, Toff, and Pc are taken as input parameters. The experiments were conducted based on L16 OA in random order for all 16 runs and measuring the response parameters in NPMEDM of AISI D3 steel workpiece (25mm x25mm x5mm). Further mathematical modeling and optimization is carried out simultaneously by combined technique of Taguchi design and GRA. Design matrix and observation table is shown in Table 2.


Figure 2. Experimental set up.

## Results & Discussions

### *TAGUCHI'S Analysis for MRR*

From the calculated result of MRR (Table 3), main effect plot graph and response table for means has been produced using MINITAB 17 software. It can be seen that MRR improves with an increment in the Ip between 5-8 A. Due to increase in the Ip, large amount of discharge energy is conducted into the discharge gap that increases heat flux on the work material surface. Thus, amount of material eroded is high.

Table 2. Design matrix and Observation table.

| **Exp. No.** | **Ip (A)** | **Ton (µs)** | **Toff (µs)** | **Pc (g/l)** | **Wt. of Workpiece (g)** | | **Run order** |
|---|---|---|---|---|---|---|---|
| | | | | | **$W_{bm}$** | **$W_{am}$** | |
| 1 | 5 | 100 | 20 | 0 | 30.92614 | 30.84553 | 8 |
| 2 | 5 | 150 | 50 | 0 | 30.94479 | 30.92614 | 7 |
| 3 | 5 | 200 | 80 | 1 | 31.14919 | 31.07424 | 16 |
| 4 | 5 | 250 | 110 | 1 | 31.28367 | 31.14919 | 15 |
| 5 | 6 | 100 | 50 | 1 | 31.47700 | 31.28367 | 14 |
| 6 | 6 | 150 | 20 | 1 | 31.59300 | 31.47700 | 13 |
| 7 | 6 | 200 | 110 | 0 | 31.02068 | 30.94479 | 6 |
| 8 | 6 | 250 | 80 | 0 | 31.1445 | 31.02068 | 5 |
| 9 | 7 | 110 | 80 | 0 | 31.55483 | 31.47038 | 4 |
| 10 | 7 | 150 | 110 | 0 | 31.73692 | 31.55483 | 3 |
| 11 | 7 | 200 | 20 | 1 | 31.69782 | 31.61735 | 12 |
| 12 | 7 | 250 | 50 | 1 | 31.91114 | 31.69782 | 11 |
| 13 | 8 | 100 | 110 | 1 | 31.96329 | 31.91114 | 10 |
| 14 | 8 | 150 | 80 | 1 | 32.12233 | 31.96329 | 9 |
| 15 | 8 | 200 | 50 | 0 | 31.94750 | 31.73692 | 2 |
| 16 | 8 | 250 | 20 | 0 | 32.01845 | 31.94750 | 1 |

Table 3. Calculation for MRR and SR.

| **Exp No** | **Ip(A)** | **Ton(µs)** | **Toff(µs)** | **Pc(g/l)** | **MRR (mm3/min)** | **SR (µm)** |
|---|---|---|---|---|---|---|
| 1 | 5 | 100 | 20 | 0 | 1.84104 | 5.675 |
| 2 | 5 | 150 | 50 | 0 | 1.09270 | 5.715 |
| 3 | 5 | 200 | 80 | 1 | 2.43960 | 5.055 |
| 4 | 5 | 250 | 110 | 1 | 1.84502 | 4.955 |
| 5 | 6 | 100 | 50 | 1 | 1.90730 | 5.750 |
| 6 | 6 | 150 | 20 | 1 | 5.91260 | 5.975 |
| 7 | 6 | 200 | 110 | 0 | 2.85680 | 6.580 |
| 8 | 6 | 250 | 80 | 0 | 2.75116 | 6.375 |
| 9 | 7 | 100 | 80 | 0 | 2.80030 | 6.650 |
| 10 | 7 | 150 | 110 | 0 | 4.04240 | 7.725 |
| 11 | 7 | 200 | 20 | 1 | 5.59220 | 5.935 |
| 12 | 7 | 250 | 50 | 1 | 4.60759 | 5.535 |
| 13 | 8 | 100 | 110 | 1 | 3.50370 | 6.680 |
| 14 | 8 | 150 | 80 | 1 | 8.54270 | 6.295 |
| 15 | 8 | 200 | 50 | 0 | 9.59580 | 7.655 |
| 16 | 8 | 250 | 20 | 0 | 5.22811 | 7.335 |

Ton is observed as the second important factor for MRR. MRR increased first with Ton initially for three machine units (100 µs, 150 µs and 150 µs) and then settles into a decreasing pattern with further rise in Ton to 200 µs. The energy supply to the work material increases with increase in Ton. But with rise in Ton value, the plasma created between the IEG obstruct the transfer of energy which result in lower MRR. The MRR decreases continuously with the rise in pulse off time between the range 20-110 µs. Increase in Toff value bring down the tool temperature much. Pc is spotted with least contribution to MRR. 13.72% improvement in MRR is estimated with powder mixed dielectric for EDM.

Table 4. Response table for means on MRR.

| Level | Ip | Ton | Toff | Pc |
|---|---|---|---|---|
| 1 | 1.805 | 2.513 | 4.643 | 3.776 |
| 2 | 3.357 | 4.898 | 4.301 | 4.294 |
| 3 | 4.261 | 5.121 | 4.133 | |
| 4 | 6.718 | 3.608 | 3.062 | |
| Delta | 4.913 | 2.608 | 1.582 | 0.518 |
| Rank | 1 | 2 | 3 | 4 |

From Table 4, response table for means on MRR show Ip with highest contribution on MRR compared to Ton, Toff and Pc. Ton and Toff are second and third significant factor respectively followed by least significant factor Pc for better MRR.

### *Regression Model For MRR*

Regression analysis has been carried out to establish the relationship between input parameters and MRR by developing a quadratic model. Regression model is developed in Minitab 17 software. According to the experimental plan L16 OA experiment are designed, with the combination of different values of input variables Ip, Ton, Toff and Pc. Each of the responses is fitted into a quadratic equation to generate a fit regression model. the derived quadratic regression equation has been developed, as shown in Eqn. (4.1).

$$MRR = -7.58 - 0.21\,Ip + 0.1317\,Ton - 0.2682\,Toff + 6.08\,Pc + 0.2261\,Ip*Ip - 0.000390\,Ton*Ton - 0.000202\,Toff*Toff - 0.00519\,Ip*Ton + 0.02041\,Ip*Toff - 0.977\,Ip*Pc + 0.000786\,Ton*Toff + 0.00299\,Ton*Pc. \quad (4.1)$$

Analysis of variance (ANOVA) is carried out to test assumptions of normality, independence and constant variance of the suggested model. Table 5 present ANOVA derived on the fitted model.

For this experiment the R-sq value show that the predictors describe 99.19 % of the response variation and adjusted R-sq for the number of predictors in the model is 95.94 %, both values indicate that the data are fitted well.

Table 5. Analysis of Variance for regression on MRR.

| Source | DF | Adj SS | Adj MS | F-Value | P-Value |
|---|---|---|---|---|---|
| **Regression** | 12 | 87.4397 | 7.2866 | 30.53 | **0.008** |
| Ip | 1 | 0.0411 | 0.0411 | 0.17 | 0.706 |
| Ton | 1 | 2.9275 | 2.9275 | 12.27 | 0.039 |
| Toff | 1 | 5.3974 | 5.3974 | 22.61 | 0.018 |
| Pc | 1 | 1.8771 | 1.8771 | 7.86 | 0.068 |
| Ip*Ip | 1 | 0.9894 | 0.9894 | 4.15 | 0.135 |
| Ton*Ton | 1 | 14.3470 | 14.3470 | 60.11 | 0.004 |
| Toff*Toff | 1 | 0.6706 | 0.6706 | 2.81 | 0.192 |
| Ip*Ton | 1 | 0.2140 | 0.2140 | 0.90 | 0.414 |
| Ip*Toff | 1 | 1.8948 | 1.8948 | 7.94 | 0.067 |
| Ip*Pc | 1 | 2.2753 | 2.2753 | 9.53 | 0.054 |
| Ton*Toff | 1 | 12.6146 | 12.6146 | 52.85 | 0.005 |
| Ton*Pc | 1 | 0.0550 | 0.0550 | 0.23 | 0.664 |
| Error | 3 | 0.7160 | 0.2387 | | |
| Total | 15 | 88.1557 | | | |

Table 6 shows verification of the tests results for MRR. To evaluate the accuracy of the suggested model, predicted MRR and experimented MRR values for few runs were recorded. The predicted values are compared with the experimented values and a good agreement is noticed between them.

Table 6. Verification of test result for MRR.

| Exp Run | Predicted Value | Experimented Value |
|---|---|---|
| 1 | 1.8657 | 1.84104 |
| 4 | 1.9218 | 1.84502 |
| 5 | 2.1106 | 1.90730 |
| 8 | 2.8326 | 2.75116 |
| 10 | 4.2979 | 4.04240 |
| 11 | 5.8985 | 5.59220 |
| 14 | 8.4205 | 8.54270 |
| 15 | 9.7554 | 9.59580 |

### *Taguchi Analysis for SR*

It can be seen that surface roughness initially increases with the increase in discharge current. The increased discharge energy develops a larger crater, resulting a higher surface roughness on the work material. Surface roughness increases first with pulse on time between 100-150 µs and then start decreasing with more increase in pulse on time between the range 150-250 µs. As the pulse off time is reduced, there is increment in number of discharges which causes reduction in surface accuracy, hence initial scaling down in SR recorded with increasing pulse off time from 20-80 µs. Then with further addition in pulse off time to 110 µs, surface roughness increases. Powder concentration plays an important role in improving surface quality. SR decreases in the existence of nano powder particles during machining when compared to machining without powder. 14.02% reduction in surface roughness is observed with powder mixed dielectric.

Table 7 include ranks for input factors that indicate discharge current with highest contribution followed by powder concentration as second important factor. Third significant factor is pulse off time and least significant one being pulse on time for reduced SR.

Table 7. Response table for means on SR.

| Level | Ip | Ton | Toff | Pc |
|---|---|---|---|---|
| 1 | 5.350 | 6.189 | 6.230 | 6.714 |
| 2 | 6.170 | 6.428 | 6.164 | 5.773 |
| 3 | 6.461 | 6.306 | 6.094 | |
| 4 | 6.991 | 6.050 | 6.485 | |
| Delta | 1.641 | 0.377 | 0.391 | 0.941 |
| Rank | 1 | 4 | 3 | 2 |

### *REGRESSION MODEL FOR SR*

From experimental results of SR the general second order model is suggested to predict the surface roughness over the experimental region and can be expressed as Eqn. (4.2).

$$SR = 1.13 + 1.107\,Ip + 0.0140\,Ton - 0.0583\,Toff + 2.941\,Pc - 0.0725\,Ip*Ip - 0.000050\,Ton*Ton + 0.000127\,Toff*Toff + 0.00080\,Ip*Ton + 0.00659\,Ip*Toff - 0.471\,Ip*Pc + 0.000014\,Ton*Toff - 0.00445\,Ton*Pc. \quad (4.2)$$

To evaluate the significance of the suggested prediction model towards surface roughness, analysis of variance (ANOVA) was performed. From Table 8, as the probability values (P) for the regression term were obtained to be 0.012 which is less than 0.05, that states that quadratic regression model has significant contributions towards the response output SR.

For this experiment the R-sq value show that the predictors describe 98.98 % of the response variation and adjusted R-sq for the number of predictors in the model is 94.90 %, both values indicate that the data are fitted well.

Table 8. Analysis of Variance for regression on SR.

| Source | DF | Adj SS | Adj MS | F-Value | P-Value |
|---|---|---|---|---|---|
| **Regression** | 12 | 10.3489 | 0.862407 | 24.26 | **0.012** |
| Ip | 1 | 0.0878 | 0.087795 | 2.47 | 0.706 |
| Ton | 1 | 0.0390 | 0.039047 | 1.10 | 0.039 |
| Toff | 1 | 0.2380 | 0.238019 | 6.69 | 0.018 |
| Pc | 1 | 0.3529 | 0.352854 | 9.92 | 0.068 |
| Ip*Ip | 1 | 0.0841 | 0.084100 | 2.37 | 0.135 |
| Ton*Ton | 1 | 0.2450 | 0.245025 | 6.89 | 0.004 |
| Toff*Toff | 1 | 0.2093 | 0.209306 | 5.89 | 0.192 |
| Ip*Ton | 1 | 0.0076 | 0.007600 | 0.21 | 0.414 |
| Ip*Toff | 1 | 0.1635 | 0.163549 | 4.60 | 0.067 |
| Ip*Pc | 1 | 0.4442 | 0.444153 | 12.49 | 0.054 |
| Ton*Toff | 1 | 0.0041 | 0.004130 | 0.12 | 0.005 |
| Ton*Pc | 1 | 0.2073 | 0.207330 | 5.83 | 0.664 |
| Error | 3 | 0.1067 | 0.035552 | | |
| Total | 15 | 10.4555 | | | |

Table 9 shows verification of the tests results for SR. To evaluate the accuracy of the suggested model, predicted MRR and experimented MRR values for few runs were recorded. The predicted values are compared with the experimented values and a good agreement is noticed between them.

Table 9. Verification of test result for SR.

| Exp Run | Predicted Value | Experimented Value |
|---|---|---|
| 1 | 5.7243 | 5.675 |
| 4 | 4.8342 | 4.955 |
| 5 | 5.6615 | 5.750 |
| 8 | 6.329 | 6.375 |
| 10 | 7.5705 | 7.725 |
| 11 | 5.8639 | 5.935 |
| 14 | 6.3134 | 6.295 |
| 15 | 7.6045 | 7.655 |

### *Multi-Objective Optimization by Grey Relational Analysis (GRA)*

The calculated value of normalised MRR and SR are presented in Table 10. The response table for grey relational grade with their ranks have been demonstrated in Table 11. According to GRG rules, all the experimental run is related to higher is better criteria. The higher grey relational grade represents first rank and indicate the corresponding experimental result is closer to the ideally normalized value. From Table 4.12, the highest value of GRG is 0.67712 with rank 1 indicates that "experiment number 4" is the optimal combination of EDM parameters to produce high MRR with minimum surface roughness during machining.

Table 10. Normalised value for MRR and SR.

| Exp No. | MRR (mm3/min) | Normalised MRR (mm3/min) | SR (µm) | Normalised SR (µm) |
|---|---|---|---|---|
| 1 | 1.84104 | 0.08801 | 5.675 | 0.74007 |
| 2 | 1.09270 | 0.00 | 5.715 | 0.72563 |
| 3 | 2.43960 | 0.15840 | 5.055 | 0.96390 |
| 4 | 1.84502 | 0.08848 | 4.955 | 1.00 |
| 5 | 1.90730 | 0.09580 | 5.750 | 0.71300 |
| 6 | 5.91260 | 0.56684 | 5.975 | 0.63177 |
| 7 | 2.85680 | 0.20747 | 6.580 | 0.41336 |
| 8 | 2.75116 | 0.19504 | 6.375 | 0.48736 |
| 9 | 2.80030 | 0.20082 | 6.650 | 0.38809 |
| 10 | 4.04240 | 0.34690 | 7.725 | 0.00 |
| 11 | 5.59220 | 0.52916 | 5.935 | 0.64621 |
| 12 | 4.60759 | 0.41337 | 5.535 | 0.79061 |
| 13 | 3.50370 | 0.28354 | 6.680 | 0.37726 |
| 14 | 8.54270 | 0.87615 | 6.295 | 0.51642 |
| 15 | 9.59580 | 1.00 | 7.655 | 0.02527 |
| 16 | 5.22811 | 0.48634 | 7.335 | 0.14079 |

Table 12 shows response table on GRG. The optimum input parameter setting for performance are calculated as Ip = 5 A, Ton= 200 µs, Toff= 50 µs and Pc= 1 g/L.
ANOVA is performed to identify the significant parameters with percent contribution on GRG. The results are given in Table 13.

Table 11. Value and Rank for GRG.

| Exp No | GRG | Rank |
|---|---|---|
| 1 | 0.50604 | 8 |
| 2 | 0.48951 | 10 |
| 3 | 0.65268 | 4 |
| **4** | **0.67712** | **1** |
| 5 | 0.49570 | 9 |
| 6 | 0.55585 | 6 |
| 7 | 0.42348 | 14 |
| 8 | 0.43846 | 11 |
| 9 | 0.41727 | 15 |
| 10 | 0.38347 | 16 |
| 11 | 0.55032 | 7 |
| 12 | 0.58248 | 5 |
| 13 | 0.42819 | 13 |
| 14 | 0.65491 | 3 |
| 15 | 0.66953 | 2 |
| 16 | 0.43056 | 12 |

A validation experiment test has been performed to confirm the influences of the optimum input parameters on multiple response characteristics. To demonstrate the method of expressing the quality improvement, the optimum machining factors for confirmatory experiment were considered as Ip= 5A, Ton= 200µs, Toff= 50µs and Pc= 1g/l. The results of the confirmatory experiments at the optimal settings of process parameters for MRR and SR are presented in Table 4.14.

Table 12. Response table for means on GRG.

| Level | Ip | Ton | Toff | Pc |
|---|---|---|---|---|
| 1 | **0.5813** | 0.4618 | 0.5107 | 0.4698 |
| 2 | 0.4784 | 0.5209 | **0.5593** | **0.5747** |
| 3 | 0.4834 | **0.5740** | 0.5408 | |
| 4 | 0.5458 | 0.5322 | 0.4781 | |
| Optimum | 1 | 3 | 2 | 2 |
| Delta | 0.1030 | 0.1122 | 0.0812 | 0.1049 |

Total mean value of GRG is 0.5222.

Table 13. Analysis of Variance for GRG.

| Source | DF | Adj SS | Adj MS | F-Value | P-Value | % Contribution |
|---|---|---|---|---|---|---|
| Ip | 3 | 0.02993 | 0.009975 | 1.34 | 0.362 | 19.67 |
| Ton | 3 | 0.02573 | 0.008576 | 1.15 | 0.415 | 16.91 |
| Toff | 3 | 0.01522 | 0.005072 | 0.68 | 0.601 | 10.00 |
| Pc | 1 | 0.04399 | 0.043988 | 5.89 | 0.060 | 28.90 |
| Error | 5 | 0.03732 | 0.007464 | | | 24.52 |
| Total | 15 | 0.15218 | | | | 100 |

Table 14. Result of Confirmatory experiment.

| Characteristics | Initial input Parameter | Predicted value | Experimental value |
|---|---|---|---|
| Optimum setting | Ip=5A, Ton=250µs, Toff=110µs, Pc=1g/l | | Ip=5A, Ton=200µs, Toff=50µs, Pc=1g/l |
| MRR ($mm^3$/min) | 1.84502 | | 3.30610 |
| SR (µm) | 4.955 | | 5.075 |
| GRG | 0.67712 | 0.7227 | 0.74218 |

With the initial input parameter setting, the experimented outcome of MRR and SR were 1.84502 mm3/min and 4.955 µm, respectively. Machining with the optimum setting of input parameters have improved MRR from 1.84502 mm3/min to 3.30610 mm3/min, whereas SR increases from 4.955 µm to 5.075 µm and there is a growth of GRG from 0.67712 to 0.74218, which is an improvement of 9.6%. The optimum predicted value were verified through confirmatory experiments on optimal input factors and the results seems to be in good agreement with each other. It can be seen that the increase in MRR and SR reported at optimum input parameters are at lower value of discharge current, pulse on time and pulse off time than initial input parameter setting. Thus, it can be agreed that the performance characteristics can be very much improved by This study.

## Conclusion

The machining of AISI D3 steel with copper electrode has been performed by NPMEDM where 1 g/l silver nano powder have been mixed in EDM oil dielectric. Based on the experimental results of the above investigations, the final conclusions have been made.

For desired result of MRR from all of the four selected input parameters, Ip with Ton are two important significant parameters respectively. Toff indicate as third significant factor and Pc as the least significant one with minimum contribution for better MRR. Ip and Ton have direct relation with MRR. From optimisation by Taguchi method, the optimal parameters settings for desired MRR is observed at Ip at 8A, Ton at 200 µs, Toff at 20 µs, and Pc at 1 g/l.

- In case of SR from all of the four selected input parameters, Ip and Pc are two important significant parameters respectively followed by Toff as third significant factor and Ton as the least significant one with minimum contribution for reduced SR. Ip and Pc possess a significant role in making better SQ by reducing surface roughness on machined surface. From optimisation by Taguchi method, the optimal input parameter settings for optimum SR are Ip at 5A, Ton at 250 µs, Toff at 80 µs, and Pc at 1 g/l.

- The multiple objective optimizations for improved MRR and reduced SR using the combination of GRA and Taguchi method approach found that the fourth experiment signifies the optimum combination of EDM parameters for best output responses of MRR and SR. Using Taguchi method, GRG values were analysed for the optimum settings of the input parameters which are Ip at 5A, Ton at 200 µs, Toff at 50 µs, and Pc at 1 g/l. On applying the input parameter values obtained above, output responses have been predicted, that may provide a guideline to pick optimum factors settings for attaining desired MRR and SR during NPMEDM of D3 steel with copper electrode.
- Presence of silver nanoparticles powder significantly affects the performance parameters in NPMEDM. Silver nanoparticles powder in machining contributes to 13.72% improvement in MRR and 14.02% reduction in SR, in contrast to machining without powder. From ANOVA for GRG, it is estimated that Pc have a major effect with a contribution of 28.91% on performance characteristics.

## References

[1] S. Singh, S. Singh, and A. Singh, "Multi objective prediction and optimization of process parameters in the NPMEDM of Nimonic 90 by using Taguchi-grey relational analysis," J. Eng. Res., vol. 10, no. 2, pp. 145-158, May 2022.

[2] R. Chaudhari, J. J. Vora, S. S. Mani Prabu, G. F. Palani, and K. Patel, "Experimental Investigations and Effect of Nano-Powder-Mixed EDM Variables on Performance Measures of Nitinol SMA," Materials, vol. 15, no. 14, p. 4880, Jul. 2022.

[3] H. P. Nguyen, T. L. Banh, and T. N. Van, "Optimization of PMEDM Process Parameters for MRR, TWR, RA, and HV Using Taguchi Method and Grey Relational Analysis for Die Steel Materials," in Decision-Making Models and Applications in Manufacturing Environments, 1st ed., Taylor & Francis, 2023.

[4] B. S. Kumar, M. M. S. Prasad, and K. V. Rao, "Optimization of PMEDM process parameters for B4C and B4C+SiC reinforced AA7075 composites with nano-graphite powder," Mater. Today: Proc., Mar. 2025.

[5] V. Singh, S. K. Singh, and R. K. Shukla, "Multi response optimization of PMEDM of Ti6Al4V using Al2O3 and SiC powder added de-ionized water as dielectric medium using grey relational analysis," SN Appl. Sci., vol. 3, no. 6, p. 696, Jun. 2021.

[6] S. G. Agebo, B. Atici, and S. Y. Ersoy, "Multi-objective optimization of process parameters... using Taguchi-based Gray relational analysis," Arabian J. Sci. Eng., vol. 49, Aug. 2024.

[7] N. T. Nguyen and Q. T. Hoang, "Multi-Objective Optimization of PMEDM Process of 90CrSi Alloy Steel... with Silicon Carbide Powder," Adv. Sci. Technol. Res. J., vol. 15, no. 1, 2021.

[8] S. Sen and S. Bhowmik, "Multi-objective Optimization of Machining Variables During Nano-powder-Mixed µ-EDM of NiTi Shape Memory Alloy," Mater. Perform. Charact., vol. 13, no. 1, Feb. 2024.

[9] R. Chaudhari et al., "Experimental Investigations... Nano-Powder-Mixed EDM... Nitinol SMA," Materials (MDPI), vol. 15, no. 20, p. 7392, Oct. 2022.

[10] M. K. Pradhan, "Estimating the effect of nano-carbon powder in electrical discharge machining of AISI D2 steel using Taguchi-GRA," Mater. Today: Proc., vol. 44, pp. 2780-2785, 2021.

[11] B. Atıcı and S. G. Agebo, "Multi-objective Optimization of Process Parameters...

Additive Manufacturing Method," ResearchGate, Jan. 2025.
[12] S. Santarao et al., "Parametric optimization... AISI D3 Die steel... Grey Relational Analysis," J. Mater. Environ. Sci., vol. 9, no. 10, 2020.
[13] T. Nguyen-Van and H. Phan-Nguyen, "Experimental study on PMEDM... Multi-objective optimization," Measurement, vol. 168, p. 108453, Jan. 2021.
[14] A. Kumar and S. Kumar, "Effect of nano-alumina powder on machining characteristics of Inconel 825 in PMEDM: A multi-objective optimization using Taguchi-Grey Relational Analysis," J. Nanopart. Res., vol. 25, no. 4, p. 112, Apr. 2023.
[15] J. Phimoolchat and A. Muttamara, "Application of Taguchi and Grey Relational Analysis... NPMEDM on Ti6Al4V," J. Manuf. Sci. Eng., vol. 143, no. 8, Aug. 2021.

*ISBN 978-81-973526-0-7*

# OPTIMIZING FUSED FILAMENT FABRICATION: NUMERICAL SIMULATION FOR RESIDUAL STRESS AND DEFORMATION REDUCTION

Jyoti shah*[1], Prashant Johri[2], Mayur P. Singh[1]
*[1]Department of Mechanical Engineering, Galgotias University
[2]Department of Computer Science Engineering, Galgotias University
*mayurpratap@gmail.com

## Abstract

*This study examines how key process parameters affect residual stress and deformation in 3D-printed parts. The main parameters considered are print speed, layer height, bed temperature, and print temperature. The specimens used in this work are ISO 527-2 Type 1A samples made using Fused Filament Fabrication (FFF), which is a material extrusion-based additive manufacturing (AM) process. FFF has great potential for producing polymer parts in an energy-efficient and sustainable way. However, its large-scale use is still limited. This is mainly due to high residual stresses that can cause defects such as warping and thermal cracking. These issues reduce both material efficiency and overall print quality. This study uses numerical simulation and machine learning to study stress and deformation in 3D-printed parts. These methods help to understand how heat and mechanical forces interact during the printing process. This interaction is important for explaining how stresses develop and how parts deform while being printed. The hybrid approach enables accurate prediction of process-induced residual stresses while significantly reducing computational time and resource consumption. The study shows that higher print speed, bed temperature, print temperature, and layer height increase residual stress and distortion in printed parts. In contrast, moderate settings give better results. The best performance was achieved with a print speed of 40 mm/min, a layer height of 0.16 mm, a bed temperature of 60°C, and a print temperature of 190°C. These results help in improving energy-efficient additive manufacturing. They provide a method for choosing process parameters to reduce thermal stress and improve strength.*

## Keywords

Additive Manufacturing, Material Extrusion, Fused Filament Fabrication (FFF), Acrylonitrile butadiene styrene, Print Speed, Layer Height, Built Orientation, Print Temperature, Bed Temperature, Residual Stress, Deformation, Machine Learning.

## Introduction

Additive manufacturing (AM) is an advanced method widely used in industry as a form of 3D printing. The process is computer-controlled and builds three-dimensional objects by depositing material in layers [1]. Unlike traditional manufacturing, which often removes material through cutting or machining, AM adds material layer by layer to form the final product. This approach provides several advantages and has transformed many industries, especially in research and development [2].

One of the main strengths of AM is its ability to produce complex shapes. Such designs are often difficult or costly to make using conventional manufacturing methods [3]. This benefit is especially useful in biomedical and aerospace fields, where lightweight and intricate parts are needed. Another key advantage is rapid prototyping [4].

AM also supports high customization. In the medical field, for instance, it enables the creation of patient-specific prosthetics and implants. This level of personalization helps improve treatment results and patient recovery [5].

Many studies have explored different AM processes through experiments. For example, Parteli and Poschel [6] created a numerical tool to simulate how powder spreads in AM. Cook and Murphy [7] emphasized the need for accurate computer models in metal AM to ensure quality and performance. Lindgren et al. [8] applied Computational Welding Mechanics (CWM) techniques to model AM. Their research examined how materials behave and change in structure during the process. Using Alloy 718 and Ti-6Al-4V, they observed that repeated heating and cooling cause phase changes in Ti-6Al-4V [9]. Shiyan Jayanath and Ajit Achuthan [10] introduced a new Finite Element (FE) method that updates geometry at regular intervals. Turner et al. [11] developed the Exascale AM simulation platform, which links different physics-based models to study melt pool movement, simulate thermal and mechanical behavior, and predict material microstructure and properties. Talagani et al. [12] proposed another simulation method using Finite Element Analysis (FEA) to study large-scale AM processes through multi-scale damage and fracture modeling. Although many studies focus on optimizing process parameters in AM, there is limited research on simulating polymer-based AM. The present study aims to address this gap. It uses machine learning techniques to estimate process parameters accurately. A thermo-mechanical finite element model is developed, where elements are activated step by step to simulate printing. Key parameters such as print speed, temperature, bed temperature, orientation, and layer height are varied. The model predicts temperature distribution, thermal stress, and part deformation during 3D printing. The material model also includes temperature-dependent properties of ABS. Finally, the study compares thermal stress and deformation results under different processing conditions.

## Methodology

This section describes the methods and materials used to simulate the Fused Filament Fabrication (FFF) process. A thermo-mechanical model was developed to study how different process settings affect distortion and residual stress. The main factors considered in this study are orientation, layer height, print speed, print temperature, and bed temperature. These parameters directly influence the amount of stress and warping in the printed part. The simulation design helps to understand how each input parameter affects the process outcome. It also allows the study of how different responses are related to one another.

In this study, Digimat software was used for numerical simulation. The finite element (FE) model of the structure was divided into 35,890 voxels, as shown in Figure 1. A mesh convergence analysis was carried out to ensure accuracy. Based on this analysis, a mesh size of 0.65 mm was chosen

Figure 1. Voxel model for additive manufacturing simulation.

Table 1 presents an overview of the testing parameters used in this study. The orientation,

*ISBN 978-81-973526-0-7*

layer height, print speed, print temperature, and bed temperature were carefully changed across three different levels. The orientation was tested in two directions. In Orientation 1, the side with the largest surface area faced the print bed, as shown in Figure 2. In Orientation 2, the side with the second largest surface area faced the bed, as shown in Figure 3.
The layer thickness was adjusted in small steps of 0.05 mm. It ranged from 0.08 mm to 0.28 mm during the tests.

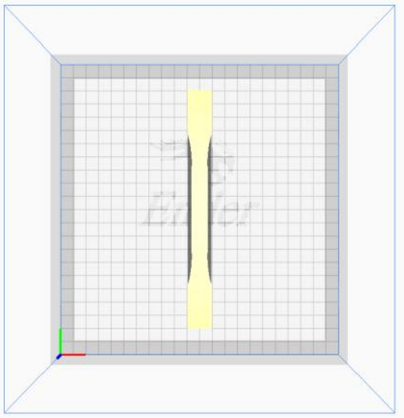

Figure 2. Orientation 1 of Specimen on Print Bed visualized from Top View.

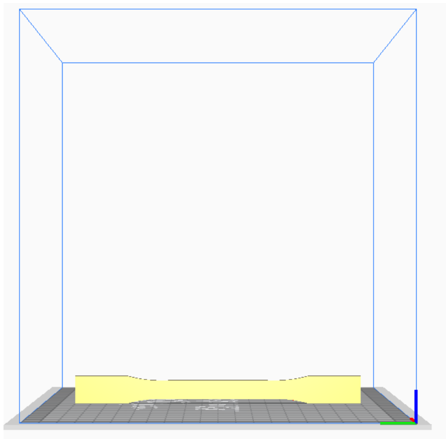

Figure 3. Orientation 2 of Specimen on Print Bed visualized from Side View.

Table 1. Testing Parameters for Orientation 1&2.

| Level | Print Speed | Layer Height | Bed Temperature | Print Temperature |
|---|---|---|---|---|
| 1 | *20* | *0.08* | *40* | *150* |
| 2 | *30* | *0.12* | *50* | *170* |
| 3 | *40* | *0.16* | *60* | *190* |
| 4 | *50* | *0.20* | *70* | *210* |
| 5 | *60* | *0.24* | *80* | *230* |
| 6 | *70* | *0.28* | *90* | *250* |

## Materials

ABS has a good balance of strength, flexibility, and thermal stability (Table-2). These properties make it a suitable material for process parameter optimization. It requires higher printing temperatures, usually between 220°C and 250°C. A heated bed is also needed to

*ISBN 978-81-973526-0-7*

prevent warping and to ensure proper layer adhesion during printing.

Table 2. ABS Specifications.

| Material | Diameter | Young's modulus | Poissons Ratio |
|---|---|---|---|
| Acrylonitrile butadiene styrene (ABS) | 1.75mm | 1.9–2.5 GPa | 0.37 |

## Result and Discussion

Residual stress and warpage are important factors that strongly affect the quality and performance of 3D-printed parts. They also influence the structural integrity of the components. A clear understanding of how residual stress and warpage form is important for improving additive manufacturing (AM) processes. This understanding allows better control of process parameters. It also helps in reducing printing defects. As a result, the reliability and performance of printed parts can be improved.

### *Influence of Process Parameters on Residual Stress*

Residual stress is an important factor that affects the quality and performance of 3D-printed parts. These stresses develop during the printing process. They occur because the material layers cool and solidify at different rates. This uneven cooling creates internal stresses within the printed part.

### *Layer Height*

Layer height significantly influences the residual stress within printed specimens. Variations in layer height can affect thermal gradients and, consequently, the development of residual stresses. Lower layer heights tend to reduce thermal stress due to smaller temperature differentials between layers.

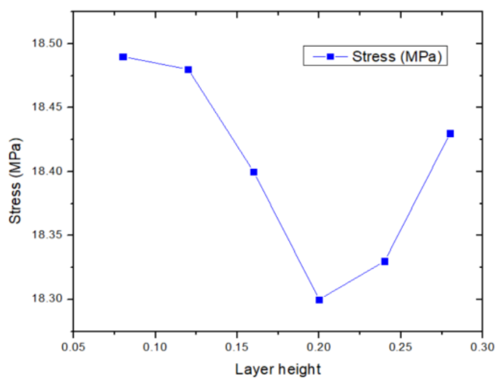


Figure 4. Layer Height vs Residual Stress for Orientation 1.

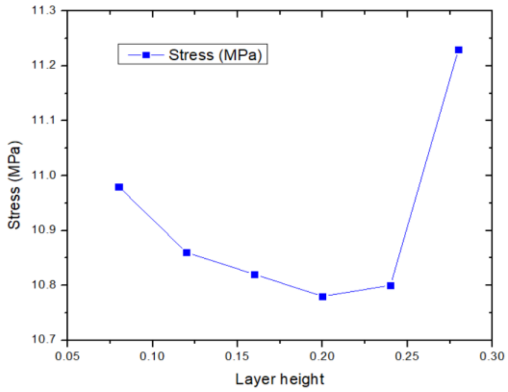


Figure 5. Layer Height vs Residual Stress for Orientation 2.

For orientation 1, figure 4, the residual stress is at its minimum when the layer height is set at 0.2 mm,

*ISBN 978-81-973526-0-7*

whereas it reaches its maximum at 0.08 mm. The change in residual stress is relatively minor when transitioning from a 0.08 mm layer height to a 0.12 mm layer height, compared to the more significant stress variation observed when progressing from a 0.16 mm layer height to a 0.2 mm layer height. For orientation 2, figure 5, the minimum residual stress is observed at a layer height of 0.2 mm, while the maximum is observed at 0.28 mm. The change in residual stress is relatively minor when transitioning from a 0.16 mm layer height to a 0.2 mm layer height, as opposed to the more significant stress variation observed when progressing from a 0.24 mm layer height to a 0.28 mm layer height.

### *Print Speed*

Changes in print speed influence the cooling rate, thereby impacting the magnitude of residual stresses. Slower feed rates allow for more controlled cooling, which reduces the levels of residual stress.

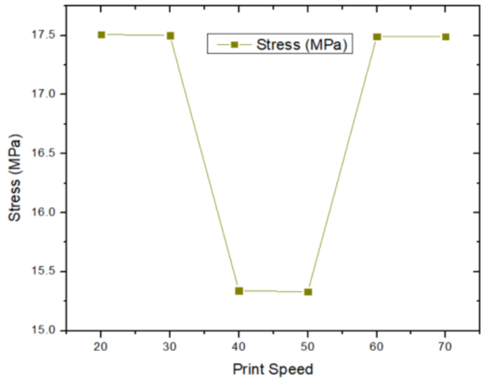


Figure 6. Print Speed vs Residual Stress for Orientation 1.

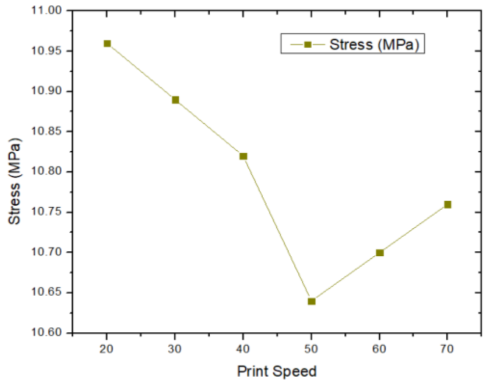


Figure 7. Print Speed vs Residual Stress for Orientation 2.

Based on the figure 6 for orientation 1, the minimum residual stress is recorded at a speed of 40 mm/min, while the maximum residual stress is observed at 20 mm/min. While for Orientation 2, according to the figure 7, the minimum residual stress is recorded at a speed of 50 mm/min, while the maximum residual stress is observed at 20 mm/min.

### *Bed Temperature*

Changes in bed temperature affect the distribution of residual stresses within the specimens. Specimens subjected to different bed temperatures exhibit distinct stress patterns, which influence their overall mechanical behavior.

As observed in the figure 8, for orientation 1, it is evident that specimens subjected to different bed temperatures exhibit distinct patterns of residual stress. Additionally, for orientation 2, as shown in the figure 9, specimens with a bed temperature of 40 degrees exhibit superior inter-layer adhesion and reduced residual stress compared to those set at 60 degrees.

ISBN 978-81-973526-0-7

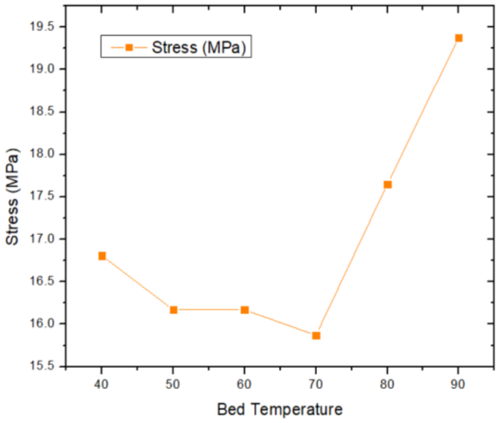

Figure 8. Bed Temperature vs Residual Stress for Orientation 1.

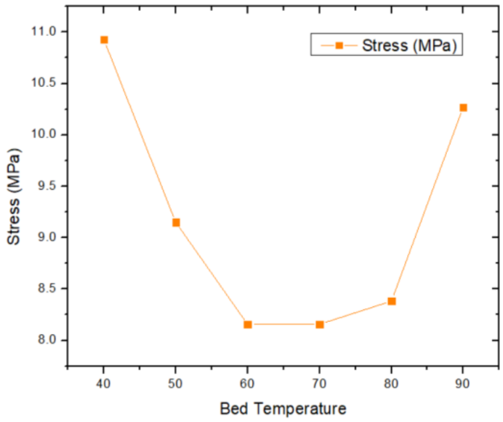

Figure 9. Bed Temperature vs Residual Stress for Orientation 2.

## *Print Temperature*

Print Temperature or nozzle temperature has a significant impact on residual stress. A high Print Temperature causes uneven or improper material deposition, leading to voids, whereas an ideal print temperature enhances material fusion, reducing stress. According to the figure 10 for orientation 1, the residual stress is at its lowest at 190 degrees, while it reaches its highest at 250 degrees. The variation in residual stress is minimal when transitioning from 130 to 150 degrees but is most pronounced when moving from 150 to 170 degrees. Additionally, the residual stresses exhibit greater variability at higher speeds.

In the figure 11 for orientation 2, the residual stress is at its lowest at 210 degrees, whereas it peaks at 250 degrees. The variation in residual stress is minimal when transitioning from 230 to 250 degrees, but it is most significant when moving from 210 to 230 degrees.

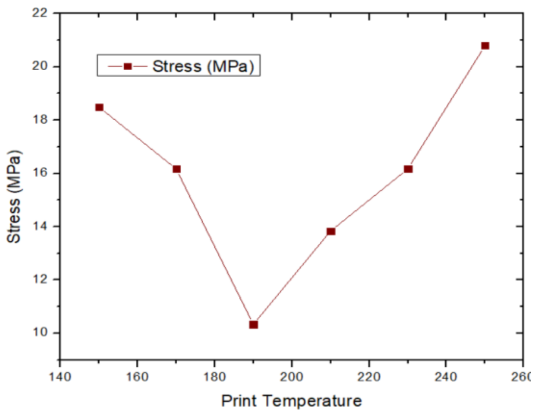

Figure 10. Print Temperature vs Residual Stress for Orientation 1.

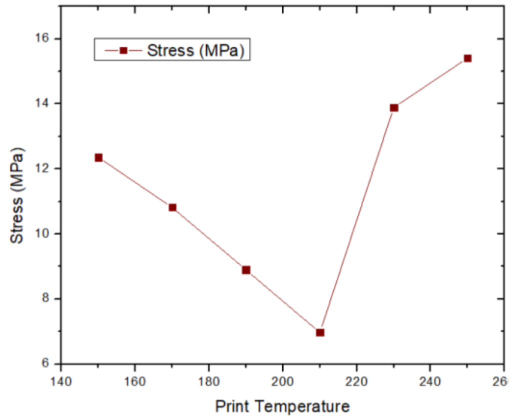


Figure 11. Print Temperature vs Residual Stress for Orientation 2.

## Effect of Orientation on Process Parameters

This section provides a detailed comparison between Orientation 1 and Orientation 2. It examines their process parameters and how they affect residual stress and deformation. The orientation of a 3D-printed model plays an important role in determining its mechanical properties. It also influences the surface finish and dimensional accuracy of the printed part. The dimensional accuracy of a print can varies based on its orientation, with flat prints generally being more accurate. Print orientation also affects the need for support structures, with overhangs and complex geometries requiring more or less support depending on orientation. Most importantly, print orientation can influence print time and material usage.

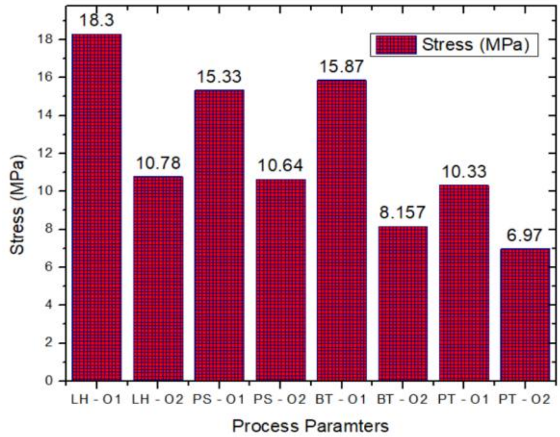


Figure 12. Different Process Parameters in both Orientations varied with Residual Stress.

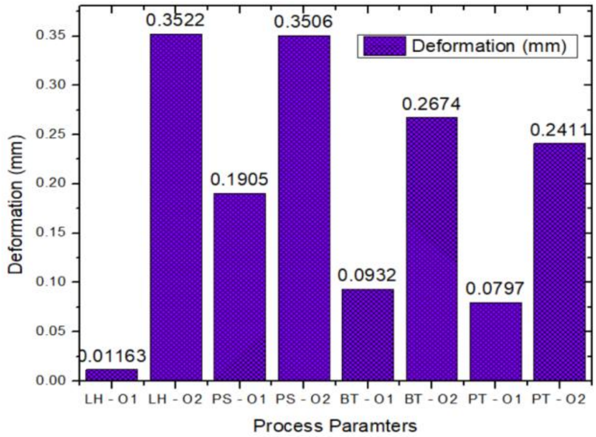


Figure 13. Different Process Parameters in both Orientations varied with Deformation.

The best result or least deformation of process parameters was noted in the parametric study of process parameters. Comparing the results from orientation 1 and orientation 2, Figure 12, it was found that orientation 2 consistently exhibited superior results with the least residual stresses overall. The most significant difference was observed in bed temperature, where the residual stresses almost doubled from 8.15 MPa to 15.87 MPa between the two orientations. In contrast, the least significant difference was noted in print speed. These findings underscore the importance of considering print orientation in additive manufacturing processes to minimize residual stresses and optimize part quality.

The parametric investigation of process parameters revealed that orientation 1, Figure 13, consistently yielded the most favorable outcomes with the least deformation. A clear difference was observed between Orientation 1 and Orientation 2. This difference was most noticeable in the residual stress values. Orientation 1 showed better overall performance compared to Orientation 2. The largest variation occurred in layer height. In this case, the residual stress increased sharply from 0.01163 mm to 35.22 mm between the two orientations. In contrast, the change in print speed had a smaller effect on residual stress.

This suggests that the choice of orientation should be based on the specific objective of the print. If the goal is to achieve precise objects without dimensional deformities, orientation 1 may be preferred. On the other hand, if the objective is to produce objects that can withstand loads or fatigue, orientation 2 might be the more suitable choice.

## Conclusion

This study shows how process parameters affect residual stress and deformation. It also explains how these factors influence the performance of the Fused Filament Fabrication (FFF) process. The analysis was carried out using ISO 527-2 Type 1A specimens. The research examined key variables such as print speed, layer height, bed temperature, and print temperature. It explored how these factors interact with each other. The study also showed how these interactions influence residual stress and deformation in the printed parts.

The results highlight the importance of selecting suitable process parameters. Proper optimization helps improve print quality and reduce defects. In addition, machine learning techniques were used to predict residual stress and deformation. These techniques also helped in reducing the overall computational time. The study showed that higher print speeds, bed temperatures, print temperatures, and larger layer heights led to greater residual stress, distortion, and porosity. In contrast, moderate parameter values produced better results. The best performance was achieved at a print speed of 40 mm/min, a layer height of 0.16 mm, a bed temperature of 60°C, and a print temperature of 190°C.

## References

[1] Bikas, P. Stavropoulos, and G. Chryssolouris, “Additive manufacturing methods and modelling approaches: a critical review,” Int. J. Adv. Manuf. Technol., vol. 83, no. 1, pp. 389–405, 2016, doi: 10.1007/s00170-015-7576-2.

[2] S. H. Huang, P. Liu, A. Mokasdar, and L. Hou, “Additive manufacturing and its societal impact: a literature review,” Int. J. Adv. Manuf. Technol., vol. 67, no. 5, pp. 1191–1203, 2013, doi: 10.1007/s00170-012-4558-5.

[3] X. Song et al., “Advances in additive manufacturing process simulation: Residual stresses and distortion predictions in complex metallic components,” Mater. Des., vol. 193, p. 108779, 2020, doi: https://doi.org/10.1016/j.matdes.2020.108779.

[4] M. Rinaldi, M. Caterino, P. Manco, M. Fera, and R. Macchiaroli, “The impact of Additive Manufacturing on Supply Chain design: a simulation study,” Procedia Comput. Sci., vol. 180, pp. 446–455, 2021, doi: https://doi.org/10.1016/j.procs.2021.01.261.

[5] M. M. Francois et al., “Modeling of additive manufacturing processes for metals: Challenges and opportunities,” Curr. Opin. Solid State Mater. Sci., vol. 21, no. 4, pp. 198–206, 2017, doi: https://doi.org/10.1016/j.cossms.2016.12.001.
[6] E. J. R. Parteli and T. Pöschel, “Particle-based simulation of powder application in additive manufacturing,” Powder Technol., vol. 288, pp. 96–102, 2016, doi: https://doi.org/10.1016/j.powtec.2015.10.035.
[7] P. S. Cook and A. B. Murphy, “Simulation of melt pool behaviour during additive manufacturing: Underlying physics and progress,” Addit. Manuf., vol. 31, p. 100909, 2020, doi: https://doi.org/10.1016/j.addma.2019.100909.
[8] L.-E. Lindgren, A. Lundbäck, M. Fisk, R. Pederson, and J. Andersson, “Simulation of additive manufacturing using coupled constitutive and microstructure models,” Addit. Manuf., vol. 12, pp. 144–158, 2016, doi: https://doi.org/10.1016/j.addma.2016.05.005.
[9] J. Baiges, M. Chiumenti, C. A. Moreira, M. Cervera, and R. Codina, “An adaptive Finite Element strategy for the numerical simulation of additive manufacturing processes,” Addit. Manuf., vol. 37, p. 101650, 2021, doi: https://doi.org/10.1016/j.addma.2020.101650.
[10] S. Jayanath and A. Achuthan, “A Computationally Efficient Finite Element Framework to Simulate Additive Manufacturing Processes,” J. Manuf. Sci. Eng., vol. 140, no. 4, Feb. 2018, doi: 10.1115/1.4039092.
[11] J. A. Turner et al., “ExaAM: Metal additive manufacturing simulation at the fidelity of the microstructure,” Int. J. High Perform. Comput. Appl., vol. 36, no. 1, pp. 13–39, Jan. 2022, doi: 10.1177/10943420211042558.
[12] M. R. Talagani, S. Dormohammadi, R. Dutton, C. Godines, H. Baid, and F. Abdi, “Unique Polyamide,” no. July, pp. 27–36, 2015.

# BARRIERS TO THE ADOPTION OF B2B TECHNOLOGIES IN CUSTOMER-DRIVEN SUPPLY CHAINS: AN ISM–MICMAC APPROACH

Nitin Kumar Chauhan*[1], Vikas Kumar[1], Sandhya Dixit[1]
*[1]J.C. Bose University of Science & Technology, YMCA, Faridabad, Haryana, India
* nitinchauhan@jssaten.ac.in

**Abstract:**
*This study develops a structural framework to analyse the barriers affecting the integration of business-to-business (B2B) technologies in e-commerce-enabled customer-driven supply chains (CDSC). RFID, EDI, point-of-sale systems, Vendor Managed Inventory (VMI), and Collaborative Planning, Forecasting, and Replenishment (CPFR) are examples of B2B technologies that enable supply chain partners to coordinate and communicate information in real time. However, organisations face multiple challenges that hinder effective adoption. In this study ten major barriers for adoption of B2B technologies were identified through literature review and expert consultation. These barriers were analysed by using Interpretive Structural Modelling (ISM) technique to develop a hierarchical structural model. Further the barriers are classified using MICMAC analysis into four groups based on their driving and dependence power. The findings from the study indicate that Lack of financial resources, high cost of implementation and inappropriate organisational are the most influential driving barriers. The study provides a prioritised roadmap to support managers and policymakers in systematically addressing these barriers.*

**Keywords:** B2B Technology, Customer-driven, ISM, Supply Chain

## Introduction:

Supply chains have evolved, as per requirement of current competitive and dynamic business environment, from traditional product-centric systems to more responsive and customer-oriented networks. Modern supply chain and customer management practices are primarily focusing to the changing needs of the final consumer rather than focusing solely on cost efficiency and product quality. This shift has led to the emergence of customer-driven supply chains (CDSC), where demand signals from end users play a crucial role in shaping production, distribution, and replenishment decisions (Hines, 2024). Few big and leading organizations have already demonstrated this transformation. For instance, Campbell Soup Company shifted its strategic focus from cost reduction to customer-centric operations and aligned their supply chain with the needs of business clients and end consumers. In the same way, Procter & Gamble has transformed its conventional manufacturing-driven supply chain into one that is customer-focused and offers a higher level of responsiveness to satisfy customer preferences. These shifts emphasise how crucial real-time information exchange, responsiveness, agility, and teamwork are to supply chain management.

To enable this transformation, firms are increasingly adopting advanced information technologies, particularly business-to-business (B2B) technologies (Bonnin & Alfonso, 2019). With the help of these technologies' integration and coordination among supply chain partners is improved. Technologies such as Vendor Managed Inventory (VMI), Collaborative Planning, Forecasting and Replenishment (CPFR) (Gomes, 2022), Point of Sale (POS) systems, Radio Frequency Identification (RFID), Electronic Data Interchange (EDI), (Jha et al., 2025) and internet-based platforms facilitate real-time information exchange which enhance supply chain visibility and enable synchronized decision making in supply chain. These technologies are considered critical enablers of digital supply chains and Industry 4.0 initiatives (Agrawal et al., 2020), which significantly improves operational efficiency and responsiveness.

Despite these advantages, the adoption of B2B technologies in e-commerce-enabled supply chains remains a complex challenge. Organizations face multiple barriers like technological complexity, lack of infrastructure, financial limitations and organizational structure (Asare et al., 2016). Recent studies have highlighted that barriers such as lack of leadership commitment, inadequate digital strategy and insufficient investment planning offer hinderance to digital supply chain transformation. Additionally, factors such as lack of knowledge, unclear benefits, and negative perceptions toward new technologies further obstruct the adoption efforts (Mouzakitis & Askounis, 2010).

Moreover, inter-organizational challenges (Hollmann et al., 2015) such as lack of trust, poor collaboration, and limited information sharing among supply chain partners also restricts an effective implementation of B2B technologies. Supply chain visibility and data-sharing barriers remain persistent issues, particularly in digitally integrated environments, where coordination among multiple stakeholders is essential. The adoption landscape of emerging technologies like blockchain and IoT become more complex due to barriers related technological readiness, organizational capabilities, and regulatory uncertainty.

Although prior research has examined various barriers to digital technology adoption in supply chains, but there is still a lack of comprehensive understanding regarding the interrelationships among these barriers (Vidani, 2024). This research studies the interrelationships among these barriers in the context of e-commerce-enabled customer-driven supply chains. Interpretive Structural Modelling (ISM) and MICMAC analysis have been widely applied in recent studies to examine hierarchical relationships and classify barriers based on their driving and dependence power which provides a broader understanding into complex systems.

Therefore, this study aims to identify and examine the important barriers affecting the integration of B2B technologies in e-commerce-enabled customer-driven supply chains. This study develops a structural framework to examine the interdependencies among barriers and to find the most influential factors by applying ISM and MICMAC analysis. The findings of this research are expected to provide a systematic roadmap for managers and policymakers to prioritize critical barriers and facilitate successful adoption of B2B technologies, thereby enhancing supply chain integration, responsiveness, and overall performance.

## Literature Review

Understanding customer needs and experiences throughout the product lifecycle is essential to digital transformation. The emergence of CDSC reflects a shift from traditional forecast-driven models to demand-responsive systems, in which real-time customer data guides operational decisions. According to the study (Chen & Lin, 2019), 74% of people on the world are connected to the internet, and around fifty percent of them engage with social media regularly. Additionally, a lot of individuals shop online using the internet. Since internet penetration and digital platform are rapidly expanding and supply chain are influenced by online consumer behaviour, hence it accelerates the adoption of e-commerce-enabled supply chain practices (Chen & Lin, 2019). Recent studies also highlight that digital technologies such as Vendor Managed Inventory (VMI), Collaborative Planning, Forecasting and Replenishment (CPFR), Electronic Data Interchange (EDI), and Radio Frequency Identification (RFID) play a crucial role in enabling CDSCs for enhancing visibility, integration, and collaboration among supply chain partners (Ivanov & Dolgui, 2020). These technologies are key enablers of agility and responsiveness in e-commerce CDSC, enabling businesses to react to changing economic circumstances in an efficient manner.

Despite these advantages, the adoption of B2B technologies remains limited due to several barriers which can be categorized into technological, organizational, financial, and inter-organizational dimensions. Technological barriers include system incompatibility, lack of standardization, and cybersecurity concerns (Kamble et al., 2020). Organizational challenges like lack of skilled workforce, resistance to change, and inappropriate organizational structure significantly affect adoption decisions (Bag et al., 2021). Financial limitation which includes high implementation costs and uncertain return on investment, further produce hinderance towards the technology adoption, especially for small and medium enterprises (SMEs) (Chauhan et al., 2023a).

Inter-organizational barriers are particularly critical in B2B environments. Lack of trust, fear of information sharing, and poor coordination among partners put a negative impact on the effectiveness of digital integration (Chauhan et al., 2023b). Additionally, environmental uncertainty, including market volatility and regulatory changes, also creates further challenges in adopting new technologies (Ivanov & Dolgui, 2020) .

Despite the fact that earlier research has found a number of obstacles, thorough studies are still lacking in to find the interrelationships among these barriers and their hierarchical influence, particularly in the context of e-commerce-enabled customer-driven supply chains. Most studies focus on individual factors rather than examining how these barriers interact and influence one another.

In order to fill this gap, the current study identifies key barriers through literature review and expert consultation and applies Interpretive Structural Modelling (ISM) and MICMAC analysis to develop a structured framework. This technique facilitates in comprehending the dependence and driving forces of barriers, thereby enabling prioritization and effective decision-making. Based on the available research and the opinions of experts, this article has identified 10 main obstacles to customer-driven supply chains in B2B technology which are lack of trust between the customer, Lack of financial resources, improper organisational structure, partner capacity, rigid business procedures, absence of information sharing anxiety, environmental uncertainties, reluctance to adoption of new technology, costly implementation and ongoing costs. A quick view of these barriers is tabulated in table 1.

Table 1: Barriers to the Adoption of B2B Technologies

| S.N. | Barriers | Category | References |
|---|---|---|---|
| 1 | Lack of Financial Resources | *Financial Barriers:* Insufficient availability of funds to invest in B2B technologies and supporting infrastructure. | (Bag et al., 2021), (Chauhan et al., 2023a) |
| 2 | High Implementation and Operational Costs | *Financial Barriers:* High initial setup and ongoing maintenance costs associated with adopting and managing digital technologies. | (Choudhury et al., 2021), (Chen & Lin, 2019) |
| 3 | Inappropriate Organisational Structure | *Organizational Barriers:* Rigid or misaligned organizational hierarchy that hinders effective decision-making and technology integration. | (Chauhan et al., 2023a), (Fawcett et al., 2015) |
| 4 | Inflexible Business Processes | *Organizational Barriers:* Existing processes are not adaptable to digital transformation and integration requirements. | (Gosain et al., 2004), (Ramesh et al., 2010), (Shukla et al., 2012) |
| 5 | Resistance to Adoption of New Technology | *Organizational Barriers:* Reluctance of employees and management to accept and implement new digital systems. | (Gardas et al., 2017), (Ramesh et al., 2010) |

*ISBN 978-81-973526-0-7*

| | | | |
|---|---|---|---|
| 6 | Lack of Digital Skills and Expertise | *Technological Barriers:* Shortage of skilled personnel capable of implementing and managing advanced B2B technologies. | (Liboni et al., 2019), (Grover & Goslar, 1993) |
| 7 | Fear of Information Sharing | *Technological Barriers:* Concerns regarding data security, privacy, and misuse while sharing information across partners. | (Sila, 2013), (Panahifar et al., 2015) |
| 8 | Lack of Trust Among Supply Chain Partners | *Inter-Organizational Barriers:* Limited confidence among partners reduces willingness to collaborate and share critical information. | (Westerman et al., 2012), (Madhani, 2019), (Sila, 2013) |
| 9 | Limited Capability of Supply Chain Partners | *Inter-Organizational Barriers:* Inadequate technological or operational capabilities of partners to support integration. | (Sila, 2013), (Liao et al., 2022) |
| 10 | Environmental uncertainty | *Environmental Barriers:* Unpredictable market conditions, regulatory changes, and external disruptions affecting adoption decisions. | (Sia et al., 2004), (Patterson et al., 2003) |

## Research Methodology:

This study employs Interpretive Structural Modelling (ISM) to analyse interrelationships among the identified barriers. MICMAC analysis is further used to classify barriers based on their driving and dependence power. Expert opinions were used to develop the Structural Self-Interaction Matrix (SSIM), which was converted into the Initial Reachability Matrix (IRM) and Final Reachability Matrix (FRM) through transitivity.

***Step 1: Identification and definition of the variables***

The barriers are used in this work as modelling inputs. There are 10 barriers, according to the B2B technology literature already in existence and the opinions of specialists from many fields of business and academics. In table 1, these impediments' descriptions are provided.

***Step 2: Determining the contextual relationship***

Following the selection of the barriers, a large number of academic and industrial experts (who are taking the initiative to digitally transform their supply chains) are questioned in order to discover the contextual relationship between each pair of barriers. In situations when barrier i affects barrier j, the "influence" contextual connection type is selected. Four symbols are used to indicate how two barriers (i and j) relate to one another. “V” denotes the direction of relationship from i to j; “A” denotes the direction of relationship from j to i; “X” indicates a two-way relationship between i and j; and “O” indicates a lack of relationship between two i and j.

***Step 3: formulation of structural self-interaction matrix (SSIM)***

The SSIM, which reflects the pairwise relationship among the detected barriers, is prepared once the contextual link between the obstacles has been established. The SSIM is also discussed with the specialists to secure their approval. The SSIM is shown in table 2.

***Step 4: Development of reachability matrix***

The step is to create an initial access matrix using SSIM. Binary numbers (ie 1s and 0s) for each SSIM member are transformed to form a matrix. Transferability is also tested in this matrix; the matrix shows "if 1$^{st}$ barrier interacts with 2$^{nd}$ barrier" and "2$^{nd}$ barrier interacts with 3$^{rd}$ barrier " then "1$^{st}$ barrier must interact with 3$^{rd}$ barrier". The final reachability matrix (FRM) shown in table 4 is formed after the initial reachability matrix (IRM) shown in table 3 has undergone transformations.

Table 2: Structural Self -Interaction Matrix (SSIM)

| | Factors | F1 | F2 | F3 | F4 | F5 | F6 | F7 | F8 | F9 | F10 |
|---|---|---|---|---|---|---|---|---|---|---|---|
| F1 | Lack of Digital Skills and Expertise (LDSE) | | **O** | **V** | **V** | **V** | **A** | **V** | **A** | **O** | **V** |
| F2 | Inflexible Business Processes (IBP) | | | **A** | **O** | **O** | **O** | **O** | **A** | **O** | **O** |
| F3 | Fear of Information Sharing (FIS) | | | | **X** | **O** | **A** | **V** | **A** | **O** | **O** |
| F4 | Limited Capability of Supply Chain Partners (LCOP) | | | | | **A** | **A** | **V** | **A** | **O** | **A** |
| F5 | Resistance to Adoption of New Technology (RANT) | | | | | | **A** | **V** | **A** | **A** | **A** |
| F6 | High Implementation and Operational Costs (HIOC) | | | | | | | **V** | **V** | **V** | **O** |
| F7 | Environmental uncertainty (EU) | | | | | | | | **A** | **A** | **O** |
| F8 | Lack of Financing (LOF) | | | | | | | | | **V** | **O** |
| F9 | Inappropriate Organisational Structure (IOS) | | | | | | | | | | **V** |
| F10 | Lack of Trust Among Partners (LOTP) | | | | | | | | | | |

***Step 5: Determination of levels by partitioning reachability matrix:***
The final matrix lists the accessibility and background of each question. While the process of reaching a problem has an impact on the problems it affects, the process before it has an impact and a potential impact. Each column with a "1" in the problem line in this study constitutes the problem reached. Therefore, every line with a "1" on the barrier of the observation line is included in the premise set. After that, access points and preset methods are combined to create the interface. Level 1 barriers will be used for those who have junction lights and reach the match. In subsequent rounds, barriers from the first stage will be removed. Likewise, the rating continues up to the level of each identified problem, as shown in table 5. The highest position in the hierarchical structure will be at the first level.
***Step 6: Developing the digraph***
The final reachability matrix is combined with the partition levels to create the digraph. The boundaries between them are depicted by nodes, and their connection is shown by arrows. Only the transitive linkages in digraph whose interpretation is important are represented.
***Step 7: Developing the interpretive structural modelling-based model***
By substituting the nodes with the interpretation of the barriers, an ISM for the B2B technological barriers in customer-driven supply chains is created as shown in figure 1.

Table 3: Initial Reachability Matrix (IRM)

| Factors | | F1 | F2 | F3 | F4 | F5 | F6 | F7 | F8 | F9 | F10 | Driving Power |
|---|---|---|---|---|---|---|---|---|---|---|---|---|
| F1 | LDSE | 1 | 0 | 1 | 1 | 1 | 0 | 1 | 0 | 0 | 1 | 6 |
| F2 | IBP | 0 | 1 | 0 | 0 | 0 | 0 | 0 | 0 | 0 | 0 | 1 |
| F3 | FIS | 0 | 1 | 1 | 1 | 0 | 0 | 1 | 0 | 0 | 0 | 4 |
| F4 | LCOP | 0 | 0 | 1 | 1 | 0 | 0 | 1 | 0 | 0 | 0 | 3 |
| F5 | RANT | 0 | 0 | 0 | 1 | 1 | 0 | 1 | 0 | 0 | 0 | 3 |
| F6 | HIOC | 1 | 0 | 1 | 1 | 1 | 1 | 1 | 1 | 1 | 0 | 8 |
| F7 | EU | 0 | 0 | 0 | 0 | 0 | 0 | 1 | 0 | 0 | 0 | 1 |
| F8 | LOF | 1 | 1 | 1 | 1 | 1 | 0 | 1 | 1 | 1 | 0 | 8 |
| F9 | IOS | 0 | 0 | 0 | 0 | 1 | 0 | 1 | 0 | 1 | 1 | 4 |
| F10 | LOTP | 0 | 0 | 0 | 1 | 1 | 0 | 0 | 0 | 0 | 1 | 3 |
| **Dependence Power** | | 3 | 3 | 5 | 7 | 6 | 1 | 8 | 2 | 3 | 3 | |

Table 4: Final Reachability Matrix (FRM)

| Factors | | F1 | F2 | F3 | F4 | F5 | F6 | F7 | F8 | F9 | F10 | Driving Power |
|---|---|---|---|---|---|---|---|---|---|---|---|---|
| F1 | LDSE | 1 | 1* | 1 | 1 | 1 | 0 | 1 | 0 | 0 | 1 | 7 |
| F2 | IBP | 0 | 1 | 0 | 0 | 0 | 0 | 0 | 0 | 0 | 0 | 1 |
| F3 | FIS | 0 | 1 | 1 | 1 | 0 | 0 | 1 | 0 | 0 | 0 | 4 |
| F4 | LCOP | 0 | 1* | 1 | 1 | 0 | 0 | 1 | 0 | 0 | 0 | 4 |
| F5 | RANT | 0 | 1* | 1* | 1 | 1 | 0 | 1 | 0 | 0 | 0 | 5 |
| F6 | HIOC | 1 | 1* | 1 | 1 | 1 | 1 | 1 | 1 | 1 | 1* | 10 |
| F7 | EU | 0 | 0 | 0 | 0 | 0 | 0 | 1 | 0 | 0 | 0 | 1 |
| F8 | LOF | 1 | 1 | 1 | 1 | 1 | 0 | 1 | 1 | 1 | 1* | 9 |
| F9 | IOS | 0 | 1* | 1* | 1* | 1 | 0 | 1 | 0 | 1 | 1 | 7 |
| F10 | LOTP | 0 | 1* | 1* | 1 | 1 | 0 | 1* | 0 | 0 | 1 | 6 |
| **Dependence Power** | | 3 | 9 | 8 | 8 | 6 | 1 | 9 | 2 | 3 | 5 | |

Table 5. Level Partitioning (LP)

| Elements | Reachability Set | Antecedent Set | Intersection Set | Level |
|---|---|---|---|---|
| 1 | 1, | 1, 6, 8, | 1, | 5 |
| 2 | 2, | 1, 2, 3, 4, 5, 6, 8, 9, 10, | 2, | 1 |
| 3 | 3, 4, | 1, 3, 4, 5, 6, 8, 9, 10, | 3, 4, | 2 |
| 4 | 3, 4, | 1, 3, 4, 5, 6, 8, 9, 10, | 3, 4, | 2 |
| 5 | 5, | 1, 5, 6, 8, 9, 10, | 5, | 3 |
| 6 | 6, | 6, | 6, | 7 |
| 7 | 7, | 1, 3, 4, 5, 6, 7, 8, 9, 10, | 7, | 1 |
| 8 | 8, | 6, 8, | 8, | 6 |
| 9 | 9, | 6, 8, 9, | 9, | 5 |
| 10 | 10, | 1, 6, 8, 9, 10, | 10, | 4 |

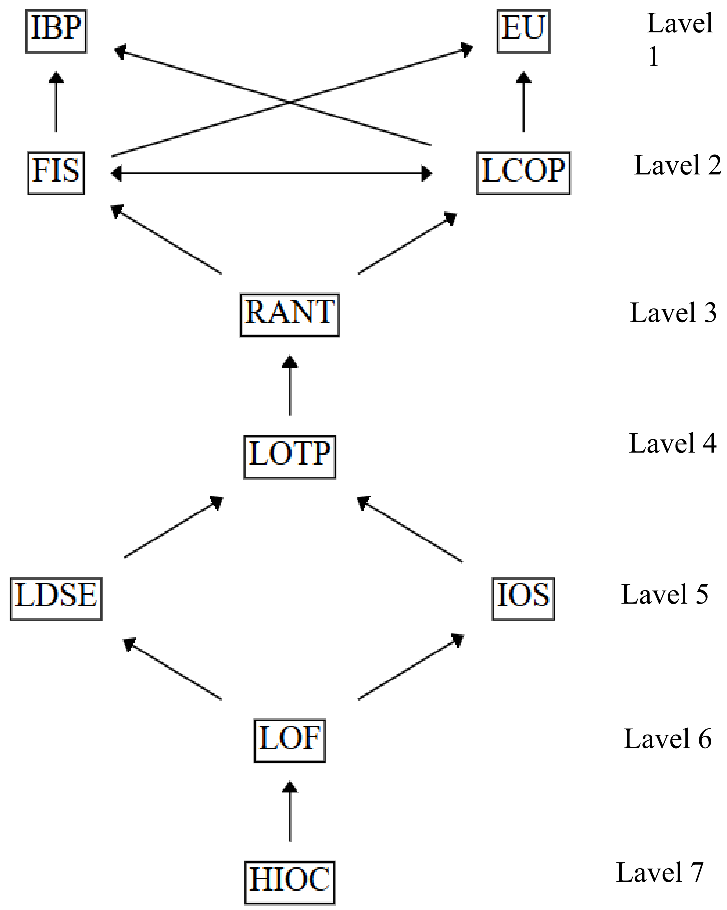


Figure 1: ISM Model

## MICMAC Analysis

The purpose of MICMAC research is to look at the driving and the dependencies of these variables. The variables are divided into four groups as shown in figure 2 based on their driving and dependencies power. Independent variables with low driving force and low dependencies constitute the first group. These variables are also isolated from the system and have little connection with the system. The difference in difference in the second group has a low driving force. The connectivity variable in the third group has a great driving force, but also a great dependency. These variables cannot be changed because every action they take has an impact on others and is interpreted by others. themselves. The fourth group has a high driving but different liberties on the line.

Autonomous Barriers, Cluster I: This category includes the difficulties associated with having reduced driving and dependency power. These obstacles are not closely connected to the system.

Dependent Barriers Cluster II: This category includes barriers with weak driving forces but substantial dependencies. By removing the barriers on which they are dependent, these barriers can be removed as well.

Linkage Barriers, Cluster III: This category includes barriers with both significant driving forces and dependencies. These are frequently unstable and interact in both directions with other obstacles.

Independent barriers Cluster IV: This category includes obstacles that are supported by both strong driving force and mild dependence. These barriers, also known as independent barriers, are thought to be important systemic hurdles because of their powerful driving forces.

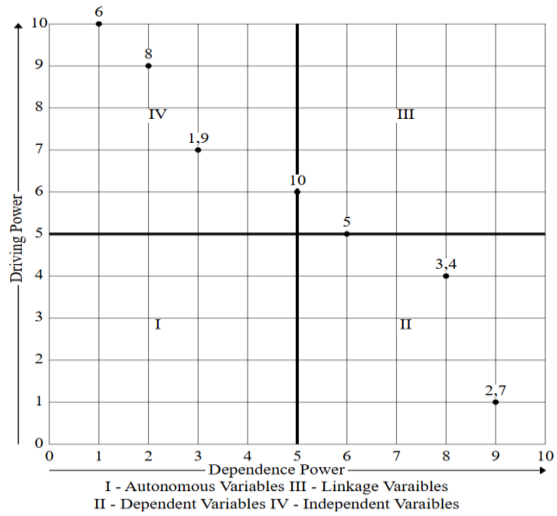


Figure 2: MICMAC Analysis

## Result and Discussion

The ISM model shows a clear structure with different levels. Lower-level barriers have strong influence, while upper-level barriers rely more on others. This barrier is placed at the bottom of the hierarchy; it indicates that it has the highest driving power. In this model the barrier high costs significantly is driving other barriers such as financial constraints, technological, organizational readiness, and environmental barriers. This finding aligns with existing literature, where cost is often identified as a primary barrier of digital transformation. Financial constraints emerge as a strong driving barrier influenced by high costs. Organizations with limited financial capacity may struggle to invest in infrastructure, training, and technology implementation. This barrier affects the various higher-level barriers and hence it becomes strategically important. These barriers indicate organizational readiness issues. A lack of skilled workforce and rigid organizational structures hinder effective implementation of B2B technologies. They are influenced by financial limitations and, in turn, affect process flexibility and technology adoption. Trust plays a critical role in inter-organizational collaboration. The model shows that lack of trust is affected by organizational and capability-related barriers and directly impacts information sharing and coordination across the supply chain. Resistance to change is a mid-level barrier in the model, which means that it is affected by both lower-level barriers (like cost, skills, and organization structure) and higher-level operational barriers. This suggests that overcoming resistance requires addressing foundational issues first. These barriers reflect inter-organizational and technological concerns. Fear of information sharing among the stakeholders due to trust issue and fear of data misuse and limited partner capabilities hinder collaboration and integration of B2B technologies. They are directly influenced by trust and resistance to adoption. These are the most dependent barriers which are positioned at the top of the hierarchy. They are outcomes of multiple underlying issues during integration of B2B technologies in e-commerce-enabled CDSC. For instance: Inflexible processes result from organizational rigidity and lack of technological skills. Environmental uncertainty raises challenges but it is less controllable internally.

The model clearly shows that cost and financial limitations are primarily responsible for impacting most other barriers. This implies that organisations have to prioritise financial planning and investment initiatives to ensure successful adoption of B2B technologies in e-commerce-enabled CDSC. Barriers such as inappropriate organizational structure and digital skills act as mediators between financial and operational challenges. Without addressing these, even well-funded initiatives may get failed. The positioning of lack of trust at the mid-level of the model emphasises its importance in facilitating information sharing and supply chain partner collaboration. Trust serves as a bridge between internal readiness and external integration. Resistance to adoption of technology is neither purely a root cause nor an outcome; instead, it is a transitional barrier which is influenced by multiple factors. This suggests the top management has to develop change management strategies. Barriers i.e. inflexible processes and environmental uncertainty are largely the result of underlying barriers and need to be addressed the core causes which will indirectly reduce these issues.

## Conclusion

This study adds to the literature by providing a hierarchical structural model for understanding of barriers rather than isolated factors. It also highlights the interdependencies among financial, organizational, and inter-organizational barriers. It also extends ISM application in the context of e-commerce-enabled customer-driven supply chains. Organizations which are ready to integrate B2B technology should prioritize their investment planning to overcome cost-related barriers. The management should develop digital skills and flexible organizational structures which is essential for successful implementation. The supply chain mangers should ensure to build trust-based relationships with supply chain partners so that it can enhance collaboration and data sharing. Managers should adopt change management practices to reduce resistance to new technologies. This study provides a systematic, bottom-up approach (starting from driving barriers) which is more effective than addressing surface-level issues. The ISM model demonstrates that barriers to B2B technology adoption in the context of e-commerce-enabled CDSC are highly inter-related, with financial and cost-related barriers acting as foundational drivers. A strategic approach to address these root barriers can significantly reduce the impact of higher-level barriers and it results in improving the adoption and performance of B2B technologies in supply chains. The future scope of B2B technologies in CDSC is promising. Businesses will leverage data analytics and AI to gain insights into customer behaviour and optimize supply chain processes. IoT and connected devices will enable real-time tracking and monitoring of products, enhancing visibility and efficiency.

## References

[1] Agrawal, P., Narain, R., & Ullah, I. (2020). Analysis of barriers in implementation of digital transformation of supply chain using interpretive structural modelling approach. Journal of Modelling in Management, 15(1), 297–317.

[2] Asare, A. K., Brashear-Alejandro, T. G., & Kang, J. (2016). B2B technology adoption in customer driven supply chains. Journal of Business & Industrial Marketing, 31(1), 1–12.

[3] Bag, S., Gupta, S., & Kumar, S. (2021). Industry 4.0 adoption and 10R advance manufacturing capabilities for sustainable development. International Journal of Production Economics, 231, 107844.

[4] Bonnin, G., & Alfonso, M. R. (2019). The narrative strategies of B2B technology brands. Journal of Business & Industrial Marketing, 34(7), 1448–1458.

[5] Chauhan, N. K., Kumar, V., & Dixit, S. (2023a). A Study of Key Challenges in Implementation of Digital Supply Chain in the Context of Indian SMEs. Lecture Notes in Mechanical Engineering, 23–32. https://doi.org/10.1007/978-981-99-1328-2_3

[6] Chauhan, N. K., Kumar, V., & Dixit, S. (2023b). To achieve sustainability in supply chain with Digital integration: A TISM approach. International Journal of Experimental Research and Review, 30, 442–451. https://doi.org/10.52756/ijerr.2023.v30.041

[7] Chen, S.-C., & Lin, C.-P. (2019). Understanding the effect of social media marketing activities: The mediation of social identification, perceived value, and satisfaction. Technological Forecasting and Social Change, 140, 22–32.

[8] Choudhury, A., Behl, A., Sheorey, P. A., & Pal, A. (2021). Digital supply chain to unlock new agility: a TISM approach. Benchmarking, 28(6), 2075–2109. https://doi.org/10.1108/BIJ-08-2020-0461

[9] Fawcett, S. E., McCarter, M. W., Fawcett, A. M., Webb, G. S., & Magnan, G. M. (2015). Why supply chain collaboration fails: the socio-structural view of resistance to relational strategies. Supply Chain Management: An International Journal, 20(6), 648–663.

[10] Gardas, B. B., Raut, R. D., & Narkhede, B. E. (2017). A state-of the-art survey of interpretive structural modelling methodologies and applications. Int. J. Business Excellence, 11(4), 505–560.

[11] Gomes, L. de C. (2022). Mitigation of supply chain vulnerability through collaborative planning, forecasting, and replenishment (CPFR). In Supply Chain Risk Mitigation: Strategies, Methods and Applications (pp. 95–119). Springer.

[12] Gosain, S., Malhotra, A., & El Sawy, O. A. (2004). Coordinating for flexibility in e-business supply chains. Journal of Management Information Systems, 21(3), 7–45.

[13] Grover, V., & Goslar, M. D. (1993). The initiation, adoption, and implementation of telecommunications technologies in US organizations. Journal of Management Information Systems, 10(1), 141–164.

[14] Hines, T. (2024). Supply chain strategies: Demand driven and customer focused. Routledge.

[15] Hollmann, R. L., Scavarda, L. F., & Thomé, A. M. T. (2015). Collaborative planning, forecasting and replenishment: a literature review. International Journal of Productivity and Performance Management, 64(7), 971–993.

[16] Ivanov, D., & Dolgui, A. (2020). A digital supply chain twin for managing the disruption risks and resilience in the era of Industry 4.0. Production Planning and Control, 0(0), 1–14. https://doi.org/10.1080/09537287.2020.1768450

[17] Jha, K. M., Velaga, V., Routhu, K., Sadaram, G., Boppana, S. B., & Katnapally, N. (2025). Transforming Supply Chain Performance Based on Electronic Data Interchange (EDI) Integration: A Detailed Analysis. European Journal of Applied Science, Engineering and Technology, 3(2), 25–40.

[18] Kamble, S., Gunasekaran, A., & Dhone, N. C. (2020). Industry 4.0 and lean manufacturing practices for sustainable organisational performance in Indian manufacturing companies. International Journal of Production Research, 58(5), 1319–1337.

[19] Liao, S.-H., Hu, D.-C., & Chen, S.-T. (2022). Supply chain integration, capability and performance–a business-to-business network cooperation. Journal of Business & Industrial Marketing, 37(5), 1127–1137.

[20] Liboni, L. B., Cezarino, L. O., Jabbour, C. J. C., Oliveira, B. G., & Stefanelli, N. O. (2019). Smart industry and the pathways to HRM 4.0: implications for SCM. Supply Chain Management, 24(1), 124–146. https://doi.org/10.1108/SCM-03-2018-0150

[21] Madhani, P. M. (2019). Building a customer-centric supply chain strategy: Enhancing competitive advantages. The IUP Journal of Business Strategy, 16(2), 28–42.

[22] Mouzakitis, S., & Askounis, D. (2010). A knowledge-based framework for measuring organizational readiness for the adoption of B2B integration systems. Information Systems Management, 27(3), 253–266.

[23] Panahifar, F., Heavey, C., Byrne, P. J., & Fazlollahtabar, H. (2015). A framework for

collaborative planning, forecasting and replenishment (CPFR) state of the art. Journal of Enterprise Information Management, 28(6), 838–871.

[24] Patterson, K. A., Grimm, C. M., & Corsi, T. M. (2003). Adopting new technologies for supply chain management. Transportation Research Part E: Logistics and Transportation Review, 39(2), 95–121.

[25] Ramesh, A., Banwet, D. K., & Shankar, R. (2010). Modeling the barriers of supply chain collaboration. Journal of Modelling in Management, 5(2), 176–193.

[26] Shukla, R. K., Garg, D., & Agarwal, A. (2012). Modeling barriers in supply chain coordination. International Journal of Management Science and Engineering Management, 7(1), 69–80.

[27] Sia, C.-L., Teo, H.-H., Tan, B. C. Y., & Wei, K.-K. (2004). Effects of environmental uncertainty on organizational intention to adopt distributed work arrangements. IEEE Transactions on Engineering Management, 51(3), 253–267.

[28] Sila, I. (2013). Factors affecting the adoption of B2B e-commerce technologies. Electronic Commerce Research, 13(2), 199–236.

[29] Vidani, J. (2024). E-Commerce Supply Chain Efficiency: A Case Study of Amazon E-Commerce Company. Available at SSRN 4849852.

[30] Westerman, G., Tannou, M., Bonnet, D., Ferraris, P., & McAfee, A. (2012). The Digital Advantage: How digital leaders outperform their peers in every industry. Capgemini Consulting. MIT Center for Digital Business Capgemini.

# REINFORCEMENTS FOR FUSED DEPOSITION MODELLING AND STEREOLITHOGRAPHY MATERIALS: MECHANICAL PROPERTIES, AND REINFORCEMENT MECHANISMS - A REVIEW

Zacharie Nankwaya Ntumba*[1], Himanshu Payal[1]
*[1]Department of Mechanical Engineering, School of Engineering & Technology, Sharda University, Greater Noida, India
*zacharientumba44@gmail.com

## Abstract
*This review investigates reinforcement mechanisms for additive manufacturing (AM) technologies, particularly for material extrusion and vat photopolymerisation materials. 3D-printed components using pure polymer are limited by poor mechanical strength, weak interlayer bonding, and anisotropic behaviour, providing unsatisfactory performance in critical environments. Hence, the need for 3D-printed materials which can perform in critical environments demonstrates the necessity for reinforced matrices (polymer composites), as they offer a satisfied strength-to-weight ratio with improved mechanical performance. The study examines the role of reinforcement types for fused deposition modelling (FDM) and stereolithography (SLA) polymer materials, and their associated reinforcement mechanisms, essential for the synthesis of composites for improved mechanical properties. It discusses the dispersion issues and processing limitations, and reinforcement approaches, aiming to guide the development of polymer composites for additive manufacturing applications. Furthermore, the influence of reinforcement type, size, and distribution on mechanical properties are also discussed.*

## Keywords
Reinforcement, SLA, polymer, 3D-printing, matrix.

## Introduction
Additive manufacturing (AM) is expected to establish itself as a dominant manufacturing technology across multiple industries in the near future. It enables the production of customised components and simultaneously reduces lead times, energy consumption, and material waste. AM, also referred to as 3D printing, is a core pillar of Industry 4.0 and facilitates the fabrication of complex geometries, supports the pull system in production, boosting reduced inventory requirements. It is applied in various fields such as aerospace, automobile, healthcare, and consumer goods [1]. Though it positively differentiates itself from traditional formative and subtractive methods, it has some limitations including the print volume, material variety, and the need for post-processing. AM covers various technologies: fused deposition modeling (FDM), stereolithography (SLA), digital light processing (DLP), multi jet fusion (MJF), selective laser sintering (SLS), selective laser melting (SLM), direct metal laser sintering (DMLS), electron beam melting (EBM), binder jetting, material jetting, polyJet, continuous liquid interface production (CLIP), laminated object manufacturing (LOM), directed energy deposition (DED), laser engineered net shaping (LENS), and robocasting (Direct Ink Writing), which uses the layer-by-layer technique for building up the entire component. They collaborate with computers, using computer aided design (CAD), in order to make the model the parts, using a set of generalised steps: CAD modelling, next conversion into an STL format, followed by the slicing of the

model then finally 3D-printed. The primary materials used in 3D printing include polymers, metals, and composites. [2]. There is a strong need to improve mechanical properties of these materials, including polymers. Polymers have weak intermolecular forces among chains, which allow flexibility, melting, and deformation [3], making it difficult to work with in critical environments. There have been various types of reinforcement of polymers, which act as stress transfer agents between the polymer matrix and reinforcement phase, limiting crack propagation and improving overall structural integrity. The reinforcement of polymers improve the polymer matrix and and helps to distribute applied loads more effectively. 3D-printed polymers experience improved stiffness, tensile strength, and the capacity to bear load [4]. The thermal stability, electrical conductivity, and impact resistance enhance, making them polymers largely suitable for structural and functional performance [5]. One of the main motivation to reinforce polymers in 3D printing is the strength-to-weight ratio that they offer, highly beneficial in industries such as aerospace, automotive, and civil infrastructure, where the weight directly affects the efficiency of structures, energy consumption, and the performance [6]. The limitations of pure polymers in AM including low strength, stiffness, and load-bearing capacity, restrict their use in applications where high performance is required. Some other limitations include a poor interlayer bonding, porosity, and anisotropic behaviour which degrade their mechanical performance, making them less reliable compared to reinforced composites [7]. Pure 3D-printed polymer alone is sometimes insufficient to provide a satisfactory impact resistance and structural performance. For this reason, the use of composite materials is essential in order to enhance the performance [8]. 3D printing technologies which use polymer include material extrusion, vat photopolymerisation, powder bed fusion, material jetting, binder jetting, and direct ink writing. It is essential to comprehend, how different reinforcement strategies influence mechanical properties across both material extrusion and vat photopolymerisation processes, and the mixing technique involved in the making of such composites.

## Reinforced Composites

Composites incorporate two phases including the dispersed and the matrix phase. The matrix defines the morphology and distribution of nanoparticles, contributes to the overall performance of the composite system. It transfers transfers the applied load, and governs the mechanical behaviour, and contributes to the viscoelastic deformation and internal friction of the whole composite ([9],[10]). In order to form composites with enhanced properties and performance, reinforcements, whose effectiveness depends on factors such as dispersion, alignment, and interconnectivity, are incorporated. However, the addition of reinforcement holds some obstacles including processing difficulties, increased viscosity, and potential interfacial incompatibility between the matrix and the reinforcement. So, it is vital to maintain the ratio between the matrix and the reinforcement [11]. The reinforcement can either be in particle form (particle reinforced composites) or fiber form (fiber reinforced composites), is primarily responsible for enhancing mechanical properties [10], as discussed in table 1 and table 2.

Table 1. Reinforcement of FDM Polymer Materials.

| Paper | Matrix | Reinforcement | Reinforcement Mechanism | Mechanical Properties |
|---|---|---|---|---|
| [13] | Polylactic acid (PLA) | Carbon fiber (CF) | The composite is prepared by pultrusion. The CF is passed through a molten PLA bath for coating. | Young's modules improved by 850% from the base material. |
| [14] | PETG-KF | Aramid fiber (AF) | This work used a pre-made AF reinforced PETG-KF. | Ultimate tensile strength: 198.6 MPa<br>Fatigue resistance: 80.1 MPa<br>Impact strength: 22.8 KJ/m^2 |
| [15] | Polypropylene | Glass fiber (GF) | Pre-made short pellets of GF-reinforced polypropylene filled with mineral fillers then pellet-based FDM was used for the printing process. | Elastic modulus: 8036 MPa<br>Tensile strength: 72.5 MPa |
| [16] | PLA | CF | The CF and PLA are 3D printed simultaneously using a two-nozzle FDM technology. One nozzle for the PLA, and the other equipped with a shearing device for the continuous CF. | Longitudinal tensile strength: 264.37 MPa<br>Tensile modulus: 4454 MPa<br>Shear modulus: 1400 MPa |
| [17] | PLA | Kevlar fiber (KF) | The KF was impregnated through a molten PLA bath, and the final result was then used for 3D printing. | Compressive strength: 69.25 MPa<br>Compressive modulus: 3.93 GPa |
| [18] | PLA | Hydroxyapatite | This work used a pre-made composite filament | Tensile strength: 34.51 MPa<br>Flexural strength: 126.17 MPa<br>Compression strength: 69.24 MPa |
| [19] | PLA | Glass powder (GP) | The PLA pellets and GP were introduced in the hopper of the 3devo composer 450 desktop extruder for the formation of the final composite. | Tensile strength: 43.71 MPa<br>Tensile modulus: 2738.50 MPa<br>Flexural strength: 50.29 MPa<br>Flexural modulus: 2760 MPa |
| [20] | PLA | Hemp fiber (HF) | The HP was ground for nanoparticle obtention, then both the PLA pellets and the HF nanoparticles passed through the extruder for the composite filament formation. | Tensile strength: 48.34 MPa<br>Ultimate tensile strength: 237 N<br>Young's modulus: 3.76 GPa |

Table 2. Reinforcement Stereolithography Material Matrix.

| Paper | Matrix | Reinforcement | Reinforcement Mechanism | Mechanical Properties |
|---|---|---|---|---|
| [21] | Resin | Waste eggshell | The eggshells are washed and dried, ground in a hammer mill fro the micro powder, sieved, and the HORIBA LA-950 was used for the particle size controller.<br>The final powder was mixed with the resin using a magnetic stirrer for the final composite formation. | Tensile strength: 39.1 MPa<br>Elastic modulus: 2331 MPa<br>Compressive strength: 50.35 MPa |
| [22] | Tripropylene glycol (TPGDA)+urethane acrylate (UA)+photo initiator phosphite oxide (TPO) | Combination of chitosan (CH), carboxymethyl chitosan (CMCH), hydroxypropyl chitosan (HPCH), hydroxyethyl chitosan (HECH) | Matrix mixture: TPGDA+UA, then later added TPO<br>The matrix was finally added with CH, CMCH, HPCH, and HECH, for the final composite material. | Compressive strength: 55.8 MPa, a 38 % reduction from the base matrix.<br>Tensile strength increased by 2.5% from the base matrix. |
| [23] | Photo curable resin | Cork powder | The cork was first boiled then dried.<br>the final cork powder result was blended with the photo curable resin. The VOS 40 paddle mixer was used for the mixing process.<br>The mixture then went through an ultrasonic bath, then lastly rested into in a vacuum filtration disiccator. | Young's modulus: 2450 ± 180 MPa<br>Tensile strength: 44.5 ± 4.1 MPa |
| [24] | Epoxy-acrylate-based resin | $BaTiO_3$ powders | The Sun resin was mixed with the $BaTiO_3$ powders. The mixture was then stirred and then went for degassing in a vacuum oven. The brookfield viscometer was used to measure the viscosity. | Interfacial shear strength: 250 N |
| [25] | FLGPCL04 polymer | Fe3O4 nanoparticles | The FLGPCL04 and Fe3O4 where mixed together manually.<br>Then, the mixture was put in an ultrasonic homogeniser for uniform composite formation. | Ultimate tensile strength: 65 MPa<br>Tensile modulus: 2.8 GPa<br>Flexural modulus: 2.2 GPa |

| | | | | |
|---|---|---|---|---|
| [26] | Elastic photopolymer resin and standard photopolymer resin | Aramid fiber (AF) | The fiber and the resins were mixed together to form the composite, using a hand blender beater. | Young's modulus: 72.50 MPa<br>Tensile strength: 7.27 MPa<br>Toughness: 7.52 MPa |
| [27] | Hard tough Acrylic-based resin | Cabalt powder | The mixture was done using the Hanchen Cantilever electrical stirrer. | Elastic modulus: 1361 MPa<br>Yield strength: 17.8 MPa<br>Ultimate tensile strength: 32.1 MPa |
| [28] | biobased methacrylate resin (MESO) | Octavinyl polysilsesquioxane (POSS), Hydroxyethyl methacrylate (HEMA), trimethylbenzoyl diphenylphosphine oxide (TPO) | The MESO was mixed with POSS, HEMA, TPO.<br>Then the mixture was sonicated, and then cured with UV lamp. | Tensile strength: 20.4 MPa<br>Toughness: 399.2 MJ/m^3<br>Elongation at break: 19.8% |
| [29] | Itaconated epoxidized soybean oil (IESO) | Itaconic acid monomethyl ester (IAME) modified cellulose nanocrstals (CNCs-IAME) | IESO was mixed with TPO photo initiator, hydroxyethyl methacrylate, and CNCs-IAME.<br>The mixture was then debubbled under vacuum and introduced into the patterning mould, and then cured with a UV lamp. | Tensile strength: 19.54 MPa<br>Elongation at break; 34.03%<br>Storage modulus: up to 3.1 GPa |

## Discussion

There are available pre-made polymer composites in the market, essential when composites synthesising is not the objective. The most performing composite using the FDM technology is the CF-reinforced PLA using the FDM technology by Z. Meng et al., 2024, and the least performing one is the hydroxyapatite-reinforced PLA by P. Aihemaiti et al. 2024; while using the SLA technology, the most performing composite is the $Fe_3O_4$-reinforced FLGPCL04 by M. Dehghan et al., 2023, and the least performing one is the Aramid fiber-reinforced resin by R. K. Saha et al., 2026. Thus, one must choose to either use the existing composites or investigate new commodities in order to achieve targeted properties.

## Conclusion

Reinforcement mechanisms are not common; however, the final mixture of the matrix and the reinforcement must be uniform, and the ratio between the matrix and the reinforcement must be carefully selected as discussed in existing works that we discussed in this study. FDM composite materials still face key limitations related to interlayer adhesion, anisotropy, and fiber integration. SLA composites encounter challenges primarily related to material compatibility and reinforcement efficiency. Hence, addressing these limitations and researching about new reinforcements is imperative.

## References

[1] G. Prashar, H. Vasudev, and D. Bhuddhi, "Additive manufacturing: Expanding 3D printing horizon in Industry 4.0," International Journal on Interactive Design and Manufacturing (IJIDeM), vol. 17, no. 5, pp. 2221–2235, 2023. doi: 10.1007/s12008-022-00956-4.

[2] A. De la Fuente, R. Castillo, A. Oñate, R. Hermosilla, B. Escudero, J. Sepúlveda, G. Vargas-Silva, M. F. Meléndrez, V. Tuninetti, and C. Medina, "Quantifying the influence of reinforcement architecture on the planar mechanical properties of 3D-printed continuous fiber-reinforced thermoplastic composites," International Journal of Advanced Manufacturing Technology, vol. 127, pp. 1575–1583, 2023.

[3] C. V. Pious and S. Thomas, "Polymeric Materials—Structure, Properties, and Applications," in Printing on Polymers, J. Izdebska and S. Thomas, Eds. Oxford, U.K.: William Andrew Publishing, 2016, pp. 21–39. doi: 10.1016/B978-0-323-37468-2.00002-6. [1] Z. Longfei, J. Miller, J. Vezza, M. Mayster, M. Raffay, Q. Justice, Z. Al Tamimi, G. Hansotte, L. D. Sunkara, and J. Bernat, "Additive manufacturing: A comprehensive review," Sensors, vol. 24, no. 9, p. 2668, 2024.

[4] I. A. Pathek Jr., J. R. F. da Silva, D. D. Lima, I. F. Limberger, A. A. Buenos, and C. J. Scheuer, "Assessment of carbon fiber incorporation effects on overall characteristics and properties of 3D-printed PLA," Journal of the Brazilian Society of Mechanical Sciences and Engineering, vol. 46, p. 640, 2024.

[5] S. Wickramasinghe, A. Manalo, O. Alajarmeh, C. D. Sorbello, S. Weerakoon, T. D. Ngo, and B. Benmokrane, "Advancing polymer composites in civil infrastructure through 3D printing," Automation in Construction, vol. 177, p. 106311, 2025.

[6] S. Kumar, D.-H. Yoo, J.-S. Song, and H.-S. Kim, "A critical review of the past, present, and future of 3D printing for continuous and short fiber composites," Composite Structures, vol. 376, p. 119819, 2026.

[7] T. Fisher, Z. Kazancı, and J. H. S. Almeida Jr., "High-velocity impact response of 3D-printed composite mechanical metamaterials," International Journal of Mechanical Sciences, vol. 286, p. 109905, 2025.

[8] O. V. Arzhakova, A. S. Khramtsovskii, I. A. Tikhonov, D. K. Chaplygin, A. A. Zvonova, A. Y. Kopnov, A. V. Bolshakova, and A. I. Aleksandrov, "Nanocomposite materials based on mesoporous polymer matrices with palladium and platinum nanoparticles via rheological explosion," Polymer, vol. 345, p. 129502, 2026.

[9] A. Premanand and F. Balle, "Significance of fracture fatigue entropy in predicting fatigue life across regimes in polymer matrix composites: A review and analysis," Composites Part B, vol. 314, p. 113489, 2026.

[10] M. Yin, M. Qiu, Y. Yuan, C. Zhu, W. Zou, and B. Yang, "Advanced polymer-based thermal interface materials: A review on matrix optimization and filler engineering for superior performance," European Polymer Journal, vol. 242, p. 114468, 2026.

[11] M. Zhang, X. Tian, L. Jia, T. Liu, P. Wang, and D. Li, "Mechanism and performance of thermal radiation recycling for in-space 3D printed continuous carbon fibre-reinforced PEEK composites," Virtual and Physical Prototyping, vol. 19, no. 1, p. e2425823, 2024.

[12] C. Suescun Gonzalez, A. Basdeo, F. A. Cruz Sanchez, C. Nouvel, J. M. Pearce, and H. Boudaoud, "Strategies for recycling multi-material polymer blends for additive manufacturing," Sustainable Materials and Technologies, vol. 44, p. e01430, 2025.

[13] M. A. Saleh, S. Olcun, M. Karam, R. Kempers, and G. W. Melenka, "High stiffness 3D-printed continuous pitch carbon fiber reinforced polymer composites," Journal of Composite Materials, vol. 58, no. 16, pp. 1873–1886, 2024.

[14] S. V. Kuchampudi, K. L. Meena, and R. B. R. Chekuri, “An experimental investigation on 3D printing of PETG-KF-based composites: optimization of process parameters for improved mechanical properties,” Cogent Engineering, vol. 11, no. 1, p. 2379989, 2024.

[15] D. Rigon, M. Ricotta, G. Ardengo, and G. Meneghetti, “Static mechanical properties of virgin and recycled short glass fiber-reinforced polypropylene produced by pellet additive manufacturing,” Fatigue & Fracture of Engineering Materials & Structures, vol. 44, pp. 2554–2569, 2021.

[16] Z. Meng, Y. Yali, L. Lu, H. Chen, S. Xu, Y. Li, R. Zhang, and T. Zhou, “Progressive damage for 3D printed composites with variable fiber volume content and ply location,” Composites and Advanced Materials, vol. 33, pp. 1–22, 2024.

[17] Z. Hou, J. He, X. Tian, W. Zhu, C. Wang, P. Liu, H. Lan, and D. Li, “Performance and failure modes of continuous fibre-reinforced energy absorption tubes by cylindrical layered 3D printing,” Virtual and Physical Prototyping, vol. 19, no. 1, p. e2367122, 2024.

[18] P. Aihemaiti, H. Jiang, W. Aiyiti, J. Wang, L. Dong, and C. Shuai, “Mechanical properties enhancement of 3D-printed HA-PLA composites using ultrasonic vibration assistance,” Virtual and Physical Prototyping, vol. 19, no. 1, p. e2346271, 2024.

[19] L. Castanon-Jano, P. Palomera-Obregon, E. Blanco-Fernandez, and I. Indacoechea-Vega, “Analysis of manufacturing and material parameters in 3D-printed polylactic acid (PLA) parts filled with glass powder: mechanical, economic, and environmental assessment,” The International Journal of Advanced Manufacturing Technology, vol. 128, pp. 1965–1979, 2023.

[20] P. Srivastava, A. B. Arumugam, A. P. Agrawal, and Z. N. Ntumba, “Development of hemp fiber reinforced PLA composites for sustainable 3D printing: Mechanical and microstructural properties,” Journal of Natural Fibers, vol. 22, no. 1, p. 2558214, 2025.

[21] G. A. Yavuz, B. G. Kıral, G. M. Gençer, and Z. Kıral, “Investigation of the effect of adding waste eggshell particles to a resin used for SLA printing applications,” Mechanics of Composite Materials, vol. 60, no. 1, pp. 103–114, 2024.

[22] N. Celikci, C. A. Ziba, M. Dolaz, and M. Tümer, “Comparison of composite resins containing UV light-sensitive chitosan derivatives in stereolithography (SLA)-3D printers,” International Journal of Biological Macromolecules, vol. 281, p. 136057, 2024.

[23] I. Romero-Ocaña and S. I. Molina, “Cork photocurable resin composite for stereolithography (SLA): Influence of cork particle size on mechanical and thermal properties,” Additive Manufacturing, vol. 51, p. 102586, 2022.

[24] L. Zhong, W. Liu, Y. Sun, F. Wang, S. Chen, Q. Sun, Y. Liu, C. Yuan, X. Li, and G. Fei, “Electrically assisted stereolithography 3D printing of graded permittivity composites for in-situ encapsulation of insulated gate bipolar transistors (IGBTs),” Materials & Design, vol. 233, p. 112220, 2023.

[25] M. Dehghan and M. Tahmasebipour, “Fabrication of peristaltic electromagnetic micropumps using the SLA 3D printing method from a novel magnetic nano-composite material,” Sensors and Actuators A: Physical, vol. 358, p. 114431, 2023.

[26] R. K. Saha, M. M. Rahman, M. T. Islam, M. M. Mumin, and N. C. Ray, “Investigating the impact of layer thickness and print orientation on strength and structural integrity of SLA 3D printed composites,” International Journal of Lightweight Materials and Manufacture, vol. 9, pp. 165–181, 2026.

[27] K. M. Gide, C. E. Tranchemontagne, M. Z. Sardar, and Z. S. Bagheri, “Precise fiber

alignment in stereolithography (SLA) 3D printing of composite polymers," Hybrid Advances, vol. 10, p. 100501, 2025.

[28] Z. Hu, M. Liu, J. Che, Q. Kang, Z. Liu, Z. Qiang, X. Liu, Y. Xia, S. Huang, J. Zhang, and Y. Chen, "SLA printing of POSS-containing, bio-based composites with low dielectric constant and shape-memory function," Composites Communications, vol. 39, p. 101566, 2023.

[29] B. Chu, X. Cui, X. Dong, Y. Li, X. Liu, Z. Guo, Y. Xia, S. Huang, J. Zhang, and Y. Chen, "SLA printing of shape memory bio-based composites consisting of soybean oil and cellulose nanocrystals," Virtual and Physical Prototyping, vol. 19, no. 1, 2024.

*ISBN 978-81-973526-0-7*

# ANALYSIS OF BARRIERS IN DIGITAL MANUFACTURING FOR SMEs

Khushi Tyagi*[1], Mahesh Chand[1], Surender Singh[1]
*[1]J.C. Bose University of Science & Technology, YMCA, Faridabad, Haryana, India
*tyagikhushi1210@gmail.com

## Abstract

*Digital manufacturing involves using computer systems and software to optimize, automate and improve various aspects of the manufacturing process from design and production to product lifecycle management. It essentially integrates technology into all stages of manufacturing to enhance efficiency, flexibility, and adaptability to market demands. For SMEs digital manufacturing means using technology automate and optimize the manufacturing processes, improve efficiency and reduce costs. Digital manufacturing involves integrating advanced technologies like Internet of Things (IoT), Artificial Intelligence (AI), Big Data Analytics and Cloud Computing to create intelligent, connected and Automated Manufacturing Systems. The paradigm of digital manufacturing is examined and contrasted with mass production and craft production. Digital manufacturing in SMEs (Small Medium Enterprises) are increasing their ability in the area of market dynamics. In this thesis different barrier of digital manufacturing in SMEs are identified. Barriers which highly affect the industries. In this thesis we analysed 20 barriers in digital manufacturing in SMEs and divide all those barriers in different categories. After analysed all this barriers we divide all these barriers into their sub category and after that we linked all these barriers with competitive index.*

## Keywords

Digital Manufacturing, Small, Medium Enterprises (SMEs), Barriers, Competitive Index.

## Introduction

Industries must embrace digitization and artificial intelligence in their operations due to the current manufacturing landscape. This landscape shifts from mass production to customized methods of production (Singh Sangwan et al., 2021; Bhosle et al., 2018). In today's digital economy, digital transformation is essential for small and medium-sized businesses (SMEs). To stay competitive and relevant as the global business environment becomes more digital, SMEs must adopt new technologies. The integration of digital technologies into every part of a business, known as "digital transformation," significantly changes how companies operate and deliver value to their clients (Emmanuel Ewim et al., 2024; Verhoef et al., 2021). The term "digital transformation" refers to many changes. This includes using e-commerce platforms, applying digital marketing techniques, and integrating digital technologies into company processes. These changes lead to better customer involvement, wider market reach, and greater operational efficiency (Nurchim et al., 2024). The digital transformation process typically begins with data integration and sharing. It then progresses to business integration and sharing promotion, and concludes with effective sharing of internal and external resources. It is important to recognize that digital transformation is a long-term, systematic effort for most organizations. Several challenges must be addressed, including rapid technological changes, resistance to organizational shifts, the need for ongoing business innovation, and the complex task of changing the organizational culture. This makes a longer timeline essential (Wan et al., 2025).
The motive of this paper is to identifying the existing barriers of digital manufacturing in

ISBN 978-81-973526-0-7

SMEs. The major upholders are found in SMEs to get a high productivity in the area of digital manufacturing with the help of digital technologies which are Artificial Intelligence (AI), Cloud computing, Internet of Things (IoT) etc. There are so many barriers in SME’s for adopting digital manufacturing in their companies to enhance their productivity, barriers like high investment cost, lack of skilled worker, requirement to upgrade software and hardware, resistance to change and many more.

## Literature Review

In today's fast-paced, technology-driven economy, small and medium-sized businesses' (SMEs') use of digital technologies has become crucial for their survival and competitiveness (Ewim et al., 2024). Manufacturing sectors should be aware of, ready for, and able to handle the challenges that come with implementing this new approach as they enter the Industry 4.0 transition phase (Sangwan et al., 2021). The review begins by examining SMEs' experiences with Industry 4.0. It then discusses demand-driven collaboration among SMEs. Finally, it highlights the research gap in supply-side collaborations for SMEs (Zolkiewski et al., 2022). Digitalization is part of an organizational information system that uses the technology available to the business. To improve user experience, efficiency, and effectiveness, people, companies, and society design and implement solutions based on information technology. This process is called digitization (Álvarez et al., 2023). The definitions most often used by regulators focus on the number of employees, sales, and loan size. However, there is no general definition on what defines an SME (Johansson et al., 2021). In contrast to large corporations, SMEs often have greater talent gaps. SMEs also usually spend less on training to improve skills (Csilla Margit Csiszár, 2023). SMEs often face significant barriers in adopting these models, particularly concerning digital infrastructure. For SMEs, digital transformation is not merely a technological upgrade but a strategic shift that impacts business models, processes, and organizational culture (Adesuyi et al., 2023; Ogunsola et al., 2021). SMEs face challenges in productivity and growth because they lack necessary skills, have greater resource needs, and struggle with access to finance (J. Mena et al., 2024). Many small and medium-sized enterprises (SMEs) need digital technologies to reduce their risk during public crises. This makes them more vulnerable than other businesses (Fernando Diogo Gouveia and Henrique São Mamede, 2022). In order to improve efficiency and gain a competitive edge, small and medium-sized businesses (SMEs) are exploring ways to integrate modern digital technologies into their production processes (M. Kamal et al., 2024).

## Barriers in Digital Manufacturing

In this paper, we studied barriers in digital manufacturing in SMEs. Here is the table of 25 barriers in digital manufacturing with their explanation as a given below:

Table 1. Barriers.

| Sr. No. | Barriers Name | Definition | Author's Name |
|---|---|---|---|
| 1. | High cost of Investment | Many SMEs cannot afford the high expense of purchasing new digital equipment, software, or training. | Vargas et al., 2024; Stentoft et al., 2021 |
| 2. | Insufficient knowledge of technology | It refers to a lack of knowledge with modern technologies, devices, or digital systems. | Soni et al., 2022; Türkeş et al., 2019 |
| 3. | Expensive technology | It refers to the high price of advance technology, software, and systems, which may make it challenging for businesses to switch to digital practices. | Thames and Schaefer, 2017; Soni et al., 2022 |
| 4. | Inadequate IT infrastructure | It indicates that companies are unable to use digital tools and smart production technologies efficiently due to outdated or inadequate computers, networks, and systems. | Soni et al., 2022; Lu, 2017 |
| 5. | Insufficient financial resources | Adopting digital technology is challenging when there is insufficient funds to purchase advanced technology, software, or employee training. | Vargas et al., 2024; Bokkens, 2021; Gupta et al., 2022; Romanova et al., 2021 |
| 6. | Inadequate digital skills | It indicates that employees or supervisors lack the skills necessary to properly use digital tools and modern manufacturing technologies. | Baig et al., 2025; Sharma et al., 2018 |
| 7. | Inadequate internet | It refers to a slow or unstable internet connection that interferes with the use of digital tools and advanced industrial systems. | Baig et al., 2025; Pei et al., 2016 |
| 8. | Inadequate standards | It refers to lacking of efficient rules or guidelines, which makes it difficult to make sure the efficiency and compatibility of digital procedures and processes. | Baig et al., 2025; A. Benešová and J. Tupa, 2017 |
| 9. | Lack of support from the government | It makes it more difficult for businesses to adopt and grow with digital technology because of the lack of financing, policies, or programs. | Gedam et al., 2022; Pham et al., 2019; Gu et al., 2019 |
| 10. | The requirement to upgrade both software and hardware | It means the digital manufacturing systems operate effectively, updated technology or regular updates are needed. Upgrades can be costly, time-consuming, and difficult to maintain, therefore this becomes a barrier. | Gedam et al., 2022; Leng et al., 2020 |
| 11. | Inadequate infrastructure for technology | It means a lack modern systems, networks, or equipment to facilitate digital manufacturing. This is a barrier due to slows down manufacturing and restricts the use of advanced digital technologies. | Gedam et al., 2022; Ingaldi and Ulewicz, 2020 |

| | | | |
|---|---|---|---|
| 12. | Lack of skilled worker | It means that there aren't enough employees with the necessary technological knowledge or digital abilities to operate, monitor, or maintain modern manufacturing technologies. This becomes a barrier because it restricts innovation in digital production processes, delays adoption, and decreases efficiency. | Gedam et al., 2022; Ahmad et al., 2020; Ingaldi and Ulewicz 2020 |
| 13. | Efforts for Standardization | It refers to establishing standard operating procedures and standards for devices, software, and data. Digital integration is slowed down when these standards are lacking or irregular since it makes it difficult for various systems to communicate or exchange data. | Barros et al., 2023; Senna et al., 2022 |
| 14. | Human Capital | It refers to employees' abilities, expertise, and experience. When workers lack the technical or digital skills needed to operate new industrial systems efficiently, it becomes a barrier. | Barros et al., 2023; Senna et al., 2022 |
| 15. | Security, Safety and Privacy Issues | It refers to risks such as machine failures, system attacks, and data theft. These turn into barriers because they make people fearful and less trusting of digital technology. | Barros et al., 2023; Senna et al., 2022 |
| 16. | Strategy for Digital | It means having a well-defined strategy for leveraging digital technologies. When businesses lack goals or direction for digital adoption, it becomes a barrier that causes implementation to be poor or ineffective. | Barros et al., 2023; Senna et al., 2022 |
| 17. | Access to technology | It refers to having the hardware, software, and tools required for digital production. When businesses cannot afford or acquire these technologies, it becomes a barrier that slows down the advancement of digital technology. | Phanden et al., 2024 Eller et al.,2020; Peillon and Dubruc, 2019 |
| 18. | lack of support from top management | It indicates that leaders do not properly support or finance modern technology. This becomes a barrier because projects lack the guidance, resources, and determination to be successful without management support. | Hussein Magdy Elhusseinya, José Crispim, 2021; Kamble et al., 2018 |
| 19. | Job interruptions | It indicates that digital issues like software glitches or network problems cause manufacturing to slow down suddenly. | Sangwan et al., 2021; Sharma et al., 2018; |
| 20. | Resistance to change | It means that employees or companies are uneasy or slower to adopt new digital technologies or procedures. | Sangwan et al., 2021; Ashok et al., 2018 |

*ISBN 978-81-973526-0-7*

## Score of barriers in digital manufacturing

Table 2. Scope of barriers in digital manufacturing.

| **Sr. No** | **Barriers** | **Sub-Barriers** | **Five point Likert Scale** | | | | | |
|---|---|---|---|---|---|---|---|---|
| 1. | High investment cost | High initial capital expenditure for new system | | | | 4.2 | | |
| | | High cost of maintenance and upgrades | | | | 4.5 | | 3.6 |
| | | Uncertainty of return of investment | | | 3 | | | |
| | | Difficult in obtaining financing for digital initiatives | | | 3 | | | |
| 2. | Insufficient knowledge of technology | Lack of awareness of emerging technologies | | | 3 | | | |
| | | Limited understanding of potential business benefits | | 2.5 | | | | 2.6 |
| | | Poor understanding of data analytics and integration | | 2 | | | | |
| | | Insufficient exposure to successful digital case studies | | | 3 | | | |
| 3. | Expensive Technology | Costly proprietary software and hardware solution | | | 3 | | | |
| | | High customization and implementation charges | | | 3 | | | |
| | | Vendor look-in leading to long term expense | | 2 | | | | 2.7 |
| | | Frequent version upgrades increasing costs | | | 3 | | | |
| 4. | Inadequate IT infrastructure | Obsolete hardware servers | | | 3 | | | |
| | | Poor data storage and management systems | | 2.5 | | | | |
| | | Unreliable network and connectivity within limit | | | 3.2 | | | 2.9 |
| | | Lack of system integration across department | | | 3 | | | |
| 5. | Insufficient financial resources | Limited budget allocation for digital projects | | 2.3 | | | | |
| | | Cash flow constrains affecting investment | | 2.8 | | | | |
| | | Dependence on external investments | | | 3 | | | 3.0 |
| | | Inability to sustain long term digital transformation program | | | | 4 | | |
| 6. | Inadequate digital skills | Employees not trained in using digital tools | | 2 | | | | |
| | | Lack of digital literacy among older worker | | | 3 | | | |
| | | Insufficient technical support staff | | | 3 | | | 2.5 |
| | | Few internal training support staff | | 2 | | | | |

*ISBN 978-81-973526-0-7*

| | | | | | | | | |
|---|---|---|---|---|---|---|---|---|
| 7. | Inadequate Internet | Slow internet connectivity | | | 3 | | | |
| | | Frequent network disruptions | | | 3.5 | | | |
| | | Limited broadband coverage | | | 3 | | | 3.3 |
| | | High internet cost | | | | 4 | | |
| 8. | Inadequate standards | Lack of information data | | | | 4 | | |
| | | Absence of industry wide guidelines for technology use | | | 3.5 | | | |
| | | Inconsistent cyber-security and privacy framework | | | | 4 | | 3.7 |
| | | Non-compliance with international benchmarks | | | 3.5 | | | |
| 9. | Lack of support from government | Limited policy incentives for technology | | 2 | | | | |
| | | Complex regulatory and approval processes | | | 3 | | | 2.8 |
| | | Lack of government funding or grants | | | 3.5 | | | |
| | | Inconsistent national digital strategies | | 2.8 | | | | |
| 10. | Requirement to upgrade software and hardware | Frequent need to purchase updated versions | | | 3 | | | |
| | | Compatibility issues with legacy systems | | | | 4.5 | | |
| | | Downtime during upgrades | | | | 4.5 | | |
| | | High upgrades costs | | | | | 5 | 4.2 |
| 11. | Inadequate infrastructure for technology | Unreliable power supply | | | 3.3 | | | |
| | | Poor data centres and network coverage | | 2.8 | | | | |
| | | Lack of climate controlled server room | | 2.5 | | | | 3.5 |
| | | Limited access to advances equipment | | | 3.8 | | | |
| 12. | Lack of skilled worker | Shortage of IT and digital engineering professionals | | | | 4 | | |
| | | Difficulty retaining skilled staff | | | | 4 | | |
| | | Lack of collaboration between industry and academia | | | 3 | | | 3.5 |
| | | Skills mismatch between graduates and market needs | | | 3 | | | |
| 13. | Efforts of standardization | Inconsistent implementation of quality standards | | | | 4 | | |
| | | Lack of coordinate among industry bodies | | | | 4.5 | | |
| | | Delays in adoption international best practice | | | 3 | | | 3.8 |
| | | Slow adoption of new technologies | | | | 4 | | |
| 14. | Human capital | Low motivation for digital learning | 1.5 | | | | | |
| | | Workforce aging and low adoptability to new digital tools | | | 3 | | | |
| | | Inefficient human resources development policies | | | 3 | | | 2.3 |

| | | | | | | | | |
|---|---|---|---|---|---|---|---|---|
| | | Poor alignment between HR and digital strategy | | 2 | | | | |
| 15. | Security, safety and privacy issues | Rising data breaches cyber attacks | | | 3.5 | | | |
| | | Insufficient cyber security protocols | | | | 4.5 | | |
| | | Lack of awareness of data privacy laws | | | | 4.2 | | 3.9 |
| | | Weak backup and disaster recovery systems | | | 3.5 | | | |
| 16. | Strategy of digital | Absence of a clear digital transformation roadmap | | 2 | | | | |
| | | Poor alignment between digital goals and business objectives | 1 | | | | | 1.7 |
| | | Absence of measurable digital transformation goal | | 2 | | | | |
| | | Fragmented or short-term planning approaches | | 2 | | | | |
| 17. | Access to technology | Limited availability of advances tools systems | | | | 4 | | |
| | | Unequal distribution of digital resources | | | | 4.4 | | 3.2 |
| | | High entry barrier for small businesses | | | | 4.7 | | |
| 18. | Lack of support from top management | Leadership not prioritizing digital initiatives | | 2 | | | | |
| | | Fear of failure or uncertainty about outcomes | | 2.3 | | | | |
| | | Limited communication of digital version to employees | | | 3 | | | 2.4 |
| | | Lack of accountability for digital outcomes | | 2.4 | | | | |
| 19. | Job interruptions | System downtime during digital migration | | | | 4 | | |
| | | Fear of job or redundancy due to automation | | | | 4.5 | | |
| | | Temporary due to productivity loss during technology adoption | | | | 4.3 | | 4 |
| | | Poor scheduling of technology rollout | | | 3.5 | | | |
| 20. | Resistance to change | Employees fear of job loss or new responsibilities | | | 3.5 | | | |
| | | Organizational culture resistance to innovation | | | | 4.5 | | |
| | | Lack of management strategies | | | | 4 | | 4.1 |
| | | Poor communication about benefits of digital transformation | | | | 4.5 | | |

## Measurement of Competitive Index

For computing the Competitive Index the mean score with their barriers in digital manufacturing for SMEs has been calculated on the basis of Table 2. After this rank, inverse rank and weight for each measure is to be finding out. For assigning weight to different measures of Competitive Index, the highest and lowest values of five point Likert scale, i.e., Five and one are mapped 100% and 0% respectively. For each of the issues of competitiveness a weight is assigned. The criteria for weight (Wi) is as under:

Wi= +1 (strength) when percentage score 60% (mean value 3)

=0 (neutral) when percentage score is between 40 60%

(mean value between two and three)

=-1 (weakness) when percentage score< 40% (mean value<2)

Sum of entries of last column (Wi Log Ki) will give CI, i.e., 13.73. Theoretically, CI value may range between –18.3 to +18.3. Computation of Competitive Index for this paper is illustrated with the help of a worksheet as shown in Table 3.

Table 3. Competitive Index.

| **Sr. No.** | **Barriers** | **Mean** | **Rank** | **Inverse Rank** | **Log Ki** | **Weight (Wi)** | **Wi X Log Ki** |
|---|---|---|---|---|---|---|---|
| 1. | Requirement to upgrade software and hardware | 4.2 | 1 | 20 | 1.30 | +1 | 1.30 |
| 2. | Resistance to change | 4.1 | 2 | 19 | 1.27 | +1 | 1.27 |
| 3. | Job interruptions | 4.0 | 3 | 18 | 1.25 | +1 | 1.25 |
| 4. | Security, safety, and privacy issues | 3.9 | 4 | 17 | 1.23 | +1 | 1.23 |
| 5. | Efforts of standardization | 3.8 | 5 | 16 | 1.20 | +1 | 1.20 |
| 6. | Inadequate standards | 3.7 | 6 | 15 | 1.17 | +1 | 1.17 |
| 7. | High investment cost | 3.6 | 7 | 14 | 1.14 | +1 | 1.14 |
| 8. | Lack of skilled workers | 3.5 | 8 | 13 | 1.11 | +1 | 1.11 |
| 9. | Inadequate internet | 3.3 | 9 | 12 | 1.07 | +1 | 1.07 |
| 10. | Access to technology | 3.2 | 10 | 11 | 1.04 | +1 | 1.04 |
| 11. | Inadequate infrastructure for technology | 3.1 | 11 | 10 | 1.00 | +1 | 1.00 |
| 12. | Inadequate financial resources | 3.0 | 12 | 9 | 0.95 | +1 | 0.95 |
| 13. | Inadequate IT infrastructure | 2.9 | 13 | 8 | 0.90 | 0 | 0 |
| 14. | Lack of support from government | 2.8 | 14 | 7 | 0.84 | 0 | 0 |
| 15. | Expensive technology | 2.7 | 15 | 6 | 0.77 | -1 | -0.77 |
| 16. | Insufficient knowledge of technology | 2.6 | 16 | 5 | 0.69 | -1 | -0.69 |
| 17. | Inadequate digital skills | 2.5 | 17 | 4 | 0.60 | -1 | -0.60 |
| 18. | Lack of support from top management | 2.4 | 18 | 3 | 0.47 | -1 | -0.47 |
| 19. | Human capital | 2.3 | 19 | 2 | 0.30 | -1 | -0.30 |
| 20. | Strategy for digital | 1.7 | 20 | 1 | 0.00 | -1 | 0 |

## Result and discussions

The major objective of this thesis is to identify major barriers which significantly affect the operation in digital manufacturing in different SMEs so that management can effectively deal with such types of barriers. In this thesis all the barriers evaluate with their sub-barriers with competitive index. First identified mean of all the sub-barrier and ranking them with their mean value and then finding their CI value. After finding CI value, the highly affected barrier

*ISBN 978-81-973526-0-7*

is strategy for digital, human capital, lack of support from top management, insufficient knowledge of technology, inadequate digital skills, expensive technology and less affected barriers are requirement to upgrade software and hardware, resistance to change, job interruptions, security, safety and privacy issues and many more. Organization needs to develop a proper strategy to reduce the impact of highly affected barriers. All the barriers value ranging from 0 to -1 are considered highly affected barriers. Industries should focus on these barriers and make efforts to minimize their impact.

## Conclusion

This study is analysing the barriers in digital manufacturing in SMEs with the Competitive Index. These barriers are common barriers in every industry of manufacturing which working on advance technologies like Artificial Intelligence, Machine Learning, Robotics and Automation, Internet of Things, Additive Manufacturing, Cloud Computing, Big Data and Analytics etc. Barriers which studied in this reports are common barriers like High Investment of Costs, Inadequate IT Infrastructure, Lack of Skilled Workers, Security, Safety, & Privacy Issues, Inadequate Infrastructure for Technology etc. After finding competitive index, the majorly focused barriers are strategy for digital, human capital, lack of support from top management, insufficient knowledge of technology, inadequate digital skills, expensive technology. The organization needs to focus on all these barriers and need to make proper strategy so they cannot affect them.

## References

[1] P. Kumar, J. Bhanu and K.S. Sangwan, 2021. Analysis of barriers to industry 4.0 adoption in manufacturing organizations: an ISM approach,

[2] S. Vaidya, P. Ambad, S. Bhosle, 2018. Industry 4,0-A Glimpse.

[3] B.M. Omowole, A.Q.O. Phillips, O.C. Ofodile, N. L. Eyo-Udo, E. Ewim, 2024. Barriers and drivers of digital transformation in SMEs: A conceptual analysis.

[4] P.C. Verhoef, T. Broekhuizen, A. Bhattacharya, J.Q. Dong, N. Fabian and M. Haenlein, 2021. Digital transformation: A multidisciplinary reflection and research agenda

[5] S. Purnomo, Nurmalitasari, and Nurchim,2024. Digital transformation in MSMEs in Indonesia: A systematic literature review.

[6] J. Xiaosheng, Z. Hua, Z. Jin, K. AL-Bukhaiti and A. Wan, 2024. Overcoming digital transformation barriers: chinese SMMEs in the sharing economy.

[7] N. Kazantsev, G. Pishchulov, N. Mehandjiev, P. Sampaio, and J. Zolkiewski, 2022. Investigating barriers to demand-driven SMEcollaboration in low volume high-variability manufacturing.

[8] L.E. Valdez-Juarez, E.A. Ramos-Escobar and E.P. Borboa-Alvarez, 2023. Reconfiguration of technological and innovation capabilities in Mexican SMEs: Effective strategies for corporate performance in emerging.

[9] C.L. Alayon, K. Safsten, and G. Johansson, 2022. Barriers and enablers for the adoption of sustainable manufacturing by manufacturing SMEs.

[10] C.M.Csizar, 2023. Unleashing the digital barrier: Obstaclesand challenges of digital transformation amidst technological roadblocks.

[11] S.O. Idemudia, O.K. Chima, O.J. Ezeilo, B.M. Ojonugwa, A. Ochefu, M.O. Adesuyi, 2023. Digital infrastructure barriers faced by SMEs in transitioning to smart business models.

[12] B.I Adekunle, E.C. Chukwuma-Eka, E.D. Balogun, and K.O Ogunsola, 2021. Predictive analytics for demand forecasting: Enhancing business resource allocation through time series models.

[13] R. Martinez-Pelaez, M.A. Escobar, V.G. Felix, R. Ostos, J. Parra-Michel, V. Garcia, A. Ochoa-Brust, P. Velarde-Alvarado, R.A. Felix, S. Olivares-Bauttisa, V. Flores and L.J. Mena, 2024. Sustainable digital transformation for SMEs: A comprehensive framework for informed decision-making.
[14] F.D. Gouveia, H.S. Mamede, 2022. Digital transformation for SMEs in the retail industry.
[15] L.J. Zheng, J.Z. Zheng, L.Y. S. Lee, S.M. Jaismuddin, and M.M. Kamal, 2024. Digital technology integration in business model innovation for carbon neutrality: An evolutionary process model for SMEs.
[16] J.A.R. Morales, J.A.A. Herrera, D.A.L. Cadavid and A.C. Vargas, 2024. Breaking the digitalization barriers for for SMEs: a fuzzy logic approach to overcoming challenges in business transformation.
[17] J. Stentoft, K. AdsbollWickstrom, K. Philipsen, and A. Haug, 2021. Driver and barriers for industry 4.0 readiness and practice: Emperical evidence from small and medium-sized manufacturers.
[18] G. Kumar, A. Bakshi, A. Khandelwal, A. Panchal, and U. Soni, 2022. Analysing industry 4.0 implementation barriers in Indian SMEs.
[19] MC. Turkes, I Hloban, A Hassan, M-P Andreea, T Dan, and C Sorinal, 2019. Driver and barriers in using industry 4.0: A perspective of SMEs in Romania.
[20] L. Thames, and D. Schaefer, 2017. Industry 4.0: An overview of key benefits, technologies and challenges.
[21] Y. Lu, 2017. Cyber physical system (CPS)-based industry 4.0: A survey.
[22] A. Bokkens, 2021. Financial inclusion and digitalization: A qualitative research into organizational solutions for financial and digital literacy.
[23] H. Gupta, A.K. Yadav, S. Kusi-Sarpong, S.A. Khan and S.C. Sharma, 2022. Strategies to overcome barriers to innovative digitalisation technologies for supply chain logistics resilience during pandemic.
[24] S. Romanova, S. Maryanova, A. Naumov, 2021. Analisis de los factores financierosclave que afectan lamrentabilidad de las empresas en el context de la digitalizacion de la economia.
[25] A. Mahmood, M.A. Habib, M. Ahmad, and S.A Baig, 2025. Barriers to adoption industry 4.0 in textile sector: Analyzing challenges in transitioning to smart manufacturing with ISM and MICMAC.
[26] S.S. Kamble, A. Gaunasekaran, and R. Sharma, 2018. Analysis of the driving and dependence power of barriers to adopt industry 4.0 in indian manufacturing industry.
[27] C. Fang, X. Liu, P.M. Paradalos and J. Pei, 2016. Optimization for a three-stage production system in the internet of things: Procurement, production and product recovery, and acquisition.
[28] A. Benesova and J. Tupa, 2017. Requirements for education and qualification of people in industry 4.0.
[29] S. Kumar, R.D. Raut, E. Aktas, B.E. Narkhede, and V.V. Gedam, 2022. Barriers to adoption of industry 4.0 and sustainability: A case study with SMEs.
[30] T.T Pham, T. Chi Kuo, M. Lang Tseng, R.R Tan, K. Tan, D. Satria Ika, and C. Joe Lin, 2019. Industry 4.0 to accelerates the circular economy: A case study of electric scooter sharing.
[31] F. Gu, J. Guo, P. Hall and X. Gu, 2019. An integrated architecture for implementing extended producer responsibility in the context of industry 4.0.
[32] J. Leng, G. Ruan, P. Jiang, K. Xu, Q. Liu, X. Zhao, and C. Liu, 2020. Blockchain-empowered sustainable manufacturing and product lifecycle management in industry

4.0: A survey.
[33] M. Ingaldi and R. Ulewicz, 2020. Problems implementation of industry 4.0 in enterprises from the SME sector.
[34] S. Ahmad, S. Miskon, R. Alabdan, and I. Tlilli, 2020. Towards sustainable textile and apparel industry: exploring the role of business intelligence systems in the era of industry 4.0.
[35] A. Ribeiro, A. Amaral, T. Barros, 2021. Project manager competencies in the context of the industry 4.0.
[36] P.P. Senna, L.M.D.F. Ferreira, A.C. Barros, J.B. Roca, and V. Magalhães, 2022. Prioritizing barrier for the adoption of industry 4.0 technologies.
[37] R. Kumar, G. Dutta, and R.K. Phanden, 2024. Digitalization adoption barriers in context of sustainability and operational excellence: Implications for SMEs.
[38] R. Eller, P. Alford, A. Kallmunzaer, and M. Peters, 2020. Antecedents consequences and challenges of small and medium-sized enterprise digitalization.
[39] S. Peillon and N. Dubruc, 2019. Barriers to digital servitization in French manufacturing SMEs.
[40] N. Suresh, K. Hemamala, N. Ashok, 2018. Challenging in implementing industry revolution 4.0 in Indian manufacturing SMEs: Insights from five case studies.
[41] S.S. Kamble, A. Gaunasekaran, and R. Sharma, 2018. Analysis of the driving and dependence power of barriers to adopt industry 4.0 in indian manufacturing industry.
[42] H.M. Elhusseiny, J. Crispim, 2022. SMEs, Barriers and opportunities on adopting industry 4.0: A review.

*ISBN 978-81-973526-0-7*

# PERFORMANCE ENHANCEMENT METHODS IN A STEPPED SOLAR DISTILLATION SYSTEM: A REVIEW

Ajay Prakash*[1], Mahesh Kumar[1]
*[1]Department of Mechanical Engineering, Guru Jambheshwar University of Science & Technology, Hisar, India
*rs220160090102@gjust.org

## Abstract

*Solar water distillation is an eco-friendly technique of obtaining clean water from brackish water. A number of designs of solar distillation systems are available out of which the stepped solar distillation system is one of the simplest and yet effective one. Stepped solar distillation systems are known for their decent productivity, compact design and economic fabrication cost. Various modifications have been done to the stepped distillation system in the past few years which are briefly reviewed. The literature suggests that use of multiple modifications such as reflectors, condensers, fins, and energy storage materials provide better results than individual modification. Studies provided that the use of reflectors (internal and external) in stepped system can improve the productivity by 125% as compared to that of conventional flat basin solar distillation system. Whereas, modifications like nano-enhanced phase change material and external condenser can enhance the yield of stepped solar distillation system by 68% and 104%, respectively.*

## Keywords

Stepped solar distillation system, phase change material, nanoparticles, condenser, reflector.

## Introduction

Clean water is a fundamental need of every human on earth. Humans consume water to regulate temperature, transport nutrients and waste removal from the body [1]. Water is also needed in day-to-day human activities like bathing, cleaning and sanitation. Consumption of impure water can cause deadly diseases like Hepatitis and cholera as it contains many harmful microorganisms, chemicals and other pollutants. Other than human consumption the agriculture and industrial sector also need and ample amount of water for growing crops and carrying out manufacturing operations, respectively. Although, the earth is majorly covered with water (71%), but a large fraction of it (97.5%) is available in the form of saline water. The freshwater availability on Earth is a very small fraction (2.5%) of the total world's water, that also is available in the form of groundwater, glaciers and ice caps [2]. Due to increasing population, over-exploitation and ill reusability of the available water resources, freshwater availability in many regions of the world has reached an alarming stage. In the arid areas the available freshwater resources are very scarce and are not sufficient for the population living there. These areas depend on rain water harvesting, water recycling and water desalination processes to meet their daily needs. So, it becomes very much important to develop a sustainable and economic water desalination technique for these areas. Globally, various desalination techniques have been developed to produce clean water from saline and brackish sources. Some of the most used techniques are vapour compression distillation, flash distillation, multi-effect distillation, Electro-dialysis, reverse osmosis and Freezing technique. The major drawback of these techniques is that, they require a huge amount of energy [3]. Generally, these systems run on electric power, which is driven from fossil fuels. Our world is well aware of the limited resources of fossil fuels and the hazards caused by them. So, as a sustainable approach, solar energy is being used from the past few decades for obtaining clean water from saline and brackish water [4].

## Stepped solar distillation system

The system used for obtaining clean water from brackish water by using solar energy is known as solar distillation systems. Research has improvised the design of the conventional solar distillation system (CSDS) by changing the basin design, by adding auxiliary unit and by optimizing operational parameters. An effective modification to the CSDS involves replacing the flat basin with a stepped basin, resulting as a stepped solar distillation system (SSDS), as illustrated in Figure 1.

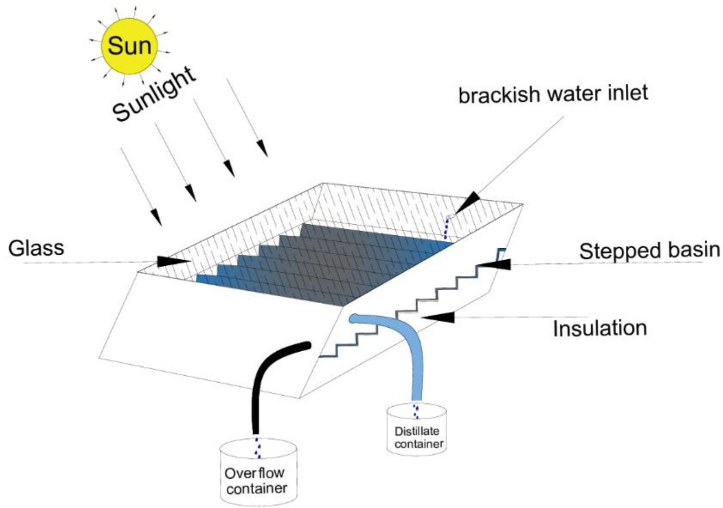


Figure 1. Stepped solar distillation system (SSDS).

The basin of the SSDS provides increased surface area, thus enhanced productivity. Till date, a number of modifications have been done on SSDS, which are shown in shown in Figure 2.

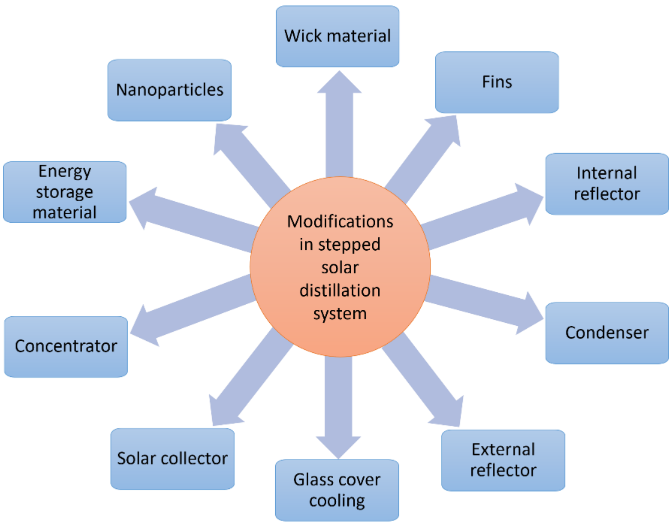


Figure 2. Modifications in stepped solar distillation system.

Baharvand et al., [5] experimentally found 6 L/m²/day in winter and 10 L/m²/day in summer as the optimal inlet water flow rate. The optimal spacing between glass and absorber plate was found to be 8 cm and 12 cm for winter and summer, respectively. The study also suggested fan-based glass cover cooling slightly more productivity than that of water film cooling. Grewal et al., [6] investigates a SSDS having nanoparticle-mixed beeswax (PCM) and an integrated collector, for desalinating RO wastewater. The SSDS yielded 4538.8 g of

distilled water with a thermal efficiency of 54.3%. Chinnasamy et al., [7] enhanced the performance of a SSS by incorporating hexagram-shaped aluminium fins, which increased its productivity by 40% achieving a peak productivity of 4.45 l/m² per day. This modification helped in reducing the payback period by 12.6%. Amiri, [8] studied an improved SSDS having a built-in passive condenser by using MATLAB software. The model was also validated by a series of experiments done under various operating conditions. The experiments showed good agreement with a maximum error of 3.7% in yield prediction. Nand et al., [9] investigated the use of glass cover cooling and external reflector on a SSDS. The modified SSDS produced a daily yield of 4.34 kg/m² with a corresponding thermal efficiency of 40.78%. Banoqitah et al., [10] improved the productivity of an SSDS by laying an energy storage material (phase change material; PCM) beneath the basin. Three different arrangements were studied, first SSDS with sand bed, second with PCM and third with Ag-nanoparticles enhanced PCM, by using ANFIS and ANFIS-PSO. It was observed that third arrangement produced maximum yield, which could be further increase by increasing the concentration of nanoparticles. Singh et al., [11] reviewed various designs of solar distillation system (single slope, pyramidal, tubular, stepped and hemispherical) accompanied by PCM and nanoparticles. The study showed that the productivity of SSDS having PCM and nanoparticles increased by 68% as compared to the CSDS. Shahdabadi et al., [12] used a sun simulator made of eight 500-watt halogen bulb to a SSDS. The steps of the basin were equipped with iron ore and granite, for absorbing additional heat and sponge pieces were placed for increasing the surface area of evaporation. It was observed that the SSDS having iron ore has 10°C higher basin temperature as compared to simple one, which gave peak distillate output and efficiency of about 34.5%.
Atteya & Abbas [13] used different color and heights of sand for improving the productivity of a SSDS. Internal reflectors, sand bed were placed on the steps of SSDS and a cooling coil was circulated from the SSDS to the feed water tank for simultaneously pre heating the inlet water and for enhancing the rate of condensation. It was reported that the SSDS yielded 8600 mL/m2. Grewal & Kumar, [14] compared a concatenated SSDS with an equivalent area SSDS. The thermal efficiency of concatenated SSDS was observed to be 33.80% which was 66.42% higher than that of equivalent area SSDS. The carbon mitigation of concatenated SSDS was observed to be 8.89 tons which was 2.97 tons higher than the equivalent area SSDS. Varun et al., [15] used ANSYS for two-dimensional analysis of SSDS. The numerical study suggested the SSDS have enhanced productivity due to its larger heat absorbing area, which can be further enhanced by using curved top glass cover and baffles in the SSDS. Jathar et al., [16] mixed magnesium oxide, aluminium oxide and titanium oxide nanoparticles in the uncleaned water for improving the rate of evaporation in a concave shape SSDS. The tests were done at 7mm, 10mm and 15mm water depth and 0.1% and 0.2% nanoparticles concentration. The magnesium oxide, aluminium oxide and titanium oxide nanoparticle with 0.2% concentration provided best distillate output of 4.950ml/day, 4.556ml/day and 4.102ml/day, respectively at 7mm water depth. Narang et al., [17] employed fourth degree Runge-Kutta method in python language to run a simulation of SSDS having pre heated inlet water from an external PV/T panel. The simulation was done for various seasons and different parameters like thickness and inclination of top glass cover, insulation thickness, water height, and salinity of water. The study reported that the system provided the best productive (12.18 kg/m2day) in summer season. Pirkandi et al., [18] designed a SSDS having pre-heated water from an ETC and external glass reflectors. The distillate production of the abovementioned SSDS was observed as 2760 ml/m2/day. Kaviti et al., [19] used permanent ferrous magnet on the steps of SSDS for magnetizing the impure water, further, activated carbon particles (70 micron)

*ISBN 978-81-973526-0-7*

were added in the inlet water to increase the evaporation rate inside the SSDS. Study revealed that the system with both magnets and activated carbon provided 900ml/day of distillate. Whereas, yield of the systems having no modifications and one having only magnets were 440 ml/day and 730 ml/day, respectively. Shmroukh & Ookawara [20] reviewed various modifications done on the SSDS. The review concluded that the SSDS are more prominent in the hot arid region and the best productivity was observed to be 8.100 l/m2/day. Samy et al., [21] developed a mathematical model for the heat transfer taking place in the SSDS by using pascal language. From the model it was seen that the performance of the SSDS was better than the CSDS, which have direct dependency on the width and height of the tray/step. The proposed optimum dimensions of the SSDS were 5 steps with 3 cm tray height, 20 cm tray width, 2 cm water height and 1 m width of SSDS. Abdelmonem Essa et al., [22] used corrugated and curved liner on the basin of SSDS. The designed experimental setup included wick material (jute), PCM with copper oxide nanoparticles and a condenser. The productivity and the efficiency of SSDS was found to be 7000ml/m2/day and 59%, which were 2600ml/m2/day and 35% for the CSDS, respectively. Adibi Toosi et al., [23] experimentally analysed the performance of a SSDS having PCM (Stearic acid) and external condenser. The experimental setup included four different arrangements for comparison purpose, first was a simple SSDS, second one loaded with PCM, third one having an external condenser and the fourth one equipped with both PCM and external condenser. The result signified that the productivity of fourth arrangement enhanced by 104% as compared to that of the first one. Sarwar et al., [24] used Microsoft excel for build a SSDS model. The build computational model was also validated with the practical experiments. The referred experimental design consisted of 5 steps each having wire mesh on it, further, external reflectors were also used for increasing the solar insolation. The study involved various optimization parameters like area and material of the steps, thickness of insulation, etc. The computational analysis revealed that the daily productivity in the month of march was 4L/day with average efficiency of 30%.

Gawande et al., [25] constructed SSDS having three different types of step designs namely, flat, convex and concave. Each SSDS consisted of 8 steps, which were provided with brackish water. The results provided that the SSDS having convex steps was 56.6% more productive than that of flat stepped one. Grewal & Kumar, [26] connected three SSDS in series and placed PCM (Paraffin wax) filled copper tubes on their steps in different quantities (15, 30 and 60 PCM filled tubes). The experiments indicated that the third case (SSDS having 60 tubes) was thermally and economically more effective as compared to the rest of cases. Grewal & Kumar, [27] tested three SSDS having PCM filled copper tubes on the steps (10,20 and 30) in parallel arrangement. The experiments showed that the performance of the SSDS increased with increase in quantity of PCM. The cost of distillate produced by the SSDS having maximum number of PCM filled tubes was $0.3 which was higher than the other two SSDS. Shyora et al., [28] constructed a SSDS and CSDS for comparing their daily efficiency and yield. The SSDS consists of 5 steps having mirrors installed on the risers of each step for reflecting the sunlight towards the tread. The efficiency and yield of stepped solar distillation system was observed to be 22.84% and 23.88% higher than that of normal CSS.

Hansen et al., [29] equipped different types of wick materials on different design of absorber plate (flat, wire mesh and stepped). The research included study of various characteristics of wick material like porosity, bulk volume, pore volume, heat transfer coefficient, water absorbance, water repellence and capillary rise. Out of all the wick materials, coral fleece, charcoal cloth, cotton and nylon were observed to be most compatible for wire meshed and stepped distillation units. The coral fleece material was found to be best for the wire meshed and SSDS El-Agouz, [30] evaluated the performance of a SSDS with cotton absorber and black cotton absorber materials for cleaning sea water and saltwater. It was perceived from the experimentations that the SSDS having cotton absorber was 53% and 47% more efficient than the CSDS for sea water and salt water, respectively. Boopalan et al., [31] used two types of PCM (paraffin wax and calcium nitrate) in a SSDS and compared their performance with each other and a simple SSDS. It was observed that the distillate production of the still with paraffin wax was 15% higher than the simple SSDS, whereas, the SSDS with calcium nitrate was 8.17% more productive than the SSDS with paraffin wax. Omara et al., [32] studied the effect of using internal and external reflectors in a SSDS. The internal reflectors were fixed on the riser of the steps and the external reflectors were affixed on the top and bottom end of the glass cover. The study revealed that, by using internal and both external reflectors the SSDS can give 125% higher distillate production. Abdullah, [33] studied the effects of certain modifications in SSDS such as using solar air collector, glass cover cooling and aluminium pieces as energy storage material. The productivity of the abovesaid SSDS enhanced by 85%, 65% and 53%, as compared to a CSDS (30.4%), respectively. Table 1. Describes some more researches on modified SSDS.

Table 1. Researches on stepped solar distillation system (SSDS).

| Sr. No. | Researcher and year | Location | Efficiency/ yield | Work done & remarks |
|---|---|---|---|---|
| 1 | Jathar & Ganesan[34] | Pune, India | 28.27% | The use of energy storage material (sand, bricks and concrete). Concrete was found to be the best |
| 2 | Kabeel et al., [35] | Tanta, Egypt | 51.82% | Usage of graphite and PCM material, internal reflectors and ETC. |
| 3 | Sathyamurthy et al., [36] | Chennai, India | 2.25 kg/ day | MgO and $TiO_2$ nanoparticles added to the water. MgO with 0.2% concentration was found with highest yield. |
| 4 | Abujazar et al., [37] | Selangor, Malaysia | 29.5% | Experimental and theoretical study of inclined type SSDS. |
| 5 | Saadi et al., [38] | Adrar, Algeria | 55.81% | The vertical side of the CSS was provided with stepped trays to hold water. |
| 6 | Naroei et al., [39] | Zahedan, Iran | 32.5% | Arrangement of pre heated water from the surface of PV/T panel. The electrical efficiency and thermal efficiency of PV/T panel and SSDS increased, respectively. |
| 7 | Muftah et al., [40] | Selangor, Malaysia | 60.2% | Various modifications like reflectors, fins and condenser were done. A significant increase in thermal efficiency was observed by the abovesaid modifications. |
| 8 | Bhalara et al., [41] | Bhopal, India | 326.66% higher than CSS | The steps of the SSDS were equipped with earthen lamps, which were used as energy storage material. |
| 9 | El-Samadony et al., [42] | Kafrelsheikh University, Egypt | 66% | The SSDS is equipped with external reflectors and condenser. |
| 10 | Kabeel et al., [43] | Kafrelsheikh University, Egypt | 53% | An ETC is connected to SSDS with wick material on the riser of each step. |

## Conclusion

The literature indicates that the combinations of multiple modifications such as PCM, nanoparticles, reflectors, fins, and preheating systems provide the highest performance improvement in stepped solar distillation system (SSDS), confirming its strong potential for sustainable freshwater production in arid regions.

- SSDS with internal and external reflectors exhibits 125% higher productivity as compared to conventional solar distillation system (CSDS), while it was 326.66% higher when earthen lamps were used as energy storage material.
- Thermal efficiency of SSDS can reach very high levels when combined with multiple modifications such as reflectors, condensers, fins, and energy storage materials. Experimental investigations reported thermal efficiencies as high as 60.2%, 59%, and 54.3%, indicating the strong potential of modified SSDS for efficient solar desalination.
- Incorporation of phase change materials (PCM) and nanoparticles can enhance productivity by up to 68%, while using an external condenser with it provides 104% higher productivity as compared to that of a simple SSDS.
- External modifications such as reflectors, solar collectors and concentrators significantly increase the basin temperature and the evaporation rate. The simulation studies had reported yield as high as 12.18 kg/m²/day.
- Integration of glass cover cooling arrangement and condensers enhances the rate of condensation, achieving overall yield up to 8600 mL/m²/day.

## References

[1] H. H. Mitchell, T. S. Hamilton, F. R. Steggerda, and H. W. Bean, "the Chemical Composition of the Adult Human Body and Its Bearing on the Biochemistry of Growth," J. Biol. Chem., vol. 158, no. 3, pp. 625–637, 1945, doi: 10.1016/s0021-9258(19)51339-4.

[2] "How Much Water is There on Earth? | U.S. Geological Survey." https://www.usgs.gov/special-topics/water-science-school/science/how-much-water-there-earth (accessed Jul. 16, 2023).

[3] A. Prakash and M. Kumar, "Experimental investigations on simple and modified concatenated stepped solar still units for the extraction of clean water: A comparative study," Renew. Energy, vol. 238, no. November 2024, p. 121957, Jan. 2025, doi: 10.1016/j.renene.2024.121957.

[4] H. Manchanda, M. Kumar, M. Gupta, and Shimpy, "No load testing of single slope solar distillation- cum-drying unit: An experimental study," Trends Adv. Mech. Eng., no. April, pp. 17–22, 2019.

[5] R. Baharvand, M. R. Assari, H. B. Tabrizi, A. J. G. Beik, and M. Setareh, "Enhanced productivity in stepped solar stills: An experimental comparative study of brine flow rates, absorber-glass distances, and cooling mechanisms," Desalin. Water Treat., vol. 323, p. 101251, 2025, doi: 10.1016/j.dwt.2025.101251.

[6] R. Grewal, A. Prakash, and M. Kumar, "Effects of nanoparticles mixed beeswax and solar collectors on the performance of a stepped solar still: An experimental study," Energy Sources, Part A Recover. Util. Environ. Eff., vol. 47, no. 1, pp. 1–15, 2025, doi: 10.1080/15567036.2025.2450006.

[7] S. Chinnasamy, K. Balasubramanian, A. Sampathkumar, P. K. Babu, and C. S. Satchi, "Feasibility assessment of a stepped solar still integrated with hexagram fin: an experimental and numerical approach toward sustainability," Environ. Sci. Pollut. Res., vol. 31, no. 41, pp. 53973–53992, 2024, doi: 10.1007/s11356-023-30726-y.

[8] H. Amiri, “Development and application of a thermal model for the improved stepped solar still with a built-in passive condenser,” Sol. Energy, vol. 270, p. 112378, 2024, doi: 10.1016/j.solener.2024.112378.

[9] A. Nand, H. Manchanda, M. Kumar, R. Grewal, and R. Kumar, “Effects of external reflector and glass cover cooling on thermo-enviro-economic performance of a stepped solar still,” Heat Transf., vol. 53, no. 1, pp. 97–114, Jan. 2024, doi: 10.1002/htj.22943.

[10] E. Banoqitah et al., “Enhancement and prediction of a stepped solar still productivity integrated with paraffin wax enriched with nano-additives,” Case Stud. Therm. Eng., vol. 49, no. March, p. 103215, 2023, doi: 10.1016/j.csite.2023.103215.

[11] D. Singh, D. Buddhi, and A. Karthick, “Productivity enhancement of solar still through heat transfer enhancement techniques in latent heat storage system: a review,” Environ. Sci. Pollut. Res., vol. 30, no. 1, pp. 44–77, 2023, doi: 10.1007/s11356-022-23964-z.

[12] R. S. Shahdabadi, A. Mortazavi, S. Ehsan Shakib, and M. M. Ghafurian, “Increasing the production of fresh water in a stepped solar still by different natural materials as photoabsorber,” pp. 1–26, 2023, [Online]. Available: https://doi.org/10.21203/rs.3.rs-2154554/v1

[13] T. E. M. Atteya and F. Abbas, “Testing a stepped solar still with different sand beds and reflectors,” Case Stud. Therm. Eng., vol. 43, no. November 2022, p. 102782, 2023, doi: 10.1016/j.csite.2023.102782.

[14] R. Grewal and M. Kumar, “Application of concatenated stepped solar still system (CS4) for RO-waste-water purification: an experimental study,” Environ. Sci. Pollut. Res., vol. 30, no. 1, pp. 1460–1476, Jan. 2023, doi: 10.1007/s11356-022-22251-1.

[15] M. Varun, S. Subhani, and R. S. Kumar, “Convection heat transfer of stepped basin single slope solar still : A numerical investigation,” vol. 17, no. 2, pp. 9433–9442, 2023.

[16] L. D. Jathar, S. Ganesan, and L. Palanimuthu, “Performance assessment of concave-type stepped desalination unit with nanoparticles and varying water depth: an experimental approach,” Int. J. Ambient Energy, vol. 43, no. 1, pp. 5041–5054, 2022, doi: 10.1080/01430750.2021.1933589.

[17] A. Narang et al., “Performance Evaluation of a Photovoltaic-Thermal Collector Coupled Stepped Solar Still for Indian Climatic Conditions,” Model. Simul. Eng., vol. 2022, pp. 1–16, 2022, doi: 10.1155/2022/4179612.

[18] J. Pirkandi, F. Kassaei, and M. Hashemabadi, “Experimental investigation of simultaneous effect of parabolic trough collector and flat external reflectors on performance of stepped solar still,” Water Supply, vol. 22, no. 3, pp. 3086–3102, 2022, doi: 10.2166/ws.2021.416.

[19] A. K. Kaviti, S. R. Akkala, and V. S. Sikarwar, “Productivity enhancement of stepped solar still by loading with magnets and suspended micro charcoal powder,” Energy Sources, Part A Recover. Util. Environ. Eff., vol. 00, no. 00, pp. 1–19, 2021, doi: 10.1080/15567036.2021.2006371.

[20] A. Shmroukh and S. Ookawara, “Stepped Solar Stills’ Development and Improvement for Seawater Desalination,” SVU-International J. Eng. Sci. Appl., vol. 2, no. 2, pp. 26–36, 2021, doi: 10.21608/svusrc.2021.86943.1012.

[21] N. Samy, A. A. El-Sebaii, S. Aboul-Enein, M. R. I. Ramadan, and A. M. Khallaf, “Mathematical modeling of the heat exchange in a stepped solar still,” Egypt. J. Solids, vol. 43, no. 1, pp. 78–97, 2021, doi: 10.21608/ejs.2021.69568.1010.

[22] F. Abdelmonem Essa et al., “Augmenting the productivity of stepped distiller by

corrugated and curved liners, CuO/paraffin wax, wick, and vapor suctioning," 2021, doi: 10.1007/s11356-021-14669-w/Published.

[23] S. S. Adibi Toosi, H. R. Goshayeshi, and S. Zeinali Heris, "Experimental investigation of stepped solar still with phase change material and external condenser," J. Energy Storage, vol. 40, Aug. 2021, doi: 10.1016/j.est.2021.102681.

[24] I. Sarwar, M. Das, M. Zahan, M. Islam, and F. N. Ani, "A Computational Model for Performance Optimization of a Stepped Solar Still," Proc. 2nd Int. Semin. Sci. Appl. Technol. (ISSAT 2021), vol. 207, no. Issat, pp. 137–144, 2021, doi: 10.2991/aer.k.211106.022.

[25] J. S. Gawande, L. B. Bhuyar, and S. J. Deshmukh, "Effect of Depth of Water on the Performance of Stepped Type Solar Still," Energy Power Eng., vol. 5, no. October, pp. 489–497, 2013.

[26] R. Grewal and M. Kumar, "Performance evaluation of a concatenated stepped solar still system loaded with different masses of energy storage material," Energy, vol. 259, Nov. 2022, doi: 10.1016/j.energy.2022.125005.

[27] R. Grewal and M. Kumar, "Comparative study on stepped solar distillers internally loaded with different masses of phase change material," Int. J. Energy Res., vol. 46, no. 9, pp. 12948–12962, 2022, doi: 10.1002/er.8071.

[28] A. Shyora, K. Patel, and H. Panchal, "Comparative analysis of stepped and single basin solar still in climate conditions of Gandhinagar Gujarat during winter," Int. J. Ambient Energy, vol. 42, no. 14, pp. 1649–1659, 2021, doi: 10.1080/01430750.2019.1612781.

[29] R. S. Hansen, C. S. Narayanan, and K. K. Murugavel, "Performance analysis on inclined solar still with different new wick materials and wire mesh," Desalination, vol. 358, no. February, pp. 1–8, Feb. 2015, doi: 10.1016/j.desal.2014.12.006.

[30] S. A. El-Agouz, "Experimental investigation of stepped solar still with continuous water circulation," Energy Convers. Manag., vol. 86, pp. 186–193, 2014, doi: 10.1016/j.enconman.2014.05.021.

[31] N. Boopalan, B. Kalidasan, K. Ranjith, B. Dhanush, S. Anbarasu, and S. Panner Selvam, "Experimental Study and Performance Analysis of Phase Change Material Integrated Stepped Slope Solar Still," IOP Conf. Ser. Mater. Sci. Eng., vol. 1059, no. 1, p. 12002, 2021, doi: 10.1088/1757-899X/1059/1/012002.

[32] Z. M. M. Omara, A. E. E. Kabeel, and M. M. M. Younes, "Enhancing the stepped solar still performance using internal and external reflectors," Energy Convers. Manag., vol. 78, pp. 876–881, Feb. 2014, doi: 10.1016/j.enconman.2013.07.092.

[33] A. S. Abdullah, "Improving the performance of stepped solar still," Desalination, vol. 319, pp. 60–65, 2013, doi: 10.1016/j.desal.2013.04.003.

[34] L. D. Jathar and S. Ganesan, "Assessing the performance of concave type stepped solar still with brick, sand, and concrete pieces," Int. J. Ambient Energy, vol. 43, no. 1, pp. 3468–3484, 2020, doi: 10.1080/01430750.2020.1839551.

[35] A. E. Kabeel, M. M. Khairat Dawood, T. Nabil, and B. E. Alonafal, "Improving the performance of stepped solar still using a graphite and PCM as hybrid store materials with internal reflectors coupled with evacuated tube solar collector," Heat Mass Transf. und Stoffuebertragung, vol. 56, no. 3, pp. 891–899, 2020, doi: 10.1007/s00231-019-02741-8.

[36] R. Sathyamurthy et al., "Experimental investigation on the effect of MgO and TiO2 nanoparticles in stepped solar still," Int. J. Energy Res., vol. 43, no. 8, pp. 3295–3305, 2019, doi: 10.1002/er.4460.

[37] M. S. S. Abujazar, S. Fatihah, E. R. Lotfy, A. E. Kabeel, and S. Sharil, "Performance

evaluation of inclined copper-stepped solar still in a wet tropical climate," Desalination, vol. 425, no. October 2017, pp. 94–103, 2018, doi: 10.1016/j.desal.2017.10.022.

[38] Z. Saadi, A. Rahmani, S. Lachtar, and H. Soualmi, "Performance evaluation of a new stepped solar still under the desert climatic conditions," Energy Convers. Manag., vol. 171, no. March, pp. 1749–1760, 2018, doi: 10.1016/j.enconman.2018.06.114.

[39] M. Naroei, F. Sarhaddi, and F. Sobhnamayan, "Efficiency of a photovoltaic thermal stepped solar still: Experimental and numerical analysis," Desalination, vol. 441, no. March, pp. 87–95, 2018, doi: 10.1016/j.desal.2018.04.014.

[40] A. F. F. Muftah, K. Sopian, and M. A. A. Alghoul, "Performance of basin type stepped solar still enhanced with superior design concepts," Desalination, vol. 435, no. July, pp. 198–209, Jun. 2018, doi: 10.1016/j.desal.2017.07.017.

[41] B. Bhalara, R. Varshney, and A. K. Yadav, "Experimental Analysis of Modified Stepped Solar Still," IOSR J. Mech. Civ. Eng., vol. 13, no. 05, pp. 147–151, 2016, doi: 10.9790/1684-130502147151.

[42] Y. A. F. El-Samadony, A. S. Abdullah, and Z. M. Omara, "Experimental study of stepped solar still integrated with reflectors and external condenser," Exp. Heat Transf., vol. 28, no. 4, pp. 392–404, 2015, doi: 10.1080/08916152.2014.890964.

[43] A. E. Kabeel, A. Khalil, Z. M. Omara, and M. M. Younes, "Theoretical and experimental parametric study of modified stepped solar still," Desalination, vol. 289, pp. 12–20, 2012, doi: 10.1016/j.desal.2011.12.023.

# NO LOAD TESTING OF PCM LOADED MODIFIED CONCATENATED STEPPED SOLAR DISTILLATION SYSTEM

Ajay Prakash*[1], Mahesh Kumar[1]
*[1]Department of Mechanical Engineering, Guru Jambheshwar University of Science & Technology, Hisar, India
*rs220160090102@gjust.org

## Abstract

*Clean water scarcity is a major global challenge, especially in the arid and semi-arid regions the water resources are often non-potable. Solar distillation offers a sustainable and simple approach for producing clean water from saline or brackish water sources. Out of the available designs of solar distillation units, stepped distillation unit is one of the economical and easy to fabricate one. In recent time various modifications have been applied to the stepped solar distillation unit (SSDU). One of most recent modification is arranging the units in series arrangement, that is known as concatenated stepped solar distillation system. In this study a parallel comparison of modified and simple concatenated stepped solar distillation systems having phase change material (beeswax)has been done under no load condition. Additionally, the modified system was equipped with external reflector and array of aluminium pin fins on the steps of each modified stepped solar distillation unit. Higher basin, glass and phase change material (PCM) temperatures were observed for the units of modified system. The maximum basin, glass and PCM temperature of values 104.3°C, 78.8°C and 85.1°C were observed from the first unit of modified system. Correspondingly the maximum temperatures observed from the units of simple system were 91.2°C, 73.6°C and 75.9°C, respectively.*

## Keywords

Concatenated stepped solar distillation system, external reflector, pin fins, phase change material

## Introduction

The earth consists of diverse ecosystems such as rainforests, grasslands and deserts, which are largely influenced by the availability of water in that particular region. Water exists in various forms on the planet, including lakes, ponds, seas and oceans [1]. Although, water is abundantly available on earth but only a fraction of it is suitable for human consumption. Clean water is one of the most essential requirements for human survival. In many arid and semi-arid regions of the world, freshwater availability is very limited and the available water resources are often non-potable. Such regions largely depend on water recycling and water desalination technologies. However, the traditional water desalination processes are highly-energy intensive and mostly rely on electricity generated from a non- renewable energy source [2]. For a sustainable future, it is therefore essential to use a renewable energy resource for water purification. Solar distillation is one of the most promising techniques of producing clean water from saline or brackish water by using renewable solar energy.
Various designs of solar distillation units have already been developed, including conventional flat basin type, stepped, hemispherical, pyramidal and cylindrical solar distillation units [3]. Among these, the stepped solar distillation unit (SSDU) can be regarded as one of the most economical and easy to fabricate one. From the past few decades many design and operational modifications have been introduced to the stepped solar distillation

units.

Pradeep et al., [4] conducted a CFD analysis of a multi-basin SSDU with modifications such as corrugated surfaces and fins, along with IoT-based monitoring. The study reported a maximum yield of 27.8 L/day which was 124% higher than conventional flat basin distillation unit. The thermal efficiency of the unit was reported to be 70%. Grewal et al., [5] experimentally investigated a SSDU having nano-enhanced PCM (Aluminium nanoparticles and beeswax) and solar air collectors for purification of RO wastewater. The modified unit produced 4538.8 g distillate with a thermal efficiency of about 54.32%. Rajesh and Chiranjeevi [6] experimentally investigated a SSDU having photovoltaic-thermal (PVT) panel and a humidification-dehumidification unit. The designed system produced average distillate between 6.4 and 7.45 L/m²/day with an overall efficiency ranging from 61 to 67% and exergy efficiency of about 17%. Hammad et al., [7] investigated a dome-shaped solar distillation unit having copper oxide nano powder mixed PCM. The unit produced 7.21 kg/m²/day of distillate which was nearly 62% higher than the conventional dome shaped distillation unit. El-Sebaey and Ganaoui [8] experimentally studied a semi-cylindrical distillation unit having stepped basin and PCM (paraffin wax). The results revealed that the distillation unit produced about 3889 mL/m²/day with a thermal efficiency of 36.86%. Davra et al., [9] studied a double-basin SSDU having a vertical wick. Results provided that the unit produces about 8 kg/m²/day freshwater with maximum thermal efficiency of 48%. Bakhtierkhalzi et al., [10] studied a pyramid solar still having stepped basin and found its productivity and energy efficiency to be 1.24 L/m²/day and 27.5%, respectively. Amiri, [11] tested a model of SSDU having a passive condenser using MATLAB. The model was validated with different meteorological data and operating conditions. Results showed good agreement with the experiments, having maximum error of about 3.7% in yield prediction. Sathyamurthy, [12] experimentally investigated a SSDU having nano-doped PCM (silver and paraffin wax). The study provided that the unit was capable of producing 7.98 kg/m²/day of distillate which was higher than 6.73 kg/m²/day with PCM and 3.61 kg/m²/day without PCM. Rajesh and Chiranjeevi [13] investigated a SSDU having a PVT module. The waste heat recovered from the PVT module was used to preheat the saline water supplied to the unit. Results showed distillate production, thermal efficiency and electric efficiency of 3460 ml/m², 49% and 15%, respectively. Muftah et al., [14] tested a SSDU having reflectors, fins, and condenser. The results revealed that the distillate productivity and the thermal efficiency of the tested unit was 6.10 kg/m²/day and 52.3%, respectively. Khalili et al., [15] studied a SSDU having angled metallic fins on the steps for enhancing the rate of absorption of solar radiations. The study revealed that the fins angled at 30° gave the best performance at 100 ml/min flow rate by increasing the efficiency by about 171% compared to a unit without fins. Grewal and Kumar, [16] investigated a SSDU having PCM (paraffin wax) tubes for increasing the brix of raw sugarcane juice while producing distilled water as a by-product. The experiments were conducted on different PCM masses (0.45, 0.9 and 1.35 kg 450 g). Results showed that the unit with 1.35 kg PCM mass produced concentrated sugarcane juice 19.6°B and 2.45 kg/day distillate with highest thermal efficiency of 43.3%. Prakash et al., [17] optimized the flow rate of a SSDU having nano-enhanced PCM (aluminium nano powder and beeswax) and a solar air collector. The unit performed best at 30ml/min flow rate and produced 3.98 kg/m²/day of distilled water.

It can be seen from the literature that SSDU are very productive in brackish water distillation. Recently, Grewal and Kumar [18] arranged three SSDU in series arrangement known as the concatenated stepped solar distillation system (CSSDS) and found that the concatenated system performed better than a single equivalent area SSDU.

Grewal and Kumar, [19] experimentally compared a CSSDS with a simple SSDU having

equivalent area. The results provided that the concatenated system had higher thermal efficiency (33.8%) and produced 2.8 kg/day of distilled water, which was 24.7% higher than that of the simple one. Grewal and Kumar, [20] studied a CSSDS having PCM (paraffin wax) tubes. The study was done for different PCM masses (0.675, 1.35 and 2.7 kg). The system having 2.7 kg of PCM performed the best by producing 2.18 kg of distillate and 25.8°Brix concentrated sugarcane juice. Prakash and Kumar, [21] compared the performance of a CSSDS having reflectors, fins, wick material, and glass cover cooling arrangement with a simple CSSDS. The systems were utilized for simultaneous obtainment of concentrated sugarcane juice and distilled water. The modified system produced 5.65 kg/day distilled water with a thermal efficiency of 45%. The concentrated sugarcane juice produced by modified system had a brix value of 38.2°. Prakash and Kumar, [22] experimentally compared a CSSDS having reflectors and glass cover cooling arrangement with a simple CSSDS for clean water production. Results provided that the modified system produced 3.43 L/day distillate which was 18.72% higher than the simple one.
It can be observed from the literature that there is no study available on the no load testing of a concatenated stepped solar distillation system having beeswax as PCM. So, an attempt is being made for evaluating the thermal response of the concatenated stepped solar distillation system under the adverse operating conditions.

## Materials and methods

The experiment was parallelly conducted on a modified concatenated stepped solar distillation system (MCSSDS) and a simple concatenated stepped solar distillation system (SCSSDS) having PCM (Beeswax) under no load condition. The MCSSDS consisted of three modified SSDU namely MSSDU-1, MSSDU-2 and MSSDU-3., respectively (Figure 1). The MSSDU-1 was equipped with an external reflector whereas, pin fins were installed on the steps of all MSSDU. Similarly, SCSSDS consisted of three simple SSDU namely, SSSDU-1, SSSDU-2 and SSSDU-3, respectively. The SSSDU were kept without any modification (Figure 1). The beeswax was layered beneath the steps of every SSDU in a stepped shape PCM chamber having uniform thickness of 1cm.

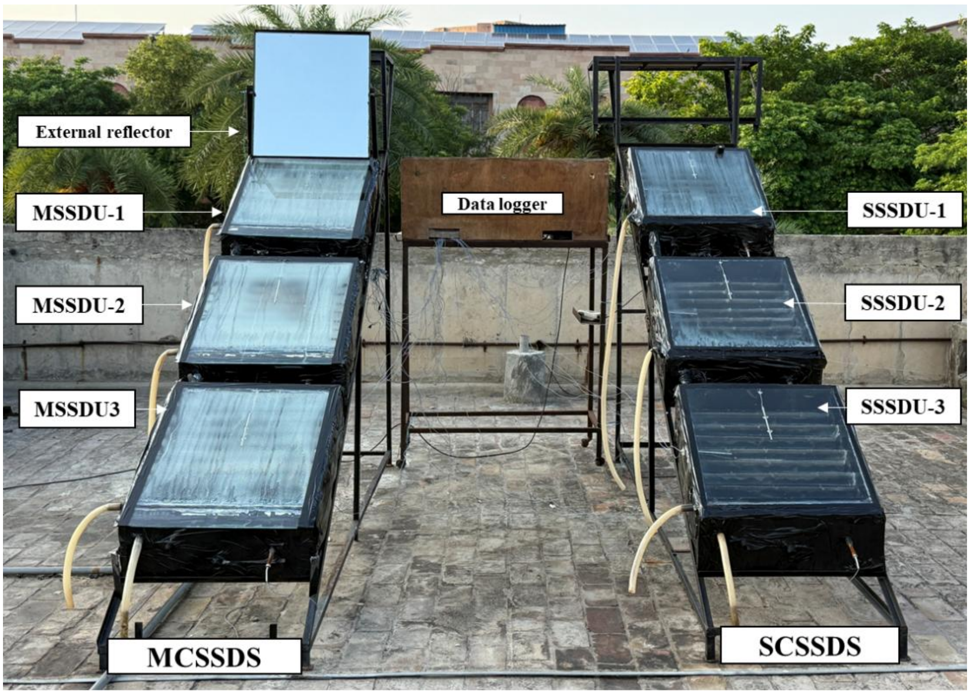


Figure 1. Picture of the modified and simple concatenated stepped solar distillation systems.

*ISBN 978-81-973526-0-7*

Each SSDU consisted of ten equal size steps (riser; 3cm, tread; 5cm and width; 50cm). The steps of the basin of SSDU were fabricated by using 2mm thick MS sheet. The basin was painted with black color to enhance its thermal absorption. The top most step of the SSDU of both MCSSDS and SCSSDS were provided with water inlet port, similarly, the bottom most step of the SSDU were provided with an outlet port. All the SSDU of MCSSDS and SCSSDS were connected end to end for a series arrangement, as shown in Figure 1. The top of the SSDU was covered by using a transparent glass, to avoid any loss of thermal radiations. The side walls and the bottom of all SSDU were insulated with respective layer of glass wool, polystyrene, thermocol and fiberglass reinforced plastic sheet.

The steps of the MSSDU-1, MSSDU-2 and MSSDU-3 were provided with an array (3×35) of hollow cylindrical aluminium pin fins for enhancing the heat transfer rate. In addition to the fins, MSSDU-1 was also equipped with a flat external reflector of thickness 4mm that directed additional heat to the basin. The external reflector was tilted backwards at an optimal angle of 15° from the vertical [23].

The experiment was conducted at Guru Jambheshwar University of Science and Technology, Hisar, India (29° 10' 11" North, 75° 44' 20" East). Both the concatenated systems (MCSSDS and SCSSDS) were placed facing south at an inclination angle of 29°, i.e., latitude angle.

The temperatures of basin (Tb), glass cover (Tg) and PCM (Tpcm) were measured using PT-100 thermocouples and gathered by using a data logger. The solar intensity (I) and ambient temperature (Tamb) were measured using solarimeter (least count 0.1 W/m2) and zeal thermometer (least count 0.1°C), respectively. The data collection was carried out on hourly basis from 07:30 am of 19th June 2025 till 07:30 am of 20th June 2025.

## Results and Discussions

The 24-hour data gathered during the no load testing of PCM loaded modified and simple concatenated stepped solar distillation system has been discussed in this section. Figure 2 and 4 respectively shows the hourly variations in the solar intensity and ambient temperature during the experimentation.

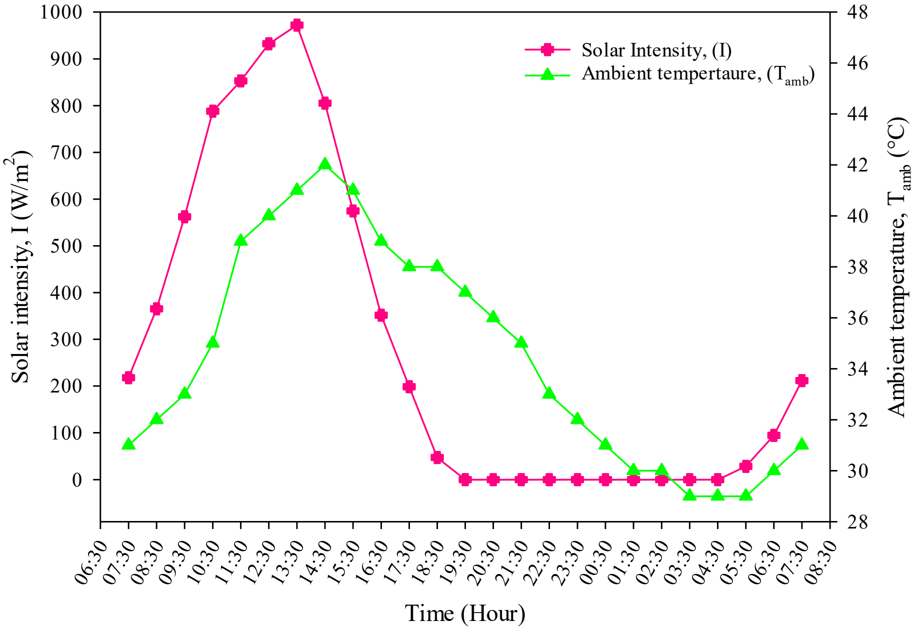


Figure 2. Solar intensity and ambient temperature.

*ISBN 978-81-973526-0-7*

It can be seen from Figure 2 that the solar intensity at 07:30 hours (19/06/2025) was 217.8 W/m2, which attained peak value of 972.1 W/m2 at 13:30 hours. Thereafter, the solar intensity diminished between 18:30 – 19:30 pm. The ambient temperature at the initiation of the experiment (07:30 am of 19/06/2025) was observed to be 31°C which reached the peak value of 42°C at 14:30 pm. The least ambient temperature (29°C) was observed from 03:30 to 05:30 hours. The hourly basin temperature of the SSDU of MCSSDS and SCSSDS are shown in Figure 3.

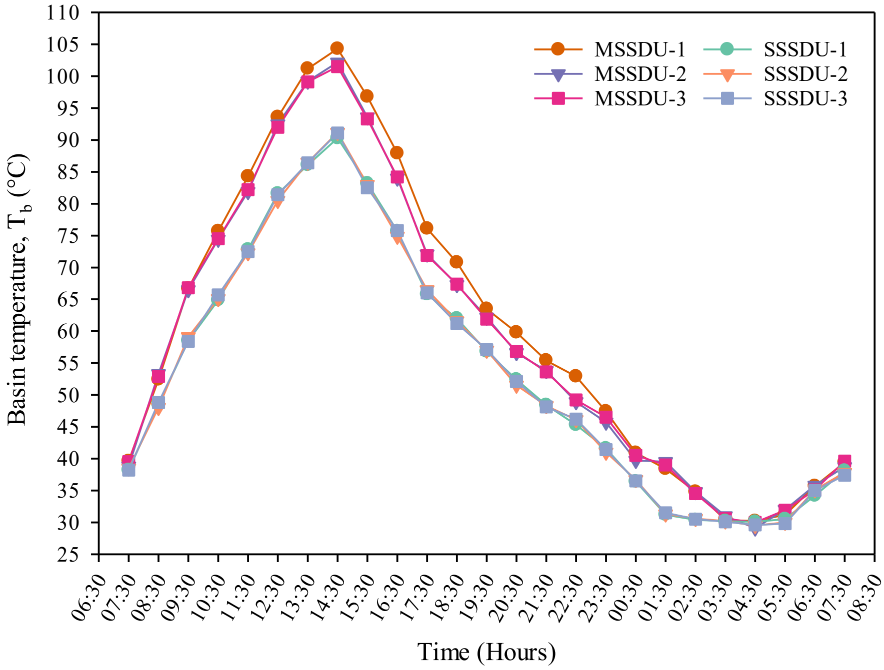


Figure 3. Basin temperatures of SSDU of MCSSDS and SCSSDS.

From Figure 3 it can be seen that, throughout the experiment the SSDU of MCSSDS had higher basin temperature as compared to that of SCSSDS due to the array of fins provided on the steps of MCSSDS. The basin temperatures of MSSDU-1 were higher than that of MSSDU-2 and MSSDU-3 due to the additional radiations provided by the external reflector. The maximum basin temperature in MCSSDS and SCSSDS were recorded in MSSDU-1 and SSSDU-2 as 104.3°C and 91.2°C, respectively, at 14:30 hours. The minimum basin temperatures were observed in MSSDU-2 and SSSDU-2 as 29.1°C and 29.5°C, respectively, at 04:30 hours. The glass cover temperatures of the MCSSDS and SCSSDS are shown in Figure 4.

From Figure 4 it can be observed that, throughout the experiment the SSDU of MCSSDS had higher glass cover temperature as compared to that of SCSSDS due to higher basin temperatures of MCSSDS. The maximum glass cover temperature in MCSSDS and SCSSDS were recorded in MSSDU-1 and SSSDU-3 as 78.8°C and 73.6°C, respectively, at 14:30 hours. The minimum glass cover temperatures were observed in MSSDU-2 and SSSDU-2 as 28.6°C and 28.8°C, respectively, at 04:30 hours. The PCM (beeswax) temperatures of MCSSDS and SCSSDS are shown in Figure 5.

It can be seen from Figure 5 that, throughout the experiment the SSDU of MCSSDS had higher PCM temperature as compared to that of SCSSDS due to higher basin temperatures. The PCM temperature in MSSDU-1 was higher than that in MSSDU-2 and MSSDU-3 due to the additional solar radiation received from the external reflector. The peak PCM temperature in MCSSDS and SCSSDS were recorded in MSSDU-1 and SSSDU-2 as 85.1°C and 75.9°C, respectively, at 15:30 hours. The minimum PCM temperatures were observed in MSSDU-1 and SSSDU-1 as 30.2°C and 29.1°C, respectively, at 06:30 hours. A delayed cooling of PCM was observed in the systems due to slow cooling of the core of PCM layer.

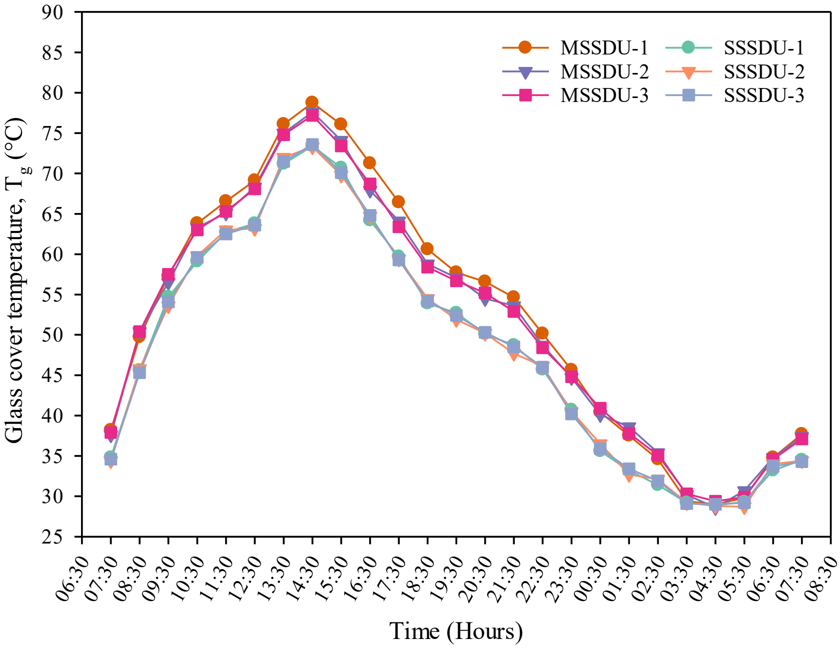


Figure 4. Glass cover temperatures of SSDU of MCSSDS and SCSSDS.

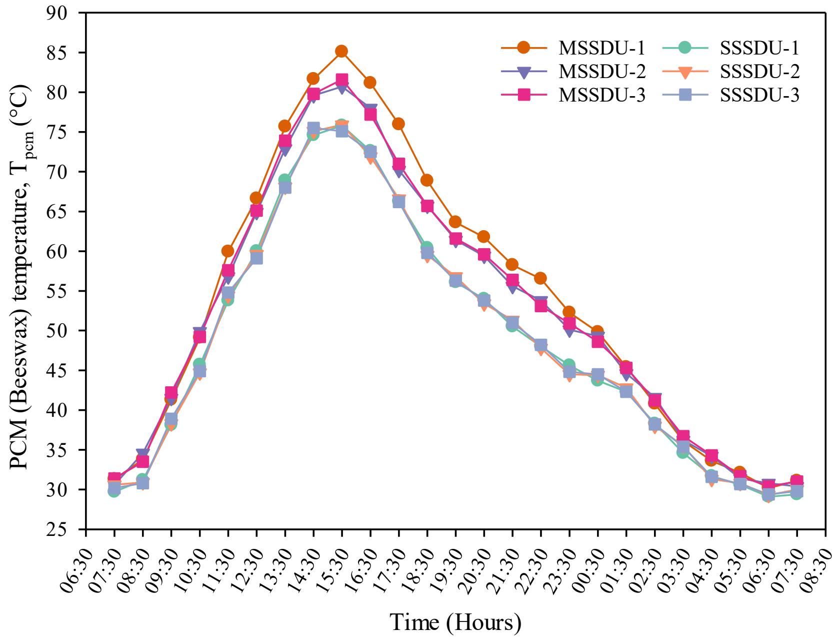


Figure 5. PCM (beeswax) temperatures of SSDU of MCSSDS and SCSSDS.

## Conclusion

Stepped solar distillation unit (SSDU) have a great potential of meeting the daily water demand of arid and semi-arid regions. The concatenated arrangement of the SSDU provides higher performance due to the fact that the second and third SSDU in the concatenated system becomes active in nature, as pre-heated water flows in them from the SSDU correspondingly above them. Simple modifications like deployment of external reflector and fins in the concatenated system can provide even more profound results. The no load testing of both modified concatenated stepped solar distillation system (MCSSDS) and simple concatenated stepped solar distillation system (SCSSDS) provides maximum attainable temperatures, thermal response and behavior of PCM under the most adverse operating conditions.

- The highest basin temperatures in MCSSDS and SCSSDS were observed in the MSSDU-1 and SSSDU-2 as 104.3°C and 91.2°C, respectively, at 14:30 hours.
- The maximum glass cover temperatures in MCSSDS and SCSSDS were recorded in MSSDU-1 and SSSDU-3 as 78.8°C and 73.6°C, respectively, at 14:30 hours.
- The peak PCM temperatures in MCSSDS and SCSSDS were recorded in MSSDU-1 and SSSDU-2 as 85.1°C and 75.9°C, respectively, at 15:30 hours.
- The basin, glass and PCM temperatures reached minimum (nearly equal to the ambient temperature) at 04:30 hours, 04:30 hours and 06:30 hours, respectively.

Results have suggested that the concatenated system can withstand adverse operating temperatures, additionally, modifications like external reflector and fins in a concatenated stepped solar distillation system provided higher basin and PCM temperatures as compared to that of simple one.

## References

[1] A. K. Sharma and D. Singh, "Solar water distillation by wick-type solar stills: a review," Environ. Sci. Pollut. Res., vol. 30, no. 16, pp. 45570–45586, 2023, doi: 10.1007/s11356-023-25930-9.

[2] D. Charitar and A. Madhlopa, "Integration of waste heat in thermal desalination technologies: A review," J. Energy South. Africa, vol. 33, no. 1, pp. 68–84, 2022, doi: 10.17159/2413-3051/2022/v33i1a5434.

[3] V. P. Katekar and S. S. Deshmukh, "A review on research trends in solar still designs for domestic and industrial applications," J. Clean. Prod., vol. 257, p. 120544, 2020, doi: 10.1016/j.jclepro.2020.120544.

[4] B. Pradeep, S. J. P. Gnanaraj, and R. S. S. Raja, "Sustainable solutions in the era of water scarcity: Multi-basin solar still innovations," Desalin. Water Treat., vol. 322, p. 101194, 2025, doi: 10.1016/j.dwt.2025.101194.

[5] R. Grewal, A. Prakash, and M. Kumar, "Effects of nanoparticles mixed beeswax and solar collectors on the performance of a stepped solar still: An experimental study," Energy Sources, Part A Recover. Util. Environ. Eff., vol. 47, no. 1, pp. 1–15, 2025, doi: 10.1080/15567036.2025.2450006.

[6] S. Rajesh and C. Chiranjeevi, "Experimental investigations on PVT-integrated hybrid desalination system: Energy, exergy, and economic analysis," Energy Sources, Part A Recover. Util. Environ. Eff., vol. 46, no. 1, pp. 3793–3806, 2024, doi: 10.1080/15567036.2024.2322682.

[7] F. A. Hammad, M. E. Zayed, E. El-Bialy, K. Irshad, Z. Lu, and S. M. Shalaby, "Performance assessment of a novel solar distiller with a fountain-shaped basin design embedded with phase change materials enriched with copper oxide nano-additives: A detailed experimental investigation," J. Energy Storage, vol. 82, p. 110555, 2024, doi: 10.1016/j.est.2024.110555.

[8] M. S. El-Sebaey and M. El Ganaoui, "Investigating the economic, energetic and exergetic aspects of semi-cylindrical solar still integrated with stepped-basins and phase change material," Process Saf. Environ. Prot., vol. 192, pp. 1455–1466, 2024, doi: 10.1016/j.psep.2024.11.027.

[9] D. Davra, P. Mehta, N. Patel, and B. Markam, "Solar-enhanced freshwater generation in arid coastal environments: A double basin stepped solar still with vertical wick assistance study in northern Gujarat," Sol. Energy, vol. 268, p. 112297, 2024, doi:

10.1016/j.solener.2023.112297.

[10] Bakhtierkhalzi, T. Islam, K. S. Asnaf, A. M. Parvej, and M. R. I. Sarker, "Comparative performance investigation of conventional and modified stepped basin pyramid solar still with improved insulation: Experimental evaluation," Desalination, vol. 587, p. 117964, 2024, doi: 10.1016/j.desal.2024.117964.

[11] H. Amiri, "Development and application of a thermal model for the improved stepped solar still with a built-in passive condenser," Sol. Energy, vol. 270, p. 112378, 2024, doi: 10.1016/j.solener.2024.112378.

[12] R. Sathyamurthy, "Silver (Ag) based nanoparticles in paraffin wax as thermal energy storage for stepped solar still – An experimental approach," Sol. Energy, vol. 262, p. 111808, 2023, doi: 10.1016/j.solener.2023.111808.

[13] S. Rajesh and C. Chiranjeevi, "Experimental investigations on a sustainable cogeneration system for power and desalination with 4-E analysis," Sol. Energy, vol. 264, p. 112046, 2023, doi: 10.1016/j.solener.2023.112046.

[14] A. F. Muftah, K. Sopian, A. Ibrahim, A. Elbreki, and A. M. Abed, "Design and evaluation of a modified basin-type stepped solar- still under Malaysia climate conditions," Energy Sources, Part A Recover. Util. Environ. Eff., vol. 45, no. 3, pp. 6756–6771, Aug. 2023, doi: 10.1080/15567036.2023.2216177.

[15] M. Khalili, M. Taheri, and A. Nourali, "Metal fins efficacy on stepped solar still performance: An experimental study," Desalination, vol. 563, p. 116706, 2023, doi: 10.1016/j.desal.2023.116706.

[16] R. Grewal and M. Kumar, "Investigations on effect of mass of phase change material on sugarcane juice concentration and distillate production in a stepped solar system," J. Energy Storage, vol. 52, Aug. 2022, doi: 10.1016/j.est.2022.104878.

[17] A. Prakash, M. Kumar, R. Grewal, and H. Manchanda, "Toward productivity enhancement of a stepped solar still using bio- phase change material , modified flat plate collector and nanoparticles," J. Brazilian Soc. Mech. Sci. Eng., vol. 47, 2025, doi: 10.1007/s40430-025-05507-y.

[18] R. Grewal and M. Kumar, "Assessment of a solar powered sustainable energy recovery system for cleaner production of concentrated sugarcane juice," Sustain. Energy Technol. Assessments, vol. 52, Aug. 2022, doi: 10.1016/j.seta.2022.102271.

[19] R. Grewal and M. Kumar, "Application of concatenated stepped solar still system (CS4) for RO-waste-water purification: an experimental study," Environ. Sci. Pollut. Res., vol. 30, no. 1, pp. 1460–1476, Jan. 2023, doi: 10.1007/s11356-022-22251-1.

[20] R. Grewal and M. Kumar, "Efficacy of mass of energy storage material on the performance of a solar driven stepped series system during sugarcane juice concentration," Sol. Energy, vol. 243, pp. 300–314, 2022, doi: 10.1016/j.solener.2022.08.009.

[21] A. Prakash and M. Kumar, "Performance assessment of an advanced solar concatenated sugarcane juice distiller," Innov. Food Sci. Emerg. Technol., vol. 104, no. June, 2025, doi: 10.1016/j.ifset.2025.104102.

[22] A. Prakash and M. Kumar, "Experimental investigations on simple and modified concatenated stepped solar still units for the extraction of clean water: A comparative study," Renew. Energy, vol. 238, no. November 2024, p. 121957, Jan. 2025, doi: 10.1016/j.renene.2024.121957.

[23] H. Tanaka, "Monthly optimum inclination of glass cover and external reflector of a basin type solar still with internal and external reflector," Sol. Energy, vol. 84, no. 11, pp. 1959–1966, Nov. 2010, doi: 10.1016/j.solener.2010.07.013.

# ADDITIVE MANUFACTURING OF NATURAL FIBRE REINFORCED BIOPOLYMER COMPOSITES: A REVIEW OF MECHANICAL PROPERTIES, APPLICATIONS AND CHALLENGES

Manjeet Chahar*[1], Rajneesh Kumar[1], Akash Ahlawat[2]
*[1]Department of mechanical engineering, DCRUST, Murthal, Sonipat, Haryana, India
[2]Department of mechanical engineering, UIET, MDU, Rohtak, Haryana, India
manjeetchahar541@gmail.com

## Abstract
*Additive manufacturing (AM), widely known as 3D printing, has emerged as a revolutionary manufacturing technology that enables fabrication of complex geometries using a layer-by-layer material deposition approach. The sustainability, biodegradability, low density, and excellent mechanical qualities of natural fiber reinforced polymer composites (NFRPCs) have led to a lot of interest from researchers in recent years. New possibilities for eco-friendly composite materials in additive manufacturing have emerged with the incorporation of natural fibers including hemp, flax, jute, kenaf, and bamboo into thermoplastic matrices. This review paper provides a comprehensive overview of the additive manufacturing techniques employed for fabrication of NFRCs, including fused deposition modeling (FDM), laminated object manufacturing (LOM) and continuous fibre 3d printing. The influence of fiber type, surface treatment, and processing variables on the mechanical characteristics of printed composites is analyzed. The applications of these materials in the production of automobiles, construction, and eco-friendly items are examined. Significant issues such as moisture absorption, inadequate fiber-matrix adhesion, and printing errors which diminished the mechanical performance of the bio polymer composites was also investigated in this review paper. It was also observed that further research is required to improve the mechanical performance of 3D-printed natural fibre reinforced biopolymers to enable their effective utilization in industries such as automotive, construction, sports equipment, and aviation.*

## Keywords
Nature fibres, Biopolymers, 3D printing, Mechanical properties, Sustainable materials.

## Introduction
Additive manufacturing (AM) is a cutting-edge production process that produces threedimensional items layer by layer from digital blueprints [1]. Additive manufacturing presents several uses across numerous sectors, such as producing models for quick prototyping, fabricating medical implants, aircraft components, automobile parts, architectural designs, and culinary creations. This methodology has transformed industrial operations by enhancing flexibility and enabling the manufacture of complex, specialized items, while minimizing waste and fostering creative design and manufacturing methods [2]. AM pledges to revolutionize the manufacturing sector by guaranteeing sustainability and accuracy at economical prices across several industries [3]. Particularly in terms of accuracy, personalization, and material choices, additive manufacturing sets itself apart from conventional techniques [4]. In contrast to subtractive methods, which include removing material from a solid block, additive manufacturing builds an object by layering on top of a digital design [5]. In order to create complicated features such as undercuts, channels, or

detailed internal geometry, the process may be applied layer after layer with greater accuracy and tighter control [6]. In a similar vein, additive manufacturing attains excellence in terms of customization as the technology enables the creation of products tailored to particular requirements, such dental crowns and bridges [7]. Existing methods allow for precise management and control of each layer to accommodate a variety of designs and properties that cannot be achieved with a subpar approach. Additionally, a single item may incorporate several materials, such as metals, polymers, ceramics, and their mixtures, thanks to additive manufacturing [8]. With ongoing advancements in excellent quality printing, nanomaterial integration, and hybrid manufacturing, 3D printing has the potential to become a fundamental component of the next-generation manufacturing framework, influencing the future of ondemand production, mass customization, and sustainable manufacturing techniques [9].

The wide-ranging usage of petroleum-based polymer mixtures has full-fledged serious environmental alarms due to their non-biodegradable nature and poor recyclability. In response, biodegradable thermoplastic polymers such as polylactic acid (PLA), polyhydroxyalkanoates (PHA), and polybutylene succinate (PBS) have amplified substantial attention for their renewable origins, low carbon footprints, and outstanding compatibility with improver manufacturing [10]. Natural fibres such as hemp, kenaf, sisal, jute, flax, and bamboo offer various benefits as reinforcement materials, including low density, biodegradability, renewability, cost effectiveness, good specific strength, and improved vibration-damping characteristics. When integrated into bio-polymer matrices, natural fibre reinforcement boosts stiffness, improves load transfer, and decreases overall material weight, making these composites attractive for sustainable engineering applications.

However, conventional manufacturing techniques for fabricating natural fibre-reinforced biocomposites, such as compression moulding and injection moulding, suffer from various limitations, including restricted design flexibility, high tooling costs, non-uniform fibre distribution, limited control over fibre orientation, and significant material wastage. These limitations hinder the fabrication of complex and customized components and restrict effective optimization of material composition. These drawbacks can be overcome by fabricaton of NFRPCs by additive manufacturing technique.

## Additive Manufacturing Techniques

Researchers have investigated that there are very few additive manufacturing techniques which can fabricate natural fiber reinforced composites. These limitation are due to less compatibility and processing problem of natural fibres. The three most common techniques are fused deposition modeling (FDM), laminated object manufacturing (LOM) and continuous fibre 3d printing. Depending on the material system and application, each approach offers advantages and disadvantages.

### *Fused Deposition Modeling*

Scott Crump of Stratasys developed Fused Deposition Modeling (FDM) in 1989. In 1992, this additive manufacturing technology was patented for the production of plastic components from solid filament. In 1992, Stratasys launched the inaugural FDM-based 3D printer. It employs material extrusion, a widely utilized additive manufacturing technique owing to its affordability and accessibility. The portable FDM head extrudes semi-viscous filament in layers. The filament temperature is established at one degree above its melting point, ensuring it solidifies immediately upon extruding onto the preceding layer. Utilizing high-quality filament, part precision can attain ± 0.05mm. The compact dimensions of FDM minimize spatial requirements and preservation expenses. Mechanical forces extrude material from the nozzle. This extrusion technique employs a heated extruder to produce thermoplastic filaments into a structure. Layers are applied incrementally. The thickness of layers during printing is typically measured in millimeters. Reduced layer thickness yields more precise and smoother outcomes; however, it extends printing duration and cost [11].

***Laminated Object Manufacturing (LOM)***

Thin sheets of biopolymer composite reinforced with natural fibers are used as raw materials in laminated object manufacturing (LOM). First, a composite material sheet is placed on the construction platform, heated, and compressed. The sheet is then sliced to the proper crosssection for the item using a laser or other cutting instrument. Another sheet is placed on top and adhered to the first layer after it has been cut. Layer by layer, this process is carried out until the finished 3D part is created. The final composite object is created by removing the excess material [12].

***Continuous fibre 3D printing***

Continuous fiber 3D printing is a state-of-the-art additive manufacturing technique that deposits continuous fibers (such flax, jute, or carbon fiber) together with a thermoplastic or biopolymer matrix using a particular print nozzle. In order to allow the fiber to become embedded in the polymer during extrusion, the printer simultaneously feeds the continuous fiber and molten polymer. To create the 3D part, the material is applied layer by layer along the intended toolpath. Continuous fibers significantly increase the printed object's strength and stiffness when compared to short-fibre composites. This method improves the mechanical performance of natural fiber reinforced biopolymer composite structures by allowing you to control the orientation of the fibers [13].

## Strengthening of Bio Polymers with Natural Fibre Reinforcements via Additive Manufacturing

Thermoplastic polymers such as PLA and ABS have relatively low mechanical strength, so they are not suitable for high load-bearing applications. This limitation can be improved by reinforcing these polymers with high-strength fibres, which enhances their overall mechanical performance. Nowadays environmental concern and sustainability are the main concern while developing a new material. Natural fibre reinforced composite (NFRCs) materials are gaining importance due to their superior properties, e.g., lightweight, high specific strength and stiffness, corrosion resistance, wear resistance, carbon neutrality, and cost-effectiveness compared to synthetic fibres. Natural fibres such as hemp, jute, flax, and sisal will be used to strengthen polymers.

Table 1. Summary of Mechanical Properties Enhancement in Additively Manufactured Biopolymers Using Natural Fibres [14-27].

| Author (et al.) | Polymer | Reinforcement | Mechanical Properties Enhanced |
|---|---|---|---|
| Billings et al., 2023 | PLA | Wood fiber | Stress–strain behavior studied; improvement in modulus |
| Ramezani Dana et al., 2022 | PLA | Flax fiber (short) | Deformability increased; tensile strength ↓ ~26% |
| Hamat et al., 2023 | PLA | Kenaf fiber (PDA coated) | Yield strength ↑13.4%, flexural modulus ↑15.3%, compressive stress ↑30% |
| Vinod et al., 2024 | Soy-PLA | Nona natural fiber | Tensile strength up to 74.82 MPa, fatigue life improved |
| Muthe et al., 2024 | PLA | Continuous flax / cellulose yarn | Tensile strength up to 356 MPa, high impact strength |
| Hinchcliffe et al., 2015 | PLA | Continuous jute / flax fiber | Tensile strength ↑116%, stiffness ↑62% |

| | | | |
|---|---|---|---|
| Rafiee et al., 2021 | PLA | Birch fiber | Moderate improvement in stiffness and printability |
| Sekar et al., 2019 | Biopolymer matrix | Natural fiber | Improved mechanical & acoustic properties |
| Agaliotis et al., 2022 | PLA | Henequen fiber flour | Maximum stress increased to 60.1 MPa |
| Siddique et al., 2024 | PLA | Wood fiber | Improved tensile modulus and strength |
| Cai et al., 2022 | Polypropylene | Continuous jute fiber | Tensile modulus ↑157%, strength ↑134% |
| Vallinayagam et al., 2021 | Polymer composite | Biomimetic fiber structure | Strength & fracture toughness ↑100% |
| Jaganathan et al., 2024 | Polymer composites | Natural fiber | Strength & toughness ↑ up to 50% |
| Ravindran et al., 2023 | PLA | Continuous flax fiber | Compressive strength ↑29%, modulus ↑522% |

## Applications

Naturally derived cellulose fibers have attracted considerable attention for their versatile applications in engineering disciplines, particularly in fields such as construction materials and structural components of vehicles, where lightweight materials are essential. These plantbased fibers exhibit numerous exceptional properties including cost-effectiveness, low density, widespread availability, significant mechanical strength, excellent thermal insulation, electrical resistivity, and environmentally friendly characteristics. Currently, a wide range of natural fibers are recognized and employed in diverse, lightweight structural applications including automotive, aerospace, and construction industries. Numerous economically feasible natural fibres, such as hemp, palm, okra, kapok, silk, coconut, alfa, bamboo, okra, jute and abaca, are extensively used in various applications such as ropes, bags, textiles, household goods, automotive components, and lightweight components in the aeronautical sectors [28].

## Limitations and future scope

Although NFRPCs have many advantages but these have limitations also. A lot of research has been done to identify those limitations. Past research showing these limitations on natural fibre–reinforced 3d-printed bio-polymer composites are depicted in the Table 2.

Table 2. Recent Research on Natural Fibre–Reinforced 3D-Printed Bio-Polymer Composites [29-38].

| Author(s), Year | Title | Key Limitations / Research Gaps |
|---|---|---|
| Jiang et al., 2024 | Mechanical Property Characterizations of Woven Natural Fiber-Reinforced Polymers 3D Printed through LOM | Long-term durability, scalability, and industrial feasibility not addressed |
| Wang et al., 2024 | Exploring Anisotropic Mechanical Characteristics in 3D-Printed Polymer Biocomposites Filled with Waste Vegetal Fibers | Limited optimization of print orientation, fibre type, and anisotropy control |

| | | |
|---|---|---|
| Thanikonda et al., 2024 | 3D Printed Composite Materials: Innovations in Additive Manufacturing | Sustainability-oriented material design and optimization not fully explored |
| Vinod et al., 2024 | 3D-Printing of Hybrid Natural Fiber Sandwich Composites | Hybrid fibre interaction and stacking sequence optimization not fully understood |
| Köllner et al., 2023 | Additive Manufacturing of Biodegradable Hemp-Reinforced Polybutylene Succinate (PBS) and Its Mechanical Characterization | Fibre type and weight fraction optimization, environmental effects, interlayer bonding, and long-term durability of 3Dprinted hemp–PBS biocomposites remain unexplored. |
| Billings et al., 2023 | Additive Manufacturing and Characterization of Sustainable Wood Fiber-Reinforced Composites | Lack of long-term durability and process parameter optimization |
| Cheng et al., 2024 | 3D Printing Continuous Natural Fiber Reinforced Polymer Composites: A Review | Performance prediction models, optimization strategies, and applicationlevel studies lacking |
| Touchard et al., 2023 | 3D Printing of Continuous Cellulose Fibre Composites | Lack of systematic optimization of printing parameters and durability assessment |
| Mugeshwaran et al., 2021 | 3D Printing of Continuous Natural Fibre Reinforced Biocomposites for Structural Applications | Fibre orientation optimization, cost analysis, and environmental impact not addressed |
| Le Duigou et al., 2020 | Tailoring Mechanical Properties of 3D-Printed Continuous Flax/PLA Biocomposites | Limited microstructure–property correlation and longterm performance studies |

The increasing demand for eco-friendly and sustainable materials renders additive manufacturing of natural fiber-reinforced biopolymer composites highly promising [39]. Further investigation is required to enhance the bonding between natural fibers and polymer matrices for improved mechanical performance. Modifications in layer thickness, printing velocity, and temperature can enhance the quality of composite printing [40]. Enhanced biobased filaments fortified with natural fibers may result in more robust, lighter structures. Investigate fiber surface treatment to enhance durability and reduce moisture absorption. To enhance mechanical properties, consider hybrid reinforcement utilizing both natural and synthetic fibers. The durability, recyclability, and environmental implications of these composites require additional investigation. The integration of nanomaterials and smart materials with natural fiber composites may enhance their functionality. These enhancements will facilitate the use of additively manufactured natural fiber composites in construction, aerospace, biomedical, and automotive sectors.

## Conclusion

This review paper summarizes the latest developments in the additive manufacturing of biopolymer composites reinforced with natural fibers, highlighting their mechanical characteristics, uses, and current challenges. This paper also provides a comprehensive overview of the additive manufacturing techniques employed for fabrication of NFRCs, including fused deposition modeling (FDM), laminated object manufacturing (LOM) and continuous fibre 3d printing. The influence of fiber type, surface treatment, and processing variables on the mechanical characteristics of printed composites is analyzed. The research gaps and limitations of use of natural fibre in additive manufacturing of polymer was discussed in detail. The increasing demand for eco-friendly and sustainable materials renders additive manufacturing of natural fiber-reinforced biopolymer composites highly promising. Further research is required to improve the mechanical performance of 3D-printed natural fibre reinforced biopolymers to enable their effective utilization in industries such as automotive, construction, sports equipment, and aviation.

## References

[1] V. Viswalingam and D. Kumar, "Additive manufacturing: a roadmap toward intellectual and industrial developments," In Additive Manufacturing of Functional Polymers and Nanocomposites, pp. 53-75, 2025.

[2] M. Srivastava and S. Rathee, "Additive manufacturing: recent trends, applications and future outlooks," Progress in Additive Manufacturing, vol. 7, no. 2, pp. 261-287, 2022.

[3] M. Alkhodair and H. Alkhudhayr, "Harnessing industry 4.0 for SMEs: Advancing smart manufacturing and logistics for sustainable supply chains," Sustainability, vol. 17, no. 3, pp. 813, 2025.

[4] I. Bahnini and et al., "Additive manufacturing technology: the status, applications, and prospects," The International Journal of Advanced Manufacturing Technology, vol. 97, no. 1, pp. 147-161, 2018.

[5] N. Yamshi and et al., "Design Methodologies and Approaches in Traditional and Additive Manufacturing Systems: A Comparative Study," Digital Manufacturing: Processes and Applications, pp. 111-136, 2025.

[6] Q. Huang and J. Huang, "Comprehensive review of edge and contour detection: from traditional methods to recent advances," Neural Computing and Applications, vol. 37 no. 4, pp. 2175-2209, 2025.

[7] F. K. Aldawood, "A Comprehensive Review of Polymeric Materials and Additive Manufacturing in Dental Crown Fabrication: State of the Art, Challenges, and Opportunities," Polymers, vol. 18, no. 6, pp. 667, 2026.

[8] X. Gao, J. Gao and W. A. Qureshi," Applications, trends, and challenges of precision weed control technologies based on deep learning and machine vision," Agronomy, vol. 15, no. 8, pp. 1954, 2025.

[9] L. Zhang and et al.," Fabrication of Organic/Inorganic nanocomposites: From traditional synthesis to additive manufacturing," Advanced Materials, vol. 37, no. 37, pp. 2505504, 2025).

[10] D. D. Kapoor and et al.,"Transition towards renewable and biodegradable polymers: a comprehensive review," Journal of Polymer Research, vol. 32, no. 10, pp. 345, 2025.

[11] V. Gupta and et al., "Additive Manufacturing of Fiber-Reinforced Polymer Matrix Composites through Material Extrusion: A Comprehensive Review on Filament Fabrication, Printing, Testing Methods, Applications, and Challenges," Advanced Engineering Materials, pp. 2500676, 2025.

[12] S. Kumar, "Laminated Object Manufacturing," In A Concise Encyclopedia of Additive Manufacturing, pp. 245-249, 2025.

[13] P. Ghabezi and et al., "Degradation characteristics of 3D printed continuous fibrereinforced PA6/chopped fibre composites in simulated saltwater," Progress in Additive Manufacturing, vol. 10, no. 1, pp. 725-738, 2025.

[14] C. Billings and et al., "Additive manufacturing and characterization of sustainable wood fiber-reinforced green composites," Journal of Composites Science, vol. 7, no. 12, pp. 489, 2023.

[15] H. Ramezani Dana and M. El Mansori, " Investigations on the mechanical properties of PLA/Flax fibre composites obtained by Fused Filament Fabrication," Plastics, Rubber and Composites, vol. 51 no. 8, pp. 393-406, 2022.

[16] S. Hamat and et al., "Experimental and multiscale analysis of volume fraction effects in tensile properties of recycled PLA-PDA/kenaf fiber 3D printing filament composites," Advanced Composite Materials, vol. 34, no. 3, pp. 463-480, 2025.

[17] A. Vinod and et al., "Advancing additive manufacturing: 3D-printing of hybrid natural fiber sandwich (Nona/Soy-PLA) composites through filament extrusion and its effect on thermomechanical properties," Polymer Composites, vol. 45, no. 9, pp. 7767-7789, 2024.

[18] L. Priya Muthe, K. Pickering and C. Gauss, "Polylactide composites reinforced with pre-impregnated natural fibre and continuous cellulose yarns for 3D printing applications," Materials, vol. 17, no. 22, pp. 5554, 2024.

[19] J. Finnerty and et al., "Effect of mechanical recycling on the mechanical properties of PLA-based natural fiber-reinforced composites," Journal of Composites Science, vol. 7, no. 4, pp. 141, 2023.

[20] M. Rafiee and et al., "Exploring the possibilities of FDM filaments comprising natural fiber-reinforced biocomposites for additive manufacturing," AIMS Materials Science, vol. 8, no. 4, pp. 524-537, 2021.

[21] V. Sekar and et al., " Additive Manufacturing: A Novel Method for Developing an Acoustic Panel Made of Natural Fiber-Reinforced Composites with Enhanced Mechanical and Acoustical Properties," Journal of Engineering, no. 1, pp. 4546863, 2019.

[22] E. M. Agaliotis and et al., "Tensile behavior of 3D printed polylactic acid (PLA) based composites reinforced with natural fiber," Polymers, vol. 14, no. 19, pp. 3976, 2022.

[23] V. U. Siddiqui and et al., "Mechanical properties and flammability analysis of wood fiber filled polylactic acid (PLA) composites using additive manufacturing," Journal of Natural Fibers, vol. 21, no. 1, pp. 2409868, 2024.

[24] R. Cai and et al., "Tailoring interfacial properties of 3D-printed continuous natural fiber reinforced polypropylene composites through parameter optimization using machine learning methods," Materials Today Communications, vol. 32, pp. 103985, 2022.

[25] S. Vallinayagam and et al., "Enhancing the Fracture Toughness of Biomimetic Composite Through 3D Printing" In High-Performance Composite Structures: Additive Manufacturing and Processing, pp. 215-244, 2021.

[26] S. Jaganathan and et al., "Advances in optimizing mechanical performance of 3Dprinted polymer composites: A microstructural and processing enhancements review," Advances in Polymer Technology, no. 1, pp. 3168252, 2024.

[27] M. Chahar and R. Kumar, " Effect of fiber weight fraction on mechanical properties of hemp, jute, bamboo epoxy composite," Green Materials, vol. 13, no. 4, pp. 259-271, 2025.

[28] M. Chahar and et al., "Factors affecting flexural and impact strength of natural fiber reinforced polymer composites: a review," Green Materials, vol. 13, no. 2, pp. 76-91, 2025.

[29] U. Punia and R. K. Garg, "Enhancing mechanical performance of 3D printable PMMA resin through strategic incorporation of SS 316 L nanoparticles for dental applications," International Journal on Interactive Design and Manufacturing (IJIDeM), vol. 18, no. 8, pp. 6317-6332, 2024.

[30] H. Wang and et al., "Exploring anisotropic mechanical characteristics in 3D-Printed polymer biocomposites filled with waste vegetal fibers," Symmetry, vol. 16, no. 1, pp. 70.

[31] A. Tyagi and et al., "Global perspective of natural fibre reinforced composites: properties, and applications" Journal of The Institution of Engineers (India): Series C, vol. 105, no. 5, pp. 1335-1350, 2024.

[32] A. Vinod and et al., "Advancing additive manufacturing: 3D-printing of hybrid natural fiber sandwich (Nona/Soy-PLA) composites through filament extrusion and its effect on thermomechanical properties" Polymer Composites, vol. 45, no. 9, pp. 7767-7789, 2024

[33] Y. Ou and et al., "Material extrusion additive manufacturing of novel lightweight collinear stayed polymer lattices: O. Yating et al," International Journal of Mechanics and Materials in Design, vol. 20 no. 5,pp. 991-1007, 2024.

[34] C. Billings and et al., "Additive manufacturing and characterization of sustainable wood fiber-reinforced green composites" Journal of Composites Science, vol. 7, no. 12, pp. 489, 2023.

[35] P. Cheng and et al., "3D printing continuous natural fiber reinforced polymer composites: A review," Polymers for Advanced Technologies, vol. 35 no. 1, pp. e6242, 2024.

[36] F. Touchard and et al., "3D printing of continuous cellulose fibre composites: microstructural and mechanical characterisation," Rapid Prototyping Journal, vol. 29, no. 9, pp. 1879-1887, 2023.

[37] A. Mugeshwaran and et al., "3D Printing of continuous natural fibre reinforced biocomposites for structural applications," In Biocomposite Materials: Design and Mechanical Properties Characterization, pp. 205-218, 2021.

[38] A. Le Duigou and et al., "Tailoring the mechanical properties of 3D-printed continuous flax/PLA biocomposites by controlling the slicing parameters," Composites Part B: Engineering, vol. 203, pp. 108474, 2020.

[39] M. Chahar and R. Kumar, "RSM-based optimization of mechanical properties of hybrid natural fiber epoxy composite," Green Materials, pp. 1-14, 2025.

[40] A. Ahlawat and et al., "Optimization of FDM 3D printing parameters for enhancing mechanical performance of carbon fiber-reinforced ABS composite through PSOANN," Engineering Computations, vol. 43, no. 2, pp. 823-836, 2026.

# SUSTAINABILITY INDEX COMPARISON OF POWER MIXED EDM PROCESS USING VARIOUS NON-EDIBLE OILS AS A DIELECTRIC FLUID

Vikas Kumar Singla[1,2], Rajesh Bajaj[3]*, Himanshu Payal[1]
[1]Department of Mechanical Engineering, Sharda University, Greater Noida, India
[2]Department of Mechanical Engineering, JSS Academy of Technical Education, Noida, India
*[3]Department of Mechanical Engineering, JSS University, Noida, India
bajajthegreat@gmail.com

## Abstract
*The present work investigates the sustainability index for nano powder mixed rotary EDM process using waste vegetable oil (WVO), Jatropha Curcas oil (JCO) & Kusum oil as a dielectric fluid for the nano powder mixed rotary EDM process. The result revels that all the three non-edible oils make the process more sustainable as compared to hydro carbon based EDM oil. Finally, the result reveals that WVO, JCO & Kusum oil shows lower sustainability index values (SI) 6.27%, 1.96% and 2.38% respectively as compared to conventional hydro carbon based EDM oil and hence making the process more efficient along with cost effective, environmentally safe and good for operator health.*

## Keywords
MRR, non-edible oils, Sustainability Index (SI), EDM oil..

## Abbreviations

| | |
|---|---|
| SWCNT: | Single Wall Carbon Nano-Tubes |
| WVO: | Waste Vegetable Oil |
| JCO: | Jatropha Curcas Oil |
| Ip: | Peak current |
| Ton: | Pulse on time |
| Toff: | Pulse off time |
| Pc: | Powder concentration |
| TR: | Tool Rotation |
| MRR: | Material Removal Rate |
| PMEDM: | Powder Mixed Electric Discharge Machining |
| SI: | Sustainability Index |

## Introduction
Over recent decades, electrical discharge machining (EDM) has emerged as a reliable non-traditional method for processing hard-to-machine materials. Its precision in creating intricate shapes has made it indispensable in fields such as biomedical devices, automotive manufacturing, mold and die production, and aerospace components [1]. EDM operates as a non-contact thermal process where material is eroded through repeated sparks generated between electrodes amid dielectric breakdown. These sparks, reaching temperatures of 8000–12000 K, form a plasma channel in the working gap that melts and vaporizes workpiece material [2]. Though EDM offers low material removal rates (MRR), it remains popular for superalloys, composites, and ceramics, with efficiency gains achieved by optimizing input parameters [3]. Researchers have enhanced basic EDM setups through innovations like specialized tool electrodes [4], advanced pulse generators [5], ultrasonic vibration of tools, workpieces, or dielectrics [6-8], tool or workpiece rotation [9,10], and dry or near-dry

machining [11,12]. Among these, micro/nano powder-mixed EDM (PMEDM) stands out for delivering superior performance. Adding fine powder particles refines the electric field distribution in the discharge zone [13]. In 1981, early work showed that mixing 4 g/l graphite powder into the dielectric boosted MRR and cut tool wear rate (TWR) when machining mild steel [14]. Smaller particles yielded smoother surfaces and thicker recast layers as reported by Fong and Chen [15]. Kansal et al. [16] found that machining with graphite PMEDM process provide better MRR, TWR, and surface roughness (SR). Peças and Henriques investigated that improved crater dimensions, recast layer thickness (RLT) and surface roughness by using silicon PMEDM process [17]. Prabhu and Vinayagam [18] achieved finer finishes, improved morphology, and fewer microcracks with multi-walled carbon nanotubes (MWCNT) on Inconel 825. Mai et al. [19] reported 66% shorter machining times and 0.09 µm SR improvement with carbon nanotubes (CNT) PMEDM process. Izman et al. [20] and Sari et al. [21], and Mohal and Kumar [22] observed improvement in SR, RLT, MRR, and energy wear ratio (EWR) while machining on alloys like Ti6Al4V, AISI-H13, and Al-10%SiCp respectively. Baseri and Sadeghian [23] found that better MRR and SR and TWR using TiO2 PMEDM technique. Bajaj et al. [24] highlighted SR reductions, MRR increases, and better topography using MWCNT PMEDM with tool rotation process. In manufacturing industries, particularly EDM as the fourth most-used process after grinding, milling, and turning, contributes heavily to pollution [25]. PMEDM is highly effective with hard materials but presents sustainability concerns, such as dielectric waste from non-recyclable powders, blocked filters, and difficulties with disposal [26-28]. Sustainable manufacturing provides better energy efficiency, operator safety and health, cost savings, and waste minimization [29-31]. In the PMEDM process, significant obstacles to sustainable manufacturing include the blending of nano powder particles and the creation of debris during machining, which is unavoidable. The sustainability issues associated with the PMEDM process can only be somewhat alleviated by utilizing cost-effective, eco-friendly, and biodegradable dielectric fluids. It has been noted that non-edible and waste vegetable oils serve as viable alternatives to hydrocarbon oil, thereby improving the sustainability aspects of the EDM process [32-34]. Mali et al. [35] reported 32% MRR gains with WVO and 8% EWR reductions with blended used vegetable oil as compared to hydrocarbon oil. Palm oil biodiesel increased MRR by 38% and reduced machining cost as compared to machining with kerosene [36]. GG Reddy et al. [37] found that sunflower oil's improved MRR, operator health and environmental safety but also higher TWR and SR. S. Das et al. [38] investigated that MRR, SR and machining time improved significantly by 22%, 17%, and 50–65% respectively with neem oil than kerosene. Bajaj et al. [39] achieved 57% MRR and 55% SR improvements by using Kusum oil as dielectric fluid along MWCNT process with tool rotation. Bajaj et al. [40] observed that by using Jatropha Curcas Oil (JCO) as dielectric with MWCNT powder and tool rotation improved the MRR by, SR by 50%, sustainability index by 9.92% better morphology and safety as compared to EDM oil [40]. Machining by WVO's as dielectric fluid provided better the machining performance and sustainability as compared to conventional EDM reported by Bajaj et al. [41]. Singla et al. [42] investigated that the PMEDM process with non-edible oils improved the material removal rate (MRR), surface roughness (SR), microhardness, corrosion resistance and biocompatibility for medical implants.

The experiments utilized a ZNC-25 die-sinking EDM machine manufactured by J K Machines in India figure 1. Nickel based alloy, Inconel 718 and pure copper electrode of 10 mm diameter, selected as workpiece and tool material respectively. while key PMEDM performance factors included peak current, pulse on time, pulse off time, powder concentration, and tool rotation with their range selected by pilot test shown in table 1. Tool rotation speed was regulated via an Arduino controller, achieving up to 2500 rpm maximum. To minimize powder consumption and experimental costs, a compact acrylic tank (30×22×13 cm) contained the process, while pre-sonicated SWCNT-mixed non-edible oils served as the dielectric fluid. A gear pump ensured proper circulation of the highly viscous non-edible at a consistent flow rate of 3.5 L/min throughout testing.

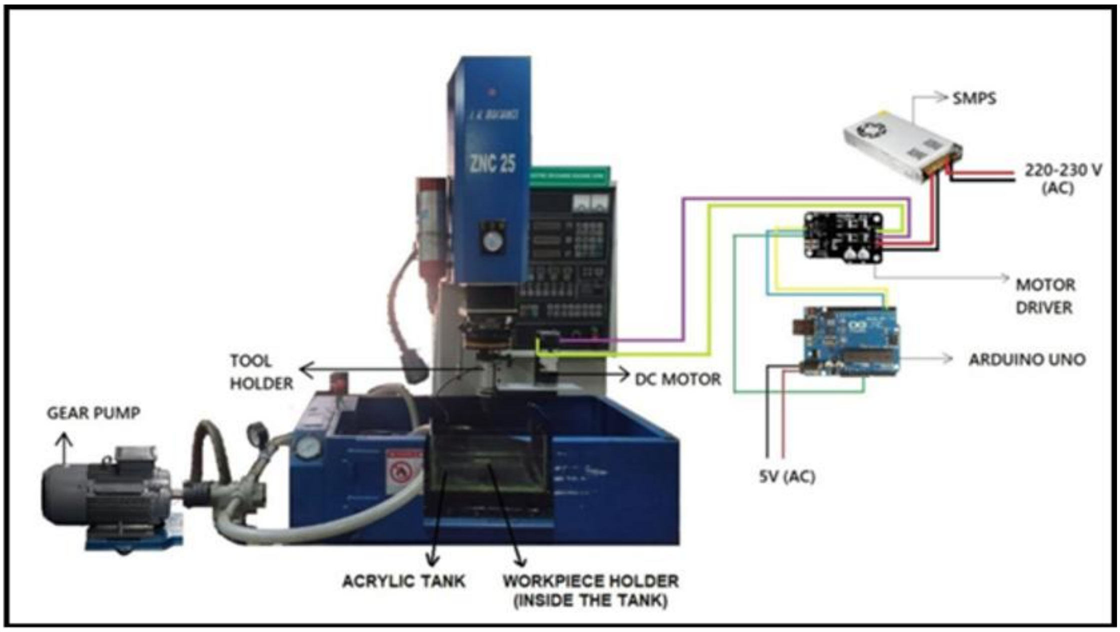


Figure 1. EDM setup machine model with tool rotation arrangement [40].

Table 1. Input process variables and their ranges.

| Variable | Symbol | Level | | |
|---|---|---|---|---|
| | | Low (-1) | Medium (0) | High (+1) |
| Peak Current (A) | $I_P$ | 3 | 5 | 7 |
| Pulse On time (μs) | $T_{on}$ | 100 | 150 | 200 |
| Pulse Off time (μs) | $T_{off}$ | 40 | 70 | 100 |
| Powder Concentration (g/l) | $P_C$ | 0.15 | 0.3 | 0.45 |
| Tool Rotation (RPM) | TR | 400 | 600 | 800 |

Table 2 compared the cost effectiveness & thermo-physical properties of the non-edible oils (WVO, JCO, Kusum oil) with EDM oil.

Table 2. Cost-effectiveness and thermo-physical properties of WVO, JCO. Kusum oil and EDM oil.

| Attributes | EDM Oil | JCO | WVO | Kusum Oil |
|---|---|---|---|---|
| Price (₹) | 91 | 41 | 0 | 60 |
| Viscosity at (40°C) | 4 | 35.8 | 9.55 | 40 |
| Density (gm/ml) | 0.824 | 0.904 | 0.893 | 0.862 |
| Specific Heat (kJ/Kg K) | 2.03 | 2.76 | 1.96 | 1.96 |
| Thermal Conductivity (W/m K) | 0.134 | 0.174 | 0.2 | 0.168 |
| Dielectric Constant (27°C) | 2.135 | 3.6 | 2.86 | 1.9 |
| Breakdown Voltage (kV) | 45 | 10 | 30 | 60 |
| Flash Point (°C) | 110 | 290 | 180 | 204 |
| Biodegradability | Low | High | High | High |

*ISBN 978-81-973526-0-7*

All tests maintained a consistent 150μm depth of cut, generating an electric field of 105–107 V/m when applying 80–320 V across electrodes. The powder-mixed dielectric modifies the fluid's thermo-physical properties, expanding the spark gap to 50–150μm [43], which produces shallower craters on the machined surface and improves overall surface finish quality. To ensure process stability, freshly prepared dielectric fluid—ultrasonically treated—was used for each experimental run listed in Table 2. Material removal rate (MRR) was determined by measuring volumetric material loss using the following calculation:

$$MRR = \frac{W_i - W_f}{\rho * t} * 1000 \qquad \text{..........(i)}$$

## Result & Discussions

On the basis of the input parameters of all three non-edible oils (WVO, JCO, Kusum oil) in table 3 the optimum values of MRR (mm3/min) predicted as well as experimental shown in figure 2.

Table 3. Optimum values of MRR with their input parameters for all three non-edible oils.

| Parameters | WVO | JCO | Kusum Oil |
|---|---|---|---|
| $I_p$ (A) | 7 | 7 | 7 |
| $T_{on}$ (μs) | 175 | 166 | 159 |
| $T_{off}$ (μs) | 40 | 38 | 46 |
| $P_c$ (gm/l) | 0.313 | 0.315 | 0.309 |
| TR (rpm) | 590 | 615 | 720 |

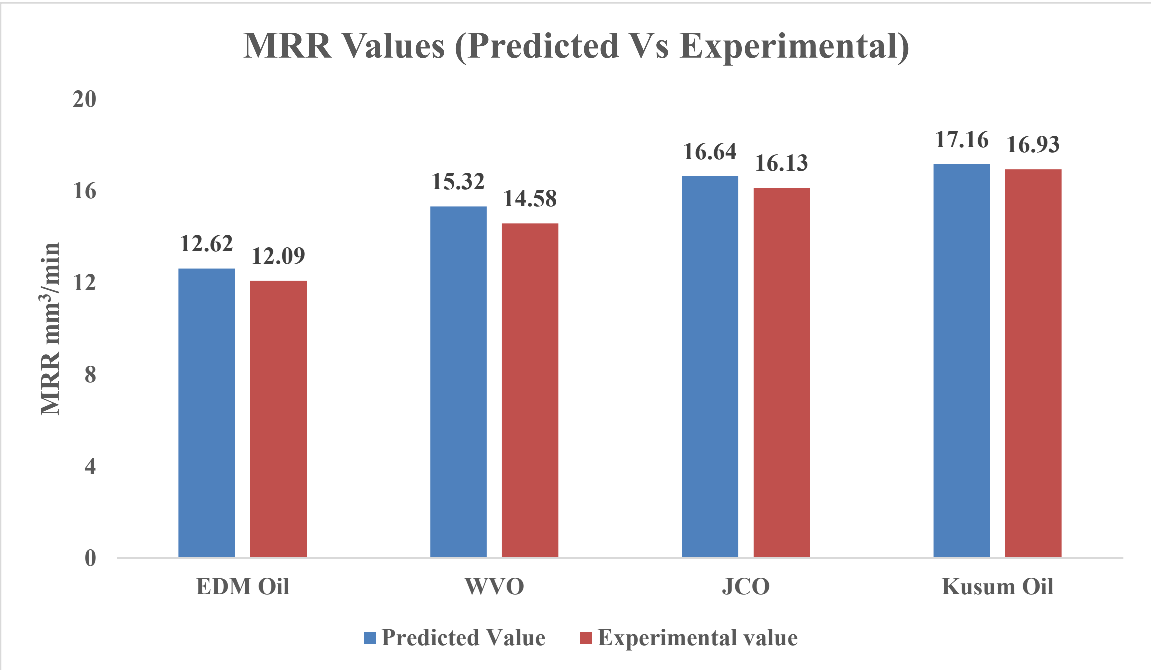


Figure 2. Comparison of Predicted and Experimental Values of MRR for all three non-edible oils.

## Sustainability Assessment

Manufacturing sustainability involves reducing costs, energy use, and negative environmental/operator health impacts while upholding product quality through reuse, reduce, and recycle principles [43].

***Sustainability Index based on Energy Consumption ($SI_{EC}$)***

It calculated in terms of rupees (₹) by the following equation

$$SI_{EC} = E_c \times C_e \quad \text{.........(ii)}$$

Where: $E_c$= Energy consumed during machining by EDM machine in kWhr;
$C_e$= Cost of electricity consumed during machining in ₹/kWhr

***Sustainability Index based on Dielectric Fluid Consumption ($SI_{DC}$)***

$$SI_{DC} = \frac{C_{DFPL} \times V_{DF} \times T_m}{T_{DFLC}} \quad \text{...........(iii)}$$

Where: $C_{DFPL}$= Cost of dielectric fluid per liter in ₹
$V_{DF}$= Volume of dielectric fluid used for per experiment
$T_m$= Machining time in minutes
$T_{DFLC}$= Dielectric fluid life cycle

***Sustainability Index based on Operator's Health and Environmental Safety ($SI_{OE}$)***

$$SI_{OE} = (1 + C_P) \times \propto \times T_m \quad \text{...........(iv)}$$

Where: $C_P$= Penalty constant, ratio of assigned values to maximum values of parameters
α= Unit value in ₹/hr, which is constant.

The sustainability index for PMEDM assesses environmental safety and societal impact—considering factors like aerosol/toxic fume emissions and operator skin health risks—via a qualitative scoring system (Table 4) where 0 indicates no risk, 1 low risk, 2 medium risk, and 3 high risk to either environment or operator health. Table 5 presents the comprehensive sustainability index, integrating energy consumption, dielectric usage, and environmental safety metrics and percentage reduction.

Table 4. Penalty Constant Analysis EDM Oil, WVO, JCO & Kusum Oil.

| Dielectric Fluid | Fire Risk | Toxic Fumes | Skin Problems | Fumes Generation | Dust Generation | Reuse of Dielectric | Total | $C_P$ |
|---|---|---|---|---|---|---|---|---|
| EDM Oil | 3 | 3 | 3 | 3 | 0 | 1 | 13 | 0.72 |
| WVO | 0 | 1 | 0 | 3 | 0 | 1 | 5 | 0.28 |
| JCO | 0 | 1 | 0 | 3 | 0 | 1 | 5 | 0.28 |
| Kusum Oil | 0 | 1 | 0 | 3 | 0 | 1 | 5 | 0.28 |

Table 5. Comparison of SI for PMEDM process WVO, JCO, Kusum Oil with EDM Oil.

| Dielectric Fluid | Optimum MRR ($mm^3$/min) | Machining Time ($T_m$) in mins | $SI_{EC}$ (₹) | $SI_{DC}$ (₹) | $SI_{OE}$ (₹) | $SI_{Total}$ (₹) | %age Reduction in SI |
|---|---|---|---|---|---|---|---|
| EDM Oil | 12.09 | 16.8 | 1.41 | 1455 | 0.48 | 1456.9 | - |
| WVO | 14.58 | 11.7 | 1.24 | 1364 | 0.25 | 1365.5 | 6.27 |
| JCO | 16.13 | 10.6 | 1.12 | 1427 | 0.23 | 1428.4 | 1.96 |
| Kusum Oil | 16.93 | 9.7 | 1.03 | 1421 | 0.21 | 1422.3 | 2.38 |

## Conclusion

The present work reveals that the non-edible oils (WVO, JCO and Kusum oil) provide better MRR as compared to EDM oil. Further, the sustainability index (SI) analysis result exposes that cost effective non-edible oils (WVO, JCO & Kusum oil) as dielectric is good alternative as compared to hydro based EDM oil in terms of machining performance, consumption of dielectric and operator health and environmental conditions.

Non-edible oils (WVO, JCO and Kusum oil) provide reduction in SI by 6.27%, 1.96% and 2.38% respectively as compared to hydrocarbon based EDM oil.

## References

[1] K. H. Ho and S. T. Newman, "State of the art electrical discharge machining (EDM)," Int. J. Mach. Tools Manuf., vol. 43, no. 13, pp. 1287-1300, 2003.
[2] G. Boothroyd, "Non-conventional machining processes," in Fundamentals of Machining and Machine Tools, 2nd ed. New York, NY, USA: Marcel Dekker, 1989, p. 491.
[3] D. K. Panda and R. K. Bhoi, "Electro-discharge machining—a qualitative approach," Mater. Manuf. Process., vol. 21, no. 8, pp. 853–862, 2006.
[4] K. Karunakaran and M. Chandrasekaran, "Investigation of machine-ability of Inconel 800 in EDM with coated electrode," IOP Conf. Ser.: Mater. Sci. Eng., vol. 183, no. 1, p. 012014, 2017.
[5] T. Muthuramalingam and B. Mohan, "A study on improving machining characteristics of electrical discharge machining with modified transistor pulse generator," J. Manuf. Technol. Manag., vol. 27, no. 1-3, pp. 101–111, 2013.
[6] Q. H. Zhang, J. H. Zhang, S. F. Ren, Z. W. Niu, and X. Ai, "A theoretical model of surface roughness in ultrasonic vibration assisted electrical discharge machining in gas," J. Manuf. Technol. Manag., vol. 7, no. 2-4, pp. 381–390, 2005.
[7] M. R. Shabgard, M. R. Farahmand, and A. Ivanov, "Mathematical modelling and comparative study of the machining characteristics in ultrasonic-assisted electrical discharge machining of cemented tungsten carbide (WC—10% Co)," Proc. Inst. Mech. Eng., Part B: J. Eng. Manuf., vol. 223, no. 9, pp. 1115–1126, 2009.
[8] J. M. Jafferson, P. Hariharan, and J. Ram Kumar, "Effects of ultrasonic vibration and magnetic field in micro-EDM milling of nonmagnetic material," Mater. Manuf. Process., vol. 29, no. 3, pp. 357–363, 2014.
[9] Y. H. Guu and H. Hocheng, "Effects of workpiece rotation on machinability during electrical-discharge machining," Mater. Manuf. Process., vol. 16, no. 1, pp. 91–101, 2001.
[10] H. Baseri, E. A. Gorban, and A. Alinejad, "Investigation of the rotary EDM process of X210Cr12," Int. J. Mach. Mach. Mater., vol. 11, no. 3, pp. 297–307, 2012.
[11] K. Dhakar and A. Dvivedi, "Parametric evaluation on near-dry electric discharge machining," Mater. Manuf. Process., vol. 31, no. 4, pp. 413–421, 2016.
[12] N. K. Singh, P. M. Pandey, and K. K. Singh, "Experimental investigations into the performance of EDM using argon gas-assisted perforated electrodes," Mater. Manuf. Process., vol. 32, no. 9, pp. 940–951, 2017.
[13] J. Kozak, M. Rozenek, and L. Dabrowski, "Study of electrical discharge machining using powder-suspended working media," Proc. Inst. Mech. Eng., Part B: J. Eng. Manuf., vol. 217, no. 11, pp. 1597–1602, 2003.
[14] M. Jeswani, "Effect of the addition of graphite powder to kerosene used as the dielectric fluid in electrical discharge machining," Wear, vol. 70, no. 2, pp. 133–139, 1981.
[15] Y.-F. Tzeng and F.-C. Chen, "Investigation into some surface characteristics of electrical discharge machined SKD-11 using powder-suspension dielectric oil," J. Mater. Process. Technol., vol. 170, no. 1-2, pp. 385–391, 2005.
[16] H. K. Kansal, S. Singh, and P. Kumar, "Application of Taguchi method for optimisation of powder mixed electrical discharge machining," J. Manuf. Technol. Manag., vol. 1, no. 2-4, pp. 329–341, 2005.
[17] P. Pecas and E. Henriques, "Electrical discharge machining using simple and powder-mixed dielectric: the effect of the electrode area in the surface roughness and topography," J. Mater. Process. Technol., vol. 200, no. 1-3, pp. 250–258, 2008.

[18] S. Prabhu and B. K. Vinayagam, "AFM surface investigation of Inconel 825 with multi wall carbon nano tube in electrical discharge machining process using Taguchi analysis," Arch. Civil Mech. Eng., vol. 11, no. 1, pp. 149–170, 2011.

[19] C. Mai, H. Hocheng, and S. Huang, "Advantages of carbon nanotubes in electrical discharge machining," Int. J. Adv. Manuf. Technol., vol. 59, no. 1, pp. 111–117, 2012.

[20] S. Izman et al., "Effects of adding multiwalled carbon nanotube into dielectric when EDMing titanium alloy," Adv. Mater. Res., vols. 463–464, pp. 1445–1449, 2012.

[21] M. Mohammadzadeh Sari, M. Y. Noordin, and E. Brusa, "Role of multi-wall carbon nanotubes on the main parameters of the electrical discharge machining (EDM) process," Int. J. Adv. Manuf. Technol., vol. 68, no. 5, pp. 1095–1102, 2013.

[22] S. Mohal and H. Kumar, "Parametric optimization of multiwalled carbon nanotube-assisted electric discharge machining of Al-10% SiCp metal matrix composite by response surface methodology," Mater. Manuf. Process., vol. 32, no. 3, pp. 263–273, 2017.

[23] H. Baseri and S. Sadeghian, "Effects of nanopowder TiO2-mixed dielectric and rotary tool on EDM," Int. J. Adv. Manuf. Technol., vol. 83, no. 1, pp. 519–528, 2016.

[24] R. Bajaj, A. R. Dixit, A. K. Tiwari, and N. K. Chauhan, "Machining performance enhancement of EN-31 die steel using MWCNT mixed rotary EDM," Indian J. Eng. Mater. Sci., vol. 27, no. 2, pp. 309–319, 2021.

[25] X. C. Tan, F. Liu, H. J. Cao, and H. Zhang, "A decision-making framework model of cutting fluid selection for green manufacturing and a case study," J. Mater. Process. Technol., vol. 129, no. 1-3, pp. 467–470, 2002.

[26] D. Nanu and A. Nanu, "Perspectives of the dimensional processing through electric erosion processing," Nonconv. Technol., vol. 3, pp. 61–64, 2008.

[27] T. Gutowski, J. Dahmus, and A. Thiriez, "Electrical energy requirements for manufacturing processes," in Proc. 13th CIRP Int. Conf. Life Cycle Eng. (LCE), Leuven, Belgium, 2006, pp. 623–628.

[28] F. N. Leão and I. R. Pashby, "A review on the use of environmentally-friendly dielectric fluids in electrical discharge machining," J. Mater. Process. Technol., vol. 149, no. 1-3, pp. 341–346, 2004.

[29] F. Modica, V. Marrocco, G. Copani, and I. Fassi, "Sustainable micro-manufacturing of micro-components via micro electrical discharge machining," Sustainability, vol. 3, no. 12, pp. 2456–2469, 2011.

[30] H. Hocheng, J.-H. Chang, and U. U. Jadhav, "Micromachining of various metals by using Acidithiobacillus ferrooxidans 13820 culture supernatant experiments," J. Clean. Prod., vol. 20, no. 1, pp. 180–185, 2012.

[31] G. Rotella, T. Lu, L. Settineri, O. W. Dillon Jr., and I. S. Jawahir, "Dry and cryogenic machining: comparison from the sustainability perspective," in Sustainable Manufacturing: Shaping Global Value Creation and Good Practice in Latin America, G. Seliger, H. Kohl, G. Quertani, and J. Hesselbach, Eds. Berlin, Germany: Springer, 2012.

[32] J. B. Valaki and P. P. Rathod, "Assessment of operational feasibility of waste vegetable oil based bio-dielectric fluid for sustainable electric discharge machining (EDM)," Int. J. Adv. Manuf. Technol., vol. 87, no. 5-8, pp. 1509–1518, 2016.

[33] J. B. Valaki and P. P. Rathod, "Investigating feasibility through performance analysis of green dielectrics for sustainable electric discharge machining," Mater. Manuf. Process., vol. 31, no. 4, pp. 541–549, 2016.

[34] J. B. Valaki, P. P. Rathod, and C. D. Sankhavara, "Investigations on technical feasibility of Jatropha curcas oil based bio dielectric fluid for sustainable electric

discharge machining (EDM)," J. Manuf. Process., vol. 22, pp. 151–160, 2016.

[35] H. S. Mali and N. Kumar, "Investigating feasibility of waste vegetable oil for sustainable EDM," in Proc. All India Manuf. Technol. Design and Res. Conf. (AIMTDR), 2016, pp. 405–410.

[36] J. B. Valaki, P. P. Rathod, B. C. Khatri, and J. R. Vaghela, "Investigations on palm oil based biodielectric fluid for sustainable electric discharge machining," in Proc. Int. Conf. Adv. Mater. Manuf. (ICAMM), Bangkok, Thailand, 2016, pp. 29–30.

[37] G. G. Reddy, B. Singaravel, and K. C. Shekar, "Experimental investigation of sunflower oil as dielectric fluid in die sinking electric discharge machining process," Mater. Sci. Forum, vol. 969, pp. 715–721, 2019.

[38] S. Das, S. Paul, and B. Doloi, "Feasibility investigation of neem oil as a dielectric for electrical discharge machining," Int. J. Adv. Manuf. Technol., vol. 106, no. 5-8, pp. 1179–1189, 2020.

[39] R. Bajaj, A. R. Dixit, and A. K. Tiwari, "Machining performance enhancement of powder mixed electric discharge machining using green dielectric fluid," J. Braz. Soc. Mech. Sci. Eng., vol. 42, p. 512, 2020.

[40] R. Bajaj, A. K. Tiwari, A. Pramanik, A. K. Srivastava, and A. R. Dixit, "Machining performance and sustainability analysis of PMEDM process using green dielectric fluid," J. Braz. Soc. Mech. Sci. Eng., vol. 44, p. 563, 2022.

[41] R. Bajaj, K. B. Mardi, A. K. Srivastava, and A. R. Dixit, "Feasibility and sustainability analysis of waste vegetable oil as a dielectric fluid for powder mixed EDM process," Int. J. Adv. Manuf. Technol., vol. 134, no. 11-12, pp. 3531–3549, 2024.

[42] V. K. Singla, H. Payal, and R. Bajaj, "Improvement in machining performance using nano powder particles mixed in bio-degradable oil as dielectric in electric discharge machining process (NPMEDM): A comprehensive review," Lett. Appl. NanoBioScience, vol. 14, no. 4, pp. 273, Dec. 2025.

[43] K. Furutania, A. Saneto, H. Takezawa, N. Mohri, and H. Miyake, "Accretion of titanium carbide by electrical discharge machining with powder suspended in working fluid," Precis. Eng., vol. 25, no. 2, pp. 138–144, 2001.

# MULTI-OBJECTIVE OPTIMIZATION OF SOLAR DRIVEN, HIGH TEMPERATURE ORGANIC RANKINE CYCLE (ORC) USING GENETIC ALGORITHM

Soumya Raj*[1], Omendra Kumar Singh[1]
*Indira Gandhi Delhi Technical University for Women, Kashmere Gate, Delhi-110006, India
*soumyaraj.me@gmail.com

## Abstract

*In the present work, multi-objective optimization of a solar-driven, high-temperature Organic Rankine Cycle (ORC) using a genetic algorithm computational model in MATLAB has been performed. Usually, an Organic Rankine Cycle works efficiently for low-temperature waste heat recovery. Contrary to this, this paper examines the potential of using ORC for utilization of the energy available at higher temperatures for searching alternative options for complicated designs of the steam Rankine cycle. The Organic Rankine Cycle was optimized, and the results for exergy and thermal stability of the working fluid were obtained at optimal conditions. Exergy efficiency of ORC, along with thermal stability of the working fluid, was considered as the objective function, while the design variable vector contained evaporator pressure, condenser pressure, and evaporator temperature. Three different siloxanes have been used as working fluid for the analysis. Therminol VP-1 was used as heat transfer fluid in the intermediate thermal oil circuit for transferring solar heat to the working fluid of ORC.*

## Keywords

High-temperature Organic Rankine Cycle, exergy, genetic algorithm, thermal stability of working fluid, optimization.

## Introduction

Organic Rankine cycles have been known for best utilization of low-temperature heat sources for generation of electricity [1]. This cycle has been in demand because of its simple design, high reliability, lower maintenance, and high thermal efficiency [2-3]. ORCs generally work for medium and low temperature heat recovery. Most of the working fluids used in the ORCs do not work effectively, they decompose at temperature above 300°C. To use this cycle for high-temperature application, working fluid selection is important [4-6]. To harness the waste heat energy available at higher temperature, the selection of a suitable working fluid has been of great interest for the researchers in the last few years. The use of thermal oil circuit for transferring high temperature waste heat to the working fluid of organic Rankine cycle has been done in some previous studies [7-9]. In a previous study, to exploit high temperature waste heat, three different combined systems which use ORC as bottoming cycle (dual loop ORC, Brayton ORC and TEG ORC) were used [10]. Comparative analysis of some key parameters namely the net power output, thermal efficiency, recovery efficiency, exergy efficiency, and turbine size parameters was performed. Concentrated solar power could also be combined with the ORC to generate power in areas where solar energy is available in abundance. Currently the operational solar thermal power plants in India could produce an output temperature of 300oC and above, and mostly use Rankine cycle with steam as working fluid for producing power. Rankine cycle requires higher maintenance, larger water resource and has comparatively complicated designs. To overcome these problems, ORC could be used as a power generating cycle for utilization of highly abundant solar energy. Vescovo and Spagnoli [1] discussed about medium and high temperature (above 300°C) ORCs and the range of working fluids suitable for these systems for power generation. For the Organic Rankine Cycle to work efficiently for the utilization of high temperature waste heat, direct contact evaporators are required, therefore the thermal stability working fluid becomes important [11,12]. NASA performed research on Organic Rankine bottoming cycle for an adiabatic diesel engine [13]. A mixture of 60 mol % pentafluorobenzene and 40 mol % hexafluorobenzene was used as the working fluid for the ORC, and thermal stability of the fluid was observed up to a temperature of 468°C. Siloxanes and cyclic siloxanes showed thermal stability up to 400°C [14-15]. Ren et.al, 2022 [16] produced a theoretical design of a high-temperature Cascade ORC power plant using concentrated solar power to eliminate the limitations of direct steam generation solar power system. This design improved the thermal efficiency of the proposed solar power plant by a significant amount.

The present work explores the possibility of using high temperature Organic Rankine cycle by combining concentrated solar thermal power source with ORC using an intermediate thermal oil circuit. The heat transfer fluid used in the thermal circuit is therminol vp-1, while three different working fluid siloxanes have been tried out for the ORC keeping in mind their thermal stability in the proposed temperature Range. The main purpose of the present study is to examine the potential of using ORC at higher temperatures as an alternative solution for complex steam Rankine cycle. Genetic Algorithm has been used as an algorithm for computational simulation in MATLAB for optimization of exergy efficiency of ORC and thermal stability of working fluid. The genetic algorithm optimization technique reduces both the cost and the time for an actual experimental analysis.

## Materials and Methods

The Schematic of a solar powered high-temperature Organic Rankine cycle (H-ORC) is shown in Figure 1. The organic working fluid of the Rankine cycle gets its heat for evaporation from the heat transfer fluid circulating in the parabolic trough collector circuit. The solar collector circuit consist of an arrangement of a number of parabolic trough collectors with Therminol VP-1 as heat transfer fluid to transport solar heat to the ORC circuit, and can achieve a temperature of 653K (produced by most of the solar thermal power plants in India).

### *System description*

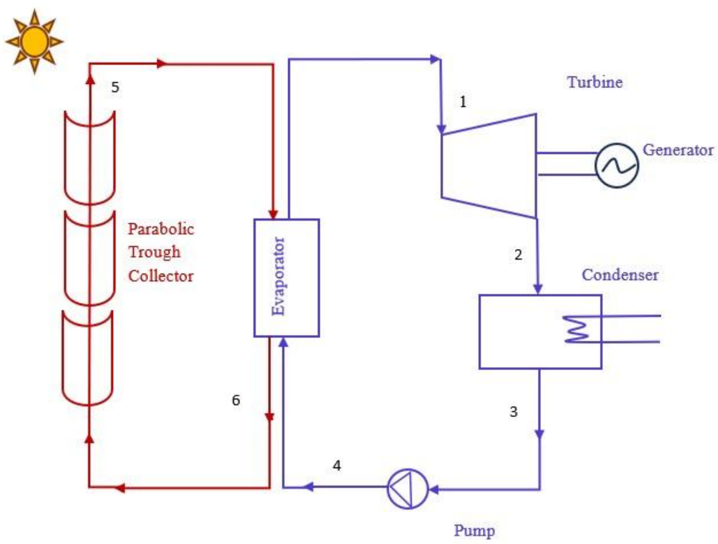


Figure 1. Schematic of solar powered high temperature organic Rankine (H-ORC) cycle.

The Organic Rankine Cycle consists of an evaporator, a turbine, a condenser, and a pump to feed the condensed working fluid back to the evaporator. Three different working fluids namely Siloxanes, MDM (octamethyltrisiloxane), MM and D5. Siloxanes have been studied in the ORC circuit. These fluids can remain thermally stable at higher temperature range up to 623 K, which is the maximum temperature of the heat transfer fluid at parabolic trough collector's outlet.

### *Thermodynamic Modelling*

It is assumed that the outlet temperature produced by the arrangement of parabolic trough collectors was 653K [17]. Below is the thermodynamic modelling for the Organic Rankine Cycle. The heat input to the ORC from the solar collector circuit is calculated by Equation 1 given below. The thermophysical properties of Therminol VP-1 were taken from Ref. [18]. Therminol vp-1 falls under the category of thermal oil and it is one of the most widely used heat transfer fluids in solar thermal power plants. The working temperature for this fluid is in the range 285K - 673K.

$$\dot{Q}_s = A_p I \tag{1}$$

$$\dot{Q}_u = \dot{m}_{htf} C_{P,htf} (T_5 - T_6) \tag{2}$$

$$\dot{m}_{htf} Cp_{htf} (T_5 - T_6) = \dot{m}_{orc}(h_1 - h_4) \tag{3}$$

$$\dot{W}_T = \dot{m}_{orc}(h_1 - h_2) \tag{4}$$

$$\dot{W}_P = \dot{m}_{orc}(h_4 - h_3) \tag{5}$$

$$\eta_{th,orc} = \frac{\dot{W}_{net}}{\dot{Q}_u} \tag{6}$$

$$\dot{W}_{net} = \dot{W}_T - \dot{W}_P \tag{7}$$

$$\eta_{exergy,orc} = \frac{\dot{W}_{net}}{\dot{Ex}_{in}} \tag{8}$$

$$\dot{Ex}_{in} = \dot{Q}_s (1 - T_0/T_s) \tag{9}$$

$$C_{P,htf} = C_p = 2.82 T_{htf} + 716 \tag{10}$$

In the above equations, $\dot{Q}_u$ , $C_{P,htf}$ , $\dot{m}_{htf}$ are the useful heat supplied from the solar circuit, specific heat of heat transfer fluid, and mass flow rate of heat transfer fluid respectively. $\dot{m}_{orc}$ is the mass flow rate of the working fluid in the Organic Rankine Cycle. $\dot{W}_T$, $\dot{W}_P$ and $\dot{W}_{net}$ are the turbine work, pump work, and the net work output from ORC respectively. $\eta_{th,orc}$ and $\eta_{exergy,orc}$ are the energy and exergy efficiencies of the Organic Rankine Cycle. $\dot{Ex}_{in}$ is the exergy input to the ORC and 'h' stands for enthalpy at a given state. $T_{htf}$ is temperature of the heat transfer fluid. $\dot{Q}_s$ solar energy incident on the collector and $T_s$ is the temperature of sun. $A_p$ and I are the aperture area of parabolic trough solar collector and the direct normal irradiance (DNI) of solar radiation, respectively. Its expression is mentioned in equation (1) mentioned above. The working parameters for the ORC as shown in Table 1, were taken from Ref. [19,20].

### *Description of Genetic Algorithm method for optimization*

Genetic algorithm (GA) which was first proposed by Holland in USA, is a computational model following the Darwin's principle of evolution [19]. It is a process of selection, crossover, and mutation like Darwin's theory of evolution [19, 21-22]. Following the steps of initial selection of a set of solution and crossover and mutation an optimal solution is obtained for a given objective. Exergy efficiency and the thermal stability of working fluid were taken as the objective functions. The aim is to maximize the exergy efficiency and maximize the stability of the working fluid.

Table 1. Operating conditions of the ORC.

| Operating Parameter | Value |
|---|---|
| Heat source temperature (K) | 653 |
| $\dot{m}_{htf}$ (kg/s) | 7.5 |
| Atmospheric Temperature (K) | 298.15 |
| Atmospheric Pressure (MPa) | 0.1 |
| Evaporator Pressure ($P_e$) | 15-25 bar [20] |
| Condenser Pressure ($P_c$) | 5kPa [20] |
| Isentropic efficiency of pump | 0.7 [19] |

The steps for optimization would start with the selection of objective function that is to be maximized or minimized, followed by the selection of design variables (the most sensitive parameters on which the objective function depends). Thereafter, we need to set up the required equality or inequality constraints. We also need to set up upper and lower bounds for the design variables. Thereafter, for the optimization of the objective function, an optimization technique, e.g., genetic algorithm computational technique would be chosen. Using GA, the best solution for a design variable vector is obtained from an initial solution. At this value of the decision variable vector, the optimal value for objective function is obtained.

The configuration of genetic algorithm is shown in Table 2, $P_e$, $P_c$ and $T_e$ are the evaporator pressure, condenser pressure, and evaporator temperature respectively.

Table 2. Configuration for Genetic Algorithm.

| GA parameter | Value |
|---|---|
| Population size | 40 |
| Objective function | $\eta_{exergy,orc}$, Thermal stability Index of working fluid |
| Decision variable vector | [$P_e$, $P_c$, $T_e$] |
| Cross over probability | 0.8 |
| Mutation probability | 0.2 |
| Maximum generation | 60 |

The computational simulation has been done in MATLAB and the fluid properties have been taken from REFPROP 7.0. [23].

## Results and Discussion

Thermodynamic analysis of high temperature Organic Rankine Cycle (ORC) with an intermediate thermal oil circuit for transferring heat from parabolic trough collectors to the ORC has been performed in this work. Multi objective optimization of the ORC has been done using Genetic Algorithm (GA) in MATLAB software. $\eta_{exergy,orc}$ and thermal stability index of the working fluid have been taken as the objective function, while evaporator pressure, condenser pressure and evaporator temperature have been taken as the part of the design variable vector [$P_e$, $P_c$, $T_e$]. A thermal stability Index parameter is defined; which is dependent on the evaporator temperature and thermal decomposition temperature of the working fluid (473K). The Pareto optimal front for the evaporator temperature ranges: (a) 413K-533K, and (b) 473K – 533K are shown in Figure 2. The best optimal values for the

exergy efficiency and the thermal stability lie on the Pareto optimal front. For the three different working fluids (siloxanes), a suitable optimal solution for exergy efficiency was found be at 56% for the case (a), and 67% for the case (b) at optimal thermal stability index of 0.3 and 0.25. In the higher
temperature range i.e case (b), the thermal stability index for the working fluid was found to be lower. The lower thermal stability index at higher temperatures may conclude that the selection of a suitable working fluid is a necessary criterion for working at higher temperatures in Organic Rankine Cycle. The results for exergy efficiency are found to be slightly higher than the results in Ref. [20]. But, the results from Ref. [20] does lie on pareto optimal front as shown in Figure 2. The error in the result values could be because of the selection of design variable vector; more variables should be selected for obtaining the best optimal solution. To avoid the complexity of the analysis, lesser parameters have been selected in design variable parameter. The results have been validated for the evaporator temperature range 413K-533K.

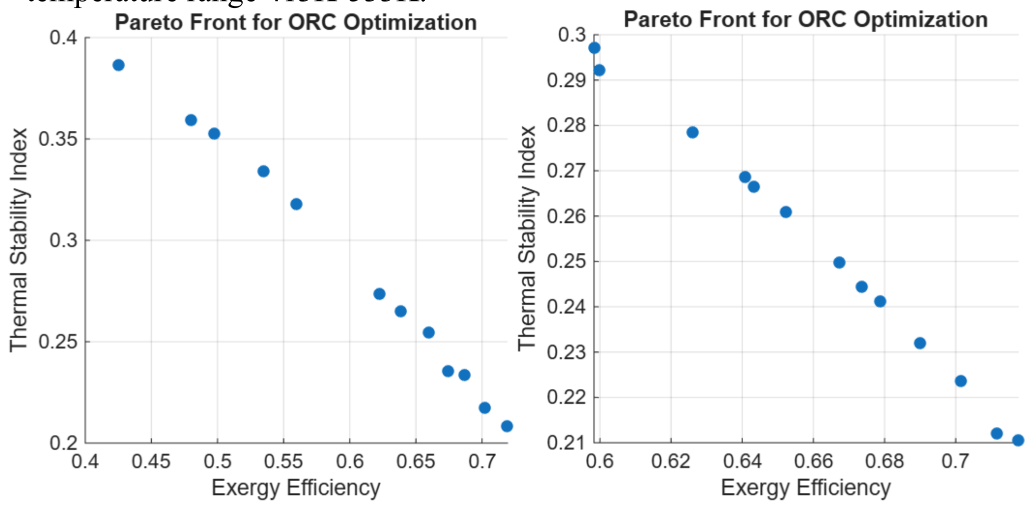


Figure 2. Pareto optimal front for (a) $T_e$ varies from 413K- 533K (b) $T_e$ varies from 473K – 533K.

## Conclusion

The multi objective optimization of high temperature organic Rankine cycle is performed using a genetic algorithm (GA) model in MATLAB. The heat source was an arrangement of parabolic trough collectors, and an intermediate thermal oil circuit was used to transfer solar heat to the evaporator of Organic Rankine Cycle. The heat transfer fluid is heated to a temperature of 653K in the collector. To carry out the multi objective optimization, the objective function is the exergy efficiency of the Organic Rankine Cycle and thermal stability index of the working fluid. The Pareto optimal front was obtained for evaporator temperature range 413K- 533K and 473K – 533K.

The exergy efficiency at optimal condition was found to be 56% and 67% for the two cases (a) and (b) at optimal thermal stability index of 0.3 and 0.25. The exergy efficiency values come out to be slightly higher, this error could be because of the chromosome variables (design variables) selected for the genetic algorithm computational analysis. To avoid this error, greater number of suitable design variables and complexity in the algorithm is required. These improvements could be done in future work in this field. The optimal thermal stability index of the working fluid decreased at higher temperatures, which suggests that there is a crucial role of selection of working fluid with good thermal stability while working at higher temperatures in Organic Rankine Cycle.

## References

[1] R. Vescovo, and E. Spagnoli, "High temperature ORC systems", Energy Procedia, Vol. 129, pp.82-89, 2017.

[2] D. Wei, X. Lu, Z. Lu, and J. Gu, "Performance analysis and optimization of organic Rankine cycle (ORC) for waste heat recovery", Energy conversion and Management, Vol. 48, No. 4, pp.1113-1119, 2007.

[3] Ö. Kaşka, "Energy and exergy analysis of an organic Rankine for power generation from waste heat recovery in steel industry", Energy Conversion and Management, Vol. 77, pp.108-117, 2014.

[4] H. Tian, G. Shu, H. Wei, X. Liang, and L. Liu, "Fluids and parameters optimization for the organic Rankine cycles (ORCs) used in exhaust heat recovery of Internal Combustion Engine (ICE)", Energy, Vol. 47, No. 1, pp.125-136, 2012.

[5] E. H. Wang, H. G. Zhang, B. Y. Fan, M. G. Ouyang, Y. Zhao, and Q. H. Mu, "Study of working fluid selection of organic Rankine cycle (ORC) for engine waste heat recovery". Energy, Vol. 36, No. 5, pp.3406-3418, 2011.

[6] T. Guo, H. X. Wang, and S. J. Zhang, "Selection of working fluids for a novel low-temperature geothermally-powered ORC based cogeneration system" Energy Conversion and Management, Vol.52, No. 6, pp.2384-2391, 2011.

[7] G. Yu, G. Shu, H. Tian, H. Wei, and L. Liu, "Simulation and thermodynamic analysis of a bottoming Organic Rankine Cycle (ORC) of diesel engine (DE)", Energy, Vol. 51, pp.281-290, 2013.

[8] D. Meinel, C. Wieland, and H. Spliethoff, "Effect and comparison of different working fluids on a two-stage organic rankine cycle (ORC) concept", Applied Thermal Engineering, Vol.63, No. 1, pp.246-253, 2014.

[9] S. Karellas, and A. Schuster, "Supercritical fluid parameters in organic Rankine cycle applications". International journal of Thermodynamics, Vol.11, No. 3, pp.101-108, 2008.

[10] [C. Zhang, G. Shu, H. Tian, H. Wei, and X. Liang, "Comparative study of alternative ORC-based combined power systems to exploit high temperature waste heat. Energy conversion and management", Vol. 89, pp.541-554, 2015.

[11] M., Preißinger, and D.Brüggemann, "Thermal stability of hexamethyldisiloxane (MM) for high-temperature organic Rankine cycle (ORC)", Energies, Vol. 9, No. 3, p.183, 2016.

[12] P. Colonna, E. Casati, C. Trapp, T. Mathijssen, J. Larjola, T. Turunen-Saaresti, and A. Uusitalo, "Organic Rankine cycle power systems: from the concept to current technology, applications, and an outlook to the future", Journal of Engineering for Gas Turbines and Power, Vol.137, No. 10, p.100801, 2015.

[13] L. R. Di Nanno, F. A. DiBella, and M. D. Koplow, "An RC-1 organic Rankine bottoming cycle for an adiabatic diesel engine" (No. NAS 1.26: 168256), 1983.

[14] P. Colonna, N. R. Nannan, A. Guardone, and E. W. Lemmon, "Multiparameter equations of state for selected siloxanes, Fluid Phase Equilibria", Vol. 244, No.2, pp.193-21, 2006.

[15] G. Angelino, and C. Invernizzi, "Cyclic methylsiloxanes as working fluids for space power cycles", 1993.

[16] X. Ren, J. Li, G. Gao, and G. Pei, "An innovative concentrated solar power system driven by high-temperature cascade organic Rankine cycle", Journal of Energy Storage, Vol.52, p.104999, 2022.

[17] T. K. Aseri, C. Sharma, and T. C. Kandpal, "Estimation of capital costs and techno-economic appraisal of parabolic trough solar collector and solar power tower based

CSP plants in India for different condenser cooling options", Renewable energy, Vol.178, pp.344-362, 2021.
[18] Y. Krishna, M. Faizal, R. Saidur, K. C. Ng, and N. Aslfattahi, "State-of-the-art heat transfer fluids for parabolic trough collector", International Journal of Heat and Mass Transfer, Vol. 152, p.119541, 2020.
[19] H. Xi, M. J. Li, C. Xu, and Y. L. He, "Parametric optimization of regenerative organic Rankine cycle (ORC) for low grade waste heat recovery using genetic algorithm", Energy, Vol. 58, pp.473-482, 2013.
[20] F. J. Fernández, M. M. Prieto, and I. Suárez, "Thermodynamic analysis of high-temperature regenerative organic Rankine cycles using siloxanes as working fluids", Energy, Vol. 36, No. 8, pp.5239-5249, 2011.
[21] J. H. Holland, "Adaptation in natural and artificial systems: an introductory analysis with applications to biology, control, and artificial intelligence. MIT press", 1992.
[22] D. Whitley, "A genetic algorithm tutorial", Statistics and computing, Vol. 4, No. 2, pp.65-85, 1994.
[23] REFPROP(NIST) version 7.0.

# DESIGN AND DEVELOPMENT OF A THERMOELECTRIC GENERATOR FOR AUTOMOTIVE EXHAUST ENERGY RECOVERY

Rone*[1], Soni Kumari[1], Sujit Kumar Verma[1]
*[1]Department of Mechanical engineering, GLA University, Mathura, India
ronie.somadder@gmail.com

## Abstract

*Utilizing waste heat from thermodynamic systems has shown to be a successful tactic for reducing environmental emissions and improving overall energy efficiency. About 40% of the chemical energy generated during fuel combustion is rejected by exhaust gases in internal combustion engines. It is possible to increase vehicle fuel efficiency and lower greenhouse gas emissions by harvesting this otherwise lost heat energy and turning it into useable electrical power. A viable answer for this kind of energy recovery is thermoelectric (TE) technology, which allows heat to be directly converted into electricity without the need for moving parts. Advantages of this technology include reduced maintenance needs, silent operation, and operational reliability. Despite these benefits, the large-scale application of automotive exhaust thermoelectric generators (AETEGs) remains constrained due to issues including temperature non-uniformity across modules, reduced conversion efficiency, and performance deterioration under variable engine operating conditions. In order to evaluate system performance under simulated exhaust circumstances typical of a light-duty vehicle, an automotive exhaust thermoelectric generator and a special experimental test facility were devised and constructed. A box-style heat exchanger, segmented cooling plates, and 44 bismuth telluride thermoelectric modules positioned on either side of the heat exchanger comprise the developed AETEG. Voltage-current (V-I) and power-current (P-I) characteristics at various thermal input levels were used to experimentally assess system performance. The peak power production of each module and the pressure drops across the heat exchanger were also measured. Degradation at the cold-side thermoelectric leg–solder contact increased internal resistance and decreased power production, according to thermal cycling studies.*

## Keywords

Waste heat recovery, thermoelectric generator, automotive exhaust energy, heat exchanger design, thermoelectric power generation.

## Introduction

For automobile exhaust heat recovery, thermoelectric generator (TEG) systems usually comprise arrays of thermoelectric modules placed between cooling plates and a heat exchanger. Automotive exhaust thermoelectric generators (AETEGs) are a promising concept, but there are a number of technical obstacles in their development. These include relatively low thermoelectric conversion efficiency, varying exhaust gas conditions, non-uniform temperature distribution across the heat exchanger surface, limited heat exchanger performance because of structural limitations, and issues with long-term operational reliability.

The efficacy of the heat exchanger and the thermoelectric modules' conversion efficiency are the main factors that determine an AETEG's overall efficiency. Depending on where each module is located in the array, uneven exhaust gas flow inside the heat exchanger frequently results in non-uniform temperature distribution. Temperature mismatch conditions thus arise, which affect the modules' electrical functioning point when coupled, resulting in decreased power output. Although a variety of flow-control structures, including baffles, diffusers, and flow straighteners, are frequently employed to enhance flow distribution, careful geometric optimization of these elements is required to improve temperature uniformity. The temperature reduction of exhaust gases along the flow direction as a result of heat extraction by the modules is another significant aspect influencing system performance. As a result, the thermoelectric materials only get a small portion of the available heat, which leads to a lower practical efficiency than theoretical material efficiency.

## Literature Review

### *Energy recovery techniques*

In order to recover energy from cars that would otherwise be lost during operation, a number of solutions have been proposed. When needed, the recovered energy can be stored and then delivered to various vehicle subsystems. Such energy recovery systems should ideally run continuously while guaranteeing that the energy is efficiently delivered when needed and stored with few losses. These systems must meet practical design requirements in addition to having great energy conversion and storage efficiency. To prevent adding to the vehicle's total bulk or packing restrictions, they should be lightweight and take up as little space as possible. Reducing parasitic losses and ensuring that the energy recovery mechanism does not adversely impact the vehicle's overall performance and fuel efficiency are two benefits of maintaining a lightweight and compact design.

### *Classification of energy recovery techniques*

The type of energy being recovered, the source of wasted energy, and the particular conversion technology used can all be used to categories energy recovery solutions in cars [1]. These categories aid in determining appropriate strategies for enhancing vehicle energy efficiency. Generally speaking, exhaust heat, braking systems, vibrations, and aerodynamic losses are the main causes of the wasted energy found in automobiles. This lost energy may be transformed into mechanical, thermal, or electrical energy that can be utilized by various vehicle subsystems, depending on the recovery process.

This wasted energy is captured and transformed using a variety of conversion technologies, such as organic Rankine cycle systems, thermoelectric generators, regenerative braking systems, and turbo-compounding devices. Regarding efficiency, complexity, cost, and viability of integration within current vehicle architectures, each method has pros and cons of its own. Researchers can more accurately assess these technologies' potential to increase overall vehicle efficiency and lower fuel consumption by classifying them according to energy source and conversion method. Figure 1 illustrates the classification of major energy recovery techniques currently being explored in modern automotive systems.

Exhaust gases, vehicle inertia, and vertical oscillations are the sources from which energy can be recovered in an automobile system. Both thermal and kinetic recovery are possible from the exhaust gases. In the former, TE technology is used to directly transform the heat present in the exhaust gas into electrical energy. In the latter, Rankine cycle or electric turbo-compounding (ETC) technologies are used to transform the exhaust gas's kinetic energy (KE) into mechanical and/or electrical energy. By using regenerative braking, the kinetic energy recovery system (KERS) transforms KE that would have been wasted as heat during braking into forms that may be used. KERS is further categorized according on the conversion method. Pneumatic and hydraulic KERS store KE as pressure energy, whereas elastomer or spring KERS store KE as elastic energy. In both situations, the stored energy is released as electrical or mechanical energy. KE is transformed into rotational energy in flywheel-based KERS and released as mechanical energy as needed. Additionally, there are alternator-control and electric KERS, which use a motor-generator system to convert KE to electrical energy.

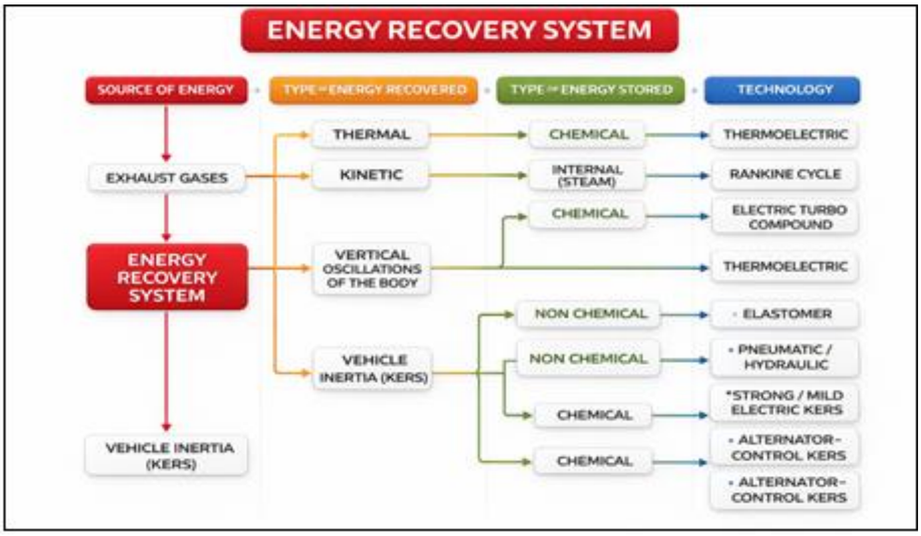

Figure 1. Classification of energy recovery techniques envisaged in automobiles.

## Experimental Methodology

### *Design and fabrication of automotive exhaust thermoelectric generator (AETEG)*

The AETEG experimental setup includes cooler plates to remove heat from the cold side of the TE modules, a heat exchanger to collect heat from the hot flowing gas and TE modules to transform the heat into electricity. Figure 2 depicts a schematic of the AETEG configuration utilized in this work. On both the top and bottom sides of the heat exchanger, the TE modules were positioned between the heat exchanger and the cooler plates.

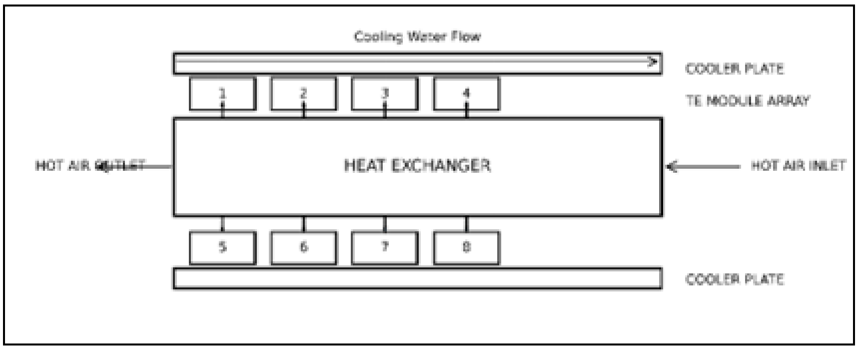

Figure 2. Schematic of the arrangement of the AETEG.

### *Heat exchanger*

The heat exchanger was constructed from stainless steel (SS 304) with a rectangular cross-section and a thickness of 2 mm. The channel's external measurements were 250 x 200 x 100 mm. The ends were joined to the hot air pipe by flanged couplings using truncated rectangular pyramids, each measuring 100 mm in length. The heat exchanger's comprehensive drawing with all of its dimensions is shown in Figure 3.

To improve the heat extraction from hot air, pin fin arrays were welded in-line to the inner surface of the rectangular channel using TIG welding. Within a particular heat exchanger volume, pin fins are among the most efficient heat transfer structures [1]. When compared to a smooth channel, the addition of pin fins increases the heat transfer coefficient by 50–100% when the Reynolds number is ≤ 20,000 [2]. Several pin cross-sections have been used to study the augmentation using these internal structures, with circular pin cross-sections being the most popular. Drop-shaped [1], elliptical [2], square [3], and other cross-sections were also examined. At higher Reynolds numbers (Re ≥ 10000), the fin shapes have less of an effect on the heat transfer properties [4].

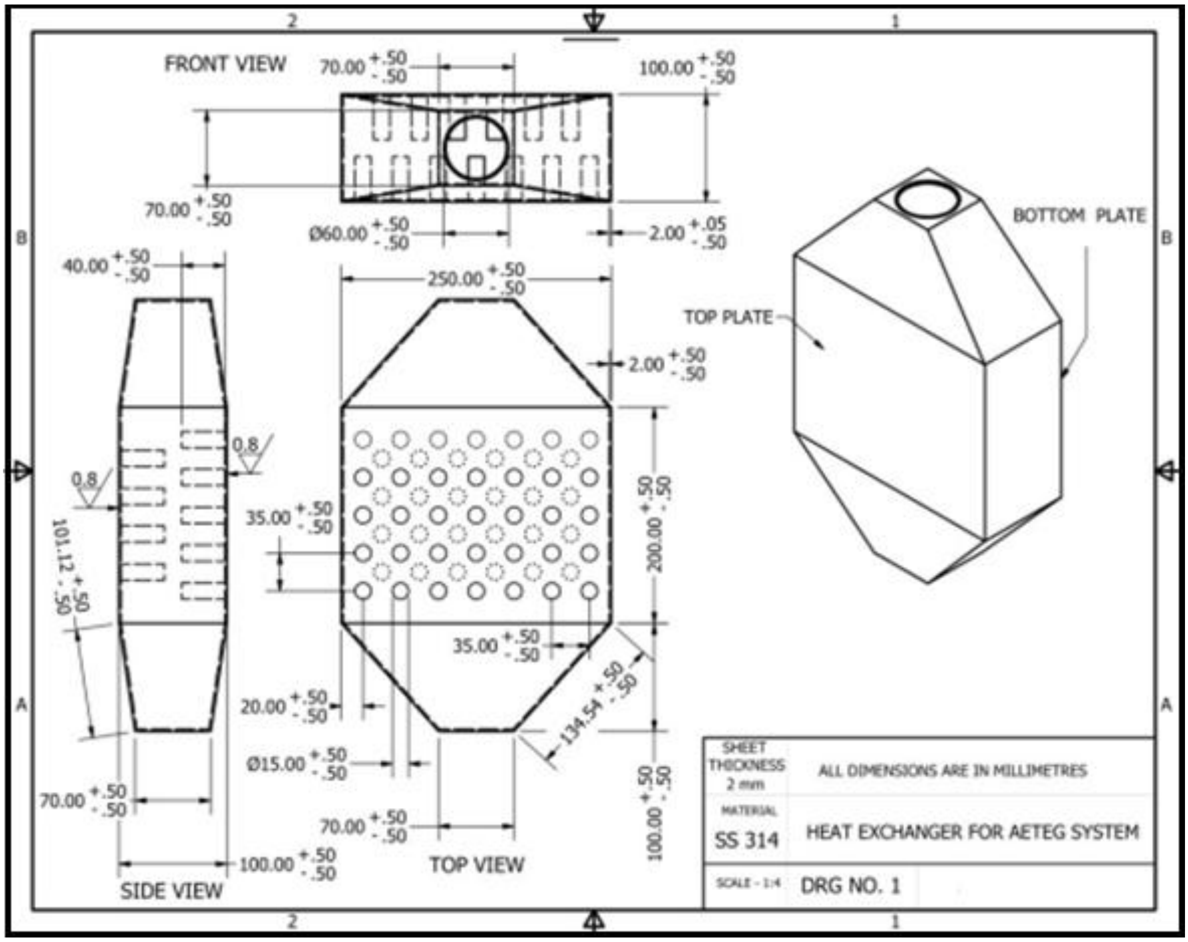


Figure 3. Dimensions of the heat exchanger channel and the pin fin arrangement in it.

There are two common arrangements for the pin fins: staggered and in-line. Because of their greater heat transfer capacity, metal pin fin arrays utilized in the integrated thermoelectric system performed better with staggered arrays than with in-line arrays [5]. On the other hand, the pressure drop in the staggered design is relatively bigger [6] [7]. Circular cross-section pin fins were chosen for the current heat exchanger design because they are easier to produce and offer a better trade-off between heat transfer and pressure loss than alternative cross-sections. The pin fin configuration of the heat exchanger intended for this investigation is depicted in Figure 4. The pin fins were positioned in a straight line. In relation to the top plate array, the fin array on the heat exchanger's bottom plate was positioned offset. The height to diameter (H/D) ratio of the pin fin was maintained at 2.7 and the stream- wise pitch to diameter ratio (ST/D) and the span-wise pitch to diameter (SP/D) ratio of the pin fin array was 2.3. L and W represent the length and width of the rectangular channel, respectively.
The actual photos of the heat exchanger and its inside are displayed in Figure 5. The fin arrangement in the rectangular channel is depicted in Figure 5 (a). Tungsten inert gas (TIG) welding was used to attach the pins to the rectangular channel's inner surface. A 50 mm length SS (SS 316) pipe with an inner diameter of 50.8 mm was used to secure the ends of the truncated rectangular pyramids on both sides. To connect the hot air pipe coming from the heat source, an SS 316 flange (ANSI, slip on the raised face (SORF) of class 150) was welded at one end. The other end was also welded with a similar flange to connect to the outlet pipe

(figure 5 (b)). A 2 mm thick SS plate with 30% area perforated was kept on the inlet region of the rectangular channel to straighten the hot air flow (figure 5 (c)).

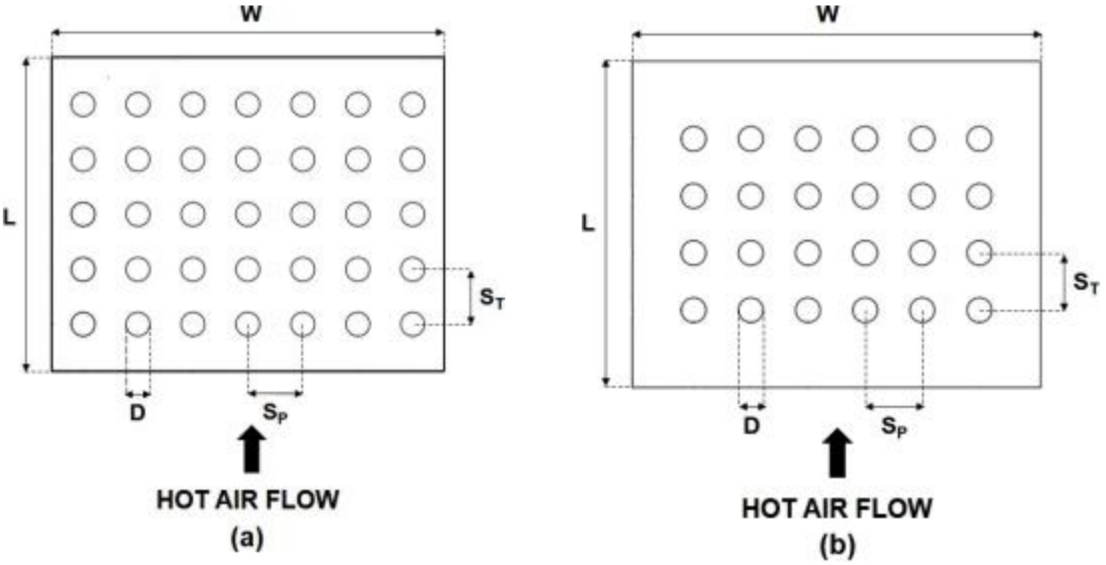


Figure 4. Pin fin arrangement on the (a) top plate and (b) bottom plate of the heat exchanger.

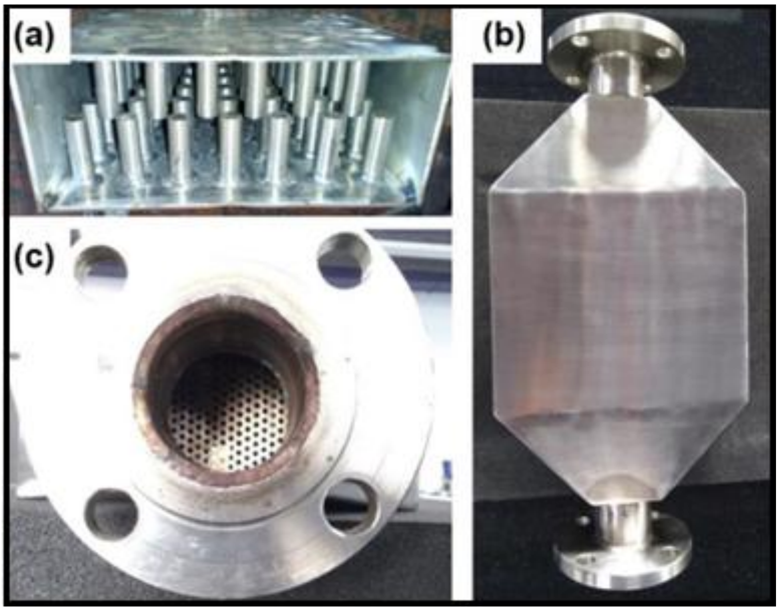


Figure 5. Actual images of the (a) pin fin arrays (b) heat exchanger (c) perforated plate at the inlet of the rectangular channel.

### *Cooler plate*

Cooler plates were used to extract heat from the TE modules' cold side. The cooler plate was made of a 2 mm thick SS 316 sheet and had external dimensions of 250 mm × 200 mm × 40 mm. Four equal parts made up the internal volume (figure 6). Three baffles, each measuring 40 mm in height and 75 mm in length, were installed in each segment to allow the coolant to flow in a serpentine pattern. The steel base plate was welded to the 2 mm thick baffles, which were sealed with a rubber gasket on top. Additionally, each portion had a 20 mm-diameter coolant input and outlet. The true image of the SS cooler plate is displayed in Figure 7. After the TE modules were positioned, two similar cooler plates were positioned, one on the heat exchanger's top and another on its bottom flat surface. The test setup had two water heads, one for each of the two cooler plates' inlets and exits.

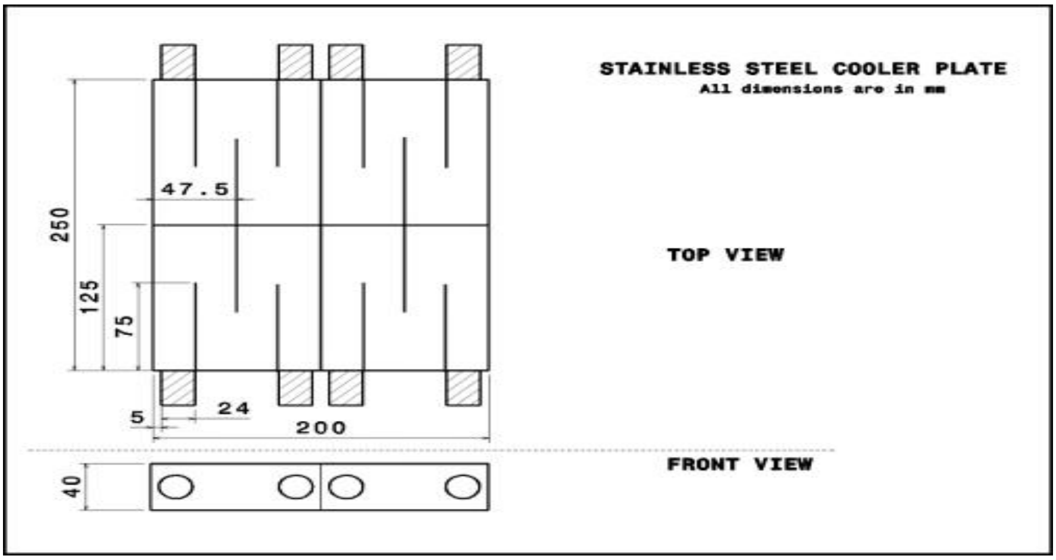


Figure 6. Drawing of the stainless-steel cooler plate.

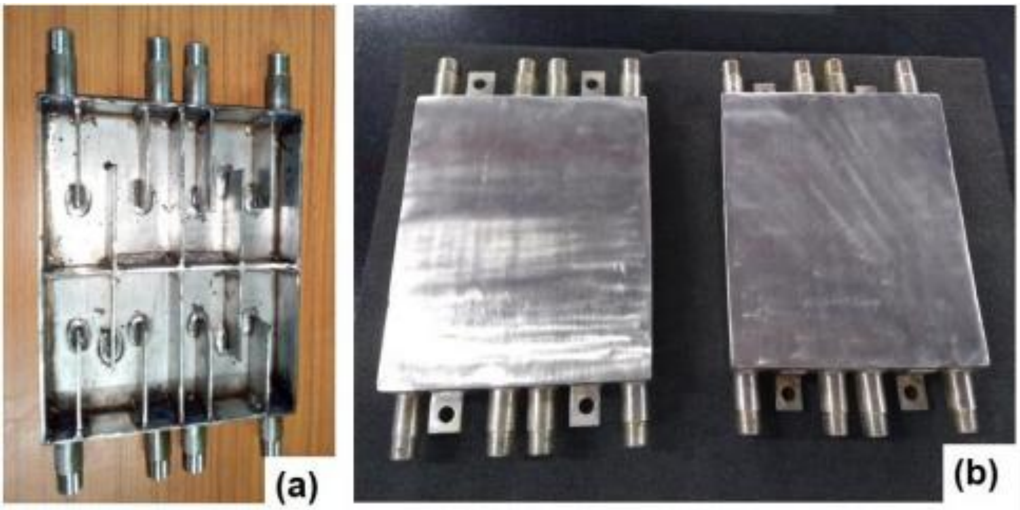


Figure 7. Actual image of the (a) baffles in the cooler plate (b) fabricated cooler plate Pin fin arrangement on the (a) top plate and (b) bottom plate of the heat exchanger.

## Experimental Setup

Eight TE modules in AETEG were used for the thermal cycling investigations. They were arranged symmetrically on the heat exchanger's upper surface (Figure 8(a)), which was covered by the aluminum cooler plate. Each of the TE modules was positioned in a distinct temperature gradient on the heat exchanger's surface. Figure 8(b) depicts the actual configuration of the TE modules on the heat exchanger surface.

### *Internal resistance and V-I characteristics of the TE modules before cycling*

Prior to the thermal cycling experiments, the Rint at room temperature (RT resistance), V-I characteristics, and HT resistance of each individual TE module in AETEG were ascertained. After the TEG system achieved the steady-state condition for a heater set temperature (THST) that matched the holding temperature of each thermal cycling profile (TCP), the VOC and V-I characteristics were ascertained.

### *Thermal cycling experiments*

Three TCPs were used for the heat cycling studies. The TEG assembly in each instance used a set of eight new TE modules. Coolant temperature and flow rate, air temperature, and air flow rate were the variables that could be changed separately in the test rig. The TCPs in this study were produced by changing the temperature of the heat source at various heating rates while maintaining a constant input air flow rate to the heater. The aluminum coolant plate's coolant temperature and flow rate were maintained at 25 l/min and 16oC, respectively.

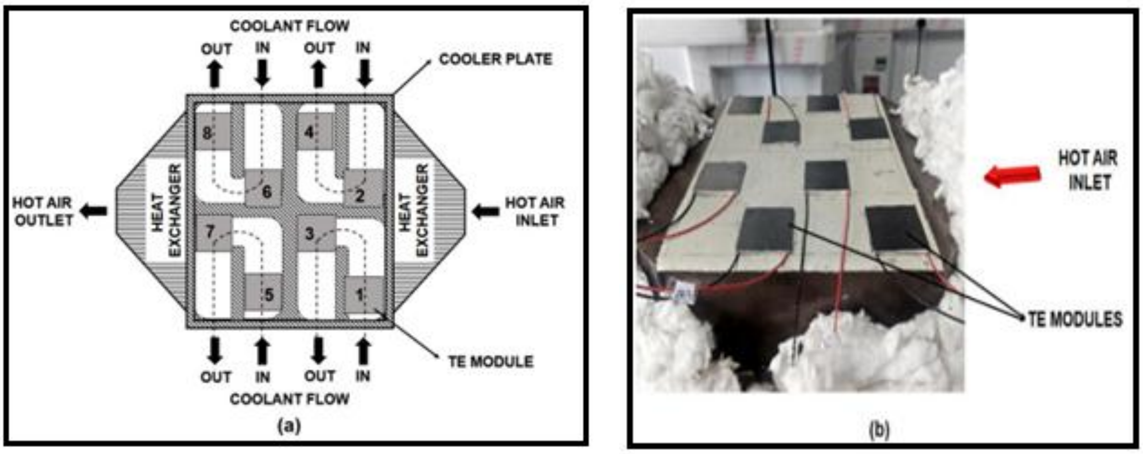


Figure 8. Schematic of arrangement of eight TE modules on the surface of the heat exchanger (b) Actual image of the arrangement.

Typical trend displays include:

- TC1 / TC2 → Temperature sensor readings
- STUD / STUM → Upper and middle surface temperatures
- GTU / GTM → Gas temperature measurements
- FLOW → Fluid flow rate
- PRESSURE → System pressure
- DPT → Differential pressure
- DC LOAD → Electrical load applied to thermoelectric modules


Figure 9. Input command entry page of the program.

*ISBN 978-81-973526-0-7*

The THST was changed from 50°C to 300°C at a rate of 50°C per minute in the initial TCP (TCP1). Similar to TCP1, the THST of the second TCP (TCP2) ranged from 50 to 300 degrees Celsius, but the heating rate was raised to about 85 degrees Celsius per minute. For the third TCP (TCP3), the air heating rate was kept at 50°C per minute while the THST was adjusted between 50°C and 350°C. The three TCPs are depicted in Figure 9, and each TCP's THST and air heating rate are listed in Table 1. The TE modules underwent 150 thermal cycles in TCP1 and TCP2, and 300 cycles in TCP3. Ten minutes was the dwell period in each of the three scenarios.

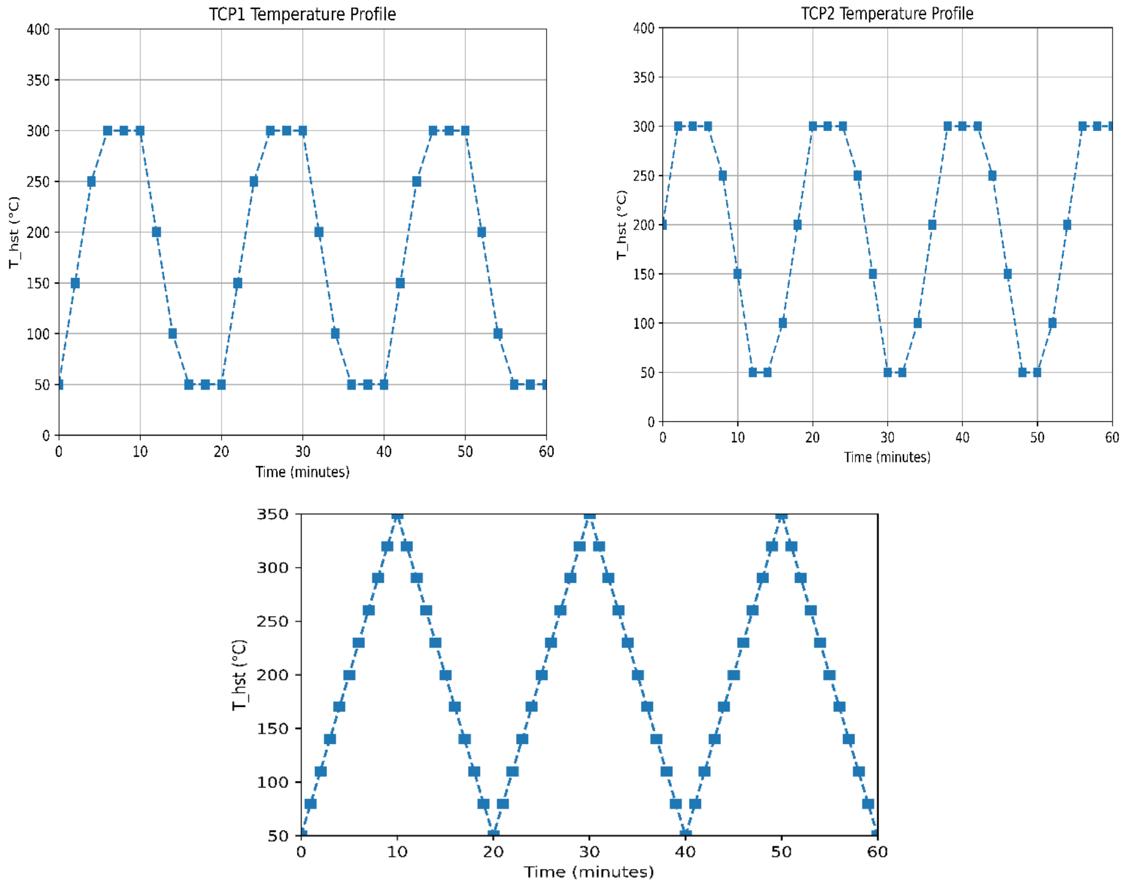


Figure 10. (a) Thermal cycling profile 1 (TCP1), (b) Thermal cycling profile 2 (TCP2) and (c) Thermal cycling profile 3 (TCP3).

Table 1. Thermal cycling profile parameters.

| Thermal cycling profile | Heater set temperature, THST (ºC) | Heating rate (ºC/min) | Dwell time at THST (minutes) |
|---|---|---|---|
| TCP1 | 300 | 50 | 10 |
| TCP2 | 300 | 85 | 10 |
| TCP3 | 350 | 50 | 10 |

## Results and Discussions

### *Temperature variation and heating rate of the TE modules*

The ~Th values measured under steady state settings that correlate to each TCP's maximum THST (holding temperature) are displayed in Figure 10(a). For all three TCPs, it was found that ~Th values exhibited the same tendency. Along the direction of hot airflow, the ~Th values displayed a declining trend. This behavior was comparable to what was seen when mapping surface temperatures. Figure 10(b) shows the heating rate of the individual TE modules at eight different locations on the heat exchanger surface, determined from the slope of the heating obtained from corresponding ~Th values.

Along the hot airflow's streamwise direction, the heating rate likewise dropped. The average heating rate of TE modules under TCP1 and TCP3 was found to be about twice that of TE modules under TCP2. The shorter residence period of hot air within the heat exchanger may be the cause of the TE modules decreased heating rate under TCP2, despite the air's quick heating rate (85°C/min) to the preset temperature in comparison to TCP1 and TCP3. Additionally, it was noted that the current study's module heating rate was significantly lower than that of the conduction setup-based tests reported in the literature [1], [2], and [3]. This would result in a slower degradation rate of the TE modules as it is proportional to the module heating rate [1].

Table 2. Variation of heating rate across thermoelectric module positions for different temperature cycling profiles (TCP1–TCP3).

| Position | TCP1 | TCP2 | TCP3 |
|---|---|---|---|
| 1 | 278 | 266 | 314 |
| 2 | 258 | 260 | 296 |
| 3 | 232 | 248 | 242 |
| 4 | 256 | 231 | 272 |
| 5 | 251 | 245 | 266 |
| 6 | 250 | 238 | 255 |
| 7 | 253 | 218 | 266 |
| 8 | 168 | 215 | 182 |

Table 3. Experimental heating rates at various TE module locations under three temperature cycling protocols.

| Position | TCP1 | TCP2 | TCP3 |
|---|---|---|---|
| 1 | 9.5 | 5.8 | 10.5 |
| 2 | 11 | 5.5 | 9.1 |
| 3 | 9.8 | 5.5 | 10.2 |
| 4 | 9 | 4.9 | 8.6 |
| 5 | 7.8 | 4.2 | 7.6 |
| 6 | 8.3 | 4.1 | 8.3 |
| 7 | 7.1 | 3.6 | 7.6 |
| 8 | 4.8 | 3.9 | 5.4 |

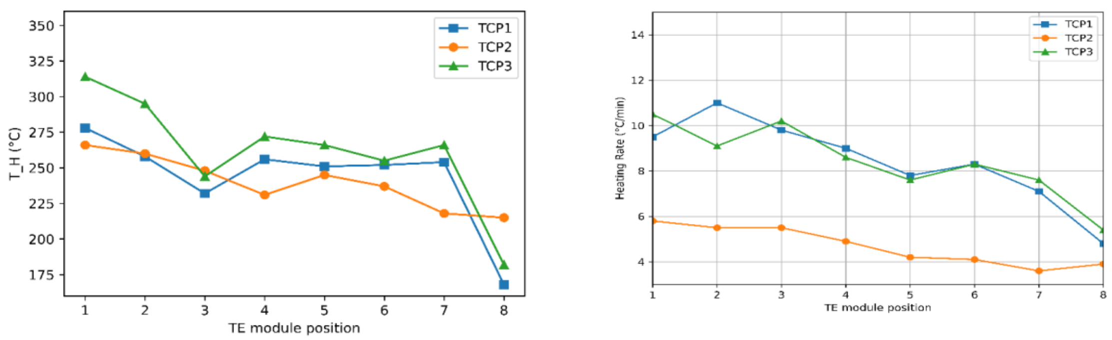


Figure 11. (a) ~Th values measured adjacent to each TE module position at the steady state conditions corresponding to the maximum THST of each TCP before thermal cycling (b) Heating rate of the modules at different positions on the heat exchanger surface when the inlet air is heated at 50°C/min (TCP1 & TCP3) and 85°C/min. (TCP2) [2].

## Conclusion

In this work, an automotive exhaust thermoelectric generator (AETEG) for light-duty vehicle applications was designed, manufactured, and tested. AETEG performance was assessed experimentally under steady state and thermal cycling circumstances in a specially designed, sturdy, and compact hot air-based test apparatus. The thermal behavior of the heat exchanger and the electrical performance of the arrays of TE modules was assessed under different operating conditions. The following are the main findings from the experimental investigations conducted in this work:

- According to the temperature distribution mapping on the heat exchanger surface, the average surface temperature peaked 75 mm from the rectangular channel's intake and then dropped as it approached the outlet. Thermal insulation reduced the spatial fluctuation in temperature.
- The maximum efficiency obtained for the present pin-fin heat exchanger design was 9.2% in bare condition at hot air inlet temperature (TiH) of 385°C and a hot air mass flow rate (MFR) of 260 kg/h. However, after assembling it in AETEG with 44 TE modules, it was 12.7%. The increase in the latter case was due to forced heat extraction from the heat exchanger by the cooler plates through the TE modules which resulted in a lower hot air outlet temperature (ToH) value.
- At the maximum TiH of 385°C and hot air MFR of 255 kg/h, the heat exchanger caused a maximum pressure drop of 0.9 kPa. This pressure drop was within an AETEG's permissible range. The expansion and contraction losses from the truncated pyramidal structures and the perforated plate placed at the heat exchanger's rectangular channel input were the main causes of the pressure reduction.
- Due to temperature mismatch conditions, the TE modules delivered varied VOC and Pmax for a given heat input depending on where they were on the AETEG. Eight TE modules produced more power than twenty-four TE modules under same heat input and experimental conditions. The percentage occupancy of the TE modules over the heat is indicated by this observation.

## References

[1] A. Gabriel-Buenaventura, J. H. Martínez, and A. García, “Energy recovery techniques in automobiles: A review,” Renewable and Sustainable Energy Reviews, vol. 49, pp. 813–824, 2015.

[2] N. Sahiti, A. Lemouedda, and F. Durst, “Thermal performance comparison of pin fin heat exchangers with different pin cross-sections,” Appl. Therm. Eng., vol. 26, pp. 1176–1185, 2006.

[3] O. von Wilmersdorf and J. S. Weigand, “Heat transfer and pressure drop in pin-fin heat exchangers for gas turbine cooling,” Int. J. Heat Mass Transf., vol. 50, pp. 1889–1899, 2007.

[4] Z. Chen, Q. Li, D. Meier, and H. J. Warnecke, “Convective heat transfer and pressure loss in rectangular ducts with drop-shaped pin fins,” Heat and Mass Transfer, vol. 33, pp. 219–224, 1997.

[5] H. Li, T. Kumada, and M. Faghri, “Experimental investigation of heat transfer in channels with elliptical pin fins,” Int. J. Heat Mass Transf., vol. 41, pp. 421–431, 1998.

[6] A. Pandit, S. Joshi, and P. K. Sharma, “Experimental study of heat transfer characteristics of pin-fin arrays under varying Reynolds numbers,” International Journal of Thermal Sciences, vol. 82, pp. 48–57, 2014.

[7] S. C. Tzeng, C. H. Chen, and Y. L. Huang, “Performance analysis of thermoelectric

generators integrated with metal pin-fin heat exchangers," Energy Convers. Manag., vol. 84, pp. 553–560, 2014.

[8] M. K. Chyu, C. H. Yen, and S. Siw, "Comparison of heat transfer from staggered pin-fin arrays with circular, cubic and diamond-shaped elements," in ASME Turbo Expo 2007: Power for Land, Sea and Air, Montreal, Canada, 2007, pp. 1–9.

[9] K. Bilen, U. Akyol, and S. Yapici, "Heat transfer and friction correlations for finned surfaces and thermal performance analysis," Energy Convers. Manag., vol. 42, pp. 1071–1083, 2001.

[10] S. Hatzikraniotis, T. Kyratsi, and K. M. Paraskevopoulos, "Thermal cycling effects on the reliability of thermoelectric modules," J. Electron. Mater., vol. 38, pp. 1173–1181, 2009.

[11] S. Park, H. Lee, and J. Kim, "Flexible thermoelectric generator for human body heat energy harvesting," Adv. Funct. Mater., vol. 30, no. 19, p. 1906257, 2020, doi: 10.1002/adfm.201906257.

[12] C. Merienne, P. D. Phelan, and S. Graham, "Thermal cycling degradation mechanisms in thermoelectric modules," J. Electron. Mater., vol. 48, pp. 356–364, 2019.

[13] S. Harish, R. R. Kumar, and P. R. Kumar, "Experimental investigation of temperature distribution and heating rate in thermoelectric modules for waste heat recovery applications," Energy Convers. Manag., vol. 245, p. 114548, 2021.

[14] A. A. Malik and A. Bilberg, "Digital twins of human-robot collaboration in production systems," Procedia Manufacturing, vol. 38, pp. 108–115, 2019.

# THERMO-ECONOMIC ASSESSMENT OF A SOLAR STILL INTEGRATED WITH PHASE CHANGE AND RECYCLED THERMAL ENERGY STORAGE MATERIALS

Raman Deep*[1], Naveen Sharma[1]
*[1]Department of Mechanical Engineering, Netaji Subhas University of Technology, Delhi, India
raman.deep.phd22@nsut.ac.in

## Abstract

*The effectiveness of the square pyramid solar still for generating freshwater in the weather of New Delhi, India (28° 35′ N, 76° 54′ E), was experimentally investigated in this work. Conventional Pyramidal Solar Still (CSS), Modified Pyramidal Solar Still (MSS), CSS with Thermal Energy Storage Material (TESMs) named CSS-ESC, and MSS with TESMs named MSS-ESC were among the four configurations that were tested in October 2025. The findings showed that freshwater production fluctuates with environmental conditions. When PCM and TESMs were added to the basin, the amount of overall freshwater produced was also increased. The freshwater productivity for CSS to CSS-ESC increased from 1.53 L/m2 to 1.88 L/m2 with addition of TESMs without any design changes. With a freshwater productivity of 2.14 L/m2, MSS-ESC is 40.5% and 17.02% more productive than CSS and CSS-ESC, respectively. For MSS-ESC, CPL of freshwater was Rs 1.69, which is around 17% less than that of CSS. Freshwater production has increased and CPL has decreased as solar energy is stored by PCMs and TESMs during day time and released it at night. In comparison to CSS with a payback period of 289 days and MSS with 264 days, MSS-ESC had a payback period of 248 days that is 41 and 16 days shorter than CSS and MSS, respectively. Therefore, MSS-ESC was found to be the most efficient solar still and exhibited the synergistic effect of PCM and TESMs with the highest freshwater productivity and the lowest CPL and payback period.*

## Keywords

Desalination, Pyramid solar still, Thermal Energy Storage Material, PCM.

## Introduction

One economical and eco-friendly strategy to fight global warming is to use solar energy. As the world's population grows, the need for clean drinking water for various purposes increases. Solar desalination plays a vital role in converting accessible salted water into drinkable water. Solar stills are affordable and convenient devices that utilize solar energy for evaporation and condensation [1]. However, due to their limited water productivity, they have not been adopted on a large scale for drinking water applications. Therefore, many researchers have worked to enhance the productivity of solar stills.

Phase change materials (PCMs) allow for continuous water generation even after sunset by absorbing solar energy during the day and at night releasing, as reported by Goel et al. [2]. Ahmed et al. [3] used PCM and fins to boost solar still (SS) productivity and findings indicated that combination could raise overall efficiency by up to 43%. Mahala and Sharma [4] experimentally examined the impact of gravel on a modified solar still (MSS). They found that using gravel together with PCM resulted in daily productivity gains of approximately 84% for MSS with gravel (MSS+G), 38% and with gravel CSS+G and 32% for MSS compared to CSS. Alshqirate et al. [5] conducted a study to compare a pyramidal SS with a CSS and with natural fibres (palm leaves). The use of natural fibres increased distillation production by 44.5%.

Pandey et al. [6] investigated a pyramidal SS, incorporating both fins and PCM. Their modified setup demonstrated a 41% higher in fresh productivity as to conventional one, along with a 47% decrease in the price per litre of freshwater produced. Vembu et al. [7] used 42 coal cylinders of identical sizes (20 mm diameter, 5 mm height), which served as TESMs and prolonged surfaces. This design improved productivity by 44.44%. Singh et al. [8] caried out a thorough analysis of various SS designs employing PCMs. Their findings revealed that incorporating PCMs in pyramid, SSs increased productivity significantly by 94%. Attia et al. [9] incorporated graphite fins in the basin of a conical solar still, increased a productivity by 42.3% compared to CSS.

Comparing the performance of CSS and MSS is the purpose of the present work, while enhancing the productivity of a square pyramid solar still using TESMs. The basin of the modified still contains a specially designed galvanized iron bed that holds the phase change material. The innovative aspect of the design lies in its optimal utilization of the energy stored in the PCM while minimizing thermal losses, thereby achieving superior performance.

## Experimental Details

The experiment was conducted on the rooftop of the Department of Mechanical Engineering at Netaji Subhash University of Technology, Jaffarpur (28° 35′ N, 76° 54′ E). Two solar stills were designed and built each with an identical square basin of area 0.49 m² and a height of 100 mm. Galvanized iron sheets with a thickness of 1.5 mm were used to construct the basins and painted black to improve solar radiation absorption. To minimize heat loss, the bottom and sides of each basin were insulated with 10 mm thick glass wool, and 18 mm thick wooden block was added to further reduce heat loss to the environment. Both stills were covered with a square pyramid glass cover of 3.5 mm thickness, having a height of 206 mm and inclined at 28° to the horizontal. This inclination angle was chosen based on the site's latitude, as previous studies have shown that the optimal tilt of the glass cover depends on the angle at which solar radiation strikes it [10]. Gaps between the basin and the glass cover were sealed with silicone. A PCM storage bed made of galvanized iron was placed inside each basin, containing approximately 15 kg of paraffin wax. To enhance heat conduction from the PCM to the water, a serpentine copper channel was embedded within the PCM storage bed. During the experiments, about 7 L of water was measured using a measuring jar and poured into each still. Solar radiation passed through the glass cover, heated the basin water, and generated water vapor. Due to the temperature difference between the vapor and the cooler glass cover, condensation occurred on the inner surface of the glass. The resulting distillate was collected through an aluminium collection channel and measured using a calibrated jar. Figure 1. shows a photograph of the experimental setup and schematic of the test rig used for experiment.

Conical shapes have special benefits in terms of heat retention and dissipation due to their geometry. A thermal gradient is produced and layered heat distribution is facilitated by the conical shape. Significant heat storage is made possible by the favourable volume to surface ratio, which also lowers losses. Better radiation efficiency, even heat transfer and natural convection for dissipation are all made possible by the sloped sides. As a result, conical structures are currently built using demolition waste and materials like concrete, marble, and ceramic. By recycling waste, these forms which were created from particles with a low-load-bearing capacity proved to be extremely effective at storing thermal energy, illustrating an environmentally responsible approach to thermal management.

Solar radiation was measured using a solar power meter with an accuracy of ±5 W/m², a percentage error of 2.5%, and an observed variation of ±0.57 W/m². Temperatures of the basin, water, glass cover, and ambient air were monitored using K-type thermocouples placed at various locations. Data were recorded automatically on interval of five minutes using a digital temperature indicator and logger with an accuracy of ±1 °C, over a range of 0-

1200 °C. The indicator exhibited an error of 0.25% and an observed deviation of ±0.57 °C. The freshwater volume was quantified using a measuring jar with an accuracy of ±10 mL, over a 0-1000 mL range, showing an error of 10% and an observed discrepancy of ±5.77 mL. Using the methodology opted by Mahala and Sharma [4], hourly yield and total daily yield uncertainties were estimated and found to be 1.5% and 2.1%, respectively.

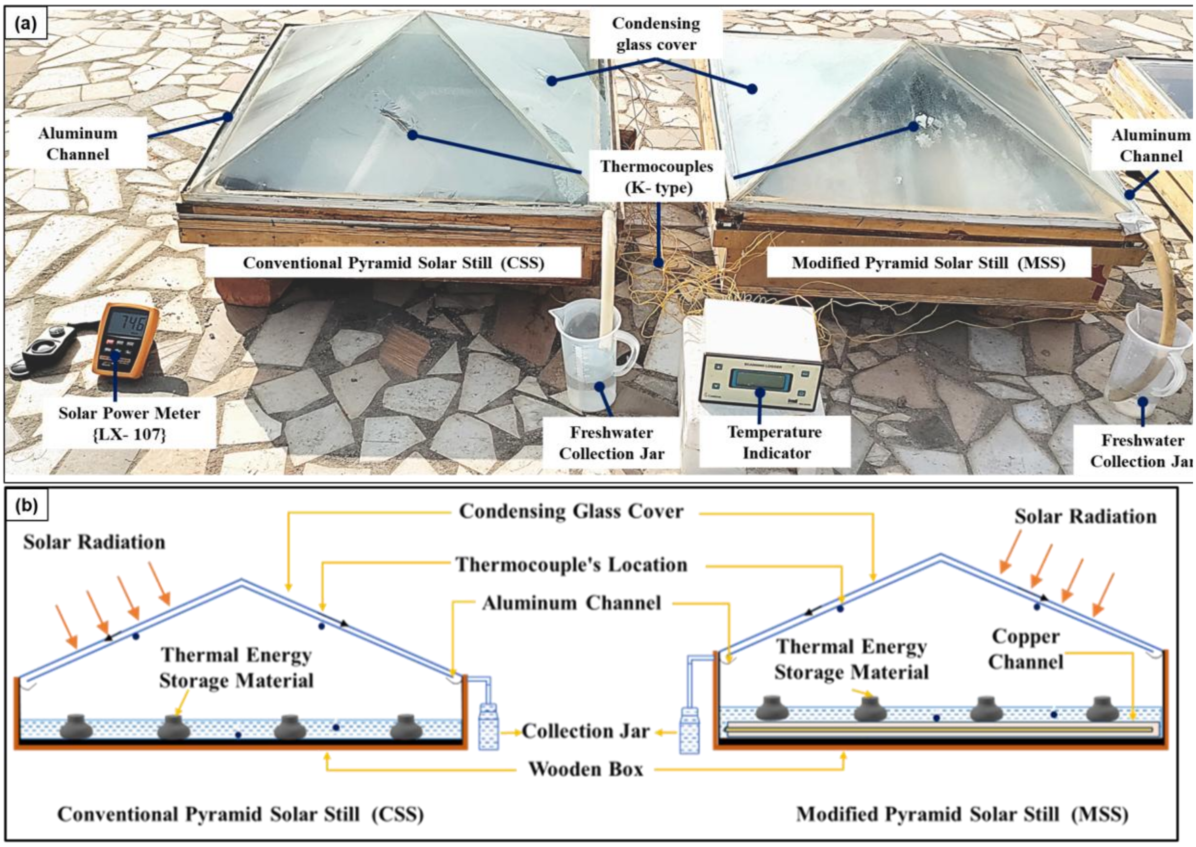


Figure 1. (a) Photograph and (b) schematic of experimental setup used for experiment.

## Economic Analysis

The methodology balances capital expenditure with long term sustainability using key metrics such as payback period and cost per liter (CPL) of freshwater, following the cost benefit approach of Mahala and Sharma [4]. Central to this assessment is the production rate (L/h), which clearly illustrates the solar still's effectiveness.
If TC, be the total amount of capital spent on SS fabrication alongside the interest rate. i, per annum (i=10%) and n be the SS's useful lifecycle in years (n= 20 years). Fabrication cost of each SS is detailed in Table 1.

The annual fixed cost ($AFC$) and capital recovery factor $CRF$ can then be computed as follows.

$$CRF = \frac{i\,(1+i)^n}{(1+i)^n - 1} \quad (1)$$

$$AFC = TC \times \text{CRF} \quad (2)$$

The annual cost of operations and maintenance $OMC_{annual}$ which includes the sum incurred on regular cleaning and feeding water, collecting freshwater, and removing scaling due to deposition of salt within the SS, is calculated as 15% of $AFC$ and presented as:

$$OMC_{annual} = 0.15 \times \text{AFC} \quad (3)$$

*ISBN 978-81-973526-0-7*

The Sinking Fund Factor ($SFF$) is computed as follows.

$$SFF = \frac{i}{(1+i)^n - 1} \tag{4}$$

The annual salvage cost $S_a$ is therefore computed as follows:

$$S_a = S \times SFF \tag{5}$$

where $S = 0.2 \times TC$ for salvage cost.

Total annual cost ($TAC$) is calculated by

$$TAC = AFC + OMC_{annual} - S_a \tag{6}$$

Average annual freshwater yield in L/m$^2$ ($M_w$) can be evaluated as:

$$M_w = m_w \times N_d \tag{7}$$

where $m_w$ refers to the average productivity of freshwater in each square unit and $N_d$ is used to describe the number of days that are clear for Delhi, India. Cost per liter ($CPL$) of fresh water is estimated as:

$$CPL = \frac{\text{Total Annual Cost (TAC)}}{\text{Average annual freshwater yield } (\mathrm{M_w})} \tag{8}$$

Annual distillate market cost.

$$AMC = M_w \times \text{Market cost of water per kg} \tag{9}$$

Annual net income $NE_a$ is computed as follows:

$$NE_a = AMC - TAC \tag{10}$$

Consequently, the payback period ($P_B$), in days, of the TSS is given by:

$$P_B = \frac{TC}{NE_a} \times 365 \tag{11}$$

Table 1. Fabrication cost of each SS.

| Component of TSS | CSS | MSS | MSS-ESC | MSS-ESC |
|---|---|---|---|---|
| Glass Cover | 2500 | 2500 | 2500 | 2500 |
| Absorber Plate (GI) | 2200 | 2200 | 2200 | 2200 |
| Wooden Frame | 2150 | 2150 | 2150 | 2150 |
| Collecting Jar | 100 | 100 | 100 | 100 |
| Aluminium Frame | 350 | 350 | 350 | 350 |
| Black Paint | 250 | 250 | 250 | 250 |
| Insulation | 220 | 220 | 220 | 220 |
| PCM Bed | 0 | 500 | 0 | 500 |
| PCM (Paraffin Wax) | 0 | 550 | 0 | 550 |
| Heat Storage Material | 0 | 0 | 550 | 550 |
| Miscellaneous | 150 | 150 | 150 | 150 |
| Total Cost (In Rs.) | 7920 | 8970 | 8470 | 9520 |

## Results and Discussion

The performance of two solar still configurations, CSS and MSS in smooth, as well as two configurations with TESMs, CSS-ESC and MSS-ESC, is being experimentally investigated. The experiments were carried out in month of October, 2025. The experiments for two consecutive days were selected to be reported in this work because the ambient temperature and solar irradiance varied very slightly during these two days.

ISBN 978-81-973526-0-7

### *Experimental conditions*

The variations with time in ambient temperature and solar radiation incident on SS during the experimental days are shown in Figures 2. and Figures 3. The experiments had very similar environmental conditions, with little variation in ambient temperature profiles and solar radiation. Beginning at 8:00 AM with around 350 W/m2 and reaching a peak of about 754 W/m2, solar radiation shows an increasing trend before progressively decreasing to its lowest value of 0 W/m2 at 7:00 PM. While ambient temperature peaks at about 2:00 PM, reaching 41°C. A direct comparison of SSs performance was made possible by the fact that the average ambient temperature and solar irradiance varied by less than 4% between the two days, confirming the stability of experimental conditions.

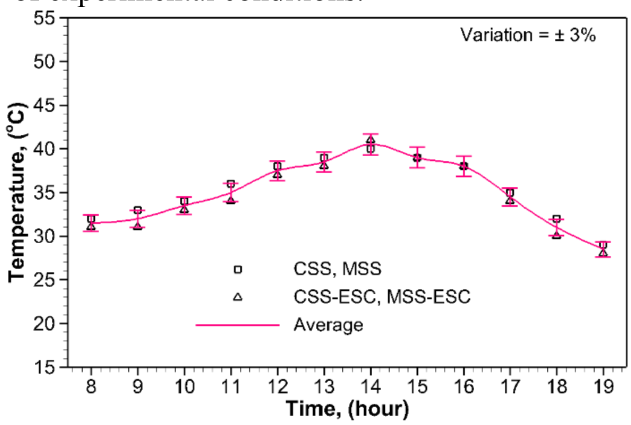


Figure 2. Ambient temperature variation on an hourly basis for studied configurations.

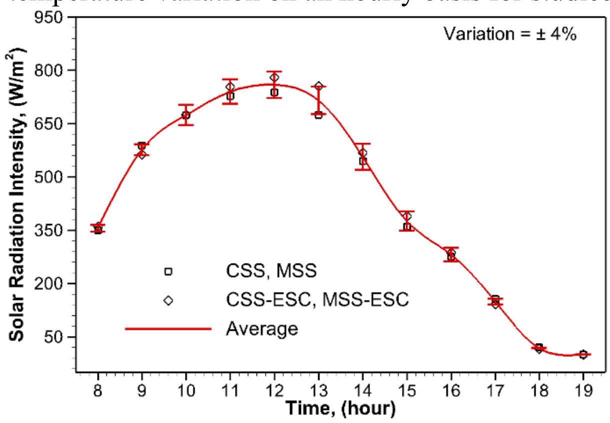


Figure 3. Solar intensity variation on an hourly basis for studied configurations.

### *Variations in temperature*

The hourly temperature variation related to the different configurations under study is shown in Figure 4. The CSS exhibits the most volatile profile, with water temperature peaking at 69 °C at 01:00 PM before rapidly declining to 32 °C by night, producing a sharp diurnal swing that promotes rapid afternoon cooling and heavy evaporation during the day. Among the four configurations, distinct thermal behaviours emerge from the interplay between PCM and the additional TESMs like cone. Integrating PCM and serpentine copper tube MSS moderates the peak to 51 °C at 03:00 PM, demonstrating the buffering effect of thermal mass. Thermal inertia is further improved by adding TESMs conical shape to CSS. As a result, the CSS-ESC peak water temperature shifts to 2:00 PM and slightly decreases to 67 °C. More importantly, CSS-ESC extends the condensation window into the evening by maintaining a positive waterglass temperature differential of 4 °C even at 6:00 PM. The peck water temperature for MSS is 51°C, which is about 18°C lower than the CSS. This is because PCM absorbs the portion of heat that still receives. For MSS ESC, the profile becomes the most damped, with peak water temperature at 48 °C leading to a diurnal curve that is almost flat. MSS-ESC, despite its modest peak driving force, offers the longest-lasting warmth, potentially facilitating overnight productivity. Overall, CSS-ESC offers a balance between strong daytime differentials and extended evening output, while MSS-ESC prioritizes thermal stability and overnight heat retention.

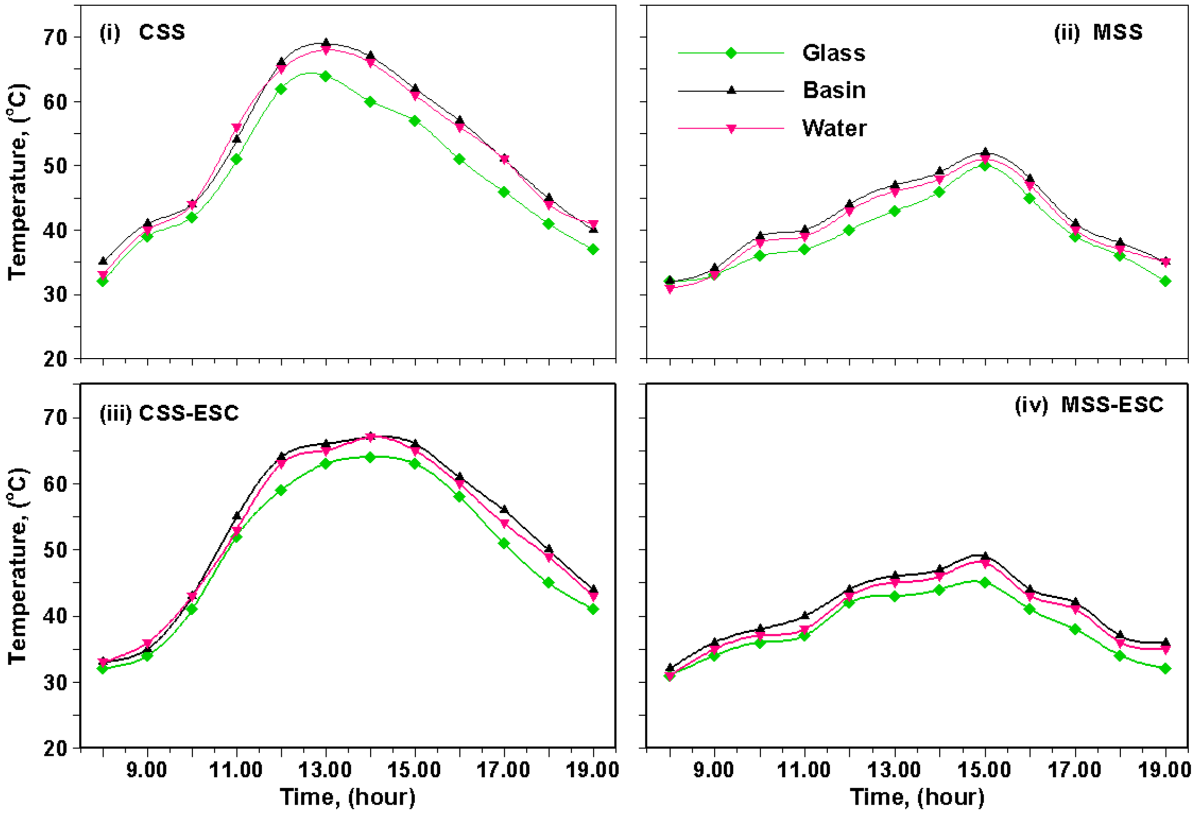


Figure 4. Hourly temperature variations throughout the day in solar stills for studied configuration.

## *Fresh water productivity*

The hourly variation in freshwater productivity as well as day, night and total productivity of all four cases studied is shown in Figure 5. The hourly production rate reveals the temporal dynamics of freshwater yield. For all configurations i.e. CSS, MSS, CSS-ESC, MSS-ESC, production peaks between 2:00 to 3:00 PM, indicating peak solar irradiance. The daytime productivities are 1.45 L, 1.43 L, 1.49 L and 1.41 L for CSS, MSS, CSS-ESC, and MSS-ESC, respectively. However, MSS-ESC exhibit a broader production curve. While CSS show a sharp decline after 4:00 PM, the MSS-ESC maintains a higher yield into the later hours (5:00 to 7:00 PM), indicating improved thermal storage brought by PCM and TESMs, which extends productivity after peak sunlight. This increased productivity in the evening has a direct impact on the overnight yields as shown in Figure 5. While all SS produce the majority of water during the day, MSS-ESC significantly outperforms others in night-time collection 0.73 L, with a 62% increase compared to CSS, which produced 0.08 L. Consequently, the MSS-ESC achieves the highest total cumulative productivity at 2.15 L/day, representing a 40.5% increase over the CSS and a 14.4% increase over MSS. The integration of TESMs and PCM proves highly effective. The synergistic effect of the MSS-ESC not only elevates peak daytime output but, more critically, sustains distillation through the night, offering the most significant enhancement in overall freshwater yield.

### ***Economic Assessment***

The CPL of freshwater and payback period are two main parameters taken into account in solar still's economic analysis, which is presented in Figure 6. For CSS, MSS, CSS-ESC, and MSS-ESC, the total cost to achieve water productivity is approximately Rs. 7920, 8970, 8470, and 9520, respectively. The freshwater productivity for CSS, MSS, CSS-ESC, MSS-ESC is 1.53, 1.88, 1.80 and 2.15 L/m2.day with the cost per litter of Rs 1.97, 1.82 1.80 and 1.69, respectively. The cost of fabrication for MSS rises by about 35% when TESMs and PCM were added. For MSS the productivity was 1.88 L/m2 and corresponding CPL was Rs 1.82. Form the figure 6 it can be seen that payback period for CSS the is 289 days which reduced by 25 days with TESMs for CSS-ESC. The payback period is reduced by 23 days from MSS to MSS-ESC.

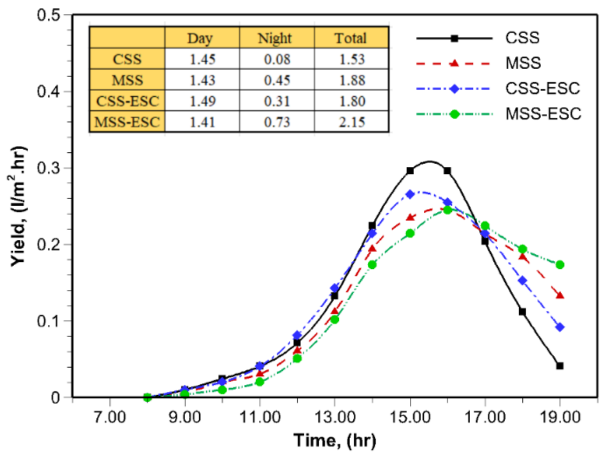


Figure 5. Hourly freshwater yield as well as day, night, and overall production for the cases under study.

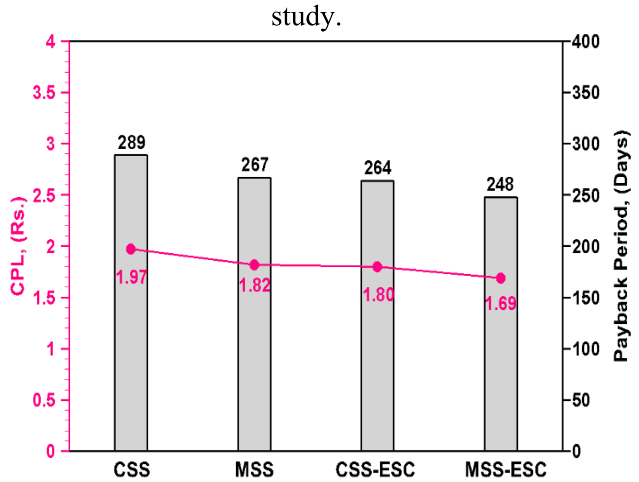


Figure 6. Variations of cost of water and payback period of studied configuration.

## Conclusion

The performance of solar stills (SSs) is evaluated in the current study using economic and productivity analyses. The following conclusions are drawn from the experimental results:

- The production of distilled water depends critically on the temperature of the glass and ambient temperature. Furthermore, TESMs have a major impact on solar still output.
- Integration of TESMs into CSS-ESC resulted in an increase of 17.02% in freshwater in contrast to CSS.
- The productivity enhancement in MSS-ESC was 40.5% compared to CSS, proving it to be a viable choice for the sustainable production of freshwater.

- The CPL and payback period decreased for CSS and CSS-ESC from Rs.1.97 to Rs. 1.80 and from 289 days to 264 days, respectively, through the use of TESMs.
- MSS-ESC was found to be the most cost-effective and sustainable method of producing freshwater, with a payback period of 248 days, the lowest CPL of Rs. 1.69, and a total cumulative productivity of 2.15 L/day.
- The freshwater generated by solar still is suitable for numerous domestic uses.

## References

[1] Sharma, N., & Mahala, T. (2026). Synergistic Enhancement of Solar Still Performance via Eco-Friendly Packed Bed Heat Storage and Natural Cloth Materials. Process Safety and Environmental Protection, 108624. https://doi.org/10.1016/j.psep.2026.108624

[2] Goel, V., Saxena, A., Kumar, M., Thakur, A., Sharma, A. and Bianco, V., 2022. Potential of phase change materials and their effective use in solar thermal applications: A critical review. Applied Thermal Engineering, Vol. 219, 119417. https://doi.org/10.1016/j.applthermaleng.2022.119417

[3] Ahmed, I. H., Al-Murshedi, T. F., Jawad, R. A. M., Hashim, A. K., & Ovuoraye, P. E. (2023). Experiment of treating polluted wastewater resulting from petroleum refineries using pyramid solar still distillation system to eliminate hydrocarbon toxicity. Desalination and Water Treatment, 313, 106-115. https://doi.org/10.5004/dwt.2023.30076

[4] Mahala, T., & Sharma, N. (2024). Experimental investigations of a novel solar still with heat storage materials-energy, exergy, economic and environmental analyses. Desalination, 578, 117467. https://doi.org/10.1016/j.desal.2024.117467

[5] Alshqirate, A., Awad, A. S., Al Alawin, A., & Essa, M. A. (2023). Experimental investigation of solar still productivity enhancement of distilled water by using natural fibers. Desalination, 553, 116487. https://doi.org/10.1016/j.desal.2023.116487

[6] Pandey, N. and Naresh, Y., 2024. Experimental study on the synergistic effects of phase change material, fins, and ultrasonic fogger in a pyramidal solar still. Journal of Energy Storage, Vol. 98, 112997. https://doi.org/10.1016/j.est.2024.112997

[7] Vembu, S., Attia, M.E.H., Thangamuthu, M. and Thangamuthu, G., 2023. Energy, exergy, and economic analysis of solar still using coal cylinder fins: an experimental study. Environmental Science and Pollution Research, Vol. 30, pp 2597–2606. https://doi.org/10.1007/s11356-022-22325-0

[8] Singh, D., Buddhi, D. and Karthick, A., 2023. Productivity enhancement of solar still through heat transfer enhancement techniques in latent heat storage system: a review, Environmental Science and Pollution Research, Vol. 30, pp 44–77. https://doi.org/10.1007/s11356-022-23964-z

[9] Attia, M.E.H., Abdelgaied, M. and Harby, K., 2024. New graphite fins efficacy on conical solar distiller performance: Experimental study with thermal, exergy, economic, and sustainability analysis. Journal of Water Process Engineering, Vol. 64, 105652. https://doi.org/10.1016/j.jwpe.2024.105652.

[10] Goshayeshi, H. R., & Safaei, M. R. (2020). Effect of absorber plate surface shape and glass cover inclination angle on the performance of a passive solar still. International Journal of Numerical Methods for Heat & Fluid Flow, 30(6), 3183-3198. https://doi.org/10.1108/HFF-01-2019-0018.

*ISBN 978-81-973526-0-7*

# EXPERIMENTAL INVESTIGATION OF DEHUMIDIFICATION PERFORMANCE OF SILICA GEL COATED CYLINDRICAL HEAT EXCHANGER (SGCHE)

Manjit Dhull[1], Sunil Nain[1], Parinam Anuradha*[1]
*[1]Mechanical Engineering Department, U.I.E.T., K.U.K. India
aparinam2015@kuk.ac.in

## Abstract

*This study examines the experimental performance of a desiccant-based dehumidifier using inlet temperature and cycle time as input parameters. Various key parameters such as enthalpy difference (ΔQ), adsorption ratio (AR), cabin supply temperature (TC-S), and dehumidification factor (dair) are used to evaluate the system performance. Experimental results show that increasing the inlet temperature increases the enthalpy difference and cabin supply temperature, while both parameters exhibit decreasing trend with respect to increase in the cycle time. The dehumidification factor increases with the inlet temperature and at a cycle time of 30 min, it achieved a maximum of approximately 12.85 g/kgdry-air. The adsorption ratio (AR) initially increases with cycle time reaches a peak (50%) and then gradually decreases to 23%, whereas with respect to inlet temperature, it increases continuously, however some fluctuations are also observed due to variation in saturation levels at different inlet temperature. Overall, it is concluded that better adsorption performance is achieved at moderate temperature and up to medium cycle time.*

## Keywords

Dehumidification Factor, Adsorption Ratio, Silica gel, Cabin Supply Temperature, Cylindrical Heat Exchanger, SGCHE.

## Introduction

Rapidly increasing global cooling demand and growing environmental concerns about conventional vapor compression refrigeration systems have shifted research focuses towards thermally driven and energy-efficient air-conditioning systems. Conventional cooling systems rely heavily on electricity and consume significant amount of electricity in hot and humid climates due to the high latent heat load required to remove moisture [1]. Desiccant-based air-conditioning systems offer a promising alternative by separating the latent and sensible processes and removing moisture directly from the air through adsorption, thereby improving thermodynamic efficiency and utilizing low-grade thermal energy for regeneration [2-3]. Solid desiccant materials are widely used in humidity control applications due to their high moisture absorption capacity, reversible sorption behaviour, and long operational life. Among various adsorbents, silica gel is one of the most widely used due to its large specific surface area, well-developed porous structure, strong moisture affinity, and good adsorption kinetics under moderate temperature and humidity conditions [4,5]. Conventional desiccant cooling systems typically use rotary desiccant wheels, in which a porous matrix filled with desiccant continuously rotates between adsorption and regeneration sectors [6]. Although rotary systems offer continuous operation and high moisture removal efficiency, they suffer from mechanical complexity, air leakage between sectors, sealing problems, and rotation-related sponging power consumption [7]. Furthermore, limitations in heat transfer within the desiccant matrix can reduce adsorption efficiency, especially at high humidity levels where rapid temperature increase reduces moisture absorption [8]. Desiccant-coated heat exchangers (DCHEs) have emerged as a promising solution to overcome the thermal resistance and structural limitations of conventional packed beds and rotary wheels. In a DCHE configuration, the desiccant layer is coated directly onto the heat exchanger surface, allowing for simultaneous heat removal and moisture absorption. This arrangement significantly improves the coupled heat and mass transfer processes by reducing thermal gradients within the dehumidifier and maintaining good adsorption conditions [9,10]. Previous studies have shown that silica gel-coated heat exchangers can achieve greater dehumidification performance due to better temperature control and improved interfacial transport [11]. Experimental investigations on fin-and-tube and plate-type heat exchangers have shown that adsorption capacity, dehumidification effectiveness, and overall system performance are strongly dependent on coating thickness, air velocity, inlet humidity ratio, and process air temperature [12–15]. Appropriate coating thickness is particularly important because higher coating thicknesses increase diffusion resistance, while lower coating thicknesses reduce absorption capacity [16]. Furthermore, transient heat and mass transfer behaviour within coating is highly nonlinear due to the strong coupling between absorption kinetics, thermal transport, and airflow characteristics [17]. Despite the growing scope of research on DCHE, most existing studies have focused on planar or fin-based geometries. Comparatively less attention has been given to cylindrical configurations, which offer several potential advantages. Therefore, the objective of this study is to experimentally investigate the performance characteristics of a silica gel-coated cylindrical heat exchanger (SGCHE). Various operating conditions such as cycle time and inlet air temperature are used to test the system performance under tropical climates of Kurukshetra, India. System performance is evaluated in terms of enthalpy difference ($\Delta Q$), adsorption ratio ($A_R$), cabin supply temperature ($T_{C\text{-}S}$), and dehumidification factor ($d_{air}$).

## Experimental System Description

The experimental setup consists of a silica gel coated cylindrical heat exchanger (SGCHE), and direct evaporative cooler, designed to simultaneously transfer heat and mass between humid air and a desiccant under controlled thermal conditions (figure 1). Specification details are provided in Table 1.

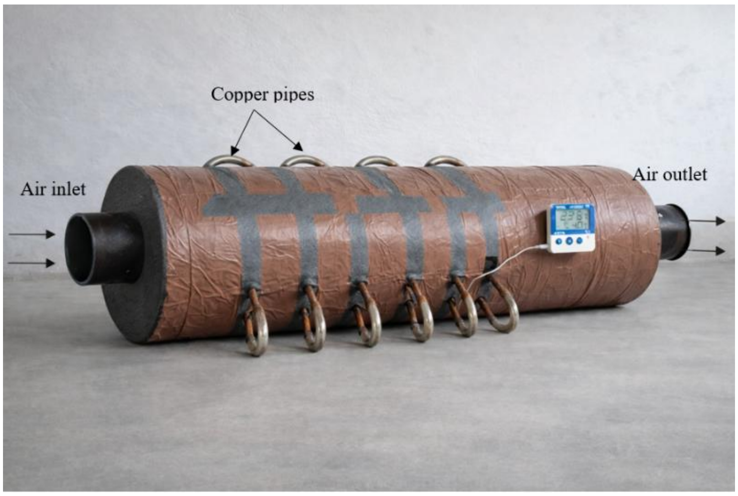


(a)


(b)

Figure 1: Experimental setup of SGCHE setup (a) dehumidifier and (b) evaporative cooler.

The setup consists of cylindrical shell containing rectangular plates coated with silica gel, and an array of copper pipes to take up the adsorption heat released during dehumidification process. Initially, humid ambient air passed to the dehumidifier through inlet section where its moisture is removed by a silica gel coating. Due to dehumidification process, adsorption heat is released which increases the temperature of process air. To address this problem, a cold-water cooler is installed which circulates cold-water through the copper pipes. As a result, dry and cold air exits the dehumidifier outlet. Silica gel is coated onto flat metallic plates using a heat-resistant glue to ensure strong bonding and minimal thermal resistance between the desiccant and the supporting structure. Further, thermal insulation is used on the outer surface of cylindrical casing to prevent heat exchange with the surrounding environment (figure 2).

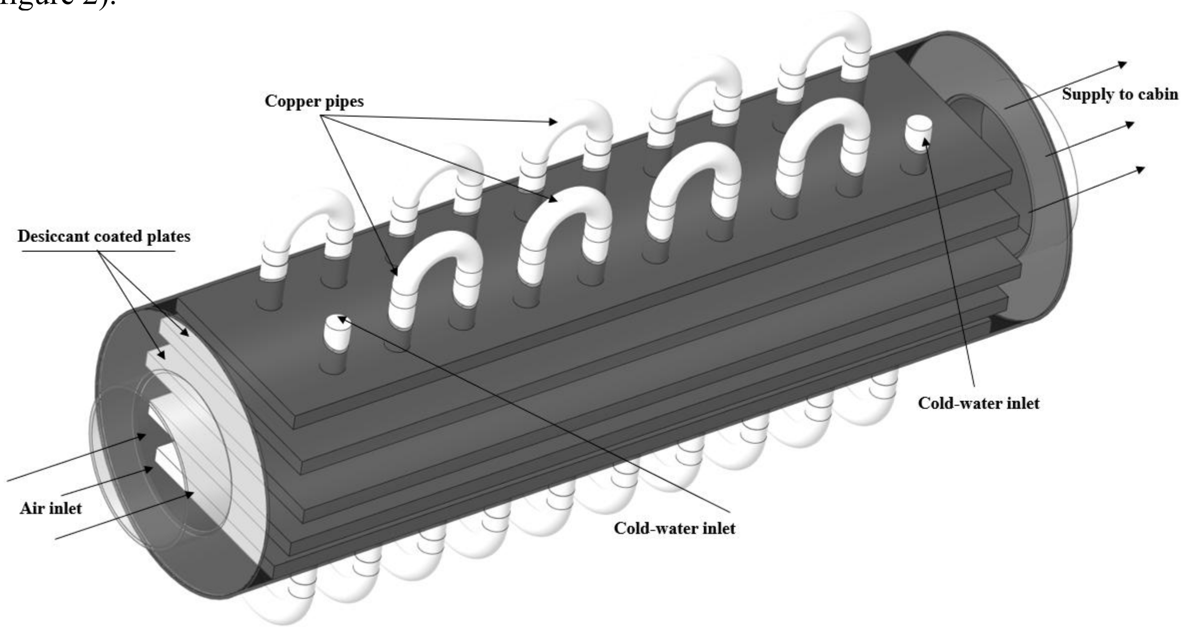


Figure 2: Schematic diagram of SGCHE dehumidifier.

Table 1: Detailed specification of SGCHE.

| S. No. | Components | Parameters | Dimension |
|---|---|---|---|
| 1. | Dehumidifier casing | Length×Diameter×thickness ($mm^3$) | 400×175×1 |
| 2. | Copper pipe | Length× Diameter ($mm^2$) | 200×9 |
| 3. | Plates | Length×Width×thickness ($mm^3$) | 320×150×1 |
| 4. | Silica gel | Quantity (kg) | 1.2 |
| | | Grain size (mm) | 4-6 |

## *Performance Parameters*

The performance of the SGCHE setup is evaluated using enthalpy difference (ΔQ), adsorption ratio ($A_R$), dehumidification factor ($d_{air}$), and cabin supply temperature ($T_{C\text{-}S}$). These parameters quantify thermal effectiveness and moisture removal capability under varying operating conditions.

## *Enthalpy Difference (ΔQ)*

The enthalpy difference represents the thermal energy change between inlet and outlet air. It is calculated as:

$$\Delta Q = m_{air}\,(h_{in} - h_{out}) \qquad \ldots 1$$

Where $m_{air}$ is the mass flow rate of air (kg/s), $h_{in}$ and $h_{out}$ are the specific enthalpies of process air at inlet and outlet (J/kg). A higher value of ΔQ indicates better thermal performance.

## *Dehumidification Factor ($d_{air}$)*

The dehumidification factor measures the decrease in the moisture content of process air.

$$d_{air} = W_{in} - W_{out} \qquad \ldots 2$$

Where $W_{in}$ and $W_{out}$ are the humidity ratio of inlet and outlet air (g/kg $_{dry\ air}$).

*ISBN 978-81-973526-0-7*

### *Adsorption Ratio ($A_R$)*

The adsorption ratio expresses the percentage moisture removal relative to saturation level. It is given by

$$A_R = d_{air} / W_{sat} \times 100\ (\%) \quad \ldots 3$$

Where $W_{sat}$ is the humidity at saturation level at a given temperature and pressure.

### *Cabin Supply Temperature ($T_{C-S}$)*

The cabin supply temperature is measured at the outlet of the system. It shows the combined effect of sensible and latent heat transfer.

## Validation study

This figure compares the dehumidification factor obtained in the present study with the experimentation results reported by Zhao et al., 2014 [18]. It can be seen that the dehumidification factor increases gradually similar operating conditions for both studies (inlet temperature). The trend of experimental results is very similar to the results reported by Zhao et al. 2014, demonstrating good agreement and validating the reliability of the experimental setup. However, small deviation between the two results may be due to the novel design of present SGCHE configuration. Overall, the comparison confirms that this study produces similar and reliable performance results.

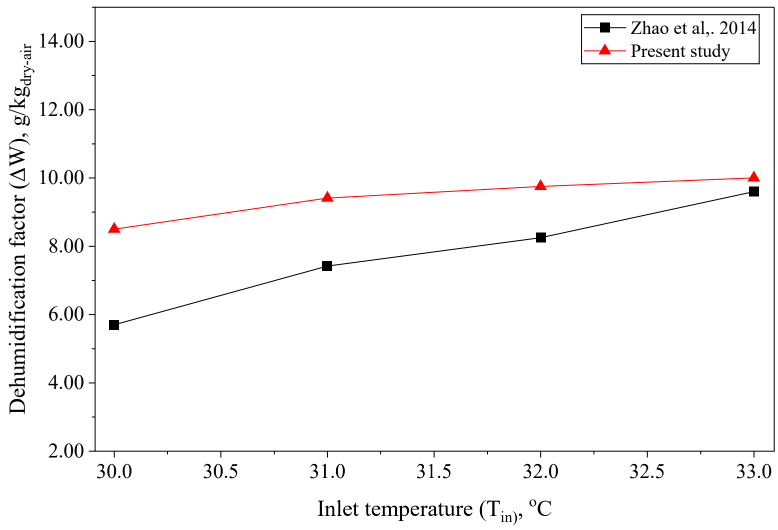


Figure 3: Comparison of dehumidification factor of present study and Zhao et al., 2014 [18].

## Results and discussion

In this study, an experimental investigation of a SGCHE is conducted to evaluate its coupled heat and mass transfer performance under tropical conditions. Multiple trials are conducted during different times of the day in order to examine the system performance under varying ambient temperature and humidity conditions and to ensure the reliability and consistency of the experimental results.

Figure 4; shows the effect of cycle time on the enthalpy difference (ΔQ) and adsorption ratio ($A_R$). It is observed that, as the cycle time increases, the enthalpy difference initially shows a slight decrease, followed by slight fluctuations and a gradual decrease with increasing cycle time, indicating a decrease in heat transfer capacity with longer operating periods. On the other hand, the adsorption ratio increases significantly at the beginning and achieved peak as the cycle time reaches 30 min, indicating better moisture absorption during the initial operating stages. Thereafter, the adsorption ratio gradually decreases and stabilizes around 34% over longer cycle durations. Overall, the results indicate that moderate cycle times provide better adsorption performance and decreases over longer cycle times. Initially, the

*ISBN 978-81-973526-0-7*

adsorption ratio is high because the desiccant has many active adsorption sites and strong pressure gradient, leading to rapid moisture uptake. As time passes, the desiccant gradually becomes saturated, reducing the available sites and reducing the adsorption rate.

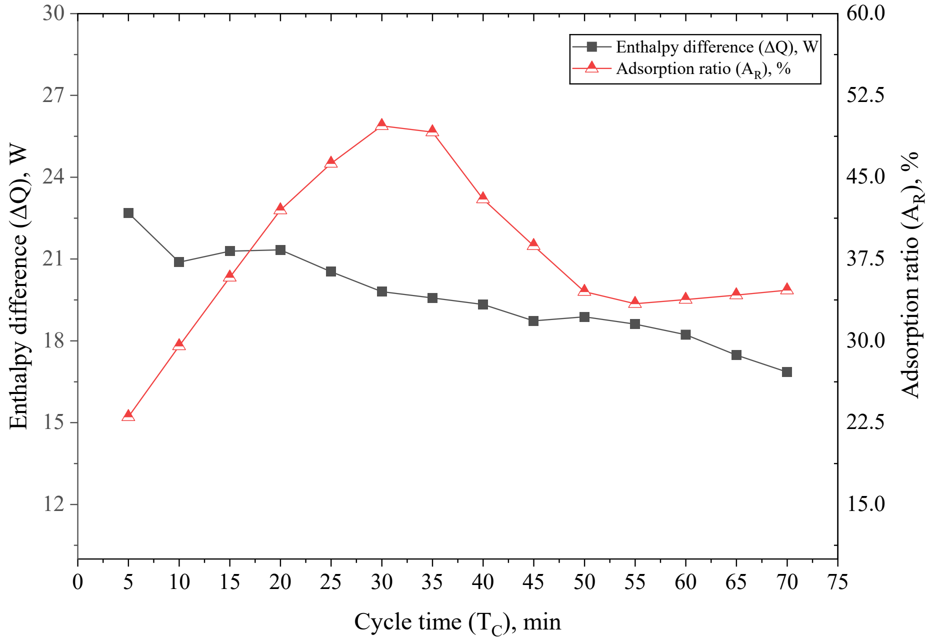


Figure 4: Effect of cycle time on the enthalpy difference and adsorption ratio.

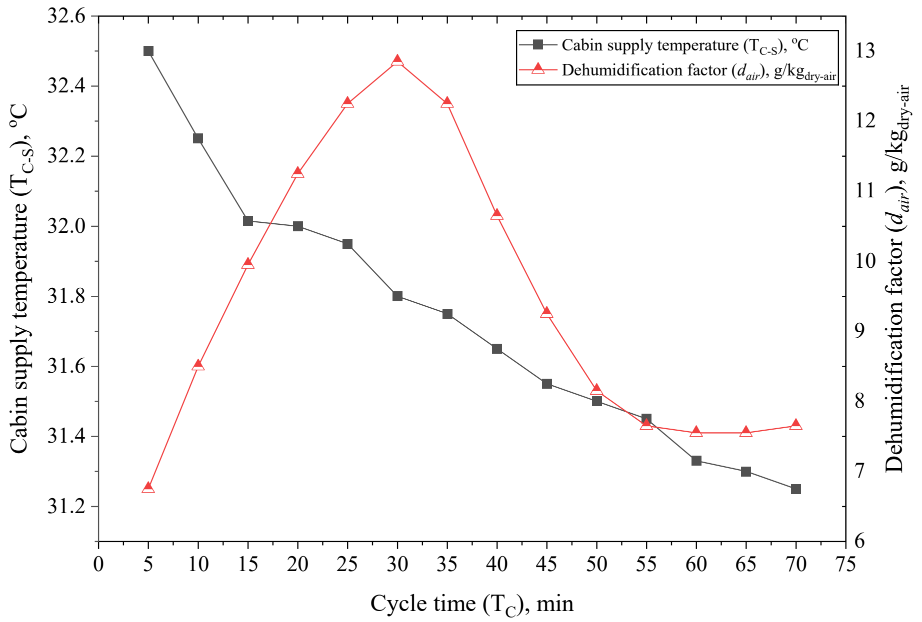


Figure 5: Effect of cycle time on the supply temperature and dehumidification factor.

Figure 5; shows the effect of cycle time on cabin supply temperature and the dehumidification factor. A marginal drop in cabin supply temperature is observed with increase in the cycle time. This can be attributed to the continuous supply of cold-water through the dehumidifier which take up the adsorption heat during dehumidification process. Thus, the cooled and dehumidified air leaves the dehumidifier. On the other hand, the dehumidification factor (g/$kg_{dry\text{-}air}$) initially increases with an increase in cycle time, reaches maximum (12.85 g/$kg_{dry\text{-}air}$) 30 min of cycle time and then decreases to a minimum of about 7.55 g/$kg_{dry\text{-}air}$ at 70 min of cycle time. This indicates that the capacity of desiccant material

*ISBN 978-81-973526-0-7*

to remove moisture from the humid air decreases as it approaches saturation conditions.
Figure 6; shows the effect of inlet air temperature on the enthalpy difference (ΔQ) and adsorption ratio ($A_R$). Experimental results indicate that both parameters increase with an increase in the inlet temperature. It is observed that as the temperature increases from 28 °C to 39.5 °C, the enthalpy difference gradually increases, from approximately 16.5 W at 28°C to 39.5 W at 39.5°C. This is due to the fact that higher inlet air temperatures increase the heat transfer rate within the system, resulting in a greater enthalpy change between the inlet and outlet air. Further, the adsorption ratio increases with temperature, although it fluctuates slightly. The adsorption ratio increases from 40% at 28°C to a maximum value of about 66% at 36°C. This behaviour indicates that the adsorption ratio improves with increasing inlet air temperature due to the greater humidity gradient between the inlet and outlet air. However, it decreases to about 60% as the inlet temperature increases to 39.5ºC, this can be attributed to the variation in saturation moisture level with increasing inlet air temperature and cold-water temperature.
Figure 7; shows the effect of increasing inlet air temperature on the cabin supply temperature and dehumidification factor. It is observed that the cabin supply temperature increases with increases in the inlet temperature. The heated inlet air exhibits more sensible heat than latent heat, resulting in a higher outlet air temperature after passing through the dehumidifier. However, concurrently, the temperature drop between the inlet and cabin supply temperature increases from 4.2 % to 9.4 %, indicating improved thermal performance. A similar increasing trend is observed for the dehumidification factor. The dehumidification factor increases from approximately 6.5 g/kg$_{dry\text{-}air}$ at 28°C to about 12.85 g/kg$_{dry\text{-}air}$ at 39.5 °C. The higher temperature increases the vapour pressure of the humid air which creates greater pressure difference around the desiccant surface, resulting in improved moisture transfer. However, at the higher inlet temperatures, the rate of moisture removal slows down, this indicate that due to thermal limitations the effectiveness of adsorption is diminishing. This is because the regeneration process is more effective at higher temperatures.

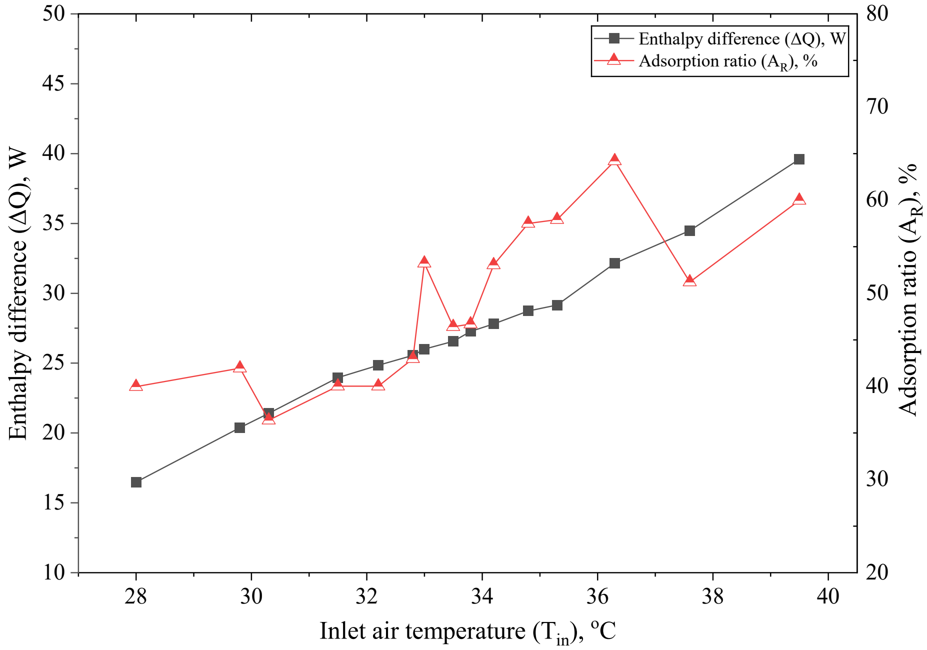


Figure 6: Effect of inlet temperature on the enthalpy difference and adsorption ratio.

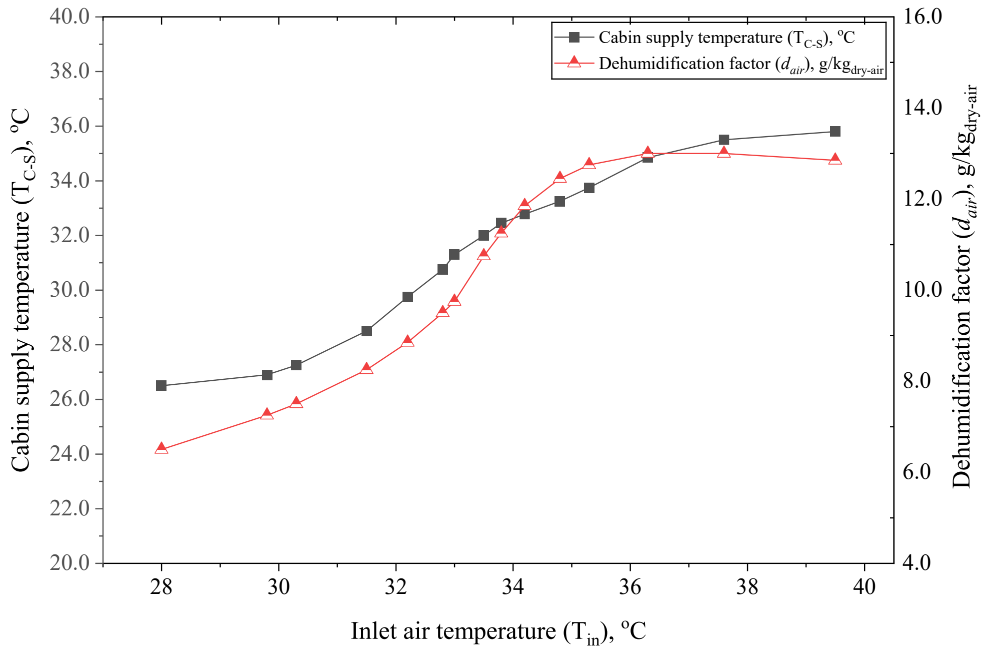


Figure 7: Effect of inlet temperature on the cabin supply temperature and dehumidification factor.

## Conclusions

In this study, an experimental investigation of SGCHE is conducted under tropical climate conditions of Kurukshetra, India. The major findings are as follows: The variation of adsorption ratio and dehumidification factor with cycle time follows a similar pattern, where both parameters increase initially, attain a peak value, and subsequently decline, reaching their minimum at approximately 70 minutes. In contrast, the enthalpy difference and cabin supply temperature exhibit a continuous decreasing trend as the cycle time increases. Furthermore, all performance parameters demonstrate an increasing tendency with respect to inlet air temperature.

The experimental observations provide a better understanding of system behaviour under real climatic conditions. These findings may help in improving the design and operation of similar dehumidification systems.

## References

[1] A. A. Pesaran, Desiccant Cooling: State-of-the-Art Assessment, National Renewable Energy Laboratory (NREL), Golden, CO, USA, Report NREL/TP-254-4147, 1992.

[2] W. M. Worek and C. G. Moon, "Performance of rotary desiccant cooling systems," Journal of Solar Energy Engineering, vol. 108, no. 2, pp. 111–119, 1986. https://doi.org/10.1115/1.3268107

[3] K. Daou, R. Z. Wang, and Z. Z. Xia, "Desiccant cooling air conditioning: A review," Renewable and Sustainable Energy Reviews, vol. 10, no. 2, pp. 55–77, 2006. https://doi.org/ 10.1016/j.rser.2004.09.010

[4] D. M. Ruthven, Principles of Adsorption and Adsorption Processes, New York, NY, USA: Wiley, 1984.

[5] S. J. Gregg and K. S. W. Sing, Adsorption, Surface Area and Porosity, 2nd ed., London, UK: Academic Press, 1982.

[6] T.S. Ge, Y. Li, R.Z. Wang 1, Y.J. Dai, "Experimental study on a two-stage rotary desiccant cooling system," International Journal of Refrigeration, vol. 32, no. 1, pp. 498-208, 2009. https://doi.org/10.1016/j.ijrefrig.2008.07.001.

[7] L. Z. Zhang, "Heat and mass transfer in a desiccant wheel," HVAC&R Research, vol.

13, no. 2, pp. 239–253, 2007. https://doi.org/10.1080/10789669.2007.10390962

[8] T. S. Ge, Y. Li, R. Z. Wang, and Y. J. Dai, "A review of the mathematical models for predicting rotary desiccant wheel performance," Renewable and Sustainable Energy Reviews, vol. 14, no. 7, pp. 1993–2000, 2010. https://doi.org/10.1016/j.rser.2010.03.009

[9] X. J. Zhang, Y. J. Dai, and R. Z. Wang, "Experimental investigation of a silica gel coated fin-tube heat exchanger," Energy Conversion and Management, vol. 46, no. 7–8, pp. 1205–1217, 2005. https://doi.org/10.1016/j.enconman.2004.06.004

[10] X. Zheng and W. M. Worek, "Numerical simulation of combined heat and mass transfer processes in a desiccant coated heat exchanger," Journal of Heat Transfer, vol. 115, no. 1, pp. 60–67, 1993. https://doi.org/10.1115/1.2910664

[11] X. H. Liu and Y. Jiang, "Performance analysis of a desiccant coated heat exchanger system," Energy and Buildings, vol. 40, no. 9, pp. 1748–1755, 2008. https://doi.org/10.1016/j.enbuild.2008.03.002

[12] L. Z. Zhang, "Design and performance of the silica gel coated fin-tube heat exchanger," International Journal of Refrigeration, vol. 31, no. 3, pp. 502–513, 2008. https://doi.org/10.1016/j.ijrefrig.2007.10.001

[13] T. S. Ge, R. Z. Wang, and Y. J. Dai, "Experimental study on silica gel coated heat exchanger for adsorption dehumidification," Applied Thermal Engineering, vol. 31, no. 17–18, pp. 3533–3541, 2011. https://doi.org/10.1016/j.applthermaleng.2011.06.015

[14] C. X. Jia and Y. J. Dai, "Experimental investigation on silica gel coated heat exchanger for adsorption cooling," Energy, vol. 32, no. 10, pp. 1932–1941, 2007. https://doi.org/10.1016/j.energy.2007.03.002

[15] S. Nain, S. Kajal, A. Parinam, Thermal performance of desiccant-based solar air-conditioning system with silica gel coating, Environ. Dev. Sustain. vol. 21, pp. 2481–2496, 2019. https://doi.org/10.1007/s10668-018-0201-4.

[16] X. D. Wang, X. H. Liu, and Y. Jiang, "Influence of coating thickness on performance of desiccant coated heat exchangers," Applied Energy, vol. 97, pp. 475–482, 2012. https://doi.org/10.1016/j.apenergy.2012.02.012

[17] T. H. Kuehn and J. W. Ramsey, "Transient heat and mass transfer in porous media," Journal of Heat Transfer, vol. 99, no. 2, pp. 196–201, 1977.

[18] Y. Zhao, T.S. Ge, Y.J. Dai, R.Z. Wang, Experimental investigation on a desiccant dehumidification unit using fin-tube heat exchanger with silica gel coating, Applied Thermal Engineering, Vol. 63, I. 1, 2014, pp. 52-58. https://doi.org/10.1016/j.applthermaleng.2013.10.018.

# CFD-BASED COMPARATIVE STUDY OF SINGLE-AXIS AND DUAL-AXIS PARABOLIC TROUGH SOLAR COLLECTORS

Manjit Dhull[1], Sunil Nain[1], Parinam Anuradha*[1]
*[1]Mechanical Engineering Department, U.I.E.T., K.U.K. India
aparinam2015@kuk.ac.in

## Abstract
*This study investigates the computational fluid dynamics (CFD) performance of single and double axis solar parabolic trough collector (PTC) setups under different inlet temperatures and velocities. The analysis emphases on the temperature difference (ΔT), entropy generation (s), and coefficient of performance (COP). Results show that with increase in inlet velocity, COP and the entropy generation of the system increases while temperature difference shows opposite trend. The COP of the system reaches a maximum value of approximately 0.37 at 9.5 m/s in case of double axis configuration. On the other hand, the temperature difference achieved a maximum value of about 102.5 K at 1.5 m/s, for double axis configuration. Further, the temperature difference in the absorber tube decreases with increasing inlet temperature for both configurations. At 300 K inlet temperature, the temperature difference is about 110 K for the double-axis and 102 K for the single-axis system, gradually decreasing to approximately 57.8 K and 54.8 K, respectively, at 360 K. Conversely, the entropy generation of the working fluid increases with inlet temperature, from 568 and 590 J/kg K at 300 K to approximately 770 and 870 J/kg K at 360 K for the single and double-axis systems. Overall, the double-axis configuration consistently shows higher thermal gain and higher entropy generation than the single-axis system due to improved solar energy capture.*

## Keywords
CFD, Solar PTC, Single Axis, Double Axis, Entropy Generation.

## Introduction
The growing global demand for clean and sustainable energy has increased research into advanced solar thermal technologies which are capable of delivering high thermal heat for power generation and industrial applications. Among renewable technologies, Concentrated Solar Power (CSP) systems play a central role because they can convert direct solar radiation into thermal energy which are suitable for electricity production through thermodynamic cycles [1-2]. Within CSP configurations, the parabolic trough collector (PTC) has achieved significant commercial placement due to its technological advancement, operational reliability, and compatibility with thermal energy storage systems [3-4]. A typical PTC employs a parabolic shape curved reflective surface that concentrates direct solar radiation onto a linear receiver tube which is positioned at the focal line, where a heat transfer fluid absorbs the heat and transports the collected energy [5].
The performance of a solar PTC system strongly depends on the optical arrangement between the collector aperture and the incident solar radiation. Because the Sun's apparent position continuously changes throughout the day and across seasons, solar tracking mechanisms are important to maximize incident radiation on the receiver [6-7]. Tracking systems are commonly classified into single-axis and double-axis configurations, each has its own distinct advantages and engineering limitations [8]. Single-axis tracking systems rotate the reflector about one main axis aligned (north–south or east–west) to capture the daily solar trajectory [9-10]. These systems are widely used in commercial installations because they offer a

favourable trade-off between energy gain and mechanical simplicity [11]. Their relatively lower cost, structural strength, and reduced maintenance requirements make them attractive for large-scale CSP plants [12]. However, single-axis trackers cannot fully payoff for seasonal variations in solar altitude, which results in residual incidence angle losses during certain periods of the year [13].

In contrast, double-axis tracking systems provide rotational choice in both azimuth and elevation directions, allowing the collector to maintain near-normal orientation to the sun at all times [14-15]. From an optical point of view, this configuration reduces cosine losses and increases concentrated flux on the heat absorbing surface [16]. Analytical and experimental investigations have stated that dual-axis tracking can significantly improve photosensitive efficiency and annual energy yield compared to single-axis configurations [17-18]. Nevertheless, the mechanical complexity of dual-axis systems results in higher installation costs, control requirements, and greater susceptibility to misalignment and wear [19].

Despite the extensive research on solar PTC and solar tracking configurations, few investigations have systematically studied the effects of inlet temperature and velocity on thermal performance parameters such as temperature difference, entropy generation, and coefficient of performance in PTC systems. Therefore, the present research aims to conduct a detailed comparative study of single and double-axis parabolic trough collectors. The study evaluates COP, entropy generation (s), and temperature difference (ΔT) to determine the most suitable tracking approach for various climatic and operational scenarios.

## Model description

A 3-dimentional CADD module (Space-claim) is used to modelled the single and double axis solar PTC. It comprises concentric tubes: glass outer tube, an absorber tube. The vacuum space between outer glass and absorber tube decreases the thermal and radiation heat losses to the outside. Figures: 1 represent the outer domain and absorber tube meshing.

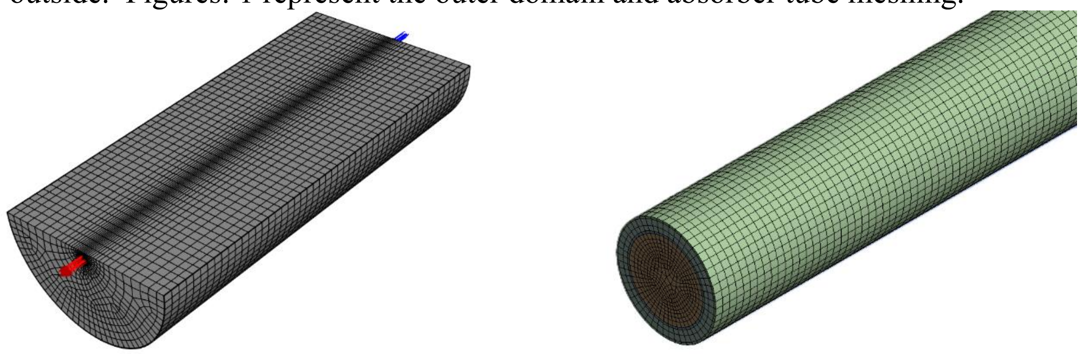

(a) (b)

Figure 1: Meshing of (a) fluid domain, (b) absorber tube.

The meshing process is performed to discretize the fluid and solid domains, three governing equations (continuity, momentum, and energy) are applied on each discretize sites to obtain accurate and real-time results. In the given figure 1 (a & b), the semi-cylindrical computational domain with its surrounding control volume and absorber tube is shown with a structured hexahedral mesh. The mesh is refined near the absorber wall and fluid interface to accurately capture the steep temperature and velocity gradients, while the outer region is shown with larger sized elements to reduce computational cost. Simple velocity-inlet and pressure-outlet boundary conditions at fluid inlet and outlet sections are used. It was ensured that further mesh refinement did not lead to any accuracy.

# Governing Equations

## *Continuity equation*

$$\frac{\partial \rho}{\partial t} + \frac{\partial}{\partial x}(\rho V_x) + \frac{\partial}{\partial x}(\rho V_y) + \frac{\partial}{\partial x}(\rho V_z) = 0 \quad \ldots(1)$$

## *Momentum equation*

$$\frac{\partial(\rho V_x)}{\partial t} + \frac{\partial\left(\rho \overline{V_x V_y}\right)}{\partial x_j} = -\frac{\partial \overline{P}}{\partial x_i} + \frac{\partial}{\partial x_j}\left[\mu_{eff}\left(\frac{\partial \overline{V_x}}{\partial x_j} + \frac{\partial \overline{V_y}}{\partial x_i}\right) - \frac{2}{3}\mu_{eff}\frac{\partial \overline{V_x}}{\partial x_i}\xi_{ij} - \rho V_x' V_y'\right] \quad \ldots(2)$$

## *Energy equation*

$$\frac{\partial}{\partial x_j}(\rho u_j T) = \frac{\partial}{\partial x_j}\left[\left(\frac{\mu}{P_r} + \frac{\mu}{\sigma_t}\right)\frac{\partial T}{\partial x_j}\right] \quad \ldots(3)$$

# Result and discussion

In this research, simulation analysis of single and double axis solar PTC model is conducted using Ansys-19.3 software. The impact of inlet parameters (inlet air velocity, temperature) is analyzed to assess the thermal performance in terms of various indices such as temperature drop (ΔT), entropy generation and COP.

Figure 2; shows the variation in the coefficient of performance (COP) for both single-axis and double-axis tracking configurations as the inlet velocity increases. It is observed that the COP increases with increasing inlet velocity in both cases, although the rate of increase slows down at higher velocities. At the lowest inlet velocity of 1.5 m/s, the COP for both configurations is approximately 0.21.

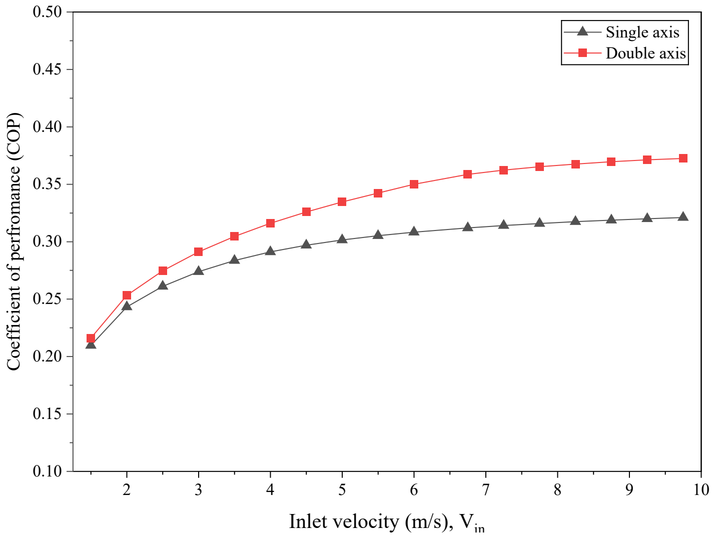


Figure 2: Effect of inlet velocity on COP of single and double axis solar PTC

Further increases in velocity to 9.5 m/s, the COP of the system increases to approximately 0.32 and 0.37 for single and double axis model, respectively. Results indicates that the double-axis tracking system consistently perform better than the single-axis configuration.

Figure 3; shows the variation in the temperature difference of the working fluid between the inlet and outlet of an absorber tube as the inlet velocity increases. The temperature difference represents the thermal gain by the working fluid as it flows through the absorber tube. It can be seen that the temperature difference decreases significantly with increasing inlet velocity for both configurations. As inlet velocity increases, ΔT decreases for both setups because higher mass flow reduces residence time, limiting energy absorption. At the lowest inlet velocity (1.5 m/s), the temperature difference is approximately 96 K for the single-axis and 101 K for the double-axis configuration. With a further increase in velocity to 9.5 m/s, the temperature difference drops to approximately 15 K for the single-axis configuration and approximately 28 K for the double-axis configuration.

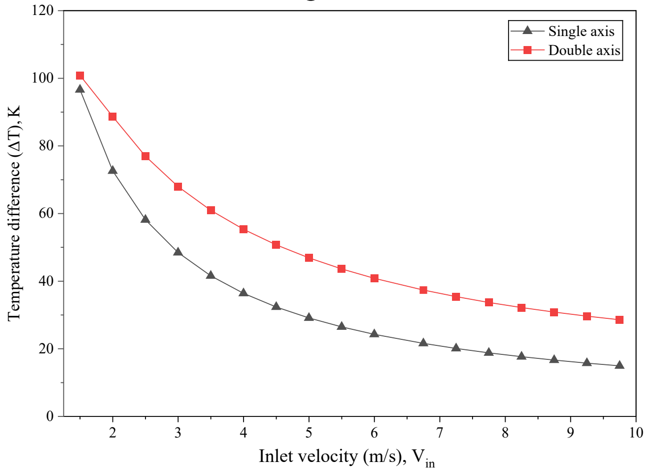


Figure 3: Effect of inlet velocity on temperature difference of single and double axis solar PTC

Figure 4; shows the variation in the entropy generation of the working fluid in a parabolic trough collector (PTC) system as the inlet fluid velocity increases.

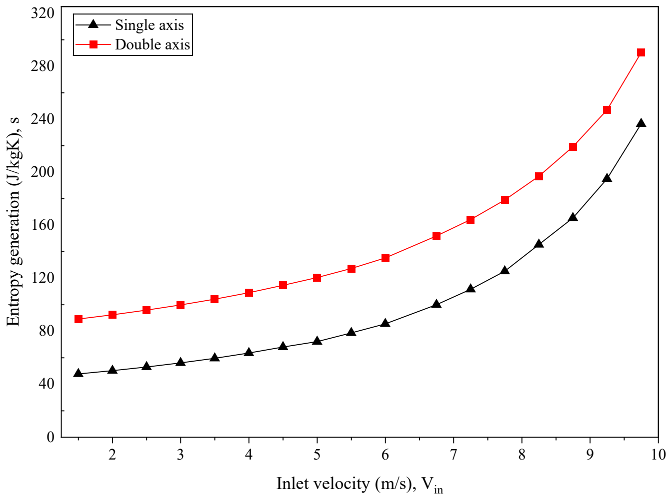


Figure 4: Effect of inlet velocity on entropy generation of single and double axis solar PTC

The entropy generation is defined as the degree of thermodynamic irreversibility of the process occurring in the absorber tube. It can be seen that the entropy generation increase steadily with increasing inlet velocity. At the lowest inlet velocity of 1.5 m/s, the entropy generation is 47.5 J/kgK and 89 J/kgK for single and double axis respectively. As the velocity increases to 9.5 m/s, the entropy generation gradually increases to approximately 236.4 J/kgK for single axis and to 290.3 J/kgK for double axis system. Result indicates that higher inlet velocities create more entropy generation due to increased irreversibility and frictional losses inside the absorber tube of the PTC.

Figure 5; shows the change in the coefficient of performance (COP) for both single and double-axis configurations as the inlet temperature increases. COP represents the ratio of useful thermal energy recovered from the working fluid to the input energy supplied to the system. It can be seen that COP gradually decreases as the inlet fluid temperature increases. At the lowest inlet temperature of 300 K, the COP is approximately 0.625 for single axis and 0.735 for double axis system. As the inlet temperature increases to 360 K, the COP decreases to approximately 0.38 and 0.47 for single and double axis configurations, respectively, indicating a gradual decline in system performance. This decreasing trend indicates that higher inlet temperatures reduce the effective heat gain of the working fluid, thereby reducing the overall thermodynamic performance of the PTC system.

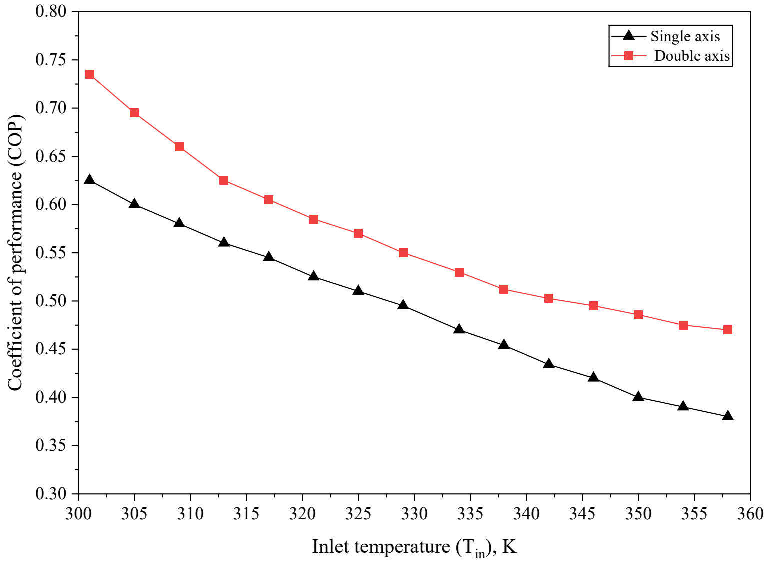


Figure 5: Effect of inlet temperature on COP of single and double axis solar PTC

Figure 6; shows the change in the temperature difference (ΔT) between the outlet and inlet of the absorber tube as the inlet temperature increases from 300 K to 360 K.

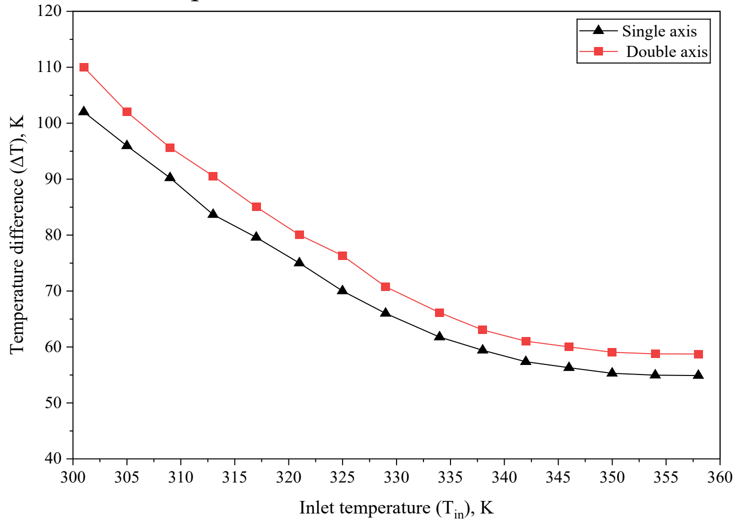


Figure 6: Effect of inlet temperature on temperature difference of single and double axis solar PTC

At an inlet temperature of 300 K, the temperature difference is approximately 110 K for the double-axis tracking system and 102 K for the single-axis system, indicating a greater thermal gain with dual-axis tracking. As the inlet temperature increases, the temperature difference gradually decreases for both configurations. For instance, at 320 K, ΔT decreases to approximately 80 K for the double-axis system and 75 K for the single-axis system. Further, as the inlet temperature increases to 360 K, ΔT stabilizes at 58.7 K for the double-axis configuration and approximately 54.8 K for the single-axis system. Figure 7; shows the variation in the entropy generation (s) of the working fluid between the inlet and outlet of the absorber tube as the inlet fluid temperature increases from 300 K to 360 K. With increase in inlet temperature, the entropy generation shows an increasing trend for both tracking modes.

At an inlet temperature of 300 K, the entropy generation is approximately 568 J/kgK for the single-axis tracking system and slightly higher, 580 J/kgK for the double-axis tracking system. As the inlet temperature increases to 360 K, the entropy generation increases to approximately 770 J/kg K for single-axis tracking and 870 J/kg K for double-axis tracking. The double-axis tracking configuration consistently shows higher entropy generation variation, this can be attributed to the rotational movement of the double axis system during tracking process, indicating better solar energy absorption and greater thermodynamic irreversibility within the collector system.

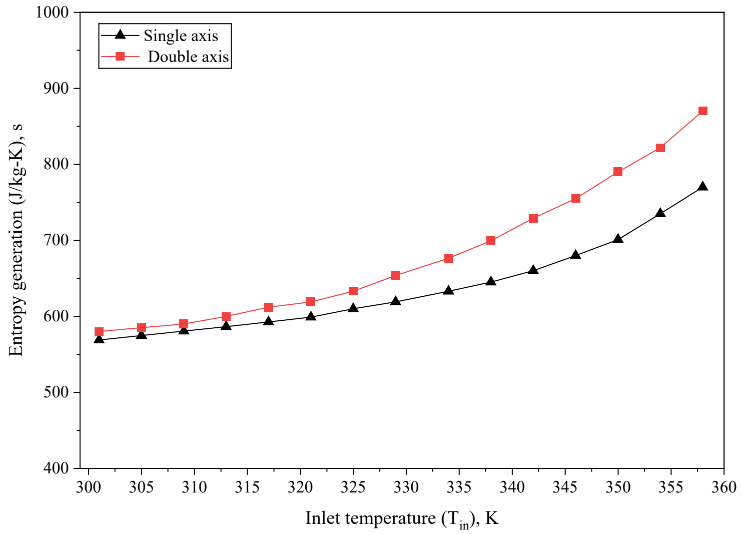


Figure 7: Effect of inlet temperature on entropy generation of single and double axis solar PTC

## Conclusions

The present study evaluates the thermal performance of a single and double axis tracking setups of solar PTC system under varying inlet temperatures and velocities. The findings may be summarised as:

- With increase in inlet velocity, it is observed that COP and entropy generation of the system increases while temperature difference shows opposite trend. The COP of the system reaches a maximum value of approximately 0.37 at 9.5 m/s in case of double axis configuration. On the other hand, the temperature difference achieved a minimum value of about 15 at 9.5 m/s, for single axis tracking system.
- It can be seen that the entropy generation increase steadily with increasing inlet velocity from 47.5 J/kgK at 1.5 m/s to 236.4 J/kgK and from 89 J/kgK to 290.3 J/kgK at 9.5 m/s for single and double axis configurations, respectively.
- With increase in inlet temperature from 300K to 360 K, it is observed that the COP decreases from 0.625 to 0.38 and from 0.735 to 0.47 for single and double axis configurations, respectively.
- The temperature difference between the inlet and outlet of the absorber tube decreases steadily with increasing inlet fluid temperature. At 300 K, the temperature difference is about 110 K for the double-axis system and 102 K for the single-axis system, which gradually reduces to nearly 58.7 K and 54.8 K, respectively, at 360 K.
- The entropy generation of the working fluid increases with increasing inlet temperature, rising from approximately 567-590 kJ/kgK at 300 K to around 770-870 kJ/kgK at 360 K.
- Overall, the double-axis configuration consistently performs better thermal

performance than the single-axis configuration due to its improved ability to capture solar radiation throughout the day.

# Nomenclature

| **Abbreviation** | **Description** |
|---|---|
| COP | Coefficient of Performance |
| CFD | Computational Fluid Dynamics |
| CSP | Concentrated Solar Power |
| PTC | Parabolic Trough Collector |
| CFD | Computational Fluid Dynamics |
| $c_p$ | Specific heat capacity of heat transfer fluid (J /kg K). |
| h | Convective heat transfer coefficient (W /m² K). |
| k | Thermal conductivity of fluid (W /m K). |
| L | Length of parabolic trough collector (m). |
| ṁ | Mass flow rate of heat transfer fluid (Kg/s). |
| p | Pressure (Pa). |
| t | Time (s). |
| ΔT | Temperature difference (K). |
| $T_{in}$ | Inlet fluid temperature (K). |
| $T_{out}$ | Outlet fluid temperature (K). |
| $V_{in}$ | Inlet velocity (m/s). |
| s | Entropy generation (J/kgK). |
| u, v, w | Velocity components in x, y, z directions (m/s). |
| ρ | Density of fluid (Kg/m³). |
| μ | Dynamic viscosity (Ns/m$^2$). |
| $y_m$ | Dilatation energy (m$^2$/s$^2$). |
| $g_k$, $g_b$ | Turbulent kinetic energy generation for fluctuation and buoyancy (m$^2$/s$^2$). |
| $Pr_k$, $Pr_\epsilon$ | Turbulent Prandtl number for k and ε respectively. |
| $Pr$ | Prandtl number. |
| V | Velocity (m/s). |
| p | Pressure (Pa). |
| $S_m$ | Source term. |
| k–ε | Turbulence model (Turbulent kinetic energy–Dissipation model) |

# References

[1] A. Fernández-García, E. Zarza, L. Valenzuela, M. Pérez, Parabolic-trough solar collectors and their applications, Renewable and Sustainable Energy Reviews, 14 (2010) 1695–1721. https://doi.org/10.1016/j.rser.2010.03.012

[2] V.K. Jebasingh, G.M. Joselin Herbert, A review of solar parabolic trough collector, Renewable and Sustainable Energy Reviews, 54 (2016) 1085–1091. https://doi.org/10.1016/j.rser.2015.10.043

[3] M. Kalogirou, Solar thermal collectors and applications, Progress in Energy and Combustion Science, 30 (2004) 231–295. https://doi.org/10.1016/j.pecs.2004.02.001

[4] M. Kalogirou, A detailed thermal model of a parabolic trough collector receiver, Energy, 48 (2012) 298–306. https://doi.org/10.1016/j.energy.2012.06.023

[5] R. Forristall, Heat transfer analysis and modelling of a parabolic trough solar receiver implemented in Engineering Equation Solver, National Renewable Energy Laboratory (NREL), NREL/TP-550-34169, 2003. https://doi.org/10.2172/15004820

[6] S.A. Kalogirou, Solar energy engineering: Processes and systems, Academic Press,

2014. https://doi.org/10.1016/C2010-0-66367-7

[7] J.A. Duffie, W.A. Beckman, Solar Engineering of Thermal Processes, 4th ed., Wiley, 2013. https://doi.org/10.1002/9781118671603

[8] M.J. Ya'u, A review on solar tracking systems and their classifications, Journal of Energy and Environmental Chemical Engineering, 2(3) (2017) 46–50. https://doi.org/10.11648/j.jeece.20170203.12

[9] T. Tomson, Discrete two-positional tracking of solar collectors, Renewable Energy, 33 (2008) 400–405. https://doi.org/10.1016/j.renene.2007.03.009

[10] A. Grena, An algorithm for the computation of the solar position, Solar Energy, 82 (2008) 462–470. https://doi.org/10.1016/j.solener.2007.10.008

[11] S. Abdallah, S. Nijmeh, Two-axis sun tracking system with PLC control, Energy Conversion and Management, 45 (2004) 1931–1939. https://doi.org/10.1016/j.enconman.2003.10.007

[12] H. Mousazadeh et al., A review of principle and sun-tracking methods for maximizing solar systems output, Renewable and Sustainable Energy Reviews, 13 (2009) 1800–1818. https://doi.org/10.1016/j.rser.2009.01.022

[13] W.T. Xie, Y.J. Dai, R.Z. Wang, Numerical and experimental analysis of a point focus solar collector, Applied Energy, 87 (2010) 1987–1996. https://doi.org/10.1016/j.apenergy.2009.11.005

[14] F. Ullah, K. Min, Performance evaluation of dual-axis tracking system of parabolic trough solar collector, IOP Conference Series: Materials Science and Engineering, 301 (2018) 012166. https://doi.org/10.1088/1757-899X/301/1/012166

[15] L. Valančius, E. Jurelionis, Optical performance analysis of parabolic trough collectors with different tracking systems, Solar Energy, 86 (2012) 365–373. https://doi.org/10.1016/j.solener.2011.10.013

[16] D. Kearney, R. Price, Solar thermal power plants, Energy Policy, 30 (2002) 727–736. https://doi.org/10.1016/S0301-4215(02)00018-1

[17] P. Heller et al., Optical performance of parabolic trough collectors, Journal of Solar Energy Engineering, 128 (2006) 1–8. https://doi.org/10.1115/1.2168051

[18] A. Montes, R. Abbas, Performance comparison of single-axis and dual-axis solar tracking systems, Applied Energy, 87 (2010) 285–292. https://doi.org/10.1016/j.apenergy.2009.07.007

[19] M. Blanco, A. Santigosa, Advances in concentrated solar thermal research and technology, Woodhead Publishing, 2017. https://doi.org/10.1016/B978-0-08-100516-3.00001-6.

# ADSORPTIVE REMOVAL OF CADMIUM FROM AQUEOUS SOLUTIONS USING GROUNDNUT SHELL-BASED ADSORBENT: LANGMUIR AND FREUNDLICH MODELLING

Bindu*[1], Rani Devi[1], Manjit Dhull[2]
*[1]Department of Energy and Environmental Sciences, CDLU, Sirsa
[2]UIET Kurukshetra University Kurukshetra
* bindumajit666@gmail.com

## Abstract

*The continued discharge of untreated industrial and domestic wastewater has significantly increased the presence of heavy metals in the marine environment, imposing a serious threat to ecosystems and public health. Among these contaminants, cadmium is particularly dangerous because it persists in water, tends to bioaccumulate, and has high mobility. This study explores the potential of using peanut shell adsorbents as a cost-effective and environmentally sustainable material for removing cadmium from water solutions. Batch adsorption experiments are conducted to determine the effect of specific operational parameters, such as solution pH and contact time. The results showed that solution pH significantly impacted adsorption efficiency, with pH 5 showing the highest removal efficiency (28.75%) and uptake capacity (40.86 mg/g). Increasing the contact time improved cadmium removal, with equilibrium achieved within approximately 60 minutes. Overall, the study confirms that peanut shells are a cost-effective and eco-friendly adsorbent for cadmium removal, showing strong potential for use in wastewater treatment processes.*

## Keywords

Uptake capacity, Removal efficiency, pH, Contact time, Batch adsorption.

## Introduction

Due to rapidly growing populations and increasing industrial activities, untreated wastewater has significantly discharged into natural water bodies, causing serious environmental pollution. Among the many contaminants present, heavy metals are of particular concern due to their toxicity, long-term persistence, and ability to accumulate in living organisms [1,2]. Heavy metals are typically characterized by a high atomic mass and a density greater than 5 g $cm^3$, and can be classified as toxic, precious, or radionuclide elements based on their chemical properties and biological effects [3]. Unlike many organic pollutants, heavy metals are non-biodegradable and accumulate in biological systems, gradually moving through the food chain and posing long-term ecological and health risks [4].

Human exposure to heavy metals is associated with a number of adverse health outcomes. Excessive zinc intake can cause gastrointestinal distress and neuromuscular disorders [5], while iron overload has been linked to tissue damage and endocrine dysfunction [6]. Arsenic exposure is widely recognized for its potential to cause cancer and its association with skin abnormalities and metabolic disorders [7]. Chromium, especially in its hexavalent state, is highly toxic and can cause liver damage, skin irritation, and genetic alterations [8]. Mercury exposure primarily affects the nervous system and vital organs, often causing severe neurological damage [9]. Of these pollutants, cadmium is considered the most dangerous due to its high mobility in the water environment and strong bio accumulative behaviour [10].

Cadmium was first identified in 1817 by Friedrich Stromeyer and is a soft, bluish-white metal commonly associated with zinc ores. It is widely used in electroplating, rechargeable batteries, pigments, coatings, and stabilizers, which contribute to its release into the environment through activities such as mining, smelting, fossil fuel burning, and improper waste disposal [11,12]. Natural processes, including volcanic emissions and rock weathering, also introduce cadmium into the environment, although human activities are the primary contributors in most contaminated areas [13]. Cadmium can enter the human body through inhalation, ingestion, or skin contact and accumulate in organs such as the kidneys and liver [14]. Long-term exposure can cause bone erosion, kidney damage, and the well-known Itai-Itai disease, while chronic toxicity is also associated with carcinogenic effects [15]. Due to these health risks, strict regulatory limits for cadmium in drinking water have been established by organizations such as the World Health Organization and the United States Environmental Protection Agency, which recommend maximum concentrations of 0.003 mg $L^{-1}$ and 0.005 mg $L^{-1}$, respectively [16].

Several technologies have been developed to remove heavy metals from water, including chemical precipitation, membrane separation, ion exchange, electrochemical treatment, and solvent extraction. However, these traditional methods often involve high operating costs, poor removal efficiency, and the generation of secondary waste streams [17]. Therefore, adsorption has emerged as an effective, inexpensive, and environmentally sustainable alternative [18]. This process involves the concentration of dissolved substances at the interface between a solid adsorbent and a liquid phase through physical or chemical interactions [19]. Synthetic adsorbents such as activated carbon, zeolites, and silica gel, as well as low-cost natural materials derived from agricultural byproducts, have been extensively investigated for this purpose [20].

In the view of above literature, the present experimental study investigated the effectiveness of a peanut shell-based adsorbent for cadmium removal from aqueous solutions. Batch adsorption experiments are conducted to investigate the effect of operational parameters such as solution pH, contact time. Further, adsorption equilibrium data are interpreted using Langmuir and Freundlich isotherm models to better understand the adsorption capacity and underlying mechanisms. The aim of this study is to help in the development of low-cost and sustainable adsorbent materials for efficient removal of cadmium in wastewater treatment systems.

## Materials and Methods

In this study, batch adsorption experiments are conducted to assess the effectiveness of an adsorbent made from peanut shells to remove cadmium from aqueous solutions. The experimental methodology involved several stages such as raw material collection, adsorbent preparation, preparation of a synthetic cadmium solution, determination of removal and adsorption capacity, adsorption experiments, optimization of operational parameters, desorption analysis, and adsorption isotherm modelling.

### *Collecting Raw Materials*

Peanut shells (Arachis hypogaea) are chosen as the precursor material for adsorbent preparation. The shells are procured from the local market in Sirsa. Careful handling and storage practices are adopted to avoid contamination before processing.

### *Preparing the Adsorbent*

The collected peels are hand-sorted to remove any foreign matter, crushed into small pieces, and thoroughly washed with distilled water to remove any adhering dirt. The cleaned material is dried in the sun for seven days to remove moisture, after which it is ground and sieved to achieve a uniform particle size of ≤ 0.5 mm. The processed adsorbent is stored in an airtight container at room temperature until further use.

*ISBN 978-81-973526-0-7*

### *Preparing the Synthetic Cadmium Solution*

A stock cadmium solution (1000 mg/L) is prepared by dissolving cadmium chloride monohydrate ($CdCl_2 \cdot H_2O$) in double-distilled water. Working solutions of the required concentration are prepared by appropriately diluting the stock solution for use in batch adsorption experiments.

### *Adsorption Isotherm Modelling*

Equilibrium adsorption data are analyzed using the Langmuir and Freundlich isotherm models. The Langmuir model, developed by Irving Langmuir, assumes monolayer adsorption on a uniform surface with a limited number of identical sites. In contrast, the Freundlich model, developed by Herbert Freundlich, accounts for adsorption on diverse surfaces and allows for multilayer formation. Model parameters are derived from linearized plots to evaluate adsorption capacity and intensity.

## Performance Parameters and optimization

The performance of the prepared peanut shell adsorbent is evaluated using removal efficiency and equilibrium adsorption capacity.

***Removal efficiency*** represents the percentage reduction in cadmium concentration after the adsorption process. The percentage removal of cadmium is calculated as:

$$Removal\ efficiency\ (\%) = \frac{C0 - Ce}{C0} \times 100 \qquad \ldots 1$$

Where $C_0$, and $C_e$ are the initial and equilibrium cadmium concentration (mg/L).

***Adsorption Capacity (Uptake)*** The equilibrium adsorption capacity describes the amount of cadmium adsorbed per unit mass of adsorbent at equilibrium. It is determined using the following expression:

The equilibrium adsorption capacity is calculated using:

$$qe = \frac{(C0 - Ce)V}{m} \qquad \ldots 2$$

where $q_e$, $C_0$, $C_e$, V, and m denoting the adsorption capacity at equilibrium (mg/g), initial and equilibrium cadmium concentration (mg/L), volume of solution (L), and mass of adsorbent used (g).

Operational variables affecting adsorption performance are systematically investigated. The pH of the solution is varied between 2.0 and 7.0, while temperature, stirring speed, adsorbent dose, and contact time are kept constant. The effects of contact time (10–180 min) are examined.

## Results and discussion

Batch adsorption experiments are conducted to assess the effectiveness of a peanut shell adsorbent for cadmium removal under different operating conditions, including varying solution pH, contact time. The experimental results obtained under these conditions are described and discussed in the following sections. The effect of solution pH on cadmium adsorption is investigated while maintaining constant experimental conditions: adsorbent dose 0.1 g per 100 mL, initial cadmium concentration 50 mg/L, contact time 180 min, temperature 26 °C, and agitation speed 150 rpm. To determine its effect on cadmium removal efficiency and adsorption capacity, the solution pH is adjusted to a range of 2.0 to 7.0.

### *Effect of pH*

As shown in Figure 1, it is observed that the uptake capacity increases with increase in the solution pH. The solution pH plays a significant role in controlling the cadmium adsorption. The highest uptake capacity achieved is 40.86 mg/g at pH 5.0. Under highly acidic conditions,

ISBN 978-81-973526-0-7

cadmium uptake is comparatively lower. This can be explained by the higher concentration of hydrogen ions ($H^+$), which compete with cadmium ions for active sites on the adsorbent surface. Strong protonation at low pH reduces the number of negatively charged binding sites, limiting cadmium adsorption.

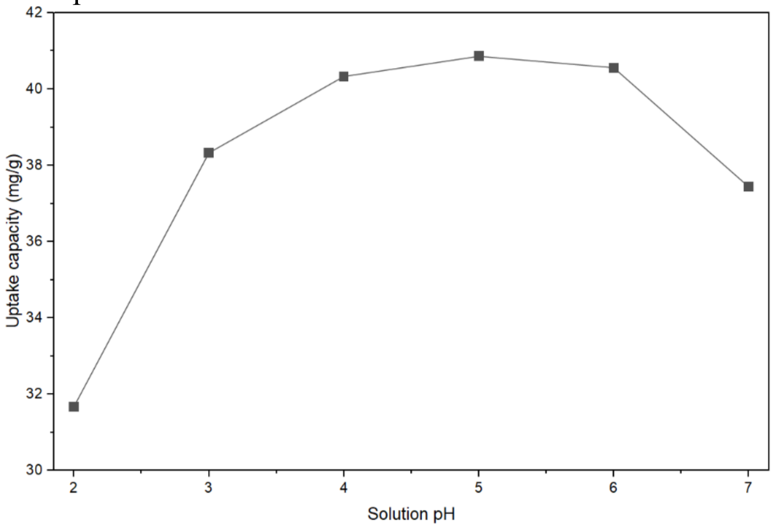


Figure 1. Effect of solution pH on the concentration of uptake capacity.

As pH increases, hydrogen ion concentration decreases, reducing competition for adsorption sites. Furthermore, deprotonation of surface functional groups increases the negative charge on the adsorbent, promoting electrostatic attraction between cadmium ions and the adsorption surface. Therefore, cadmium absorption gradually increases with increase in the pH of the solution. Further increases in pH beyond this range are generally avoided because metal hydroxide deposition can occur, which can hinder the adsorption process and lead to inaccurate interpretations of removal performance.

On the other hand, cadmium removal efficiency shows opposite trend with increase in the solution pH value (figure 2). The removal efficiency decreases by approximately 4.5%, as the solution pH vary from 2.0 to 7.0. However, minimum removal efficiency is observed at pH 5.0, thereafter it shows little increment of about 2.5% with increase on solution pH. Overall pH 5.0 is identified as the optimal condition for maximal cadmium removal and minimum cadmium removal efficiency using peanut shell adsorbent.

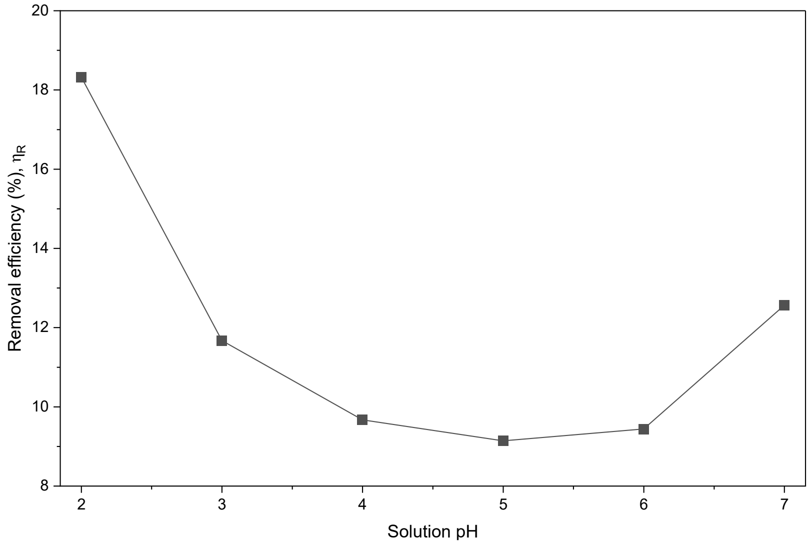


Figure 2. Effect of solution pH on the concentration of cadmium removal efficiency.

## *Effect Contact Time*

As shown in Figure 3, uptake capacity showed a positive correlation with contact time. It is observed that the uptake capacity exhibits increasing trend with increase in contact time. However, the increasing rate slows down after 120 min of contact time. The uptake capacity increased from 11.22 to 40.99 mg/g, as contact time increased from 15 to 180 minutes. The adsorption process is rapid in the initial stage and gradually reached equilibrium after approximately 60 minutes, after which no significant increase in removal efficiency is observed.

The initial rapid uptake may be due to the large number of active adsorption sites available on the adsorbent surface at the beginning of the process. As the contact time increased, these sites became more occupied, leading to saturation and reducing the number of vacant binding sites. Consequently, the adsorption rate decreased over time, making further metal uptake less beneficial after equilibrium is reached.

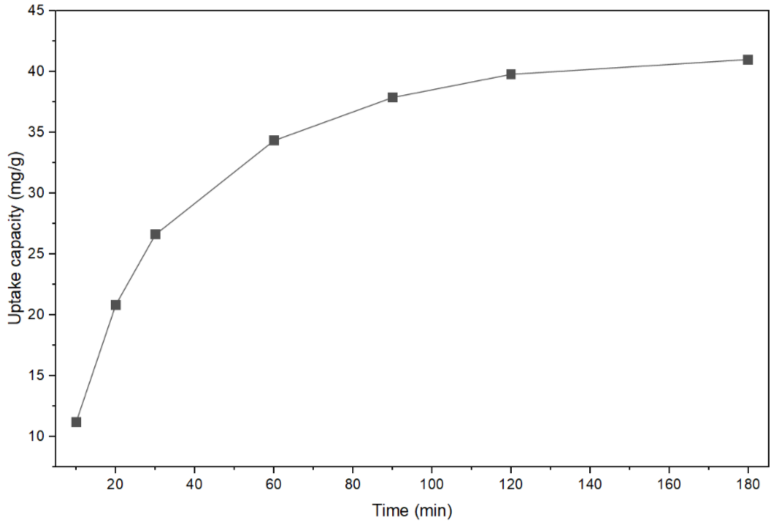


Figure 3. Effect of time on the uptake capacity.

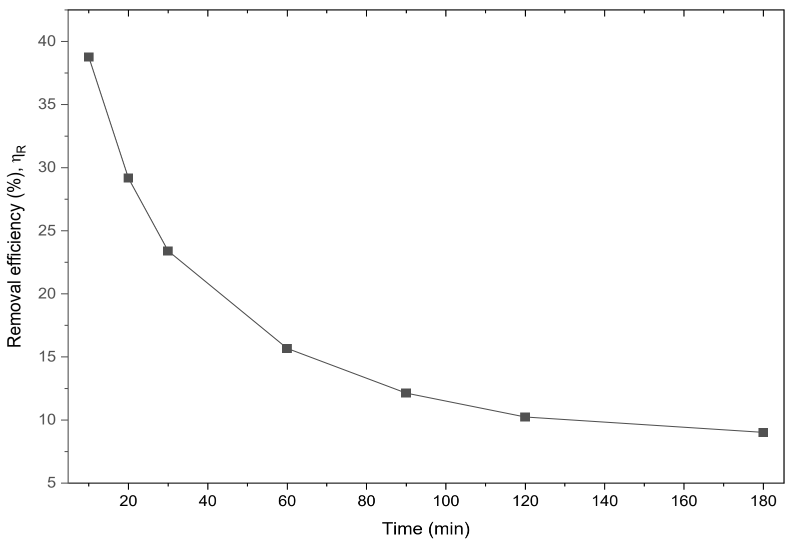


Figure 4. Effect of time on the cadmium removal efficiency.

Figure 4, shows the variation in cadmium removal efficiency with contact time. Initially, the removal efficiency is approximately 38%, thereafter decreases to approximately 8.5 %, as the contact time increases. This rapid change indicates the greater presence of active adsorption sites initially. As contact time increases, the removal rate gradually decreases, indicating that the system approaches equilibrium as adsorption sites gradually become saturated.

## Conclusion

In this study, the batch adsorption experiments are conducted to assess the effectiveness of a peanut shell adsorbent for cadmium removal under different operating conditions, including varying solution pH and contact time. Experimental results reported that the peanut shell adsorbent is an effective, inexpensive, and environmentally sustainable material for removing cadmium from aqueous solutions. Adsorption performance is highly dependent on operational parameters. The adsorption uptake shows similar behaviour with respect to solution pH and contact time, it increases with both parameters, reaches a peak of approximately 41 mg/g at higher contact time. However, the rate of increase slows down at higher contact time. On the other hand, the cadmium removal efficiency exhibits decreasing trends with respect to solution pH and contact. The maximum decrease in residual concentration is about 28.75 % as the contact time increases from 10 to 180 min.

## References

[1] Fu Fenglian, Wang, Q., Removal of heavy metal ions from wastewater: A review. Journal of Environmental Management, 92 (3) (2011) 407–418. https://doi.org/10.1016/j.jenvman.2010.11.011

[2] Babel Sandhya, Kurniawan, T.A., Low-cost adsorbents for heavy metals uptake from contaminated water: A review. Journal of Hazardous Materials, 97 (1–3) (2003) 219–243. https://doi.org/10.1016/S0304-3894(02)00263-7

[3] JarupLars, Hazards of heavy metal contamination. British Medical Bulletin, 68 (1) (2003) 167–182. https://doi.org/10.1093/bmb/ldg032

[4] Godt Jochen, Scheidig, F., Grosse-Siestrup, C., Esche, V., Brandenburg, P., Reich, A., Groneberg, D.A.,The toxicity of cadmium and resulting hazards for human health. Journal of Occupational Medicine and Toxicology, 1 (2006) 22. https://doi.org/10.1186/1745-6673-1-22

[5] Nordberg Gunnar F, Fowler, B.A., Nordberg, M., Handbook on the Toxicology of Metals, 3rd ed., Academic Press, Burlington, 2007. https://doi.org/10.1016/B978-012369413-3/50001-3

[6] Barakat Mohamed A, New trends in removing heavy metals from industrial wastewater. Arabian Journal of Chemistry, 4 (4) (2011) 361–377. https://doi.org/10.1016/j.arabjc.2010.07.019

[7] Pyrzynska Katarzyna, Removal of cadmium from wastewaters with low-cost adsorbents. Environmental Chemistry Letters, 17 (2) (2019) 665–681. https://doi.org/10.1007/s10311-018-00841-7

[8] Sud Dhiraj, Mahajan, G., Kaur, M.P., Agricultural waste material as potential adsorbent for sequestering heavy metal ions from aqueous solutions – A review. Bioresource Technology, 99 (14) (2008) 6017–6027. https://doi.org/10.1016/j.biortech.2007.11.064

[9] Demirbas Ayhan, Heavy metal adsorption onto agro-based waste materials: A review. Journal of Hazardous Materials, 157 (2–3) (2008) 220–229. https://doi.org/10.1016/j.jhazmat.2007.12.071

[10] Bhatnagar Amit, Sillanpää, M., Utilization of agro-industrial and municipal waste materials as potential adsorbents for water treatment—A review. Chemical Engineering Journal, 157 (2–3) (2010) 277–296.

https://doi.org/10.1016/j.cej.2010.01.007

[11] Ruthven Douglas M, Principles of Adsorption and Adsorption Processes. John Wiley & Sons, New York, 1984. ISBN: 978-0471866060

[12] Yu Ming-Ho, Environmental Toxicology: Biological and Health Effects of Pollutants, 2nd ed., CRC Press, Boca Raton, 2011. https://doi.org/10.1201/b10796

[13] Sharma Rakesh Kumar, et al., Industrial applications and environmental implications of cadmium and its compounds. Journal of Industrial Pollution Control, 31 (2) (2015) 245–252.

[14] World Health Organization, Guidelines for Drinking-Water Quality, 4th ed., WHO Press, Geneva, 2017. ISBN: 978-9241549950

[15] United States Environmental Protection Agency, National Primary Drinking Water Regulations. EPA 816-F-09-004, Washington DC, 2009.

[16] Rangabhashiyam Selvaraju, Balasubramanian, P., The potential of biosorbents for heavy metal removal from aqueous solutions: A review. Chemical Engineering Journal, 359 (2019) 1251–1266. https://doi.org/10.1016/j.cej.2018.11.020

[17] Mohamed A Barakat, New trends in removing heavy metals from industrial wastewater. Arabian Journal of Chemistry, 4 (4) (2011) 361–377. https://doi.org/10.1016/j.arabjc.2010.07.019.

[18] Amit Bhatnagar, Sillanpaa, M., Utilization of agro-industrial and municipal waste materials as potential adsorbents for water treatment—A review. Chemical Engineering Journal, 157 (2–3) (2010) 277–296. https://doi.org/10.1016/j.cej.2010.01.007.

[19] Douglas M Ruthven, Principles of Adsorption and Adsorption Processes. John Wiley & Sons, New York, 1984. ISBN: 978-0471866060.

[20] Alireza Karimi, et al., Natural and synthetic adsorbents for water treatment: A review. Environmental Technology Reviews, 8 (1) (2019) 1–16. https://doi.org/10.1080/21622515.2019.1578349.

# ECO-FRIENDLY UTILISATION OF STUBBLE THROUGH PELLETIZATION: STELLETS

Masooma Gour*[1], Sonam Khera[1], Vivek Rawat[1]
*[1]J.C. Bose University of Science & Technology, YMCA, Faridabad, Haryana, India
*khushmaitri03@gmail.com

## Abstract

*India's rapid advancement in the field of technology and infrastructure has portrayed it amongst the fastest growing nations in the world. Yet the pace of development has brought immense opportunities and progress but pose a significant threat to the environment. With Delhi being the heart and driving force of the nation, it has deeply contributed to pollution measures in India. The study deals with the growing intensity of pollution in Delhi NCR region and ways to combat it. Every year during winters, significant stubble burning is performed in this region which releases immense amounts of smoke and dust. This is further accompanied by naturally slow wind patterns that lead to deterioration of the air quality in the region. Stubble (parali) is typically the short, leftover parts of cereal crops remaining in the field after harvesting. The objective of the study is to convert this agricultural waste into an eco-friendly usable form known as "Pellets". Pellets, in general, are compactly compressed organic materials which serve as high-density fuel and can be used for various purposes. The whole idea of converting stubble into pellets and then using it for various purposes comes under "Circular Economy" and is aligned with sustainable development goals such as "SDG 7" (Affordable and Clean Energy), "SDG 12" (Responsible Consumption and Production) and "SDG 13" (Climate Action). Thus, the study provides the foundation for re-envisioning waste as fuel reconciling with the principles of circular economy and sustainable development goal.*

## Keywords

Stubble; Pellets; Circular Economy; SDG.

## Introduction

### *Stubble*

India is known as the 2nd biggest agro-economy-based country [1]. It stands second in rice and wheat production after China and produces 175.58 Mt of rice and 101.29 Mt of wheat per annum [2]. According to Ministry of New and Renewable Energy (MNRE), every year on an average, India generates 500 Million tons of crop residue [3]. Hence, counting as one of the leading producers of stubble globally. Agricultural Stubble, also known as parali, is typically the short, leftover parts of cereal crops remaining in the field after harvesting. It has calorific as well as economic value. Paddy and wheat are the major types of agricultural stubble found in northern and north western regions of India. "According to the Indian Agricultural Research Institute (IARI) in New Delhi, cereal crops produce the most residues, with 352 Mt. Paddy and wheat account for 34% and 22% of total production" [2]. It is because rice–wheat cropping cycle is dominant in the region, thus, farmers are left with a very short period of time between the harvesting of rice in October and the sowing of wheat in November. Also limited access to technology and lack of awareness collectively drive the farmers towards rapid clearance methods. Secondly, unlike ancient manual harvesting practices, modern machines, especially combine harvesters have led to a significant increase in the proportion of stubble production in India. Harvesting through combine harvesters leaves behind tall stalks that are difficult to remove manually or ploughed back which in turn results in generation of solid waste. To combat the management of this generated waste, farmers tend to burn the produced stubble leading to emissions. Primarily for rice-wheat cropping system, the in-situ burning of stubble can significantly alter the physical and chemical properties of soil, particularly in the top layer of soil [4].

***Affected Region***

Northern and north western region of India are majorly affected by stubble burning. India's leading rice-producing states I.e., Punjab and Haryana, account for nearly half of the total stubble burned (Gadde et al., 2009) [2]. Punjab contributes 1.5% of the total geographical area in India and shares 13-14% of total grain production, including 25.5% rice and 35.5% wheat, which is significantly high compared to all other states in the available area [5]. Every year, in Punjab, nearly 20 million tonnes of paddy stubble are burnt across an area of about 17,900 sq. km [5].

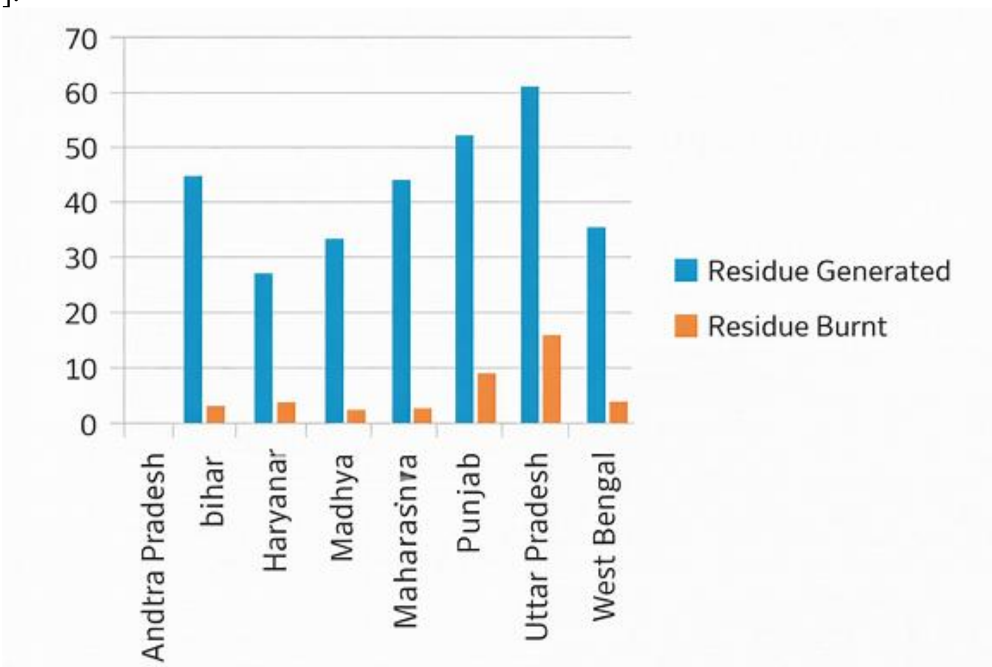


Figure 1. Stubble burning and residue generation in some states of India.

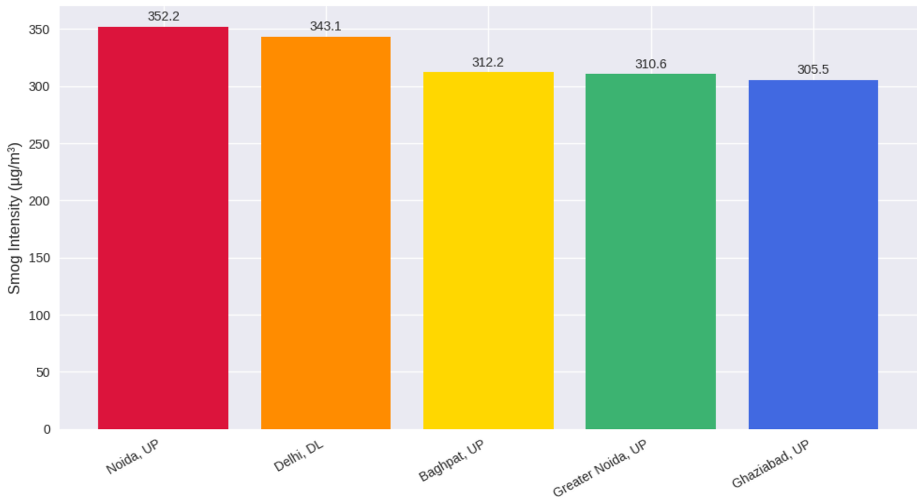


Figure 2. Smog intensity in Delhi NCR region during December 2025.

Since 2016, every year, the state has witnessed the highest number of cases of stubble burning while in 2021 there were over 8000 cases of fire in the Sangrur district of Punjab [6]. Coming to Delhi's pollution, the direction of the plume is from northwest to southeast over Delhi NCR during October-November, when the stubble burning is at its peak [5]. The pollution problem in Delhi may be viewed as a regional issue rather than a problem confined within Delhi [7]. Uttar Pradesh followed by Punjab leads in residue generation as well as stubble burning in India (Figure 1), according to Indian Agricultural Research Institute (IARI), every year around 14 Mt out of 22 Mt rice stubble (about 63.6%) is burnt [8].

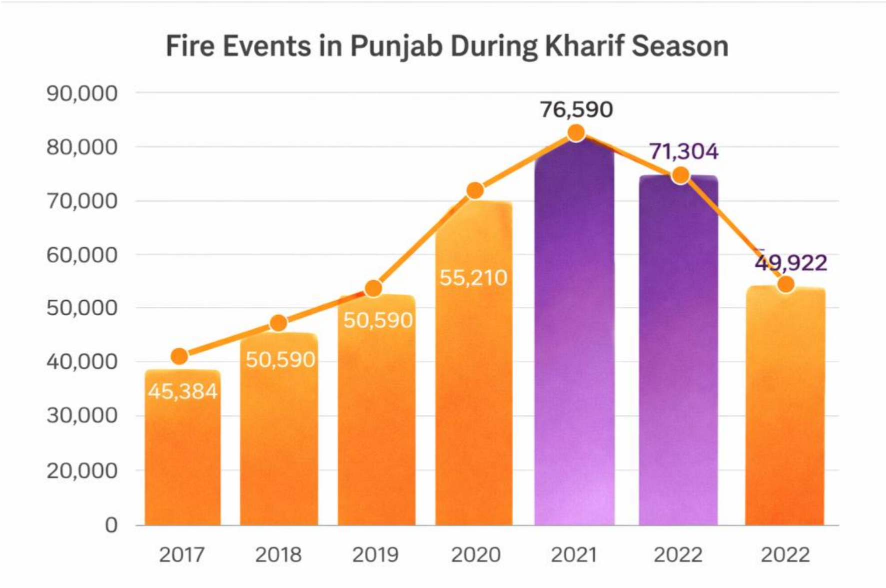


Figure 3. List of fire events in Punjab.

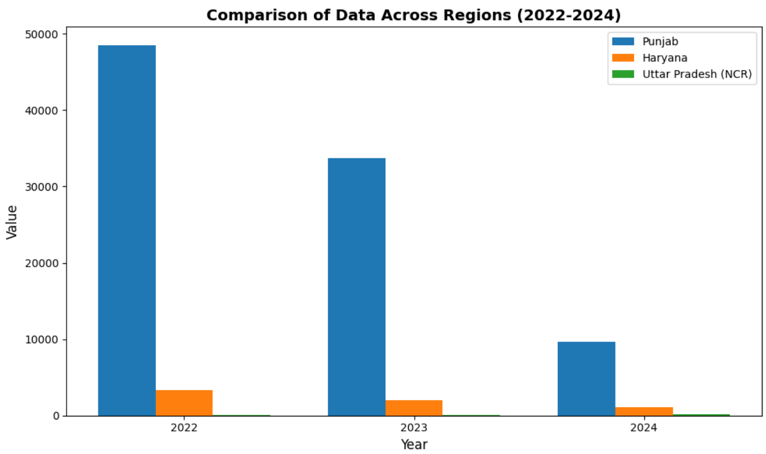


Figure 4. Stubble Burning (paddy) events (Period: 15th September- 18th November).

## ***Combustion: Stubble Burning***

Combustion, in general, acts as both source and sink for pollutants as a result of which it has created turbulence in society. The oxides of carbon, nitrogen and sulphur along with aromatic compounds, volatile organic compounds (VOCs), soot, and other fine particles are some of the prominent byproducts of combustion [9]. Crop residue management is a major challenge for farmers for the sake of which burning is seen as a cost-effective method by them [7]. From the farmers' perspective, burning also acts as a pest control measure, eliminating leftover straw and stubbles that could interfere with tillage and seeding operations [4]. Although stubble burning is a crime under Section 188 of the Indian Penal Code (IPC) and the Air and

ISBN 978-81-973526-0-7

Pollution Control Act (APCA) of 1981, a lack of implementation of these government acts has been witnessed across the country [10].

### *Effects of Stubble Burning*

From Indian perspective stubble burning has always been a concerning issue as it leads to poor Air Quality Index (AQI). It is one of the major contributor of air pollution as it emits CH4 SOx, PM of 10 (PM10) and 2.5 (PM2.5) microns, nitrogen oxides (NOx), CO2, and CO, mostly in every South Asian country such as India, Nepal, Bangladesh, and Pakistan and China (Figure 4)[9]. The effect of crop residue burning in northwest India can be directly evaluated with a study stating 149 million tonnes (Mt) of carbon dioxide (CO2), 9.0 Mt of carbon monoxide (CO), 0.25 Mt of sulfur oxide (SOX), 1.28 Mt of particulate matter (PM), and 0.07 Mt of black carbon (BC), which has found to be directly affecting Delhi's air quality index (AQI) [9]. Also in-situ burning of crop residue results in the depletion of 27–73 % of nitrogen in the soil and deteriorates the microbial population i.e., bacteria, fungi present on the upper layer of soil i.e., 2.5 cm which is most fertile layer [2]. According to SAFAR (System of Air Quality and Weather Forecasting) 46% of air pollution in Delhi and surrounding areas is caused by stubble burning in Punjab and Haryana [5].

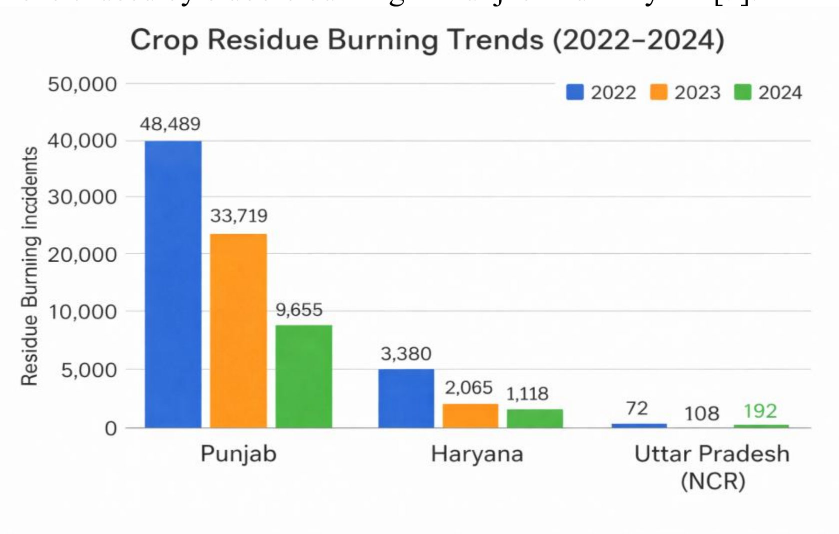


Figure 5. Statistics depicting the stubble burning of crops in tonnes from the year 2022–2024.

### *External Factors*

Anthropogenic factors such as vehicular emissions, industrial effluents and burning of firecrackers also contributes in the increased levels of emissions. Similarly natural factors such as slow wind patterns during the season tends to worsen the situation already posed by Stubble burning.

### *Mitigation*

Stubble can be converted into a valuable resource by several methods [1]. Incorporating crop residues into the soil can enhance its physical, chemical, and biological properties in various ways [1]. In southern states of India, paddy straw is used as bedding material in cattle shed while it is also preferred for mushroom making as it has high lignocellulosic content and is cheap [2]. Lignocellulosic and algal biomass is an emerging technology used for making green plastics as they emit no pollutants and reduce stubble burning [9]. The Pusa Decomposer is a microbial spray (a consortium of seven different microorganisms) designed to decompose crop residues in a short span of time, thereby clearing the land for the next crop [5].

### *Pelletization*

Biomass pelletization is the process of compressing agricultural, forestry, or industrial waste residues into small, dense cylindrical pellets that can be used as fuel [11]. The core principle behind pelletization is densification. Loosebiomass materials have low bulk density, which makes them difficult to handle, store, and transport. Through the pelletization process, the density of biomass is increased significantly, making it easier to store and burn efficiently [11].

Advantages of pellets include: -

- Cost-Effectiveness: They are cheaper than coal or any other fuel
- High Density Energy: They have a calorific value of around 4000-4500kcal/kg
- Sustainability: They are carbon neutral and renewable in nature etc.

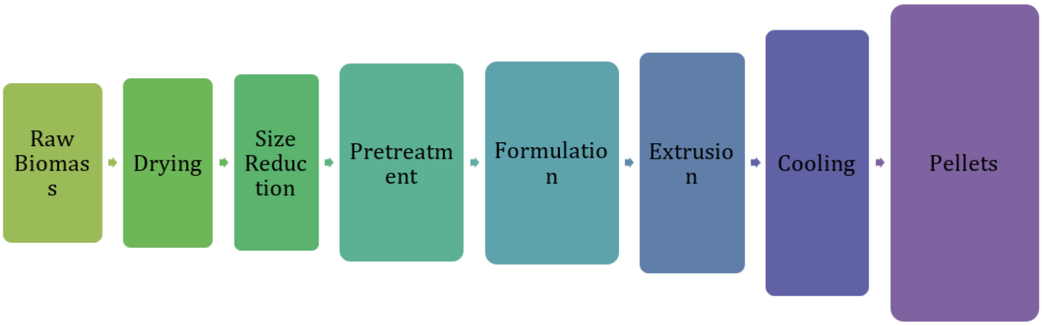


Figure 6. Statistics depicting the stubble burning of crops in tonnes from the year 2022–2024.

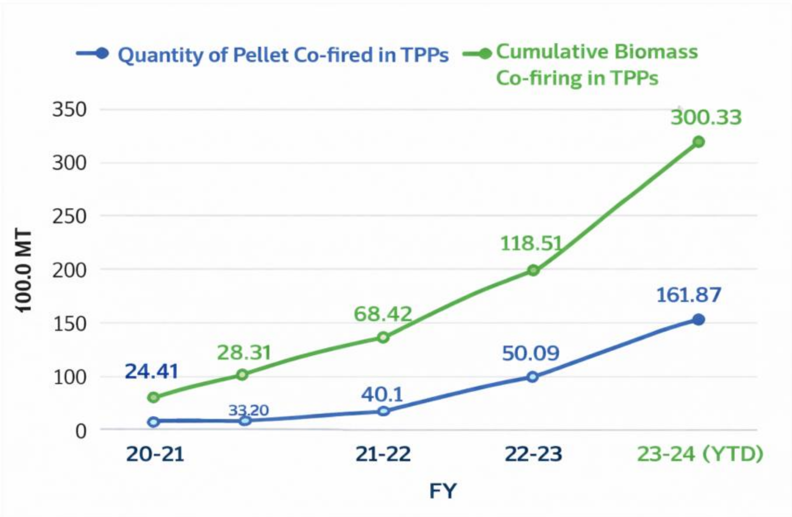


Figure 7. Annual data of pellet co-fired in TPSs.

## *Pelletization vs. Combustion*

Table 1. Combustion vs. Pelletization [9, 10, 12, 13, 14].

| Aspect | Combustion (Stubble Burning) | Pelletization of Stubble |
|---|---|---|
| Environmental Impact | Releases large amounts of $CO_2$, CO, $CH_4$, $N_2O$, and particulate matter, contributing to smog and climate change [9,12] | Reduces emissions by converting residue into densified biofuel pellets, lowering particulate and GHG release [10] |
| Soil Health | Causes loss of organic carbon and essential nutrients (N, P, K, S), degrading fertility [12] | Preserves soil nutrients by avoiding burning; ash from pellet use can be recycled as fertilizer [10] |
| Air Quality & Health | Major contributor to respiratory illnesses, eye irritation, and cardiovascular risks in Northern India [9,14] | Cleaner combustion in controlled facilities; reduces direct exposure to harmful pollutants [10] |

| | | |
|---|---|---|
| Energy Potential | No energy recovery; biomass is wasted [12] | Pellets serve as renewable bioenergy, usable in power plants, industries, and households [10] |
| Economic Value | Farmers save time but incur hidden costs via soil degradation, health impacts, and regulatory fines [13] | Generates marketable products (pellets, briquettes), offering farmers additional income streams [10] |
| Scalability & Adoption | Widespread due to ease and low immediate cost, despite bans and penalties [12] | Requires collection, processing infrastructure, and investment, but scalable with policy support and subsidies [13] |

### *Environmental Ethics*
STELLETS not only promotes sustainability but is also an ecocentric approach towards the environment. Combustion of agro residue-based pellets does not increase CO2 concentration in the atmosphere and thus it is also termed as carbon neutral fuel, hence, making it a renewable source of energy [15]. It implies circular economy and adheres to various sustainable development goals, such as “SDG 7” (Affordable and Clean Energy), “SDG 12” (Responsible Consumption and Production) and “SDG 13” (Climate Action). Hence, providing an ethically sound environment.

## Materials and Methods
The objective of the study is to provide a holistic approach of utilizing stubble as a fuel rather waste. It includes the level of stubble burning in India with major focus on north India. Literary and Experimental data relevant to study were collected, and results were interpreted according to the objectives of the study.

## Results and Discussion
After the evaluation and interpretation of data and information included in the study, key findings could be summarised as a shift from anthropogenic approach to ecocentric approach. In which a new perspective towards waste is presented in the society so as to achieve sustainability. One of such perspective could be utilising stubble as pellets and reusing them to mitigate conventional techniques that leads to huge amount of carbon emissions. Hence, achieving carbon neutrality. Prominent regions of India such as Punjab, Haryana and Uttar Pradesh constituting surplus amount of stubble are significant for initiating the ideology and spreading awareness. Emerging techniques like Pelletization are vital in providing foundation for achieving goals like SDGs and circular economy. The study “STELLETS” if implemented could be vital in various spheres such as solid waste management, circular economy, energy security, sustainability, ecocentrism, global SDGs, etc.

## Conclusion
With continuous development in infrastructure and technology, it is the need of the hour to emphasize on the idea of sustainability. Hence, in this regard the work named “STELLETS” is introduced. Wherein the idea of converting stubble into viable product is presented. The study focuses majorly on northern and north western regions of India which are dominant by rice-wheat cropping cycle. These crops, during harvest, produces large amounts of stubble due to various reasons including time constraints and lack of technology. Yet the burning of them by the farmers for the sake of ease pose a greater threat. Thus, comes into play “STELLETS” that provides a new perspective in the utilisation of stubble. It encompasses the idea of converting stubble into pellets which can be further utilised for various purposes. Hence, promoting circular economy and achieving SDGs.

# References

[1] S. Saxena and T. T. Thomas, "A Comprehensive Review on Tackling the Problem of Stubble Burning - An Indian Perspective," MATEC Web of Conferences, vol. 419, ICMME 2025, Art. no. 01006, 2026. doi: 10.1051/matecconf/202641901006

[2] R. Gottipati, B. Raghavendra, M. N. Pavan, and S. Menon, "Stubble burning: Root cause, impacts and its management in Indian scenario, "Environment Conservation Journal, vol. 22, no. 3, pp. 37–45, 2021. doi: https://www.environcj.in/

[3] M. Barman and A. Mukhopadhyay, "Stubble Burning in India: Problems and Mitigation Strategies, "ICAR–Indian Agricultural Research Institute, New Delhi, India, Article ID: 33181, 2021.

[4] P. Pradhan, A. K. Sinha, and T. K. Pandit, "The Effect of Stubble Burning and Residue Management on Soil Properties: A Review, "International Journal of Plant & Soil Science, vol. 36, no. 6, pp. 36–49, 2024, Art. no. IJPSS.116015. doi:10.9734/IJPSS/2024/v36i64604

[5] S. Kumar, "Stubble burning in Punjab: Causes, effects, and sustainable solutions," Wikifarmer, 2025. https://www.wikifarmer.com

[6] S. Misra, "Stubble Burning – An Environmental Threat in Delhi and NCR: An Overview, "International Journal of Research and Analytical Reviews (IJRAR), vol. 10, no. 2, pp. 36–49, May 2023. https://www.ijrar.org

[7] Commission for Air Quality Management in NCR and Adjoining Areas, "Framework for Development of Emission Inventory and Emission Based Source Apportionment in Delhi NCR, "Apr. 2025.

[8] A. Omer and A. Singh, "Sustainable agriculture and Stubble Burning approaches: A step towards clean environment, "International Journal of Innovative Research in Technology (IJIRT), vol. 8, no. 10, Mar. 2022. https://www.ijrar.org

[9] I. Chanana, A. Sharma, P. Kumar, L. Kumar, S. Kulshreshtha, S. Kumar, and S. K. S. Patel, "Combustion and Stubble Burning: A Major Concern for the Environment and Human Health, "Fire, vol. 6, no. 2, p. 79, Feb. 2023. doi: 10.3390/fire6020079

[10] G. K. Porichha, Y. Hu, K. T. V. Rao, and C. C. Xu, "Crop Residue Management in India: Stubble Burning vs. Other Utilizations including Bioenergy, "Energies, vol. 14, p. 4281, Jul. 2021. doi: 10.3390/en14144281

[11] Lehra Fuel Tech Pvt. Ltd., "Biomass Pelletization Process," https://www.lehrafuel.com

[12] G. Singh, "The environmental impact of stubble burning," International Journal of Science and Research Archive, vol. 12, no. 2, pp. 114–116, Jul. 2024, doi: 10.30574/ijsra.2024.12.2.1206.

[13] M. D. Saifuddin, T. Hussain, S. Sidharth, and K. Manasa, "Stubble burning in northern India: factors, technological solutions and management strategies—A comprehensive review," Bhartiya Krishi Anusandhan Patrika, vol. 40, no. 1, pp. 13–22, 2025, doi: 10.18805/BKAP837.

[14] Z. Yang, K. Ueda, T. Umemura, K. Onishi, H. Terasaki, T. Nakayama, Y. Matsumi, K. Vatta, H. Araki, S. Hayashida, and P. K. Patra, "Perceptions of air pollution from stubble burning and its health risks in Punjab, India," Scientific Reports, vol. 15, Art. no. 37455, Oct. 2025, doi: 10.1038/s41598-025-21235-8.

[15] Ministry of Power, Government of India, Standard Operating Procedure for Biomass Co-firing in FBC Boilers, National Mission on Use of Biomass in Thermal Power Plants (SAMARTH), New Delhi, India, 2025. https://samarth.powermin.gov.in/content/policies/80e5db53-014e-4dbf-ad85-a9d0ce9b654a.pdf.

*ISBN 978-81-973526-0-7*

# PERFORMANCE INDICATOR OF MONOCRYSTALLINE AND POLYCRYSTALLINE PHOTOVOLTICS SYSTEM

Rishika Ranawat*[1], Sheilza Jain[1], Sakshi Bangia[1], Arvind Gupta[1]
*[1]J.C. Bose University of Science & Technology, YMCA, Faridabad, Haryana, India
*rishikaranawat06@gmail.com

## Abstract
*Solar PV systems are advanced energy that converts raw solar energy into a clean and polished form of Electrical energy. Its process begins as disorganized photons, which are then harnessed through advanced forms of either monocrystalline or cost-effective polycrystalline or flexible thin-film humanoid solar cells. This is possible through the photoelectric effect, where the photons are converted into a directional flow of DC electricity through the panel's internal circuitry. This is then converted into Alternating Current (AC), a clean and compatible form of energy for our modern settings and use. This transformation of solar energy to electrical energy is done through the process known as Fabrication that converts raw materials, primarily silicon, into functional photovoltaic cells and assemble them into panels. Fabrication transforms raw silicon into efficient energy converters through precise texturing, phosphorus diffusion, and anti-reflective coating to create a functional P-N junction. In this paper, a comparison of monocrystalline and polycrystalline has been done on the basis of the performance indicators such as Performance ratio (PR), Specific Yield, and Efficiency (EFF).*

## Keywords
Photovoltaic Systems (PV Systems), Monocrystalline, Polycrystalline, Thin Film, Performance Efficiency, Degradation Rate.

## Introduction
Solar energy is a clean, renewable, and limitless source of power. In one hour, the sun provides more energy than all human needs for a whole year. Solar energy is used through solar cells and solar thermal systems to produce electricity, which plays a big role in making the world more sustainable, reducing the greenhouse effect, and ensuring energy security despite the challenges. Photovoltaic systems mainly use monocrystalline, polycrystalline, and thin film solar panels.

Monocrystalline PV panels are made from a single piece of silicon, so electricity flows easily through them. They have a pyramid cell structure, allowing them to cover a large surface area and collect more sunlight. Solar panels collect sunlight and turn it into electricity. A typical solar panel has cells made of layers of silicon, boron, and phosphorus. The positive charge comes from the boron layer, the negative from the phosphorus layer, and the semiconductor from the silicon. The solar cells in monocrystalline panels are tiny but work very efficiently when grouped together. They produce more energy in the same area as other panels and are good for large-scale projects [1]-[4].

Polycrystalline solar panels, also known as multi-crystalline, are a type of photovoltaic technology used to generate electricity from sunlight. They are made from solar cells that come from multiple silicon crystals fused together. These solar panels function as semiconductors with different photovoltaic cells. Each cell uses melted silicon to generate electricity. Unlike other solar panels that are black, these polycrystalline panels are blue because of the melted silicon inside. This allows them to capture more sunlight in less time [1]-[5].

Thin film solar panels are type of photovoltaic technology that is a layer of material, measuring from tiny fraction of a nano meter to several micrometres in thickness. They are light weight, adaptable and flexible PV devices that are made by layering photovoltaics substances. They are highly suitable for Building Integrated Photovoltaics (BIPV), installations on roofs and portable energy solution, providing excellent performance in low-light conditions and reduced manufacturing expenses in comparison to conventional silicon. Structure of thin film, polycrystalline and monocrystalline PV Systems is given in Figure 1 [1],[6].

The technical characteristics include efficiency, fill factor, temperature coefficient, degradation rate.

Efficiency is the percentage of sunlight energy that a panel can turn into electricity. It is usually between 15% and 22% for commercial panels. It depends on the panel's electrical power output compared to the solar energy input and is affected by technology, temperature, shading, and dirt [7]-[10].

Fill factor is the ratio of the actual maximum power output to the theoretical maximum power. The Fill Factor of typical commercial silicon solar cells ranges from 0.7 to 0.85 [10].

Temperature coefficient is the rate at which power output drops as the panel temperature rises above 25 degrees Celsius. It is the percentage change in power for each degree of temperature change. It usually ranges between -0.29% and -0.5% per degree Celsius [11].

Degradation rate is the gradual loss of power over time. It is the rate at which a panel loses its power. It typically drops by about 0.5% annually, so the panel retains about 80-90% of its capacity over 25-30 years [12].

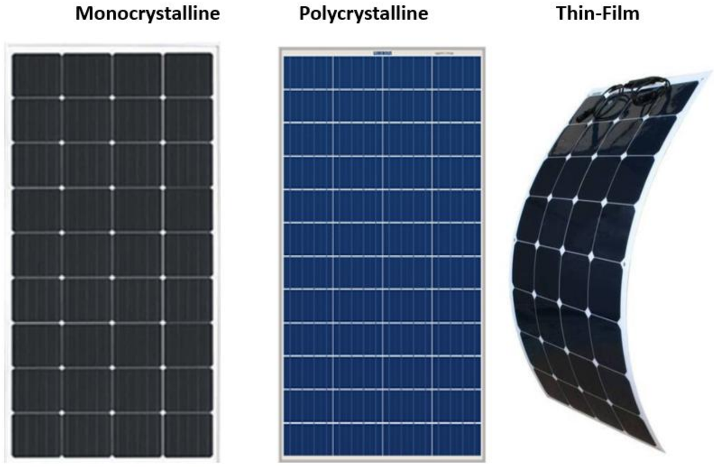


Figure 1. Structure of Monocrystalline, Polycrystalline and Thin-film PV Systems.

## Steps of Fabrication of PV Modules

Fabrication is the manufacturing and transformation of raw silicon into electricity generating photovoltaics panels through a multi stage process. It includes steps such as silicon purification and ingot formation in which silicon is purified through methods like carbothermic reduction and siemens process and Mold into solid ingot according to the module requirement. After that these ingots are sliced into thin wafers and are cleaned and textured to remove damage and to create a rough surface to increase the light absorption and reduces reflection. And then doped and assembled into modules [13].

***Detailed explanation of fabrication of PV modules***

Step 1: Raw Material Extraction and Purification

The production of a solar panel begins with the collection of silica sand (quartzite), which serves as the source of silicon. Silicon functions as a semiconductor, able to conduct electricity under specific conditions, making it suitable for solar applications. To be suitable, quartzite must be heated in an electric arc furnace to remove oxygen, producing metallurgical-grade silicon. This silicon then undergoes a thorough chemical purification process known as the Siemens process, essential for achieving "solar-grade" purity. The process of conversion from sand to silicon and silicon to ingot is Shown in Figure 2. This stage is crucial since even minor impurities can disrupt electron flow, significantly impacting the efficiency of the final cell.

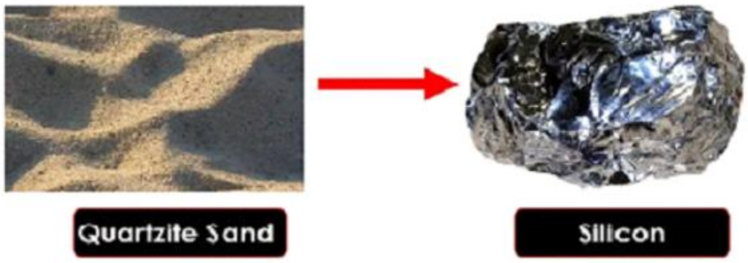


Figure 2. Sand to Silicon Formation.

Step 2: Ingot Formation and Wafer Cutting
After purification, the silicon is melted and formed into solid blocks called ingots. For monocrystalline production, a seed crystal is submerged in molten silicon and slowly pulled out while rotating, resulting in a single, continuous cylindrical crystal. Polycrystalline ingots are shaped into squares, yielding a more varied crystal structure. Once cooled, these ingots proceed to the wafer cutting process. The Silicon Ingot formation and Silicon Wafer formation are shown in Figure 3 and Figure 4. Here, highly precise diamond-wire saws slice the silicon into thin sheets, approximately 160 to 190 microns thick. These wafers are extremely fragile and serve as the essential base for the complete solar cell.


Figure 3. Silicon to Silicon Ingot formation.


Figure 4. Formation of Silicon Wafer from Silicon Ingot.

Step 3: Doping and the P-N Junction
Pure silicon does not conduct electricity effectively on its own, so a doping process is necessary to create an internal electric field. During this stage, the wafers are treated with chemical elements like phosphorus (n-type) and boron (p-type). Phosphorus introduces additional electrons to the upper layer, while boron creates "holes" (electron deficiencies) in the lower layer. This difference forms a "p-n junction" at the boundary. This is shown in Figure 5. When sunlight hits the cell, it releases electrons, and the internal electric field directs them to flow in a specific direction, generating a direct electrical current.
Step 4: Surface Treatment and Anti-Reflective Coating
To ensure the wafer does not reflect sunlight away, the surface is chemically etched to create a microscopic texture, often resembling tiny pyramids, which helps capture light. Following this, a silicon nitride anti-reflective coating is applied. This layer gives solar cells their distinctive blue or black appearance and ensures that the silicon absorbs the maximum number of photons. This anti reflecting coating on solar wafer is shown in Figure 6. Without this treatment, a significant portion of incoming sunlight would be reflected off the glossy silicon

 *ISBN 978-81-973526-0-7*

surface and lost.

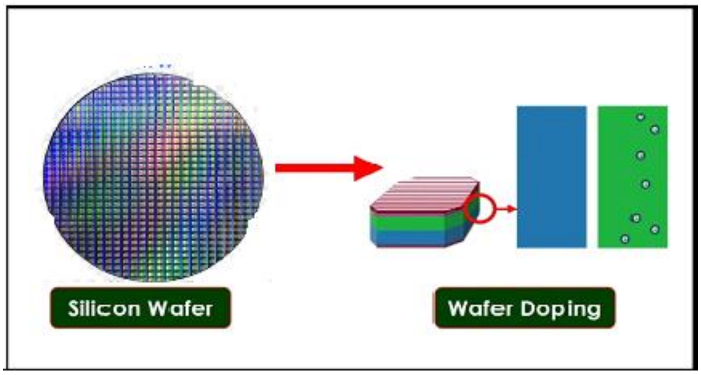


Figure 5. Wafer Doping from Silicon Wafer.

Step 5: Electrical Contact Printing and Testing

At this stage, the doped and coated wafers are transformed into functional solar cells by incorporating electrical contacts. Metal fingers along with larger busbars (typically made from silver paste) are screen-printed onto the surface to serve as pathways for the electrons produced. Each cell then undergoes a Flash Test, where it is exposed to artificial sunlight to evaluate its specific power output and efficiency as shown in Figure 7. Only cells that meet stringent performance criteria are sorted and sent to the final panel assembly stage.

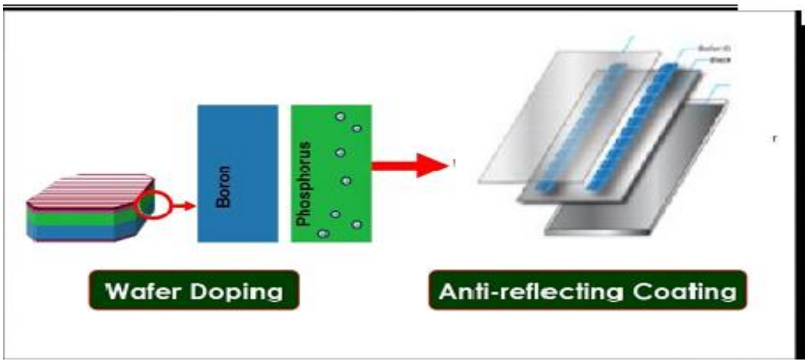


Figure 6. Anti-Reflecting Coating on Solar Wafers.

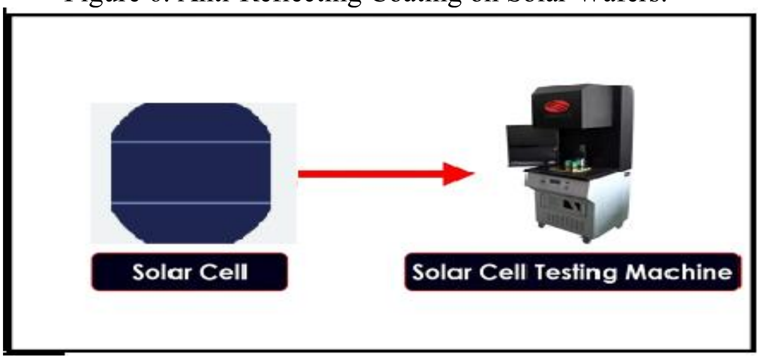


Figure 7. Solar cell Testing before cell assembling.

Step 6: Stringing, Lamination, and Framing

During assembly, multiple individual cells are connected in series using copper strips and arranged in a matrix as shown in Figure 8. To ensure these delicate components last for twenty-five years, they are laminated. The cells are encased between a piece of tempered glass and a strong polymer back sheet, held together by a transparent encapsulant such as Ethylene Vinyl Acetate (EVA) as shown in Figure 9. After being vacuum-sealed and cured, the laminate is fitted into an anodized aluminium frame. This frame provides essential structural support to withstand wind and snow pressure while offering a stable mounting point during installation as shown in Figure 10.

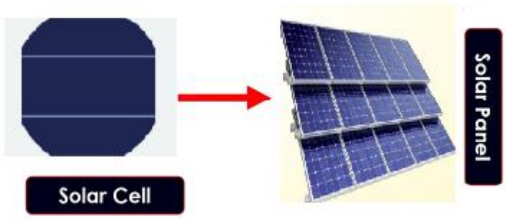


Figure 8. Solar cell assembling in solar panels.

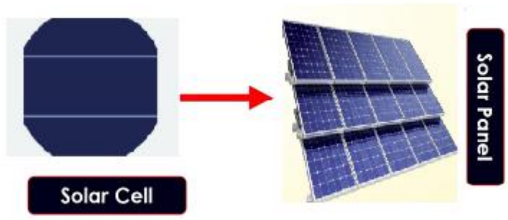


Figure 9. Solar Panel Lamination of solar panels.

Step 7: Final Quality Control

The final stage involves a series of quality control checks to verify that the panel meets global safety and performance standards. This includes Electroluminescence (EL) imaging, a process similar to an X-ray that detects hidden micro-cracks or "defective areas" within the cells that could lead to future issues. Additionally, the panel undergoes insulation resistance and grounding tests. Only after passing these rigorous evaluations is the panel marked with its final wattage specification and shipped for use in residential or commercial solar installations.


Figure 10. Solar Panel Framing.

## Performance Indicators

Performance indicator in PV Systems are the standards primarily defined by the IEC 61724-1 that measure a solar power plants efficiency, quality and reliability. These indicators include performance ratio, specific yield, capacity factors, availability and more [14],[15].

### *Performance Ratio (PR)*

Performance Ration is the ratio of total energy produced to the predicted energy output depending on solar irradiation and panel rating. It shows the systems efficiency once losses (such as temperature loss, shading loss, soiling loss) are taken into consideration. For different PV systems like monocrystalline, polycrystalline and thin film there are different values. for monocrystalline it is 18 -24% and it is the highest efficiency and high average dc performance ratio around 90.1%. for polycrystalline it is around 15-19% efficient with typical performance ratio around 90.64%. and lastly for thin film the performance ratio typically ranges between 70% and 85% and it has the lowest efficiency i.e. around 10 -18%, but have superior high temperature reliance 0.87 -0.96 PR [7],[16].

$$\text{Performance Ratio (PR): } \frac{\text{Actual Energy Output}}{\text{Expected Energy Output}} X\ 100 \qquad (1)$$

### *Capacity Factor (CF)*

Capacity Factor is the ratio of total energy produced to the predicted energy production if the system operated at full rated capacity for 24 hours a day. It evaluates the efficiency which the plant utilizes the sunlight it receives, typically falling within range of 0.1 to 0.2. For monocrystalline it is typically around 15-20% and produce more electricity per square foot thus leading to higher total system yield. For polycrystalline it is typically around 14-18% but have slightly lower efficiency than monocrystalline silicon and for thin film solar cells it is typically around 10-15% [7],[14].

Capacity Factor (CF): $\frac{\text{Actual Energy Output}}{\text{Expected Energy Output}}$ (2)

### *Specific Yield (Energy Yield)*

Specific energy yield is the total energy generated per installed Kilowatt- peak over a specific period. It allows the comparison of PV systems of different types. Monocrystalline offers highest yield per square meter which is typically ~1400-1700+ kWh/kWp annually. For polycrystalline it is lower energy yield per square meter than monocrystalline typically ~1200–1500 kWh/kWp annually and for thin film it has excellent low-light and high temperature performance around 1,300 to 1,700 kWh/kWp/year, depending heavily on climatic conditions [7],[15].

Specific yield ($Y_f$): $\frac{\text{Total Energy Generated (E)}}{\text{Installed DC Capacity } (P_{DC})}$ (3)

### *Availability*

Availability is the proportion of time a system is functional and capable to generate power, taking into account the times when not operational. It is about 98% for monocrystalline, 95-97% for polycrystalline, and typically 90-95% for thin film solar.

### *Degradation Rate*

Degradation rate is the measure of annual decline of power output over time. Average Annual degradation rate for monocrystalline, polycrystalline and thin film is 0.3% to 0.5%, 0.5% to 0.7% and 1% to 1.5% respectively. [12]

Annual Degradation Rate (%): $\frac{(\text{Power Year 1} - \text{Power Year N})}{\text{Power Year } 1 \times (\text{N} - 1)} \times 100$ (4)

Where,
Power Year 1: The actual power output (or performance ratio) measured at the end of the first year.
Power Year N: The power output (or performance ratio) measured in a later year
N: The year for which the calculation is being made (e.g., year 5, year 20)

### *Solar Fraction (SF)*

Solar Fraction is defined as the ratio of energy supplied by a solar system to the total energy required. For monocrystalline solar fraction is high due to high efficiency as they yield the highest energy output per square meter. For polycrystalline solar fraction is moderate. They typically produce 10-13% less energy than monocrystalline, requiring more area to achieve the same percentage of solar energy production. For thin film the solar fraction is variable.[13],[17]

Solar Fraction (SF): $\frac{\text{Solar Energy Supply}}{Solar\ Energy\ Demand}$ (5)

### *Efficiency*

Efficiency is the percentage of sunshine that reaches a solar panel and is transformed into usable electrical energy. Monocrystalline solar panels possess the highest efficiency usually 18%–24%+, followed by thin-film 7%–15% and polycrystalline 13%–18%.[7]-[10]

η: $\frac{P_{Max}}{A \times G} \times 100$ (6)

Where:
$P_{Max}$: Maximum power output in watts (W).
$A$: Surface area of the module in square meters.

$G$: Solar irradiance in watts per square meter, typically 1000W under Standard Test Conditions (STC).

## Comparison of Monocrystalline, Polycrystalline, Thin-Film PV Systems

This comparison table shows the comparative analysis of Monocrystalline, Polycrystalline, and Thin Film Solar Technologies by evaluating their features such as Efficiency, Performance Ratio, and Specific Yield.

| **Feature** | **Monocrystalline** | **Polycrystalline** | **Thin-Film** |
|---|---|---|---|
| **Material** | Single high-purity crystal | Multiple crystals | Various (a-Si, Cd-Te, etc.) |
| **Manufacturing** | Czochralski method | Silicon purification/casting | Deposition on substrate |
| **Efficiency (η)** | Highest (avg. 14%) | Moderate | Lowest (avg. ~7%) |
| **Performance Ratio (PR)** | 90.10% | 90.64% | 70% and 85% |
| **Capacity Factor (CF)** | 15-20% | 14-18% | 10-15%. |
| **Degradation Rate** | 0.3% to 0.5%, | 0.5% to 0.7% | 1% to 1.5% |
| **Specific Yield ($Y_f$)** | High | Lowest | Highest |

Monocrystalline solar panels are known for their high efficiency and long-lasting performance, but their production requires more energy. Polycrystalline panels offer a good balance between cost and performance, with consistent energy output. Thin-film panels, while less efficient and more prone to performance loss over time, are well-suited for certain applications and perform better in varied weather conditions. The choice between these options depends on which factors are most important: power output, cost, or adaptability to different environments [1]-[7],[9],[10].

## Conclusion and future Scope

To Conclude, the comparison of monocrystalline, polycrystalline, and thin-film technology, highlight their own advantages depending on the requirements, environment and conditions. Monocrystalline technology is one of the best technologies available, with an efficiency rate of 18-24% and average DC performance ratio of 90.1%. This technology consumes a lot of energy to produce, but it is the one that produces the most energy per square meter. This technology is best used when space is a problem. On the other hand, polycrystalline technology, it is expensive as compared to thin-film technology, but is a balanced technology having an efficiency rate of 13-18%. It offers an average performance ratio of 90.64%. While least preferred is thin-film technology, with an efficiency rate of 7-15% and degrades faster, with an annual degradation rate of 1-1.5%. It is best used when high temperatures and low light are required, such as in BIPV applications. The choice of technology is also based on the level of complexity involved in its manufacturing, level of degradation, and climatic conditions.

The future scope of investigations should focus on the optimization of the Siemens process, ingot formation, and surface treatment to reduce the production costs and improve the absorption of photons. Moreover, improvements in lamination techniques, EL images, and

IEC 61724-1 monitoring are essential to improve the long-term efficiency of thin-film solar cells.

# References

[1] O. Ayadi, R. Shadid, A. Bani-Abdullah, and M. Alrbai, "Experimental comparison between Monocrystalline, Polycrystalline, and Thin-film solar systems under sunny climatic conditions," Energy Rep., vol. 8, pp. 218–230, Jun. 2022, Doi: 10.1016/j.egyr.2022.06.121.

[2] L. Jiang, S. Cui, P. Sun, Y. Wang, and C. Yang, "Comparison of Monocrystalline and Polycrystalline Solar Modules," Results Eng., vol. 27, Art. no. 106113, Sep. 2025, Doi: 10.1016/j.rineng.2025.106113.

[3] E. Alam and X. Xu, "Life cycle assessment of photovoltaic electricity production by mono-crystalline solar systems: a case study in Canada," Environ. Sci. Pollut. Res., vol. 30, pp. 27422–27440, 2023, doi: 10.1007/s11356-022-24077-3.

[4] A. Sherwani, J. A. Usmani, and V. Goel, "Life cycle assessment of solar PV based electricity generation systems: A review," Renew. Sustain. Energy Rev., vol. 14, no. 1, pp. 540–544, Jan. 2010, doi: 10.1016/j.rser.2009.08.003.

[5] Y. Fu, X. Liu, and Z. Yuan, "Life-cycle assessment of multi-crystalline photovoltaic (PV) systems in China," J. Clean. Prod., vol. 86, pp. 180–190, Jan. 2015, Doi: 10.1016/j.jclepro.2014.07.057.

[6] S. Sakthinathan et al., "A Review of Thin-Film Growth, Properties, Applications, and Future Prospects," Processes, vol. 13, no. 2, Art. no. 587, Feb. 2025, Doi: 10.3390/pr13020587.

[7] S. Odeh, "Analysis of the Performance Indicators of the PV Power System," J. Power Energy Eng., vol. 6, no. 6, pp. 59–75, Jun. 2018, Doi: 10.4236/jpee.2018.66005.

[8] A. Saleem, K. Mehmood, and F. Rashid, "The Efficiency of Solar PV System," in Proc. 2nd Int. Multi-Disciplinary Conf., Gujrat, Jul. 2019.

[9] S. D. Bazyomo, C. Manirakiza, A. Bayala, A. Ouedraogo, and E. Lawin, "Comparative efficiency assessment of polycrystalline, monocrystalline, and thin-film photovoltaic technologies under Burkina Faso’s climatic conditions," World J. Adv. Res. Rev., vol. 29, no. 1, pp. 814–823, Jan. 2026, Doi: 10.30574/wjarr.2026.29.1.0095.

[10] L.-G. Hua et al., "Comparative Analysis of Power Output, Fill Factor, and Efficiency at Fixed and Variable Tilt Angles for Polycrystalline and Monocrystalline Photovoltaic Panels-The Case of Sukkur IBA University," Energies, vol. 15, no. 11, Art. no. 3917, May 2022, Doi: 10.3390/en15113917.

[11] D. T. Cotfas, P. A. Cotfas, and O. M. Machidon, "Study of Temperature Coefficients for Parameters of Photovoltaic Cells," Int. J. Photoenergy, vol. 2018, Art. no. 5945602, Apr. 2018, Doi: 10.1155/2018/5945602.

[12] A. Boretti and S. Castelletto, "Annual relative performance degradation in photovoltaic solar plants," Sustain. Energy J. Adv., vol. 4, Oct. 2024, Doi: 10.1016/j.seja.2024.100074.

[13] A. Yadav et al., "Advancements in Solar Cell Fabrication Techniques: A Comprehensive Review," Preprints, May 2024, Doi: 10.20944/preprints202405.1591.v1.

[14] N. Bolson, P. Prieto, and T. Patzek, "Capacity factors for electrical power generation from renewable and nonrenewable sources," Proc. Natl. Acad. Sci. U.S.A., vol. 119, no. 52, Art. no. e2205429119, Dec. 2022, Doi: 10.1073/pnas.2205429119.

[15] S. Gulkowski, "Specific Yield Analysis of the Rooftop PV Systems Located in South-Eastern Poland," Energies, vol. 15, no. 10, Art. no. 3666, May 2022, Doi:

10.3390/en15103666.

[16] C. Haydaroglu, H. Kiliç, and B. Gumus, "Performance Analysis and Comparison of Performance Ratio of Solar Power Plant," Turk. J. Electr. Power Energy Syst., vol. 4, no. 3, pp. 190–199, Sep. 2024, Doi: 10.5152/tepes.2024.24009.

[17] "Annual Solar Fraction - an overview," ScienceDirect Topics. [Online]. Available: https://www.sciencedirect.com/topics/engineering/annual-solar-fraction.

# MECHANICAL BEHAVIOUR ANALYSIS UNDER CONVENTIONAL TURNING PROCESS OF MAGNESIUM ALLOY

Deepak*[1], Puneet Katyal[2], Rajender Kumar[2]
*[1]Department of Mechanical Engineering, Guru Jambheshwar University of Science & Technology, Hisar
[2]Department of Basic Engineering, Chaudhary Charan Singh Haryana Agricultural University, Hisar
* deepaksuthar035@gmail.com

## Abstract
*The lightweight, high strength, and great damping properties of magnesium alloys make them popular in architecture. Nevertheless, the alloy's inflammability is a constraint in the machining process. In the current investigation, a traditional turning under machining was conducted on Magnesium alloy AZ91 to determine response traits, including roughness of the surface (SR) and rate of metal removal (MRR), and fragment morphology. In order to examine the impact of turning workflow variables including feed rate (F), cutting speed (V) and depth of cut (D), a L9 orthogonal array was contemplated. Results showed that turning factors affect MRR, surface integrity, and chip shape of AZ91 Mg alloy. The influence of turning settings on machining performance was assessed using scanning electron microscopy. All process factors affect surface roughness synergistically. Cutting speed greatly affects chip kinds. Results show that multi-objective optimization grey relational analysis's most affecting qualities are cutting speed with minimizing SR and increasing MRR to reduce Mg alloy deterioration. The GRA approach shows that V1(1500 rpm)- D3(0.75 mm)-F3(250 mm/min) is the best parametric setting for rotating AZ91 for low SR and highest MRR. This arrangement is suggested for in-vitro mechanical integrity and degradation*

## Keywords
Magnesium alloys, Turning, GRA technic, Chip form, MRR, Roughness.

## Introduction
The expanding potential of Biomaterials using magnesium and alloys has challenged academics and industry experts in recent years. Biomaterials that are biocompatible with bone regeneration, mechanical, wear, and corrosion resistant, and biocompatible are needed [1]. Bioproduct metabolite magnesium ion is absorbed daily in 250–300mg from bones [2,3]. Their reason small weight, high strength-to-density ratio, low elastic modulus (45GPa), and mechanical qualities similar to real human bone (10-30GPa), magnesium and its alloys may be biodegradable implants [4-5]. With these qualities, many biodegradable development of magnesium-implantation alloys in humans and animals. H2 evolution under physiological settings causes Mg alloys to rapidly lose mechanical strength and acquire toxicity at the implantation site, limiting their medicinal potential [6-8]. Product failure frequently starts at the surface, whether from wear, corrosion, or fracture propagation [9]. Surface integrity-dependent degrading behavior must be studied to reduce corrosion. Medical device manufacturing relies on mold adhesion, which is affected by surface roughness [10]. Surface texture and circumstances below the surface affect the device functionality and performance manufactured by material removal processes, notably machining procedures [11].
Low density magnesium alloys are better for machining owing to their lower power consumption, prolonged tool life, and higher surface quality. In processing Mg-alloy

biomedical implants, conventional machining must be emphasized [12]. Traditional turning procedures affect removal rate and surface integrity with chopping speed, feeding rate, and depth. In AM series Mg alloys examined by Dutta and Narala [13], higher speeds with lower feeds and depth of cut increase surface quality. Grey relational analysis helped Vasu et al.,2021[14] enhance without-coated carbide cutting tools for AZ91 Mg alloy in dry circumstances. High cutting-edge angle carbide tools showed increased surface roughness regardless of cutting speed or feed rate. Danish et al.,2021[15] processed Mg alloys using environmentally friendly cooling techniques and found that a modest feed rate of 50-150 m/min produced the best surface polish and high material removal rate. Viswanathan et al., 2020[16] analyzed MRR, flank wear, cutting force, SR when converting dry PVD- treated carbide insert magnesium alloy utilizing grey-based Taguchi. Turning Mg alloy at low speed produced little chips. Cutting factors affect surface roughness in AZ31 magnesium alloys, according to Asal,2019[17] using Taguchi's L9 model, feed rate affects SR more than cutting speed.

Experiments on turning Magnesium alloys with particular depth, coolant, modeling and chip creation, predicting, cutting tools, and various metallic materials based on surface roughness have been conducted [18-21]. There is little study on improving turning settings for biodegradable Mg alloy. To fill the research gap, L9 orthogonal Taguchi array (OA) was chosen to analyze MRR and SR turning process factors with chip shape of AZ91 magnesium alloy. The GRA approach was used to combine various replies to improve MRR and minimize SR. Machining surface topography has been investigated using our process conditions.

## Experimental specifications and methodology

Table1 shows the composition of AZ91 Magnesium alloy plate utilized in the investigation. A 100x100x30 mm plate was machined to offer a smoother surface for sample preparation. A 10x10x2 mm specimen was cut from the original material for SEM composition testing. SEM (JSM-7610F Plus) employs high-resolution imaging to determine material sample chemical composition. The SEM chemical makeup of Mg alloy is shown in Fig. 1 and Table 1.

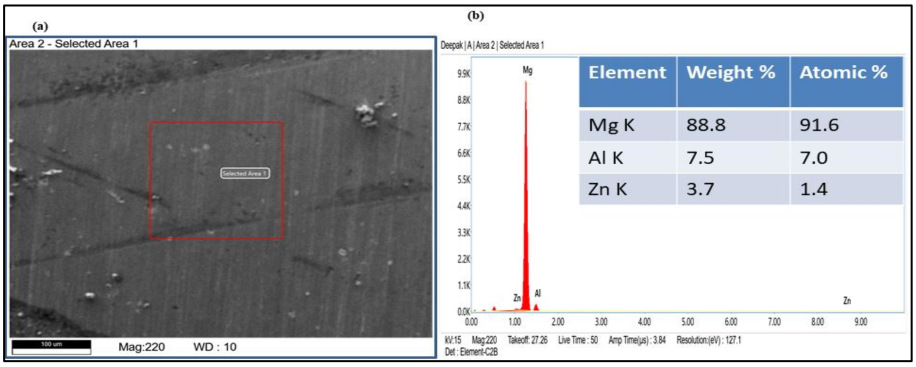

Figure 1. SEM/EDS analysis of machined AZ91 alloy specimen.

Without cooling in the machining zone, turning tests were done on a Computer numerical control rotating lathe (Hi-tech automation, variant SLT-100 Computer numerical control, in conjunction alongwith a Siemens advanced controller) with accurate tolerances. Specimens measuring 30 mm length and 27.5 mm diameter were fabricated adding WEDM techniques. In Table 2, cutting speed (1500, 2000, 2500 rpm), depth of cut (0.25, 0.5, 0.75mm) and feed rates (150, 200, 250 mm/min) were tested under dries conditions after refining. SR and MRR response parameters were examined after each experiment with chip evolution. Minitab analyzes L9 orthogonal array trials and GRA optimizes multi-response. The Mitsubishi SJ410 surface roughness tester measures roughness by averaging turning surface values. To measure chip thickness (average µm) and length (mm), a stereomicroscope was utilized with scale. Fig. 2 shows the experiment's flow.

Table 1. The AZ91 Mg alloy's chemical composition.

| Element | Magnesium | Zinc | Aluminium |
|---|---|---|---|
| Wt.% | 91.6 | 1.4 | 7.0 |

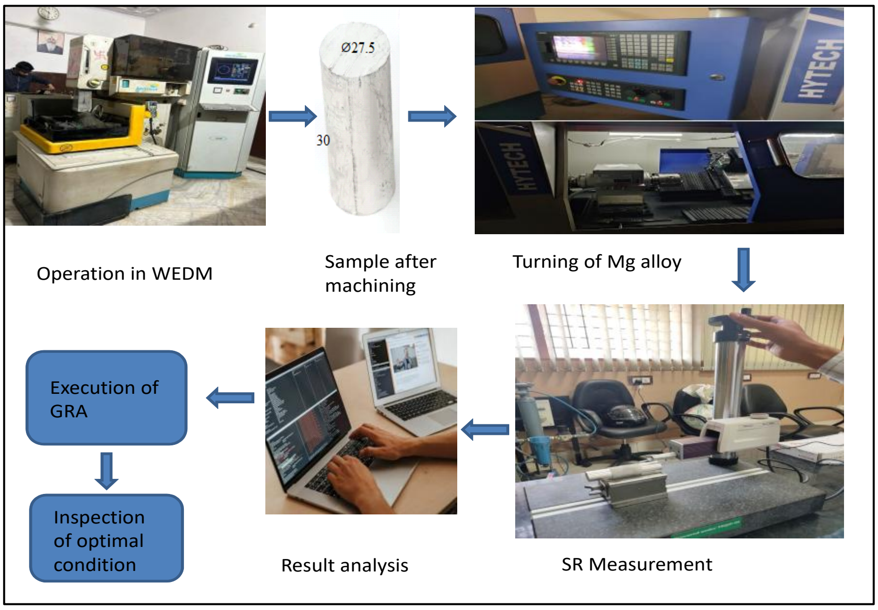


Figure 2. The experiment's process flow.

Table 2. Process settings being turned with level.

| Cutting Parameters | Symbol | Units | Level | | |
|---|---|---|---|---|---|
| | | | Level 1 | Level 2 | Level 3 |
| Depth of cut | D | Mm | 0.25 | 0.5 | 0.75 |
| Cutting speed | V | RPM | 1500 | 2000 | 2500 |
| Feed Rate | F | mm/min | 150 | 200 | 250 |

## Results and Discussion

Table 3 lists MRR and SR values for each parametric combination using L9 orthogonal array. Using Minitab-21, ANOVA was used for proportion contribution and significant results. The following sections show how process parameter affects response parameter level of operations.

Table 3. Taguchi technique experimentation employing L9 OA layout.

| | Process parameters | | | Response Parameters | |
|---|---|---|---|---|---|
| Exp. No. | Cutting speed | Depth of cut | Feed rate | Surface roughness ($R_a$) | MRR |
| 1 | 1500 | 0.25 | 150 | 1.782 | 3254.5 |
| 2 | 1500 | 0.50 | 200 | 2.187 | 7537.9 |
| 3 | 1500 | 0.75 | 250 | 2.675 | 15126.8 |
| 4 | 2000 | 0.50 | 150 | 0.564 | 1231.3 |
| 5 | 2000 | 0.75 | 200 | 1.599 | 11507.9 |
| 6 | 2000 | 0.25 | 250 | 2.034 | 4627.2 |
| 7 | 2500 | 0.75 | 150 | 1.244 | 8103.6 |
| 8 | 2500 | 0.25 | 200 | 1.629 | 4280.4 |
| 9 | 2500 | 0.50 | 250 | 2.136 | 8756.4 |

## *Single response optimization of Material Removal Rate*

Fig. 3 demonstrates just how process parameter affects MRR. MRR value falls from 1500 to 2000 rpm owing to cutting forces involved in surface hardening, then rises from 2000 to 2500 rpm due to thermal softening. MRR constantly rises with cut depth and feed rate increased from 0.25 to 0.75 mm and 150 to 250 mm/min, respectively. Chip thickness and material sheared by the tool increase with cutting speed per unit area. Increased depth of cut increases shearing area, coarser chips, greater cutting and thermal stresses [12]. This boosts MRR. In AZ91 Mg Alloy turning, cut depth and feed rate are more important than CS.

ANOVA was used with a 5% significance threshold to examine process parameter effects [22]. In Table 4, D hold the largest Delta value, demonstrating its greatest importance. Except for cutting speed, Table 5 shows that all process factors affect MRR. F 29.10% and D contributes 61.40% to MRR, rendering their greatest important process parameters. Taguchi analysis found that V1: 1500 rpm, D3: 0.75 mm and F3: 250 mm/min provide the highest MRR value for single response optimization (Figure 3). Signal-to-Noise (S/N) ratio is estimated to be 86.1813 and mean is 15405.7 for the setup.

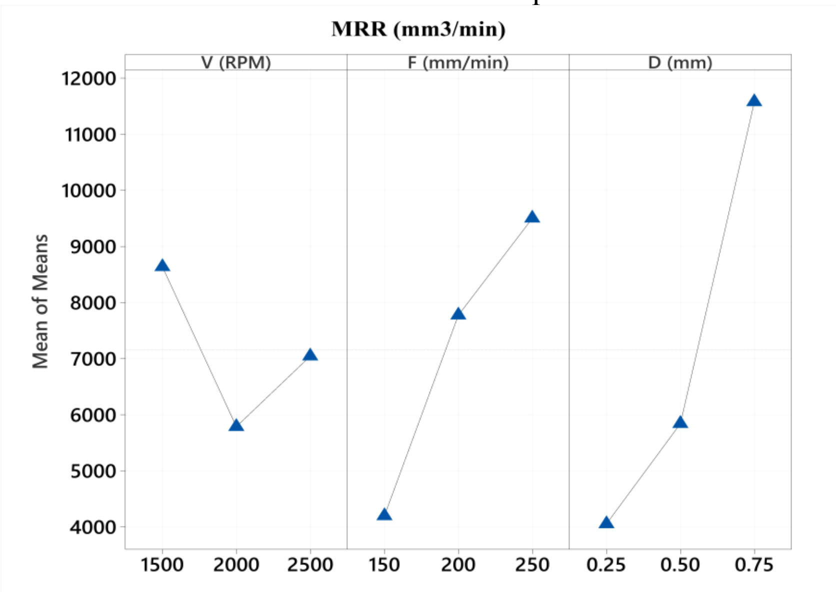


Figure 3. The MRR major impacts plot.

Table 4. Response Table for Mean.

| Level | V (rpm) | D (mm) | F (mm/min) |
|---|---|---|---|
| 1 | 8640 | 4054 | 4196 |
| 2 | 5789 | 5842 | 7775 |
| 3 | 7047 | 11579 | 9503 |
| Delta | 2851 | 7525 | 5307 |
| Rank | 3 | 1 | 2 |

Table 5. Anova for MRR.

| *Factor* | D.F | SS | Contribution | MS | F-Value | P-Value |
|---|---|---|---|---|---|---|
| *V (rpm)* | 2 | 12247821 | 8.11% | 6123911 | 5.80 | 0.147 |
| *F (mm/min)* | 2 | 43959227 | 29.10% | 21979614 | 20.83 | 0.046 |
| *D (mm)* | 2 | 92747664 | 61.40% | 46373832 | 43.94 | 0.022 |
| *Error* | 2 | 2110670 | 1.40% | 1055335 | | |
| *Total* | 8 | 151065383 | 100.00% | | | |
| S: 1027.29; R-sq.: 98.60%; R-sq(adj): 94.41% | | | | | | |

### *Single response optimization of Surface Roughness*

Surface defects increase corrosion site susceptibility, making surface integrity crucial for Mg-alloy component performance forecasts [23]. The material's composition, cutting settings, and machining working conditions greatly affect surface roughness. Fig. 4 indicates that SR reduces from 1500 to 2000 rpm and subsequently rises to 2000 to 2500. Increasing cutting speed values increase job surface heat, which degrades material and reduces cutting forces. As CS rises, SR falls. Later, high-speed, dry cutting raises the temperature due to heat accumulation [24]. Tool face stickiness chipped due to friction and SR rise. SR depends on feed rate, cutting speed, and depth of cut. Figure 4 shows that SR drops constantly as FR goes up 150 to 250 rev/mm. SR decreases with higher F due to fracturing and vibrations. Higher feed rates seem to stick chips for raked head, reducing surface quality. The accuracy of magnesium alloy machined surfaces depends on feed (Rubio et al.,2013) [25]. When cut from 0.25 to 0.50 mm, thermal softening reduces surface roughness. From 0.50mm to 1.0mm, the D boosts the labor needed to cut metal, resulting in a tool edge buildup for cutting and increased roughness [26]. ANOVA reveals that the F parameter significantly affects surface roughness, attributed 59.62%, accompanied by pace of cutting with 34.80% (Table 6). Taguchi analysis yields the smallest SR value for individual reply optimization with these parameter settings: V2: 2000 rpm, F3: 150 mm/min, D2: 0.50 mm. Minitab-21 software predicts a S/N ratio of -8.76472 and a value mean of 0.350733 for specified setup.

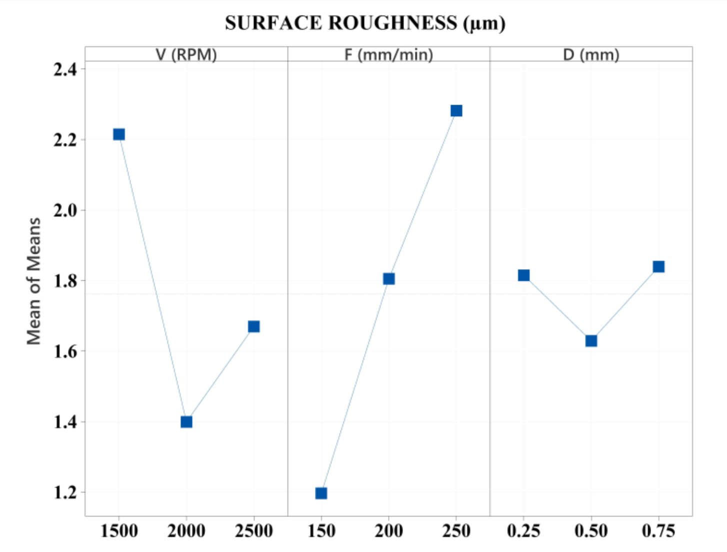


Figure 4. Plot of the SR major effects.

Table 6. Table of Mean Responses for SR.

| Level | V (rpm) | D (mm) | F (mm/min) |
|---|---|---|---|
| 1 | 2.215 | 1.815 | 1.197 |
| 2 | 1.399 | 1.629 | 1.805 |
| 3 | 1.670 | 1.839 | 2.282 |
| Delta | 0.816 | 0.210 | 1.085 |
| Rank | 2 | 3 | 1 |

### *Influence of Chip Morphology*

Chips greatly affect titanium and Mg alloy machinability. In addition, chip shape affects heat behavior at the workpiece-tool contact, which affects tool life. The effect of chip formation on machinability must be studied to improve Mg-based alloy productivity and tool life. Chip types created at various experimental operation conditions are shown in Fig. 5. Exp. 1 shows low-cutting-speed shorts chip formation. Rubbing on the tool's rake-face breaks the chips into many little, fractured bits at lower cutting speeds [12,16]. The sorts of chips generated did not vary much with cutting thickness. Figure 5: Experiments 6, 9, chip production is ongoing and lengthy as speed, feed rate, and cut depth increase. The heat from turning magnesium alloy melts chips, which stick to the tool edges. Due to decreasing rotating feed rates, chip edges lose sharpness. However, as F grows, chip thickness linear speed per unit area increases, and material shearing area increases with depth [12]. This increases the thickness of the chip and bearing tension hardening. After chip removal, material shrinking at grain boundaries causes residual pressures on the machined surface. These residual stresses degrade and cause micro-cracking on the turned surface [12,22]. SEM and EDS inspection of turned AZ91 Mg-alloy in Fig. 7 (a and b). Heat production rises with chip thickness, reducing tool life. Fig. 6 shows the chips' Standard ISO 3685-1977(E) [27] characteristics, whose similar to findings. Chips attach to cutter faces due to friction, affecting surface morphology and tool life [24]. For various process settings, chip anatomy may compare mechanical cutting powers, tool degradation, and manufactured surface texture [28]. Thus, feed rate in chip creation is ineffective. Cutting speed is the main determinant in chip creation. Short chips improve worker safety whereas long chips reduce material roughness and risk operators' health.

Figure 5. Experimental chip creation at varied parametric parameters.

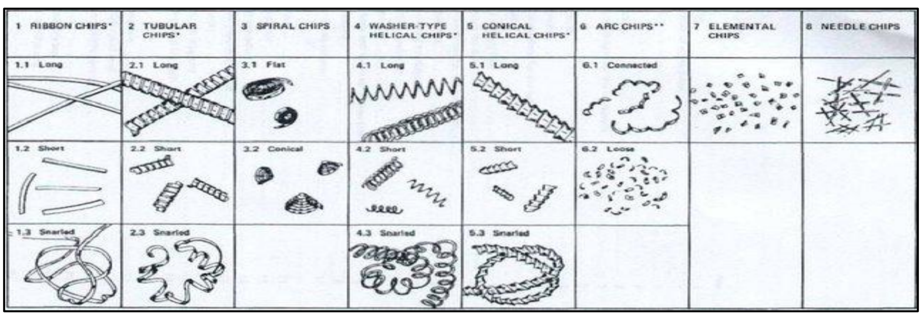


Figure 6. Standard ISO 3685-1977(E) chip formation.

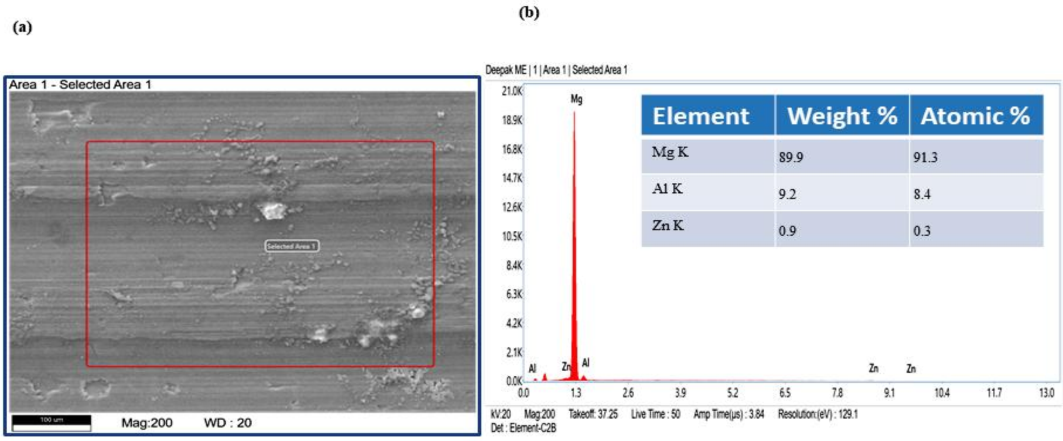


Figure 7. SEM/EDS analysis of machined AZ91 alloy specimen after turning.

## Multi-response optimization using grey relation analysis

Multi-functional optimization is done using GRA math in this work. The approach uses GRA to improve many response properties concurrently by Kumar et al.,2022 and Kumar et al.,2023 [12,29]. GRA flow is shown in Fig 8. The ideal process variable solution and improved response parameter are recommended by higher GRG values, as shown in Experiment No 3. Table 8 displays GRG/GRC calculations. The investigation's current goal is to find the ideal parameter settings to increase GRG, which optimizes SR and MRR.

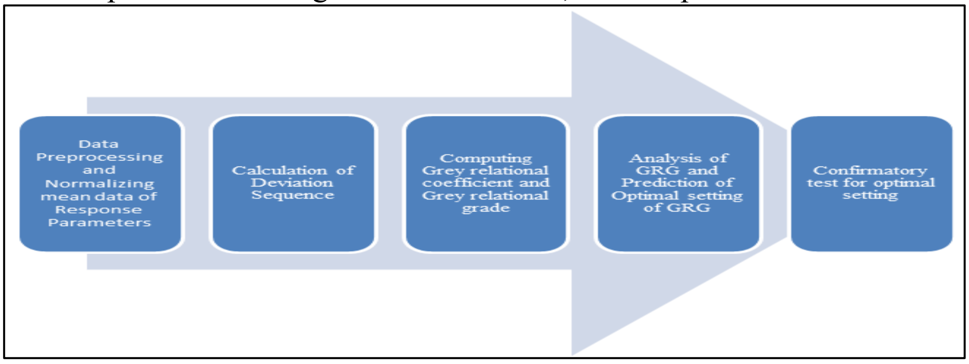


Figure 8. SEM/EDS analysis of machined AZ91 alloy specimen after turning.

Table 8. Pre-processing and GRG calculation.

| Exp. Run | Normalization of response mean data | | Deviation sequence | | GRC | | GRG | Rank |
|---|---|---|---|---|---|---|---|---|
| | **MRR** | **SR** | **MRR** | **SR** | **MRR** | **SR** | | |
| 1 | 0.39 | 0.739 | 0.61 | 0.26 | 0.449 | 0.657 | 0.553 | 8 |
| 2 | 0.72 | 0.871 | 0.28 | 0.13 | 0.643 | 0.794 | 0.719 | 3 |
| 3 | 1.00 | 1.000 | 0.00 | 0.00 | 1.000 | 1.000 | 1.000 | **1** |
| 4 | 0.00 | 0.000 | 1.00 | 1.00 | 0.333 | 0.333 | 0.333 | 9 |
| 5 | 0.89 | 0.669 | 0.11 | 0.33 | 0.821 | 0.602 | 0.712 | 4 |
| 6 | 0.53 | 0.824 | 0.47 | 0.18 | 0.514 | 0.740 | 0.627 | 5 |
| 7 | 0.75 | 0.508 | 0.25 | 0.49 | 0.668 | 0.504 | 0.586 | 6 |
| 8 | 0.50 | 0.681 | 0.50 | 0.32 | 0.498 | 0.611 | 0.555 | 7 |
| 9 | 0.78 | 0.855 | 0.22 | 0.14 | 0.696 | 0.776 | 0.736 | 2 |

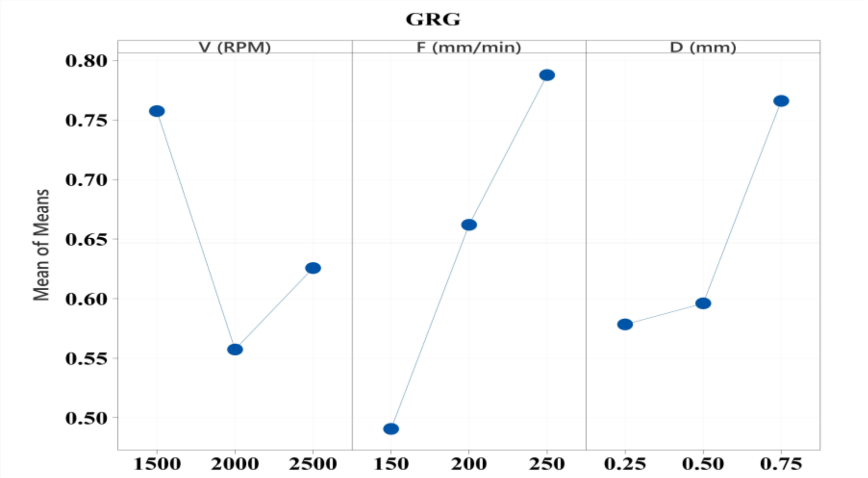


Figure 9. Grade value effect on turning process parameters (Mean of means).

Analysis of variance was used to assess process factors that significantly affect process response with 95% confidence. The "larger the better" technique was used to examine multiple iteration outcomes. In Table 9, F holds largest Delta value, showing that it has the greatly impact on the GRG, followed by V and D. ANOVA Table 10 shows that D (24.60%), F (50.91%), and V (23.67%) constitute the GRG calculation. Therefore, the best parameter pair is D3 (0.75 mm) - V1 (1500 rpm)- F3 (250 mm/min) (Fig. 9). In this case, Taguchi projected a grade average of 1.01744 and S/N ratio of 0.778895 from minitab-21.

Table 9. GRG Means Feedback Table.

| **Level** | **V (rpm)** | **D (mm)** | **F (mm/min)** |
|---|---|---|---|
| 1 | 0.7573 | 0.5783 | 0.4907 |
| 2 | 0.5573 | 0.5960 | 0.6620 |
| 3 | 0.6257 | 0.7660 | 0.7877 |
| Delta | 0.2000 | 0.1877 | 0.2970 |
| Rank | 2 | 3 | 1 |

Table 10. Anova for GRG.

| *Factor* | D.F | Contribution | SS | MS | F-Value | P-Value |
|---|---|---|---|---|---|---|
| *V (rpm)* | 2 | 23.67% | 0.062006 | 0.031003 | 28.67 | 0.034 |
| *F (mm/min)* | 2 | 50.91% | 0.133356 | 0.066678 | 61.66 | 0.016 |
| *D (mm)* | 2 | 24.60% | 0.064431 | 0.032215 | 29.79 | 0.032 |
| *Error* | 2 | 0.83% | 0.002163 | 0.001081 | | |
| *Total* | 8 | 100.00% | 0.261956 | | | |

S: 0.0328853; R-sq.: 99.17%; R-sq(adj): 96.70%

## ***Finding GRG's optimal value with confirmation***

The ANOVA model predicted GRG optimum values using pertinent variables. The ideal GRG may be determined using equation 1.

$$\Psi_{Opt} = \Psi_m + \sum_{k=1}^{n}(\Psi_k - \Psi_m) \quad \text{------ Eq.1}$$

$\Psi_{Opt}$ represents optimum grade, $\Psi_k$ represents GRG level means, $\Psi_m$ represents, and n represents process. If process settings are many, important ones could be considered. The ideal GRG is predicted using three process parameters. Equation yields 1.01740, the necessary grade.

$\Psi_{Opt}$ (anticipated) = 0.6467 + (0.7573-0.6467) + (0.7877-0.6467) + (0.7658-0.6467)= 1.0174

For MRR:

The aggregate mean MRRμ = 7158.444 $mm^3$/min, hence an projected MRR is predicted as follows:

MRRp = ($Vm_1$+ $Fm_3$+ $Dm_3$) - (j-1) MRRμ (j= utilized process parameters)

= (8639.733+9503.467+11579.43) -2*7158.444 = 15405.74 $mm^3$/min

Similarly, SR: SRp = 2.8134 μm

Table 9, which provides process parameters for each phase, predicts the GRG from experimental data. Test No. 3 in Table 8 has the greatest GRG of the nine trials employing the optimum processes set of V1-F3-D3, showing the finest qualities multiple outcomes. Using an optimum set of parameters, V1 (1500 rpm)- D3 (0.75 mm) and F3 (250 mm/min) Taguchi-based GRA yielded Metal removal rate: 15126.8 mm3/min and Surface roughness: 2.675 mm, which were closest to Table 11's anticipated values.

Table 11. Taguchi optimization using grey relations confirms experiments.

| Strategy | Response | Ideal condition | | %age deviation = ±(P-E)/P*100 |
|---|---|---|---|---|
| | | Value predicted optimally (P) | Value of experiment (E) | |
| Multi response optimization | Metal removal rate($mm^3$/min) | 15405.74 | 15126.8 | 1.8106 |
| | Surface roughness (μm) | 2.8134 | 2.675 | 4.9193 |

## Conclusion

This research examines AZ91 magnesium alloy machining without lubrication under various cutting conditions. The feedback factors inspected in the currently machining include surface roughness(SR) and material removal rate, together with the influence of chip shape. General linear optimization optimizes process parameters. The following major findings were made during AZ91 magnesium alloy turning.

- Increasing cutting speed reduces Metal removal rate and Surface surface. However, increasing rate of feed and cut depth increases MRR and SR simultaneously. Depth of cut is more important for MRR, whereas feed rate is most important for SR in single response optimization. Additionally, chip morphology is primarily affected by cutting speed.
- Short chips are suggested for comparing cutting applied force, quality of surface, and tool damage for varied process parameters.
- For maximum MRR, F3: 250 mm/min; V1: 1500 rpm; and D3: 0.75 mm; for minimal SR, F3: 150 mm/min; V2: 2000 rpm; and D2: 0.50 mm were tuned using Taguchi approach for single response characteristics.
- For multi-response optimization, Taguchi-based GRA recommends V1 (1500 rpm)-D3 (0.75 mm)-F3 (250 mm/min). According to GRA value analysis of variance, multi-objective optimization's most important factors are V (23.67%), D(24.60%), and F(50.91%).
- Further study may examine chip shape, surface properties, fracture density, and mechanical integrity loss to determine Mg-alloy implant turning process.

## References

[1] S. Kumar and P. Katyal, "Factors affecting biocompatibility and biodegradation of magnesium based alloys," Mater. Today Proc., vol. 52, pp. 1092--1107, 2022. https://doi.org/10.1016/j.matpr.2021.10.499.

[2] R. Kumar, P. Katyal, K. Kumar, and V. Singh, "Multiresponse optimization of end milling process parameters on ZE41A Mg alloy using Taguchi and TOPSIS approach," Materials Today, vol. 56, pp. 2497-504, 2022. https://doi.org/10.1016/j.matpr.2021.08.271.

[3] R. Kumar, P. Katyal, "Effects of alloying elements on performance of biodegradable magnesium alloy," Materials Today, vol. 50, pp. 56:2443, 2022. https://doi.org/10.1016/j.matpr.2021.08.233.

[4] T.T. Trang, J.H. Zhang, J.H. Kim, A. Zargaran, J.H. Hwang, B.C. Suh and N.J. Kim, "Designing a magnesium alloy with high strength and high formability," Nature communications, vol. 9, pp. 2522, 2018. https://doi.org/10.1038/s41467-018-04981-4.

[5] F. Witte, V. Kaese, H. Haferkamp, E. Switzer, A. Meyer-Lindenberg, C.J. Wirth and H. Windhagen, "In vivo corrosion of four magnesium alloys and the associated bone response," Biomaterials, vol. 26(17), pp. 3557-63, 2005. https://doi.org/10.1016/j.biomaterials.2004.09.049.

[6] K. Kumar, R.S. Gill and U. Batra, " Challenges and opportunities for biodegradable magnesium alloy implants," Materials technology, vol. 33(2), pp. 153-72, 2018. https://doi.org/10.1080/10667857.2017.1377973.

[7] M..P Staiger, A.M. Pietak, J. Huadmai, G. Dias, "Magnesium and its alloys as orthopedic biomaterials: a review,"Biomaterials, vol. 27(9), pp. 1728-34, 2006. https://doi.org/10.1016/j.biomaterials.2005.10.003.

[8] B.R. Sunil, K.V. Ganesh, P. Pavan, G. Vadapalli, C. Swarnalatha, P. Swapna, P. Bindukumar and G.P. Reddy, " Effect of aluminum content on machining characteristics of AZ31 and AZ91 magnesium alloys during drilling," Journal of Magnesium and alloys, vol. 4(1), pp. 15-21, 2016. https://doi.org/10.1016/j.jma.2015.10.003.

[9] M. Yasir, M. Danish, M. Mia, M.K. Gupta and M. Sarikaya, "Investigation into the surface quality and stress corrosion cracking resistance of AISI 316L stainless steel via precision end-milling operation," The International Journal of Advanced Manufacturing Technology, vol. 112, pp. 1065--76, 2021. https://doi.org/10.1007/s00170-020-06413-4.

[10] V. Singh, P. Katyal, K. Kumar and R. Kumar, "Surface integrity and biological response of Ti-alloy implants after surface modification," Materials Today, vol. 56, pp. 2451--2468, 2022. https://doi.org/10.1016/j.matpr.2021.08.235.

[11] F. Pusavec, H. Hamdi, J. Kopac and I.S. Jawahir, "Surface integrity in cryogenic machining of nickel based alloy—Inconel 718," Journal of Materials Processing Technology, vol. 211(4), pp. 773-83, 2021. https://doi.org/10.1016/j.jmatprotec.2010.12.013.

[12] R. Kumar, P. Katyal, K. Kumar and N. Sharma, "Investigating machining characteristics and degradation rate of biodegradable ZM21 magnesium alloy in end milling process," International Journal of Lightweight Materials and Manufacture, vol. 5(1), pp. 102-12, 2022. https://doi.org/10.1016/j.ijlmm.2021.11.002.

[13] S. Dutta and S.K. Narala, "Optimizing turning parameters in the machining of AM alloy using Taguchi methodology," Measurement, vol. 169, pp. 10834, 2021. https://doi.org/10.1016/j.measurement.2020.108340.

[14] C. Vasu, A.B. Andhare and R. Dumpala, " Multiobjective optimization of performance characteristics in turning of AZ91 Mg alloy using grey relational analysis," Materials Today: Proceedings, vol. 42, pp. 642-9, 2021. https://doi.org/10.1016/j.matpr.2020.11.049.

[15] M. Danish, S. Rubaiee and H. Ijaz, "Predictive modelling and multi-objective optimization of surface integrity parameters in sustainable machining processes of magnesium alloy," Materials, vol. 14(13), pp. 3547, 2021. https://doi.org/10.3390/ma14133547.

[16] R. Viswanathan, S. Ramesh, S. Maniraj and V. Subburam, " Measurement and multi-response optimization of turning parameters for magnesium alloy using hybrid combination of Taguchi-GRA-PCA technique," Measurement, vol. 159, pp. 107800, 2020. https://doi.org/10.1016/j.measurement.2020.107800.

[17] Ö. Asal, "Optimization of surface roughness in turning of AZ31 magnesium alloys with Taguchi method,"Gazi University Journal of Science Part A: Engineering and Innovation, vol. 6(1), pp. 25-32, 2019.

[18] M. Danish, T.L. Ginta, A.M. Rani, D. Carou, J.P. Davim, S. Rubaiee and S. Ghazali, " Investigation of surface integrity induced on AZ31C magnesium alloy turned under cryogenic and dry conditions," Procedia Manufacturing, vol. 41, pp. 476-83, 2019. https://doi.org/10.1016/j.promfg.2019.09.035.

[19] S. Tekumalla, M. Ajjarapu and M. Gupta, "A novel turning-induced-deformation based technique to process magnesium alloys," Metals, vol. 9(8), pp. 841, 2019. https://doi.org/10.3390/met9080841.

[20] B.B. Buldum, A. Şık, A. Akdağlı, M.B. Biçer, K. Aldaş and İ. Özkul, " ANN surface roughness prediction of AZ91D magnesium alloys in the turning process," Materials Testing, vol. 52, pp. 59(10), 2017. https://doi.org/10.3139/120.111088.

[21] X.H. Guo, L.J. Teng, W. Wang and T.T. Chen, "Study on the cutting properties about magnesium alloy when dry turning with kentanium cutting tools," Advanced Materials Research, vol. 102, pp. 653-7, 2010. https://doi.org/10.4028/www.scientific.net/AMR.102-104.653.

[22] R. Kumar, P. Katyal and S. Mandhania, "Grey relational analysis based multiresponse optimization for WEDM of ZE41A magnesium alloy," International Journal of Lightweight Materials and Manufacture, vol. 5(4), pp. 543-54, 2022. https://doi.org/10.1016/j.ijlmm.2022.06.003.

[23] M.S. Sukumar, P.V. Ramaiah and A. Nagarjuna, "Optimization and prediction of parameters in face milling of Al-6061 using Taguchi and ANN approach," Procedia Engineering, vol. 97, pp. 365-71, 2014. https://doi.org/10.1016/j.proeng.2014.12.260.

[24] S. Dinesh, V. Senthilkumar, P. Asokan and D. Arulkirubakaran, " Effect of cryogenic cooling on machinability and surface quality of bio-degradable ZK60 Mg alloy," Materials & design, vol. 87, pp. 1030-6, 2015. https://doi.org/10.1016/j.matdes.2015.08.099.

[25] E.M. Rubio, J.L. Valencia, A.J. Saá and D. Carou. (2013) , " Experimental study of the dry facing of magnesium pieces based on the surface roughness," International Journal of Precision Engineering and Manufacturing,2013, pp. 995-1001, 2013. https://doi.org/10.1007/s12541-013-0132-9.

[26] W. Akhtar, J. Sun and W. Chen, " Effect of machining parameters on surface integrity in high speed milling of super alloy GH4169/Inconel 718,"Materials and Manufacturing Processes, vol. 31(5), pp. 620-7, 2016. https://doi.org/10.1080/10426914.2014.994769.

[27] ISO 3685:1993 Tool-Life Testing with Single-Point Turning Tools. International

Organization for Standardization (ISO): Geneva, Switzerland.

[28] M. Nurhaniza, M.K. Ariffin, F. Mustapha and B.T. Baharudin, " Analyzing the Effect of Machining Parameters Setting to the Surface Roughness during End Milling of CFRP-Aluminium Composite Laminates," International Journal of Manufacturing Engineering, vol. 1, pp. 468038, 2016. https://doi.org/10.1155/2016/4680380.

[29] R. Kumar, P. Katyal and K. Kumar, " Effect of end milling process parameters and corrosion behaviour of ZE41A magnesium alloy using Taguchi based GRA," Biointerface Res. Appl. Chem, vol. 13(3), 2023. https://doi.org/10.33263/BRIAC133.214.

# NANOSTRUCTURE-INDUCED THERMOELECTRIC ENHANCEMENT IN $Bi_2Te_3$ NANORODS DESIGN, ANALYSIS, AND PERFORMANCE EVALUATION

Manish Kumar*[1], Rone[1]
*[1]Department of Mechanical engineering, EIT, Faridabad
*manishkumar@eitfaridabad.co.in

## Abstract
*Thermoelectric materials capable of efficient energy conversion near room temperature are critical for waste heat recovery applications. In this work, solution-grown $Bi_2Te_3$ nanorods were synthesized via a trioctylphosphine-assisted thermal decomposition route, and the influence of surfactant-induced nanostructuring on their thermoelectric properties was systematically investigated. Structural analysis using X-ray diffraction and Rietveld refinement confirmed the formation of rhombohedral $Bi_2Te_3$ with the emergence of $Bi_2Te_3$–BiTe nanocomposites at higher surfactant concentrations. Electron microscopy revealed one-dimensional nanorods with crystallite sizes tunable down to ~40 nm. Raman spectroscopy showed the appearance of IR-active $A_1u$ modes, indicating a ligand-induced breakdown of inversion symmetry due to the formation of sub-quintuple layers along the nanorod axis. Thermoelectric measurements demonstrated n-type conduction with a significant enhancement in Seebeck coefficient attributed to carrier energy filtering at grain boundaries and quantum confinement effects. An optimized surfactant concentration yielded a maximum power factor of 348.7 $\mu W\ m^{-1}\ K^{-2}$ at 300 K, exceeding values reported for comparable solution-processed $Bi_2Te_3$ systems. The combined effects of reduced crystallite size, controlled barrier height, and nanocomposite formation establish surfactant-engineered $Bi_2Te_3$ nanorods as promising candidates for high-performance near-room-temperature thermoelectric applications. Furthermore, the role of surfactant-mediated growth in tailoring the electronic transport and phonon scattering mechanisms was examined to understand the origin of the enhanced thermoelectric response. The presence of nanoscale interfaces and heterophase boundaries in the $Bi_2Te_3$–BiTe nanocomposites introduces additional phonon scattering centers, which can potentially suppress lattice thermal conductivity while maintaining favorable electrical transport. Such hierarchical nanostructuring provides a viable pathway for optimizing the thermoelectric figure of merit in solution-processed materials. In addition, the scalable wet-chemical synthesis approach employed in this study offers advantages in terms of cost-effectiveness, compositional control, and compatibility with large-area device fabrication. These findings highlight the importance of surfactant engineering as an effective strategy for designing nanostructured thermoelectric materials with improved performance near room temperature, thereby opening new opportunities for efficient waste heat harvesting in practical energy conversion systems.*

## Keywords
Thermoelectric materials, $Bi_2Te_3$ nanorods, Solution growth, Energy filtering, Nanocomposites.

## Introduction
Research on effective energy conversion technology has accelerated due to the world's expanding energy needs and the quick depletion of fossil fuel supplies. Waste heat accounts for a sizable portion of global energy production, especially in electronic gadgets, vehicle exhaust systems, and industrial operations. Thermoelectric (TE) materials present a viable

way to directly transform waste heat into electrical energy, allowing for solid-state power generation that is silent and free of hazardous emissions and moving parts. With a rhombohedral crystal structure made up of quintuple layers that are weakly connected by van der Waals forces, $Bi_2Te_3$ is a semiconductor with a low bandgap. Despite having a respectable Seebeck coefficient and strong electrical conductivity, bulk $Bi_2Te_3$'s very high lattice thermal conductivity prevents future advancements in thermoelectric efficiency. In order to suppress lattice thermal transport without compromising electrical characteristics, a lot of work has been done. Due to the depletion of fossil fuels and the advantages of electronic cooling devices, the quest for alternative energy sources is currently the most popular area of study. Efficient thermoelectric (TE) devices have become one of the best options for solving the energy scarcity issue because to advancements in materials synpaper methods. Without emitting any hazardous gases or byproducts, it may use waste heat to generate energy in a silent manner. The dimensionless figure of merit ZT, which is inversely proportional to κ and directly proportional to α2σ, is used to calculate the efficiency of TE devices [1-4]. Thus, to improve ZT, one must increase α2σ and decrease κ, indicating that the best TE materials should have ε and σ that are glass-like and crystal-like, respectively. It is challenging to decouple the parameters α, σ, and κe since they are intercorrelated in a bulk material due to its charge concentration [5]. Two popular methods for increasing ZT in recent years are (i) choosing a complex crystal structure that effectively scatters phonons through voids and rattlers (heavy elements occupy voids), which minimises atomic vibration frequencies [1,6]; and (ii) using nanostructuring [2,5,7-11], which reduces κL by phonons-scattering from grain boundaries (GBs) with little effect on σ. Current state-of-the-art materials based on (Bi,Sb)2Te3 can obtain a ZT value above 1 close to room temperature, indicating that Bi2Te3 has enormous potential to attain better efficiency under various situations.

The strongest covalently ionic link in the quintuple is the Bi–Te(1) bond, whereas the Bi–Te(2) bond is covalent in this [12]. There are three methods for nanostructuring: first, the particle or grain itself can be made smaller; second, nanomaterials can be added as an impurity phase to bulk or nano host materials. A significant benefit for improving ZT is that, in addition to decreasing κL on nanostructuring because of the growing number of GBs scattering phonons, α also rises as a result of quantum confinement [2,3] and carrier energy filtering [4,5,13-17]. When the particle size is too small to be similar to the electron's De Broglie wavelength, quantum confinement is typically seen. This leads to a rise in enhanced α, which is the energy difference between the Fermi level and the average mobile charge carrier energy [2,3,18]. Longer wavelength charge/heat carriers are typically filtered out when nanostructured impurities with a little different band gap than the host are inserted. This is because only charge carriers with higher energy and larger effective mass (m*) can get through the barriers at the interface [4,5,13-17]. This leads to an increase in ZT and the α/κ ratio.

## Literature Review

Because they can directly transform waste heat into electrical energy, thermoelectric materials have garnered a lot of interest as a sustainable option for energy recovery close to room temperature. Because of their small bandgap, high carrier mobility, and advantageous Seebeck coefficient, bismuth telluride ($Bi_2Te_3$) and its alloys are commonly considered benchmark materials for low- to mid-temperature applications among diverse thermoelectric systems. However, additional improvement of its thermoelectric efficiency is limited by the comparatively high lattice thermal conductivity of bulk $Bi_2Te_3$. In order to get over this restriction, a lot of research has been done on nanostructuring techniques that try to separate thermal and electrical transport. Lattice thermal conductivity can be decreased by introducing nanoscale features that improve phonon scattering at grain boundaries using methods like ball milling, melt spinning, spark plasma sintering, and solution-based synthesis. Simultaneously, it has been demonstrated that nanostructuring enhances the Seebeck coefficient via carrier energy filtering and quantum confinement. Through the selective scattering of low-energy charge carriers, the incorporation of secondary phases or nanoinclusions into the $Bi_2Te_3$ matrix improves thermoelectric performance even further.

The benefits of bottom-up chemical synthesis techniques, which provide exact control over particle size, shape, and surface chemistry, have been emphasised in recent publications. Because of their enhanced interface density and anisotropic transport characteristics, one-dimensional nanostructures like nanowires and nanorods show great promise. An efficient method for customising interfacial potential barriers and defect structures is surfactant-assisted synthesis, which has been shown to significantly increase power factor and overall thermoelectric performance.

## Experimental Section

### *Thermal decomposition technique for $Bi_2Te_3$ synpaper*

Two distinct complex solutions of sources of Bi and Te are prepared independently for the synpaper of $Bi_2Te_3$ nanorods and combined to create the nanorods, just like in a standard thermal decomposition approach for Ni NP synpaper [23,24]. In order to do this, 5 mL of oleylamine (OA, Aldrich, 70%) is mixed with 2 millimole (mmol) of Bi(NO3)2.5H2O (Aldrich, 98%) and degassed in a test tube at 140 oC for 30 minutes. This results in a yellowish Bi-OA complex. In another, a blackish Te-TOP complex is created by heating 3 mmol of TeCl4 (Alfa Aesar, 99.9%) and 2 ml of trioctylphosphene (TOP, Sigma Aldrich, 70%) in a three-necked round-bottom flask at 180 °C for 30 minutes under constant Ar-gas flow. After that, it is chilled to 100 degrees Celsius. The beginning of the synthesis of Bi2Te3 NPs is then confirmed by injecting the Bi-OA complex at 140 oC into the Te-TOP complex (at <100 oC), which results in a black precipitate (ppt). After that, the reaction temperature is raised to 220 °C and kept there for 1.5 hours while Ar gas is continuously flowing. After cooling to 27 degrees Celsius, a large amount of n-hexane (20–25 mL) is added. For 12 minutes, the fluid is centrifuged immediately at 12,000 rpm.

### *Polyol technique for $Bi_2Te_3$ synpaper*

One sample is made using the straightforward polyol approach [7] without the use of any extra complicated surfactant because both TOP and OA are surfactants with lengthy hydrocarbon chains. Using a standard procedure, 50 mL of diethylene glycol (DEG, ≥98.5%) in a three-neck round-bottom flask containing 2 millimoles (mmol) of Bi(NO3)2.5H2O (98%, Aldrich) and 3 mmol of K2O3Te.H2O (97%, Alfa Aesar) are heated at a rate of 6 ℃/min to 220-230 ℃ for two hours. A constant flow of N2-gas is kept in order to avoid any oxidation. At or above 220 degrees Celsius, a black precipitate (ppt) began to form, suggesting that Bi2Te3 may occur above this temperature. After allowing it to cool naturally, the chilled product is centrifuged for 12 minutes at 1200 rpm. After removing the supernatant, the black ppt is suspended in ethanol and subjected to a 5-minute sonication utilizing probe ultrasonication to ensure uniform dispersion. These washing procedures are repeated twice with a 4-minute centrifugation and a 2-minute sonication in between to completely remove DEG. The PowerPoint is then given time to calm down. After decantation, the ethanol is eliminated, and the ppt is vacuum-dried for three hours at 60 degrees Celsius. The powder sample that is produced is immediately used for additional characterizations.

### *Removal of ligands from Bi2Te3 NPs made using the thermal breakdown technique*

A typical ligand removal procedure involves two precipitation processes to further purify the black precipitate (ppt) of Bi2Te3 nanoparticles after they have been washed (using hexane and ethanol). Following a 2-minute ultrasonication of approximately 800 mg of Bi2Te3 ppt in 20 mL of 90% Aldrich oleic acid, stirring is continued for the entire night. Oleic acid is eliminated by centrifuging the mixture for four minutes at 12,000 rpm, discarding the supernatant, and then washing the resulting material twice with n-hexane. Second, a two-phase system is created by dissolving the resultant ppt in a 1:1 mixture of fresh n-hexane (20 mL) and hydrazine hydrate (20 mL). This solution, which contains insoluble black ppt, is ultrasonically agitated for two minutes and stirred overnight to ensure adequate mixing. The supernatant is then extracted once more following centrifugation at 12,000 rpm for 4 minutes, and ppt is recovered using new hydrazine. Again, for homogeneous dispersion, a 2-minute ultrasonification is carried out, followed by a 30-minute wait, and after the supernatant is decanted, the ppt is extracted. After two washes, fresh ethanol is finally applied. It is subsequently vacuum-dried for two hours at 60°C. These powder samples are utilised straight away for additional characterisations. Their electrical resistivity and Seebeck coefficient data are gathered using four linear point contact resistivity measurements in a specially made, commercially available Dewar [28] and a load-based thermopower measurement setup utilising the differential direct current approach [27].

## Results and Discussion

### *X-ray diffraction and energy dispersive X-ray analysis*

Bi2Te3 NPs' powder X-ray diffraction (XRD) patterns, which were made with varying amounts of TOP (Fig. 3.1a), closely resemble JCPDS#892009 of rhombohedral crystal-structured Bi2Te3 with space group R-3m. There is no detection of the peaks that match to any impurity phases. Using Rietveld refinement fitting with necessary initial parameters derived from the literature, the phase purity of the resultant products is investigated [29]. The characteristics required to characterise the rhombohedral crystal structure of Bi2Te3 are determined from the Rietveld refinement of BTp, which is displayed in Fig. 3.1b (Table 7.1). These cell parameters (Table 7.1) closely resemble bulk values [29–31]. The CIF file from the refinement of BTp is used to create a representative crystal structure of a unit cell using VESTA [32] software in order to better understand the bond length and bond angle between Bi and Te in rhombohedral symmetry (Fig. 3.1 c,d). In this case, Te can occupy two distinct positions 6c (0, 0, 0.209) for Te1 and 3a (0, 0, 0) for Te2, but Bi only occupies one Wyckoff (Z = 3) position 6c (0, 0, 0.4) [30, 31]. The bond lengths between Te1-Bi, Te2-Bi, and Te1-Te2 are 3.063(4) Å, 3.255(3) Å, and 3.639(4) Å; the angles between Bi-Te1-Bi, Te2-Bi-Te2, and Te1-Te1-Te1 are 91.39(1)o, 84.66(9)o, and 74.01(8)o, respectively, are quite similar to those of bulk Bi2Te3 [30,31].In this, five alternate layers of Bi and Te atoms of the -Te1-Bi-Te2-Bi-Te1- form constitute a layered structure along c axis in which atoms are bonded with covalent bond and known as quintuple. This quintuple is bonded with other nearby quintuples with van der Waal (vdW) forces along c-axis (Fig. 3.1d). These arrangements of quintuples make it highly anisotropic and suitable for TE applications.

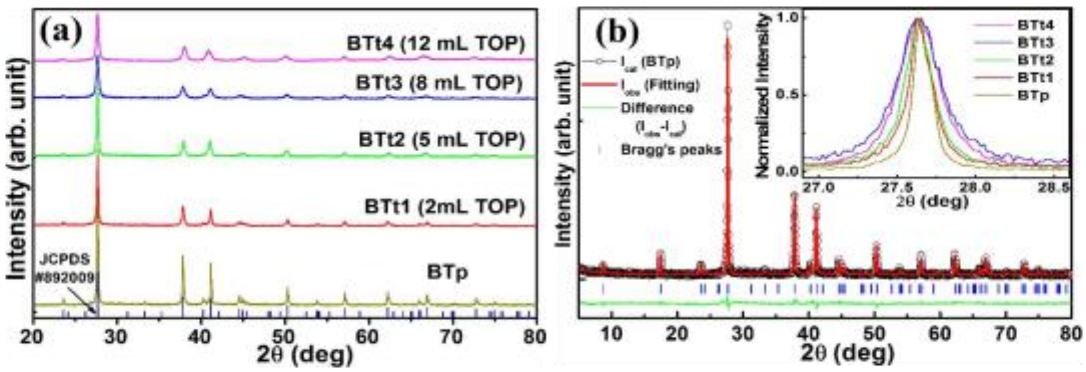

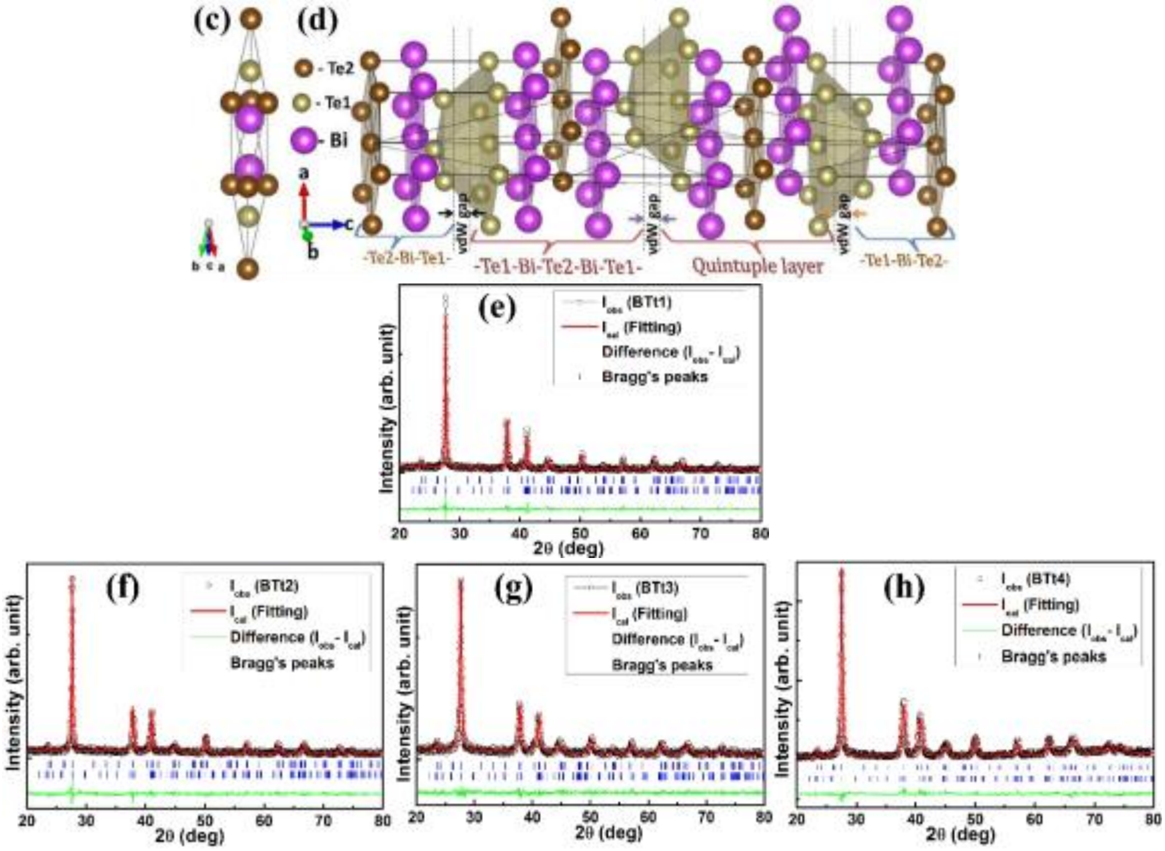


Figure 1. BTp, BTt1, BTt2, BTt3, and BTt4 powder X-ray diffraction; (b) Rietveld refinement of BTp nanoparticle (Inset: Normalised peaks of the most prominent peak for all samples); (c) rhombohedral unit cell of Bi2Te3 without taking any atoms outside of unit cell; (d) the quintuple representation of layered hexagonal structure of Bi2Te3, with dotted lines showing the rhombohedral cell and van der Waal gap (vdW gap); and (e-h) dual-phase Rietveld refinement of BTt1, BTt2, BTt3, and BTt.

Table 1 calculated crystallite size and mass density for every sample, and obtained cell characteristics for both phases, rhombohedral (R) Bi2Te3 and hexagonal (H) BiTe, with corresponding errors mentioned in the study.

Table 1. A comparison of the main technological elements in Industry 5.0 smart manufacturing systems.

| Sample | TOP Concentration (mL) | Crystallite Size (nm) | Seebeck Coefficient (µV/K) | Electrical Resistivity (mΩ·cm) | Power Factor (µW m⁻¹ K⁻²) | Relative Density (%) |
|---|---|---|---|---|---|---|
| BTp | 0 | 62 | -108 | 0.85 | 210 | 89 |
| BTt1 | 2 | 48 | -132 | 1.05 | 265 | 88 |
| BTt2 | 5 | 41 | -152 | 1.12 | 340 | 86 |
| BTt3 | 8 | 30 | -165 | 1.45 | 295 | 82 |
| BTt4 | 12 | 28 | -178 | 1.85 | 255 | 77 |

## Conclusion

Several approaches have been used to characterize the Bi2Te3 nanorods that were successfully synthesized utilizing the thermal decomposition method, and their thermoelectric properties have been examined. The conversion of single phase Bi2Te3 into BiTe-Bi2Te3 nanocomposites with increasing TOP concentration was verified by their Rietveld refinement. The stoichiometric production of Bi2Te3 is revealed by Raman spectra analysis, which also supports a regular decrease in crystallite size found in XRD. For the first time, Bi2Te3 nanorods' inversion symmetry is broken by ligands. FTIR is used to investigate if ligands are present on the surface of as-synthesized NPs. Utilizing XRD, TEM, FESEM, and DLS, the development of particle size with TOP concentration was examined. The production of ligand-capped Bi2Te3 with varying thicknesses is compatible with zeta potential measurements. Together with electrical resistivity and Hall measurements, the thermopower analysis verified that these nanocomposites are n-type semiconductors.

## References

[1] F. J. DiSalvo, Science 285, 703 (1999).
[2] B. Poudel, Q. Hao, Y. Ma, Y. C. Lan, A. Minnich, B. Yu, X. A. Yan, D. Z. Wang, A. Muto, D. Vashaee, et al. Science 320, 634 (2008).
[3] L. D. Hicks and M. S. Dresselhaus, Phys. Rev. B 47, 12727 (1993).
[4] S. V. Faleev and F. Leonard, Phys. Rev. B 77, 214304 (2008).
[5] Tarachand, S. Hussain, N. P. Lalla, Y.-K. Kuo, A. Lakhani, V. G. Sathe, U. Deshpande and G. S. Okram, Phys.Chem.Chem.Phys. 20, 5926 (2018).
[6] X. Shi, J. Yang, J. R. Salvador, M. Chi, J. Y. Cho, H. Wang, S. Bai, J. Yang, W. Zhangand L. Chen, Multiple-filled skutterudites: J. Am. Chem. Soc. 133, 7837 (2011).
[7] A. Soni, Z. Yanyuan, Y. Ligen, M. K. K. Aik, M. S. Dresselhaus and Q. Xiong, Nano Lett. 12, 1203 (2012).
[8] G. Zhang, B. Kirk, L. A. Jauregui, H. Yang, X. Xu, Y. P. Chen and Y. Wu, Nano Lett.12, 56 (2011).
[9] S. Sumithra, N. J. Takas, D. K. Misra, W. M. Nolting, P. F. P. Poudeu and K. L. Stokes, Adv. Energy Mater. 1, 1141 (2011).
[10] R. J. Mehta, Y. Zhang, C. Karthik, B. Singh, R. W. Siegel, T. Borca-Tasciuc, G. Ramanath, Nat. Mater. 11, 233 (2012).
[11] M. Scheele, N. Oeschler, K. Meier, A. Kornowski, C. Klinke, and H. Weller, Adv.Funct. Mater. 19, 3476 (2009).
[12] K. M. F. Shahil, M. Z. Hossain, V. Goyal and A. A. Balandin, J. Appl. Phys. 111, 1-8 (2012).
[13] M. Liu and X. Y. Qin, Appl. Phys. Lett. 101, 132103 (2012).
[14] J. Martin, L. Wang, L. Chen, and G. S. Nolas, Phys. Rev. B 79, 115311 (2009).
[15] S. Hwang, S.-I. Kim, K. Ahn, J. W. Roh, D.-J. Yang. S.-M. Lee and K.-H. Lee, J.Electronic Mater. 42, 1411 (2013).
[16] Tarachand, V. Sharma, R. Bhatt, V. Ganesan and G. S. Okram, Nano Research 9, 3291 (2016).
[17] Y. C. Dou, X. Y. Qin, D. Li, L. L. Li, T. H. Zou and Q. Q. Wang, J. Appl. Phys. 114, 044906 (2013).
[18] J. Chen, T. Sun, D. H. Sim, H. Peng, H. Wang, S. Fan, H. H. Hng, J. Ma, F. Y. C.Boey, S. Li, et al., Chem. Mater. 22, 3086 (2010).
[19] G. Yuan, Y. Li, N. Bao, J. Miao, C. Ge,Y. Wang, Mater. Chem. Phys. 143, 587 (2014).
[20] B. Madavali, H. S. Kim, K. H. Lee, and S. J. Hong, J. Appl. Phys. 121, 225104 (2017).
[21] W. J. Xie, X. F. Tang, Y. G. Yan, Q. J. Zhang, and T. M. Tritt, J. Appl. Phys. 105, 113713 (2009).
[22] A. Purkayastha, F. Lupo, S. Kim, T. Borca-Tasciuc, and G. Ramanath, Adv. Mater.18,

496 (2006).
[23] J. Singh, Tarachand, S. S. Samatham, D. Venkateshwarlu, Netram Kaurav, V. Ganesan and G. S. Okram, Appl. Phys. Lett. 111, 201904 (2017).
[24] Tarachand, V. Sharma, J. Singh, C. Nayak, D. Bhattacharyya, N. Kaurav, S. N. Jha and G. S. Okram, J. Phys. Chem. C 120, 28354 (2016).
[25] K. Wang, H.-W. Liang, W.-T. Yao, S.-H. Yu, J. Mater. Chem. 21, 15057 (2011).
[26] Y. Zhao, J. S. Dyck, B. M. Hernandez, C. Burda, J. Phys. Chem. C 114, 11607 (2010).
[27] Tarachand, M. Saxena, B. Mukherjee and G. S. Okram, Rev. Sci. Instrum. 90, 063904 (2019).
[28] A. Soni and G. S. Okram, Rev. Sci. Instrum. 79, 125103 (2008).
[29] S. Nakajima, J. Phys. Chem. Solids 24, 479 (1963).
[30] Y. Feutelais, B. Legendre, N. Rodier, V. Agafonov, Mat. Res. Bull., 28, 591 (1993).
[31] M. Gharsallah, F. Serrano-Sánchez, J. Bermúdez, N. M. Nemes, J. L. Martínez, F. Elhalouani and J. A. Alonso, Nanoscale Res. Lett. 11, 142 (2016).
[32] K. Momma and F. Izumi, J. Appl. Crystallogr. 44, 1272 (2011).

# GREEN SYNTHESIS OF SILVER NANOPARTICLES USING AZADIRACHTA INDICA LEAF EXTRACT: STRUCTURAL AND OPTICAL CHARACTERIZATION

Abhishek Sharma*[1], Agriya Mukherjee[1], Krishna Tewatia[1], Anuradha Sharma[1]
*[1]J.C. Bose University of Science & Technology, YMCA, Faridabad, Haryana, India
*abhishekstudyvlogs@gmail.com

## Abstract
*This study offers an eco-friendly and sustainable approach for the synthesis of silver nanoparticles (AgNPs) using Azadirachta indica (neem) leaf extract as a reducing and stabilizing agent, eliminating the need for toxic chemicals commonly used in conventional methods. The formation of AgNPs was initially indicated by a visible colour change in the reaction mixture from pale yellow to dark brown. UV–visible spectroscopy further confirmed nanoparticle synthesis through a characteristic Surface Plasmon Resonance peak at 438 nm. Scanning Electron Microscopy (SEM) analysis revealed a clustered morphology, attributed to nanoparticle aggregation during sample preparation, while confirming the presence of Nano scale particles. The particle size was estimated to range between 15–30 nm, consistent with previously reported findings. The optical band gap, determined using Tauc's plot, was approximately 2.49 eV, indicating the influence of Nano scale dimensions on electronic properties. The results demonstrate that neem-mediated synthesis yields stable and functional AgNPs with desirable structural and optical characteristics. This method provides a simple, reproducible, and scalable strategy for nanoparticle fabrication, with potential applications in biomedical, environmental, and industrial fields. The study contributes to the advancement of green nanotechnology by offering an efficient and sustainable synthesis route.*

## Keywords
Green synthesis, Silver nanoparticles, Azadirachta indica, UV–Vis spectroscopy, Optical band gap.

## Introduction
Nanotechnology is rapidly growing field due to its ability to change materials property at the Nano scale, where unique physical, chemical, and biological properties are seen. At this scale, material shows enhanced surface area, quantum effects, and improved reactivity, making them highly suitable for applications in medicine, electronics and environmental remediation [1], [2]. Among various nanomaterial, silver nanomaterial (AgNPs) have gain high attention because of their unexpected antimicrobial, electrical, and optical properties. Even all metal nanoparticles have received considerable attention in recent years because of their unique properties and potential applications in catalysis, photonics, optoelectronics, biological tagging and pharmaceutical applications. Their performance depends critically on their size, shape and composition [3]. Their high surface area to volume ratio enables strong interaction with biological systems, which has applications in drug delivery, bio-sensing, and water purification [4]. On the other hand traditional methods for synthesizing nanoparticles, such as chemical reduction and physical techniques, involves toxic chemicals, high energy consumption, and complex instrumentation. These drawbacks raise concerns towards environmental safety and sustainability [5], [6]. To overcome these problems green synthesis is a better alternative that utilizes biological systems such as plant extract, bacteria, and fungi. This approach cuts off the need of hazardous reagents making it cost effective and sustainable [1], [7]. Due to presence of bioactive compounds such as flavonoids, terpenoids, and

polyphenols, which act as both reducing and stabilizing agents [1], [8]. Among various plants, Azadirachta indica (neem) is widely used for its rich photochemical composition and medicinal properties. Neem leaf extract contains compounds such as quercetin, Azadirachta, and nimbolide, which facilitate efficient reduction of silver ions and stabilization of nanoparticles [5], [9]. Although it has advantages, neem based synthesis is not without limitations. Some studies have noted inconsistency in particle size depending on leaf age, extract concentration and pH [10], also some pointed out the need for better purification technique and stability under storage [11]. Neem AgNPs have also promise as an antibacterial agent effective against MDR pathogens [12]. Nanoparticle-bound drugs are easily suspended in liquids and are able to penetrate deep in organs and tissues [13]. But still several gaps still exist in current literature like, lack of standardized protocols for neem based AgNP synthesis, scalability and stability under practical conditions remain underexplored [14],15. Therefore this study aims to develop an efficient, systematic, reproducible and sustainable method for the synthesis of silver nanoparticles using Azadirachta indica (neem) leaf extract, and to characterize their structural, optical, and biological properties. All this study will help to find the biological potential of synthesized AgNPs, focusing on their antimicrobial, antioxidant, or cytotoxic activity and scalability for possible future biomedical or environmental applications [16], [17].

## Experimental Details

Fresh leaves of Azadirachta indica (neem), analytical grade silver nitrate ($AgNO_3$), distilled water, 70% ethanol, and filter paper were used for the green synthesis of silver nanoparticles. Neem leaves were washed thoroughly with distilled water to remove impurities and air-dried for 30–60 minutes. Approximately 20 g of dried leaves were ground and boiled in 100 mL distilled water at 60–70°C for 15 minutes. The mixture was cooled and filtered to obtain a clear extract, which was stored at 4°C.
Silver nanoparticles were synthesized using the neem extract, which acted as both reducing and stabilizing agent, converting $Ag^+$ ions into $Ag^0$ nanoparticles [18],[19]. Formation of nanoparticles was indicated by a colour change in the reaction mixture. The synthesized nanoparticles were purified and characterized using standard techniques such as UV–Visible spectroscopy and scanning electron microscopy (SEM) to determine their optical properties, size, and morphology, consistent with reported green synthesis methods.

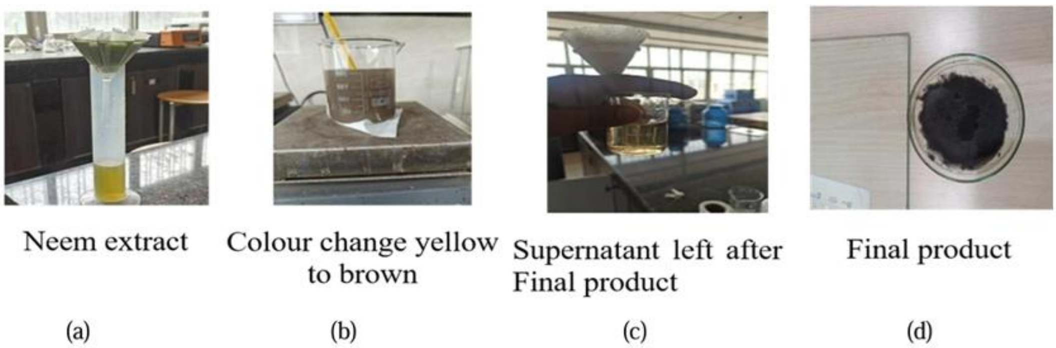


Figure 1. Synthesis process.

### *Green synthesis of silver nanoparticles*

A 0.01 M silver nitrate (AgNO3) solution was prepared using distilled water. For synthesis, 10ml of neem extract was added drop wise into 50ml of AgNO3 in interval of 5 seconds under continuous stirring at 50 - 60°C and was stirred for 30 minutes to ensure complete mixing and reduction. The formation of AgNPs firstly indicated by visible colour change from pale yellow to brown [18] (Figure 1(b)). Then mixture was left to cool down at room temperature to allow complete synthesis and stabilization of nanoparticles.

### *Purification of Silver Nanoparticles*

The synthesized silver nanoparticles were purified using ethanol-assisted centrifugation. The process involved the following steps:

- The synthesized colloidal silver nanoparticle solution was first mixed with 70% ethanol in a 1:1 volume ratio, transferred into sterile centrifuge tubes, and centrifuged at 7,000 rpm for 15 minutes to obtain a pellet.
- Then the supernatant (figure 1(c)) was carefully separated without disturbing the pellet and the pellet was washed again with 70% ethanol; the suspension was centrifuged again at 7,000 rpm for 15 minutes to obtain a pellet.
- The dried nanoparticles were then stored in sterile containers (figure 1(d)) for further analysis.

## Characterization techniques

### *UV- Visible spectroscopy*

The formation of silver nanoparticles was confirmed by analysing the colloidal solution using UV- Visible spectroscopy in the range of 300 – 700 nm. The surface Plasmon resonance (SPR) peak observed near 438 nm indicated successful nanoparticle formation.

(a) (b)

Figure 2. (a) Inside view (b) Outer view of UV-Visible Spectrometer.

### *Scanning Electron Microscopy (SEM)*

SEM (Figure 3) was used to examine the morphology, shape and size distribution of the synthesized nanoparticles. The dried sample were coated with gold to improve conductivity for imaging.


Figure 3. SEM (Scanning Electron Microscope).

## Characterization techniques

### *UV-Visible Spectroscopy Observations*

The UV-Visible spectrum was recorded between 300 and 800 nm (Figure 4(a)). A distinct absorption peak was observed at 438 nm, confirming the formation of silver nanoparticles through SPR. The solution remained stable and no significant shift was observed upon repeated measurement, suggesting good particle stability. However a biological Nano synthesis system is always less controllable compared to chemical methods [13], [14]. The sharpness and symmetry of the peak indicate a relatively uniform size distribution of nanoparticles.

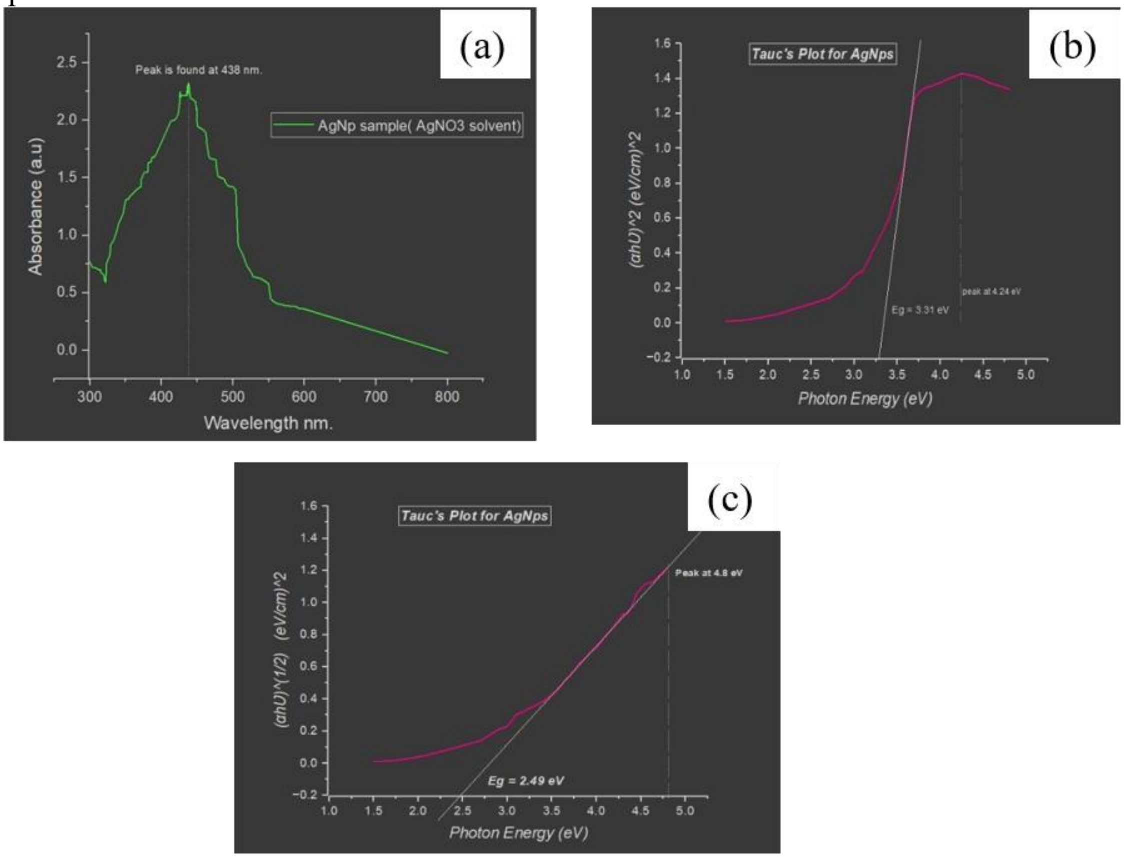


Figure 4. (a) UV-Visible spectrum (b) Tauc's Plot for direct band Gap and (c) for indirect band Gap for AgNPs.

Using UV–Visible spectroscopy data, a Tauc's plot was constructed to estimate the optical band gap of the biosynthesized silver nanoparticles. The calculated band gap values were approximately 2.49 eV for direct allowed transitions (Figure 4(b)) and 3.31 eV for indirect allowed transitions (Figure 4(c)). These values are in close agreement with previously reported studies, where biosynthesized AgNPs typically exhibit band gaps in the range of 2.4–3.3 eV depending on particle size and synthesis conditions [14], [18]. The results confirm the semiconducting nature of the nanoparticles and highlight their size-dependent optical properties and potential applications.

### *Scanning Electron Microscopy (SEM) Observations*

SEM micrographs (figure 4.) showed an irregular size distribution of particles, formation of particle clusters, which generally observed in green synthesized nanoparticle due to capping done by phytochemicals present in neem extract [15],[18].

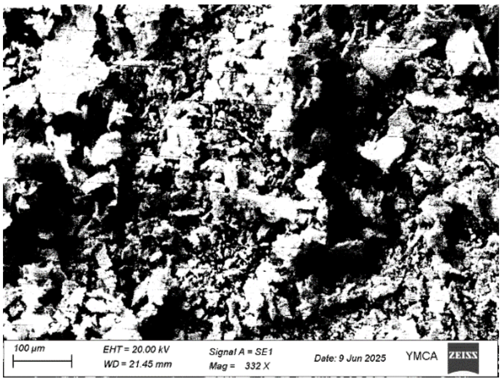


Figure 4. SEM at 100 µm.

## Conclusion

The present study successfully established a simple, effective, and environmentally friendly method for synthesizing silver nanoparticles utilizing Azadirachta indica (neem) leaf extract, which functioned both as a reducing and stabilizing agent. The synthesis was carried out under mild experimental conditions, avoiding the use of hazardous chemicals, aggressive reducing agents, or complex instrumentation. This green synthesis route provides a sustainable alternative to conventional chemical synthesis, aligning with global efforts to advance environmentally conscious nanotechnology. During the synthesis, the reduction of silver nitrate to silver nanoparticles was visually monitored through a gradual colour transformation from pale yellow to dark brown, serving as an initial indication of nanoparticle formation. The successful generation of nanoparticles was subsequently confirmed and thoroughly analysed through a series of characterization techniques. The UV-Visible spectroscopy revealed a prominent Surface Plasmon Resonance (SPR) peak at 438 nm, characteristic of silver nanoparticles, indicating successful synthesis and excellent colloidal stability with minimal particle aggregation. Analysis using Tauc's plot, derived from UV-Vis data, estimated the optical band gap of the nanoparticles to be approximately 2.49 eV, reflecting the influence of Nano scale size and modified electronic properties. Overall, this study not only validated the potential of neem extract for green synthesis but also demonstrated a reproducible, cost-effective, and scalable method for silver nanoparticle production. The approach offers multiple benefits, including simplicity, environmental safety, economic viability, and suitability for large-scale manufacturing.

## References

[1] Ahmed, S., et al. (2016). A review on plants extract mediated synthesis of silver nanoparticles for antimicrobial applications: A green expertise. Journal of Advanced Research, 7(1), 17–28. https://doi.org/10.1016/j.jare.2015.02.007

[2] Irvine, S. (2014). Green synthesis of metal nanoparticles using plants. Green Chemistry, 16(6), 2638–2650. https://doi.org/10.1039/C3GC41886H

[3] Begum, N. A., et al. (2009). Biogenic synthesis of Au and Ag nanoparticles using aqueous solutions of black tea leaf extracts. Colloids and Surfaces B: Bio interfaces, 71(1), 113–118. https://doi.org/10.1016/j.colsurfb.2009.01.012

[4] Ray, M., et al. (2009). Silver nanoparticles as a new generation of antimicrobials. Biotechnology Advances, https://doi.org/10.1016/j.biotechadv.2008.09.002 27(1), 76–83.

[5] Song, J. Y., & Kim, B. S. (2009). Rapid biological synthesis of silver nanoparticles using plant leaf extracts. Bioprocess and Bio systems engineering, 32(1), 79–84. https://doi.org/10.1007/s00449-008-0224-6

[6] Bar, H., et al. (2009). Green synthesis of silver nanoparticles using latex of Atrophy

carcass. Colloids and Surfaces A: Physicochemical and Engineering Aspects, 339(1–3), 134–139. https://doi.org/10.1016/j.colsurfa.2009.02.008

[7] Mittal, A. K., et al. (2013). Synthesis of metallic nanoparticles using plant extracts. Biotechnology Advances, https://doi.org/10.1016/j.biotechadv.2013.01.00331(2), 346–356.

[8] Roy, P., et al. (2017). Green synthesis of silver nanoparticles using Azadirachta indica leaf extract and its antimicrobial study. Applied Nano science, 7(8), 843–850. https://doi.org/10.1007/s13204-017-0621-8

[9] Vera, A., & Mehta, M. S. (2016). Controllable synthesis of silver nanoparticles using neem leaves and their antimicrobial activity. Journal of Radiation Research and Applied https://doi.org/10.1016/j.jrras.2015.11.001Sciences, 9(1), 109–115.

[10] Rajesh Kumar, S., & Naik, P. (2014). Synthesis and biomedical applications of silver nanoparticles using Azadirachta indica (neem) bark extract. Journal of Nano materials, 2014, Article ID 476810. https://doi.org/10.1155/2014/476810

[11] Kumara, S. A., et al. (2022). Biosynthesis of silver nanoparticles using Azadirachta indica and their antioxidant and anticancer effects in cell lines. Micro machines, 13(9), 1416. https://doi.org/10.3390/mi13091416

[12] Alqahtani, O., et al. (2022). In vitro antibacterial activity of green synthesized silver nanoparticles using Azadirachta indica aqueous leaf extract against MDR pathogens. Molecules, 27(21), 7244. https://doi.org/10.3390/molecules27217244

[13] Bhatt, R. S., et al. (2019). Biosynthesis of silver nanoparticles using Azadirachta indica leaves: Characterisation and impact on Staphylococcus aureus. IET Nano biotechnology, 13(5), 498–502. https://doi.org/10.1049/iet-nbt.2018.51333

[14] Prathna, T. C., et al. (2011). Kinetic evolution studies of silver nanoparticles in a bio-based green synthesis process. Colloids and Surfaces A: Physicochemical and Engineering Aspects, https://doi.org/10.1016/j.colsurfa.2011.01.027377(1–3), 212–216.

[15] Kharat, S. N., & Mendhulkar, V. D. (2016). Synthesis of silver nanoparticles by using Azadirachta indica leaf extract at room temperature. International Journal of Biological Macromolecules, https://doi.org/10.1016/j.ijbiomac.2015.11.00284 , 298–301.

[16] Ramar, K., et al. (2019). Environmental and antimicrobial properties of silver nanoparticles synthesized using Azadirachta indica leaves. SN Applied Sciences, 1(1), Article 128. https://doi.org/10.1007/s42452-018-0143-3

[17] Chand, K., et al. (2019). Green synthesis and antimicrobial activity of silver nanoparticles using extracts of neem, onion, and tomato. RSC Advances, 9(30), 17002–17015. https://doi.org/10.1039/C9RA01407A

[18] Shankar, S. S., et al. (2004). Rapid synthesis of Au, Ag, and bimetallic Au core Ag shell nanoparticles using neem leaf broth. Journal of Colloid and Interface Science, 275(2), 496–502. https://doi.org/10.1016/j.jcis.2004.03.003

[33] Jena, S., et al. (2019). Green synthesis of silver nanoparticles using Azadirachta indica and Ocimum sanctum leaf extract. Current Science, 117(8), 1300–1308.

# DESIGN AND DEVELOPMENT OF LIFTER NOVA: AN IOT-BASED SMART ROBOTIC SYSTEM FOR AUTOMATED MATERIAL HANDLING

Avinash Raj Sinha*[1], Kameshwar Chaudhary[1], Pravin Kumar Singh[1], Viveksheel Yadav[1]
*[1]Department of Mechanical Engineering, Galgotias University, Greater Noida, India
* pravinsingh.phd@gmail.com

## Abstract

*The ESP32 microcontroller facilitates real- me control, wireless communication, and remote monitoring. The adaptable gripping assembly enhances versatility in object handling. The invention reduces manual effort, improves operational accuracy, and provides IOT- based monitoring capabilities. The system is suitable for educational institutions, offices, laboratories, and small- scale industries, offering scalable and efficient smart material handling solutions. ESP32 microcontroller allows real-me control, wireless communication and remote monitoring. Flexible / gripping assembly allows ease the handling of objects. This invention minimizes manual work and ensures operational accuracy as well as IOT-based monitoring. Its smart automation can suffice material handling solutions for educational institutes, offices, labs, and small-scale conveying needs.*

## Keywords

Adaptive Multi-Geometry Robotic Gripper, Intelligent Material Handling Robot, Gripping Force Optimization and Control, Mechatronic System Prototype Development.

## Introduction

Material handling and lifting mechanisms have been part of human civilization in some form or other since ancient days. Early societies created rudimentary contraptions like levers, pulleys and inclined planes that helped transport heavy objects with less energy. The crane would be among the oldest known lifting system, used in Greece and Rome; pulley blocks and windlasses were used to raise construction materials for monuments or buildings. In the Industrial Revolution (18th–19th century), lifting mechanisms – achieved by steam-powered hoists, mechanical jacks and gear-driven lifting systems – underwent significant evolution. These advancements allowed industries to manage more significant loads with improved efficiency and accuracy.

Because of its ease of use, dependability, and precise linear motion conversion, the rack and pinion system is one of the most popular lifting mechanisms. This mechanism allows for controlled vertical or horizontal movement by converting a pinion gear's rotational motion into a rack's linear motion. When precise positioning is needed, rack and pinion drives are frequently used in automated industrial systems, lifting tables, elevators, and machine tools [4]. This mechanism is appropriate for contemporary automated lifting devices because it can provide controlled displacement with low slippage.

Lifting systems have changed from being solely mechanical structures to becoming electromechanical and intelligent systems as automation and robotics have advanced. To handle loads in manufacturing settings, industrial automation introduced robotic manipulators, sensors, and programmable logic controllers (PLCs). Conventional lifting devices have been further transformed into intelligent, networked systems with data-driven decision-making, remote operation, and real-time monitoring thanks to the Internet of Things (IoT) in recent years. These systems can communicate with networks thanks to microcontrollers and wireless communication modules, which improve operational effectiveness and security.

Compact and intelligent material handling systems are frequently needed in modern indoor settings like offices, labs, schools, and small-scale industries. Large industries typically use bulky, costly, and inappropriate traditional lifting equipment for cramped interior spaces. The need for automated and safer alternatives is further highlighted by the ergonomic risks, physical strain, and workplace injuries that can result from manual object lifting . Consequently, the need for small robotic lifting solutions that incorporate sensing, navigation, and communication technologies is growing.

The ESP32, which supports wireless connectivity, real-time control, and IoT integration within a small hardware footprint, is one example of a powerful yet affordable microcontroller made possible by recent developments in embedded systems. Robotic platforms can follow predetermined routes using machine navigation techniques like QR-code-based path guidance, which eliminate the need for costly sensors or intricate mapping algorithms. This method keeps operational efficiency and dependable positioning while streamlining indoor navigation.

In this regard, the current invention presents "Lifter NOVA," a smart robotic weight-lifting system enabled by the Internet of Things. The suggested system combines a flexible gripping fixture that can handle objects of various sizes and shapes with an ESP32 microcontroller-based control architecture, a rack-and-pinion-based vertical lifting mechanism, and QR-code-guided navigation. The design seeks to offer a small, economical, and clever indoor material handling solution. The system lowers manual effort, increases ergonomic safety, and boosts operational accuracy by fusing mechanical precision with IoT-enabled monitoring and control. When effective and scalable material handling solutions are needed, such a system may find use in offices, labs, educational institutions, and small-scale businesses.

## Methodology

Mechanical design, embedded electronics, and Internet of Things-based control architecture are all integrated in the development of the Lifter NOVA smart robotic weight-lifting system. The system's goal is to create a small robotic platform that can lift and move light objects in indoor settings like offices, labs, and educational institutions. To accomplish controlled and automated material handling, the system combines a rack-and-pinion lifting mechanism, an ESP32 microcontroller-based control unit, and QR-code-based navigation.

### *Mechanical Design*

A rigid base frame, a vertical lifting assembly, a mobile drive system, and an adaptive gripping fixture make up the Lifter NOVA robot's mechanical structure. Lightweight aluminum or mild steel components are used in the construction of the robot's frame to guarantee adequate structural strength while keeping the system weight under control. In order to minimize friction and mechanical wear during operation, shafts, gears, and structural members must be properly aligned.

The rack and pinion system that powers the vertical lifting mechanism transforms the DC motor's rotational motion into linear vertical displacement. The lifting platform moves upward or downward as a result of the pinion gear's rotation engaging with the rack teeth. During lifting operations, this mechanism offers accurate control, stable load handling, and dependable positioning.

The robot's ability to lift things depends on the torque of the motor, the gear ratio, and how well the rack and pinion work. If the motor is rated at 100 W and the overall mechanical efficiency is 70%, the effective lifting power is about 70 W.

The robot needs to be able to lift 10 kg, which means it needs to be able to lift this much weight:

F = m × g = 0.5 × 9.81 = 4.9" N"

The lifting assembly is on a stable chassis that is held up by wheels, which lets the robot move around in indoor work areas. The motors, electronic control units, and power supply parts are all inside the base platform. The Lifter Nova is shown from different angles in Figure 1. The design was made using Solid Works Software.

### *Adaptive Gripping Mechanism*

The robot has a flexible gripping fixture that can hold things of all shapes and sizes. The gripping unit is the robotic system's end-effector and can hold cylindrical, rectangular, and oddly shaped objects. The gripper mechanism has adjustable arms that make it easy to hold onto things without them slipping while you lift them.

This adaptive gripping system makes the robot more flexible by letting it pick up different kinds of materials that are often found in labs, offices, or small factories. Motor actuation controls the gripping force, which makes sure that the load stays stable while it is being lifted and moved.

Figure 1. Various views of Lifter NOVA.

### *Electronic Control System*

The ESP32 microcontroller is the most important part of the Lifter NOVA system's electronic control architecture. The ESP32 controls the communication modules, sensors, drive motors, and lifting motors. The controller lets you communicate wirelessly and keep an eye on how the system is working from a distance because it has built-in Wi-Fi and Bluetooth.

Motor driver modules control the speed and direction of the DC motors that move the robot and lift things. A regulated power supply makes sure that the voltage levels for the microcontroller and other electronic parts are safe and stable. The system also has sensors, like ultrasonic sensors that measure distance and find obstacles, which make moving around safer.

***QR-Code Based Navigation***

The robot uses a path identification system guided by QR codes for indoor navigation. In the operating environment, QR codes are positioned at particular spots on the walls or floor. These QR codes are detected by a camera or scanning module installed on the robot, which then recognises the location data they contain.

The robot can follow predetermined paths using this navigation method without the need for pricey navigation sensors or intricate mapping algorithms. The QR-based guidance system is appropriate for controlled environments like labs and warehouses because it offers a straight forward and dependable way for structured indoor navigation.

## Experimental Setup

The purpose of the experimental setup was to assess the Lifter NOVA prototype's gripping efficiency, lifting performance, and navigational capability. A mobile base platform, a rack-and-pinion lifting assembly, an ESP32 control module, DC motors, motor drivers, and an adaptable gripper mechanism make up the robot prototype.

QR codes were positioned at specific locations along the robot's operating path during testing. The robot was directed toward target locations by these codes, which functioned as navigation markers. The robot was designed to recognize the QR codes, decipher the location information, and make appropriate movements.

To test the lifting mechanism, various objects were placed inside the gripping fixture. The rack moved vertically and raised the object when the ESP32 controller turned on the DC motor that drove the pinion gear. Lifting stability, motion smoothness, and load handling capacity were used to assess the lifting system's performance.

Lightweight items that are commonly used in office and laboratory settings could be lifted by the designed prototype. The adaptive gripping mechanism guaranteed stable object handling, while the rack-and-pinion mechanism produced smooth vertical motion, according to experimental observations. The electrical connection and real pictures of the Lifter NOVA are displayed in Figure 2. Through an Internet of Things-based interface, control commands are sent to the Smart Weight-Lifter Robot. After being turned on, the ESP32 interprets commands from the input and manages the drive motors to move the robot. The robot can locate itself and precisely move to the desired location thanks to QR-based navigation. The lifting motor smoothly raises or lowers the load by operating the rack-and-pinion mechanism in response to a lifting command.

Table 1. Summarizes the main components used in the development of the Lifter Nova system.

| **Component** | **Specification** | **Function** |
|---|---|---|
| ESP32 Microcontroller | 32-bit dual core | System control and IoT communication |
| DC Motor | 10 W | Driving wheels and lifting mechanism |
| Rack and Pinion | Steel gear system | Converts rotational motion to linear lifting |
| Ultrasonic Sensor | Distance sensing | Obstacle detection |
| Battery | 9V power supply | Electrical power for electronics |
| Adaptive Gripper | Multi-geometry fixture | Object gripping and handling |

 ISBN 978-81-973526-0-7

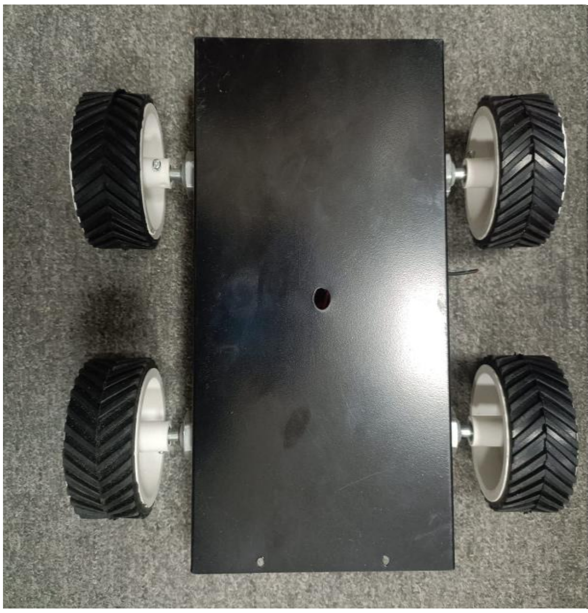

(a) Chassis

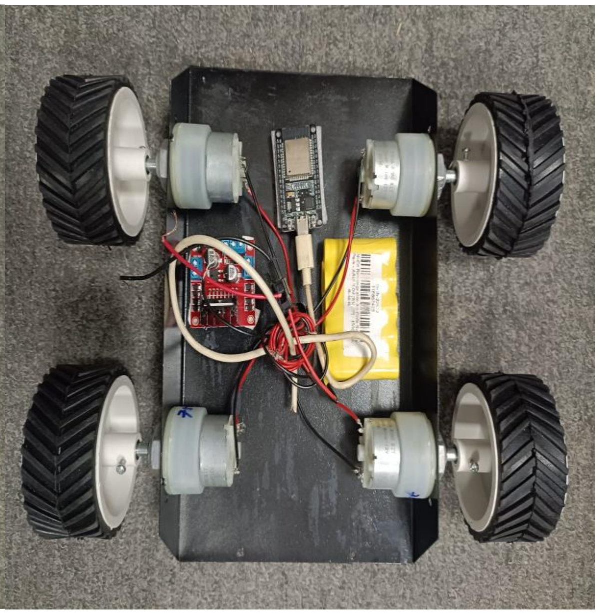

(b) Electronic Control Unit.(ECU)


(c) ESP32 Microcontroller

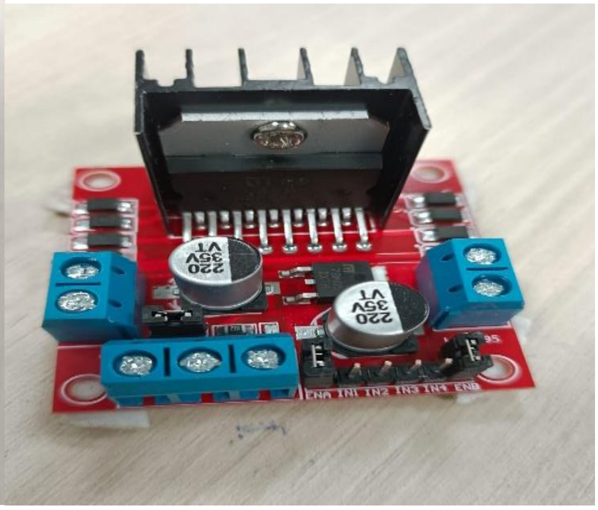


(d) L298N Motor Driver Module

Figure 2. Components.

Description of Figure 2:

Figure 2.a: The Chassis of the robot is fabricated using lightweight aluminium or mild-steel sections to ensure sufficient structural strength while maintaining a manageable system weight.

Figure 2.b: An Electronic Control Unit (ECU) is an embedded electronic system that controls and manages different functions of a robotic system using a microcontroller and programmed logic.

Figure2.c: ESP32 Microcontroller, a powerful and versatile microcontroller designed for the Internet of Things (IoT). It features a dual-core processor, making it much faster and more capable than a standard Arduino. It has both Wi-Fi and Bluetooth (Dual- Connectivity).

Figure2.d: L298N Motor Driver Module, a high-power dual H-bridge controller, which is used in Lifter NOVA to drive DC and stepper motors.

*ISBN 978-81-973526-0-7*

## Results and Discussion

The performance of the adaptive robotic gripper and the rack-and-pinion lifting mechanism was assessed using the Lifter NOVA prototype. The system was built to lift a 0.5 kg load, and F=mg was used to determine the necessary lifting force, which came out to be roughly 4.9 N. To guarantee steady gripping and dependable operation, a safety factor was considered.

Through a series of prototype tests, the Lifter Nova smart robotic weight-lifting system's lifting capacity, gripping stability, and navigational performance were assessed. These tests were designed to ascertain whether the developed system could carry out dependable load lifting and transportation in an indoor setting. . These tests aimed to assess if the designed system can perform accurate and safe lifting and transportation in an indoor environment.

The lifting motion of the rack-and-pinion showed stability and smooth operation. The pinion gear's rotational motion was effectively transformed into linear displacement of the rack when the lifting motor was activated via the ESP32 controller. The platform seemed to rise gently without overt vibration, indicating decent.

## References

[1] L. Atzori, A. Iera, and G. Morabito, The Internet of Things: A survey Computer Networks vol. 54 no. 15, p. 27872805, Oct. 2010.

[2] D. B. Chaffin, G. B. J. Andersson and B. J. Martin, Occupational Biomechanics, 4 th edition Hoboken, NJ, USA: Wiley-Interscience, 2006.

[3] M. P. Groover, Automation, Production Systems and Computer-Integrated Manufacturing, 4th ed. New Delhi, India Pearson Education, 2016.

[4] Mechanical engineering design J. E. Shigley, C. R. Mischke, and R. G. Budynas, Mechanical Engineering Design, 10th ed. McGraw-Hill Education, New York, NY, USA, 2015.

[5] B. Siciliano and O. Khatib, Springer Handbook of Robotics. Berlin, Germany: Springer, 2016.

[6] W. Bolton, Mechatronics: Electronic Control Systems of Mechanical and Electrical Engineering, 6 th edition. Harlow, U.K.: Pearson Education, 2015.

# GLOBALIZING INDIAN KNOWLEDGE: OPPORTUNITIES AND CHALLENGES FOR QUALITY EDUCATION

Rohit Sinha*[1]
*[1]J.C. Bose University of Science & Technology, YMCA, Faridabad, Haryana, India
* rohitsinha644@gmail.com

## Abstract
*As the world is becoming more and more interconnected, the globalization of Indian knowledge is providing a unique opportunity to enhance the quality of education globally. India has a rich heritage of ancient sciences, mathematics, philosophy, and indigenous technology, which has immense potential to meet the contemporary educational and societal needs of the world. However, there are also many challenges involved in the globalization of Indian knowledge. Challenges include the complexities involved in the translation of ancient texts, the need to match indigenous practices with contemporary standards, and the problems of intellectual property rights, cultural appropriation, and the risk of watering down the original knowledge. However, the opportunities involved in the globalization of Indian knowledge are immense. Globalizing Indian knowledge seeks to discuss some of the strategies, policies, and models for effectively globalization of Indian knowledge without compromising its authenticity. By confronting the challenges of globalization of knowledge in India, it is possible to work towards an education system that is both inclusive, relevant, and of high quality for the future.*

## Keywords
Indian knowledge system, quality education, globalization, indigenous technologies, cultural diversity.

## Introduction: The Renaissance of Indigenous Knowledge
The 21st century is witnessing a paradigm shift where "Global" no longer exclusively means "Western." As one of the oldest continuous civilizations in the world, India has a stock of knowledge that is not only historical but also functional. Indian stuff really changed the way people think all over the world. I mean everything from the decimal system we all use now to Yoga, which is all about holistic health and balance.
When it comes to SDG 4 on quality education, spreading Indian knowledge globally seems like it could bring this pluralistic way of learning into the mix. Its not meant to take over modern science or anything, but more like it fills in some gaps, especially with environmental ethics and how we handle mental well-being, I think that adds a lot of depth there. Sometimes people might see it as just old traditions, but actually, it complements what we already have pretty well, even if its not always straightforward to blend them.

## Theoretical Framework: The Pillars of Indian Knowledge
To really get what globalization means here, it helps to break down the kinds of knowledge that got shared around.

### *Pillar I: Mathematical and Astronomical Sciences (Ganita-Shastra)*
Indian mathematics spreading out globally, that is not something from just recent times. It seems like it started way earlier, with the Silk Road trade routes and then the House of Wisdom in Baghdad where ideas mixed. I might be missing some details on how exactly that worked, but it feels important. Things like that make you see connections across places.

### The Concept of Shunya (Zero) and Place Value

I guess the decimal place-value system stands out as one of the biggest things India gave to the world in math. You know, that system with zero in it really changed everything. From what I remember, theres this old text called the Bakhshali Manuscript, dating back to around the 3rd or 4th century CE, and it shows they were using a dot to represent zero early on. That seems pretty important, since zero wasnt always a thing like that. The Greeks thought of numbers more in terms of shapes and geometry, sort of abstract stuff, but Indian folks like Aryabhata saw zero differently, as an actual number you could use in equations and algebra. It had its own properties, I think that part gets a bit tricky to explain fully because of this change, they could build up more complicated ways of doing math, the kind that eventually led to computers today. Its wild how something so basic ties into all that modern tech, even if Im not totally sure on every detail. Zero just makes everything positional and easier, right.

### The Sulba Sutras and Geometry

India came up with the decimal place value system, and honestly, that feels like one of their huge gifts to math. It totally flipped how people deal with numbers back then, making everything easier to work with. I think the Bakhshali Manuscript is where it starts showing up, from maybe the 3rd or 4th century CE. They used a dot for zero in there, which was way ahead of time. Aryabhata and those Indian mathematicians treated zero like a real number, something you could plug into equations and calculations.The Greeks handled numbers differently, more tied to shapes and geometry stuff. But with zero as its own thing in India, arithmetic got so much better, like it opened doors for bigger ideas.That setup with place values and zero, it laid the groundwork for computers today, even if its tough to imagine math without it now. Some details about how it all connected still seem fuzzy to me, not totally clear.

### The Kerala School of Mathematics

Between the 14th and 16th centuries, the Kerala School, led by Madhava of Sangamagrama, developed the foundations of calculus, including infinite series for sine and cosine, nearly 250 years before Newton and Leibniz. The globalization of this knowledge—potentially through Jesuit missionaries—remains a significant area of modern historiographic debate.

### Pillar II: Life Sciences, Wellness, and Ecology (Ayurveda & Yoga)

The world demand for “Wellness” has put Indian Life Sciences at the center stage of global health discussion.

### Ayurveda: The Science of Longevity

- The two most important books of Ayurveda are the Charaka Samhita and the Sushruta Samhita Ayurveda is a Systems Biology approach, while Western “allopathy” is more of a symptom-remedy approach. It divides people into three groups based on their constitution Vata, Pitta and Kapha. It also accentuates Prakriti or the individual quality.
- Globalization Challenge: Literature states that although Ayurveda is popular around the world, it is often reduced to “herbalism”. The challenge is to maintain its status of a comprehensive medical system with surgery (Shalya-tantra), in which Sushruta is recognized as the “Father of Plastic Surgery”.

### Yoga and Consciousness Studies

Yoga has evolved from a spiritual practice (Moksha-dharma) to a global health commodity. Patanjali's Yoga Sutras give us a structured "Psychology of the Mind." Researchers at schools like Harvard are studying the "Relaxation Response" that Pranayama (breath control) causes. This connects ancient practice with modern neuroscience.

### Environmental Ethics and Sustainability

Prakriti (Nature) is considered a mother figure in the Vedic literature. This differs from the

Anthropocene (human-centered) view of the environment. A major example of how Indian indigenous knowledge affects global climate activism is the spread of the "Chipko Movement" philosophy, which is based on the idea that trees are sacred.

***Pillar III: Linguistic Science and Philosophy (Shabda-Bramhan)***

Linguistics in India was a highly developed "meta-science" used to preserve the oral integrity of the Vedas.

***Panini's Ashtadhyayi and Formal Language***

Panini's Ashtadhyayi (circa 4th Century BCE) is a complete, generative grammar of Sanskrit. It uses a system of 4,000 rules that function like a modern computer program.

Modern Relevance: Leading computer scientists, such as Rick Briggs (NASA), have argued that Sanskrit's structure is the most suited for Natural Language Processing (NLP) and Artificial Intelligence because it is unambiguous. The globalization of Panini's logic has fundamentally influenced Western structural linguistics (Saussure) and formal language theory (Chomsky).

***Tarkashastra: The Logic of Debate***

The Indian logic (Nyaya) is based on the "Five-membered Syllogism . Indian logic needs a 'Example' (Drishtanta) which is based on something which can be seen in the real world. Aristotelian logic has three parts (All men are mortal...). And this makes Indian philosophy more "empirical" than "abstract," a special way for people everywhere to learn how to think on the basis of evidence.

***Tarkashastra: The Logic of Debate***

Summary of Literature Trends

Current academic literature (e.g., Kapila, 2022; Subbarayappa, 2013) highlights a "Decolonial Turn." There is now a shift from viewing Indian knowledge as "mythology" to acknowledging it as a "Rational Science," which has been intentionally marginalized throughout the colonial period. The globalization of such systems in the current context is utilized to further the aim of Inclusive Education (SDG 4).

## Opportunities in the Global Market

In the 21st century, knowledge is the most important thing that people can use to influence others around the world. India was the Vishwaguru (World Teacher) for hundreds of years. It was an intellectual hub where scholars from across the Silk Route flocked to study in institutions such as Nalanda and Taxila. With climate change, mental health issues, and challenges associated with purely materialistic education being some of the biggest challenges for humanity today, the entire world is now looking up once again at Indian Knowledge Systems (IKS). However, globalization of Indian knowledge is not merely a form of cultural narcissism but also an opportunity to redefine the concept of 'Quality Education' worldwide. Nevertheless, this is a difficult path fraught with systemic challenges that require a judicious balance between the new and old.

There is a big change happening in the global education market. There is a growing need for learning that is holistic, sustainable, and based on values. Indian culture is great at these things.

**A. The "Holistic Wellness" Economy**

The best known examples of the dissemination of Indian knowledge to the rest of the world are Yoga and Ayurveda. These systems provide not only physical fitness but also a framework for mental health and preventive healthcare. India can lead the trillion dollar global "well-being" market by introducing these into medical and psychological programs across the world.

**B. Ethics and Sustainable Teaching**

A lot of times modern education is about "what to think" instead of "how to live." Indian philosophy is based on concepts like Vasudhaiva Kutumbakam (The World is One Family) and Prakriti (Harmony with Nature), which offer a paradigm for Global Citizenship Education (GCED). The UN is promoting the Sustainable Development Goals (SDGs) and Indian wisdom has been used for centuries to protect the environment and live ethically.

**C. Math and Language**

The rising popularity of Vedic Mathematics and the linguistic correctness of Sanskrit in cognitive science and computational linguistics. The algorithmic structure of Sanskrit grammar is often regarded as an important resource for Artificial Intelligence (AI) and Natural Language Processing (NLP), creating a technologically advanced market for traditional Indian scholarship.

**The Quest for Quality Education**

- Indian knowledge needs to be globally accepted by following contemporary notions of "Quality Education," defined by global standards such as the QS rankings and the UNICEF frameworks. It should not be limited to translation, it should fuse Tradition and Technology.
- Multidisciplinary Learning: The NEP 2020 encourages multidisciplinary learning, which is in consonance with the ancient Gurukul system that had science, arts and ethics in a single frame.
- Competency Based Learning vs Rote Learning: Quality Education in India is moving from memorization to gaining wisdom and applied sciences, known as Jnana and Vijnana. It fits in with the global move towards "problem-solving" and "critical thinking."

## Challenges to Globalization

In the 21st century, knowledge is the most important thing that people can use to influence others around the world. India was the Vishwaguru (World Teacher) for hundreds of years. It was an intellectual hub where scholars from across the Silk Route flocked to study in institutions such as Nalanda and Taxila. With climate change, mental health issues, and challenges associated with purely materialistic education being some of the biggest challenges for humanity today, the entire world is now looking up once again at Indian Knowledge Systems (IKS). However, globalization of Indian knowledge is not merely a form of cultural narcissism but also an opportunity to redefine the concept of 'Quality Education' worldwide. Nevertheless, this is a difficult path fraught with systemic challenges that require a judicious balance between the new and old.

Indian knowledge has vast potential but faces many obstacles that prevent its full acknowledgment in the world community.

**A. The Colonial Hangover and the Gap in Perception**

Much of India's deep knowledge is written in Sanskrit or other regional languages. It can't reach as many people, because there are not many good, standardized translations into English, Spanish or Mandarin, which are all global languages. There are not enough trained teachers to help people learn the difference between old and new scientific terms.

**B. Language and Access**

Much of India's deep knowledge is written in Sanskrit or other regional languages. It can't reach as many people, because there are not many good, standardized translations into English, Spanish or Mandarin, which are all global languages. There are not enough trained teachers to help people learn the difference between old and new scientific terms.

**C. Making sure quality and standardization**

The world market does not trust “pseudo-science.” India needs to have robust accreditation bodies to ensure quality of IKS. Degrees in Ayurveda or certifications in Vedic Math should be recognized globally for students to travel and for professionals to trust each other.

**D. The Digital Divide and Infrastructure**

India is a digital power house but traditional schools often lack the smart classrooms, research labs and global connectivity needed to compete with Ivy League or European schools. What we need is a world class digital delivery system to get knowledge to everyone.

## Strategic Solutions for the Future

To turn these challenges into milestones, a multi-pronged strategy is required:

| Strategy | Action Point | Expected Outcome |
|---|---|---|
| Research & Validation | Fund interdisciplinary research labs (e.g., Ayurveda + Modern Medicine). | Scientific legitimacy and global patents. |
| Digital Expansion | Create high-quality MOOCs (Massive Open Online Courses) on IKS. | Global reach and affordable access. |
| International Collaborations | Joint degree programs between Indian and Foreign Universities. | Cultural exchange and standardized curriculum. |
| Teacher Training | Develop "IKS Ambassadors" proficient in both tradition and modern pedagogy. | High-quality instructional delivery. |

## Critical Challenges: The Barriers to Global Integration

**A. The Validation and “Science” Argument**

The empirical gap is the main problem. The underpinning of modern global academia is the Western scientific temperament, which values experiments that are repeatable and physical. Many IKS are holistic and metaphysical in nature, especially in the fields of Ayurveda and Yogic Science.

The Challenge: Indian knowledge often has to be ‘proven’ according to Western standards for it to be published in medical or scientific journals around the world. This process sometimes removes context from the knowledge and thus makes it less useful than it was before.

**B. Quality Control and Standardization**

The market is flooded with unproven practitioners and institutions as the demand for “Vedic” or “ancient” knowledge grows.

- The Challenge: There is no single global accrediting body for IKS as in case of MBAs or MDs. Without strict quality control you get “fast-food” versions of complicated ideas. This can lead to wrong information, and in medical cases, physical harm. This non-standardization endangers the credibility of real Indian scholarship in the world arena.

**C. The Language and Translation Barrier**

The depth of Indian knowledge often is inextricably bound up with the Sanskrit language, which has a technical precision that’s difficult to replicate in English.

The Challenge: Most of today’s translations are either too literal (losing the philosophical nuance) or too poetic (losing the scientific rigor). Furthermore, there is a lack of scholars who are equally proficient in ancient languages and modern disciplines (such as Quantum Physics or Neuroscience), which makes it difficult to "translate" these concepts into a vocabulary that the modern world understands.

**D. Intellectual Property and Bio-Piracy**

Knowledge globalised, there is a danger of exploitation.

*ISBN 978-81-973526-0-7*

- The Challenge: Traditional Indian knowledge like the benefits of Neem or Turmeric has often been patented by foreign companies. It's difficult to protect the traditional intellectual property, and try to share it with the world. India has to navigate complex patent laws across the globe to ensure that "globalizing" does not mean "giving away" its culture without credit or remuneration.

**E. Institutional and Digital Infrastructure**

- For Indian knowledge to provide "Quality Education," it must be provided through state-of-the-art platforms.

The Challenge: Many of the centers of learning from the traditional era in India lack the digital tools for delivering education in terms of high-speed Internet access, sophisticated LMS software systems, and global reach through marketing. The knowledge which is the most genuine is found at locations which are not capable of reaching out globally.

**Summary of Hurdles**

| **Challenge Category** | **Root Cause** | **Impact** |
|---|---|---|
| **Epistemological** | Conflict between holistic and reductionist science. | Marginalization as "pseudo-science." |
| **Regulatory** | Lack of international certifications. | Proliferation of low-quality "fake" gurus. |
| **Legal** | Weak international IP protections. | Bio-piracy and loss of cultural credit. |
| **Pedagogical** | Shortage of bilingual, multi-disciplinary experts. | Poor delivery and misunderstood concepts. |

## Strategic Models for Effective Globalization

To ensure authenticity while expanding reach, the following strategies are proposed:

- The "Glocal" Policy Framework

India needs to follow the National Education Policy (NEP) 2020 model and adopt a "Glocal" (Global + Local) approach. This involves setting up digital repositories like the Traditional Knowledge Digital Library (TKDL) to prevent biopiracy and also to make data accessible to researchers globally.

- Digital Literacy and Open Access

Offering MOOCs (Massive Open Online Courses) on IKS through digital platforms. This keeps the "source" of the knowledge in Indian academia while the "reach" is global.

- Collaborative Research Centers

Establishing collaborative research programs involving Indian institutions and foreign organizations like Harvard University's Sanskrit Department or Oxford University's Center for Hindu Studies, to establish an academic connection between ancient and modern science.

## Case Study: The Global Success of Yoga and Its Lessons

(In this section talk about how Yoga grew to become a multi-billion dollar global industry but also emphasize the loss of the spiritual and philosophical roots in the "Western Fitness" model. Let this be a lesson for other Indian sciences.)

First of all, flexibility is key. Yoga worked because it was presented in a modular fashion. Its spiritual essence lives on, but it has been adapted into many forms – Hatha, Vinyasa and even therapeutic Yoga – to make it accessible to many cultures without requiring a total lifestyle change. This "secular accessibility" enabled it to overcome religious barriers and to penetrate mainstream healthcare and fitness markets.

Secondly, Scientific Validation comes to bridge the gap that exists in terms of credibility. This was the element that caused Yoga to gain popularity throughout the world. From being

described as a "mystical art," it transformed into a "validated science" when Western medical establishments began documenting the effects it had on reducing stress, promoting cardiovascular wellness, and managing chronic pain.
Finally, Soft Power and Branding Do Matter. The strong brand was built through pro-active diplomacy by the Indian government and a "bottom-up" demand from global celebrities and influencers. The lesson for future knowledge exports is clear: success requires a mix of grassroots authenticity and strategic high-level promotion.

## Conclusion

The world is getting more connected and complicated these days, with all sorts of stresses piling up. I think shifting education away from just material stuff toward something more holistic and based on values makes a lot of sense now. Its not optional anymore, really. Indias old knowledge systems could fit right into that. These systems cover everything from ethical ways to live sustainably to precise ancient sciences. They seem like a good toolkit for dealing with big problems today, like mental health issues or the environment falling apart. India has this rich intellectual history that might help globally. Take Yoga as an example. Its a case where moving from traditional roots to something everyone accepts worldwide takes careful balancing. You cant just push it out there without adjustments. To make quality education happen on a bigger scale, India needs to push hard for scientific checks, standard ways to accredit it, and making it easy to access online. That way its not stuck in the past. We have to connect those ancient ideas with modern research methods. Otherwise it stays as cultural nostalgia, not something useful practically around the world. I am not totally sure how smooth that bridge will be, but it feels necessary. The aim is building an educational setup where old wisdom and new innovations work together, sort of symbiotically. India could step up as a real hub for knowledge again. That might lead to a future that more mindful and sustainable for everyone, though its hard to say exactly how it all plays out.

## References

[1] Agrawal, A. (2025). Artificial Intelligence and Indian Knowledge Systems. International Journal of Innovation in Engineering Research & Management, 12(4), 146–149.

[2] Ancient Indian Knowledge Tradition, Colonialism, Globalization and Challenges: A Study. (2025). Knowledgeable Research. https://knowledgeableresearch.com/index.php/1/article/view/551

[3] Datta, R., & Mete, J. (2024). Indian Knowledge System: Analysis of traditional wisdom and modern integration. Integrated Journal for Research in Arts and Humanities, 4(5), 82–90. https://ijirah.dvpublication.com/uploads/66edb4f19aee4_424.pdf

[4] Government of India. (2020). National Education Policy 2020. Ministry of Education. https://www.education.gov.in/sites/upload_files/mhrd/files/NEP_Final_English_0.pdf

[5] Indian Knowledge Systems (IKS): Historical Foundations, Contemporary Relevance, and Integration in Modern Research and Education. (2026). RJ Wave, 3(1). https://rjwave.org/ijedr/papers/IJEDR2601373.pdf

[6] Revitalizing Education: Embracing India's Knowledge System in Mid 21st Century. (2026). RJ Wave. https://rjwave.org/jaafr/papers/JAAFR2512541.pdf

[7] Sahoo, P. (2026). Revitalizing higher education through Indian Knowledge System in the light of NEP-2020. Critical Journal of Social Sciences, 1(1), 77–89. https://criticaljournalofsocialsciences.com/index.php/CJSS/article/view/v1n1-article5

[8] Scientific Approach to Indian Knowledge System and NEP 2020. (2024). International Journal of Advanced Research and Multidisciplinary Trends, 1(2), 173–179. https://www.ijarmt.com/index.php/j/article/view/215

[9] Taneja, D. K. (2014). Yoga and health. Indian Journal of Community Medicine, 39(2), 68–72. https://doi.org/10.4103/0970-0218.132716

[10] Tripathy, D. (2025). Introduction. Journal of Indian Knowledge Systems, 1(1). https://brill.com/view/journals/jiks/1/1/article-p1_1.xml

[11] Ydo, Y. (2022). Reaching SDG 4: Our shared responsibility and renewed commitment to action. PROSPECTS, 52(1-2), 223–229. https://doi.org/10.1007/s11125-022-09628-3

[12] UGC Guidelines on the integration of Indian Knowledge Systems (2023).

# SURROGATE-ASSISTED GENETIC OPTIMIZATION OF HONEYCOMB SANDWICH STRUCTURES BASED ON FINITE ELEMENT ANALYSIS

Sushil Kumar Singh*[1], Mayur Pratap Singh[1], Navin Kumar[2]
*[1]School of Mechanical Engineering, Galgotias University, Greater Noida, Uttar Pradesh, India
[2]AICTE, New Delhi, India
*sushil.acet@gmail.com

## Abstract

*In this research paper machine learning system and finite element systems are added together to grab the advantage of varying orientation, under compressive load on a Honeycomb sandwich structures to calculate the mechanical behaviour of the structure. Listed input parameters are chosen Thickness t, Cell size s, Geometric ratio t/l, Relative density ρ*/ρs, Elasticity E, Poisson ratio μ, Density ρ and Case ID to determine the output parameter Von Mises stress(S-Mises). Abaqus based finite element analysis is used for deformation properties under various geometric dimensions. Five machine learning models were trained and the best model a Random Forest regressor is trained as a stand-in model to predict Von Mises stress (S-Mises). Stratified cross-validation coefficient of determination (R2) of 0.805, the surrogate model has good predictive power. Additionally, the model is inherently coupled with a genetic algorithm to perform stress-driven optimization in a high-dimensional design space. The optimization process exhibits rapid convergence, reducing the minimum von Mises stress from 5.4619 to 3.2843 within 20 generations, corresponding to an improvement of approximately 39.9% compared to the best initial design. The optimized configuration favours reduced effective density and enhanced geometric stiffness, highlighting the effectiveness of the proposed ML-assisted optimization framework for the efficient design of lightweight sandwich structures.*

## Keywords

Honeycomb Structures, Compression, Abaqus Simulation, Mechanical Behaviour, Optimization, Printing.

## Introduction

Introduction of honeycomb-shaped materials in aerospace design was first noticed in the 20th century due to its super-stiffness-to-weight ratio characteristics[1], [2]. With the introduction of new advanced computational tools, finite element analysis (FEA) has become a new tool to predict the failure mechanism and performance analysis of these architected structures[3]. Abaqus Software for modelling honeycomb geometries has been widely applied due to its strength in simulating nonlinear material response and large deformations. Former studies modelled accurate finite element analysis models to identify relevant failure modes under compressive test. [4] augmented a machine learning model with dimensional analysis and physical laws to predict the quality of additively manufactured high-entropy alloys, enhancing its generalizability beyond empirical data. [5]developed a novel framework for predicting porosity in 3D printing using reinforcement learning to autonomously optimize process parameters. [6]demonstrated the use of ML for the real-time monitoring and optimization of 3D printing process parameters to enhance product quality. [7]provide a comprehensive review of the progress and significant opportunities for ML across all aspects of 3D printing materials and processes. [8]employed ML to predict and optimize the mechanical properties of Ti6Al4V alloy fabricated via laser powder bed fusion, linking process parameters to performance outcomes. Combining FEA with ML techniques offer significant potential for the optimization and design of advanced materials.[3], [9]. Comprehensive FEA models are developed to predict mechanical characteristics and structural performance. The generated simulation datasets establish quantitative relationships between geometric parameters and corresponding mechanical properties [10]. Tree based Random Forest algorithm was developed for comparison of practical and theoretical framework [11]. To develop quantitative correlations between processing parameters and performance characteristics, mechanical nature of composite materials has been systematically evaluated [12]. Architectural based, accurate prediction of lattice structures response was developed by the aid of ML models [13]. A computationally efficient surrogate model based on the Random Forest algorithm for structural optimization of honeycomb structure by employing FEA simulations was tested [14]. Results revealed that both wall thickness and material type significantly influence mechanical performance, with ABS exhibiting superior ductility and dimensional stability [15]. This research totally enlightens the integration of FEA and ML to develop an effective lightweight structural optimization. Many research studies in 3D printing for the application of honeycomb structures were carried out still a clear research gap remains in accurately predicting the mechanical response of honeycomb-sandwich structures under varying orientation using an integrated FEA–ML framework. A Random Forest regression model is trained to predict von Mises stress distributions, enabling efficient lightweight structural optimization is selected with simulation-based data driven mechanical performance metrics, material characteristics and geometric parameters to fill the research gap.

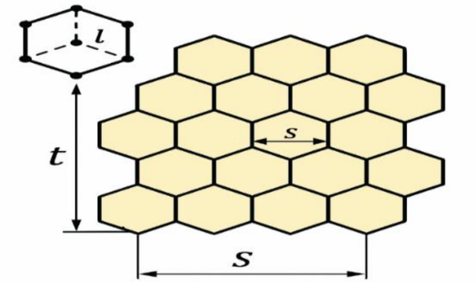


Figure 1. Honeycomb structure along with geometric dimensions.

## Methodology

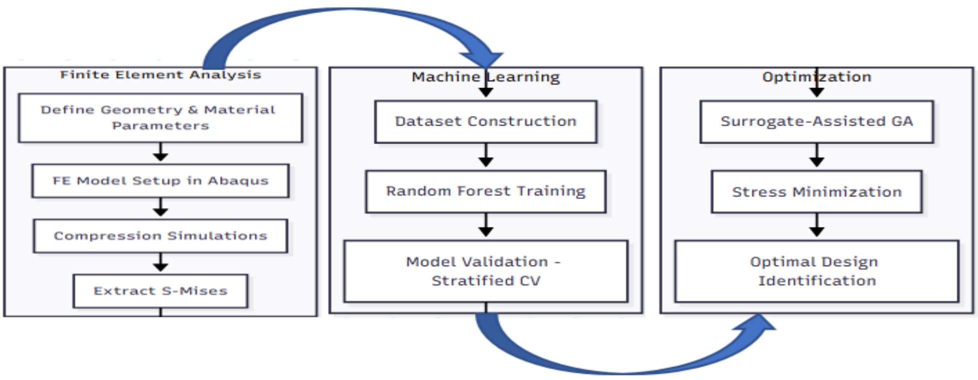


Figure 2. Systematic representation of combined FEA, ML SM, and GA optimization path for stress-driven design of honeycomb-inspired sandwich structures.

As shown in the Figure 2. Flowchart of the integrated FEA, ML surrogate modelling, and genetic algorithm optimization framework for stress-driven design of honeycomb-inspired sandwich structures, describes the methodology of this research study. Input parameters such as (t, s, t/l, ρ*/ρs, E, μ, ρ) are chosen to determine the output parameter Von Mises stress(S-Mises), to guarantee feasible circumstances for light-weight load-bearing applications on PLA, ABS and PETG material. using Abaqus based FEA simulations were performed to

*ISBN 978-81-973526-0-7*

determine distortion points and stress distribution in honeycomb sandwich structure under uniaxial compression. Boundary conditions were applied, while loading was introduced along different orientations to capture the directional dependence of the response. The von Mises stress (S-Mises) was identified as the principal output variable. A comprehensive dataset was applied on various geometric configurations and material properties to establish the relationship between design parameters and structural response. Large dataset was generated to incorporate machine learning. The Python-based scikit-learn library was employed to implement the data-driven machine learning component. To address the influence of multiple nonlinear relationships among the parameters, a Random Forest Regressor was employed. For model training and validation, a stratified cross-validation strategy was implemented to ensure consistency, robustness, and accuracy across the dataset. Machine learning assisted surrogate model shows strong prediction of stress response of previously excluded honeycomb structure and minimizes the dependency of finite element simulation.

## Results and Discussion

Abaqus simulated data regarding stress distribution and distortion/deformation nature of honeycomb sandwich cells under uniaxial compression provides valuable insights by combining FEA and ML. It also incident impactful geometrical properties like as wall thickness and size of the cell. Fast calculation is possible by combining the FEA and ML framework over stress responses, rapid design exploration, physical and experimental accuracy.

### *Finite Element Simulation*

PLA, ABS and PETG Honeycomb structure of Cell size and wall thickness (8 mm,0.93 mm wall Thickness) and PLA, ABS and PETG Honeycomb structure of Cell size and wall thickness (12 mm, 1.2 mm wall Thickness) data is used to generate figure 3(a) and 3(b) in Abaqus as the main computational tool, finite element computations were performed on the honeycomb sandwiched configurations shown. To specify the three-dimensional geometry of the buildings, the program imported the CAD models, Abaqus enables rigorous handling of nonlinear deformation and exact description of complicated cellular geometries.

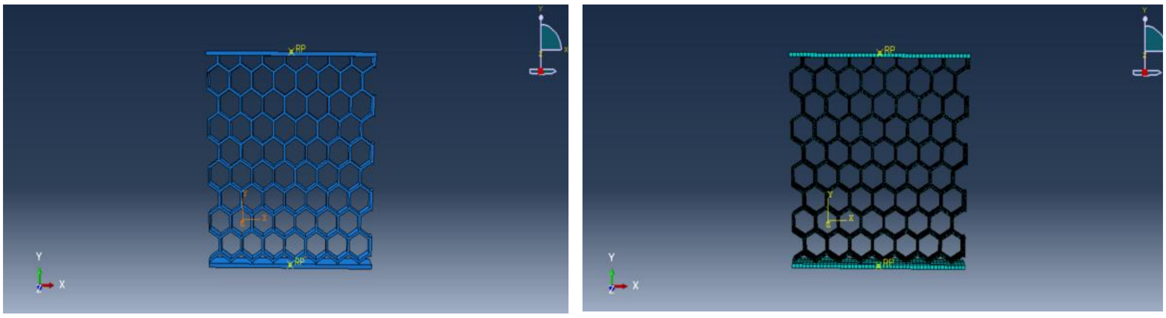

Figure 3. (a) ABS honeycomb Structure (b) PETG honeycomb Structure.

The honeycomb core was meshed with a fine element size of 0.47 mm, while the plates used a 2 mm mesh, resulting in approximately 129,129 elements for the core and 610 for the plates. Boundary conditions were applied using the Abaqus Limit Condition Manager. After an initial stabilization step, a general static compression step of 1 s was performed. The simulation allowed up to one million increments with an initial increment of 0.1, a minimum of $1 \times 10^{-9}$, and a maximum of 1, using the full Newton solution method for convergence. Compression was simulated using a displacement-controlled loading, where the top plate was displaced by 10% of the specimen height (e.g., 10 mm for a 100 mm sample). Method enables the realistic modelling of progressive deformation, stress redistribution, and buckling behaviour in the honeycomb structure. Static analysis with convergence.

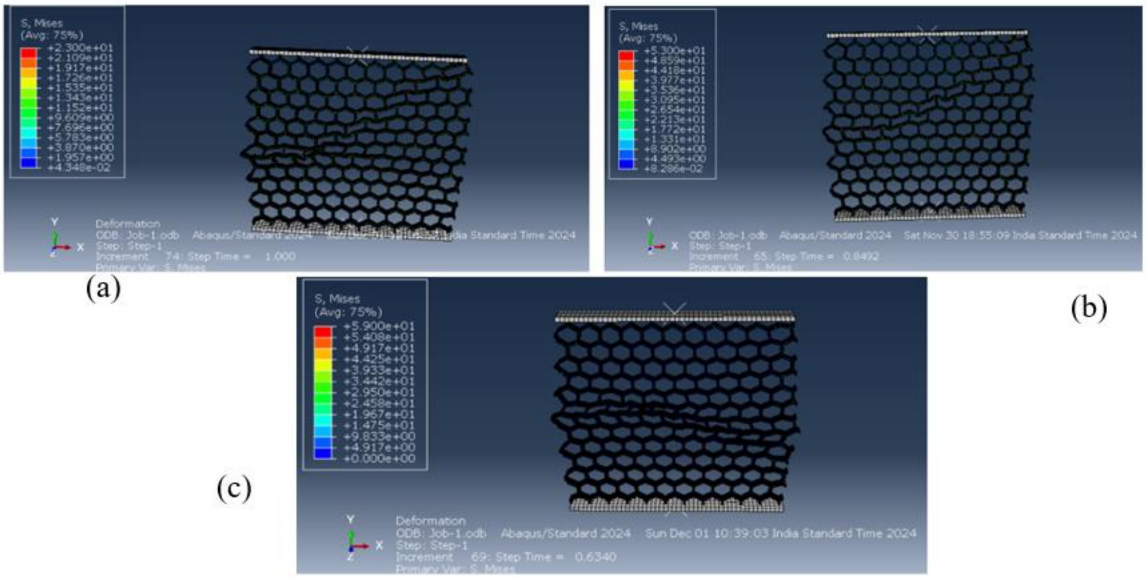


Figure 4. (a) ABS, (b) PETG, (c) PLA Von Mises Stress Distribution of Honeycomb Structure (Cell Size = 8 mm, Thickness = 4 mm, Wall Thickness = 0.93 mm).

In the finite element simulations conducted using Abaqus/CAE 2022, the von Mises stress distribution patterns revealed significant material-dependent variations under compressive loading, as illustrated in Fig. 4 for the configuration with cell size = 8 mm, thickness = 4 mm, and wall thickness = 0.93 mm. For this geometry, in Fig. 5 (cell size = 12 mm, thickness = 6 mm, wall thickness = 1.2 mm) showed notably different behaviour.

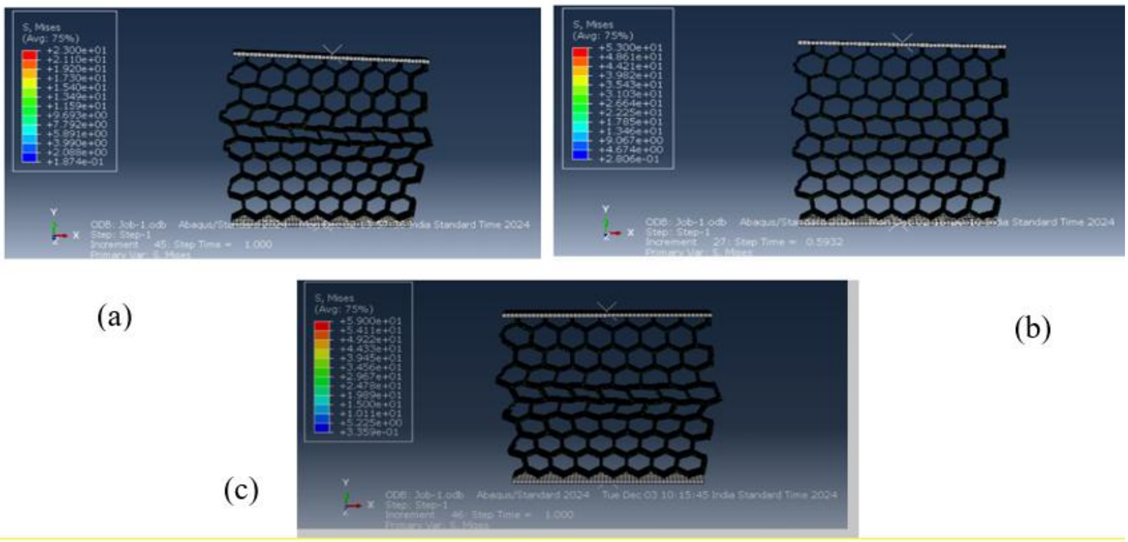


Figure 5. (a) ABS, (b) PETG, (c) PLA Von Mises Stress Distribution of Honeycomb Structure (Cell Size = 12 mm, Thickness = 6 mm, Wall Thickness = 1.2 mm).

ABS show significant reduction in stress concentration, PETG moderate reduction with improved stress distribution and PLA large reduction but still highest stress among materials.

Table 1. Percentage change in maximum von Mises stress with increased cell size and wall thickness.

| Material | Stress in cell size 8mm in (MPa) | Stress in cell size 12mm (MPa) | Change in Stress (MPa) | Percentage Change (%) |
|---|---|---|---|---|
| ABS | 18.7 | 14.2 | −4.5 | −24.06% |
| PETG | 22.3 | 19.8 | −2.5 | −11.21% |
| PLA | 35.6 | 28.4 | −7.2 | −20.22% |

### *Machine Learning Model*

In machine learning Scikit-learn was used to create the prediction model in Python library. The finite element simulations produced the dataset utilized for training and assessment, which contained important morphological attributes (t, s, t/l, ρ*/ρs, E, μ, ρ) The output variable was the von Mises stress level that was taken out of the simulations.

### *Data Preparation*

Data extracted from Abaqus finite element simulations was used for machine learning. Every simulation was run for honeycomb sandwich constructions with different geometric parameters, such as wall thickness, overall thickness, and cell size, with ABS serving as the basis material. The von Mises stress distribution, the main output of interest, was noted after each instance of compression loading. The mentioned input variables are (t, s, t/l, ρ*/ρs, E, μ, ρ) and case ID for the maximum von Mises stress (S-Mises).

### *Model Selection and Implementation*

Out of 5 regression model only Random Forest Regressor is chosen best prediction model to calculate S, Mises. Python assisted scikit-learn is used. Input features used for the model are: (t, s, t/l, ρ*/ρs, E, μ, ρ) and case ID Numerical features were standardized using standard scaling, and the dataset was split into 80% training and 20% testing sets with a fixed random state for reproducibility.

### *Model Evaluation*

The predictive performance of the developed Random Forest regressor was evaluated using an unseen test dataset. The model achieved an RMSE of 7.196 and an $R^2$ value of 0.748, indicating good agreement between predicted and actual von Mises stress values. To assess robustness, stratified five-fold cross-validation was conducted with balanced stress distributions across folds. The cross-validation produced an average $R^2$ of 0.805 with a standard deviation of ±0.049, showing stable predictive accuracy. A representative prediction of 9.07 MPa further confirms the model's reliability for integration into the genetic algorithm optimization framework.

### *Analysis of Results and Visualizations*

Fig. 6 show that for random forest model density of the material is a dominating factor for prediction of maximum von Mises stress in ABS honeycomb structure contributes about 80%. Relative density ratio, young's modulus and Poisson's ratio have minimum effect, Geometric features like as cell size and wall thickness show minor influence. Case ID have low importance in stress prediction. Actual vs Predicted Plot(fig.7) show solid predictive performance confirms for, the random forest model achieved R2 values of 0.748 test set and 0.805 cross validation. At higher stress level little deviation were listed, overall, model effectively captures non-linear stress nature, validating reliable surrogate for simulation based mechanical analysis.

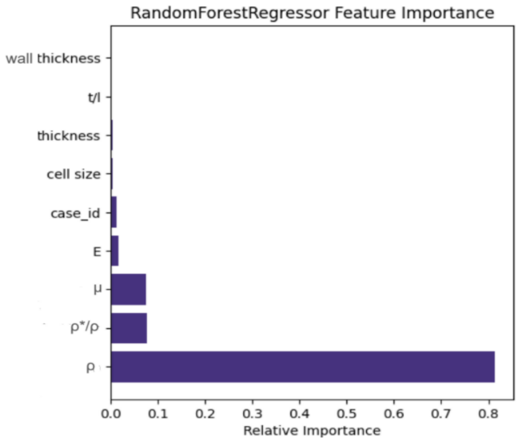


Figure 6. Feature importance of R F R.

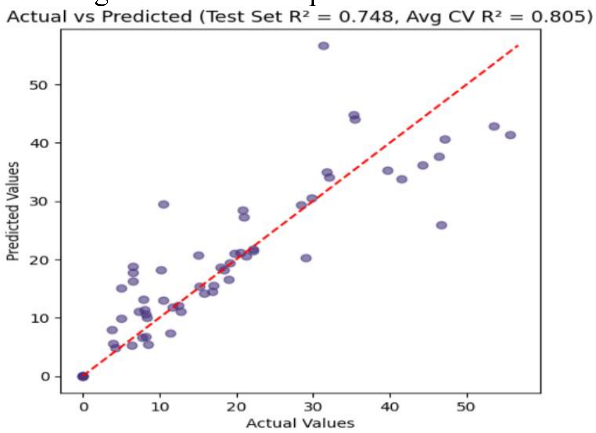


Figure 7. Actual vs Predicted Response of RFR.

Distribution of Residuals (Fig.8) show that no systematic bias and random error dispersion, symmetrically distributed around zero for Random Forest model residuals. Accurate von Mises stress prediction outcome reflects for close clustering of data points near the zero line, only few negligible outliners. Overall, model is best suited for capturing complex relation between geometry, material characteristics and stress response in honeycomb sandwich structures.

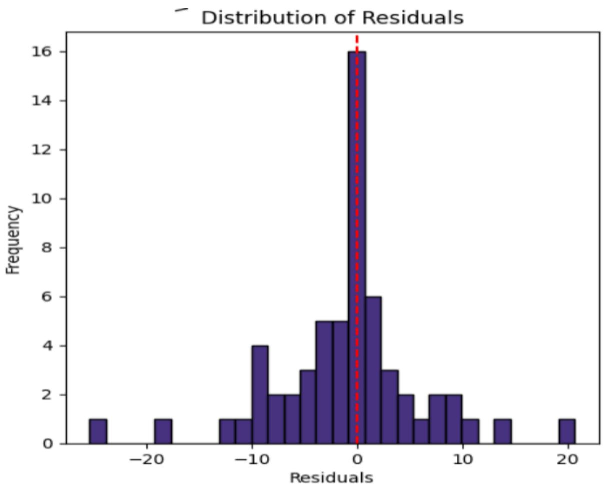


Figure 8. Distribution of Residuals for R F R.

Fig.9 show the pairwise scatter and kernel density distributions of Young’s modulus (E), density (ρ), thickness-to-length ratio (t/l), and von Mises stress. Young’s modulus and density display bimodal distributions, with dominant ranges of E ≈ 2.1–2.3 and 2.8–3.2, and ρ ≈ 1.05–1.10 and 1.25–1.35, while t/l mainly clusters around 0.10 and 0.12. The resulting von Mises stress varies widely from 5 to 60, with most samples below 30. More density and stiffness lead to more stress, while increasing t/l reduces stress, showing the combined nonlinear influence of material and geometric parameters.

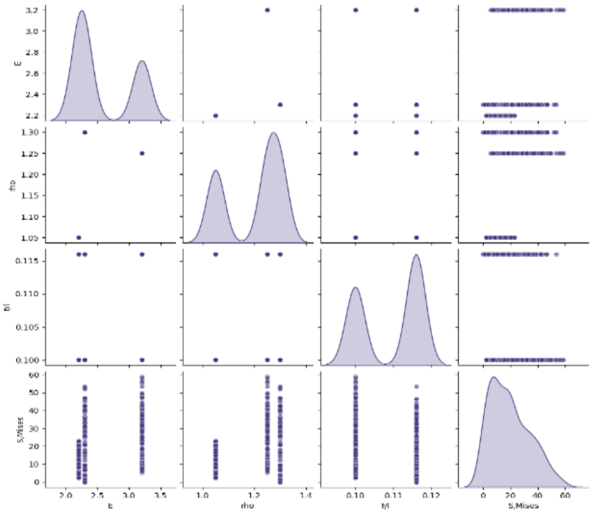

Figure 9. Pair plot of top Correlated Feature.

### *GA Optimization*

Population-based stochastic genetic algorithm, optimization method is used to minimize stress in multidimensional design spaces, reduce computational cost, with a Random Forest surrogate model. The design vector includes geometric and material parameters: x = [t, c, $t_n$, t/l, $\rho/\rho_s$, E, μ, ρ]. The objective function is defined as min $f(x) = \sigma_v M(x)$, subject to physical bounds for each design variable. The optimization declines rapidly, with stress decreasing from 5.46 in the initial population to 3.28 by the 15th–20th generations, achieving a 39.9% reduction. The optimal design includes t = 5.97, c = 10.62, $t_n$ = 1.09, and t/l = 0.1129. Corresponding material properties include $\rho/\rho_s$ = 0.0847, E = 2.22, μ = 0.369, and ρ = 1.06. Results indicate that reduced material density and stiffness combined with improved geometric stiffness effectively minimize stress concentration. The smooth convergence confirms the robustness of the machine learning–assisted GA optimization framework.

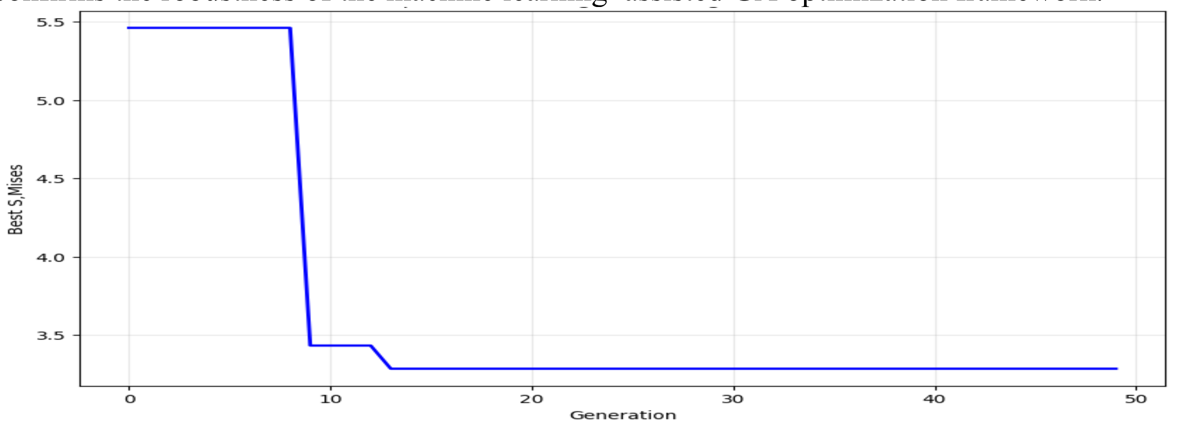


Figure 10. GA optimization convergence history using the Random Forest surrogate model.

## Conclusion

A combined module of FEA simulation, machine learning based Random Forest surrogate modelling along with genetic algorithm-based optimization is developed for honeycomb structure designed with PLA, ABS and PETG material to minimize Von mises stress. The traditional techniques of optimization become less efficient as simulation results showed strong nonlinear interactions between geometric and material parameters, making conventional optimization approaches less effective. The regression model showed sound prediction with RMSE = 7.196 and $R^2$ = 0.748, and cross-validation confirmed its robustness (average $R^2$ = 0.805). An improvement of About 39.9% is achieved to align genetic algorithm and surrogate model by minimising stress from5.46 to 3.28. The optimal design favoured lower density, moderate stiffness, and higher geometric stiffness larger t/l ratio. Collectively the proposed Machine learning based GA module provides an efficient and reliable approach for optimizing complex material–geometric systems while significantly reducing computational cost.

## References

[1] N. Samadiani, A. S. Barnard, D. Gunasegaram, and N. Fayyaz, "Best practices for machine learning strategies aimed at process parameter development in powder bed fusion additive manufacturing," J. Intell. Manuf., Oct. 2024, doi: 10.1007/s10845-024-02490-4.

[2] O. El Khatib, S. Kumar, W. J. Cantwell, and A. Schiffer, "Effective Elastic Properties of Hierarchical Honeycombs with Corrugated Sandwich Walls," in Key Engineering Materials, Nov. 2024, pp. 75–81. doi: 10.4028/p-mwwHv1.

[3] L. Lv, Y. Huang, J. Cui, Y. Qian, F. Ye, and Y. Zhao, "Bending properties of three-dimensional honeycomb sandwich structure composites: experiment and Finite Element Method simulation," Textile Research Journal, vol. 88, no. 17, pp. 2024–2031, Sep. 2018, doi: 10.1177/0040517517703602.

[4] H. Wang, B. Li, and F.-Z. Xuan, "A dimensionally augmented and physics-informed machine learning for quality prediction of additively manufactured high-entropy alloy," J. Mater. Process. Technol., vol. 307, p. 117637, Sep. 2022, doi: 10.1016/j.jmatprotec.2022.117637.

[5] A. M. Faizan Mohamed, F. Careri, R. H. U. Khan, M. M. Attallah, and L. Stella, "A novel porosity prediction framework based on reinforcement learning for process parameter optimization in additive manufacturing," Scr. Mater., vol. 255, p. 116377, Jan. 2025, doi: 10.1016/j.scriptamat.2024.116377.

[6] T. S. Tamir et al., "Machine-learning-based monitoring and optimization of processing parameters in 3D printing," Int. J. Comput. Integr. Manuf., vol. 36, no. 9, pp. 1362–1378, Sep. 2023, doi: 10.1080/0951192X.2022.2145019.

[7] T. Yi, "Mechanical properties of a hierarchical honeycomb with sandwich walls," Proc. Inst. Mech. Eng. C J. Mech. Eng. Sci., vol. 230, no. 16, pp. 2765–2775, Oct. 2016, doi: 10.1177/0954406215602284.

[8] Z. Cao, Q. Liu, Q. Liu, X. Yu, J. J. Kruzic, and X. Li, "A machine learning method to quantitatively predict alpha phase morphology in additively manufactured Ti-6Al-4V," NPJ Comput. Mater., vol. 9, no. 1, p. 195, Oct. 2023, doi: 10.1038/s41524-023-01152-y.

[9] Z. Wei, C. Zhou, F. Zhang, and C. Zhou, "Reliability Optimization of the Honeycomb Sandwich Structure Based on A Neural Network Surrogate Model," Materials, vol. 16, no. 23, p. 7465, Nov. 2023, doi: 10.3390/ma16237465.

[10] X. Shen and others, "Dynamic mechanical response prediction model of honeycomb structure based on machine learning method and finite element method," Int. J. Impact Eng., vol. 184, p. 104825, Feb. 2024, doi: 10.1016/j.ijimpeng.2023.104825.

[11] M. Zhao, H. Jin, Z. Yun, Z. Meng, and W. Zhang, "Investigation of the Mechanical

Properties of Composite Honeycomb Sandwich Panels after Fatigue in Hygrothermal Environments," Polymers (Basel)., vol. 16, no. 17, p. 2497, Sep. 2024, doi: 10.3390/polym16172497.

[12] Q. Liu, W. Chen, V. Yakubov, J. J. Kruzic, C. H. Wang, and X. Li, "Interpretable machine learning approach for exploring process-structure-property relationships in metal additive manufacturing," Addit. Manuf., vol. 85, p. 104187, Apr. 2024, doi: 10.1016/j.addma.2024.104187.

[13] J. Liu, J. Ye, D. Silva Izquierdo, A. Vinel, N. Shamsaei, and S. Shao, "A review of machine learning techniques for process and performance optimization in laser beam powder bed fusion additive manufacturing," J. Intell. Manuf., vol. 34, no. 8, pp. 3249–3275, Dec. 2023, doi: 10.1007/s10845-022-02012-0.

[14] A. Moradi, S. Tajalli, M. H. Mosallanejad, and A. Saboori, "Intelligent laser-based metal additive manufacturing: A review on machine learning for process optimization and property prediction," The International Journal of Advanced Manufacturing Technology, vol. 136, no. 2, pp. 527–560, Jan. 2025, doi: 10.1007/s00170-024-14858-0.

[15] S. K.Singh, M. P.Singh, and N.Kumar, ""Compression Analysis and Mechanical Assessment of Bioinspired 3D-Printed Honeycomb Sandwich Structures Using Abaqus-Based Simulation"." Macromolecular Symposia (2025): e70178. https://doi.org/10.1002/masy.70178.

*ISBN 978-81-973526-0-7*

# AI & FEM – BASED PIPE RACK OPTIMIZATION FOR CARBON REDUCTION

Lalit Mohan Singh*[1], Subbarao Chamarti[1]
*[1]Lingayas Vidyapeeth, Faridabad India
*lalitbisht01@live.in


## Abstract
*Industrial pipe racks account for a substantial portion of structural steel consumption in large-scale facilities such as water treatment plants, oil and gas installations, pharmaceutical plants, and data centers. Conventional design approaches rely heavily on conservative load assumptions and standardized layouts, often resulting in structural oversizing and increased embodied carbon emissions. This study proposes an integrated computational framework combining Finite Element Method (FEM)-based structural analysis, topology optimization, and Artificial Intelligence (AI)-assisted layout and section selection. A representative three-tier industrial pipe rack was analyzed under combined dead, live, wind, and seismic loading conditions. The objective was mass minimization subject to stress, deflection, and stability constraints. The optimized design achieved a 16.7% reduction in steel weight, resulting in 38 tons of embodied $CO_2$ reduction and 17% cost savings compared to the baseline configuration. Furthermore, AI-assisted automation reduced engineering design time by approximately 37%. The results demonstrate that integrating structural mechanics with data-driven algorithms provides a viable pathway toward sustainable and economically efficient industrial infrastructure design.*



## Keywords
Structural Optimization; Finite Element Method; Embodied Carbon; Industrial Pipe Rack; Artificial Intelligence; Steel Reduction.


## Introduction
Pipe racks are critical structural systems used to support process pipelines, cable trays, instrumentation lines, and maintenance walkways in industrial plants. In conventional engineering practice, pipe racks are frequently designed using standardized layouts and conservative load combinations. While this ensures safety, it often results in unnecessary material consumption.

With global emphasis on carbon neutrality and sustainable infrastructure, reducing embodied carbon in steel-intensive systems has become essential. Structural steel production contributes significantly to industrial $CO_2$ emissions. Therefore, optimizing steel usage directly impacts environmental performance.

Although FEM enables accurate structural behavior prediction, and AI algorithms improve design efficiency, most existing studies treat these methods independently. This research integrates FEM-based topology optimization with AI-assisted layout refinement into a unified workflow and evaluates their combined impact on weight, cost, and carbon reduction.

## Materials
### *Structural Material*
The pipe rack structure was modeled using ASTM A36 mild structural steel.

### *Mechanical Properties*

| Property | Value |
|---|---|
| Yield Strength (fy) | 250 MPa |
| Modulus of Elasticity (E) | 200 GPa |
| Density | 7850 kg/m³ |
| Poisson's Ratio | 0.30 |

Steel behavior was assumed linear-elastic within permissible stress limits, following Hooke's Law:
Stress = Modulus of Elasticity x Strain

### *Corrosion Protection*

Since pipe racks are usually outdoors, we considered:

- Epoxy protective coating
- Small corrosion allowance
- Galvanized bolts

This ensures long service life of the structure.

## Methodology

### *Case Study Description*

Figure 1. A Typical Industrial Pipe rack in large plant.

A representative industrial pipe rack with the following parameters was modeled:

- Length: 30 m
- Width: 6 m
- Height: 8 m
- Three-tier pipe arrangement
- Material: ASTM A36 steel

Design loads included

- Dead load (self-weight)
- Pipe load: 8 kN/m per tier
- Cable tray load: 2 kN/m
- Walkway live load: 3 kN/m²
- Wind load: 1.2 kN/m²
- Seismic load (medium zone)

### *Baseline Structural Design*

The initial pipe rack configuration was developed using conventional industrial design practice. Standard steel sections were selected based on:

- Code-based load combinations
- Conservative safety factors
- Typical span assumptions
- Manual section selection methods

After modeling the full structure, the total steel volume was calculated from the cumulative volume of all structural members (columns, beams, bracings, secondary supports).
The structural mass was computed using the fundamental mass–density relation:

$$M = \rho V$$

Where:
M = total mass (kg)
ρ = steel density (7850 kg/m³)
V = total steel volume (m³)
For the baseline design:
Total steel volume ($V_1$) = 15.3 m³
Therefore:
$M_1 = 7850 \times 15.3$
$M_1 \approx 120{,}000$ kg
$M_1 \approx 120$ tons
This configuration satisfied safety requirements but showed significant under-utilization in several members.

### *EM-Based Structural Analysis*

A three-dimensional finite element model (Figure 2) of the pipe rack was developed using beam elements. Linear static analysis was performed under the following load combinations:

- Dead Load + Live Load
- Dead Load + Live Load + Wind
- Dead Load + Live Load + Seismic

The FEM results revealed:

- Several beams were operating at only 55–65% of allowable stress
- Some columns had high safety margins (>2.0)
- Bracing members showed low axial utilization
- Deflection values were significantly below L/250 limits

This indicated overdesign in multiple components.

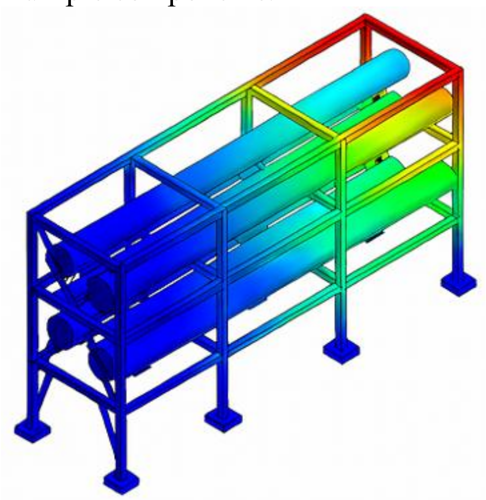

Figure 2. Finite Element Method analysis.

 ISBN 978-81-973526-0-7

### *FEM-Based Structural Optimization*

A 3D computer model of the pipe rack was created (Figure 2).

- The following steps were performed:
- The structure was divided into beam elements.
- The base of the columns was fixed.
- Different load combinations were applied:
    - Dead Load + Live Load
    - Dead Load + Live Load + Wind
    - Dead Load + Live Load + Seismic

Linear static analysis was performed to check stresses and deflections.
Mesh convergence was also checked to make sure the results were accurate.

### *Pipe rack members Optimization Process*

The optimization was performed in the following structured steps:

**Step 1: Member Utilization Assessment**

Each structural element was evaluated using:
Utilization Ratio = Actual Stress / Allowable Stress
Members with utilization < 0.75 were flagged for resizing.

**Step 2: Section Downsizing**

Oversized sections were replaced with lighter alternatives while ensuring:

- $\sigma\_actual \leq \sigma\_allowable$
- $\Delta\_actual \leq L/250$
- Stability constraints satisfied

For example:

- Columns reduced from heavier ISMB 450 to ISMB 400
- Primary beams reduced one section grade
- Secondary beams replaced with lighter channels
- Bracing sizes optimized

**Step 3: Topology Optimization**

Density-based topology optimization (SIMP method) was applied to remove unnecessary material in low-stress zones while preserving load paths.
This reduced redundant steel near connection regions and secondary framing.

**Step 4: Recalculation of Total Volume**

After resizing and topology refinement:
Total optimized volume ($V_2$) = 12.7 m$^3$
New mass:
$M_2 = 7850 \times 12.7$
$M_2 = 100{,}000$ kg
$M_2 = 100$ tons

### *Final Weight Reduction*

Weight reduction = 120 − 100 = 20 tons
Percentage reduction ≈ 16.7%
This reduction was achieved without violating stress, deflection, or stability constraints.

### *Artificial Intelligence and Machine Learning*

FEM alone improves structural accuracy. However, AI and ML were introduced to enhance design efficiency and reduce conservative decision-making.

### *Dataset Preparation*

A dataset of 42 industrial pipe rack projects was compiled. Input features included:

- Span length

- Number of pipe tiers
- Pipe diameters
- Load intensity
- Wind zone
- Seismic zone

Output variable:

- Optimal section size selection
- Recommended column spacing

***Random Forest Regression for Section Prediction***

A Random Forest model was trained to predict suitable steel sections based on input loading parameters.

Why Random Forest?

- Handles nonlinear relationships
- Reduces overfitting
- Suitable for structural parameter prediction

Model performance: $R^2 = 0.89$

This indicates strong predictive capability. The model reduced manual trial-and-error iterations during section selection.

***Genetic Algorithm for Spacing Optimization***

Column spacing significantly influences bending moment and material demand.

A Genetic Algorithm was implemented to:

- Minimize total structural mass
- Maintain stress constraints
- Maintain deflection constraints

The algorithm iteratively evolved spacing combinations and selected the best-performing configuration. This improved load distribution and further reduced steel consumption.

***AI Reduced Engineering Time***

AI automated:

- Preliminary section selection
- Iterative layout modification
- Utilization ratio prediction

Conventional design required approximately 4 weeks due to repeated manual recalculations.

AI-assisted workflow reduced design duration to 2.5 weeks (37% reduction).

***Carbon Reduction Mechanism***

Embodied carbon was estimated using (Figure 3):

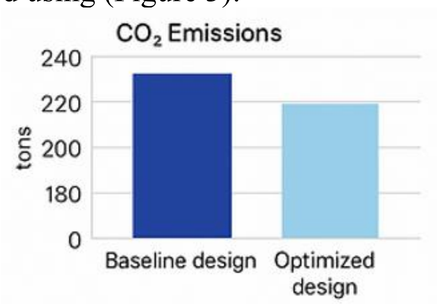


Figure 3. $CO_2$ saving.

CO2= Steel Weight x Emission factor (1.9 tCO2 @ ton steel)

Baseline design $CO_2$: $120 \times 1.9 = 228$ tons

Optimized design $CO_2$: $100 \times 1.9 = 190$ tons

Carbon saving: 38 tons $CO_2$
Since embodied carbon scales linearly with material usage, steel reduction directly translates to carbon reduction.

***Engineering Interpretation (Strong Academic Statement)***

The 16.7% reduction in structural weight was achieved through a systematic process involving:

- Accurate stress redistribution using FEM
- Identification of under-utilized members
- Controlled section downsizing
- Topology-based material removal
- AI-assisted intelligent section prediction
- Genetic algorithm-based spacing refinement

The integration of physics-based modeling with data-driven optimization reduced structural redundancy while maintaining safety, serviceability, and constructability requirements.

## Results

| Parameter | Baseline | Optimized | Reduction |
|---|---|---|---|
| Steel Weight | 120 tons | 100 tons | 16.7% |
| $CO_2$ Emission | 228 tons | 190 tons | 16.6% |
| Steel Cost ($900/ton) | $108,000 | $90,000 | $18,000 |
| Design Time | 4 weeks | 2.5 weeks | 37% |

## Discussion

The combined FEM–AI framework demonstrated significant material and environmental benefits. FEM enabled accurate stress distribution analysis, ensuring safety compliance. AI eliminated conservative design redundancies and accelerated section selection.
The 20-ton steel reduction translated directly into proportional carbon and cost savings. These findings align with reported optimization studies showing 10–20% material reduction in structural systems.
This methodology is particularly relevant for water treatment plants, data centers, oil & gas installations, and pharmaceutical facilities where steel-intensive pipe racks are common.
Future work may include real-time sensor-based adaptive optimization and life-cycle carbon assessment.

## Conclusion

This study confirms that integrating FEM-based structural analysis with AI-driven optimization significantly enhances industrial pipe rack efficiency.
Key findings:

- 16–17% steel weight reduction
- 38 tons $CO_2$ reduction
- $18,000 cost savings
- 37% reduction in design time

The proposed framework offers a practical pathway toward sustainable and economically optimized industrial infrastructure.

## References

[1] Hibbeler, R. C., Structural Analysis, 9th ed., Pearson, 2014.
[2] Reddy, J. N., An Introduction to the Finite Element Method, McGraw-Hill, 2005.
[3] Rao, S. S., Engineering Optimization, Wiley, 2009.

[4] Deb, K., Multi-Objective Optimization Using Evolutionary Algorithms, Wiley, 2001.
[5] ASTM International, ASTM A36/A36M-19, 2019.
[6] Sigmund, O., Bendsoe, M. P., Topology Optimization, Springer, 2003.

*ISBN 978-81-973526-0-7*

# AI-ENHANCED COMPUTATIONAL MECHANICS FOR DIGITAL ENGINEERING DESIGN USING CFD AND FEA

Somya Joshi*[1], Arti Mehta[1]
*[1]G.B. Pant University of Agriculture and Technology, Pantnagar, Uttarakhand
* somyajoshi070705@gmail.com

## Abstract

*The work described in this paper details a combined computational fluid dynamics (CFD), finite element analysis (FEA) and artificial intelligence (AI) based optimization process within a digital engineering workflow context to inform design through simulation based processes, as is increasingly performed within the design process in modern engineering as a means of avoiding redundant prototyping. In order to illustrate the flow and structural interaction issues and the principle of the coupling approach, a simplified mechanical system is considered. Computational Fluid Dynamics (CFD) tools are used to compute the pressure and velocity field while Finite Element Analysis (FEA) tools are used to compute the stress and deformation fields. In this step, parametric optimization loops using AI tools are executed to improve the quality of the design parameters and reduce the number of iterations. This step combines physics based simulations with data driven approaches in order to improve computational efficiency, accuracy in the prediction of results, and virtual prototyping in early-stage engineering design. The study also highlights the necessity for multiphysics interaction, and the role of digital engineering practices in mechanical systems design in modern engineering. Despite being conceptual, the proposed framework shows how clever simulation environments may be utilized in future engineering design and optimization.*

## Keywords

Computational Mechanics, Computational Fluid Dynamics (CFD), Finite Element Analysis (FEA), Artificial Intelligence in Engineering Design Optimization, Multiphysics Simulation, Digital Engineering, Virtual Prototyping.

## Introduction

The process of engineering design has changed dramatically in the past few decades, largely as a result of improved computer capabilities. In the early 1980s new product development based on physical prototyping and experimentation was slow, expensive, inflexible. Computational mechanics is now a relevant tool in the engineering cycle by allowing an engineer to forecast the behavior of a complex mechanical system before its construction, using Computational Fluid Dynamics (CFD) and Finite Element Analysis (FEA) in conjunction for fluid flows, structural deformations, heat transfers and Multiphysics [6,7,8]. Computation Fluid Dynamics (CFD) enables numerical assessments of fluid flow problems such as the Navier Stokes equations and Finite Element Analysis (FEA) enables such analyzes of stresses, strains and deformations on solids [6,14]. These numerical trials allow for more accurate design assessments without the need for endless rounds of physical testing. Such high-fidelity simulations usually require important computing power to iterate towards a final solution.

The use of AI and ML in computational mechanics has enabled simulation driven analysis and optimization of designs [2,3,4] . AI can be trained on simulation data to predict system behavior and assist in determining design variables with the desired characteristics, decreasing the time required for simulations in the design process. By harnessing the capabilities of digital engineering, industry is transforming its processes with CAD modeling, simulation, optimization and virtual prototyping in a powerful digital environment. This allows the use of digital twins and multiphysics modeling to simulate the multi-physical effects and the behavior of systems over time, from a design to a production phase [9,10]. This single approach minimizes risk, speeds time to market, and adds value to cost-effective product development.

The use of integrated CFD, FEA, AI based design optimization and multiphysics simulation in a digital engineering environment is discussed. A case study illustrates the advantages of AI improved simulation workflows that can improve the performance of a mechanical system. The aim of this research is to show the benefits and challenges of the use of computational mechanics and ai in future generation engineering design.

## Literature Review

The beginning of applied computational mechanics was very slow to develop, struggling to get from paper to screens. Engineers relied on experimentation. They relied on wind tunnels, Physical models, Long waiting times, High cost. Then came CFD and FEA, everything started changing and Computational Fluid Dynamics allows engineers to visualize the air flow over a wing before it is built. A heat transfer fluid travelling through a pipe. This science investigates Stress, Strain, Deformation and Structures and it is numerically solved using Finite Element Analysis. CFD and FEA were introduced together influential in the development of simulation driven design and have been thoroughly researched with the aim of reducing prototypes and achieving greater accuracy [1,8,13]. Even detailed simulations take time, sometimes a lot more time. Iterations increase Resources get stretched. The research question thus became, Will we be able to make the simulations faster, smarter, maybe even predictive?

This is what makes AI come to the rescue quietly at first then everywhere. Machine Learning models started learning by example from simulations. Alternatively a prediction model can be more easily computed and while not perfectly accurate and it is usually accurate enough to be useful in an optimization loop. Neural networks, surrogate models and genetic algorithms to name a few are widely used in the literature to solve optimization problems with better shapes, better parameters, better performances [4,5]. Humans are still guided on their decisions by engineers but AI can suggest paths humans might miss. The field of multiphysics modeling has also emerged since all real systems are coupled, fluids affect structures, heat affects materials and vibrations affect flow and vice versa. More recently coupling fluid structure interaction (FSI), thermomechanical and multiphysics has attracted interest. These multiphysics approaches provide accurate predictions within the researchers' community but are computationally demanding. That tradeoff is always there and digital engineering workflows are attempting to address the complexity by using CAD models directly in simulation. Optimization routines are supplied by simulations typically generated iteratively in the context of virtual prototype development and validation. Some researchers argue that digital twins are digital representations of physical systems in real time. This sounds futuristic but the idea is being implemented in aerospace, automotive and energy systems.

Despite all progress challenges remain. Computational cost is still high for detailed simulations. AI models sometimes lack physical interpretability. Integration between physics based and data driven methods is not always smooth. At present hybrid methods are being developed that combine physics based accuracy and AI's efficiency [11]. This paper builds upon these efforts to look at CFD and FEA AI based optimization and digital engineering into one unit, not as separate tools but as parts of one workflow. Thus a simple but meaningful example can be given as case study. Today modern engineering design is no longer just about solving equations. It is about connecting tools making them talk to each other and designing smarter systems before they physically exist.

## Research Methodology

Though not so complex as to be difficult to understand this is a simulation driven workflow. The first goal was to study the interaction between CFD, FEA and an AI based optimizer in a digital engineering environment. The study started with the definition of a simplified mechanical geometry and something generic. While a flexible tool for fluid and structural simulations it was not meant to be a copy of a real industrial product but rather a system designed to be seen interacted with, from there it went to simulation.

A First CFD based analysis was performed. The flow around the component was conceptually explained using the governing equations of mass and momentum conservation[6,14]. Assumed boundary conditions for steady state flow allowed determination of pressure regions, velocity distribution and possible irregularities in potential flow. Nothing too extreme but enough to understand interaction trends.This was then followed with the structural analysis wherein the geometry was divided into smaller structural elements (FEA) and appropriate material properties and loads corresponding with operational conditions were assumed [1,13]. Stress concentration points and deformation patterns corresponded to those we would expect. Following simulation output observation the workflow moves into optimization. Here the AI assisted thinking steps in to avoid multiple parameter tinkering sessions, a conceptual predictive loop was introduced, adapting parameters according to the simulation results in an iterative process [2,4,5]. Adjustments are made and the loop repeats.


Figure 1. Simplified digital engineering workflow integrating CFD, FEA, and AI-based design optimization.

Another approach is rather multiphysics since fluid and structure in real life systems do not behave independently fluid pressure affects structural response and structural change affects flow pattern but even assuming simplified models to couple these yields a more complete picture. Not perfect but closer to reality.In general the method forms a digital iteration cycle that is quiet, efficient and slightly messy but effective enough to show integration of computational mechanics and artificial intelligence assisted decision support.

## Results

Meaningful results were obtained from this combined workflow. The CFD analysis highlighted that some model surfaces were pressurized. These same regions also experienced increased stress values during structural evaluation which was expected and thus helpful.After installation of the optimization adjustments, load pressure uniformity improved and stress peaks decreased. The performance increases though small is important in that fewer passes are necessary to achieve an acceptable performance. That alone suggests efficiency gain. Also the flow structures were noticeably stabilized and the patterns of structural deformation were more evenly spread out. This is also where the multiphysics interaction was revealed, it is all connected

The workflow demonstrated:

- Improved design stability
- Reduced stress concentration
- Better flow distribution
- Fewer manual design iterations

Although these results are only conceptual they show how integrated simulation and AI guided refinement can improve early stage decisions.

## Discussion

The study is consistent with the emerging consensus in engineering practice that simulation is very powerful. AI (Artificial Intelligence) by itself is promising. Together they become practical but customarily CFD and FEA involve a human [2,4]. Engineers run a simulation, change the inputs and repeat, effective but time consuming. The AI assisted optimization accelerates this process effectively learning from past trials rather than blind guesses [5] . The approach suggests better parameters which, while not always correct are directionally helpful. Saves effort and sometimes saves resources. Also as all real mechanical systems are multiphysical that is subject to more than one type of physical phenomenon, structures are loaded by fluid flow. The material has a temperature dependence of course any interactions we miss can destroy the picture we are developing but the simplified coupling we have considered can help.

There are limitations. The optimization in this study was conceptual and not based on large datasets. Although high fidelity multiphysics simulation is costly and may not be feasible in an academic environment, the work flow direction is still valid.

What this research shows is simple:

- The engineering design tools are becoming integrated.
- Simulation dataand optimization all working together.
- Not isolated anymore.

## Conclusion

In this paper we implement a framework of CFD, FEA with AI assisted optimization in the digital engineering workflow, showing the ways in which a simulation based design frame work can be cleverly iterated. These findings thus show the benefit of employing physics based modeling principles combined with optimization techniques to create a more efficient design process. They further indicate the strength of using a simplified approach to modeling fluid and structural interactions to gain a preliminary understanding of the system while easing parameter tuning in the AI assisted loop.

The future trend in engineering design is to eventually move to clever simulation environments with digital prototypes as a first step. This research illustrates the transition, modest in scope but substantial in implication

## Recommendations

Future work in this area could take the work further by matching experimental results to the simulation results, making the framework more concrete by comparing it to observations [6,11]. More advanced machine learning models can be used for non linear systems and large scale data sets. Future work could focus on a fully multiphysics coupling using specialized simulation software and on linking with digital twin environments for real time monitoring and prediction of engineering systems [10,12]. Furthermore additional computational resources could allow for more refined models and better optimizations. It is however also applicable to aerospace automotive and thermal system design and can be extended to other complex engineering systems.

## References

[1] Ziemkiewicz. O. C., Taylor, R.L., & Zhu, J.Z. (2013). The finite element method: Its basis and fundamentals (7th ed.). Elsevier.
[2] Brunton, S. L., & Noack, B. R. (2020) Machine learning for fluid mechanics. Annual Review of Fluid Mechanics, 52, 477-508. https://doi.org/10.1146/annurev-fluid-010719-060214
[3] Raissi, M., Perdikaris, P., & Karniadakis, G. E. Physics-informed neural networks: A deep learning framework for solving forward and inverse problems involving nonlinear partial differential equations. Journal of Computational Physics, 378,686-707. https://doi.org/10.1016/j.jcp.2018.10.045
[4] Goodfellow, I., Bengio, Y., & Courville, A. (2016). Deep Learning. MIT Press.
[5] Deb, K. (2012). Optimization for Engineering Design: Algorithms and examples (2nd ed.) PHI Learning.
[6] Anderson, J. D., Jr. (1995). Computational Fluid Dynamics: The basics with applications. McGraw-Hill.
[7] Versteeg, H. K., & Malalasekera, W (2007). An introduction to computational fluid dynamics: The finite volume method (2nd ed.). Pearson.
[8] Reddy, J. N. (2019). An introduction to the finite element analysis. (Updated ed.). McGraw-Hill.
[9] Grieves, M., & Vickers, J. (2017). Digital twin: Mitigating unpredictable, undesirable emergent behavior in complex systems. In F.-J. Kahlen, S. Flumerfelt, & A. Alves (Eds.), Transdisciplinary perspectives on complex systems (pp.85-113). Springer. https://doi.org/10.1007/978-3-319-38756-7_4
[10] Tao, F., & Zhang, M. (2017). Digital twin shop-floor: A new shop-floor paradigm towards smart manufacturing. IEEE Transactions on Industrial Informatics, 13(6), 3625–3633. https://doi.org/10.1109/TII.2017.2756650
[11] Chinesta, F., Cueto, E., & Ryckelynck, D. (2017). Reduced order modeling of complex systems. Archives of Computational Methods in Engineering, 24(4), 713–747.
[12] Quarteroni, A., & Valli, A. (2008). Numerical approximation of partial differential equations. Springer.
[13] Bathe, K. J. (2006). Finite element procedures. Klaus-Jürgen Bathe.
[14] Ferziger, J. H., and Perić, M. (2002). Computational methods for fluid dynamics (3rd ed.) Springer.
[15] Tu, J., Yeoh, G. H., and Liu, C. (2018). Computational fluid dynamics: A practical approach (2nd ed.). Butterworth-Heinemann.
[16] Bishop, C. M. (2006). Pattern recognition and machine learning. Springer.

# A REVIEW ON PREDICTION OF MECHANICAL AND WELD PROPERTIES OF TIG WELDING BY ARTIFICIAL INTELLIGENCE

Amaan Naseh*[1], Ravi Butola[1]
*[1]Guru Gobind Singh Indraprastha University, India
*naseh.amaan@gmail.com

## Abstract

*Welding is a very common manufacturing process which is used to join a vast variety of materials including metals (Aluminum, Magnesium, etc.), alloys (stainless steel, Inconel, etc.) and polymers (thermoplastics, bio-polymers, etc.). There are a lot of welding technologies available, including Arc welding, Gas welding, Resistance welding, Solid-State welding and Modern welding, respectively. Out of all the welding technologies, Gas Tungsten Arc Welding, GTAW also known as Tungsten Inert Gas, TIG is the best welding technology as it requires less investment, performs fast welding, produce nearly non-contaminated or defect-free welds, shows compatibility with a variety of materials including dissimilar metals and alloys as well as it covers vast range of applications. This study aims to review the recent advancements in TIG welding in the new industrialization era, i.e., Industry 4.0 by utilizing modern technologies such as artificial intelligence, machine learning (ML), deep learning, neural networks (NN), digital twin, and robotics. It is found that most of the recent works focused on optimization of TIG welding by predicting mechanical and weld properties such as tensile strength, micro-hardness, defects and bead geometry (width, height, penetration, etc.). Comparative analysis of many ML methodologies is employed in few researches which showed that Random Forest algorithm shows exceptional results as both classification and regression model. Similarly, for deep learning, neural networks like XGBoost outperforms other algorithms and it can be further fine-tuned by coupling it with fuzzy algorithms. This study compares such researches in detail which can be further utilized to develop a novel system.*

## Keywords

GTAW/TIG Welding, Mechanical Properties Prediction, Machine Learning, Deep Learning.

## Introduction

Welding is defined as a material joining operation which joins materials using heat either supplied externally ("ex-situ") or generated on-site ("in-situ"). There is a vast range of materials that can be joined using welding, including metals (such as Aluminum, Magnesium, etc.) alloys (such as stainless steel or SS, Inconel, etc.) and polymers (thermoplastics, bio-polymers, etc.). The criteria for material selection depends mostly on the application and the required outcome of welding operation. Some of the most common welding applications include equipment of aerospace, nuclear and automobile industry, repair of mechanical parts, micro-precise surgical instruments and medical equipment [1]. There are a lot of welding technologies available, including Arc welding, Gas welding, Resistance welding, Solid-State welding and Modern welding, as shown in Figure 1.

Choice of welding operation depends on lot of factors including application, materials, time, money, labour and efficiency. TIG welding is the best welding technology as it requires less investment, fast welding operation and it is compatible with a variety of materials as well as it covers vast range of applications. Also, there are some benefits unique to TIG welding, i.e., it produces accurate weld beads with least or minimal defects (due to the shielding effect of inert gases), pollution-free welds and it has the ability to weld dissimilar metals [2-6].

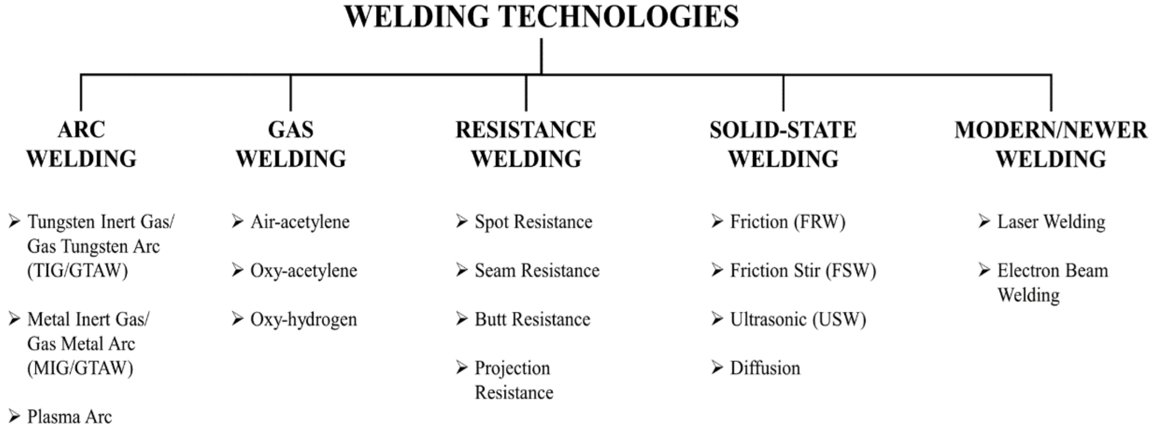


Figure 1. Welding technologies.

## Literature Review

The following work has been done by authors in the recent years, which can also be seen in Table 1.

Table 1. Summary of literature review on TIG welding, (*) denotes model with best results.

| Welding Type | Material | Input/Process parameters | Output parameters | ML methodology | Ref. |
|---|---|---|---|---|---|
| A-TIG | SS304L | Current, Welding speed, Flux, Gas flow rate, Arc length and Voltage | Surface temperature | 5 algorithms: LR, SVR, DT, RF*, XGBoost | [7] |
| Twin-TIG | SS316L | Current, Arc length, Welding speed, Tungsten angle, frequency & spacing, Gas flow rate and Nozzle diameter | Weld penetration and width | 3 algorithms: LR, GPR*, BPNN | [8] |
| A-TIG | SS304 L/LN, SS316 L/LN | Current, Voltage, Travel speed, Flux, Gas flow rate, Sample thickness and Flux | Weld penetration depth, width and their ratio | RF | [9] |
| Robotic TIG | SS304L | Gas flow rate, Voltage, Travel speed and Arc length | Burn-through, Good weld, Partial penetration and Undercut | 2 algorithms: ResNet*, SVM | [10] |
| TIG | SS316L | Gas flow rate, Welding speed, Wire feed rate, Voltage, Current and Nozzle diameter | Welding anomaly/ defect | 2 algorithms: KNN*, IF | [11] |
| TIG and YAG Laser | SS304 | Weld power, Travel speed and Hole depth | UTS and micro-hardness | 2 algorithms: ANFIS, UCNN | [12] |
| Vibratory-assisted TIG | Al6063 | Vibromotor voltage and Vibration time | Hardness and microstructure | 2 algorithms: ANN, GRNN | [13] |

| | | | | | |
|---|---|---|---|---|---|
| Ultrasonically-assisted TIG | Inconel 625 | Arc length, Ultrasonic power, Current, Gas flow rate and Filler wire | Micro-hardness and Hot crack length | 4 algorithms: RFR*, ANN, ANFIS, MLR | [14] |
| TIG, A-TIG and Autogenous TIG | SS304H | Arc gap, Root gap, Torch angle, Welding speed, Filler wire, Flux, Heat input and Gas flow rate | Bead width, height, penetration, Weld tensile strength, % elongation and Rockwell hardness | 6 algorithms: ANN, KNN, SVR, RF, GBR, XgBoost* | [15] |

Chandra et al. [7] performed Activated TIG (A-TIG) welding on SS304L plates with dimensions 100 mm x 50 mm x 6 mm. The experimental setup includes TIG315P power source, 99.95% pure argon and FLIR TG287 thermal camera. The process parameters include variable parameters and constant parameters. Variable parameters include current (100-130 A), welding speed (4-6 mm/s) and fluxes (CaO, SiO2, Al2O3 and TiO2) whereas constant parameters include gas flow rate (10 L/min), arc length (5-6 mm), open-circuit voltage (20 V) and a DC power source. Using these parameters, 40 experiments were conducted, mainly to record thermal images of size 180 x 120 pixels with temperature reaching maximum up to 1030 °C. After data collection and 25-75% test-train splitting, 5 ML algorithms, including Linear Regression (LR), Support Vector Regression (SVR), Decision Tree (DT), Random Forest (RF) and Extreme Gradient Boosting (XGBoost) were used to predict surface temperature and relationship among independent variable parameters. It was seen that RF model performed best by achieving highest R2 value (approx. 0.95) and lowest errors, i.e., Root Mean Square Error, RMSE (19.93 °C) and Mean Absolute Error, MAE (16.45 °C), respectively. Future scope include consideration of more process parameters for achieving generalization of the ML model to optimize A-TIG welding using ML.

Zhang et al. [8] performed 100 Twin-TIG welding experiments on 20 plates of SS316L with dimensions 200 mm x 100 mm x 5 mm, and produced 100 defect-free weld beads. The process parameters include welding current (150-300 A), arc length (1-3 mm), welding speed (5-10 mm/s), tungsten angle (30-60 °), frequency (5-500 Hz), tungsten spacing (1-5 mm) and some less-contributing factors such as gas flow rate and nozzle diameter. All these parameters were used to conduct 100 experiments to obtain weld penetration (0.8-4.4 mm) and weld width (6.8-12.7 mm). After data collection, 3 ML algorithms, including Linear Regression (LR), Gaussian Process Regression (GPR) and Backpropagation Neural Network (BPNN) were used to predict weld penetration and weld width. It was seen that GPR model performed best by achieving the R2 value for weld penetration and weld width as 0.9680, 0.9696 and Mean Squared Error (MSE) for weld penetration and weld width as 0.0384, 0.0819, respectively. Based on the results, a novel Twin-TIG welding power source and a software for testing ML models was developed which can be utilized for further research and development.

Munghate et al. [9] utilized the data from different literatures on A-TIG welding to develop a ML model for prediction of bead geometry (i.e., penetration depth (D), bead width (w) and D/w ratio). The data of different varieties of steel was taken, including 316L, 304L, 316LN, 304LN, to finally obtain 318 data points consisting of 6 input parameters as current, voltage, travel speed, gas flow rate, sample thickness and flux type. The data was split into test and train in the ratio of 30-70% and Random Forest (RF) algorithm was used to train regression and classification models. The regression model achieved R2 value for penetration, width and D/w as 88.8%, 89.8% and 51.4%, respectively. The classification model achieved accuracy for penetration, width and D/w as 97.7%, 85.5% and 94.12% as well as Area Under Curve (AUC) value for the same as 0.94, 0.84 and 0.92, respectively. Other metrics were also used to further evaluate the performance of ML models, which finally suggests that both the regression and classification models can be adopted to predict bead penetration and D/w ratio effectively. This study can be utilized for broadening the scope to dissimilar metals.

Zhang et al. [10] performed robotic TIG welding on SS304L plates with dimensions 250 mm x 150 mm x 10 mm. The process parameters include gas flow rate of pure Argon (30 L/min), travel speed (20 cm/min), operating voltage (20 V), Tungsten-Lanthanum electrode (6.5 mm diameter), arc length (2.5 mm) and a camera (Basler ace acA1920-40gm inclined at 45°) to capture weld pool images. Nearly 4,000 images of dimensions 1280 x 1240 pixels were captured and grouped into 4 categories, including burn-through, good weld, partial penetration and undercut, which was further grouped into 2 categories, i.e., defective and good welds. K Singular Value Decomposition (K-SVD) algorithm was employed to enhance captured images. The enhanced dataset images was split into the ratio of 6:2:2 as training, testing and validation for training and cropped to different dimensions for compatibility, i.e., initially 880 x 680 pixels and further 256 x 256 pixels. It was seen that low currents (< 450 A) or high currents (> 460 A) resulted in defects. The accuracy of ResNet model for burn-through, good weld, partial penetration and undercut was found to be 1.000, 0.948, 0.996 and 0.981, respectively whereas for Support Vector Machine (SVM) based models, it was found to be 0.295, 0.914, 0.97 and 0.985, respectively. It was concluded that neural networks can be used to deduce complex patterns in the weld pool images as compared to traditional algorithms. Future scope includes robust real-time defect detection and welding monitoring systems in industry which can enhance the production efficiency of overall welding process.

Boutin et al. [11] performed TIG welding on SS316L plates with dimensions 250 mm x Ø278 mm x 28 mm using automatic GTAW wire process (50 passes). The process parameters include interpass temperture (150 °C), 3.2 mm tungsten electrode, 3.2 mm 316L filler wire, Ø20 mm nozzle diameter, gas flow rate of pure tungsten as 20L/min, welding speed, wire feed rate, voltage and current. A camera of Alvium model with Sony sensor sensitive to near-infrared light was used to capture 8100 images at 25Hz frequency and record data using different types of electronic devices. After data collection and test-train 20-80% splitting, 2 ML algorithms, K-Nearest Neighbor (KNN) and Isolation Forest (IF) were used to develop ML models for anomaly detection. It was found that KNN model performed better by achieving 94% accuracy and 0.034% standard deviation as compared to IF model with 93% accuracy and 0.056% standard deviation, respectively. Other metrics were employed to further evaluate ML models. Future scope includes real-time inspection and monitoring in welding by advanced sensors and algorithms which further leads to automation in welding.

Kumar et al. [12] performed TIG welding and YAG Laser welding on SS304 plates with dimensions 300 x 150 x 2 mm. The process parameters for TIG welding include weld power (180-190 W), travel speed (5-8 mm/s) and hole depth (3-8 mm), whose effect on ultimate tensile strength (UTS) and micro-hardness was studied. The UTS before and after welding was found to be 501 MPa and 532 MPa. Similarly, the micro-hardness before and after welding was found to be 162 and 221 Hv, respectively. After collecting data, 2 ML algorithms, Adaptive Neuro-Fuzzy Inference System (ANFIS) and Universal Convolutional Neural Network (UCNN) were used to train ML models. ANFIS was trained on 45 data pairs to predict UTS and micro-hardness, with Mean Absolute Percentage Errors (MAPE) as 13.0598% and 13.0663% using gaussmf membership function. UCNN was trained on optical images to predict microstructures, i.e. Fusion Zones (FZ) and Heat Affected Zones (HAZ) with an accuracy of 91.64% and 92.62% for TIG welding, respectively. Similar results are available for YAG Laser welding. Thus, ANFIS model can be used to select and optimize

process parameters whereas UCNN model can be used for defect detection and monitoring.
Rao et al. [13] performed vibratory-assisted TIG Welding on Al6063 alloy (having max 0.9% Mg and 0.6% Si) with dimensions 300 x 100 x 5 mm. The process parameters include vibromotor voltage (50-230 V) and vibration time (60-100 s). After welding, Rockwell hardness testing (with 100 Kg load) was used to calculate hardness without vibration at 0 V, with vibration at 140 V and 230 V. Leica DMI optical microscope was used to capture images of the specimen at 200x magnification. It was observed that voltage in the range 50-140 V enhanced vibrational energy for increasing hardness whereas above 140 V caused significant decrease in the hardness. Also, fine granules/smaller dendrites was observed in microstructure in the range 0-140 V whereas coarse grains/long dendrites was observed beyond 140 V. After collecting data, 2 deep learning algorithms were selected to develop ML models, i.e., Artificial Neural Network (ANN) on 44 data items and Generalized Regression Neural Network (GRNN) for 57 data items for hardness prediction. The precision for the ANN model was found to be 99.9% and the validation accuracy of GRNN model was found to be 97.46%, respectively.
Dhilip A. et. al. [14] performed ultrasonically-assisted TIG welding on Inconel 625 alloy (Houldcroft specimen) with dimensions 76 mm x 44.5 mm x 2 mm (with 9 slots of 0.8 mm width). The experimental setup includes TIG 315BP AC/DC machine, 2.4 mm tungsten electrode, ERNiCrMo-3 manually fed filler metal (1.6 mm thick) and a magneto-restrictive ultrasonic transducer (RELTEC). The process parameters include arc length of 1.5 mm, ultrasonic power (at 1kW, 20.1 kHz), current (80-120 A) and gas flow rate of pure argon (5-7 L/min). Micro-hardness was calculated using Vickers hardness test by applying 500g load for 10s. Finally, 2 continuous parameters (current and gas flow rate) with 3 levels and 2 categorical parameters (ultrasonic vibration and filler) with 2 levels (not included-0, included-1) were used to perform 52 experiments to collect the data. After data collection and 20-80% test-train split, 4 ML algorithms, including Random Forest Regression (RFR), Artificial Neural Network (ANN), Adaptive Neuro-Fuzzy Inference System (ANFIS) and Multiple Linear Regression (MLR) were used to train ML models for micro-hardness and hot crack length prediction. Among all the ML models, RFR model performed best by achieving R2 value for crack length and micro-hardness as 0.9612 and 0.9772 as well as Root Mean Square Error (RMSE) value for crack length and micro-hardness as 2.4095 and 2.9535 for testing stage, respectively. Future scope includes parametric augmentation, real time monitoring and control using better algorithms like XGBoost and thermal imaging.
Saha et al. [15] performed TIG, autogenous TIG and activated TIG welding on SS304H with dimensions 50 mm x 50 mm x 8mm (butt-welded). The experimental setup includes Qineo GLW 322 TIG machine by CLOOS with a Promotech Gecko auto magnetic carriage, MOGRA CWF 04 cold wire feeder, Kalling's reagent 2 (for etch test), MITUTOYO tool maker's microscope, METSCOPE PRO optical microscope, JEOL JSM IT500 Scanning Electron Microscope, INSTRON 8862 machine (for tensile test), LABQUIP and UHL-VHMT Vickers micro-hardness tester. The process parameters include constant parameters and variable parameters. The constant parameters include arc gap (2 mm), root gap (0 mm), torch angle (75° best so fixed), welding speed (1.22 mm/s), filler wire (1.2 mm diameter, 20 mm/s flow speed) and activated flux (TiO2) in some trials. The variable parameters include heat input (0.768-1.52 KJ/mm) and gas flow rate (10-14 mm/s). The mechanical properties before welding include tensile strength as 582.08 MPa, percentage elongation as 30.48% and Rockwell hardness as 31.33 HRC. A total of 50 experiments were performed by altering these parameters to calculate bead characteristics (width, height and penetration) and mechanical properties (tensile strength, % elongation and Rockwell hardness). After data collection, 6 ML algorithms were used to train ML models, including Artificial Neural

Network (ANN), K-Nearest Neighbor (KNN), Support Vector Regression (SVR), Random Forest (RF), Gradient Boosting Regression (GBR) and Extreme Gradient Boosting (XGBoost). Among them, XGBoost performed best by achieving R2 values for all the outputs in the range 0.85-0.90 as well as least errors. Therefore, this work can be considered as a generic approach for different types of TIG welding considering vast range of parameters to predict a variety of outputs as a holistic view.

## Results and Discussion

From the previous literature, it can be seen that a lot of work has been done on different types of welding technologies, including TIG welding on a vast range of materials, in accordance with newer technologies and trends of Industry 4.0 such as thermal sensors, artificial intelligence, machine learning and deep learning. The commonly used machine learning and deep learning algorithms are Random Forest (RF), Extreme Gradient Boosting (XGBoost), Artificial Neural Network (ANN), Convolutional Neural Network (CNN), Adaptive Neuro-Fuzzy Inference System (ANFIS), Support Vector Machine (SVM) and Linear Regression (LR). These algorithms performed very well by achieving high accuracy and low errors and were successful in deducing patterns in dataset and complex relationships among process parameters. A lot of predictive/diagnostic systems were developed targeting different process parameters to optimize TIG welding as well as real-time monitoring and control systems were proposed as future scope.

The following gaps were observed from the research:

- Comparatively lesser work is done on dissimilar metals as they are hard to weld as well as their chemical composition necessitates a good understanding of welding's material science.
- Most of the researches are only focusing on optimization of TIG welding for sheets or bars of workpieces, which is very generic in nature. Specific applications are not fulfilled but proposed as an upscaling task for future references.
- Most of the developed systems are diagnostic in nature, i.e., they are able to detect the output but there is nearly no work after output detection for its real-time monitoring, control and optimization.
- There are very few real-time analytics system to optimize and correct welding parameters during the welding. Also environmental noise cancellation mechanism is not fully employed to eradicate the effect of unpredictable noise factors from the environment.

The thermal imaging techniques, advanced sensors, parametric augmentation and comparative analysis of different machine and deep learning algorithms with mathematical modelling is concluded as areas of further research a result of this literature review.

## Conclusion

TIG welding is considered as one of the best welding technologies due to its enormous capabilities, especially the ability to weld dissimilar metals and less-polluted welds due to the shielding effect of inert gases. A lot of work has been already done on TIG welding to optimize the process parameters using various traditional techniques such as Taguchi analysis, Response Surface Methodology (RSM) as well as some modern technologies such as Machine learning, Deep learning, etc. It is found that Random Forest, Artificial Neural Network and XGBoost algorithms perform very well to generalize welding data. Therefore, they were mostly used to develop ML models for predicting a vast range of outputs, including mechanical properties (tensile strength, micro-hardness, % elongation), bead geometry (penetration, width, depth) and defects (burn-through, undercut, hot cracks). Also, it was found that current, travel speed, gas flow rate, torch angle and arc length are one of the most contributing factors acting as input to produce these outputs. These studies proposed real-time analytics system for welding monitoring and control to enhance production efficiency which will eventually lead to automation in welding technology.

## References

[1] N. Jeyaprakash, A. Haile, and M. Arunprasath, "The parameters and equipments used in TIG welding: A review," The International Journal of Engineering and Science (IJES), 2015.
[2] R. P. Singh, S. Kumar, S. Dubey, and A. Singh, "A review on working and applications of oxy-acetylene gas welding," Materials Today: Proceedings, Elsevier, 2020.
[3] P. Stavropoulos and K. Sabatakakis, "Quality assurance in resistance spot welding: State of practice, state of the art, and prospects," Metals, MDPI, 2024.
[4] D. K. Rajak, D. D. Pagar, P. L. Menezes, and A. Eyvazian, "Friction-based welding processes: Friction welding and friction stir welding," Journal of Adhesion Science and Technology, Taylor & Francis, 2020.
[5] D. Y. You, X. D. Gao, and S. Katayama, "Review of laser welding monitoring," Science and Technology of Welding and Joining, 2013.
[6] A. Biber, R. Sharma, and U. Reisgen, "Robotic welding system for adaptive process control in gas metal arc welding," Welding in the World, Springer, 2024.
[7] M. Chandra, S. Kumar, K. Ankit, S. K. Rajak, and S. Rajak, "A machine learning approach for prediction of surface temperature of the weld region in A-TIG welding," Transactions of the Indian Institute of Metals, Springer, 2023.
[8] S. Zhang, H. Zhao, Y. Liu, B. Zhang, H. Dong, and Y. Chang, "Machine learning-based optimization of process parameters in high efficiency twin-TIG welding," Welding in the World, Springer, 2025.
[9] A. A. Munghate and S. Thapliyal, "Process parameters based machine learning model for bead profile prediction in activated TIG welding using random forest machine learning," Proceedings of the Institution of Mechanical Engineers, Part B: Journal of Engineering Manufacture, 2023.
[10] X. Zhang, S. Zhao, and M. Wang, "Deep learning-based defects detection in keyhole TIG welding with enhanced vision," Materials, MDPI, 2024.
[11] T. Boutin, I. Bendaoud, J. Delmas, D. Borel, and C. Bordreuil, "Development of machine learning model for anomaly detection in multi-pass TIG welding," Welding in the World, Springer, 2025.
[12] V. Kumar A, P. Krishna R, M. F. Hasanabadi, and S. K, "Evaluation of machine learning techniques for the Nd:YAG laser and TIG welded stainless steel 304," FME Transactions, 2024.
[13] M. V. Rao, K. V. Reddy, B. V. Suresh, C. V. Babu, S. Chiranjeevarao, and M. V. N. V. Satyanarayana, "Investigation of vibratory-assisted TIG welding on Al6063 alloy: Microstructural behavior, mechanical properties, and machine learning based hardness prediction," Journal of The Institution of Engineers (India), Springer, 2024.
[14] D. A, J. Nampoothiri, and S. K, "Leveraging machine learning to predict welding quality in ultrasonically assisted TIG (UA-TIG) welded Inconel 625 joints," Journal of Materials Engineering and Performance, ASM International, 2025.
[15] S. Saha, B. Haldar, H. Joardar, S. Das, S. Mondal, and S. Tadepalli, "Supervised machine learning models for predicting SS304H welding properties using TIG, autogenous TIG, and A-TIG," Crystals, MDPI, 2025.

# AI-BASED PREDICTIVE DETECTION OF AIRCRAFT ICING USING PITOT TUBE SENSOR DATA: A REVIEW

Chetna Diwakar*[1], Shruti Mittal
*[1]J.C. Bose University of Science & Technology, YMCA, Faridabad, Haryana, India
*chetnadiwakar227@gmail.com

## Abstract

*Aircraft icing condition is a major safety hazard, particularly pitot tube icing, which can alter airspeed data and cause aircraft accidents. Conventional detection techniques are reactive, identifying ice only after it has developed. This analysis looks at how ice detection technology has evolved, with an emphasis on the move to artificial intelligence and machine learning-based prediction systems that use temperature, humidity, and pressure data to offer early warning. This study uses experimental studies, computer simulations, and integrated artificial intelligence techniques to show how lightweight machine learning models, specifically Random For est and XGBoost, provide accurate real-time icing predictions with over 94% accuracy and sub-second latency. The intro duction of a voice-activated AI co-pilot is a step towards a more intelligent, proactive flight safety system that increases situational awareness and has the potential to shift aircraft icing control from reactive to preventative.*

## Keywords

Pitot Tube, Artificial Intelligence, Aircraft Icing, Machine Learning, Predictive Detection, Embedded Systems, Aviation Safety.

## Introduction

One of the most hazardous and enduring problems affecting aviation safety is aircraft icing. Supercooled water droplets can drastically reduce aerodynamic efficiency and jeopardize sensor reliability when they freeze on aircraft surfaces, particularly on vital parts like wings, propellers, and pitot tubes. Pitot tube icing is the most dangerous of these because it interferes with dynamic air pressure monitoring, resulting in erroneous airspeed estimates and potentially devastating flight control failures. Numerous major aircraft tragedies, including as Air France Flight 447 and Saratov Airlines Flight 703, have been connected to pitot probe blockage brought on by undetected ice. This highlights the critical need for more proactive and dependable detection techniques.

Figure 1. Visual of an icing in pitot tube [9].

One of the most hazardous and enduring problems affecting aviation safety is aircraft icing. Supercooled water droplets can drastically reduce aerodynamic efficiency and jeopardize sensor reliability when they freeze on aircraft surfaces, particularly on vital parts like wings, propellers, and pitot tubes. Pitot tube icing is the most dangerous of these because it interferes with dynamic air pressure monitoring, resulting in erroneous airspeed estimates and potentially devastating flight control failures. Numerous major aircraft tragedies, including as Air France Flight 447 and Saratov Airlines Flight 703, have been connected to pitot probe blockage brought on by undetected ice. This highlights the critical need for more proactive

and dependable detection techniques.

However, recent developments in artificial intelligence (AI) and machine learning (ML) have brought about a new era of predictive ice detection, where environmental factors such as air temperature, humidity, and pressure are continuously analyzed to anticipate ice danger before accretion begins, supported by the proven effectiveness of ML in other complex prediction domains [8].

The transition from reactive to predictive systems is a turning point in aircraft safety research. The viability of employing data-driven algorithms for early ice detection and severity classification is demonstrated by studies by [3], [4], and [2]. Additionally, the adoption of real-time prediction systems on embedded platforms is supported by recent research on lightweight AI models [5], opening the door for intelligent onboard monitoring and AI-assisted pilot support.

With a focus on pitot tube sensor integration, machine learning techniques, and human-AI interaction in flight safety systems, this paper investigates the state of AI-based aircraft icing detection. In order to build autonomous, self-aware air craft systems that can anticipate and mitigate icing dangers in real time, the study highlights technological advancements, assesses current discoveries, and identifies unfilled research.

## Literature Review

### *Aim of the review*

With an emphasis on pitot tube sensor integration, machine learning prediction, and pilot assistance systems, this paper explores current developments in AI-based aircraft icing detection. By combining new findings from the fields of experimental, computational, and artificial intelligence, it il lustrates how predictive modeling could change the detection of ice from reactive to proactive. The research is separated into five sections: pitot icing threats and accidents, experimental and computational breakthroughs, AI-based warning systems, lightweight AI integration in aviation safety, and existing limitations vs future prospects for intelligent, real-time aircraft icing prevention.

Because it directly affects aerodynamic performance and sensor dependability, aviation icing has long been a concern for both human and unmanned aircraft. The research literature demonstrates a persistent trend of pitot tube icing leading to serious accidents, an ongoing development of computational and experimental detection techniques, and a recent surge in applications of artificial intelligence (AI) and machine learning (ML) for predictive risk assessment. This section looks at notable contributions to five major challenges that outline the technological and scientific progress of AI powered predictive icing detection.

### *Pitot Tube Icing: Risks and Accidents*

One of the biggest and most avoidable risks to con temporary aviation is pitot tube icing. [1] carried out one of the first major studies of pitot tube icing. According to their research, supercooled water droplets in stratiform or cumuliform clouds may quickly freeze inside the pitot probe, obstructing airflow and producing erroneous airspeed readings. Sensor malfunctions have been a direct cause of loss of control in flight (LOC-I) events, as shown by historical case studies like Air France Flight 447 and Saratov Airlines Flight 703.

[2] extended on this concept by focused on High-Altitude Ice Crystals (HAIC), a type of micro-ice particle that commonly bypasses standard heating systems. Their findings revealed that Total Air Temperature (TAT) anomalies often occur before to pitot probe blockage, hinting that early temperature deviations might serve as prognostic indicators of ice formation. This finding emphasizes how crucial it is to continuously and intelligently monitor sensor abnormalities in order to prevent cascade data failure and deliver timely cockpit notifications. The significance of switching from passive detection to predictive systems that can comprehend early warning signals from environmental sensors is highlighted by our

ISBN 978-81-973526-0-7

collective findings.

### Experimental and Computational Advances in Detection

Predictive ice detection is now achievable because to developments in computer modelling and laboratory testing.

A low-cost pitot tube-based detection prototype was created by [3] using Arduino and differential pressure sensors to differentiate between glazing, rime, and non-ice obstacles. They found that every variety of ice has a distinct pressure signature that allows for real-time classification using simple computer logic. According to their findings, low-cost, lightweight sensor arrays could perform on par with commercial-grade technology, which makes them appropriate for unmanned aerial vehicles and tiny airplanes.

[1] expanded on the experimental findings by modelling ice formation under varied airflow and temperature conditions using Computational Fluid Dynamics (CFD). In order to simulate real-world icing events in silico, their study incorporates crucial modelling techniques such boundary conditions, turbulence models, and droplet distribution patterns.

By combining CFD simulations with data-driven machine learning techniques, [4] expanded on these initiatives. Li trained Random Forest, XGBoost, and Logistic Regression models using NASA's icing datasets to forecast ice area, thickness, and severity with above 90 per cent accuracy. This work set a precedent for combining AI-driven analytics with physics-based modelling to create hybrid systems that can foresee and simulate ice conditions. These studies show that combining sensor experiments with computer modelling is the foundation of accurate, predictive icing detection systems.

### AI/ML-Based Warning Systems and Pilot Assistance

The increasing use of AI and ML has transformed ice detection from simple sensing to sophisticated predictive warning systems. [4] showed that when it comes to predicting the severity of icing based on environmental characteristics like air temperature, velocity, and humidity, ensemble algorithms like XGBoost perform better than classic thermodynamic models. Such models produce interpretable, high-accuracy outputs that may be used aboard for real-time monitoring.

[2] proposed an operational strategy in which cockpit devices identify TAT anomalies and offer early warnings of impending icing. Their methodology is similar to unsupervised anomaly detection techniques in AI, in which sensor variances automatically generate alarms without requiring ongoing pilot supervision.

In the meanwhile, [5] widened the scope by investigating AI-assisted pilot systems and voice-activated copilots that improve situational awareness and minimize cognitive burden. These tools evaluate incoming data, anticipate potential threats, and use natural language to give the pilot useful information. The confluence of predictive modelling and human-AI communication reveals a revolutionary trend towards intelligent flight safety ecosystems in which AI not only detects dangers but also assists with decision-making.

### Integration of Lightweight AI in Aviation Systems

Models need to be precise and computationally efficient in order to apply AI to aviation systems. The emergence of lightweight AI architectures optimized for mobile and embedded systems that can operate in restricted resource situations such as UAVs and micro-aerospace is highlighted by [5]. Such models maintain real-time inference capabilities while minimizing computing latency, which is crucial for airborne systems where every millisecond matters.

Simultaneously, [4] demonstrated how combinations of algorithms like Random Forest and Logistic Regression combine predictive power with processing speed. These models don't require a lot of onboard computation and can be directly implemented on microcontrollers and low-power CPUs. Scalable, onboard predictive icing systems can be achieved through the combination of lightweight AI algorithms and sensor integration.

*ISBN 978-81-973526-0-7*

The emphasis on small, high-efficiency models is consistent with the current research, which intends to integrate AI driven detection on embedded hardware platforms such as Raspberry Pi or Arduino, bringing predictive safety intelligence right to the aircraft level.

***Gaps, Open Problems, and Future Directions***

There are still several gaps in the existing studies, despite considerable progress. initially, integrated real-time systems that incorporate pilot engagement, AI prediction, and data collection into a cohesive system are currently lacking. Current methods often handle these parts separately, which causes delays and issues with communication between models, sensors, and cockpit interfaces.

Second of all, the quantity of quality icing datasets is fairly limited. It is impossible to generalize learnt AI models since most datasets are either limited to research environments or proprietary to specific aircraft designs. In order to expedite comparison and standardization, forthcoming studies should give priority to open-source icing data sets.

Third, the computational trade-off between model complexity and energy efficiency continues to hinder real-time implementation. Even though deep neural networks may effectively record nonlinear interactions, they are often not suitable for embedded aircraft hardware. Random Forests and other lightweight models offer a compromise, but they still require further optimization for low-latency inference.

At last, the incorporation of human-AI integration systems, such voice-assisted copilots and AR/VR-based visualization, still has a lot of work to do. These technologies have the potential to revolutionize pilot training and in-flight awareness by visualizing and vocalizing expected icing hazards before they become serious.

Resolving these challenges will enable fully autonomous, self-diagnosing airplane safety systems, transforming icing detection from a reactive process to an intelligent, anticipatory role within aviation ecosystems.

Table 1. Summary of Reviewed Literature.

| Author, year | Purpose | Key findings | Gaps |
|---|---|---|---|
| Jäckel et al., 2021 | Examination of probe behaviour and pitot tube icing and de-ice phenomena. | found design deficits, SLD mechanisms, and probe vulnerabilities. | AI/ML not used; primarily concentrating on physics. |
| Ayra et al., 2023 | Study of HAIC affecting pitot/TAT sensors. | TAT anomalies accurately forecast the risk of early icing. | No ML modelling; only sensor anomaly correlation. |
| Lv et al., 2020 | Prototype for inexpensive pitot tube icing detection. | Pressure indications for non-ice obstructions, glaze, and rime ice. | Just reactive sensing; no model for prediction. |
| Li, 2021 | AI-driven prediction of aircraft icing risk. | ML models had > 90% accuracy in predicting ice thickness and severity. | Limited dataset diversity; requires in-flight data. |
| Wild et al., 2025 | Real-time aviation safety systems using lightweight AI. | Voice AI improves situational awareness and supports onboard inference. | AI for general aviation, not for just icing. |

## Methodology

xIn order to guarantee that the chosen literature accurately reflects recent developments in AI-based aircraft icing detection, the methodology used for this review takes a structured, methodical approach. It is especially focused on pitot tube sensor systems and machine learning applications in aviation safety. The process involved defining the study goals, locating appropriate keywords, selecting trustworthy sources, and applying inclusion and exclusion criteria in order to reduce the final collection of articles studied.

### *Research Scope and Objectives*

The primary objective of this review was to analyze and compile scholarly and commercial studies on the use of artificial intelligence and machine learning for aircraft icing detection and prediction, with a focus on pitot tube icing phenomena. Because these years represent the most active time of technical progress in predictive aviation systems and embedded AI applications, the scope was restricted to works published between 2018 and 2025.

### *Literature Search Strategy*

An extensive literature review was conducted using a number of academic databases, including IEEE Xplore, ScienceDirect (Elsevier), SpringerLink, and MDPI Open Access Journals. Additional verification and additional data were gathered from the NASA Technical Reports Server (NTRS) and the AIAA (American Institute of Aeronautics and Astronautics) digital library to confirm domain relevance. Boolean operators and a combination of keywords were used to conduct searches, such as:

- “Aircraft icing” AND “machine learning”
- “Pitot tube icing detection” AND “artificial intelligence”
- “Real-time icing prediction” AND “embedded systems”
- “AI co-pilot” OR “intelligent aviation safety”

These combinations made sure that research on the technical and human-AI interface sides of aviation icing detection was retrieved.

### *Inclusion and Exclusion Criteria*

Inclusion and Exclusion Criteria To guarantee relevance, scientific rigour, and variety of approach, the inclusion criteria were created:

- Works published between 2018 and 2025 in peer reviewed journals, conferences, or dissertations.
- Studies that directly use AI, ML, or computational modelling in sensor-based detection or aviation icing.
- Research on aircraft safety that addresses pitot tubes, TAT sensors, or associated environmental equipment.

Exclusion criteria included:

- Research that only looked into icing aerodynamics without using AI.
- Patents or non-scientific papers with opaque methodology.
- Articles lacking full-text access or not available in English.

Based on their relevance, technological innovation, and experimental or computational rigour, five primary research articles and a number of secondary references were selected for in-depth assessment following preliminary screening.

### *Selection and Evaluation Process*

Each shortlisted paper underwent a two-stage evaluation:

- Abstract Screening: To verify congruence with the study’s emphasis on intelligent or predictive ice detection systems.
- Full-Text Review: To extract details regarding issue formulations, methods, procedures, datasets, and experimental outcomes.

A comprehensive analysis was conducted to identify prevalent practices, technology gaps, and emerging trends in the integration of AI with aircraft safety systems. The five chosen publications include an overview of contemporary aviation AI frameworks [5], computational modelling investigations [4], experimental sensor implementations [2][3], and theoretical reviews [1].

***Data Extraction and Thematic Categorization***

The information gathered from each study was organized into a literature review that summarized crucial elements such as aims, techniques, outcomes, and importance. The reviewed papers were separated into five topic categories to facilitate more structured discussion:

- Pitot Tube Icing- Risks and Accidents.
- Experimental and Computational Advances.
- AI/ML-Based Warning Systems and Pilot Assistance.
- Integration of Lightweight AI in Aviation Safety.
- Gaps, Open Problems, and Future Directions.

This topic synthesis meant that the study not only summarized previous research but also identified trends, constraints, and potential for the development of predictive, AI assisted flight safety systems.

## Conclusion

As evidenced by several past incidents and sensor malfunctions, aircraft icing—especially pitot tube icing—remains a serious danger to aviation safety, as this paper demonstrates. A distinct development can be seen across the literature: early studies concentrated on comprehending icing mechanisms and the aerodynamic effects of probe blockage, followed by computational and experimental methods that investigated pressure responses, icing physics, and CFD based modelling. Researchers have shown that environmental factors like temperature, humidity, and pressure may be utilized to predict ice risk well before accretion begins, indicating a clear move towards artificial intelligence and machine learning. The integration of AI with lightweight embedded systems and real-time anomaly detection represents a major advancement toward proactive safety systems capable of providing early alerts to pilots.

Overall, the reviewed work demonstrates that predictive, AI-assisted icing detection is no longer theoretical—it is technically viable, computationally efficient, and more aligned with modern aviation's automation push. At the same time, the research indicates persistent obstacles, such as the scarcity of open-access icing datasets, the necessity for multi sensor fusion, and the absence of holistic frameworks that incorporate sensing, prediction, and human-AI interaction. These flaws highlight the need for additional study to develop more reliable, scalable, and pilot-focused solutions. Overall, the results demonstrate that AI-enabled predictive detection can change ice control from reactive to proactive, opening the door for more intelligent, autonomous, and safe aircraft systems.

## Discussion

The studied literature demonstrates a steady advancement in the field of aviation icing detection, from traditional mechanical and thermal monitoring to complex computational and AI-driven prediction systems. Early research, such as [1], identified the underlying dangers connected with pitot tube icing, emphasising the need for more proactive and dependable detection approaches. [3] showed that even low-cost sensor sets can efficiently discriminate ice kinds using pressure signatures, while [4] proposed machine learning as a potent technique for forecasting icing severity using environmental factors. These developments are consistent with the emerging trend of incorporating lightweight AI systems into real time aircraft operations, as noted by [5], who demonstrated that integrated AI and intelligent pilot interfaces may dramatically increase situational awareness.

Every study has one thing in common: as compared to traditional reactive systems, AI and machine learning greatly increase accuracy, responsiveness, and predictive capabilities.

However, the lack of fully integrated end-to-end systems, the shortage of open-source icing datasets, and the requirement for validated frameworks that include sensing, prediction, and pilot communication impede the research. The research indicates that whereas predictive icing detection is theoretically feasible, full adoption requires multidisciplinary development involving sensor design, embedded AI optimization, and human-AI collaboration. Intelligent flight safety ecosystems that can predict threats rather than just respond to them are made possible by this convergence.

## Future Scope

The assessment reveals that, while great progress has been achieved in understanding and forecasting aircraft icing, some key chances for growth remain. initially, the development of large-scale, open-access icing datasets that capture real flight conditions at different altitudes, climates, and aircraft types is urgently needed. The generality of most current models is limited because they are based on data from simulations or laboratories.

Secondly, in order to create better dependable and fault tolerant prediction models, future studies should examine multi-sensor fusion frameworks that integrate pressure, temperature, humidity, optical, and infrared data. In rapidly changing air conditions, integrating these numerous sensor inputs may greatly improve early detection accuracy. thirdly, even though models based on machine learning have shown promising performance, further work is required to build lightweight, energy-efficient AI architectures that can reliably operate on integrated aircraft hardware with rigorous computation and power constraints. Model pruning, quantization, and edge-optimized algorithms will be critical in enabling real-time predictive icing detection for small aircraft and UAVs. Furthermore, there is great potential for improving human-AI interaction, notably through voice assisted copilots and augmented or virtual reality interfaces that can improve pilot situational awareness during icing situations.

Lastly, fully interconnected real-time systems that com bine sensing, prediction, and pilot communication into a single, coherent safety module should be the focus of future study. Researchers' cooperation with the aircraft industry and regulatory bodies such as the FAA or EASA will be required to ensure certification, reliability, and large-scale implementation. As aviation adopts intelligent automation, these advancements will play an important role in developing autonomous, self-aware, and safer aircraft systems capable of anticipating and mitigating icing hazards proactively.

## References

[1] M. Jäckel, C. Lensch-Franzen, and M. Janser, "A review on pitot tube icing in aeronautics: Research, design, and characterization– Future trends," Aerospace Science and Technology, vol. 116, pp. 106859, 2021.

[2] R. Ayra, M. B. Bragg, and D. Miller, "Detection and warning of ice crystals clogging pitot probes from TAT anomalies," in Proc. AIAA Aviation Forum, 2023, pp. 1–12.

[3] X. Lv, X. Zhang, and Z. Yang, "Pitot tube–based icing detection: Effect of ice blocking on pressure," International Journal of Aerospace Engineering, vol. 2020, pp. 1–9, 2020.

[4] S. Li, "Investigation of aircraft icing based on numerical modeling and machine learning methods," Ph.D. dissertation, Univ. of Illinois at Chicago, Chicago, IL, USA, 2021.

[5] G. Wild, S. Austin, and M. Romero, "Lightweight and mobile artificial intelligence and immersive technologies in aviation," Visual Computing for Industry, Biomedicine, and Art, vol. 8, no. 1, pp. 203, 2025

[6] Federal Aviation Administration, "Aircraft icing handbook," U.S. Dept.

Transportation, Washington, DC, USA, Tech. Rep., 2022.
[7] NASA Glenn Research Center, "In-flight icing research and data resources," NASA Technical Reports Server (NTRS), 2021.
[8] V. Bhardwaj, "Role of ML in Cancer Prediction," in Advances in Artificial-Business Analytics and Quantum Machine Learning", K. Santosh, P. Nandal, S. K. Sood, and H. M. Pandey, Eds., Lecture Notes in Networks and Systems, vol. 1053. Singapore: Springer, 2024.
[9] Jackel, R.; Gutierrez-Urueta, G.; Tapia, F., "A review on Pitot tube icing in aeronautics: Research-design and characterization-future trends.", Flow Meas. Instrum. 2021, 81, 102033.

# Text-Driven Knowledge Extraction for Data-Driven Engineering Simulation Using Natural Language Processing

Chandra Kanta Yadav*[1]
*[1]Department of Computer science, Banasthali Vidyapith, Rajasthan, India
*chanduyadav443@gmail.com

## Abstract
*In Computational Fluid Dynamics (CFD) and Finite Element Analysis (FEA) simulations, technical reports and experimental reports are essential. A weakness is however encountered when there is no technical information that is in a structured form and, this makes it difficult to perform data-driven simulations. This study presents a suggestion of NLP-based techniques that could be used to extract engineering text information. These processes that include text pre-processing, feature extraction and machine learning processes enable the extraction of important information in the form of engineering materials and simulation parameter. The retrieved information simplifies modeling and digital engineering processes using data. In addition, the proposed framework, in contrast to current methods, aims at recognizing engineering features that are relevant to simulation and connecting them to computational models that are founded on data, which is the case with CFD and FEA. This facilitates the automatic exploitation of the knowledge contained in text to the aim of simulating engineering. The suggested work illustrates the contribution of NLP towards the aid of the computational engineering and intelligent design systems.*

## Keywords
Engineering Systems, Natural Language Processing, and Data-Driven Models, Machine Learning Techniques

## Introduction
Digital Engineering is a digital tool that bridges the computation tools, simulation technology, and data analytics in an attempt to design, analyze, and optimize complex engineering systems [1]. In this modern world, engineers, who are affected by the development in the field of computational engineering, are making more use of digital models. This helps them to make predictions on the behavior of the system even before making any physical changes a feature that is not only useful at all levels, but also efficient in designing the system in a much more efficient way with minimal costs at the same time [2]. Critical simulation techniques such as Finite Element Analysis (FEA) and Computational Fluid Dynamics (CFD) are used in engineering and aerospace applications to study the fluid dynamic, heat conduction, abrasion of the skeletons, and collapse extensively[3]. The primary results of these standardized simulation techniques are vast amounts of conceptual and experimental data and they are used to enhance forecasting and system analysis using data based techniques of computation. Moreover, through the process of integrating machine learning with data analysis tools, engineers are able to come up with important discoveries during the experiments and real-world data thus facilitating the process of intelligent engineering design and decision making [4]. These facts disclose that much of the critical knowledge is not expressed in structured data, but in unstructured data- this is a scenario that is a great challenge to digital engineering. The critical information about the system design, operation performance and failure analysis can be found in research articles, simulation reports, maintenance logs and technical design documents. Despite the fact that the amount of the simulation results produced with the help

of computational tools like Finite Element Analysis and Computational Fluid Dynamics is enormous, numerous technical hints, assumptions, and contextual interpretations are still hidden in the written documents. Data engineering is not very structured and therefore it will be challenging to automate the process of analysis, extraction and integration into the IT processes [1]. The further the engineering documentation increases, the inefficient and time-consuming is the analysis done manually. In order to enhance the knowledge management and advance data-driven engineering design and decision-making processes, advanced methods are increasingly gaining importance, such as the Natural Language Processing, which operates on extracting useful information to be stored in the text-based engineering sources automatically [5].

Natural Language Processing (NLP) remains a key field to date in order to compute and analyze the vast volumes of unstructured text information that is intertwined with the modern engineering tasks. With the assistance of the NLP methods, now it is possible to extract important information in technical papers, including research articles, simulation reports, maintenance records, and design specifications automatically [6]. Also, NLP simplifies the retrieval of information since unstructured text can be easily transformed into a standard form that can be readily incorporated into data-driven engineering systems. Automated text summary techniques are also used to enable engineers to grasp lengthy technical documents of interest in a short summary of the key findings and specifications of a design [7]. Since NLP-based systems can be used to smartly make decisions in digital engineering processes, engineering design, and predictive maintenance, these features enhance efficiency of working with complex engineering data and reduce human intervention.

The given paper provides a framework, which utilizes Natural Language Processing (NLP) methods to facilitate the process of information extraction and integration in the setting of digital engineering. To derive the relevant engineering knowledge with the use of unstructured text, such as technical documents, simulation reports, and research articles, the first suggestion of the study is an NLP-based architecture. Second, there are data-driven modeling processes that are applied to structure and combine the textual information that is retrieved to streamline engineering simulation and analytical processes. Third, the proposed framework enhances the digital engineering processes through effective knowledge management and data-driven decision-making capabilities in the computational design and simulation framework. The proposed solution is hoped to increase the ease of accessing engineering information and facilitate engineering design processes based on intelligent engineering design by transforming unstructured engineering language into structured knowledge. The paper has introduced a new approach to the application of Natural Language Processing (NLP) and data-driven modeling in the engineering processes. The proposed research is the initial attempt at filling the gap between natural language processing (NLP) in general text mining application and machine learning in engineering simulation. The key contributions of this work are the following ones:

***Engineering-Specific Extraction of Knowledge***

As opposed to blanket provisions in NLP, the present study pays ample attention to takeout narrow information using unstructured information in the engineering literature- constituent aspect, boundary restriction, and computational pretension framework.

***Simulation Workflow Integration (CFD/FEA)***

The proposed architecture establishes a direct relationship between the methods of engineering simulation and the knowledge of linguistics learned, which allows the systematic support of Finite Element Analysis (FEA) and Computational fluid dynamics (CFD).

***Whole NLP Process of Engineering Applications***

All of these processes, preprocessing, feature extraction (TF-IDF, Word2Vec, BERT), and knowledge extraction (NER, LDA), can be linked into one pipeline to create decision support systems.

### *Collaboration based on data design*

The framework can improve digital engineering by converting textual knowledge that is not structured into structured information which may be immediately utilized in the simulation-based design and analysis. A significant improvement of this fusion of NLP and simulation based engineering processes as compared to the existing techniques that consider text mining and simulation as distinct processes.

Although the text mining with Natural Language processing and machine learning with engineering simulations have been previously researched, there are very few studies that explicitly use NLP-based knowledge extraction along with the engineering simulation processes. This gap demonstrates the need to have a standard framework that would be able to convert unstructured technical jargon into structured inputs of the simulation systems. This study is aimed at bridging that gap.

## Related Work

Recent advancements in natural language processing (NLP) and artificial intelligence (AI) have significantly impacted engineering research, as they have facilitated the automated extraction of information from unstructured technical documents and the enhancement of data-driven simulation processes.

### *NLP in Engineering Documents*

NLP-based text mining algorithm can be used to extract useful information in research journals and engineering reports. These methods are used to transform unstructured technical data into structured information to be studied by identifying important technical words, parameters, and engineering concepts [8]. The organized data makes technical decision-making and the management of digital documents simple.By combining five modules-design cost prediction, error and change analysis, ITB analysis utilizing natural language processing, and equipment maintenance forecasting-the study created a data-driven decision support system for the engineering, procurement, and construction (EPC) sector [2]. Throughout the course of a project, these modules make use of historical engineering big data to support informed decision-making, improve risk management, and increase efficiency.

### *AI in Engineering Simulation*

Machine learning approaches are often used to accelerate simulations in finite Element Analysis and Computational Fluid Dynamics by building surrogate models that mimic complex numerical processes [9]. In a similar vein, the combination of machine learning with finite element analysis (FEA) has made it possible to predict structural responses and material behavior in engineering systems more quickly. Without doing complete numerical simulations, data-driven models can identify trends in simulation datasets and forecast stress, deformation, and other structural characteristics [10].Data-driven engineering techniques utilize the vast information obtained from experiments and simulations to construct predictive models, which aid in performance analysis, system design, and optimization[11].This advancement has led to an increased utilization of Artificial Intelligence (AI) within contemporary computational engineering systems, enhancing simulation efficiency and facilitating the process of making informed engineering decisions.

### *NLP for Scientific Literature Mining*

Latent Dirichlet Allocation and other topic modeling approaches can be utilized to extract research trends and hidden themes from vast databases of scientific journals. Through the identification of significant components and connections from research papers, information extraction techniques aid in the systematic discovery of knowledge. Large collections of technical and scientific literature can now be efficiently mined thanks to recent developments in natural language processing. Topic modeling is a popular method that automatically finds

*ISBN 978-81-973526-0-7*

latent thematic structures in massive text corpora. Latent Dirichlet Allocation (LDA) and Non-Negative Matrix Factorization (NMF) are two popular methods for identifying research patterns and grouping massive scientific datasets into relevant topic groups [12].Moreover, it has been indicated by recent studies that big language models and transformer-based language models can significantly increase the process of extracting structured information out of scientific publications, which can help in knowledge discovery and automation of literature review processes [13]. There are a few studies that have focused on the use of natural language processing (NLP) to derive engineering information in textual form, although previous studies have been done on machine learning in engineering simulations.

Nevertheless, the majority of current research does not specifically address the integration of NLP-extracted knowledge with engineering simulation parameterization; instead, it concentrates either on text mining or simulation modeling separately. This gap is intended to be filled by the proposed work.

## Proposed Framework

The proposed framework provides a structured framework for the use of natural language processing techniques to convert engineering documentation into structured knowledge.

Figure 1 show how Natural Language Processing is used to convert technical documents into structured information. Key engineering information is found using knowledge extraction techniques after pre-processing, tokenization, and feature extraction (using TF-IDF or embeddings). After that, this data is kept in a knowledge base to help with simulations like computational fluid dynamics and finite element analysis.

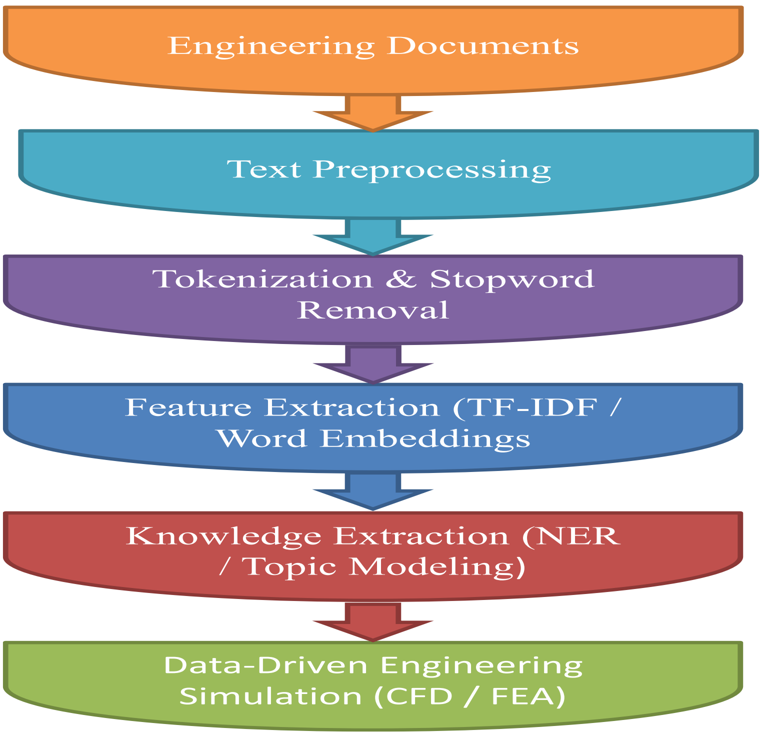


Figure 1. NLP framework for texts-based information extraction

## Methodology

In this paper, the author is going to suggest an NLP-based information extracting system in the field of engineering in text data. The system achieves this task in four phases which are data collection, pre-processing of the text, feature extraction and extraction of the information through Natural Language Processing techniques. Simulation reports, research papers, technical manuals and maintenance logs are used to collect text data. The sources are important in terms of giving critical data about the engineering systems and design processes.

Pre-processing of text is done to normalize, analyze and improve the quality of text found within the document corpus. It is a technique that includes different processes, namely, tokenization, stopword removal, stemming, and lemmatization. After completing the pre-processing of the textual data, it is translated into a numerical representation that can be easily manipulated by feature engineering; Word2Vec, Term Frequency / Inverse Document Frequency (TF-IDF), and BERT are the most common techniques used to draw out the features. The knowledge extraction methods are identified as keywords through Named Entity Recognition (NER) and topic modeling through Latent Dirichlet Allocation (LDA) to extract the key concepts and topics contained in the text. Such processes are applied in order to glean out relevant engineering data, including simulation parameters, engineering components, and design constraints.

### *Engineering Simulation Usage*

The information obtained with the help of Natural Language Processing (NLP) methods that automatically locate important information related to design in scientific studies is used in engineering simulations. The resulting textual data are used to determine parameters that are critical in the simulation of the Computational Fluid Dynamics (CFD) simulations, including the flow velocity, turbulence models, and the boundary conditions. When these parameters can be automatically read out of the technical documentation, it helps the engineer to set up simulation frameworks more effectively, and therefore save them the time to interpret the data smeared across the manual processing step[3]. On the same note, in the case of Finite Element Analysis (FEA), NLP-derived information extraction process interfaces directly with the manuals and design specifications to obtain required structured information, such as material properties, overall load, and stress limits. This information together can then be put into consideration into simulations, and therefore simplifies design analysis as well as its verification.

## Results & Discussion

The present paper has assessed in theory the application of an architecture based on Natural Language Processing (NLP), which demonstrated that valuable engineering-specific data could be obtained, with respect to a technical documentation. This discussion demonstrates that NLP algorithms can be effectively employed to find key words in engineering reports, the use of topic modeling to divide research content into clusters of themes and the ensuing ideas can be arranged in a knowledge graph. These elements enable inputting of unstructured engineering language to be structured to be used in design and simulation.Consequently, the framework enhances engineers' access to knowledge and facilitates more effective decision-making in engineering simulations like Finite Element Analysis and Computational Fluid Dynamics.

The field of digital engineering and data-oriented models processes can greatly benefit from NLP-based knowledge extraction, as shown in Figure 2.The suggested methodology minimizes manual labor in the analysis of extensive technical information by proactively identifying engineering characteristics, resources, and restrictions on design from textual data. The knowledge that has been extracted can help engineers make better decisions pertaining to engineering and configure simulation models. Thus, a viable method for improving contemporary engineering design and simulation environments is the integration of NLP with computational tools used in engineering.

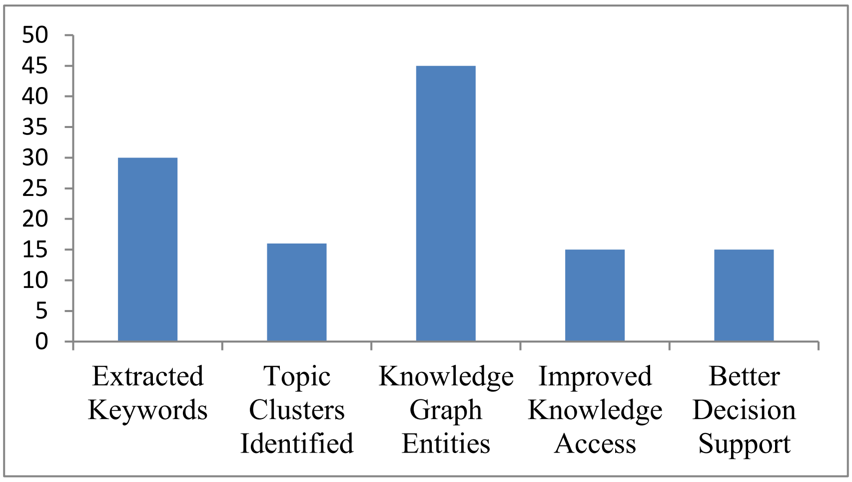


Figure 2. Conceptual Results of NLP-based engineering knowledge extraction

The given framework, a language processing technique-based one, has a number of benefits in the context of knowledge management in professions. First of all, these methods do not require manual review since they allow extracting knowledge automatically in large repositories of research papers.

More so, manual textual analysis is minimized through this method, thus helping the engineer to quickly recognize important aspects and design requirements. This framework enables to model and research by translating unstructured textual input into formatted information and eventually enables a more efficient workflow of digital engineering.

However, there are still some limitations because engineering publications often use specialized words or buzzwords that may complicate the process of extracting specific information. It has also been noted that the available high-quality and big datasets to train NLP models on the engineering field are scarce. These issues need to be considered in order to increase the effectiveness of NLP-based systems in the further use of engineering.

## Conclusion

The study is rooted in the methodology that aims to convert unstructured research data in architecture into well-organized knowledge, where the use of NLP is very helpful in the digital engineering systems. The applicability of such data is usually put into perspective by simulation needs and architectural limitations; these are systematically incorporated into engineering analysis and documentation procedures. NLP techniques ensure successful access to correct information at the same time with the reduction of manual work to a large extent. Moreover, this method produces parameters to be used in models to aid simulations in both the Computational Fluid Dynamics (CFD) and Finite Element Analysis (FEA). Essentially, this approach to work, through the competent control of data, will play an important role in making engineering processes leaner and the design process more efficient overall.

## References

[1] D. Adamenko, S. Kunnen, and A. Nagarajah, "Digital Twin and Product Lifecycle Management: What Is the Difference?," in *Product Lifecycle Management Enabling Smart X*, F. Nyffenegger, J. Ríos, L. Rivest, and A. Bouras, Eds., Cham: Springer International Publishing, 2020, pp. 150–162. doi: 10.1007/978-3-030-62807-9_13.

[2] G. Cascini, A. Fantechi, and E. Spinicci, "Natural Language Processing of Patents and Technical Documentation," in *Document Analysis Systems VI*, S. Marinai and A. R. Dengel, Eds., Berlin, Heidelberg: Springer, 2004, pp. 508–520. doi: 10.1007/978-

3-540-28640-0_48.

[3] S. L. Brunton, B. R. Noack, and P. Koumoutsakos, "Machine Learning for Fluid Mechanics".

[4] S. L. Brunton and J. N. Kutz, *Data-Driven Science and Engineering: Machine Learning, Dynamical Systems, and Control*. Cambridge University Press, 2022.

[5] I. Beltagy, K. Lo, and A. Cohan, "SciBERT: A Pretrained Language Model for Scientific Text," in *Proceedings of the 2019 Conference on Empirical Methods in Natural Language Processing and the 9th International Joint Conference on Natural Language Processing (EMNLP-IJCNLP)*, K. Inui, J. Jiang, V. Ng, and X. Wan, Eds., Hong Kong, China: Association for Computational Linguistics, Nov. 2019, pp. 3615–3620. doi: 10.18653/v1/D19-1371.

[6] Y. Liu and M. Lapata, "Text Summarization with Pretrained Encoders," in *Proceedings of the 2019 Conference on Empirical Methods in Natural Language Processing and the 9th International Joint Conference on Natural Language Processing (EMNLP-IJCNLP)*, K. Inui, J. Jiang, V. Ng, and X. Wan, Eds., Hong Kong, China: Association for Computational Linguistics, Nov. 2019, pp. 3730–3740. doi: 10.18653/v1/D19-1387.

[7] Y. Kim, J. Lee, E.-B. Lee, and J.-H. Lee, "Application of Natural Language Processing (NLP) and Text-Mining of Big-Data to Engineering-Procurement-Construction (EPC) Bid and Contract Documents," in *2020 6th Conference on Data Science and Machine Learning Applications (CDMA)*, Mar. 2020, pp. 123–128. doi: 10.1109/CDMA47397.2020.00027.

[8] J. Dagdelen*et al.*, "Structured information extraction from scientific text with large language models," *Nat Commun*, vol. 15, no. 1, p. 1418, Feb. 2024, doi: 10.1038/s41467-024-45563-x.

[9] S. L. Brunton, B. R. Noack, and P. Koumoutsakos, "Machine Learning for Fluid Mechanics".

[10] T. Maric, M. E. Fadeli, A. Rigazzi, A. Shao, and A. Weiner, "Combining machine learning with computational fluid dynamics using OpenFOAM and SmartSim," *Meccanica*, vol. 60, no. 6, pp. 1831–1850, Jun. 2025, doi: 10.1007/s11012-024-01797-z.

[11] F. M. A. Altalbawy*et al.*, "Computational fluid dynamic and machine learning modeling of nanofluid flow for determination of temperature distribution and models comparison," *Sci Rep*, vol. 15, no. 1, p. 19073, May 2025, doi: 10.1038/s41598-025-03187-1.

[12] R. Albalawi, T. H. Yeap, and M. Benyoucef, "Using Topic Modeling Methods for Short-Text Data: A Comparative Analysis," *Front. Artif.Intell.*, vol. 3, p. 42, Jul. 2020, doi: 10.3389/frai.2020.00042.

[13] J. Dagdelen*et al.*, "Structured information extraction from scientific text with large language models," *Nat Commun*, vol. 15, no. 1, p. 1418, Feb. 2024, doi: 10.1038/s41467-024-45563-x.

# PERFORMANCE AND ROBUSTNESS EVALUATION OF DNA-BASED IMAGE ENCRYPTION METHODS

Yashika Tanwar*[1], Shailender Gupta[1], Krishnansh Gupta[2]
*[1]J.C. Bose University of Science & Technology, YMCA, Faridabad, Haryana, India
[2]National Institute of Technology, Delhi
*yashika.tanwar567@gmail.com

## Abstract
*The secure transmission and storage of digital images have become significant due to their widespread use in communication, healthcare and surveillance systems. DNA based image encryption has emerged as a powerful technique due to its high storage capacity, parallel processing capability and complex encoding structure. In order to ensure reliability and security of such methods, a comprehensive performance evaluation is required. In this paper, we have analyzed the effectiveness of DNA based image encryption techniques with the help of various parameters where robustness analysis is kept as a crucial parameter. The evaluation framework includes differential attack using NPCR and UACI, robustness assessment using chi-square, noise and geometric attacks, statistical analysis based on entropy and correlation coefficients. Furthermore, brute-force resistance is examined through key space analysis and key sensitivity metrics, while computational time complexity is analyzed to determine feasibility of encryption technique for real-world applications. The results demonstrate that DNA based encryption technique provides strong security characteristics along with acceptable computational efficiency, making them suitable for secure image communication applications.*

## Keywords
DNA Image Encryption, Robustness Analysis, Differential Attack, Statistical Analysis.

## Introduction
The transmission of medical data is increasing at a rapid speed, the data transmitted consists of sensitive patient information thus making security a critical component. This concern is further emphasized by the fact that healthcare data breaches in 2025 affected an average of 168,647 individuals per day, thus highlighting the scale of exposure of confidential medical data [1].Traditional encryption methods which are effective for textual data, face limitations when applied to large-scale image data due to strong inter-pixel correlations. Due to which, DNA based image encryption has emerged as a promising alternative, having high storage capacity, parallel processing capability and complex encoding mechanism to enhance security and efficiency.

The effectiveness of DNA based encryption techniques is determined by their ability to resist various attacks. Robustness analysis is an important parameter to check the efficiency of an encryption technique to withstand noise attack, compression and geometric distortions during data transmission and storage. Therefore, encryption techniques are evaluated on multiple parameters like robustness, differential, statistical and brute-force attacks to provide a better understanding for real-world applications.

This paper shows a comparative analysis of DNA based image encryption techniques using multiple evaluation metrics which includes:

- Differential Attack Analysis: It measures the sensitivity of encryption scheme against small changes in input image, even a small change should produce a different encrypted image. It is evaluated using NPCR and UACI [2].

- Robustness Attack Analysis: Evaluates the ability of an encrypted image to withstand disturbance and attacks like noise, compression and geometric distortions [3].
- Statistical Attack Analysis: Assesses the randomness and correlation between pixel values to check for no visible patterns in encrypted image. It is evaluated using entropy and correlation coefficients [4].
- Brute-force Attack Analysis: It determines the strength of an encryption technique against systematic key search. It is evaluated based on key space and key sensitivity [5].
- Computational complexity: Analyzes the efficiency of the encryption technique with respect to time for real-world applications [6].

The aim of this paper is to identify techniques which provide both strong theoretical security and efficiency for real world applications.

The rest of the paper is organized as: Section II comprises of DNA Encryption Technique Used, section III comprises of Comparative Analysis of DNA based Encryption Methods, Section IV includes conclusion.

## DNA Encryption Technique Used

DNA based encryption techniques uses nucleotide encoding, where each pixel values can be represented in the form of A, T, C and G nucleotides.

The following subsection describes DNA based encryption techniques considered in this study, highlighting their core design principles and operational workflow.

### *DNA Encoding with Spatiotemporal Chaos*

This technique uses DNA encoding with spatiotemporal chaotic system to enhance security. The plain image is transformed using XOR operations, followed by selected DNA encoding mapping rules. A chaotic system is then used for row and column permutation of the encoded data, thus generating an encrypted image, and achieving strong randomness and resistance against statistical and differential attacks. Fig-1 shows the entire encryption mechanism.

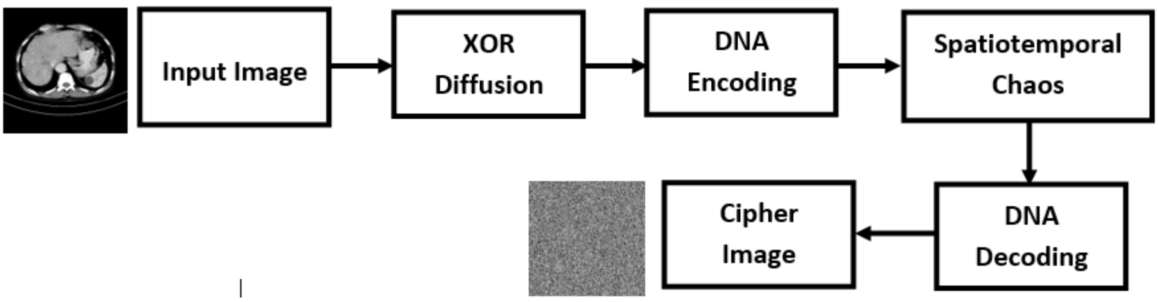


Figure 1. Encryption Mechanism.

### *Hyper chaotic DNA Encryption with Multi-Level Scrambling*

This method employs a 5D hyper chaotic system for generating chaotic sequences for encryption. The image undergoes both pixel and bit level permutation to reduce correlation. DNA encoding is then applied, followed by XORing and other operations for diffusion. The combination of multi-level scrambling and DNA operations enhances security against known-plaintext and differential attacks. Fig-2 shows the entire encryption mechanism.

### *Bit-Level Diffusion Based DNA Cryptosystem*

This approach introduces a DNA based image encryption using enhanced bit level diffusion. The image is transformed to increase randomness and then shuffled using Arnold's Cat Map. DNA encoding rules are applied to modify pixel values and diffusion is performed at both pixel and plane level using dynamic DNA encoding rule selection. This improves key sensitivity and ensures lossless decryption, making it suitable for medical images. Fig-3 shows the entire encryption mechanism.

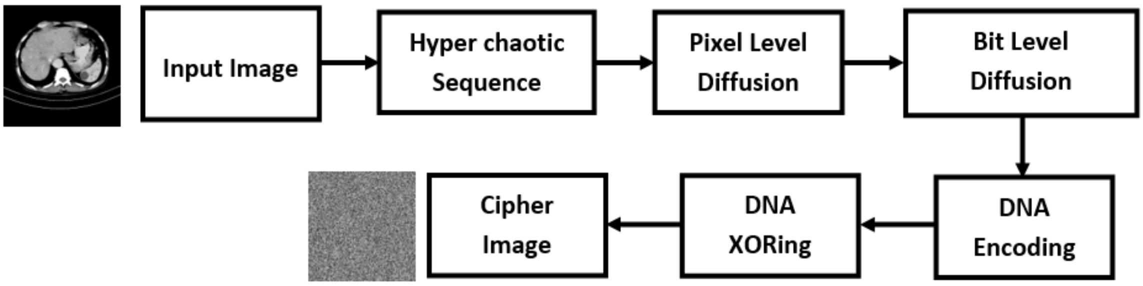


Figure 2. Encryption Mechanism.

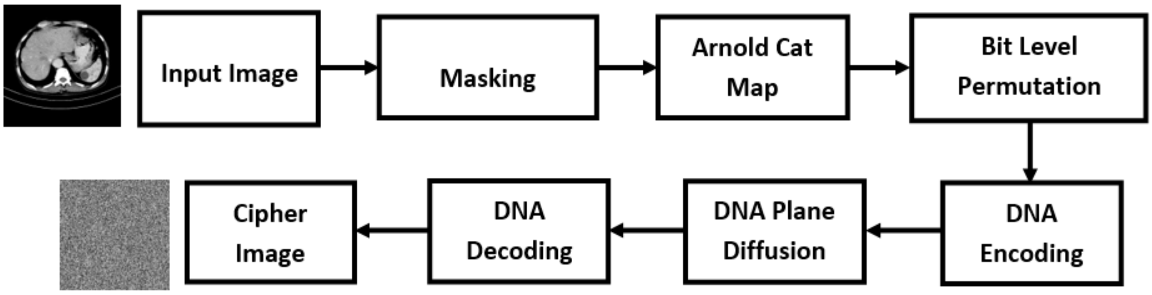


Figure 3. Encryption Mechanism.

### *Content-Aware DNA Encryption*

This technique integrates content aware mechanism into DNA based encryption using random DNA encoding rules to shuffle the actual data of image, which is then followed by permutation and diffusion processes. This introduces non-linearity in input image, thus making it less predictable and more resistant to attacks. Fig-4 shows the entire encryption mechanism.

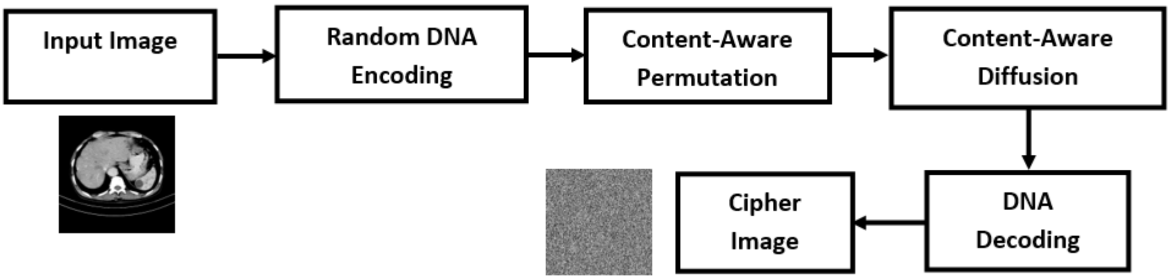


Figure 4. Encryption Mechanism.

## Comparative Analysis of DNA based Encryption Methods

A systematic evaluation of DNA based image encryption techniques is performed to determine their suitability for secure and robust image transmission. The analysis include differential attack analysis (NPCR and UACI), robustness attack analysis (Chi-Square, Noise and geometric Attack), statistical attacks (Entropy and Correlation), brute-force attack using key space analysis and Key sensitivity, and time complexity. The results are summarized in Table-1, where H and W are the dimensions of the image and M being the size of dataset for which the process has been evaluated.

Table 1. DNA Based Encryption Method Analysis.

| **Ref.** | **Differential Attack Analysis** | | **Robustness Attack Analysis** | | | **Statistical Attack** | | **Brute Force Attack** | | | **Time Complexity** |
|---|---|---|---|---|---|---|---|---|---|---|---|
| | **NPCR** | **UACI** | **Chi-Square** | **Noise Attack(dB)** | **Geometric Attack** | **Entropy** | **Correlation** | **Key Space Analysis** | **Key Sensitivity NPCR** | **Key Sensitivity UACI** | |
| **[7]** | 99.64 | 41.76 | 260.664 | ✘ | ✘ | 7.4084 | -0.00096 | 268 | 99.62 | 33.78 | $O(MHWlog(HW)$ |
| **[8]** | 99.60 | 33.43 | 247.561 | ✔ | ✘ | 7.9988 | -0.00021 | 298 | 99.61 | 33.43 | $O(KRMN)$ |
| **[9]** | 99.58 | 33.42 | 260.528 | ✔ | ✔ | 7.9987 | -0.01599 | 256 | 99.60 | 33.54 | $O(Kmnlog(mn))$ |
| **[10]** | 99.36 | 33.42 | 252.507 | ✔ | ✘ | 7.9902 | 0.00534 | 398 | 99.61 | 33.41 | $O(Kn^3)$ |

## Conclusion

This paper presented a comparative analysis of four DNA-based image encryption techniques using multiple evaluation parameters, including differential attack resistance, robustness, statistical analysis, brute-force resistance, and computational complexity. Based on the analysis of these techniques, the following inferences can be made:

- Strong differential and statistical performance across all techniques: All methods exhibit high NPCR and UACI values along with entropy values close to the ideal, indicating effective resistance against differential and statistical attack.
- Robustness as a key differentiating factor: Although all techniques exhibit strong resistance against differential, statistical and brute-force attacks. Some techniques were not able to withstand noise and geometric distortions, highlighting robustness as an important factor for real-world applications.
- Balanced performance achieved by advanced hybrid approaches: Techniques using dynamic rule selection and chaotic systems shows overall better performance, results computed for Ref. [9] provides an optimal balance between security, robustness and computation efficiency making it feasible for real-world applications.

## References

[1] https://www.hipaajournal.com/healthcare-data-breach-statistics/ accessed on 23/03/2026.

[2] Z. Hou, J. Ren, and S. Chen, “Machine learning-aided differential-linear attacks with applications to DES and Speck32/64,” Journal of King Saud University – Computer and Information Sciences, vol. 37, p. 228, 2025, https://doi.org/10.1007/s44443-025-00241-w

[3] J. DeMarchi et al., "Evaluation of Robustness Metrics for Defense of Machine Learning Systems," 2023 International Conference on Military Communications and Information Systems (ICMCIS), Skopje, North Macedonia, 2023, pp. 1-12, https://doi.org/10.1109/ICMCIS59922.2023.10253593

[4] K. Mahalakshmi and S. Nagarajan, "Comprehensive Review and Analysis of Image Encryption Techniques," in IEEE Access, vol. 13, pp. 109783-109813, 2025,

https://doi.org/10.1109/ACCESS.2025.3578158

[5] P. Ahlawat, "Key Management in Space Integrated Terrestrial Network: A Cybersecurity Perspective," 2024 2nd International Conference on Recent Trends in Microelectronics, Automation, Computing and Communications Systems (ICMACC), Hyderabad, India, 2024, pp. 129-133, https://doi.org/10.1109/ICMACC62921.2024.10894511

[6] S. A. M. A. Junid, M. S. Reffin, Z. A. Majid, N. M. Tahir and M. A. Haron, "Implementation of genetic algorithm for optimizing DNA sequence alignment," 2012 IEEE Business, Engineering & Industrial Applications Colloquium (BEIAC), Kuala Lumpur, Malaysia, 2012, pp. 80-85, https://doi.org/10.1109/BEIAC.2012.6226111

[7] C. Song and Y. Qiao, "A novel image encryption algorithm based on DNA encoding and spatiotemporal chaos," Entropy, vol. 17, no. 10, pp. 6954–6968, Oct. 2015, https://doi.org/10.3390/e17106954

[8] S. Sun, "A Novel Hyperchaotic Image Encryption Scheme Based on DNA Encoding, Pixel-Level Scrambling and Bit-Level Scrambling," in IEEE Photonics Journal, vol. 10, no. 2, pp. 1-14, April 2018, Art no. 7201714, https://doi.org/10.1109/JPHOT.2018.2817550

[9] P. Mishra, C. Bhaya, A. K. Pal, and A. K. Singh, "A medical image cryptosystem using bit-level diffusion with DNA coding," Journal of Ambient Intelligence and Humanized Computing, vol. 13, no. 5, pp. 2637–2654, 2022, https://doi.org/10.1007/s12652-021-03410-7

[10] D. Huo, Y. Qiu, C. Han, L. Wei, Y. Hong, Z. Zhu, and X. Zhou, "A visually meaningful double-image encryption scheme using 2D compressive sensing and multi-rule DNA encoding," Complex & Intelligent Systems, vol. 9, pp. 4783–4803, 2023, https://doi.org/10.1007/s40747-023-00989-6.

# A COMPARATIVE PERFORMANCE ANALYSIS OF DNA-BASED AND QUANTUM-BASED MEDICAL IMAGE ENCRYPTION TECHNIQUES

Vyoma Vaish*[1], Kakoli Dutt[1], Ashutosh Dixit[1]
*[1]J.C. Bose University of Science & Technology, YMCA, Faridabad, Haryana, India
*vyoma873@gmail.com

## Abstract
*The generation and transmission of medical images have been significantly increased in the healthcare system due to rapid digitization, making data security a critical concern. To secure medical data and images, an efficient image encryption algorithm is essential need of hour. Two most prominent and advanced approaches include DNA-based and quantum-based encryption. The former show special behavior by using biological encoding and chaotic systems to achieve strong security with low computational cost, whereas the later scheme relies on quantum principles such as superposition and randomness, offering high theoretical security but with greater computational complexity. The experimental analysis in this paper shows comparison between DNA-based and quantum-based medical image encryption techniques using various key performance parameters, which includes entropy, correlation coefficients, Number of Pixel Change Rate (NPCR), Unified Average Changing Intensity (UACI), and computational efficiency. The results show that DNA-based encryption achieves high entropy, low correlation, and efficient NPCR and UACI values with lower computational complexity. Quantum-based methods provide comparable security performance but face challenges in real-time applicability. By closely comparing, the study concludes that DNA-based encryption is more emerging technique for current healthcare applications, while quantum-based techniques remain promising for future secure systems.*

## Keywords
Chaos Theory, DNA Computing, Medical Image Encryption, Quantum Encryption

## Introduction
The increased creation and sharing of medical images such as X-rays and MRIs of healthcare system through communication and internet technology improves diagnosis and expands access to care, but also introduces serious data security concerns. These images are important information carrier containing sensitive patient information, making them vulnerable to unauthorized access and cyberattacks. Any alteration or leakage of such data from illegal access can compromise both patient safety and privacy. Furthermore, the use of cloud platforms and telemedicine heightens these risks during transmission. Therefore, strong security measures are essential to safeguard medical image data and ensure its confidentiality and reliability [6], [9].

To overcome these challenges and thus to protect the medical image data from unauthorized access, researchers have developed various encryption algorithms. Two prominent strategies are DNA-based encryption, which uses biological encoding rules, and quantum-based encryption, which leverages quantum mechanical principles for high security. Quantum encryption facilitates the encoding of image data into quantum states, allowing the efficient storage and processing of quantum images using a flexible structure that can adapt to different image sizes and formats.[5]
The combination of multiple techniques in hybrid scheme enhances both the security and

 *ISBN 978-81-973526-0-7*

efficiency, offering a balanced solution to address evolving cyber threats. [7][10][11].
This paper focuses on DNA-based and quantum-based image encryption techniques as the two prominent techniques. Due to unique properties of DNA and complexity of its sequence, DNA-based encryption has been applied in many fields like medical science, healthcare system, information science, providing high security, efficiency, adaptability and developmental potential, while quantum image encryption based on quantum principle offers superior speed and theoretical security. In this paper, an effort has been made to comparatively analyze these two approaches by selecting representative methods from recent literature. The comparison is carried out using key performance metrics such as entropy, correlation, NPCR, UACI, and computational complexity to evaluate their suitability for medical image security. The remainder of this paper is organized as follows: Section 2 describes the methodology of the selected techniques. Section 3 gives the performance metrics used. Section 4 discusses the performance analysis and results. Finally, Section 5 concludes the paper with future research directions.

## Methodology

This study presents a comparative evaluation of DNA-based and quantum-based medical image encryption techniques using standard security and performance metrics. The methodology is designed to ensure a fair and consistent comparison based on recent research contributions.

### *DNA-Based Encryption Model*

The DNA-based encryption process generally consists of three major stages (See Fig-1):

- DNA Encoding: It is a technique in which the pixel values of the input image are converted into DNA sequences using encoding rules (A, T, C, G). It is widely used in secure image encryption because of its high randomness, parallelism, and complexity.
- Permutation (Scrambling): The process involves the shuffling of pixels without changing its actual value in image encryption. To achieve better permutation, Chaotic maps are widely used due to its inherent properties which includes sensitivity to initial condition, unpredictability and randomness. The shuffling of pixel positions reduces the spatial correlation among neighboring pixels, resulting in complete distortion of an image, making it inaccessible to unauthorized users.
- Diffusion: This is the process in which pixel values of an image are modified to reduce statistical relationship between original and encrypted image. In image encryption, diffusion is achieved through arithmetic operations such as XOR and complementary rules, ensuring strong confusion and diffusion properties. Consequently, this process helps to strengthens the encryption by achieving high entropy, optimal NPCR, UACI values and reducing pixel correlation, thereby increasing the robustness against cryptanalytic attacks.

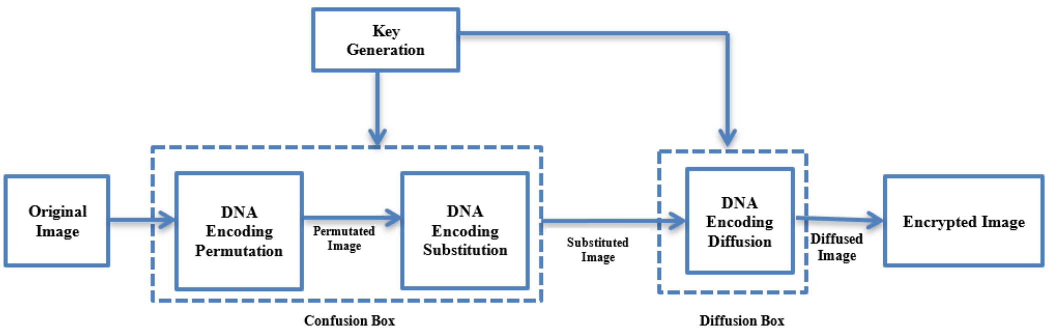


Figure 1. DNA Encryption Process.

These steps collectively enhance randomness and resistance to attacks while maintaining computational efficiency [1][3].

***Quantum-Based Encryption Model***

Quantum-based image encryption involves the utilization of quantum principles like randomness and entanglement aiming to generate encryption keys that are impossible to break, thereby enhancing the efficiency and security of the system. This scheme is typically implemented using simulation environments providing framework for secure processing of image. The process includes the following stages:

- Quantum Image Representation: In this, the image data is encoded into quantum states using specialized models such as Flexible Representation of Quantum Images (FRQI) or Novel Enhanced Quantum Representation (NEQR), which allows the efficient storage and manipulation of information by representing pixel positions and intensity values using qubits.
- Quantum Key Generation: In this true random sequences keys are generated using Quantum True Random Number Generators (QTRNG) or quantum chaotic systems, thereby significantly enhancing the security of the encryption process.
- Quantum Operations: Encryption is performed using quantum gates, superposition, and entanglement-based transformations, enabling simultaneous processing of multiple states while introducing high levels of complexity and randomness, making the encrypted image highly resistant to cryptographic attacks.

Although these methods provide high security, they require complex computations and specialized environments due to limited availability of quantum hardware system. [4][6]

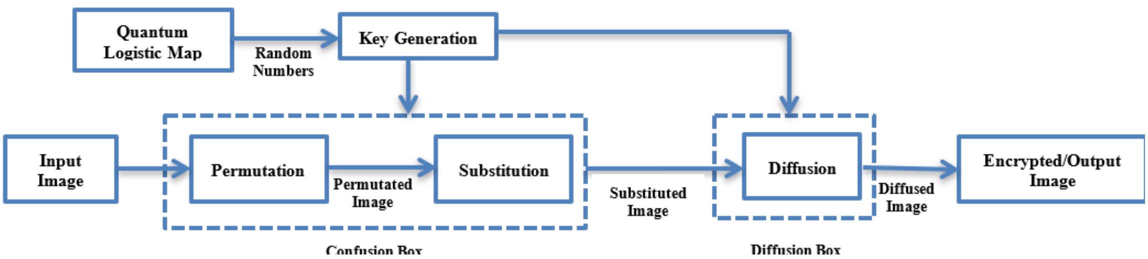


Figure 2. Quantum Based Encryption Process.

## Evaluation Metrics

The performance of the encryption techniques is evaluated using standard metrics commonly used in image security analysis as shown in Table-1. These metrics are widely used in image encryption analysis [2][5].

Table 1. Performance Metrics with desirable range.

| **Analysis Type & Category** | **Performance Parameter (Name, Definition & Units)** | **Desired / Pass–Fail Range** |
|---|---|---|
| **Quantitative Security Analysis –** Metric-based numerical evaluation to objectively assess encryption strength, distortion, randomness and statistical independence. | **Peak Signal-to-Noise Ratio (PSNR):** Measures distortion between original and encrypted images. [8] (Express in dB) | **Pass (P):** < 7.5 dB desirable |
| | **Shannon Entropy:** Measures randomness of gray-level distribution in the encrypted image. [9] | **Pass (P):** ≥ 7.9 (Ideal ≈ 8) **Fail (F):** < 7.9 |
| | **Correlation Coefficient (H, V, D):** Measures pixel dependency in | **Pass (P):** \|r\| ≤0.05 otherwise **Fail (F)** |

| | | |
|---|---|---|
| | horizontal, vertical, and diagonal directions. [12] | |
| **Differential Attack Analysis –** Measures sensitivity of encryption to minor plaintext changes, ensuring resistance against differential cryptanalysis. | **NPCR:** Measures percentage of pixel changes due to a one-pixel change in plaintext. (Express in percentage) | **Pass (P):** ≥ 99.61%<br>**Fail (F):** otherwise |
| | **UACI:** Measures average intensity difference between two encrypted images. (Express in percentage) | **Pass (P):** ≥ 33.33%<br>**Fail (F):** otherwise |
| **Computational Time** | Represents the time required to encrypt the image, indicating the efficiency of the algorithm. | |

## Results and Discussion

The comparative study of both DNA-based and quantum-based encryption using key performance metrics, as shown in Table-2, achieves high entropy, indicating strong randomness, and show excellent resistance to differential attacks with similar NPCR values. DNA-based techniques provide more stable UACI values, reflecting consistent diffusion.
Both approaches effectively reduce pixel correlation to near zero, ensuring secure encryption. However, DNA-based encryption is faster and more suitable for real-time applications, while quantum-based methods are slower and computationally intensive, limiting their practical use at present.

Table 2. DNA-based vs Quantum-based Encryption (Performance Metrics).

| Performance Metric | DNA-Based Encryption | Quantum-Based Encryption |
|---|---|---|
| **Entropy** | 7.98 – 7.999 (High randomness) | ≈ 7.999 (Very high randomness) |
| **NPCR** | ≈ 99.5% – 99.7% (Excellent) | ≈ 99.6% (Excellent) |
| **UACI** | ≈ 30% – 33% (Stable, near ideal) | ≈ 27% – 33% (Slight variation) |
| **Correlation Coefficient** | ≈ 0 (Very low correlation) | ≈ 0 (Very low, slightly better) |
| **Execution Time** | Fast | Slow / Resource-intensive |
| **Real-Time Applicability** | Suitable for real-time use | Not practical currently |

## Conclusion

The work done in this paper provides a comprehensive comparison of DNA-based and quantum-based medical image encryption techniques using standard performance metrics. The analysis shows that both approaches achieve high levels of security and randomness. The following inferences can be drawn from the results

- Entropy: In terms of entropy Quantum based mechanism have edge on DNA based security mechanisms indicating high randomness of data in Quantum security mechanisms
- Differential Parameters: Almost, both are equivalent with DNA based having slight advantage over its counter part
- Real Time Applicability: Quantum-based encryption provides superior theoretical security due to its foundation in quantum mechanics. In contrast, DNA-based encryption offers an effective balance between security and performance. It achieves high entropy, strong resistance to attacks, and efficient execution on classical

systems. These characteristics make DNA-based techniques more suitable for real-time medical image protection.

Therefore, it can be concluded that DNA-based encryption is currently the most practical solution for securing medical images, while quantum-based approaches represent a promising direction for future research.

## References

[1] Kumaran, V. N. S., Manikandan, T., Dhanaraj, R. K., Al-Shehari, T., Alsadhan, N. A., & Selvarajan, S. (2025). A secure medical image encryption technique based on DNA cryptography with elliptic curves.

[2] Aljaedi, A., Jamal, S. S., Aljuhni, A., Alharbi, A. R., & Shah, T. (2025). Fusion cryptography for secure medical data transmission using mathematical quantum computing operations.

[3] Shafique, A., Naqvi, S. A. A., Raza, A., Ghalaii, M., Papanastasiou, P., McCann, J., Abbasi, Q. H., & Imran, M. A. (2024). A hybrid encryption framework leveraging quantum and classical cryptography for secure transmission of medical images in IoT-based telemedicine networks.

[4] Gao, J., Wang, Y., Song, Z., & Wang, S. (2023). Quantum image encryption based on quantum DNA codec and pixel-level scrambling. Entropy, 25(6), 865.

[5] Ali, Z. A., Atia, T. S., Yousuf, A. Y., & Khahdim, A. J. (2024). A comprehensive review of quantum image encryption methods. Quantum Information Processing.

[6] Kumar, D., Mishra, D. C., & Guleria, V. (2025). Survey on medical image encryption: From classical to deep learning-based approaches. Computers & Electrical Engineering, 123, 110011.

[7] Levaillant, C. (2025). A novel approach to multi-image quantum encryption/decryption using qudits. https://arxiv.org/abs/2506.23039

[8] Anand, A. N., Muni, S. S., & Kaushik, A. (2025). DICOM compatible 3D multimodality image encryption using hyperchaotic signal. https://arxiv.org/abs/2504.20689

[9] Zhang, Y., Liu, H., & Wang, X. (2024). Secure medical image transmission in cloud-based healthcare systems. IEEE Access, 12, 45678–45690.

[10] Chen, J., Xu, L., & Li, P. (2023). Chaos-based image encryption: A review and new directions. Information Sciences, 640, 119–135.

[11] Singh, R., & Sharma, P. (2024). Hybrid cryptographic techniques for secure image communication. Journal of Information Security and Applications, 76, 103512.

[12] Wang, S., & Li, Q. (2023). Advances in quantum cryptography for secure communication. IEEE Communications Surveys & Tutorials, 25(2), 987–1012.

# DESIGN, DEVELOPMENT AND EXPERIMENTAL INVESTIGATION OF A SQUARE PYRAMID SOLAR STILL FOR DESALINATION APPLICATIONS

Abhishek Bhardwaj*[1], Raj Kumar[1], Nitin Panwar[1]
*[1]J.C. Bose University of Science & Technology, YMCA, Faridabad, Haryana, India
*abhishek.bhardwaj99@gmail.com

## Abstract

*Using sustainable solar energy, solar desalination is a practical and eco-friendly way to produce drinkable water. In order to produce freshwater, a square pyramid solar still (SPSS) was devised, built, and experimentally examined. The solar still is made up of a 350 mm by 350 mm square basin made of galvanized iron sheet that is coated in a clear, pyramid-shaped glass structure that is 4 mm thick. Throughout the day, solar radiation can enter the still from a variety of directions due to the pyramid glass surfaces' 30° inclination. In Faridabad (Latitude 28.368° N, Longitude 77.374° E), the experimental setup was put up and tested in an outdoor climate. Black paint was applied to the basin's surface to enhance evaporation and solar absorptivity. Throughout the trial, performance metrics such basin temperature, water temperature, glass temperature, and freshwater productivity were noted. Compared to traditional solar stills, the pyramid design offers a greater condensation surface area, which improves the evaporation–condensation process. The results demonstrate that the proposed technique is a simple, cost-effective and efficient approach for freshwater production and desalination, particularly suitable for remote and rural areas with limited access to clean drinking water.*

## Keywords

Solar desalination, Solar Still, Pyramid solar still, Renewable energy, Freshwater production.

## Introduction

Freshwater scarcity has emerged as one of the most critical global challenges, driven by rapid urbanization population growth and climate change. Safe drinking water is unavailable in many parts of the world, particularly in isolated and rural places [1]. Conventional water purification techniques are inappropriate for decentralized applications because they frequently require a large energy input and complicated infrastructure. [2]

Because solar desalination uses abundant solar energy to turn contaminated or salted water into drinkable water through evaporation and condensation processes, it is a promising alternative. One of the most straightforward and affordable solar desalination systems is a solar still [3]. They work on the basis of the natural hydrological cycle, in which distilled water is created when water condenses on a cooler surface after evaporating due to solar warmth [4].

Due to their small surface surfaces for condensation and evaporation, traditional basin-type solar stills are not very productive [5]. Researchers have suggested a number of design changes, including multi-basin stills, stepped stills, wick-type stills, and pyramid solar stills, to enhance the performance of solar stills. Compared to traditional designs, a pyramid solar still has a number of advantages [6]. The pyramid-shaped glass cover enables solar radiation to enter the basin from multiple directions throughout the day, thereby enhancing heat absorption. Furthermore, the inclined glass surfaces provide an increased condensation area, which improves the collection efficiency of distilled water [7].

The objective of this study is to design, fabricate and experimentally investigate a SPSS using locally available materials and to evaluate its performance for desalination applications.

## Design and Fabrication of Square Pyramid Solar Still

### *Basin Design*

The basin of the solar still was fabricated using a galvanized iron (GI) sheet. The vessel is 350 mm by 350 mm and has a square shape. Black paint was applied to the basin's interior surface to enhance heat transmission to the water and increase solar radiation absorption [8].
The square design was chosen to distribute heat evenly over the basin and sustain the pyramid-shaped glass framework. Fig. 1 shows a schematic illustration of the square pyramid solar still. The basin's square base, measuring 350 mm by 350 mm, acts as the saline water evaporation chamber. The pyramid glass cover, which is positioned above the basin, is made up of triangular glass plates that are angled around 30 degrees from the horizontal surface [9]. The basin structure's height of roughly 150 mm gives the still's evaporation and condensation operations enough room. The inclined glass surfaces downwards facilitate the condensation of water vapor, allowing the formed droplets to flow smoothly downward into the collection channel [10]. This arrangement enhances both the condensation efficiency and overall solar energy absorption, thereby improving the performance of the desalination process.

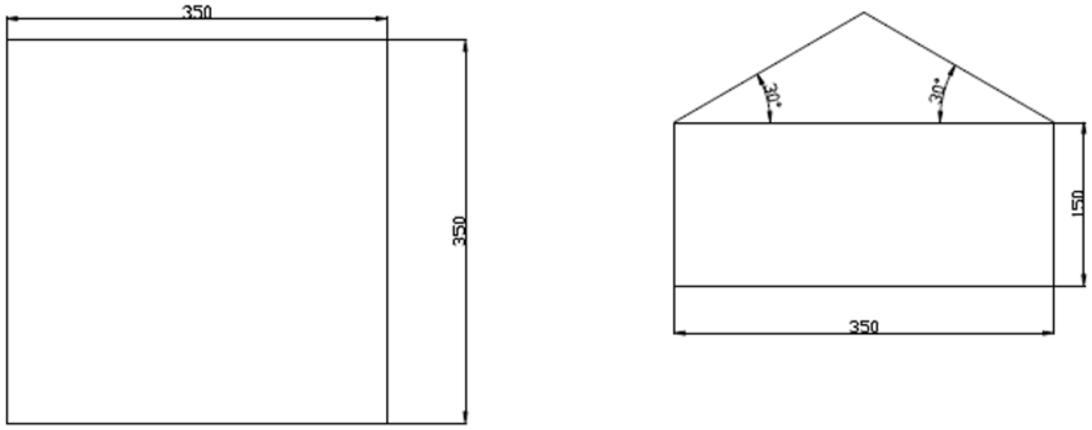


Figure 1. Schematic views of the square pyramid solar still.

### *Pyramid Glass Cover*

The transparent cover of the solar still consists of four triangular glass panes arranged in a pyramidal configuration. Each pane has a thickness of 4mm, providing adequate structural strength while ensuring high transmittance of solar radiation. The glass surfaces are inclined at an angle of approximately 30° to the horizontal, which facilitates efficient condensation of water vapor on the internal surfaces [11]. The condensed droplets then flow smoothly downward into the collection channel under the influence gravity. The pyramid configuration offers several advantages over conventional single-slope solar still designs [12]. It allows solar radiation to enter the basin from multiple directions throughout the day, thereby increasing the total solar energy absorbed within the system and enhancing the day. Furthermore, the pyramid design increases the condensation surface area, which enhances the condensation process and boosts the effectiveness of freshwater collection [13]. Additionally, the design lessens the effects of shade at different times of the day, which enhances the solar still's overall distillate yield and thermal performance. As seen in Fig. 2, galvanized iron (GI) sheet was used to construct the solar still's basin.

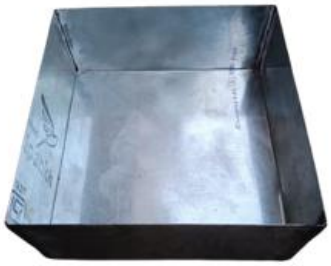

Figure 2. Fabricated GI sheet basin used in the square pyramid solar still.

### *Supporting Structure*

The glass panels and basin were supported by a wooden frame. The pyramid configuration's correct alignment and structural stability are guaranteed by the frame as shown in Fig. 3. The solar still structure's overall height of about 150 mm offers enough room for the condensation and evaporation processes. To stop heat loss and vapor leakage, silicone sealant was applied to all gaps between the glass panels and the basin [14].

Figure 3. Wooden frame to cover square pyramid solar still.

### *Distillate Collection System*

The basin water is heated by solar radiation during operation, which results in evaporation. On the inside surfaces of the inclined glass cover, the produced water vapor rises and condenses [15]. As seen in Fig. 4, the condensed water droplets are collected through a condensate collecting channel at the base of the glass panels after sliding lower due to gravity. After that, the distilled water is sent to an exterior collection container via an exit pipe.

Figure 4. Distillate collection system of square pyramid solar still.

## Materials and Methods

### *Materials Used*

Several readily available and reasonably priced materials were used in the construction of the square pyramid solar still. Galvanized iron (GI) sheet, which offers good durability and corrosion resistance, was used to build the solar still's basin. The transparent cover of the solar still was fabricated using 4mm thick glass to ensure effective transmission of solar radiation

ISBN 978-81-973526-0-7

while maintaining structural strength. A wooden frame was used to support both the glass panels and the basin structure. The inner surface of the basin was coated with black paint to enhance solar radiation absorption and promote rapid water evaporation [16]. All joints and connections were carefully sealed using silicone sealant to prevent vapor leakage during operation. A plastic pipe was employed as the distillate collection channel to convey the condensed water from the still to an external storage container [17]. These materials were selected based on their availability, low cost and ease of fabrication making the system suitable for practical implementation, particularly in remote and rural areas.

### *Fabrication Procedure*

There were several stages involved in building the square pyramid solar still. First, a square basin with the required dimensions was created by cutting and shaping the GI sheet. After the basin was built, its interior surface was painted black to enhance solar energy absorption and speed up the evaporation process [18]. A hardwood frame was then used to provide structural support for the basin and the pyramid glass cover. The triangular plates made of glass required to form the pyramid construction were carefully cut and assembled above the basin [19]. These glass plates were affixed at the required inclination angle to facilitate efficient condensation and the effortless movement of condensed water droplets. Every junction between the glass panels as well as the basin was sealed with silicone to prevent vapor leaks and maintain the system's internal temperature [20]. Finally, a condensate collection channel and an outlet pipe were constructed to collect the distilled water produced during operation. The final result was a tiny, portable solar desalination apparatus suitable for testing.

## Experimental Setup

Experimental research on the square pyramid solar still was conducted in the outside atmosphere of Faridabad. Several productivity and thermal parameters were tracked during the trial to evaluate the solar still's effectiveness. These factors included basin temperature, water temperature, glass temperature, ambient temperature, and freshwater yield [21]. Digital thermometers were placed at key locations throughout the solar still to detect temperature in order to accurately monitor the system's thermal activity. The amount of distilled water produced was measured using a calibrated measuring flask that was fastened to the collection route. Observations were conducted at regular hourly intervals throughout the day to assess the solar still's thermal performance and freshwater productivity under natural sun radiation.

Figure 5. Designed square pyramid solar still.

## Results and Discussion

The experiment's findings demonstrate that basin and water temperatures increase with solar radiation intensity during the day. Maximum temperatures were usually recorded during midday, when solar energy was at its highest.

As the temperature of the basin water increased along with the rate of evaporation, the still produced more vapor [22]. The vapor condensed on the interior surfaces of the glass panels due to the temperature difference between the vapor and the glass surface [23].

The pyramid-shaped glass cover provided more surface area for condensation than conventional solar still designs, which improved the condensation process [24].

The freshwater productivity of the still increased gradually throughout the morning and reached its peak in the afternoon, often between 12:00 and 3:00 PM, when solar radiation strength was at its highest [25].

Overall, the results of the experiment demonstrate that the square pyramid solar still can efficiently provide freshwater using renewable solar energy.

## Conclusion

A square pyramid solar still was successfully designed, built, and tested for desalination applications. The pyramid design allows solar energy to enter from multiple directions and enhances the condensation surface area.

The primary findings of the study are as follows:

- The condensation and evaporation processes are improved by the pyramid glass structure.
- Low-cost, locally accessible materials can be used to manufacture the system.
- The solar still offers an eco-friendly and sustainable way to produce freshwater.
- Rural and isolated locations with little access to clean drinking water can use the established system.

Future research might concentrate on enhancing the solar still's efficiency by adding fins, phase-change materials, or nanofluids.

## References

[1] Kabeel, A. E., and Mohamed Abdelgaied. 2020. "Enhancement of pyramid-shaped solar stills performance using a high thermal conductivity absorber plate and cooling the glass cover." Renewable Energy 146: 769-775.

[2] Fath, Hassan ES, M. El-Samanoudy, K. Fahmy, and A. Hassabou. 2003. "Thermal-economic analysis and comparison between pyramid-shaped and single-slope solar still configurations." Desalination 159, no. 1: 69-79.

[3] Wassouf, Peter, Tom Peska, Randeep Singh, and AliakbarAkbarzadeh. 2011. "Novel and low cost designs of portable solar stills." Desalination 276, no. 1-3: 294-302.

[4] Omara, Z. M., Mohamed A. Eltawil, and ElSayed A. ElNashar. 2013. "A new hybrid desalination system using wicks/solar still and evacuated solar water heater." Desalination 325: 56-64.

[5] Shalaby, S. M., E. El-Bialy, and A. A. El-Sebaii. 2016. "An experimental investigation of a v-corrugated absorber single-basin solar still using PCM." Desalination 398: 247-255

[6] Kabeel, A. E., and Mohamed Abdelgaied. 2016. "Improving the performance of solar still by using PCM as a thermal storage medium under Egyptian conditions." Desalination 383: 22-28.

[7] Kabeel, A. E., Mohamed A. Teamah, Mohamed Abdelgaied, and Gmal B. Abdel Aziz. 2017. "Modified pyramid solar still with v-corrugated absorber plate and PCM as a thermal storage medium." Journal of Cleaner Production 161: 881-887.

[8] Elamy, M. I., Alawee, W. H., Basem, A., Mohammed, S. A., Abdullah, A. S., Majdi, H. S., ... & Younes, M. M. (2024). An experimental comparison for thermos-economic performance of five different designs of solar stills. Case Studies in Thermal Engineering, 59, 104561.

[9] Zakaria, M. M., Esmail, M. F., Abdel-Fadeel, W. A., Abdel-Ghany, A. M., & Hares, E. (2025). Latest Advanced Techniques Applied to Solar Still Configurations to Enhance Performance: A Review. Process Safety and Environmental Protection, 106806.

[10] Kumar, V., Das, B., & Gupta, R. (2025). Energy, exergy, economic and environmental analyses of single slope solar still employing cylindrical cement fins and wick material for thermal energy storage. Journal of Energy Storage, 110, 115360.

[11] Mankai, S., Chemkhi, S., Madiouli, J., Saad, F. O., Shigidi, I., & Sghaier, J. (2025). Performance Optimization of Solar Still Employing Red-Bricks as Sensible Heat Storage Material and Interfacial Evaporation Area. Case Studies in Thermal Engineering, 105798.

[12] Sibagariang, Y. P., Rosyid, O. A., Ambarita, H., Sudrajat, A., Ridlo, M. R., Lande, N. M., & Fudholi, A. (2025). Solar still double slope evaporation improvement using palm kernel as sensible heat storage material. Case Studies in Thermal Engineering, 66, 105705.

[13] Bhardwaj, A., Panwar, N., & Kumar, R. (2025). Influence of wick material, pyramid shape and phase change material on performance enhancement of solar stills-a review. Environment, Development and Sustainability, 1-58.

[14] Veeramanikandan, K., & Somasundharam, S. (2026). A critical review on thermal energy storage enhanced solar stills: Evaluation of energy, exergy, cost-effectiveness and environmental impact. Journal of Energy Storage, 141, 119084.

[15] Abbaspour, M., Esmaili, Q., & Ramiar, A. (2024). Improving vertical solar still performance for efficient Desalination: Investigating the influence of Wick, condensate plate and device dimensions. Solar Energy, 272, 112468.

[16] Elfasakhany, A. (2016). Performance assessment and productivity of a simple-type solar still integrated with nanocomposite energy storage system. Applied energy, 183, 399-407.

[17] Mahala, T., & Sharma, N. (2024). Experimental investigations of a novel solar still with heat storage materials-energy, exergy, economic and environmental analyses. Desalination, 578, 117467.

[18] Attia, M. E. H., Eisa, A., Mahroogi, F., & Elazab, M. A. (2025). Enhancing conical solar still water production through surface tension reduction with floating plastic tubes: A comparative study and sustainability analyses. International Communications in Heat and Mass Transfer, 165, 109081.

[19] Farouk, W. M., Abdullah, A. S., Mohammed, S. A., Alawee, W. H., Omara, Z. M., & Essa, F. A. (2022). Modeling and optimization of working conditions of pyramid solar still with different nanoparticles using response surface methodology. Case Studies in Thermal Engineering, 33, 101984.

[20] Dubey, A., Dubey, A., & Arora, A. (2026). Machine learning based prognostic analysis of a hybrid solar still coupled with evacuated tube collector and stearic acid: A comprehensive 4-E assessment. Solar Energy Materials and Solar Cells, 298, 114165.

[21] Awad, A. M., El-Said, E. M., Abdelgaleel, M., Abdelrehimd, O., & Hegazi, A. A. (2025). Enhancement of the solar still performance using bitumen, iron, copper and

aluminum filings: Energy, exergy and economic analysis. Renewable Energy, 124520.

[22] Bacha, H. B., Joseph, A., Abdullah, A. S., & Sharshir, S. W. (2025). Synergizing water desalination and hydrogen production using solar stills with novel sensible heat storage and an alkaline electrolyzer. Case Studies in Thermal Engineering, 65, 105663

[23] Elmghari, N., Rachidi, M. B., Salihi, M., Chebak, A., Al-Dahhan, M. H., & Chhiti, Y. (2025). Enhancing solar still productivity using phase change material: Experimental investigation under the climatic conditions of Benguerir, Morocco. Applied Thermal Engineering, 269, 126056.

[24] Ahmadian, Z., Khanmohammadi, S., & Khanjani, S. (2025). Experimental investigation of sustainable solar desalination with pulsed air–water injection: Energy, exergy, and image processing-based analysis. Case Studies in Thermal Engineering, 107443.

[25] Kanka, S. D., Kibria, M. G., Anika, U. A., Das, B. K., Hossain, M. S., Roy, D., & Mohtasim, M. S. (2024). Impact of various environmental parameters and production enhancement techniques on direct solar still: A review. Solar Energy, 267, 112216.

# QLM BASED AUDIO STEGANOGRAPHY USING CHAOTIC LSB SUBSTITUTION

Dikshant Sharma*[1], Neelam Turk[1], Shailender Gupta[1]
*[1]J.C. Bose University of Science & Technology, YMCA, Faridabad, Haryana, India
*dikshant112@gmail.com

## Abstract
*The rapid growth of digital audio transmission in applications like secure communication, multimedia sharing and IOT systems has increased the need for effective audio steganography techniques to ensure data confidentiality and secure communication. Traditional methods often face limitations in balancing security, transparency and robustness, where as many existing techniques rely only on a limited set of evaluation metrics, restricting a detailed assessment of performance. This paper presents a novel audio steganography technique based on the Quantum Logistic Map (QLM) and Least Significant Bit (LSB) substitution. The proposed method utilizes chaotic sequences generated using QLM to determine embedding positions, thereby enhancing randomness and security. By integrating chaos-driven positioning with LSB embedding, the method achieves improved resistance against statistical and differential attacks while maintaining high audio quality. Experimental results shows high perceptual transparency with a PSNR of 117.65 dB and a low BER of $3.06\times10^{-5}$. Furthermore, comparative analysis with recent state-of-the-art techniques shows that the proposed method achieves superior performance while also incorporating a broader set of evaluation parameters for detailed analysis. These results highlight its suitability for secure and reliable audio data transmission in real-world applications.*

## Keywords
Audio steganography, QLM, chaotic maps, LSB, security.

## Introduction
The widespread and faster adoption of communication platforms, streaming services and IOT enabled systems has led to huge amount of data being generated and exchanged over open networks. In 2025, global audio streaming alone reached a market value of nearly USD 46.9 billion, with a rapid growth following by smartphones and internet based services [1]. Furthermore, digital audio consumption has reached significant levels, with users spending around 4 hours per day listening to music, podcasts and streaming services [2]. In 2025, global audio streaming activity exceeded 5 trillion streams, highlighting the huge amount of audio data being transmitted [3]. The exponential growth makes audio data vulnerable to unauthorized risks and highlighting the need for effective security mechanism like audio steganography. Unlike traditional techniques, audio steganography embeds secret information within audio signals, which conceals the existence of the message. Any changes to the stego signal can modify the embedded data, which can be easily detected during the extraction process, which helps in analyzing if any unauthorized user has made any change to the original data, thus enhancing confidentiality and resistance to interception. Traditional LSB methods suffer from consistency and weak security. To overcome these limitations, chaotic systems like Quantum Logistic Map (QLM) [4] are used for enhancing randomness. This paper proposes a QLM-driven LSB embedding technique to improve security and imperceptibility. To evaluate the effectiveness, multiple performance parameters are considered.

- Peak Signal to Noise Ratio (PSNR): It measures the similarity between modified and original audio signal, where higher PSNR means better quality [5].

- Mean Squared Error (MSE): It evaluates the average squared difference between the original and stego audio signals, where lower value corresponds to better audio quality [6].
- Signal to Noise Ratio (SNR): It evaluates the original signal to the noise introduced during data embedding.
- Bit Error Rate (BER): Assess total number of bits incorrectly recovered after extracting the hidden data.
- Mean Absolute Error (MAE): It determines the average absolute difference between the original and stego signals, lower MAE corresponds to better quality.
- Root Mean Square Error (RMSE): It is the square root of MSE and measures the average difference between the original and stego audio signals.
- Percentage Root Difference (PRD): It evaluates the percentage difference between the original and stego signals.

Together, all these parameters offer a comprehensive evaluation of the performance and reliability of audio steganography techniques [7]. Rest of the paper is organized as: Section 2 comprises of Proposed Methodology, Section 3 comprises of Experimental Results, Section 4 consists of Comparison with Existing Works and Section 5 consists of Conclusion.

## Proposed Methodology

The proposed technique is designed to achieve high perceptual quality and enhanced security using chaos-based technique to securely embed the data. Initially, the input audio signal is transformed into WAV format to ensure that the samples are taken at a constant rate. A chaotic sequence is generated, which shows high sensitivity against initial conditions and pseudo-random behavior. The chaotic sequence generated is further used to determine positions for embedding data using a nonlinear sinusoidal mapping function as shown in Eq-1.

$$\sin\left(\frac{\pi}{2} * x_n * N\right) \quad (1)$$

Here $x_n$ denotes the chaotic value and N represents the total number of samples.

The mapping ensures randomness and unpredictable selection of embedding positions which enhances resistance against statistical and brute-force attack. The data is embedded into least significant bits (LSB) of the selected audio samples, ensuring efficient data hiding with minimal perceptual distortion. LSB substitution ensures that the modifications remain unnoticeable while maintaining high embedding capacity. After embedding, the modified audio samples are reconstructed to generate the final stego-audio signal. The resulting stego signal maintains the original audio quality while providing robustness against potential attacks, making the proposed method suitable for secure audio communication applications. The algorithm for the proposed technique is mentioned in Table-1.

Table 1. Proposed Algorithm.

| ***Embedding***: | |
|---|---|
| **Step 1:** | Convert secret message to binary.(1024 bits) |
| **Step 2:** | Generate chaotic sequence using QLM key.(equal to the size of audio file) |
| **Step 3:** | Select random audio sample positions. (Least Significant Bit location Selection) |
| **Step 4:** | Embed bits into LSB of selected samples. |
| **Step 5:** | Obtain stego audio. |
| ***Extraction:*** | |

| | |
|---|---|
| **Step 1:** | Generate same chaotic sequence using key. |
| **Step 2:** | Identify embedding positions. |
| **Step 3:** | Extract LSB bits. |
| **Step 4:** | Reconstruct original message. |

## Experimental Results

The proposed technique was evaluated using standard audio datasets, against a detailed set of performance metrics. Results computed are shown in Table-2.

Table 2. Comparative Results.

| Ref. | PSNR (dB) | MSE | SNR | BER | Entropy | Correlation | MAE | RMSE | PRD |
|---|---|---|---|---|---|---|---|---|---|
| **[8]** | 12.1723477 | 0.0671156 | -6.178 | - | - | - | - | - | - |
| **[9]** | 74.87 | 0.083 | 0.0083 | - | - | 0.003 | - | - | - |
| **Proposed** | 117.65 | 0.00049 | 102.16 | $3.05*10^{-5}$ | 5.93 | 0.9999 | 0.0005 | 0.022 | 0.0007 |

## Comparison with Existing Works

To ensure the effectiveness of the proposed method a detailed is conducted against existing audio steganography techniques as shown in Table-2. The results evaluated using Ref. [1] shows moderate performance with a PSNR value of 74.87 dB and MSE of 0.083, it provide a partial assessment as it does not include other important parameters such as entropy, BER and correlation, which are essential for analyzing randomness and security. Similarly, the hybrid steganography approach used in Ref. [2] uses both LSB and QIM techniques, which generates low PSNR value of 12.17 dB and a negative SNR value, indicating visible distortion in stego audio signal.

The proposed technique shows improved performance across all evaluation parameters, achieving a PSNR of 117.65 dB, MSE of 0.00049 and minimal distortion. The SNR value further confirms superior signal quality, where as BER ensures reliable data extraction and robustness against transmission errors. Furthermore, it uses additional evaluation metrics like entropy, RMSE, MAE and PRD, to provide a detailed analysis against existing techniques. The overall results shows that the proposed technique outperforms existing techniques in terms of perceptual transparency and robustness thus making it more suitable for secure audio data transmission.

## Conclusion

This paper presents a secure and efficient audio steganography method which combines QLM with LSB substitution. The proposed method implements chaos based embedding along with LSB method to improve security while maintaining high audio accuracy. Based on experimental evaluations and comparison with existing techniques, the following inferences can my made:

- Limited evaluation in existing techniques: Most existing methods do not utilize all necessary performance parameters required to evaluate efficiency, robustness and reliability, and instead focus on only basic parameters like PSNR and MSE.
- Improved performance of the proposed method: The proposed technique performs better in terms of transparency, signal quality and robustness, which is shown by low

BER, high PSNR and high SNR values.

- Comprehensive performance analysis: The proposed method uses a wider range of evaluation metrics like entropy, MAE, RMSE and PRD, for providing a reliable assessment of system performance.

## References

[1] https://www.mordorintelligence.com/industry-reports/audio-streaming-market accessed on 23/03/2026.

[2] https://www.nielsen.com/insights/2025/the-record-q1-audio-listening-trends accessed on 23/03/2026.

[3] https://apnews.com/article/music-listening-habits-2025-christian-rock-latin-a5e06a001705cd7e5d3854d8fab901b8 accessed on 23/03/2026.

[4] N. Mittal, S. Dhall, L. Rai, et al., “Logistic map-based deterministic random number generators: A survey,” SN Computer Science, vol. 7, p. 265, 2026, doi: 10.1007/s42979-026-04853-5.

[5] Y. Liu, X. Zhu, J. Wang and J. Xiao, "A Quantitative Metric for Privacy Leakage in Federated Learning," ICASSP 2021 - 2021 IEEE International Conference on Acoustics, Speech and Signal Processing (ICASSP), Toronto, ON, Canada, 2021, pp. 3065-3069, doi: 10.1109/ICASSP39728.2021.9413539.

[6] D. K. Sharma, M. Chatterjee, G. Kaur, and S. Vavilala, “Deep learning applications for disease diagnosis,” in Artificial Intelligence for COVID-19, Elsevier, 2021, pp. xx–xx, doi: 10.1016/B978-0-12-824145-5.00005-8.

[7] A. Pradhan, A. K. Sahu, G. Swain and K. R. Sekhar, "Performance evaluation parameters of image steganography techniques," 2016 International Conference on Research Advances in Integrated Navigation Systems (RAINS), Bangalore, India, 2016, pp. 1-8, doi: 10.1109/RAINS.2016.7764399.

[8] T. Srinivasa Padmaja and S. Mahaboob Basha, “A novel hybrid steganography approach for securing text, images, and audio with robust encryption in audio steganography,” Journal of Engineering and Technology for Industrial Applications (ITEGAM-JETIA), vol. 11, no. 52, pp. 136–147, Mar./Apr. 2025, doi: 10.5935/jetia.v11i52.1235.

[9] A. S. Abd, O. Q. J. Al-Thahab, and A. A. Hamad, “New approach in steganography algorithm by using audio and image as secure information based on chaotic method,” International Journal of Safety and Security Engineering, vol. 15, no. 2, pp. 349–358, 2025, doi: 10.18280/ijsse.150216.

# IMT Industries Association Faridabad

## For the Industry ~ By the Industry

## IIAF Governing Body

- Shri Parmod Rana - President
- Shri H.S. Shekon - Vice President
- Shri Nitin Bareja - Vice President
- MS. Rashmi Singh - GENERAL SECRETARY
- Shri Ajay Abrol - Add. General Secretary
- Shri Rajendar Kalra - Joint Secretary
- Inder Chand Jain - Chairman Media
- Shri. D.P. Yadav - Chairman Environment
- Shri Devender Goyal - Chairman Sanitation and Water Works
- Shri Tej Chaudhary - Chairman Law and Order
- Shri V.P. Goyal - Chairman Infra
- Shri V.P Dalal - Chairman New Project

Let's Talk +91 9289293999
Mail us: info@iiaf.co.in
Visit : www.iiaf.co.in

J.C. BOSE UNIVERSITY OF SCIENCE AND TECHNOLOGY, YMCA, FARIDABAD

*NAAC 'A+' Grade Accredited State Govt. University*

NH-2, Sector 6, Faridabad (Haryana) 121006

jcboseust.ac.in /JCBoseUST